Assessment and Modelling of Chromium Release in Minerals Processing Waste Deposits

by

Joachim Petersen

Thesis Presented for the Degree of

DOCTOR OF PHILOSOPHY

in the Department of Chemical Engineering

UNIVERSITY OF CAPE TOWN

March 1998

Abstract

The minerals processing industry is by far the largest generator of mineral solid wastes, which are commonly stored in large scale landfill deposits. The potential environmental impact of these is directly linked to the time-dependent process of leachate generation within these deposits. Rainwater draining through the porous matrix of a deposit creates a slowly moving aqueous environment within the deposit. Heavy metal species that may be contained in trace amounts in the waste material can be mobilised into the aqueous phase by various chemical reactions and be transported by mechanisms of diffusion and convection to the base of the deposit and from there further into the surrounding environment.

Laboratory assessment methods aim to provide indicators to the leachate generation potential of a particular waste material, often based on "worst case" assumptions, but generally fail to offer a meaningful appreciation of the time-dependent leach behaviour of the material in a full scale deposit. This is to a large part due to the lack of a thorough description - in terms of a rigorous mathematical model - of the leachate generation process itself.

Such a model is developed in the present work, building on an existing model for heap leaching, which, conceptually, is very similar to the leachate generation process. The model is based on the continuity equation formulated for reaction-diffusion processes at the level of an individual porous particle and for convection-dispersion transport at the bulk level. This is combined with a number of reaction models, both kinetic rate expressions and thermodynamic equilibrium models, to describe the release process of individual species at the solid liquid interface and also within the aqueous phase. The model has been translated in the WASTESIM computer code within which waste

material and disposal scenario are characterised by a number of parameters, such as those describing reaction modes and constants, particle size and pore diffusion effects as well as bed transport and saturation. The program was found to be a versatile tool for modelling a wide range of multi-species, multi-reaction deposit and batch leach scenarios.

However, for modelling real waste materials the model parameters have to be established from a systematic laboratory investigation. An assessment methodology is proposed which aims to combine lysimeter studies with bench scale leach and physico-chemical characterisation experiments to enable determination of all model parameters entirely on the basis of laboratory experiments and validate them at this level against the results from independent lysimeter studies with the modelling tool. It is argued that, if all model parameters are validated at the laboratory scale in this way, modelling of full scale scenarios involving the same waste material can be conducted with some confidence.

This approach has been put to the test with two waste materials from the ferro-alloy industry - a furnace emission control dust and a smelter slag. The contaminant species of particular interest for both these materials was chromium, especially Cr(VI), and therefore it was the release behaviour chromium on what much of the work presented herein has focused. The aqueous and environmental chemistry of chromium is extensively reviewed and, as a side aspect, the long-term atmospheric oxidation of Cr(III) to Cr(VI) has been positively identified by experimental work with a third chromium-containing waste material.

The two test materials have been subjected to intensive characterisation in terms of column and batch leach experiments, adsorption studies, column tracer studies and physical characterisation experiments. The results are carefully interpreted with a view to establishing a complete set of parameters to simulate the leachate generation behaviour with respect to chromium species in a deposit scenario. It is demonstrated

that the modelling tool can in fact also be used for the interpretation of batch leach data through curve fitting exercises.

For both materials the WASTESIM code, calibrated with parameters established entirely through the laboratory experimentation, has been used to simulate the leach curves of two independent lysimeter experiments, which are then compared to the measured data. In both cases the modelled and measured curves compared reasonably well and in most regards discrepancies can be explained by insufficient characterisation in the bench-scale experiments. The overall approach is therefore seen as valid in principle, but it is acknowledged that further experimental work and model development would be needed to take account of the remaining discrepancies.

Two aspects were found to be particularly significant. The first relates to slow reaction mechanisms, which may go unnoticed in short-term laboratory experiments, but may become significant in full scale deposits given their long life-span. The slow atmospheric oxidation of chromium is a point in case. The second aspect relates to the hydro-dynamic characterisation of flow through unsaturated beds. Both model and laboratory assessment methods are insufficiently developed to account for effects such as dead pore diffusion and a distribution of flows.

Recommendations for further development work should focus on these two aspects and on expansion of the approach to heavy metal species other than chromium. It is hoped that the modelling and assessment methodology will ultimately find welcome application in the environmental risk assessment of mineral processing waste disposal operations.

Acknowledgements

So many people have helped me, in one way or another, to achieve the enormous task of completing this PhD work. To all of them I would like to extend my deepest feeling of gratitude. More specifically I would like to thank the following:

- Prof. James G. Petrie for inviting me to come and work on his team and for giving me the freedom to approach this work in my own way and yet providing guidance wherever it was needed. I have great admiration for Jim's vision, and if there is one thing I have learned through working with him, it is never to lose sight of the broader implications of the work I am doing, yet always to question critically the details.

- The Foundation for Research and Development (FRD) in South Africa for funding the final year of my research project.

- All the members of "The Greenhouse" for fun, fights and fish! Special thanks go to Harro von Blottnitz, Brett Cohen and Shehnaaz Moosa for being such good friends.

- All the members of staff at the Department of Chemical Engineering for their friendly support, but especially Suzana Vasic and Katarina Johannson for their tireless efforts in analysing the uncountable number of samples.

- Richard Walsh, Brett Paton, Andrea MacDonald, Derek Delmar and Yvonne Hansen for helping out with the experimental work at various stages.

- My parents, Ingrid and Harro Petersen, for their love and unconditional support and for making it possible for me to be in South Africa.

- Caroline for all her patience, for believing in me and for her never-ending love.

Table of Contents

Appendices

A 3.5" disk, labelled DATA & WASTESIM, containing all files listed in Appendix C is supplied in the sleeve in the back-cover of this volume

List of Figures

List of Figures (cont.)

List of Figures (cont.)

List of Figures (cont.)

List of Figures (cont.)

List of Figures (cont.)

List of Figures (cont.)

List of Tables

List of Tables (cont.)

Roman (cont.)

Symbol	Description	Units
h	hydraulic head	[m]
I	total ionic strength	[mol/l]
j_D	Chiltom-Colburn factor	diml.
k, k_p, k_s	(pore, surface) reaction kinetic constant	var.
k_c	film mass transfer coefficient	[m/s]
K	hydraulic conductivity	[m/s]
K_{ads}	Langmuir adsorption constant	[l/mol]
K_{eql}	general equilibrium constant	var.
K_d	partition coefficient	[l/kg]
K_{sol}	solubility product	var.
L(t)	surface leach rate	[mol/m^{2}s]
m	empirical constant	diml.
m_i	molality of species i	[mol/kg $_{solute}$]
M_i	molar mass of species i	[g/mol]
M_{liq}	total liquid mass in a stirred tank experiment	[kg]
M_{part}	total mass of particles in a stirred tank experiment	[kg]
N_i	molar flux of species i	[mol/m^{2}s]
p	pressure	[N/m^2]
Pe	Peclet number for mass transport	diml.
Q	volumetric flow rate	[m^3/s]
Q_C	source/sink rate term	[mg/l·s]
r	radial dimensional variable	[m]
R	particle radius	[m]
$\overline{R}$	radius of reference size class, mean radius	[m]
R_d	retardation factor	diml.

Greek

Symbol	Description	Units
α	empirical constant	var.
α_L	dynamic dispersivity	[1/m]
β	dimensionless stoichiometric ratio	diml.
γ_i	activity coefficient of species i	var.
δ_i	effective pore diffusivity ratio	diml.
δ_s	surface layer thickness	[m]
δ_{STR}	STR liquid volume to total particle surface area ratio	$[m^3/m^2]$
Δe	discrete incremental concentration shift	[mg/l]
Δt	discrete time interval	[s]
ε	porosity	$[m^3_{void}/m^3_{total}]$
ε_b	bulk fluid void ratio	$[m^3_{fluid}/m^3_{bed}]$
ε_h	heap voidage ratio	$[m^3_{void}/m^3_{bed}]$
ε_p	particle porosity	$[m^3_{void}/m^3_{part}]$
ζ	normalised bed height	diml.
θ	moisture content	$[m^3_{fluid}/m^3_{bed}]$
θ	fractional adsorption	diml.
ϑ	dimensionless bulk flow time variable	diml.
κ	dimensionless reaction rate to diffusion ratio	diml.
λ	heap solids to fluid volume ratio	$[m^3_{solids}/m^3_{bulkfluid}]$
μ	local liquid volume to solid mass ratio	$[l_{fluid}/g_{solid}]$
μ'	local liquid volume to solid surface area ratio	$[l_{fluid}/m^2_{solid}]$
μ_f	fluid viscosity	$[Ns/m^2]$
ν	stoichiometric coefficent	diml.

Superscripts (where used consistently)

Symbol	Description
ads	referring to Langmuir adsoprtion isotherms
eql	referring to equilibrium reactions
f	in feed
j	reaction index
kin	referring to kinetic reactions
(n)	in size class n
sol	referring to solubility product equilibria
(t)	at time t
0	initial
*	reference

Greek (cont.)

Symbol	Description	Units
ξ	normalised radial variable	diml.
Ξ	normalised particle radius	diml.
ρ_f	fluid mass density	[kg/m^3]
ρ_t	true solid mass density	[kg/m^3]
σ	normalised solid concentration	diml.
τ	dimensionless pore diffusion time variable	diml.
τ_D, τ_r, τ_S,...	characteristic time constants	[s]
τ_T	tortuosity factor	
Y	volumetric solid to liquid ratio in a CSTR	[m^3_{solids}/m^3_{liq}]
ϕ	kinetic reaction order	diml.
Φ	fluid potential	[m^2/s]
χ	normalised dissolved concentration	diml.
ψ	pressure head	[m]
ω	dimensionless transport parameter, inverse Peclet number	diml.

Subscripts (where used consistently)

Symbol	Description
i	chemical species index
j	reaction index
n	particle size class index
b	referring to bulk fluid
s	referring to particle surface
p	referring to particle pore fluid

1

Introduction

1.1 Background

The minerals processing industry is concerned with the primary extraction of mineral values from mined raw ores to produce a beneficiated concentrate or a primary commodity for sale. Since the exploitable mineral grade in many ore types is fairly low, beneficiation processes invariably result in large volumes of residues and waste products, the majority of which are present in the form of solids. These include tailings from separation processes, leach residues, smelter slags and flue dusts and precipitates from wastewater treatment, amongst others. Stripped of their mineral values these materials have little immediate economic value and are therefore discarded, usually by disposal to landfill. Historically, such disposal sites have been abandoned after closure of the associated minerals processing operation with little regard being given to their impact on the local environment.

The presence of trace amounts of various heavy metals in many solid minerals processing waste materials constitutes a considerable environmental risk for this form of disposal. Rainwater percolating through a deposit can induce a variety of chemical processes that can potentially lead to the release of heavy metal species and their transport to the bottom of the deposit. From there they can enter and spread through the subsoil and underlying groundwater aquifers (Figure 1-1). The eco-toxicity of dissolved heavy metals, even at relatively small concentrations, is well established (Alloway and Ayers, 1993). Thus the gradual generation and transport of an environmentally harmful leachate from minerals processing waste deposits can turn these into long-term environmental hazards.

1

Introduction

1.1 Background

The minerals processing industry is concerned with the primary extraction of mineral values from mined raw ores to produce a beneficiated concentrate or a primary commodity for sale. Since the exploitable mineral grade in many ore types is fairly low, beneficiation processes invariably result in large volumes of residues and waste products, the majority of which are present in the form of solids. These include tailings from separation processes, leach residues, smelter slags and flue dusts and precipitates from wastewater treatment, amongst others. Stripped of their mineral values these materials have little immediate economic value and are therefore discarded, usually by disposal to landfill. Historically, such disposal sites have been abandoned after closure of the associated minerals processing operation with little regard being given to their impact on the local environment.

The presence of trace amounts of various heavy metals in many solid minerals processing waste materials constitutes a considerable environmental risk for this form of disposal. Rainwater percolating through a deposit can induce a variety of chemical processes that can potentially lead to the release of heavy metal species and their transport to the bottom of the deposit. From there they can enter and spread through the subsoil and underlying groundwater aquifers (Figure 1-1). The eco-toxicity of dissolved heavy metals, even at relatively small concentrations, is well established (Alloway and Ayers, 1993). Thus the gradual generation and transport of an environmentally harmful leachate from minerals processing waste deposits can turn these into long-term environmental hazards.

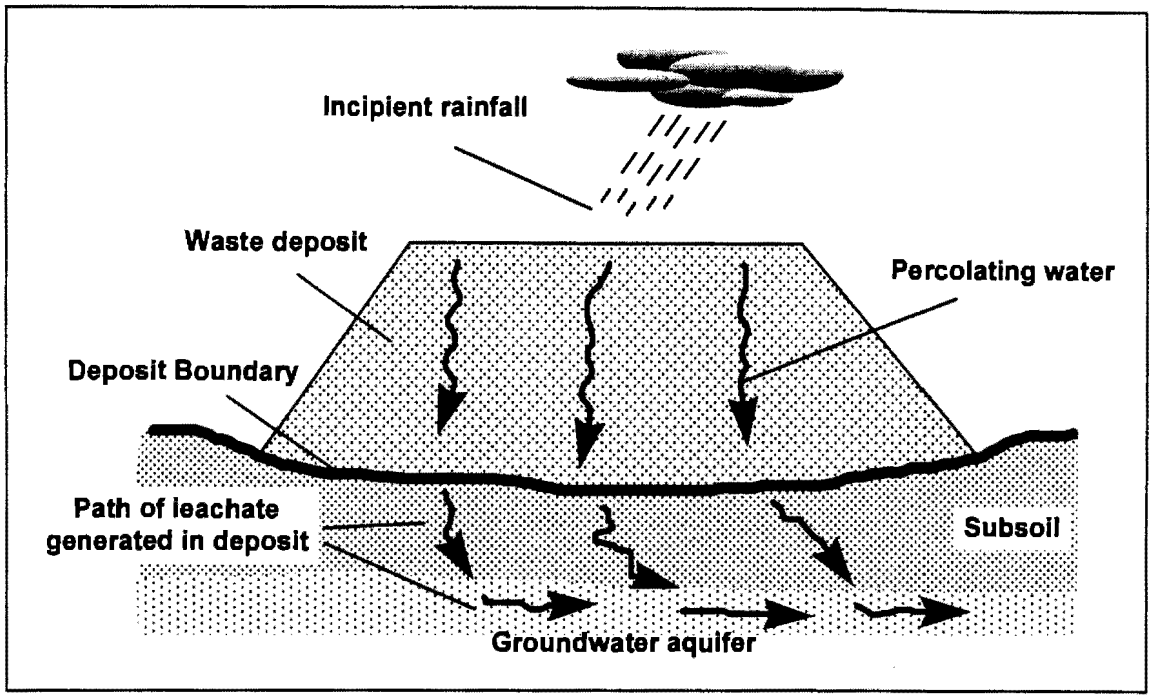

Figure 1-1: Conceptual process of leachate generation in a landfill waste deposit

With environmental concerns growing world-wide over the past 30 years, many types of minerals processing wastes have been identified as major sources of pollution. In many countries legislation has been introduced which is placing the onus on the operators of disposal sites to ensure environmentally sound disposal practice and long-term stability of the site, even beyond closure. This legislative incentive has prompted a substantial growth of geo-technical expertise in constructing environmentally sound waste deposits sites in recent years (Daniel, 1993). Much of this is focused on minimising the flow of leachate from deposits into the ground, for example by the introduction and improvement of liner and leachate collection systems.

While such practice ensures that leachate from a waste deposit is captured and treated before it can enter the surrounding environment, the processes that lead to the generation of such leachates within the deposit are still largely unexplored. In the absence of such an understanding it is difficult to estimate the extent and time a particular deposit is likely to generate environmentally hazardous leachate. With the legal liability for long-term environmental stability of a disposal site resting with its operators, it is now becoming increasingly more important to be able to estimate this leachate generation behaviour. An

understanding of this will allow estimation of the time frame over which pollution control measures around a disposal site can be gradually relaxed up to its final abandonment - with minimal risk of further environmental damage.

The leachate generation process is a complex interaction of transport processes of fluid moving through the solid bed and chemical reaction processes, both within the percolating fluid and between fluid and the solids. Although there are a number of established test procedures available to assess the toxicity or leach potential of a waste material, such as the Toxicity Characteristic Leaching Procedure (TCLP, US EPA, 1992), these tend to concentrate on short-term chemical characterisation and do not take cognisance of the complex interactions likely to be experienced by the material in a deposit situation over extended periods of time. Geochemical models, on the other hand, generally focus on transport of a leachate through soils and aquifers, but are usually less well suited to account for its generation in a waste deposit scenario.

Thus there is a lack of a suitable tool to predict the long-term leachate generation potential of a waste material within a deposit scenario based on a rigorous model and suitably chosen set of waste characterisation methods. The development of such a tool, providing it is reasonably simple to apply and at the same time reasonably accurate over extended periods of time, would benefit not only an industry which is challenged with increasingly stringent environmental legislation, but also society as a whole which would be less likely to be burdened with the legacy of environmentally unsound waste disposal and resulting cases of unforeseen pollution.

The ferro-alloy industry, which encompasses the production of ferro-chromium, ferro-manganese, ferro-silicon as well as stainless steel making, is one branch of minerals processing that continues to enjoy tremendous growth potential in South Africa and world-wide (Barcza, 1996). In South Africa the products of this industry are largely aimed for export, while the wastes and the associated environmental impacts remain in the country. Recognising a global responsibility for the environmental impacts of product cycles, the consumer nations (mostly in the so-called first world) have begun to

exert pressures on raw material producing countries (which often are developing countries) to maintain similar environmental standards as those found in the consumer countries. This directly challenges industry to consider potential environmental burdens of their activities already at the planning stage of new projects and thus consider technology choices and waste management practices, which minimise these potential impacts (Petrie and Raimondo, 1997). The waste assessment methodology proposed herein can greatly help in this regard.

Many of the solid wastes generated in the ferro-alloy industry are characterised by their potential to mobilise chromium, particularly as the toxic Cr(VI), when deposited in landfills. Thus, testing the proposed methodology with such materials and with specific focus on chromium mobilisation, appears a sensible choice in order to immediately demonstrate the relevance of such a tool for its envisaged application.

1.2 Scope of Work

A comprehensive method or tool which allows assessment of the potential for leachate generation of solid minerals processing waste materials and prediction of leachate generation with time within landfill deposits of such waste materials does not exist currently.

The development of such a tool is the central objective of this thesis. As indicated above, the desired predictive method has to incorporate a rigorous model of the chemical and transport processes likely to take place in a waste deposit, and laboratory methods to assess chemical and physical parameters for a certain waste material. These, in combination with such a model, allow meaningful prediction of the generation and transport of leachate within a deposit of this waste material over extended periods of time. Thus the method has two stages: assessment of the waste and deposit modelling.

There exists a substantial body of knowledge on each of these two stages. Waste assessment tests and laboratory procedures are well established and in some cases even form part of legal frameworks, such as the TCLP (US EPA, 1992). Such methods, however, generally fall short of providing meaningful data for the prediction of dynamic leachate generation as it occurs over time within a deposit scenario, but only provide crude yardsticks to the total potential leach capacity or the "worst case" leach potential.

Deposit modelling, on the other hand, can draw from geochemical transport models, which describe groundwater transport through porous media and interactions of chemical species dissolved therein. Such models have been successfully applied to describe and predict leachate transport from contaminated sites. But while rigorous in modelling solution transport, such models generally fall short of comprehensively incorporating chemical interactions with the specific solids the solution is in contact with. Thus there is a clear gap between waste assessment methods on the one hand, and models to incorporate parameters established from such methods on the other. The work presented in this thesis aims to bridge this gap and to synthesise a combined methodology for waste assessment *and* deposit modelling.

A suitable modelling approach for this purpose must take cognisance of the complexity of the process, which is a combination of hydro-transport processes through porous media and multi-species multi-reaction processes, both at the solid-liquid interface and within the moving pore solution. The complexity of the mathematical equations describing such a system is likely to preclude analytical solution and the development of a robust computer algorithm must be considered.

Providing such a rigorous, computer-based modelling tool can be developed, it is postulated here that it can be used to assess the leachate generation potential of a particular waste material in a particular disposal scenario *a priori* (i.e. independent of field data), if all parameters that inform the model can be established from a methodical experimental programme at the laboratory scale.

For this to be achieved, an experimental methodology needs to be devised which ensures that the waste material in question is characterised in terms of all aspects pertaining to its behaviour in a deposit leach situation. Methods that are commonly employed in this context are (Jones, 1995):

- Lysimeter Column Studies. These intend to mimic a deposit situation. The material is exposed to a percolating aqueous phase in a packed bed very similar to what is likely to occur in a full-scale deposit. The chemical environment that exists in such columns (in terms of dissolved concentrations in the aqueous phase, pH, redox potential etc.) can be taken as a good indicator for the chemical conditions likely to prevail in a full scale deposit. However, lysimeter experiments tend to be long-winded and costly.

- Bench Scale Experiments. These aim to establish the leach characteristics of a particular waste material within short-term batch leach studies and thus allow an insight into the chemical behaviour at the particle level. However, while such bench scale studies can be conducted with relative ease, relating the leach behaviour of the material at this scale to the leachate generation process in a full-scale deposit is not straightforward.

- Physico-Chemical Characterisation Studies. These characterise the material in question in terms of its physical properties, such as particle size distribution, shape, porosity, packing and wetting behaviour, as well as in terms of its chemical characteristics, such as chemical composition and mineralogy. Although this characterisation reveals little about the leach behaviour of the material, it provides important background information required for meaningful description of a deposit leach scenario.

Quite clearly, none of these methods is alone sufficient to provide all the information required to calibrate the model for a meaningful prediction of the overall transport and leaching process in a waste deposit. It is therefore postulated further, that a systematic laboratory assessment of a waste material will have to combine all three types of experimental methods to establish characteristic parameters which, when incorporated in

the model, allow predictive simulation of leachate generation process in a full deposit scenario. This approach is illustrated in Figure 1-2.

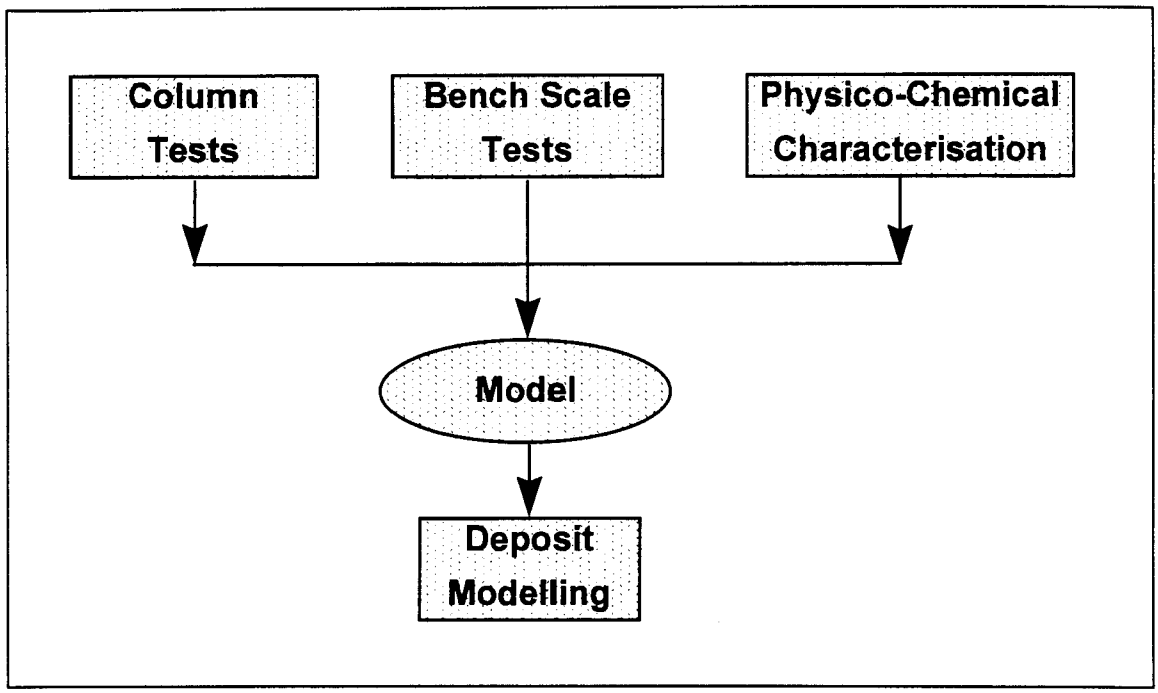

Figure 1-2: Approach to experimental waste characterisation in combination with a model to simulate waste deposit leach scenarios

This combined modelling and assessment methodology needs to be developed and verified through work with real waste materials. Two waste materials from a South African ferro-alloy producer - an emission control dust and a smelter slag - were used in this study. In both of these materials chromium, mainly as the highly toxic Cr(VI), was the major heavy metal species of environmental concern. Chromium was therefore chosen as the focal species for establishing laboratory assessment techniques to characterise release and chemical interactions with the test materials. The behaviour of the materials in a deposit situation was simulated in large lysimeter columns. Further parameters were obtained from laboratory batch leach tests and physico-chemical characterisation methods. In order to test the model with the parameters obtained from these studies, the leach curves of independent lysimeter experiments were simulated. These were compared to the measured data in order to validate or disqualify the overall approach.

Once proven successful for the case of chromium , it then needs to be established in what way and to what extent the methodology established can be redefined to apply for the prediction of the leaching behaviour of other heavy metal species. The potential mobility of chromium in deposits of wastes from this type of minerals processing industry is thus considered as a test case for the development of a general waste assessment and modelling methodology, which may ultimately be expanded for application with one or several species in any type of solid minerals processing waste. This expansion, however, falls beyond the scope of the present work.

A potential limitation to the present approach lies in the the long-term nature of the leach process in a full scale waste deposit, given its likely life span. Kinetically slow chemical reactions may determine the leach process in these, while such reactions may go undetected in the relatively short-term laboratory tests proposed here.

With respect to chromium such a reaction was indeed identified. The potential oxidation of trivalent chromium to its toxic and highly mobile hexavalent form by atmospheric oxidation is a phenomenon that has not been fully explored, but has been subject to much speculation. Without deviating too much from the main objectives of this thesis formulated above, this particular aspect, pertaining more specifically to the type of chromium containing waste materials considered in this study, is investigated in some more detail.

As it is impractical to assess such long-term effects specifically for a specific waste material (given the long time it would take to assess these), incorporation or omission of such reactions in the model needs to be experience-based or dependent on some form of indicative tests. As the primary objective here is the fundamental formulation and validation of the model, such methods are not explored further, but should form part of further work in the future.

1.3 Thesis Structure

The thesis begins with a detailed background studies in Chapters 2 and 3. Chapter 2 focuses on general chromium chemistry, chromium cycles in natural environments and a more detailed experimental study of the atmospheric oxidation of Cr(III) to Cr(VI). Chapter 3 begins with a conceptual introduction to wastes, waste management and pollution before embarking on a review of solid waste management practice in general. Types of chromium containing wastes and aspects of their management, treatment as well as pollution case studies are then discussed more specifically.

Chapter 4 focuses on model development. The theory of aqueous flow through porous media, contaminant transport in aqueous phase and release mechanisms is briefly reviewed. Against this theoretical background, existing modelling strategies in the fields of waste leaching, hydro-geochemical transport and heap leaching are reviewed and discussed in terms of their applicability in the given context. A heap leach model was chosen as the starting point for the formulation of a new model. This is expanded to include multiple reaction mechanisms and various bulk transport phenomena. With minor adaptation the model can also be used to describe batch leach scenarios. The model, which has been translated into the WASTESIM computer code, is subjected to a sensitivity study, investigating the effect of varying various model parameters, such as bed residence time, particle size effects and reaction mechanisms, on model output. Further expansions and limitations of the model are discussed.

Detailed description of the assessment methodology in terms of both, experimental methods and analytical tools for data interpretation is given in Chapter 5. This begins with a review of existing assessment methods and their limitations in the given context, before describing methods for physico-chemical material characterisation, lysimeter studies and various types of batch leach experiments in the specific context of the present study. The interpretation of experimental data in order to obtain material characteristic parameters is discussed in detail. The three-pronged approach indicated in Figure 1-2 is refined in such a way that the preliminary results from the laboratory assessment can be immediately

validated against the lysimeter experiments. Direction and design of further experimental work can be deducted, if the validation is unsuccessful at this level.

Column tracer studies are a useful tool to identify the hydrodynamic behaviour of the waste material under consideration in a packed bed situation. The interpretation of such data in terms of a simple two stream model is elaborated and the incorporation of this approach in the overall modelling strategy is discussed.

Chapter 5 closes with an overview of the experimental work conducted on the two waste materials investigated in the context of this study. Chapters 6 and 7 give detailed account of all experimental results, interpretation of laboratory data, extraction of kinetic and diffusion related parameters using the WASTESIM code, tracer studies and simulation of the lysimeter data for each of the two materials. A critical discussion of the successes and failures of specific experimental and analytical tools and the overall methodology is given in each case.

Conclusions are then drawn in Chapter 8. The overall approach is re-iterated and a detailed chapter-by-chapter summary of specific approaches taken and the key features and findings is given. This is followed by a critical discussion of the work as a whole in terms of the objectives set out in Section 1.2. Some recommendations for further work are made and an overview is given where the model and the proposed methodology might find application in the future.

Appended to the main body of text are three appendices. Appendix A focuses on analytical methods and instrumentation used for the experimental work. Appendix B contains numerical methods and computer algorithms as well as brief introduction to the computer code WASTESIM which is included on the 3.5" disk included in the sleeve on the back-cover to this volume. Appendix C gives a detailed table of contents of all analytical data and simulation results available in Microsoft EXCEL Ver 6.0 spreadsheets contained on the attached disk.

2

Chromium in the Environment

Chromium is counted amongst the toxic heavy metals whose uncontrolled release into the natural environment can cause cases of severe pollution. The phrase "heavy metals" is a general collective term for the group of metals with an atomic density greater than 6 g/cm^3. Although it is only a loosely defined term it is widely recognised and applied to elements such as Cd, Cr, Cu, Hg, Ni, Pb and Zn which are commonly associated with pollution and toxicity problems (Alloway and Ayres, 1993). A more suitable, but less used term for these elements is "trace metals", indicating that they are omnipresent in natural environments at low background concentrations. Only if their local concentrations exceed these background levels beyond certain tolerance levels do these trace metals become toxic. Such increases are usually a direct consequence of anthropogenic processes such as waste disposal.

Chromium occurs naturally only in two forms, the trivalent Cr(III), which is nearly insoluble at a pH between 5 and 10, and the hexavalent Cr(VI) which is soluble in large concentrations at all pH and highly mobile. Cr(VI) is a strong bio-oxidant and carcinogen and therefore considered highly toxic.

It will be shown in the following sections that the chromium chemistry of natural environments such as soils and waters is complex, and involves a range of reactions such as oxidation/reduction, adsorption/desorption and dissolution/precipitation (Palmer and Wittbrodt, 1991). Account needs to be taken carefully of various possible physico-chemical interactions between the two oxidations states to understand fully the

dynamics of chromium in the natural environment, which have been described as cyclic in both, soils and natural water bodies. Out of such an understanding some insight can be gained into the likely effects of imbalances imposed through the "polluting" release of chromium from waste deposits.

One aspect of chromium chemistry that has continued to be the subject of much speculation is the oxidation of Cr(III) to Cr(VI) by atmospheric oxygen (Schroeder and Lee (1975), Saleh *et al.* (1989), van der Weijden and Reith (1982)). While there is sufficient indication in the literature that such a reaction is indeed possible, it is generally taken to be kinetically too slow to warrant consideration in the study of natural environments. In deposits of chromium containing wastes, however, this reaction could give cause for concern, as continued oxidation could lead to a continued release of Cr(VI) from the disposal site into the adjacent natural surroundings, although the waste material may initially not have contained any leachable Cr(VI).

An experimental investigation was therefore conducted to provide more evidence for the chemical conditions and rates at which atmospheric oxidation of Cr(III) to Cr(VI) can take place. Further evidence was also collected from a long-term column leach experiment with a real chromium containing waste material (a stainless steel smelter slag). Experimental results would suggest that the slow atmospheric oxidation of chromium is significant only over extended periods of time, but can indeed be a source of slow pollution through continued Cr(VI) generation and mobilisation associated with certain chromium containing waste materials.

2.1 Environmental Chromium Chemistry

2.1.1 Occurrences, Uses and Toxicity of Chromium

Occurrence

Chromium is the seventh most abundant element on Earth (average concentration 3700 mg/kg), with most of it found in the core and mantle. It is the 21st most abundant element in the Earth's crust. The average concentration in the crust is about 100 mg/kg, but may be as high as 3400 mg/kg in certain ultramafic rock types (Nriagu, 1988).

The most important chrome-containing ore is chromite ($FeO{\cdot}Cr_2O_3$), which is in the form of spinel type crystals, and is highly stable and resistant to chemical attack. Chromium content of this ore can be as high as 46%, making it the most attractive species for chrome processing. At least another 40 chromium minerals are known. In addition, Cr appears as a contaminant in numerous other minerals, often responsible for its colouring, such as in gemstones like ruby and emerald. Most Cr minerals contain Cr(III), whereas Cr(VI) minerals are rare - they mostly occur as types of lead chromate, $PbCrO_4$ (Richard and Bourg, 1991).

Known chromium resources amount to 5.75 billion tons of ore, with recoverable chromium reserves estimated at about 1.5 billion tons of ore. Almost 90% of this reserve is situated in southern Africa (Nriagu, 1988).

Trace amounts of chromium appear virtually everywhere. It has been identified as an essential nutrient for plant, animal and human life in small concentrations (dietary intake <200 μg/day, Nieboer and Jusys, 1988), but may quickly become toxic if consumed in larger amounts. Chromium also appears in virtually all soils at an average concentration of 35-100 mg/kg, but huge variations have been reported (concentration from 0.3 to 10,000 mg/kg, McGrath and Smith, 1991). Similarly chromium is present in all natural waters

(median concentration < 50x 10^{-9} M in fresh water (Richard and Bourg, 1991); between 10^{-8} to 10^{-9} M in oceans (Mayer, 1988)). Through industrial pollution, levels of airborne chromium mobilisation have increased markedly during this century (emissions between 7 340 to 53 610 tons per annum world-wide (Nriagu and Pacyna, 1988)).

Industrial Uses

It is estimated that current production of chromium from ore processing is in the region of 10 million tonnes per annum, of which 76% is consumed in the metallurgical industry (stainless steel and other ferro-alloys), 13% for making refractory linings and 11% for chemical uses such as metal finishing, corrosion control, leather tanning, dies, pigments, wood-preservation, photographic, etc. (Nriagu, 1988).

In general there are no satisfactory substitutes for chromium in any of its major industrial applications, a fact which will ensure its continued demand in the foreseeable future. As resources and reserves are large, little concern has been given to chromium recovery from either scrap metal or process residues. In the USA, for example, only 15% of the chromium consumed annually is recycled (Nriagu, 1988).

Toxicity

Although chromium in trace amounts has been identified as an essential nutrient in all plant, animal and human life, intake of larger amounts of Cr may quickly become toxic, even lethal (McGrath and Smith, 1991; Sheehan *et al.*, 1991). Generally Cr(VI) is considered as the toxic form of Cr, whereas the toxicity of Cr(III) remains somewhat nebulous.

The highly mobile Cr(VI) species can migrate into living cells, causing oxidation of organic components contained therein. Ross *et al.* (1981) have shown that soil concentrations of Cr(VI) in the low range of 0.1 to 10 mg/kg are toxic to soil bacteria. In

studies by McGrath and Smith (1991) plant life was found to be strongly inhibited near chromium contaminated landfill sites. Human contact with Cr(VI) components has been reported to lead to skin dermatitis and mucosal ulceration (Calder, 1988). Ingestion and dermal adsorption has caused kidney failure, whereas breathing of chromate dust has been linked to incidence of lung cancer (Sheehan *et al.*, 1991). Most of these cases, however, occurred as a direct result of long term exposure to high concentrations of Cr(VI) compounds, particularly by workers in the chromate industry (Calder, 1988; Sheehan *et al.*, 1991).

The lethal dose of Cr(VI) intake has been identified as 0.1 g per kg of body weight (Mertz in Richard and Bourg, 1991). The recommended drinking water level of chromium have been set to 0.05 ppm for Cr(VI) and 0.5 ppm Cr(III) by several world bodies (Sheehan *et al.*, 1991). Similarly for air pollution a limit of 0.1 mg/m_N^3 has been set.

The toxicity of Cr(III) is less well established and therefore often tends to be ignored in hazard studies. Cr(III) is largely insoluble in most environments and hence relatively immobile (Ross *et al.*, 1981). Sheehan *et al.* (1991) report that doses of Cr(III) as high as 1468 mg/kg/day in the diet of rats have not produced any adverse effects. Ross et al. (1981) state that the tendency of Cr(III) to form large hydrolysed species prevents its diffusion through cell membranes, but that its adsorptive behaviour with proteins may very well have toxic implications. Excessive concentrations of Cr(III) in soils have led to inhibition of soil bacteria growth (Ross *et al.*, 1981). McGrath and Smith (1991) conducted experimental work which showed that, where mobile Cr(III) species are present in soils at concentrations similar to Cr(VI) levels, equivalent damage to certain types of food seedlings resulted. Schroeder and Lee (1975) report Cr(III) to be potentially hazardous to certain forms of aquatic life. It can therefore be concluded that, although the immediate toxicity of Cr(III) is less than that of Cr(VI), it cannot be ignored as a potential environmental hazard.

The adverse effects of Cr(VI) accumulation in polluted soils have been described by Calder (1988) and Bartlett (1991) in the "chromate bloom" phenomenon that results from upward mobility of Cr(VI) in soils and basement walls due to capillary action, particularly in the dry season. It tends to accumulate on surfaces and crystallise as chromate salt. The surface concentration of Cr(VI) due to this effect can be orders of magnitude higher than in the underlying soils. The adverse effects of such deposition are aggravated in the dry season, when this chromium can become airborne thereby provoking major concern over respiratory ingestion.

2.1.2 Aqueous Cr Chemistry: Speciation and Solubility

Chromium is a d-block transition metal of Group VIB in the Periodic Table. It has the atomic number 24 and an atomic weight of 51.996. Of the five known radioisotopes, ^{51}Cr (half-life 27.8 days) is the most commonly used in experimental work (McGrath and Smith, 1991).

Oxidation states of -2 to +6 can occur, although in aqueous solutions only the +2, +3 and +6 states are of concern (Hartford, 1979), with the latter two being the only ones of interest in natural aqueous environments. The +4 and +5 states can occur as intermediates of limited stability in chemical reactions involving Cr(III)/Cr(VI) interconversions (Eary and Rai, 1987). Ionic radii are 0.052 nm for Cr(III) and 0.064 nm for Cr(VI) (McGrath and Smith, 1991).

Cr metal appears as grey-white, brittle, but highly polishable substance of cubic crystalline structure. It is chemically not stable at atmospheric conditions, but passivates readily with a thin oxide layer (Deltombe *et al.*, 1966), which justifies its widespread use in corrosion protection.

Cr(III) Speciation and Solubility of Cr(OH)3

The free, unhydrolysed Cr^{3+} species is predominant only at a pH below 3. Trivalent chromium shows a strong affinity to oxygen centres, which, in aqueous solution, are readily supplied by water molecules or hydroxide ions. Hence at pH above 3, Cr(III) tends to hydrate with water to various extents (as a function of pH), establishing covalent bonds between Cr and O. In this sense Cr(III) is a Lewis acid. Hydrated Cr(III) displays amphoteric character, i.e. it can act as acid as well as base, depending on solution pH. Hydrolysed species can agglomerate and form polynuclear species with hydroxyl bridges.

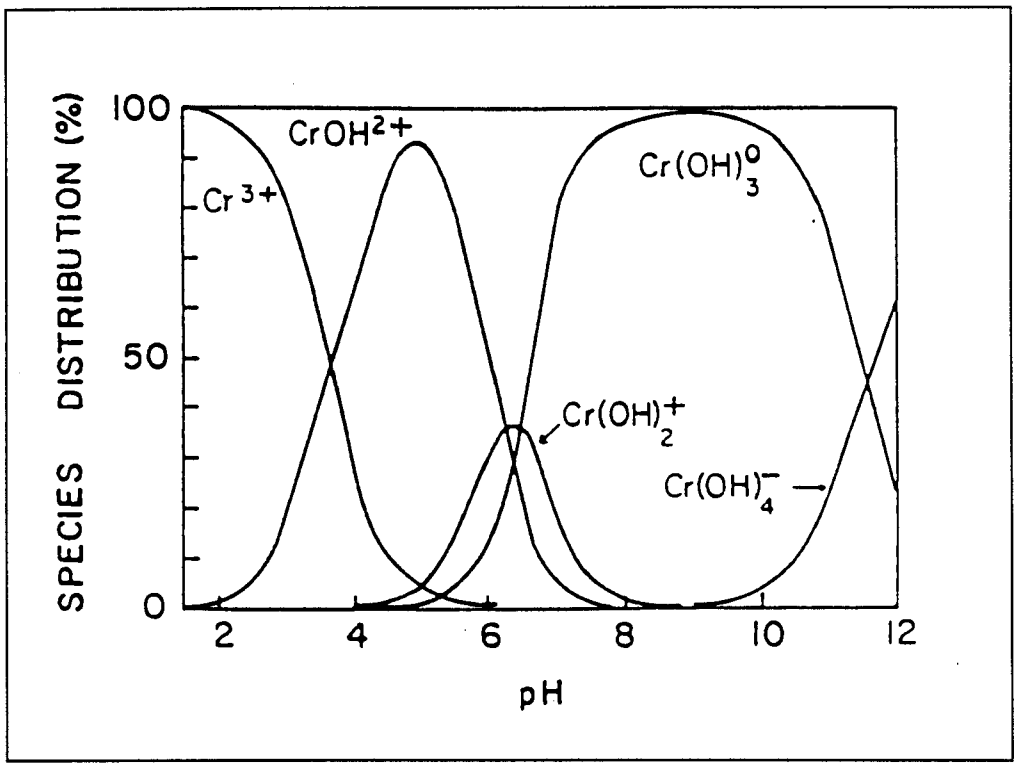

Figure 2-1: Distribution of Cr(III) species as function of pH (after Rai et al., 1987)

Until recently there has been no agreement in the literature over which Cr(III) species occur and which predominate at different pH levels (Rai *et al.*, 1987). Baes and Mesmer (1976), by reviewing available hydrolysis data, identified the following principal species: $Cr(OH)^{2+}$, $Cr(OH)_2^+$, "probably" $Cr(OH)_3^0$ (i.e. soluble, non precipitated species), and

$Cr(OH)_4^-$. Furthermore, polynuclear species of the type $Cr_2(OH)_2^{4+}$ and $Cr_3(OH)_4^{5+}$ occur to a minor extent. Rai *et al.* (1987) accept this speciation, but assign different weighting to their prominence. Stuenzi and Marty (1983) identified even higher order polymeric species up to Cr_5. Hartford (1979) speaks of a species $Cr(OH)_6^{3-}$. Deltombe *et al.* (1966) have identified CrO_2^- at pH > 7 and CrO_3^{3-} at a pH > 15. The species distribution as a function of pH, computed from data by Rai *et al.* (1987), is presented in Figure 2-1.

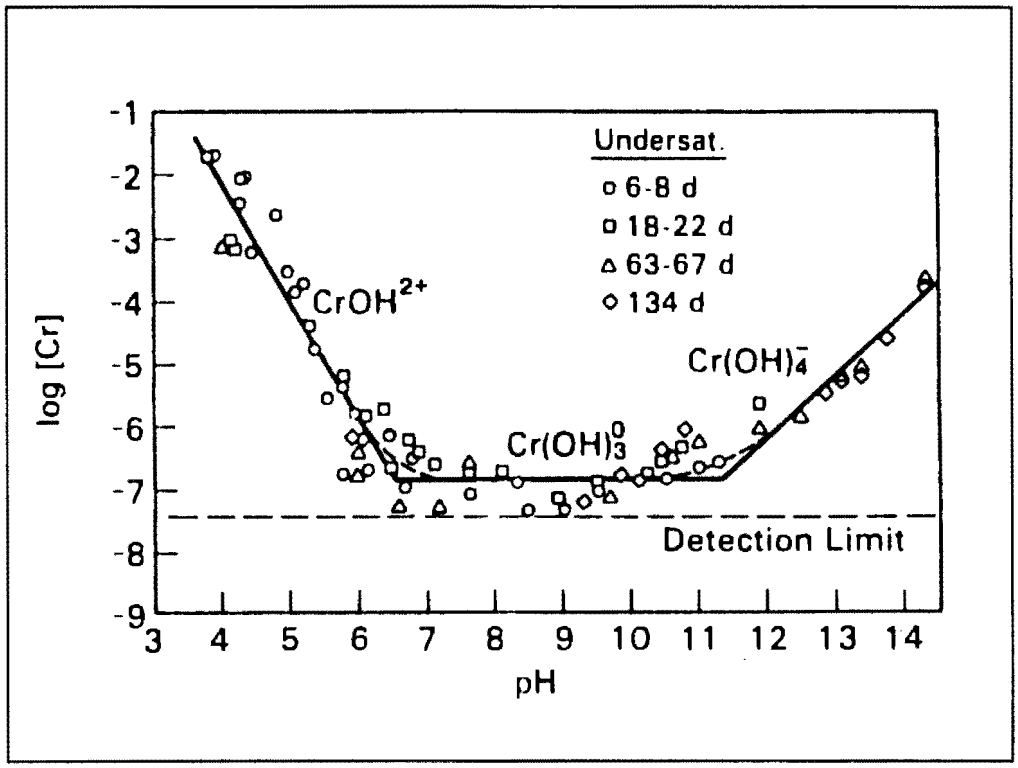

Figure 2-2: Cr(III) solubility and speciation as function of pH. The lower curve is based on data by Rai et al. (1987), the upper on data by Baes and Mesmer (1976).

Irrespective of these diverse speciations of Cr(III) in the soluble phase, the concentration of Cr(III) above a pH 4-5.5 is mainly limited by the solubility of $Cr(OH)_3$. Rai et al. (1987) showed a computer generated solubility chart using both their data and those of Baes and Mesmer (1976). These data sets have been accepted most widely. As can be seen in Figure 2-2, the solubility of $Cr(OH)_3$ is about 10^{-7} M between pH 6 and 11.5, with $Cr(OH)_3^0$ as the predominant dissolved species. At lower pH values, Cr(III) becomes increasingly more soluble with decreasing pH, existing mainly as $CrOH^{2+}$ for pH 4-6, and Cr^{3+} below pH 3.8.

At high pH, an increase in solubility can be noted with $Cr(OH)_4^-$ as the soluble species. As indicated in Figure 2-2, the data of Baes and Mesmer (1976) suggest somewhat higher solubilities and different speciation.

Rai et al. (1987) report that solubility equilibria are established slowly; about 6 days in the lower pH range and significantly longer above a pH of 12. This can be explained by the characterisation of the $Cr(OH)_3$ "precipitate", which was the feedstock base for all their experiments. At moderate concentrations the hydroxide remains in solution as a "solid solution" consisting of individual $Cr(OH)_3$ molecules or clusters which agglomerate and precipitate only slowly.

$Cr(OH)_3$ appears in various forms, depending on the way it is precipitated and its age. Initially $Cr(OH)_3$ forms macro-molecules consisting of several Cr centres linked by hydroxy-bridges (Spiccia and Marty, 1986). Upon ageing and temperature influence the macro-molecules agglomerate into a gel-type structure often described as $Cr(OH)_3 \cdot aq$. Further ageing and higher temperatures result in a more crystalline structure referred to as $Cr_2O_3 \cdot aq$ or $Cr_2O_3 \cdot xH_2O$ (Gmelin (1962)). The exact mechanisms of this ageing procedure are not well understood. The various forms, however, can be distinguished by their solubilities in acids, which decrease with increasing age and temperatures of formation (Gmelin, 1962).

The data established by Rai et al. (1987) are accepted generally today and the solubilities and speciation of Cr(III) shown in Figures 2-1 and 2-2 are considered sufficiently accurate. In summary, and based on these data, it can be concluded that for Cr(III)

- the un-hydrolysed species is predominant at below pH 3
- the ion progressively hydrolyses with increasing pH
- the uncharged $Cr(OH)_3^0$ species is dominant pH between 5 and 9
- the hydrolysed anionic species becomes significant above pH 10 and dominant above pH 11.5

Furthermore, $Cr(OH)_3$ initially exists as a solid suspension (gel), which gradually changes its structure towards $Cr_2O_3 \cdot x\ H_2O$. While the reactivity of the various soluble species does not appear to be influenced by their hydrolysis, the reactivity of the precipitated Cr(III) oxides/hydroxides is limited by its capacity to redissolve, which decreases with age.

It needs also to be mentioned that Cr(III) exhibits co-precipitation behaviour with other metal cations. If Fe(III) ions are present, Cr(III) and Fe(III) precipitate together in a common matrix of $[Fe, Cr](OH)_3$ (Rai *et al.* as quoted by Richard and Bourg, 1991). It is not fully understood whether this phenomenon is based on adsorption of one phase onto the other, or whether there is a mutual mechanism. Nevertheless, this co-precipitate is considered a stable form of Cr(III) and an effective method for scavenging Cr(III) from solution. A more detailed discussion of Cr(III) adsorption behaviour is given in Section 2.1.3. Further aspects of Cr(III)/Fe(II) co-precipitation are detailed in Sections 2.1.7 and 3.3.2.

Complexes of Cr(III)

Cr(III) is known to form thousands of aqueous complexes, both organic and inorganic (Hartford, 1979). Its character as a "hard" Lewis acid underlines its affinity to hydroxyl, sulphate, cyanide and sulpho-cyanide, chloride and fluoride groups (Deltombe *et al.*, 1966). Complexes are considered meta-stable and ligand exchange generally proceeds at slow rates (Hartford, 1979). This may have an effect on the reactivity of Cr(III), as any reaction partner would have to replace one of the current ligands to approach a Cr(III) centre.

Organic complexes of Cr(III) are of particular importance in any discussion of its environmental chemistry. James and Bartlett (1983a) showed that Cr(III) forms complexes with soil organics such as citric and fulvic acid. The most important feature of these complexes is their ability to solubilise Cr(III) with an increase in mobility up to a pH of 7, whereas in their absence, Cr(III) precipitates as the immobile hydroxide at a pH of about

5. Co-precipitation with $Fe(OH)_3$ no longer occurs (Nakayama et al., 1981c). The citrate complex was found to remain stable even after one year (James and Bartlett, 1983a) and thus it can be assumed that Cr(III) remains largely mobile in soils where the pH is slightly acidic. As Cr(III) is only slowly released from the citric complex (James and Bartlett, 1983b), its reactivity is somewhat reduced in spite of its higher mobility.

Other organic complexes of Cr(III) are known (Bartlett and James, 1988), but occur to a lesser extent. Complexes with high molecular weight organics can immobilise Cr(III). For example, Cr(III) forms very stable complexes with proteins, the effect of which is utilised in the leather tanning process (Nriagu, 1988).

Cr(VI) Speciation and Solubility

Cr(VI) appears in aqueous solution only as chromic acid, H_2CrO_4, and its anions, the chromate oxo-anions. The solid form of chromic acid is CrO_3, the anhydride, which vigorously hydrolyses upon contact with water and has a solubility of 6.25 mol/l. Dissolution and hydrolysis occur as follows (Deltombe *et al.*, 1966):

$$CrO_3 + H_2O \rightleftharpoons H_2CrO_4$$

$$H_2CrO_4 \rightleftharpoons HCrO_4^- + H^+ \qquad (HCrO_4^- \text{ dominates at pH} > 0{,}75)$$

$$HCrO_4^- \rightleftharpoons CrO_4^{2-} + H^+ \qquad (CrO_4^{2-} \text{ dominates at pH} > 6{,}45)$$

Chromic acid is a strong acid and predominates in aqueous solution only at pH < 0.6, whereas the $HCrO_4^-$ anion predominates in mildly acidic solutions, the chromate anion CrO_4^{2-} above a pH of about 6.5 (see Figure 2-3). At total Cr(VI) concentration >0,01 M and acidic pH, the hydrogen-chromate dimerizes to di-chromate according to

$$2\ HCrO_4^- \rightleftharpoons Cr_2O_7^{2-} + H_2O$$

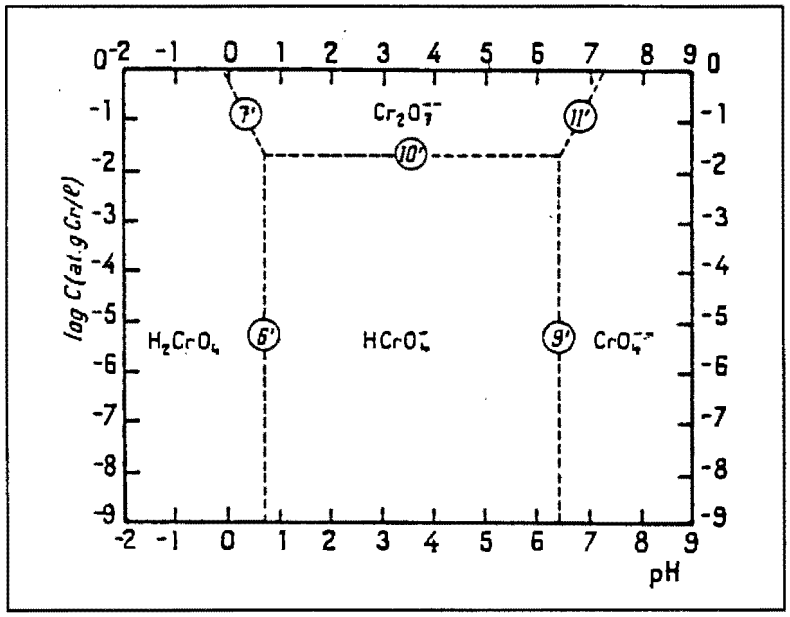

Figure 2-3: Domains of relative predominance of the various Cr(VI) anions (from Deltombe, 1966)

Ligand free Cr(VI) (i.e. Cr^{6+}, as Cr(VI) is often mistakenly referred to) has never been identified, and few stable complexes other than those mentioned above are known - chromylchloride Cl_2CrO_2 is one exception. The oxygen bond can therefore be considered as strong. The inner co-ordination sphere is fixed and cannot be replaced by other ligands.

Metal chromates fall into three categories of solubility (Nieboer and Jusys, 1988). The highly soluble type (solubility > 1 M) comprises Na and K chromates, Na di-chromate and Ca di-chromate. The class of intermediately soluble chromates (solubility 0.1 to 1 M) contains Ca chromate and K di-chromate. The sparingly soluble chromates (solubility < 0.01 M) include various types of Zn, Pb and Ba chromates (for example, solubility of $BaCrO_4$: $4.3 \cdot 10^{-3}$ M). $PbCrO_4 \cdot PbO$ is considered a completely insoluble chromate mineral.

2.1.3 Adsorption of Cr from Aqueous Solution

The tendency of dissolved chromium species, both Cr(III) and Cr(VI), to adsorb onto oxide minerals, particularly those of Fe, Mn, Si and Al, is significant in natural environments. Metal oxides tend to form surface hydroxyl groups through the dissociative sorption of water (Dzombak and Morel, 1990) as is illustrated in Figure 2-4. This sorption process is kinetically slow and usually it can take several days for a surface to reach maximum coverage of hydroxyl sites. Also the density of such sites depends on a number of factors such as solid cation type, crystal structure and surface structure and is difficult to estimate accurately from theoretical considerations alone.

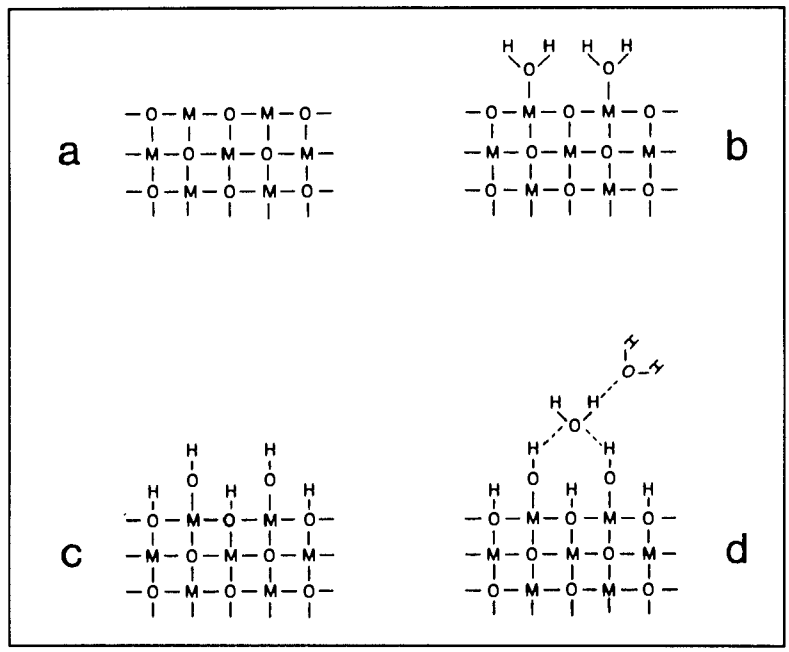

Figure 2-4: Schematic cross-section of the surface layer of a metal oxide: (a) surface ions are not fully coordinated; (b) surface metal ions coordinate H_2O molecules in the presence of water; (c) protons dissociated from the sorbed H_2O molecules. leading to the formation of an uniformly hydroxylated surface; (d) sorption of water on the hydroxylated surface (figure taken from Dzombak and Morel, 1990)

The surface hydroxyl groups of a hydrated metal oxide can bind and release protons as a function of solution pH, thus showing amphoteric behaviour. This can be described as follows (Dzombak and Morel, 1990):

$$\equiv XOH_2^+ \leftrightarrows \equiv XOH^0 + H^+$$
$$\equiv XOH^0 \leftrightarrows \equiv XO^- + H^+$$

where $\equiv XOH_2^+$, $\equiv XOH^0$ and $\equiv XO^-$ represent positively charged, neutral and negatively charged surface sites, respectively. These equilibrium reactions can be described by suitable mass law constants. As a consequence, the solid surface can become positively or negatively charged, depending on the pH of the surrounding aqueous phase.

These surface charges can be measured by acid-base titration methods. An important characteristic in this context is the "point of zero charge" (PZC), the pH at which the net surface charge due to proton transfer reaction is zero. The tendency of such a surface to be positively charged in acid media and negatively in alkaline solution accounts, at least in part, for the attraction and adsorption of cations or anions from solution as a function of pH. The net surface charge of the solid results in the retention of counter ions in the diffuse layer near the surface, i.e. cations are retained near a negatively charged surface at higher pH levels and anions are retained near a positively charged surface at lower pH levels. This phenomenon is sometimes referred to as non-specific adsorption (Stollenwerk and Grove, 1985).

Adsorption of ionic species onto solid oxide surfaces is best described as a sorption process to surface hydroxyl groups. These can be described for anions:

$$\equiv XOH^0 + A^{3-} + H^+ \leftrightarrows \equiv XA^{2-} + H_2O$$

where A^{3-} represents a hypothetical trivalent anion. For cations one can write similarly:

$$\equiv XOH^0 + M^{2+} \leftrightarrows \equiv XOM^+ + H^+$$

where M^{2+} represents a divalent cation (Dzombak and Morel, 1990). Ion adsorption onto surface hydroxyl groups is thus described as equilibrium reactions and an equilibrium constant can be written for each reaction. The above equations indicate that ion sorption onto hydrated surfaces is strongly dependent on pH. Cation sorption increases with increasing pH and the fraction sorbed increases from 0 to 1 over a narrow pH range. Anion sorption, on the other hand, is greatest at low pH and gradually decreases as pH increases (Dzombak and Morel, 1990). Tendencies of cation and anion adsorption as function of pH are shown in Figure 2-5.

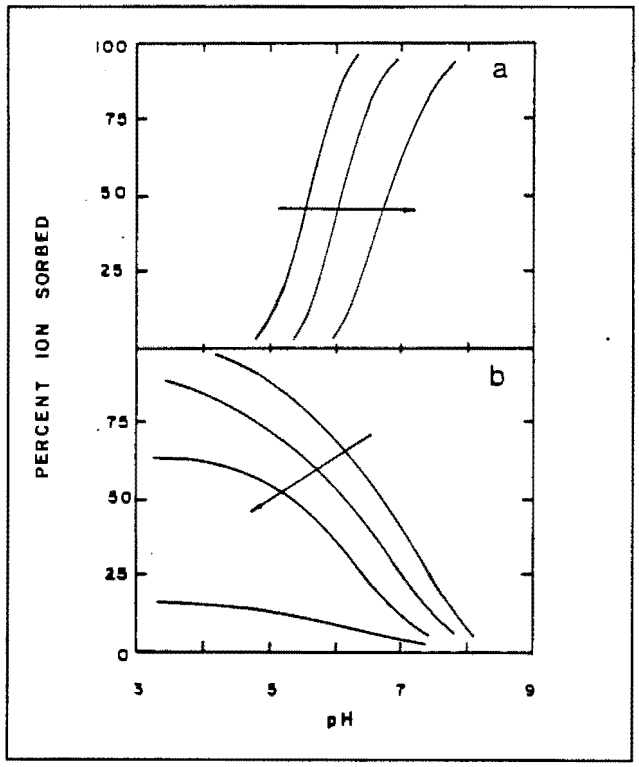

Figure 2-5: Typical pH edges for (a) cation sorption and (b) anion sorption. Arrows indicate direction of increasing sorbate/sorbent ratio.

Adsorption behaviour is usually expressed either in "pH edges", such as used in Figure 2-5, where the fraction adsorbed is plotted versus solution pH for different solute to sorbate ratios, or as adsorption isotherms (Figure 2-6) which show adsorbed concentration plotted against solution concentration. Ionic adsorption onto hydrated surfaces is usually best described by either Langmuir or Freundlich isotherms. Such isotherms are usually

established for a single dissolved species in much smaller concentrations relative to the available number of surface sites. Care needs to be taken with systems where several ionic species compete for a limited number of surface sites. Also, at high concentrations of dissolved ions, surface precipitation can occur, resulting in the integration of adsorbed ions into the solid lattice under the formation of a new hydrated surface.

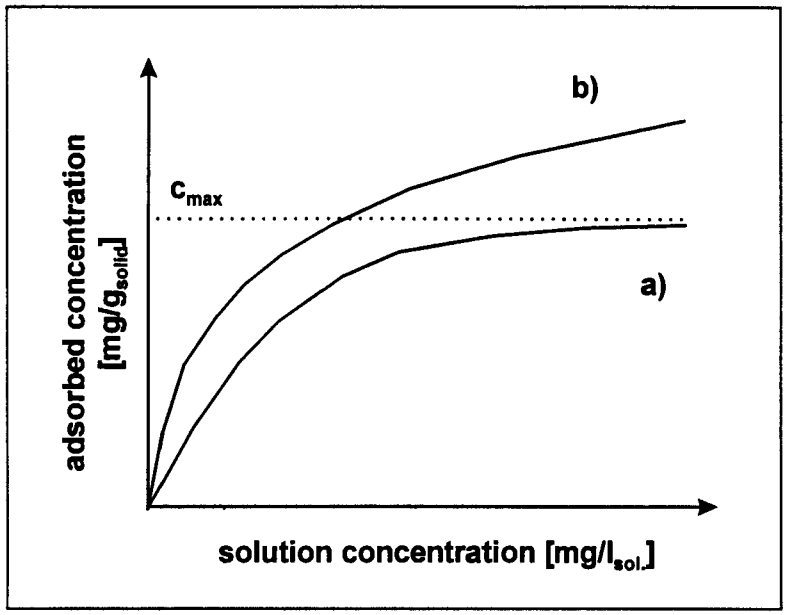

Figure 2-6: Typical adsorption isotherms: (a) Langmuir type and (b) Freundlich type.

In the light of the foregoing discussion, the adsorption tendencies of chromium species reported in the literature are straightforward. Cr(III) is generally considered to strongly adsorb to mineral Fe and Mn (Bartlett and Kimble, 1976a), which usually arise as hydrated oxides in natural environments. Strong chromium adsorption onto natural alumina-silicate minerals has been reported for feldspar (Singh et al., 1992), kaolinite and montmorillonite (Griffin et al., 1977) and china clay (Sharma et al., 1990). The hydroxy-complexes of Cr(III) appear to adsorb particularly strongly (James and Healy as quoted in van der Weijden and Reith, 1982). Schroeder and Lee (1975) report Cr(III) adsorption on natural solids such as sand, bentonite, MnO_2 and $Fe(OH)_3$, as well as glassware (boro-silicates), during their experiments.

The adsorption tendency increases with increasing pH (Richard and Bourg, 1991) as would be expected. Competing cations reduce the adsorption of Cr(III) (Richard and Bourg, 1991), possibly due to higher charge densities. Adsorbed Cr(III) species are stable, with desorption rates slow, particularly in the absence of competing cations. Dzombak and Morel (1990) have successfully modelled data of Cr(III) adsorption onto ferric hydrous oxide obtained by various workers and extracted equilibrium constants for this process. An interesting point to consider would be Cr(III) adsorption behaviour at pH above 10, where it mainly appears as the negatively charged $Cr(OH)_4^-$ (see Figure 2-1).

Cr(VI), which is present only in chromate oxo-anions, should show strong adsorption tendencies in acidic environments but be largely desorbed in alkali media. Chromates are reported to adsorb onto Fe and Al-oxides (James and Bartlett, 1983c; Bartlett, 1991), alumina-silicates (Griffin *et al.*, 1977; Sharma et al., 1990; Singh *et al.*, 1992) and onto $Fe(OH)_3$ and $Cr(OH)_3$ (James and Bartlett, 1983c). In the latter case there is some uncertainty whether Cr(VI) actually adsorbs or co-precipitates with Cr(III), but adsorption is the generally favoured mechanism. Richard and Bourg (1991) state that Cr(VI) species are adsorbed at specific surface sites, notably those occupied by hydroxyl species, with each Cr(VI) covering 3-4 hydroxyl groups. Competing anions decrease the adsorption tendency of Cr(VI). Adsorbed Cr(VI) species are protected from reductive attack, for example by Fe^{2+} (Bartlett and James, 1988), i.e. they are chemically 'masked'. Dzombak and Morel (1990) also modelled the adsorption of chromate onto ferric hydrous oxide.

Little information was found in the literature on the characteristics of desorption reactions of Cr species once they have been adsorbed (permanent or fully reversible), and very little on the kinetics of adsorption/desorption reactions. Rai *et al.* (1987) indicate that equilibrium reactions involving chromium may take several weeks to reach equilibrium. Eary and Rai (1987) suggest slow Cr(VI) desorption to be rate limiting in surface reactions involving Cr, but fail to offer any quantitative description.

2.1.4 Aqueous Electrochemistry of Chromium

In aqueous chemistry, the thermodynamic redox equilibria and speciation of ionic components are most conveniently expressed in an Eh (or pEh) - pH diagram also known as Pourbaix-diagrams (Deltombe et al., 1966). Figure 2-7 shows such a diagram for chromium, here in the revised form by Rai et al. (1987). Figure 2-7 indicates that Cr(III) is the predominant form in redox-neutral solutions (i.e. Eh = 0) for pH values <11. In a reducing environment, i.e. Eh < 0, Cr(II) or even Cr metal (Eh < -1.0 V) can become the predominant species, but such conditions are not normally encountered in natural environments.

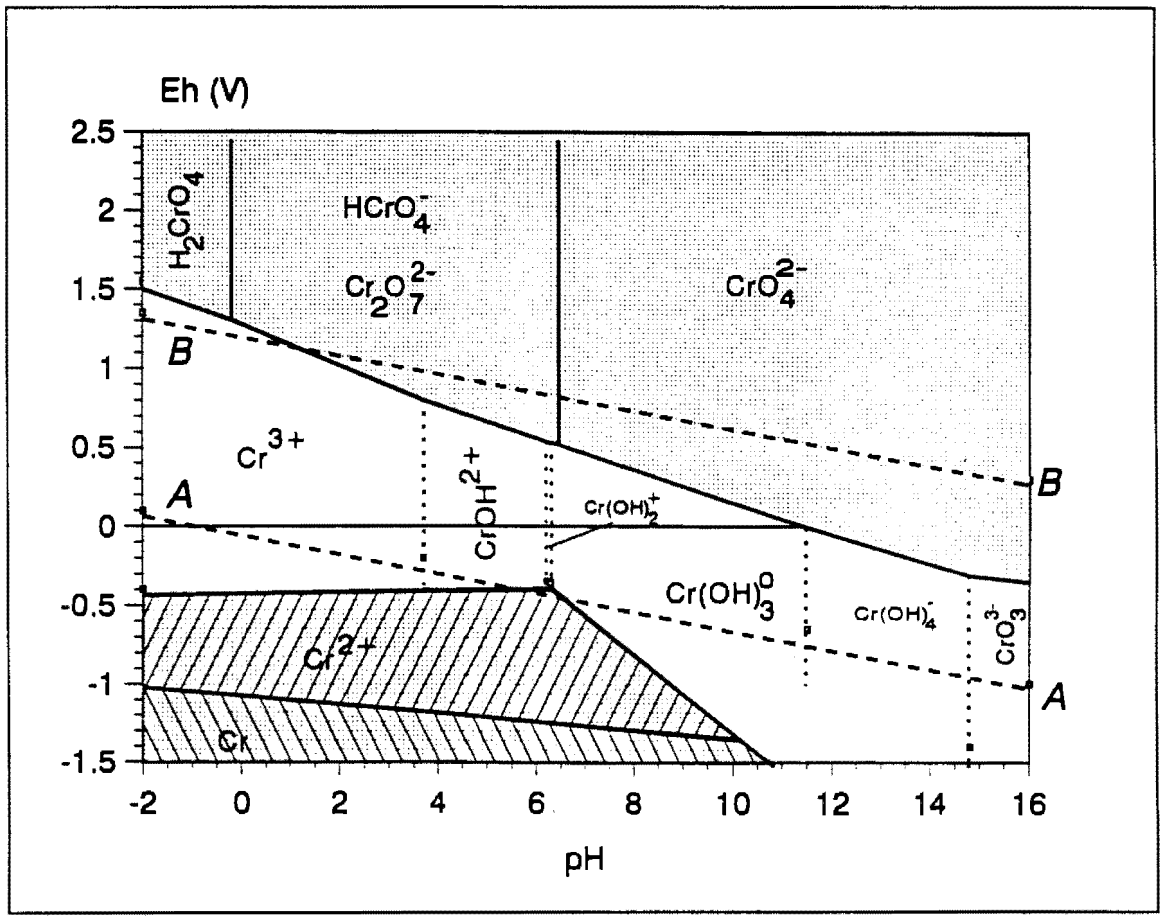

Figure 2-7: Eh-pH diagram for Cr in aqueous solution (after Delcombe (1966) and Rai et al. (1987))

Line B in Figure 2-7 indicates the redox-potential of oxygen dissolved in water (at 1 atm) according to the half reaction

$$O_2 + 4H^+ + 4e^- \leftrightharpoons 2\,H_2O \qquad Eh\,(V) = 1.229 - 0.0592\,pH$$

Strongly aerated aqueous solutions therefore show a high oxidising potential at which Cr(VI) can become the thermodynamically predominant form for pH values above 2. It has thus been postulated that, from a thermodynamic perspective, the predominant Cr species in oceans, which are well aerated and have a pH of about 8, should be Cr(VI) (Elderfield, 1970). For soils this is similarly true, at least for the upper, well aerated layers (Bartlett, 1991).

The actual Cr(III)/Cr(VI) redox potential can be calculated from the Nernst equation and standard chemical solution potentials of the species involved. This redox potential is a function of pH and chemical speciation of the chromium ions as well as of the Cr(III) to Cr(VI) concentration (or, more correctly, activity) ratios. Such thermodynamic equilibrium calculations make no prediction about the kinetics of a particular reaction, i.e. it does not indicate whether, and how fast, the theoretical equilibrium is reached. In fact, as will be shown further below, Cr(III) to Cr(VI) oxidation by oxygen proceeds so slowly under natural conditions that, in general, a state of non-equilibrium needs to be assumed for natural environments (Elderfield, 1970). This renders Cr(III) as a principally meta-stable oxidation state in these environments.

Chromate species are considered to be strong oxidising agents, particularly towards organics, due to the high redox potential of Cr(VI). The mechanism involved often proceeds via an esterification with an organic hydroxyl or sulpho-hydroxyl group, with subsequent oxidation. Cr(VI) is reduced to Cr(III) in these reactions. The esterification tendency of chromates is highlighted in the dimerization reaction (see above) which is a kind of self-esterification. Organic oxidations by Cr(VI) are often catalysed by light (Bartlett and James, 1988). The strong oxidising potential of Cr(VI) towards organics is

the main reason for its bio-toxicity (see section 2.4.2). Inorganic reduction of Cr(VI) to Cr(III) occurs rapidly with Fe^{2+} (see for example Schroeder and Lee, 1975), a reaction which is frequently used for the removal of Cr(VI) from waste-waters (see Section 3.3.2).

2.1.5 Cr(III) Oxidation in the Presence of Oxygen

The oxidation of dissolved Cr(III) by atmospheric oxygen in a mildly acidic environment is given by

$$4CrOH^{2+} + 3O_2 + 6H_2O \leftrightharpoons 4HCrO_4^- + 12H^+$$

and for oxidation from the precipitated $Cr(OH)_3$ one could write

$$4Cr(OH)_3^0 + 3O_2 \leftrightharpoons 4CrO_4^{2-} + 2H_2O + 8H^+$$

and in the alkaline region:

$$4Cr(OH)_4^- + 3O_2 \leftrightharpoons 4CrO_4^{2-} + 6H_2O + 4H^+$$

As protons are generated in these reactions it appears they should proceed further at higher pH. This is in line with the Pourbaix-chart (Figure 2-7). As Cr(III) appears as the neutral hydroxide species in the second reaction and the bulk of Cr(III) will be "precipitated" as inert $Cr(OH)_3$ there may be a kinetic limitation to this reaction. In support of this, Hartford (1979) suggests that oxidation by air should proceed at "hydrothermal" conditions (i.e. in an aqueous environment at elevated temperatures), elevated pressures and alkaline pH.

The slow atmospheric oxidation of freshly precipitated $Cr(OH)_3$ in strongly alkaline solutions (0.5 to 2 M NaOH) has been observed by Wood and Black (1916), but noticeable extents were only reached after two months at room temperature. Ipatiew and

Platonowa (1931) describe direct oxidation of Cr(III) solutions with pressurised air at 200 to 300 °C which proceeds to completion within 18 to 48 hours. Nyholm (1947) reports experiments on Cr(III) oxidation in strongly alkaline solutions (0.25 to 2.5 M NaOH) bubbled with air, using $MnSO_4$ as a catalyst, achieving equilibrium conversions within 2 to 3 hours at room temperature. Farrow and Burkin (1973) explored the use of alkali pressure leaching of Cr_2O_3 and chromite mineral at elevated temperatures (210 to 280 °C) using compressed air. Dissolution of the solid Cr(III) was rate-limiting, particularly from the spinel type chromite mineral (Section 2.1.2), whereas oxidation, both in the presence and absence of MnO_2 as catalyst, was fast.

Rates for the oxidation reaction at natural pH levels (pH 4 to 9) are known to be slow. Indeed, several workers reported zero (or only marginal) oxidation of Cr(III) solutions sparged with air, after as long as 137 days (Bartlett and Kimble, 1976a; Saleh *et al.*, 1989; v. d. Weijden and Reith, 1982; Nakayama *et al.*, 1981c; Eary and Rai, 1987). None of these studies discredited the feasibility of Cr(III) oxidation by O_2, but rather assumed kinetics were so slow that detection could only take place after long periods of time.

Saleh *et al.* (1989) quote a half-life (time taken for 50% conversion, based on first order kinetics) of 2 - 9 years. Van der Weijden and Reith (1982) established a speculative first order rate law with k=0.35/yr, leading to a half-life of 1.75 years.

However, Schroeder and Lee (1975) report successful oxidation in experiments by Canter and Gloyna, in which "appreciable" amounts of reagent are oxidised at pH 8-10 within five days. In their own experiments, they sparged solutions of Cr(III) in a carbonate buffer (pH = 10.5) for as long as 50 days at 25, 35, and 45 °C. They found appreciable oxidation in all experiments and were able to establish a first order rate law, with an activation energy of ca. 92.5 kJ/mol.

In order to put some time scales on the Schroeder and Lee data, a rate expression of the following form is proposed here:

$$-\ln(1-x) = kt$$

with

x = fractional conversion

$k = k_0 \exp\{-E/RT\}$

$k_0 = 1.4 \cdot 10^{13}$ 1/d

$E = 92.564$ kJ/mol

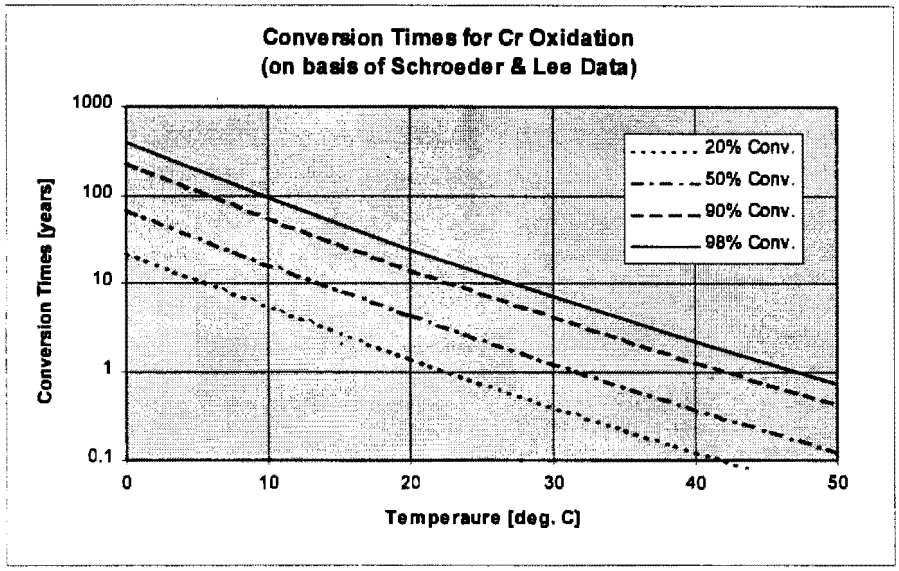

Figure 2-8: Projection of conversion times Cr(III) to Cr(VI) as a function of temperature (based on data from Schroeder and Lee, 1975)

A graphical representation of conversion time versus temperature is given in Figure 2-8. At 20 °C the reaction constant would be $k = 4.4 \cdot 10^{-4}$ d^{-1} and the half-life of the conversion 4.46 years. Thus it can be concluded that the oxidation under aerobic conditions does take place, but at rates so slow that it is generally neglected in environmental studies. This logic has prevailed on the grounds that Cr(III) is considered likely to get involved in other reactions more rapidly (Richard and Bourg, 1991). However, several studies indicated that other oxidation mechanisms, such as that involving MnO_2, proceed somewhat slower under anaerobic than aerobic conditions (Eary and Rai, 1987; Saleh *et al.*, 1989).

Therefore it appears that chromium oxidation by dissolved oxygen in aqueous environments can never be discounted completely.

Atmospheric oxidation of Cr(III) can also occur from the solid chromic oxide, in the presence of lime:

$$4CaO + 2Cr_2O_3 + 3O_2 \rightleftharpoons 4CaCrO_4$$

This reaction has been shown to be thermodynamically feasible at ambient temperatures (Hattori *et al.*, 1978) and has been assumed to play a role in chromium mobilisation, specifically in furnace slags containing chromium oxides and lime in separate crystal phases (Kilau and Shah, 1984). There appears to be little evidence in the literature that this reaction has been quantified further.

The apparently slow kinetics of chrome oxidation by oxygen need to be treated with some care. Oxygen is known to exhibit large over-potentials in direct reaction as well as on many surfaces (Deltombe, 1966), thus significantly reducing the thermodynamic driving force of a reaction. The presence of suitable surfaces might, however, sufficiently reduce this over-potential and give rise to increased rates of chrome conversion. No effort appears to have been made to investigate the influence of certain surfaces in catalysing the direct oxidation of Cr(III) to Cr(VI).

In summary it can be said that, although atmospheric oxidation of Cr(III) to Cr(VI) under natural conditions appears kinetically slow or inhibited, this should not give rise to any undue confidence in the long-term stability of Cr(III), particularly in the context of waste landfill disposal. Despite its slow rate, Cr(VI) production may become significant considering the extended periods of time such waste material may remain exposed to the open (aerated) atmosphere. This trend can potentially be exacerbated further in environments which are highly alkaline due, for example, to the presence of lime or limestone.

Quite clearly the atmospheric oxidation of Cr(III0 to Cr(VI) requires further investigation to identify under which conditions the reaction is likely to proceed, particularly with respect to conditions likely to be encountered in solid waste deposits. An experimental study has been conducted to clarify aspects of the oxidation reaction, which is described in more detail in Section 2.3.

2.1.6 Cr(III) Oxidation by Manganese Dioxide

Cr(III) can be oxidised by solid MnO_2 under acidic conditions:

$$2CrOH^{2+} + 3MnO_2 \leftrightharpoons 2HCrO_4^- + 3Mn^{2+}$$

and in alkaline conditions:

$$2Cr(OH)_4^- + 3MnO_2 + 4H^+ \leftrightharpoons 2CrO_4^{2-} + 3\,Mn^{2+} + 6H_2O$$

During adsorption studies of Cr(III) Schroeder and Lee (1975) identified the capability of MnO_2 to oxidise Cr(III) to Cr(VI) at meaningful rates. Bartlett and James (1979) found that all soils rich in manganese readily oxidised Cr(III) spiked to them. This reaction seemed to proceed better at pH 3 than at higher pH 7-9. They concluded that MnO_2, present in virtually all soils, is the main oxidising constituent for chrome in soil environments. Nakayama (1981b) spiked MnO_2 and Cr(III) into an aerated solution and found 10% of the Cr(III) oxidised after 100 hours, suggesting that the reaction proceeds only slowly. Saleh et al. (1989) experimented with Cr(III) oxidation on MnO_2 and arrived at first order half-lives of 2 to 3.5 years. Schroeder and Lee (1975) found half-lives of between 3 and 43 minutes depending on the concentration of MnO_2 added. Bartlett and James (1988) describe slow zero order kinetics on the surface of δ-MnO_2 at low temperatures (attributed to low mobility of Cr(III)), and faster rates of first order kinetics at higher temperatures. In more thorough investigations, Eary and Rai (1987) investigated

oxidation with β-MnO_2, Fendorf and Zasoski (1992) with δ-MnO_2, Johnson and Xyla (1991) with γ-MnOOH (manganite). Eary and Rai (1987) found that oxidation did occur on the surface of β-MnO_2 at higher pH, indicating mobilisation of Cr(III) hydroxide, even though the reaction rate was slow.

All workers in this field have noted a distinct fall-off in reaction rate before either the Cr(III) or the solid MnO_2 phases are consumed. Although the initial oxidation is fast, the reaction slows down drastically with time, though not quite ceasing (Schroeder and Lee (1975), v. d. Weijden and Reith (1982), Eary and Rai (1987)).

It is accepted generally that only a few sites on the Mn surface are available for oxidation. This explains the large excess of MnO_2 required (Schroeder and Lee (1975)). The fall-off in reaction rate is attributed to declining availability of these sites, though no unanimous explanation exists for this phenomenon. Bartlett and James (1988) quote Anmacher and Baker suggesting that Mn^{2+} ions become re-adsorbed onto the Mn surface, thereby inhibiting further Cr(III) adsorption due to a reversal in surface charge. They further suggest that Mn(II) is readily re-oxidised by atmospheric oxygen on the MnO_2 surface allowing further chrome oxidation to proceed although at a significantly slower rate. This mechanism is consistent with the oft-described "catalytic" role for MnO_2 in this reaction with atmospheric oxygen. Other workers (Schroeder and Lee (1975), v. d. Weijden and Reith (1982)) attribute the surface blinding to adsorption of other cations. Eary and Rai (1987) cast some doubt on the re-adsorption of Mn^{2+} since their Mn balances were stoichiometric, which suggests that all Mn^{2+} ions remain in solution. As an alternative, they attributed the cessation of the reaction to the rate-limiting slow de-sorption of Cr(VI), but fail to offer a quantitative description of this effect. Fendorf and Zasoski (1992), by way of further explanation, concluded that the MnO_2 surface is altered by surface precipitation of Cr(III), thereby inhibiting further reaction. No cessation was observed in reactions with manganite (MnOOH), a phenomenon which remains unexplained.

With respect to oxidation in alkali media, the work of Nyholm (1947) should be noted. This shows that the atmospheric oxidation of Cr(III) in strongly alkaline solutions (0.25 to 2.5 M NaOH) is catalysed by Mn^{2+}. The pathway involves oxidisation of Mn^{2+} by air to MnO_2, which then precipitates and oxidises the Cr(III) thereby being reduced back to Mn^{2+}.

In summary, it can be said that MnO_2 is a suitable oxidant for chromium (III), but reaction rates are only fast in fresh solutions owing to a rapid blinding of the few suitable surface sites. This "blinding" is thought to occur either by re-adsorption of Mn^{2+}, Cr(VI) or competing cations, or by surface precipitation of $Cr(OH)_3$. Following an initially fast reaction, oxidation proceeds only slowly, either due to re-oxidation of adsorbed Mn^{2+} and/or continued Cr(III) oxidation on the remaining few suitable sites. MnOOH appears to be a fast oxidant for Cr(III) with no observable decrease in reaction rate. In strongly alkali media MnO_2 can act as a catalyst for the atmospheric oxidation of Cr(III).

2.1.7 Cr(VI) Reduction

The removal of Cr(VI) from industrial waste waters frequently involves a reduction step to Cr(III) before the actual removal by precipitation or adsorption. Frequently used reductants are SO_2, sodium meta-bisulfite or ferrous ion, supplied from ferrous sulphate or electrochemically from consumable iron electrodes (Beszedits, 1988). In natural environments only reduction by ferrous ion and soil organics are of importance.

A prominent reaction for the reduction of Cr(VI) is that by ferrous iron (Fe^{2+}):

$$CrO_4^- + 3Fe^{2+} + 5H^+ \rightleftharpoons Cr(OH)_3^0 + 3Fe^{3+} + H_2O$$

This reaction should be favoured under acidic conditions.

Saleh *et al.* (1989) reported rapid reduction of CrO_4^- added to natural water which, additionally, had been spiked with Fe^{2+}. Half-lives of 99 to 173 days were recorded against a first order rate expression. Schroeder and Lee (1975) used Fe(II) solutions to reduce Cr(VI), but their reaction reached completion only at low pH and large excess of Fe(II) (4:1 to 12:1 w/w). Rapid oxidation of Fe(II) by O_2 in aerated solution was reported, particularly at higher pH. Under similar conditions, Richard and Bourg (1991) identified reduction of Cr(VI) with a resulting co-precipitate of [Fe, Cr]$(OH)_3$. Most workers have reported that reductions proceed faster under anaerobic conditions than aerobic conditions, giving rise to the assumption that Fe(II) oxidation by O_2 does not compete under these conditions.

The reduction of Cr(VI) by ferrous ion and subsequent co-precipitation of Cr(III) with Fe(III) has found widespread use in the removal of Cr(VI) in industrial waste waters and has been thoroughly investigated by numerous workers (Beszedits, 1988; Eary and Rai, 1988; Aldrich, 1984; Anderson *et al.*, 1984). In acid environment the reduction is described as rapid and going to completion and rate laws have been determined (Espenson, 1970; Espenson and King, 1963). Reduction above a pH of 8 is not considered feasible because of precipitation of Fe(II) hydroxide. However, Aoki and Munemori (1982) report successful reduction at pH values as high as 11.6 from interaction with the solid Fe(II) hydroxide.

An area for concern in this process is the observed tendency of small quantities of Cr(VI) to adsorb onto the forming precipitate and thus escape reduction (section 2.4.4) (Petersen and Petrie, 1997), particularly if the initial Cr(VI) concentrations are high and Fe(II) concentrations employed are not significantly more than stoichiometric. Subsequent landfill disposal of the [Fe, Cr]$(OH)_3$ sludge could result in remobilisation of this adsorbed phase.

Soil organic matter readily reduces Cr(VI) (Bartlett and Kimble, 1976b) at neutral pH. This reaction is accelerated under acidic conditions (James and Bartlett, 1983c). Viable

organics include humic and fulvic acid (Ross et al., 1981). Bartlett (1991) quotes Anmacher and Baker who have shown that Cr(VI) reduction by soil organics is a straightforward first order reaction with half lives of several weeks. Cr(VI) reduction is also reported for sulfides and organic sulpohydryl groups (Richard and Bourg, 1991). The tendency of Cr(VI) to act as a strong oxidant towards organics (Section 2.1.1) is clearly evidenced in this trend.

2.2 Chromium Cycles in Natural Environments

The foregoing description of Cr(III) and Cr(VI) chemistry permits an assessment of the possible fate of chromium in natural environments such as soils or water systems. It will be shown that, in both cases, a dynamic cycle between Cr(III) and Cr(VI) is the only way to explain the behaviour of chromium in these environments.

2.2.1 Chromium Cycle in Soils

Figure 2-9 illustrates the chromium cycle in soil environments as postulated by Bartlett (1991). Cr(III) at soil pH (normally between 5 and 9) will be mostly present as $Cr(OH)_3$, which is either precipitated, or occurs as an immobile solid suspension in a polynuclear network (Section 2.1.2), depending on the age of the hydroxide. Other species will be largely adsorbed to soil surfaces such as Fe oxides and silicates (Section 2.1.3). However, since the suspended solid is in immediate contact with the soluble phase, small concentrations of soluble Cr(III) species will always be maintained.

Organic ligands which readily complex with Cr(III) species, such as citrates, can react with the soluble phase, however small in concentration, and render a portion of Cr(III) mobile (Section 2.1.2). This Cr-citrate complex can readily migrate to a suitable MnO_2 site

present in almost all soils (mostly as Λ-MnO_2). Although Cr(III) release from these organic complexes is slow, some Cr(III) will eventually be able to adsorb on the manganese oxide surface and be oxidised to Cr(VI) (Section 2.1.6).

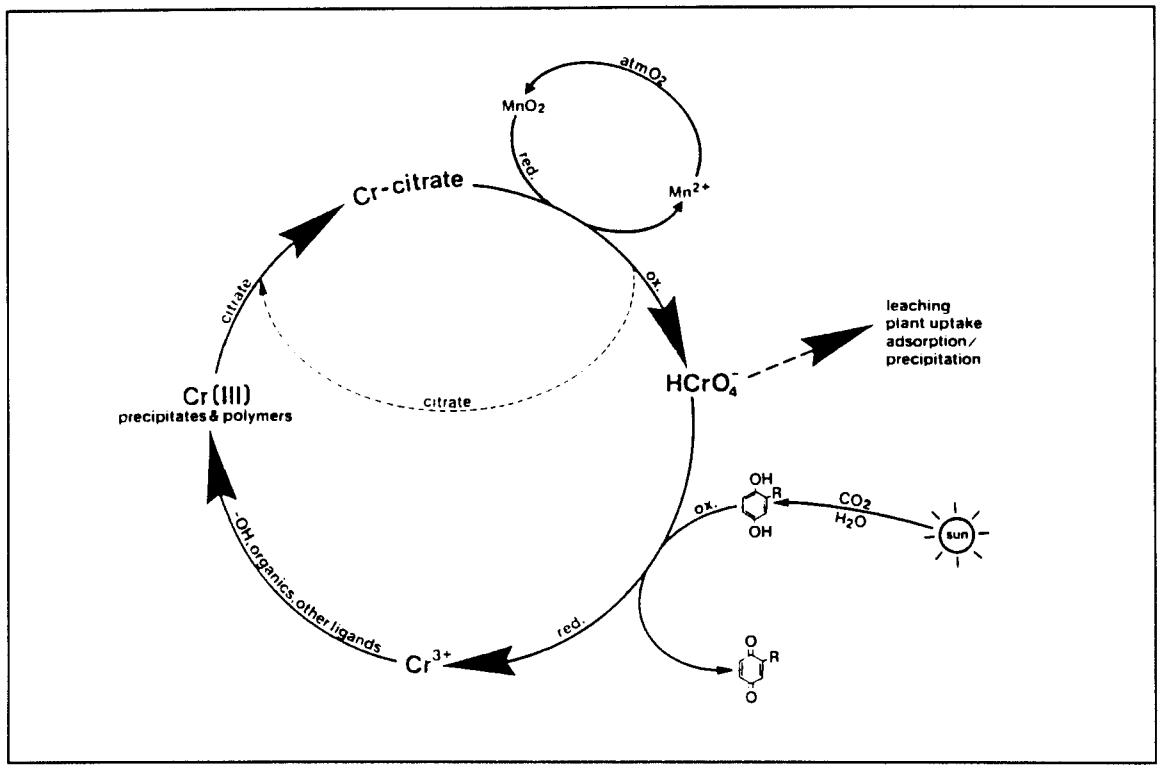

Figure 2-9: Chromium cycle in natural soils (after Bartlett, 1991)

The fate of the reduced Mn^{2+} ion follows the previous discussion i.e. it can re-adsorb at the MnO_2 surface, where it will be re-oxidised by atmospheric oxygen which is present at sufficient concentrations in the upper soil layers (Section 2.1.4). Thus, indirectly, MnO_2 acts as a catalyst for the oxidation of Cr(III) to Cr(VI) by atmospheric oxygen (Section 2.1.6).

The oxidised Cr(VI) is very mobile and can migrate through porous ground matter relatively quickly, reaching groundwater level, from where it can be transported into drinking water or rivers. Because of its toxicity (Section 2.1.1) it thereby poses an environmental threat. It can also enter plants through the roots, and soil bacteria through

the cell membrane. In unpolluted grounds these levels will remain small and may provide for the necessary chromium intake of plants.

A portion of the Cr(VI) will also be reduced by soil organic matter (Section 2.1.7) or Fe^{2+}, although the latter does not occur in soils at significant concentrations. The resulting reduced Cr(III) will now precipitate as hydroxide or be adsorbed by soil surfaces - thus closing the cycle.

The effective chromium balance in any soil depends very much on the local conditions, such as pH, presence of organic ligands, sorption surfaces, MnO_2 surfaces, amount of aeration, water pathways, rain, temperature, presence of other ions, soil geometry etc. (Bartlett and James, 1988). Predictive modelling of the chromium cycle, on a general basis, is thus almost impossible. Even with adequate soil characterisation, only an estimate of Cr(III) - Cr(VI) interconversion is possible. No estimates for cycle time or mean residence time of chromium in soils are available.

Furthermore, this cycle by no means provides an exhaustive description of all potential mechanisms. For example, direct oxidation of Cr(III) by atmospheric oxygen may proceed slowly, (Section 2.1.5), or Cr(III) might be permanently retained in either a complexed or adsorbed form as an immobile phase (Section 2.1.3). Another possibility is that Cr(VI) precipitates as insoluble chromate compounds (Section 2.1.2).

It is important to note that the chromium balance depends also on the chromium loading of the soil. Excessive loading, for example by waste sludges, may temporarily upset the natural balance until a new equilibrium is found. As all reactions involved proceed slowly, this may take many years. It can, however, lead to high concentrations of Cr(VI), even if the load was initially all as Cr(III).

2.2.2 Chromium Cycle in Natural Waters

The chromium cycle in natural waters is not as fully understood as that in soils, largely because chromium appears in only minute concentrations in large-volume water bodies, particularly oceans (10^{-9} M). Chromium has been ignored in the past because its presence was not considered relevant to any of the natural processes in water. It is only with the recent identification of chromium pollution problems that interest in the chromium-water cycle has arisen.

Saleh et al. (1989) claim that Cr(III) should be the most stable Cr species in water, whereas Schroeder and Lee (1975), v. d. Weijden and Reith (1982) and Elderfield (1970) claim that Cr(VI) is. Elderfield (1970) used simple thermodynamic calculations involving both theoretical and measured redox potentials, to show that, in water, all chromium should be present as Cr(VI). Measurements have shown that this is not the case and considerable amounts of chromium are present in the trivalent form. Analysis is complicated by the fact that Cr(III) species may adsorb on suspended particles or complex with available organics (Nakayama, 1981a). It should be noted that, due to the low concentrations of Cr in these natural waters, Cr(III) will not form a precipitate as $Cr(OH)_3$ (Section 2.1.3).

Oxidation in natural waters by mechanisms other than the slow process of dissolved oxygen (Section 2.1.5) is generally associated with MnO_2, in a similar manner to the way in which it functions in soils (v. d. Weijden and Reith, 1982; Richard and Bourg, 1991; Nakayama et al., 1981c). However, the amount of MnO_2 suspended in water columns is generally negligible, even in view of the small concentration of Cr(III). Large amounts of MnO_2 and manganite (MnOOH) are usually found only in sediments at the bottom of lakes and oceans. Mayer (1988) indicates that chromium concentrations in oceans are usually higher near the sediment layer than in the upper regions of a column. This may indicate that chromium is accumulated and "regenerated" in this region.

The strong adsorption of Cr(III) (Section 2.1.3) to particles suspended in the water column may lead to a slow downward transport into the sediment as the particles settle (Richard and Bourg, 1991). There it can desorb and be oxidised on MnO_2 or MnOOH to Cr(VI) (Section (2.1.6). The oxidised form is freely mobile and can re-enter the water column.

Before Cr(VI) can be scavenged from the water column by sediment, it needs to be reduced, as Cr(VI) is not strongly adsorbed in the more alkaline conditions of ocean water (Section 2.1.3). However, it is not clear what species are active in the reduction of Cr(VI) in the water phase. Van der Weijden and Reith (1982) cite three possibilities:

- biological activity
- diffusion into oxygen-depleted layers of the sediment
- reduction in anoxic basins.

Cr(VI) is less stable in anaerobic environments, but the actual reducing reagent is not identified in the literature. The importance placed on the amount of dissolved oxygen in the water column for the stability of Cr(VI) indicates that direct oxidation of Cr(III) by O_2 (Section 2.1.5) in the column should not be discounted, particularly since the residence time of chromium in the ocean has been quoted in the order of 20 000 to 40 000 years (Mayer, 1988).

In summary, the chromium cycle in waters can be schematically described as shown in Figure 2-10. Cr(III) travels down the water column adsorbed to particulate matter. It is deposited in the sediment, where it can become oxidised on the surface of MnO_2 or MnOOH. The freely mobile Cr(VI) re-enters the column and travels upwards, where it is reduced by biochemical action or unknown reducing agents in oxygen depleted regions. The reduced Cr(III) readily adsorbs to particulates - which close the cycle. Here, however, account needs to be taken of the potential for "short-cutting" i.e. by direct oxidation of Cr(III).

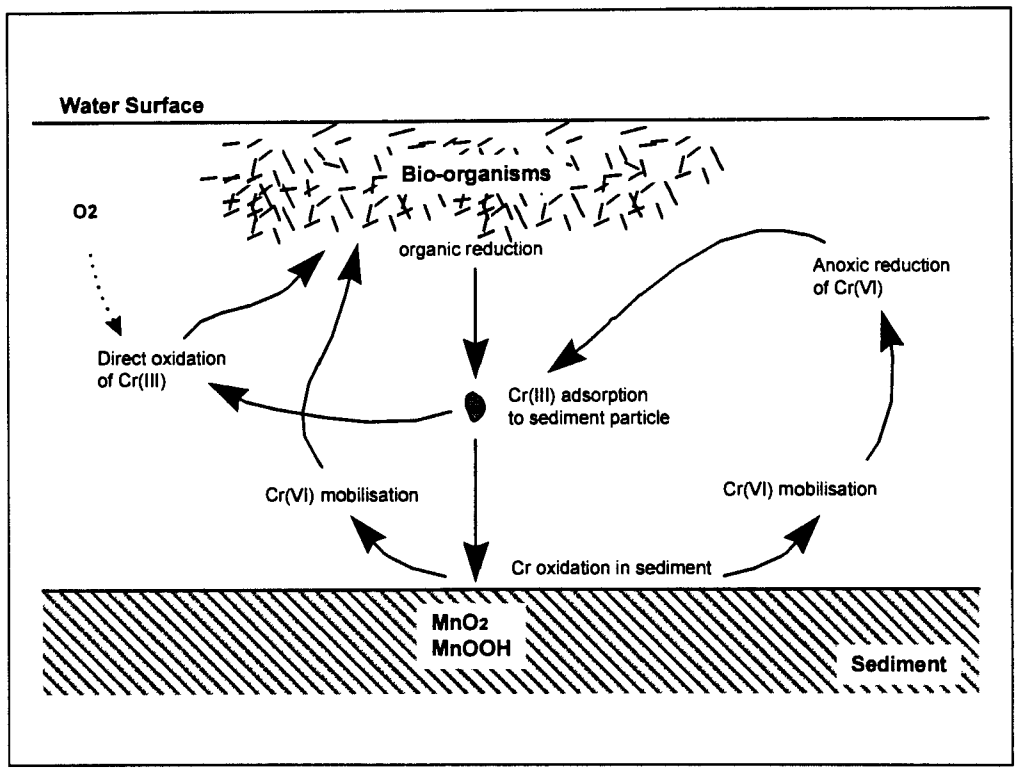

Figure 2-10: Proposed chromium cycle in oceans and natural waters

Chromium cycling in natural water columns follows principally the same mechanism as that in soils, and is equally dependent on local conditions such as pH, Eh, dissolved oxygen, temperature, Mn presence etc. (Elderfield, 1970). Due to extremely low concentrations and long residence times, equilibrium in oceans is attained only very slowly.

In lakes or rivers, mechanisms may be similar, but residence times, and thus cycle times, may be significantly shorter. The interconvertability between Cr(III) and Cr(VI) under these conditions is more rapid. This implies that, in principle, the total chromium concentration rather than simply that of Cr(VI) should be used as a "hazards index" (Schroeder and Lee, 1975).

2.2.3 Imbalances

There is little reported information in the literature on chromium cycles in soils which are heavily loaded with chromium compounds (irrespective of their oxidation state) or, indeed, on chrome laden landfills, where these can form their own micro-environment. There is a real need to explore the mechanisms already described in order to predict the fate of chromium in these "loaded" environments.

As has been stated above, excessive chromium loading of a soil environment might upset the natural dynamic balance of the cycle with an unknown outcome. Bartlett and James (1988) stated in this regard:

> *"Both oxidation of Cr(III) and reduction of Cr(VI) are thermodynamically favourable in soils and, because of the non-equilibrium between O_2 and organic matter, both take place at the same time in the same soil. Because oxidation so strikingly increases the mobility of Cr in soils and because oxidation is kinetically fast compared with reduction, reduction of Cr(VI) can be expected to occur at an infinitely later time and perhaps at some point far from its place of formation. Therein lies the possibility of chromium pollution of ground or surface water."*

It was also stated that only time will tell when soils will arrive at a new balance after being loaded with excessive amounts of chromium - since the cycle is slow and predictive modelling virtually impossible.

Weng *et al.* (1994) describe analyses conducted on soils sampled from sites contaminated by chromate processing facilities (Hudson County, New Jersey, USA, see Section 3.3.5). Although the majority of chromium was present as the original insoluble chromite mineral phase, the mobile concentrations of both Cr(VI) and Cr(III) were significantly higher than normally expected for this type of soil. Cr(VI) was readily leachable from the samples at pH > 4.5. Significant attenuation due to adsorption onto soil organics and mineral oxides

was only observed at pH below 2.5, a value unlikely to be obtained in natural environments.

The chromium cycle is strongly dependent on both the oxidising and reducing potential of a soil. Oxidation is mostly achieved through MnO_2, which, as shown in Section 2.1.6, acts only as a catalyst between atmospheric oxygen and chromium. Thus, in well aerated soils (usually within the layers near the surface), oxidation potential is unlimited, since atmospheric oxygen is freely available. If Cr(III) is also in sufficient supply near the surface (as for example in grounds adjacent to a disposal site) it can be readily oxidised.

On the other hand, the reducing capacity of a soil is limited to the amounts of oxidisable soil organics present. These are supplied by micro-organisms and decomposing plants, or, in some cases, by organic products of industrial activity co-disposed in landfills along with chromium compounds. If soil organics are consumed rapidly due to excessive amounts of reducible Cr(VI) present, they might deplete. At the same time chromium poisoning (through both Cr(VI) and Cr(III), Section 2.1.2) might destroy soil organisms and plant life removing the source of replenishment, thus leading to total exhaustion of the soil's reducing capacity.

Hence excessive chromium loading on a soil might not only upset but destroy the natural balance of a soil, giving way to extensive Cr(VI) production, even if the original load was exclusively Cr(III).

If Cr(VI) is present in a waste material, its mobilisation due to dissolution into an aqueous phase and transport into a soil environment is highly likely and must be avoided at all cost. More indirect and unexplored are the risks associated with the potential mobilisation of Cr(III), which, as has been stated above, is relatively immobile. Citrate complexation is only a feasible mechanism if the Cr(III) is already dispersed in the soil, and only if citrate is in sufficient supply, which again depends on the organic microcosm in the soil. In deposits that do not contain domestic type wastes, organic content can be considered as

generally low. Mobilisation of $Cr(OH)_3$ precipitate is slow unless enhanced by dissolution in strongly acidic or strongly alkaline environments. Such an environment might be created by acidic deposition ("acid rain") or the phenomenon of acid rock drainage (oxidation of sulphide minerals). Such acid attack will be a strong function of the physical state (particle size, crystallinity, porosity) of the chromium compounds. Likewise, the presence of alkaline materials, particularly lime and limestone, can result in an atmosphere that favours the mobilisation of Cr(III) due to alkali leaching (Section 2.1.2) and the associated danger of direct atmospheric oxidation.

Even under the most favourable conditions, dissolution of aged $Cr(OH)_3$ or chromium minerals will be slow, and a rapid movement of Cr(III) can generally not be expected. However, an assessment of environmental stability requires a more extended time scale analysis. The postulated upset of chrome stability within a soil may take considerable time (years or decades), but should never be totally discounted. Over such long time periods, however, another factor needs to be considered. Direct oxidation of Cr(III) by atmospheric oxygen, even from $Cr(OH)_3$ or chromic oxides, may reach significant extents over long periods of time (Sections 2.1.5), leading to a gradual accumulation of Cr(VI). In this context it becomes mandatory to substantiate the as yet only tentatively defined oxidation reaction by atmospheric oxygen by further experimental evidence and quantify this effect in terms of a kinetic rate expression. This is pursued in the following section.

2.3 Experimental Study of Chromium Oxidation by Atmospheric Oxygen

As indicated in the previous section, the oxidation of Cr(III) to Cr(VI) forms an integral part of the chromium cycle in natural environments. The oxidation reaction proceeds on the surface of MnO_2, which is believed to be regenerated by subsequent atmospheric oxidation of the resulting Mn^{2+}. Thus MnO_2 acts as a catalyst to the oxidation of Cr(III) by oxygen. No clarity exists, however, whether Cr(III) can also be directly oxidised by

atmospheric oxygen in the absence of suitable MnO_2 surfaces. This reaction, although thermodynamically feasible, has only been observed by a few workers (Schroeder and Lee, 1975; Saleh *et al.*, 1989; van der Weijden and Reith, 1982; Kilau and Shah, 1984) and is generally described as kinetically extremely slow.

In the context of chromium bearing waste deposits it is, however, very important to shed more light on this potential reaction, since the generation of the highly mobile and toxic Cr(VI), however slowly it may proceed, can constitute a long-term environmental burden associated with such deposits. Moreover, precisely because the reaction proceeds so slowly, it may easily be overlooked during an initial assessment of waste toxicity, but could nonetheless result in ever increasing Cr(VI) loading in the environment surrounding a chromium containing disposal site after some decades.

Available knowledge on the chemistry of direct atmospheric oxidation of chromium has been reviewed in Sections 2.1.5 and 2.1.6. From this, the following two reaction conditions seem to favour the reaction:

- aqueous solutions at very high pH values (pH 12 and higher). At these pH values Cr(III) becomes soluble in significant amounts and the oxidation reaction is thermodynamically favoured. Since such high pH values are not encountered in natural environments, this reaction path appears of little relevance for natural Cr oxidation. In highly alkaline waste materials, however, the situation might be different. Such high pH values have been observed in the interstitial pore water of deposits of certain smelter slags that contain a considerable portion of free lime (UCT, 1994).

- a mixture of lime and chromic oxide can oxidise to calcium chromate in the presence of oxygen:

$$2\ CaO + Cr_2O_3 + 1.5\ O_2 \rightarrow 2\ CaCrO_4$$

This reaction proceeds freely at high temperatures (and is in fact used in the glazing of ceramics), but is thermodynamically feasible also at atmospheric temperatures. Some of the waste materials analysed in the context of this work show high contents of both Cr and Ca, which are presumed to be largely in the form of oxides and therefore could show a potential for oxidation along this pathway.

Some preliminary experimental work has been conducted to identify whether atmospheric Cr oxidation can indeed be verified along either of these two pathways and what rates and extents of the reaction can be observed, which is detailed in the following sections.

2.3.1 Oxidation in Aqueous Solution

As reviewed in Section 2.1.5, Wood and Black (1916) have observed that strongly alkaline solutions of Cr(III) (in 0.25 to 2 M NaOH) left exposed to air for 2 months gradually turn yellow indicating the formation of some Cr(VI). Ipatiew and Platonowa (1931) report much more rapid conversions of such solutions at temperatures between 200 and 300 °C. Schroeder and Lee (1972) report gradual oxidation of Cr(III) in a carbonate buffer (pH 10.5) at slightly elevated temperatures.

In this study, it was aimed to investigate the atmospheric oxidation of Cr(III) solutions over the pH range from 2.5 to 12.4, the lower limit being the limit at which this reaction is thermodynamically feasible as stipulated in the Pourbaix chart for Cr (Figure 2-7) and the upper limit chosen as the pH likely to prevail in an environment with high concentrations of lime present.

Experimental Procedure

All experiments were carried out at 90 °C in closed 2 l glass vessels immersed in a water bath. The solution was continuously agitated by an epoxy coated impeller and air was gently bubbled through the solution through a submerged sparger. The vessel was fitted with a reflux condenser to ensure minimal losses to evaporation. The experimental temperature of 90 °C was chosen such that maximum acceleration of the reaction could be achieved without the need for a pressure vessel.

The Cr(III) source material was chromic nitrate $Cr(NO_3)_3$ which readily dissolves in water, resulting in a pH between 2.5 and 3 - depending on concentration - due to the hydrolysis of Cr(III). The reactor charge was prepared under nitrogen by dissolving under constant stirring the required amount of chromic nitrate in de-ionised water or a buffer solution, then adjusting the pH by using 1M NaOH where required. If the solution pH was driven above about 5.5, most Cr would precipitate as a finely dispersed $Cr(OH)_3$ gel as expected. In these cases the solution was allowed to stabilise for 2 hours before proceeding further.

The prepared solution was then transferred into the reactor vessel, where it was allowed to heat up to reaction temperature overnight under constant stirring and bubbling with nitrogen. At the beginning of the experiment the nitrogen supply was switched to air supply and 10 ml samples were taken in regular intervals, centrifuged to remove residual $Cr(OH)_3$, and analysed for the concentration of Cr(VI) using the spectrophotometric method described in Appendix A. Runs were continued for a maximum of 7 days (180 hours) but generally started to become unstable after about 100 hours due to technical problems with equipment or unreasonably high evaporation losses.

The experimental matrix was chosen as follows. Runs using 50 mg/l solutions of Cr(III) were conducted at pH 12.2 (experiment CrOx 1-1), pH 10 in a carbonate buffer (experiment CrOx 1-2), pH 9 (experiment CrOx 1-3), pH 4.2 in a citrate buffer (experiment CrOx 2-1) and at pH 2.7 (no pH adjustment of the initial Cr(III) solution)

(experiments CrOx 2-2 and 2-3). A further experiment was initially prepared at a pH of 6 (experiments CrOx 1-4), but slipped to pH 8 upon heating the solution, assumed due to some re-dissolution of $Cr(OH)_3$. pH adjustment in the neutral region was found to be extremely difficult due to the fickle nature of the formed precipitate and was therefore abandoned. External pH control during the run was not attempted in this preliminary series of experiments.

Further runs were conducted using initial Cr(III) concentrations of 10, 100 and 500 mg/l in acidic (i.e. not pH adjusted) solution (experiments CrOx 3-1 to 3-3). Finally the effect of small MnO_2 concentrations was also investigated using 50 mg/l Cr(III) solutions spiked with MnO_2 at Mn:Cr ratios of 1.5 (stoichiometric in terms of the oxidation reaction) and 10 (experiments CrOx 4-1 and 4-2). Also in these experiments the solutions were continuously bubbled with air. The pH of these solutions adjusted itself to around 3.5.

Results

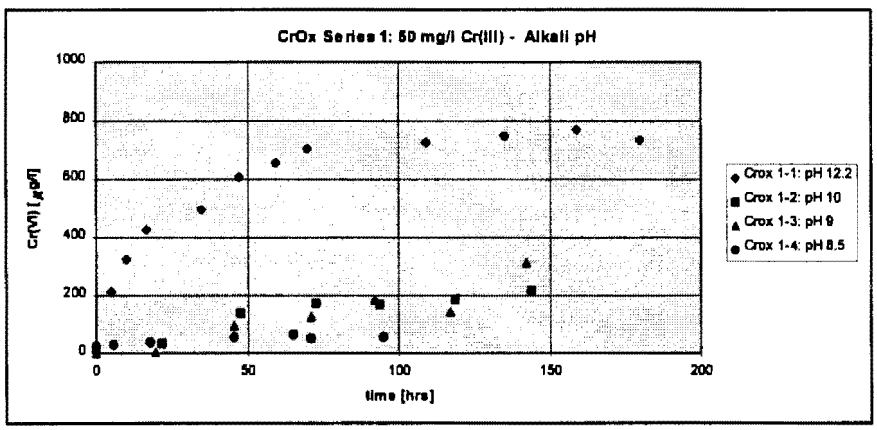

Figure 2-11a: Results from Cr oxidation experiments in alkali media

The experimental results of the alkali runs with 50 mg/l Cr(III) (CrOx 1-1 to 1-4) are given in Figure 2-11a, those of the acid runs (CrOx 2-1 to 2-3) in Figure 2-11b. Most prominent is the reaction curve at pH 12.2, which shows a clear, first order type development reaching a final extent of around 750 µg/l. At lower pH the development is

less clearly defined, but in all experiments there is a definitive increase in Cr(VI) concentrations as the experiment progresses. Also the rate of Cr(VI) formation decreases with decreasing pH. The repeat of run 2-2 in 2-3 indicates good repeatability of the experiment with fairly identical results.

For all these runs the conversion achieved (calculated relative to the 50 mg/l Cr(III) initially charged) after 100 hours is plotted versus the experimental pH value in Figure 2-12. Although there are too few data points to make definitive statements, the trend to higher conversions with increasing pH is clearly demonstrated. It must be pointed out here that taking conversion relative to the total Cr(III) charge is somewhat misleading, since in the alkali experiments only a small fraction of this is likely to be in solution, the rest being precipitated as $Cr(OH)_3$.

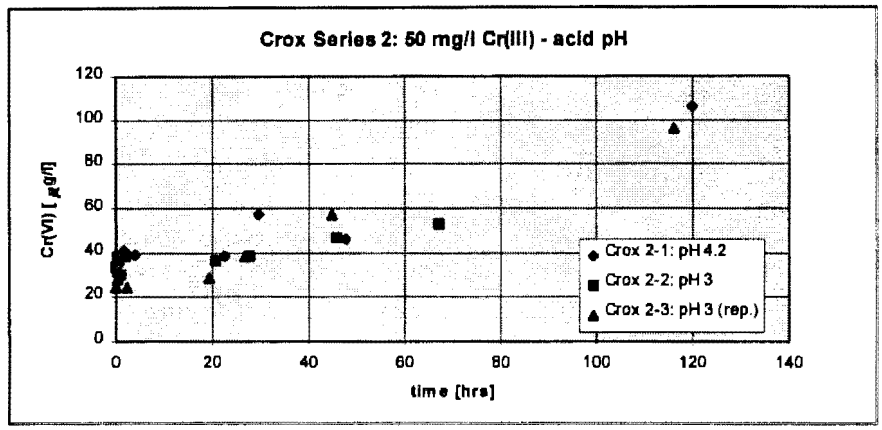

Figure 2-11b: Results from Cr oxidation experiments in acid media

The dissolved Cr(III) concentrations in these experiments was not established for lack of sufficiently accurate analytical equipment. On the other hand, there exist the possibility that the oxidation reaction is not restricted to the dissolved Cr(III) species, but may also involve the finely dispersed hydroxide gel, which, as was indicated in Section 2.1.2, when freshly precipitated initially exists only as individual $Cr(OH)_3$ compounds and polynuclear clusters before forming a precipitate upon ageing. Since the experimental solutions were

all freshly prepared, ageing may have not progressed far enough and unagglomerated $Cr(OH)_3$ may still have participated in the reaction.

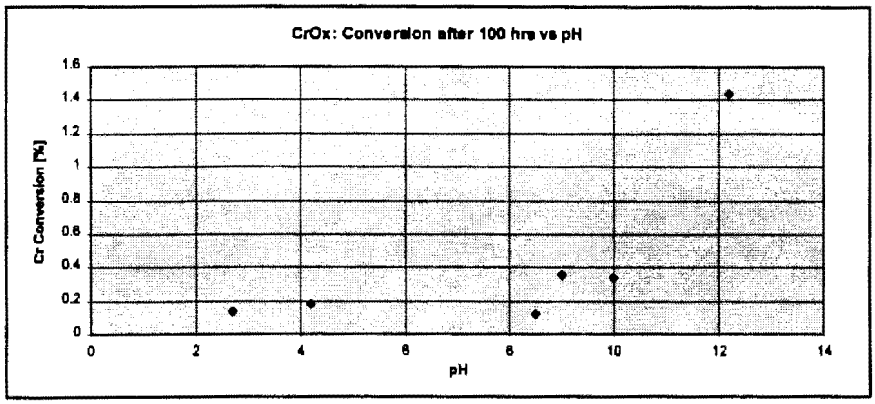

Figure 2-12: Cr(III)/Cr(VI) conversion after 100 hrs as function of reaction pH

The effect of Cr(III) concentration on oxidation is indicated by the results of experiments CrOx 3-1 to 3-3 given in Figure 2-13. Since the experiments were all conducted in the acidic region, all Cr(III) was in solution. Comparing reaction extents after 100 hours (Table 2.1) shows percentage conversion is not a significant function of the initial Cr(III) concentration.

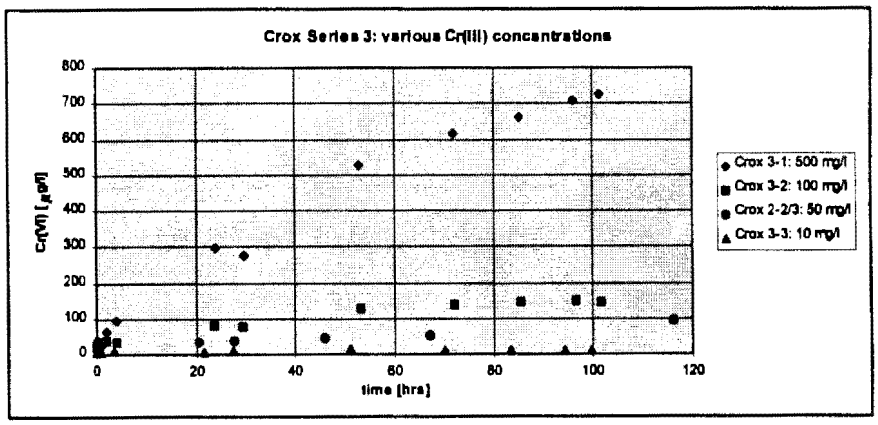

Figure 2-13: Cr(III)/Cr(VI) oxidation reaction at various Cr(III) initial concentrations

Table 2.1: Cr(III)/Cr(VI) conversion as function of initial Cr(III) concentration

initial Cr(III) conc. in feed [mg/l]	Cr(VI) conc. after 100 hrs [µg/l]	conversion of initial conc. [%]
500	727	0.145
100	144	0.144
50	75	0.150
10	11	0.110

The effect of adding MnO_2 to a 50 mg/l Cr(III) solution is shown in the results from experiments CrOx 4-1 and 4-2 given in Figure 2-14. Cr(VI) conversion occurs rapidly after MnO_2 addition, but comes to a virtual standstill after about 1 day with only marginal increases thereafter. The extent of the initial conversion is governed by the amount of MnO_2 present, but bears no relation to the total Mn concentration (which was stoichiometric and 6.6 times stoichiometric), indicating that only a small portion of the MnO_2 does react with the remainder staying inert. This is in agreement with findings of other research (see Section 2.1.6). The marginal increase in Cr(VI) after the first day could be attributed to continuing direct oxidation by oxygen as indicated by a comparison with data from experiment 2-1, which was run under similar conditions but without MnO_2 present.

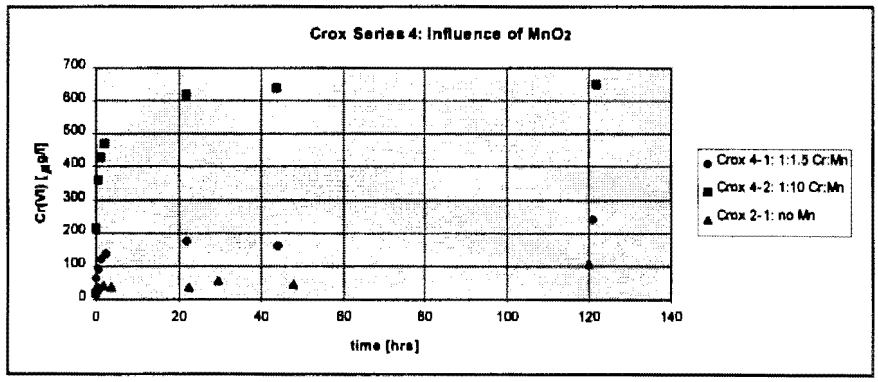

Figure 2-14: Influence of MnO_2 on the Cr(III)/Cr(VI) oxidation reaction

Discussion

It must be pointed out again, that the present series of experiments served only as a preliminary study into the general nature of the oxidation reaction in the aqueous phase. It is acknowledged that the experimental procedure is somewhat superficial, for example by not establishing the Cr(III) concentrations actually dissolved at the various pH values, by not continuing experiments over extended periods of time and running at lower (or higher) temperatures or by more rigorous pH control during the run.

Nonetheless, the results clearly demonstrate that Cr(III) does indeed oxidise to Cr(VI) in aqueous solutions at all pH in the presence of oxygen, but the reaction rates are extremely slow even at the elevated temperature used. Furthermore, there appears to be a limit to the reaction extent in the experiments at high pH, although it is not clear in what way this is related to the concentration of dissolved Cr(III) at the various pH values for lack of accurate analytical data. In the experiments under acidic conditions reactions rates are so slow, that no clarity with respect to reaction extents could be obtained within the experimental period. The experiments confirm the observations by Wood and Black (1916) that at pH values above 10 increasing pH significantly increases rate and extent of the oxidation reaction. The presence of MnO_2 dramatically increases the rate of oxidation but rapidly reaches a limiting extent, probably due to surface precipitation effects as was reported by other research (see Section 2.1.6).

The experimental results are insufficient to quantify the oxidation reaction in terms of a kinetic model. A more in-depth and rigorous experimental study is however strongly recommended to assess this potentially serious long-term effect in the context of environmental concerns.

2.3.2 Oxidation of Solid Chromic Oxide

The paper by Kilau and Shah (1984) directly hints at the possibility of atmospheric oxidation of solid Cr_2O_3 in the presence of lime (CaO) if these are in separate solid phases as could be the case in certain furnace slags. Hattori *et al.* (1978) point out that this reaction is thermodynamically feasible also at ambient temperatures. There appears to be little evidence in the literature that this effect has been investigated further as a potential source of Cr(VI) from waste materials which may contain such phases.

It was decided therefore to investigate the effect on an artificial mixture of Cr_2O_3 and lime exposed to ambient air over an extended period of time. Again this investigation was only of a preliminary nature in order to assess the extent of the reaction if it does take place and no further details were studied.

Analytical grade chromic oxide powder was mixed dry with analytical grade hydrated lime ($Ca(OH)_2$) powder and slurried with some distilled water to form a workable paste. This was rolled into spherical balls which were placed on a pad of moistened glass fibre and sealed in polyethylene bags allowing for a sufficiently large volume of air to be enclosed. The purpose of this was to ensure a closed environment in which the moisture contained in the balls would be maintained over an extended period of time. Balls not enclosed in this way would dry out completely in ambient air within one day. Although the reaction should proceed in the absence of water, it was felt that maintaining the presence of water would hold the separate grains of chromic oxide and hydrated lime closer together and would provide a medium through which ion and oxygen migration is facilitated. It is acknowledged that the same experiment should also have been carried out on dry samples for comparison.

Three experimental runs were conducted with the mixtures prepared as follows:

a) 90% Cr_2O_3 mixed with 10% $Ca(OH)_2$ as dry powder and then slurried with 20% distilled water (mass water relative to mass of the resulting paste).

b) 100% Cr_2O_3 mixed with 20% 0.1 M NaOH solution (mass solution relative to mass of the resulting paste)

c) 89% Cr_2O_3 mixed with 10% $Ca(OH)_2$ and 1% MnO_2, again slurried with 20% distilled water.

The rationale for the choice of mixtures was partly based on experiences gained from the aqueous phase oxidation experiments reported in Section 2.3.1. If oxidation takes place in experiment a) then this could be based either on direct solid phase oxidation or on aqueous phase oxidation of Cr(III) which dissolves into the residual pore water from the solid Cr_2O_3, promoted by the high alkalinity provided by the lime, or a combination of both effects. In experiment b), where lime is absent, only the aqueous oxidation could take place at a pH similar to that which could be expected from dissolved lime. By comparing the two experiments the two mechanisms can be clearly distinguished. Since the role MnO_2 can play in catalysing Cr(III) oxidation is well known, experiment c) was conducted with a small addition of MnO_2, to see to what extent (if any) this might promote the reaction.

For each experiment a batch of about 250 g of the respective paste was prepared and rolled into 10 balls of about 25 g each, which were packed into individual bags and stored on a shelf in an area of constant temperature of 22 ± 2 °C. For sampling, one bag from each batch was picked randomly and the ball subjected to analysis. Each of the three experiments was conducted in two parallel runs.

For analysis the ball was weighed moist, then dried in an oven at 60 °C overnight, and again weighed dry to establish the residual moisture content. The dry ball was then ground up into powder form using pestle and mortar. The powder, after weighing (usually yielding about 20 g), was then slurried in 1 M NaOH for exactly 1 hour. A sample of the leachate was filtered and analysed for Cr(VI) using the spectrophotometric method described in Appendix A. The Cr(VI) yield was then calculated back per unit mass of dry Cr_2O_3 originally present in the sample.

It should be annotated here that the commercially obtained reagent grade Cr_2O_3 powder was pre-washed once in 2 M NaOH and 3 times in distilled water in order to remove any Cr(VI) that might be present in the material as received. The total Cr(VI) yield from these washes was in the order of 0.8 mg/g, indicating a considerable amount of Cr(VI) initially present. It is speculated that this is residual from the manufacturing process as Cr_2O_3 is prepared from chromate solutions.

The results of the six experimental runs are presented in Figure 2-15. The results show a remarkably clear trend. Those samples containing 10% $Ca(OH)_2$ show a clear increase of Cr(VI) content with increasing age of the sample, whereas those prepared with 0.1 M NaOH show only a small initial increase and stay more or less constant thereafter. The initial offset of 0.015 mg/g corresponds to a residual Cr(VI) concentration contained in the Cr_2O_3 material used in the sample preparation and applies for all six data series.

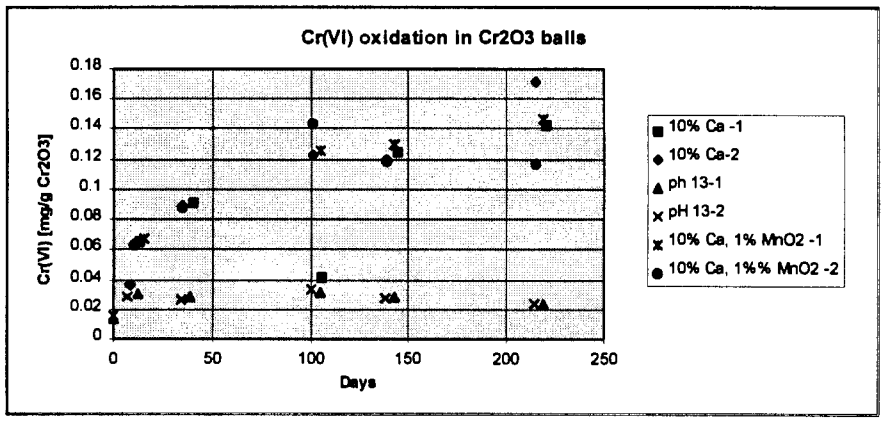

Figure 2-15: Results from long-term Cr_2O_3 oxidation experiments

It should be remarked here that the initial moisture content of the balls gradually decreased with time due to inefficient sealing of the container bags. This resulted in the balls becoming virtually dried up after about 150 days. As can be seen from the last set of data points in Figure 2-15 (after around 215 days), this did not seem to inhibit the oxidation reaction with time, although the fall-off of the conversion curve may be releated to the gradual drying up.

As was pointed out above, this investigation is only of preliminary nature and therefore insufficient data has been collected for any more in-depth analysis of the potential reaction mechanisms. Nonetheless the data measured for the experiments that did indicate some oxidation were correlated in order to obtain a first order rate constant in similar fashion as was done with the Schroeder and Lee (1975) data in Section 2.1.5. Initially this was done taking the measured conversion as fraction of total Cr present in each ball. For this the rate constant k (at 22 °C) was calculated as $6.3 \cdot 10^{-7}$ d^{-1}, which is several orders of magnitude lower than that established for the oxidation in aqueous solution from the Schroeder and Lee data ($k = 4.4 \cdot 10^{-4}$ d^{-1}, Section 2.1.5).

The experimental data did, however, suggest that the reaction falls off after very low conversions (Figure 2-15). Although this might be possibly due to the drying up of the balls, it was speculatively assumed, only a small fraction of the Cr(III) contained in the ball is available for oxidation. That this assumption is not totally unreasonable may be supported by the similar fall-off noticed for the oxidation at the surface of MnO_2, attributed to a limited availabiliy of suitable surface sites (Section 2.1.6). Thus, assuming no more than 1 mg/g of Cr(III) contained in the ball can potentially be oxidised, the first order rate constant was recalculated from the experimental data as $6.5 \cdot 10^{-4}$ d^{-1}, which is remarkably similar to that established from the Schoeder and Lee (1975) data and would imply similar reaction scenarios to those indicated in Figure 2-8, bearing in mind that only a small fraction (0.1 %) of the total Cr available can be oxidised.

Again, it must be pointed out that these projections are very speculative and a more detailed investigation with respect to meachanisms and conditions of the atmospheric oxidation reaction is required. Nonetheless, the trends observed thus far clearly illustrate that Cr(III) in chromic oxide does indeed gradually oxidise to Cr(VI) in air at ambient conditions in the presence of lime, probably irrespective of the presence of pore water, and that this Cr(VI) can be mobilised in an alkaline wash. Pore water alkalinity supporting an aqueous oxidation reaction, however, does not or only very marginally contribute to this effect. Also the presence of small amounts of MnO_2 does not appear to contribute to enhanced Cr oxidation.

In the context of wastes containing both chromic oxide and calcium oxide phases in intimate vicinity this trend gives reason for serious concern. In a waste deposit the reaction can proceed unhindered over the years and thus continuously generate small concentrations of Cr(VI) which can be mobilised by percolating water. But, even if the deposit remains relatively dry, Cr(VI) is still generated and can be mobilised when the material is ultimately contacted with water, for example if the deposit is reworked. In the long term, a waste material initially presumed environmentally benign could thus become hazardous.

2.3.3 Long-term Cr(VI) Generation In A Column Experiment

The potential long-term Cr oxidation effect postulated in the previous section has been investigated using a real chromium containing waste material under conditions conducive to the oxidation reaction (i.e. presence of free lime, well aerated and moist conditions).

The waste material used in this investigation is a slag material from a stainless steel smelter process, consisting of an electric arc furnace (EAF) and an argon-oxygen decarburization (AOD) vessel. The slag phases from both theses processes are poured into pits and left to solidify before being removed and co-disposed on the slag heap.

The EAF/AOD slag sample consists of a production related mixture of samples from the respective processes. The EAF slag occurs mainly in large and medium sized chunks (from 10 cm up to 1 m in size), whereas the AOD slag tends to disintegrate into smaller particles and fine powder after cooling. The samples were collected by random point sampling and crushed on site in a jaw crusher set to 20 mm gap.

The photograph of the slag mix (Figure 2-16) shows the widely differing types and sizes of particles present. The larger particles are either glass-like, dark grey in colour, or quite porous, brownish grey in colour and more brittle in nature. Interesting were metallic globular inclusions of about 5mm in diameter in the larger particles, which are considered to be metal droplets that were entrapped in the slag phase at pouring. The finer fraction (<1mm) consists partly of splinters of large particles, probably originating from the crushing process, and partly of a fine white powder, mainly attributed to disintegrated AOD slags.

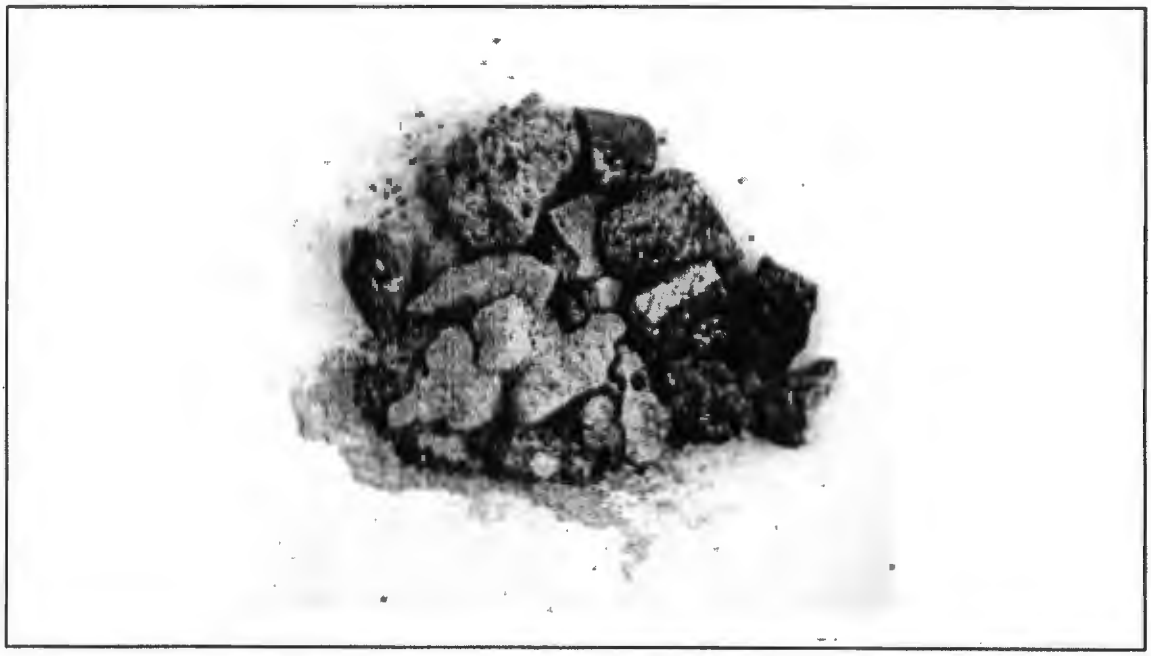

Figure 2-16: Picture of EAF/AOD slag sample mixture

Chemical analysis of the main metal components of the two slag phases are given in Table 2.2. Of note are the relatively high concentrations of Mg and Ca (assumed to be present as their oxides) which is understandable since they are used as fluxes in the process. The fine, disintegrated fraction of the AOD slags is mainly associated with these. The only metal components of significant concentrations are Fe, Cr and Ti, but many other metal species (particularly Na and K) are present in trace amounts. The balance of the material composition (>50%) is assumed to be made up mainly of silicates and alumina-silicates, which were not analysed for. These are considered responsible for the more glassy type of particles (Figure 2-16).

The material was tested for an initial presence of Cr(VI) by washing in distilled water at a solids to liquid ratio of 1:20, but measured concentrations remained below the analytical limit of 0.01 mg/l, thus confirming that the material would be environmentally benign with respect to chromium. The pH measured in the water wash was around 12.3, which corresponds well with what be expected from the dissolution of free lime.

Table 2.2: Concentration of main components of EAF/AOD slag phases*

	EAF	AOD
Fe	2.53	0.40
Cr	3.34	1.14
Ca	20.0	25.9
Mg	10.1	8.10
Ti	1.94	1.00

* all concentrations in %

The mixture was placed into a lysimeter column, 225 mm in diameter and approximately 1 m in height. Set-up and operation of such column experiments are described in more detail in Section 5.3. The bed was sprinkled with daily charges of distilled water, acidified with a sulphuric/nitric acid mix to a pH of 4 to simulate "acid rain" as it is frequently encountered in the area where this material is normally deposited (Mpumalanga Province in north-eastern South Africa). As will be clarified in subsequent chapters of this thesis, the rationale of this experiment is to simulate the behaviour of the waste material in a deposit scenario. The feed liquor gradually percolates through the porous matrix of the bed in similar fashion as to how incipient rain water would migrate through a deposit. On its

path chemical species can dissolve from the solid matrix into the aqueous phase and be transported within it to the base of the bed and enter into the surrounding environment as a potentially hazardous leachate. In the lysimeter experiment the effluent from the column is collected in beaker and analysed for dissolved constituents.

After an initial leach run of 40 days at a daily feed of about 500 ml of acid rain leachant, the column was left standing open to the atmosphere. After about 6 months it was restarted for a second run with a daily feed of fresh acid rain leach liquor of about 200 ml which continued for another 6 months. The column was then again left to stand for 6 months, before a third leach run of 6 months at 200 ml acid rain leachant per day was conducted.

In all three runs the only constituents found in significant concentrations in the effluent from the column were Na, K and Ca as well as traces of Cr(VI). The three leach curves for Na and K are given in Figure 2-17 a-c and those for Cr and Cr(VI) in Figure 2-18 a-c overleaf.

At the beginning of each run the concentrations start at a peak before relatively quickly levelling off to smaller concentrations. While for Na and K those peaks become smaller with each new run, they actually increase each time for Cr(VI). Furthermore, the Cr(VI) curves level off at a higher level in each consecutive run (0.1, 0.22 and 0.54 mg/l), whereas the final levels of Na and K actually decrease from run to run.

This behaviour is a clear indication that the availability of Cr(VI) in the bed has actually increased with time, whereas that of Na and K has continuously decreased as would be expected with continued leaching. Although this increased availability could, in principle, be assigned to a very slow release mechanism, this is unlikely considering the normally very high solubility and mobility of Cr(VI). The leach curves from this experiment are therefore taken as a strong indicator for continuing Cr oxidation.

The following scenario is hypothesised explaining the leach curves. The first leach run was conducted when the material was still relatively new (about 3 months after sampling "fresh" production). The low Cr(VI) levels observed were small and could be attributed to background contamination initially present in the sample. Likewise the Na and K concentrations can be attributed to the washing off of small salt concentrations included in the material.

When the bed then undergoes the 6 months rest phase a migration of residual concentrations is likely to take place from stagnant zones into the main flow channels (which are likely to exist in the highly inhomogeneous material, see Section 4.1). This takes place in the pore water entrapped in the bed after the first leach run, which, as was observed, does not dry up entirely during the rest phase. More Cr(VI) is formed by oxidation in the well aerated bed, which also migrates into the flow channels.

When the column is then started up again, initial effluent concentrations are at a new peak as the flow channels have been replenished, but quickly fall off as these are washed out. Thereafter, recovery proceeds at the rate at which further migration into the flow channels takes place. This way the available Na and K is gradually diluted within the bed and levels continuously decrease from run to run. For Cr(VI), however, which is assumed to be continuously generated in the bed, the opposite effect occurs and measured concentrations increase from run to run as less Cr(VI) is removed than is generated over the total time of the experiment (i.e. rest and leach periods combined).

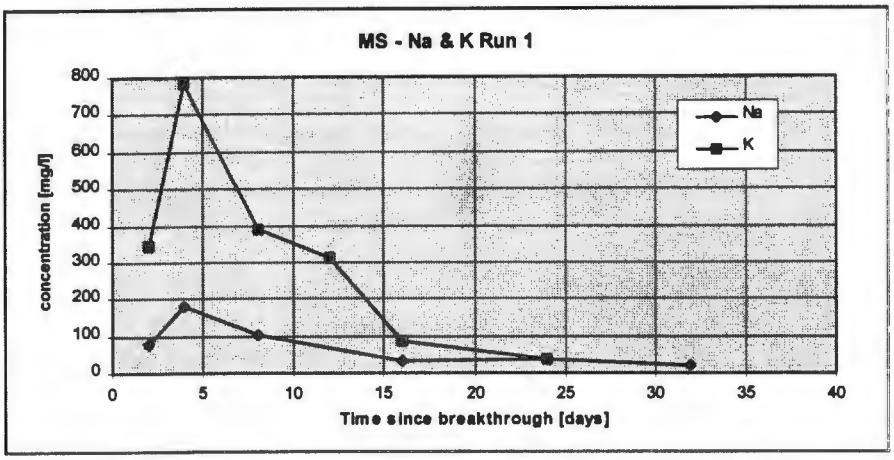

Figure 2-17a: Leach profile of Na and K from MS lysimeter, 1st run

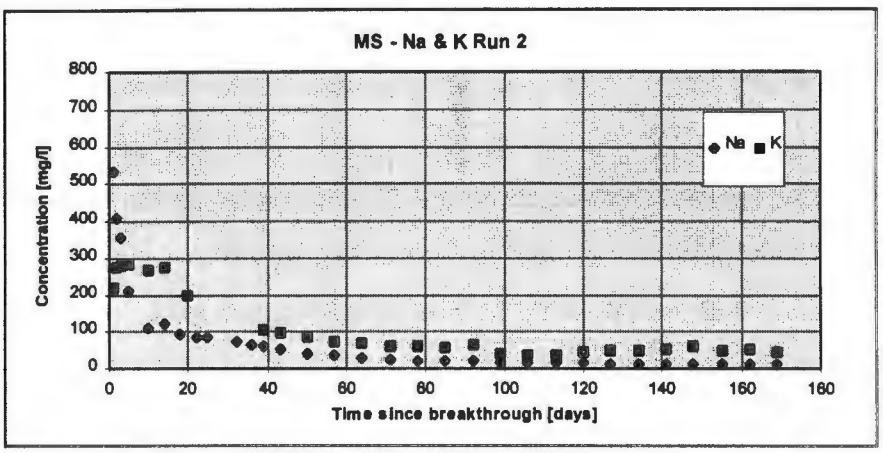

Figure 2-17b: Leach profile of Na and K from MS lysimeter, 2nd run

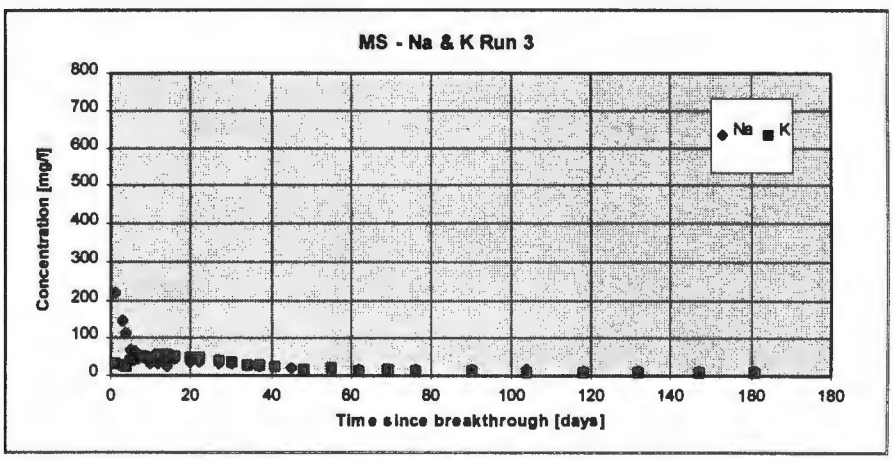

Figure 2-17c: Leach profile of Na and K from MS lysimeter, 3rd run

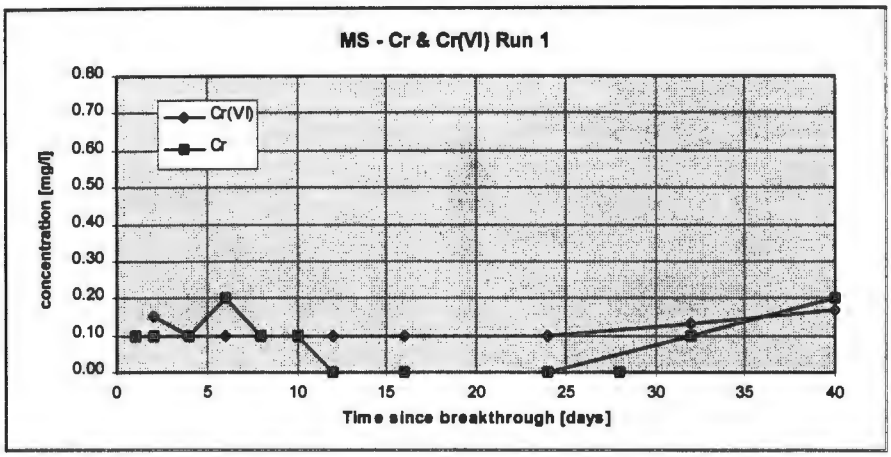

Figure 2-18a: Leach profile of Cr and Cr(VI) from MS lysimeter, 1st run

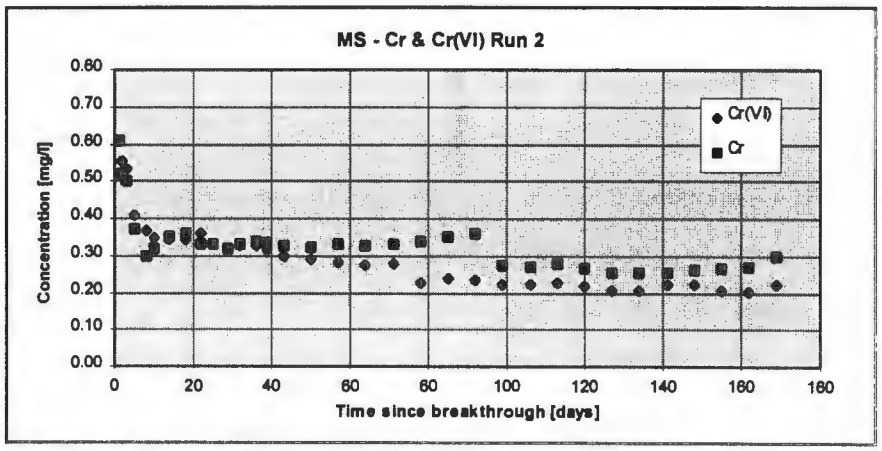

Figure 2-18b: Leach profile of Cr and Cr(VI) from MS lysimeter, 2nd run

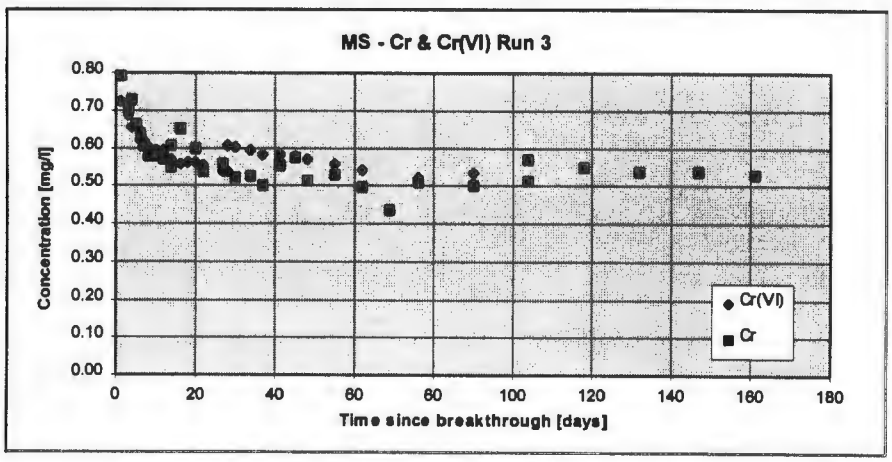

Figure 2-18c: Leach profile of Cr and Cr(VI) from MS lysimeter, 3rd run

This trend confirms the environmental concern associated with this type of waste materials raised in Section 2.2 above. Cr oxidation continues irrespective of the rate of removal by leaching. If this removal rate is small (as was the case in the rest phases in the column study), Cr(VI) is likely to gradually accumulate in a deposit over time. If leaching does eventually take place (for example by water percolating through the deposit after a rainstorm), this accumulated Cr(VI) could then be suddenly mobilised at peak concentrations, as was observed at the beginning of the second and third runs. The hazardous Cr(VI) could thus suddenly emerge in significant concentrations from a waste deposit that was originally deemed environmentally benign.

2.4 Closure

This chapter gives a detailed review of chromium chemistry and the chemical interactions of chromium in natural environments such as soils and natural water bodies. As a trace metal chromium is omnipresent is these environments at low background concentrations, mainly as the trivalent Cr(III) and the hexavalent Cr(VI). While the former is mostly immobilised at natural pH levels, Cr(VI) is soluble at all pH values and can become toxic if its dissolved background concentration exceeds 0.1 mg/l. In natural environments there exist complex cycles of dissolution/precipitation, adsorption/desorption and oxidation/reduction between Cr(III) and Cr(VI), the mechanisms of which have been discussed in detail.

These natural chromium cycles are likely to be disturbed if excessive amounts of additional chromium are introduced as a result of anthropogenic processes, particularly through uncontrolled leaching from deposits of chromium containing wastes. Not only can the natural background levels of chromium be exceeded beyond levels which are tolerable to certain forms of plant and microbial life, but also can the oxidation/reduction cycle between the relatively innocuous Cr(III) and the toxic Cr(VI)

be upset in such a way, that an increased presence of Cr(VI) results, even if a chromium imbalance is initially introduced exclusively as Cr(III).

Of particular interest in this context is the oxidation of Cr(III) to Cr(VI), which is assumed to be facilitated by MnO_2 surfaces, but may also proceed through the direct action of atmospheric oxygen albeit at very slow rates. While this may be of minor consequence in natural chromium cycles, it may become significant in deposits of chromium containing waste materials. Although the chromium in such materials is mostly present as the relatively immobile Cr(III), gradual oxidation to Cr(VI) may result in the mobilisation of chromium into the natural environment surrounding the deposit and a potentially harmful disturbance of the chromium balance of these.

Chromium oxidation by atmospheric oxygen has been confirmed experimentally and was found to proceed faster and to increasing extents with increasing pH in an aqueous environment as well as directly with solid Cr_2O_3 in the presence of lime. A column leach experiment with a waste slag material from the ferro-alloy industry, characterised by significant concentrations of both Cr(III) compounds and free lime further corroborated the potential for atmospheric chromium oxidation, as leachable concentrations of Cr(VI) continuously increased with time, whereas those of other species decreased as expected. This study clearly illustrates how chromium can be mobilised from a waste deposit, although the material contained therein may be perceived initially as environmentally benign.

The remainder of the present work is focused on providing an understanding of the principles of leachate generation in waste deposits in general and, more specifically, on the development of a predictive modelling tool and waste assessment methodology. This has been tested with chromium containing waste materials mainly focussing on the mobilisation of Cr species from deposits of such materials. The review in this chapter has illustrated that a thorough appreciation of the often complex chemical interactions involving this heavy metal species is important for meaningful predictions of the potential impacts such waste deposits can have on their surrounding environment. Thus

the case of chromium interactions is used as an example here for the likely interactions involving other heavy metal species in the context of waste materials where these are of concern. Therefore these interactions need to be understood with similar detail as is illustrated here in the case of chromium in order to allow meaningful assessment of the long-term mobilisation of the respective species from waste deposits and their impact on the surrounding natural environments.

3

Management of Solid Minerals Processing Wastes

Solid wastes from industrial processes have historically been deposited in ways that have resulted in the mobilization of hazardous constituents contained in these. Natural processes, such as leaching by rainwater seeping through a waste deposit, can effect the release and transport of hazardous constituents out of the deposit into the surrounding natural environment. Where such release has exceeded the natural attenuation capacity of these environments, cases of pollution have been experienced, at times taking a serious toll on biotic and human health.

This chapter serves as a background study to aspects of handling, disposal and treatment of solid wastes as well as the mechanisms of pollution resulting from such practice, pollution case studies and remedial action. The focus here is on solid wastes arising from the minerals processing industry, which accounts for by far the largest volumes of industrial waste world-wide. As chromium containing waste materials from the ferro-alloy industry are the subject of experimental work in this thesis, specific attention is given here on these types of waste, but it should be pointed out that, in most respects, they can be taken as representative of minerals processing wastes in general.

Section 3.1 contains a more general introduction to the concepts of waste, waste management and pollution and to the fundamental mechanisms that lead to the mobilisation of contaminants within solid waste deposits. Waste disposal practice in the minerals processing industry is then investigated in more detail in Section 3.2. Types of chromium containing wastes, their generation and treatment as well as options for recycle

or recovery are discussed in Section 3.3. This section also covers some case studies of pollution arising from such wastes and some aspects of clean-up and remediation of such pollution. The chapter closes with some remarks (Section 3.4) regarding the need to be able to appreciate the process of leachate generation from solid waste deposits in more depth for environmentally (and economically) sound waste management practice.

3.1 Waste, Waste Management and Pollution - A Conceptual Introduction

Within the natural environment, physical and chemical conversions are taking place continuously through both biological activity and geological transformations. This results in a continuous movement of material between these natural processes with the chemical constituents produced by one becoming the feed material for the next. All organisms and physical components within a given geographical area and their interactions in terms of material and energy flows are termed an *ecosystem* (Moran *et al.*, 1986). Through the exchange of material each element is moving between soils, aqueous systems and the atmosphere in complex, often cyclic pathways, within and between ecosystems at various scale, very localised (for example a meadow or a pond), regional (an area comprising a number of meadows, ponds, forests and fields) or global.

For example the pathway of phosphorus, an essential nutrient for all organic life is illustrated in Figure 3-1. Plants take up phosphorus from the soils through their roots. When these plants die, the phosphorus is returned to the soil by decomposition through bacterial action. As plants do not move, this cycle is very localised. If animals take up phosphorus by feeding on plants, the cycle is widened to a regional scale as they move around over a much larger area. Some phosphorous is lost from the soil through run-off and leaching and transported through water ways (ground and surface waters) to the ocean, where it may be taken up by aquatic biosystems (i.e. other localised ecosystems). It may be returned to the soil by geological transformation (settling in ocean sediments,

geological uplift and subsequent weathering of phosphate rocks). At this scale the phosphorus cycle becomes global and is exchanged between individual, more localised ecosystems.

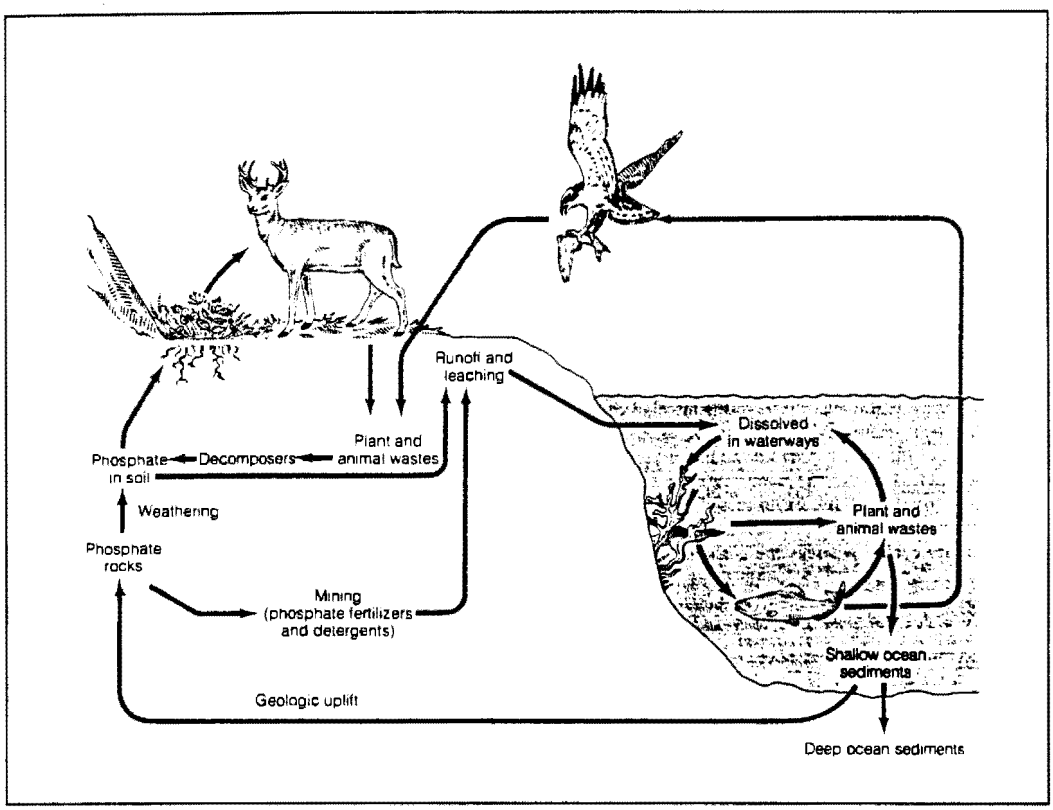

Figure 3-1: The phosphorous cycle (taken from Moran et al., 1986)

The interactions between these natural processes within and between ecosystems at various scales result in complex balances of uptake, dispersion and return of the elements, which are characterised by apparent equilibria which tend to shift only on a geological time scale. On the other hand, industrial, i.e. anthropogenic processes, have no such equivalent. While also here there exists a chain of products - for example a mineral is mined, extracted, refined, turned into a product and so forth - each of these processes is likely to generate wastes, i.e. substances which are unwanted, unnecessary or incompatible within the boundaries of this process and have no immediate economic value for any subsequent process (Figure 3-2). Thus material flows within the industrial chain of processes results in a number of "dead ends", which are returned to the natural

environment in the form of deposited solids, liquid effluents and gaseous exhausts with no further consequence to the industrial process chain.

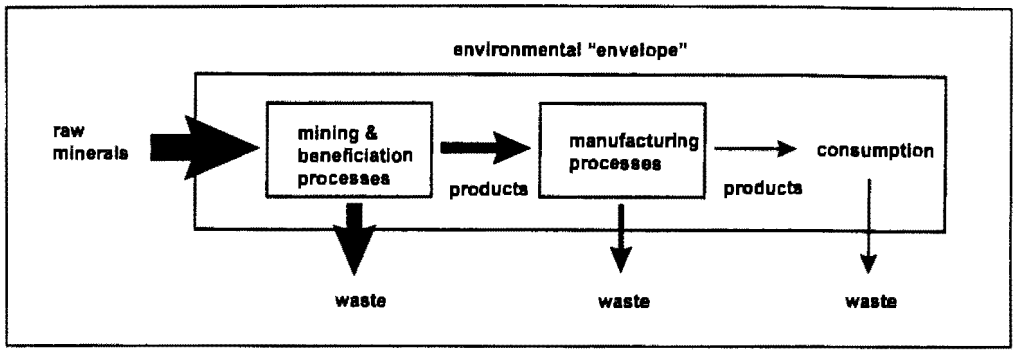

Figure 3-2: Industrial product chain and waste generation

However, by returning anthropogenic wastes to the natural environment, chemical substances contained in these waste streams can re-enter into natural process cycles by a number of physical and chemical processes, often with unforeseen consequences. The often sensitive balances in ecosystems can be disturbed through the introduction of such substances, either because their concentrations are unnaturally high or because they are altogether alien and potentially toxic to certain organisms. This shifting of balances can in consequence lead to the establishment of new equilibria within an ecosystem or lead to its complete destruction. In any event, changes in the natural environment are a potential consequence of the disposal and dispersion of wastes from industrial processes.

Depending on the scale of introduction of such ecological disturbances, changes in the natural environment can be very localised, regional or even global. As an example, one may take the continuous release of SO_2 into the atmosphere as a result of industrial burning of fossil fuels, particularly in pyrometallurgical processes and power generation over the last century. "Acid rain", the increasing acidity of precipitation in areas of high industrial activity, is attributed to this process. This in turn will effect gradual changes in local ecosystems, such as the acidification of soils and lakes, sometimes far away from the original source of the SO_2 exhaust gases and often with a considerable time lag (Stigliani, 1993).

Ultimately such changes, local or global, affect humans through our participation in ecological systems - through the food we eat, the water we drink and the air we breathe. The changing quality of these natural "products" we consume may adversely affect our health. When human well-being is thus infringed on, through the direct and indirect consequences of waste disposal or dispersion, we begin to talk of "pollution" and refer to the chemical species that cause it as "contaminants" (Alloway and Ayres, 1993).

Just as products of natural processes are not normally polluting but form part of a complex cycle, the generation of waste from an industrial process need not in itself be an act of pollution. Only once chemical species - introduced into the natural environment as a direct consequence of a particular waste disposal practice - become a disturbance to existing ecosystems to an extent which is detrimental to human well-being, does generating waste constitute pollution.

The way contaminants are introduced into and dispersed within the natural environment is dependent on waste management practice, i.e. the form and manner in which waste from a particular process is disposed. Venting of gaseous wastes and directing of liquid effluents into natural waterways will result in an immediate dispersion and transport of chemical species far from their source and consequently potential contaminants can directly interfere with ecosystems on local, regional and, in the case of gaseous wastes, even on a global level. Thus it is an obvious choice for pollution prevention to minimise dispersion of contaminants by containing the waste stream or removing them from the waste stream such that they are rendered less mobile, preferably in the form of solids. Examples of this "de-contamination" of waste streams are the scrubbing of toxic components and electrostatic precipitation of fine particulates from flue gases and the precipitation of heavy metal species and subsequent filtration from industrial waste waters.

If the waste is in solid form, storage in landfill deposits could be perceived as "safe" disposal practice since any potential contaminants are practically immobilised in the solid

state and therefore unlikely to interfere with any adjacent ecosystem. This perception can be seriously misguided, however, as there exist mechanisms, by which contaminant species can become mobilised within solid waste deposits and transported into the surrounding environment.

Deposits of solid waste are never entirely dry but are usually exposed to some extent of water migration. Where the waste material was deposited dry originally, rainfall onto the deposit surface will result in at least some water entering the waste matrix. In solid wastes deposited as a slurry or dewatered filter cake, residual moisture will gradually drain through the deposit in addition to incipient rainwater entering from the top. In buried wastes, moisture migrating from the surrounding soils will also gradually permeate the waste matrix.

Water migrating through a waste deposit will create an aqueous environment within the deposit into which chemical species, toxic and non-toxic, can be released from the solid matrix by a number of chemical mechanisms, such as dissolution, desorption and leaching, and within which they can be transported away from their source to the bottom of the deposit by bulk movement and diffusion. From there dissolved species may disperse further into underlying subsoils and aquifers (Figure 3-3). This process is commonly referred to as leachate generation and transport, resulting in the mobilization of potentially harmful constituents in the (anthropogenic) waste material into the surrounding natural environment.

Thus, a certain risk exists for contaminant mobilisation, dispersion and potential pollution also for solid waste disposal, but these effects are likely to much more localised and less immediate than what can be expected from the dispersion of unmodified gaseous and aqueous wastes. By recognising the potential for leachate generation, however, potential pollution from solid waste disposal sites is controlled relatively easily by appropriate waste management and even if pollution has already taken place it is cleaned up much more easily relative to pollution at a regional or global level. Solid waste management

with respect to disposal practice, pollution monitoring and control is discussed in detail in the following section.

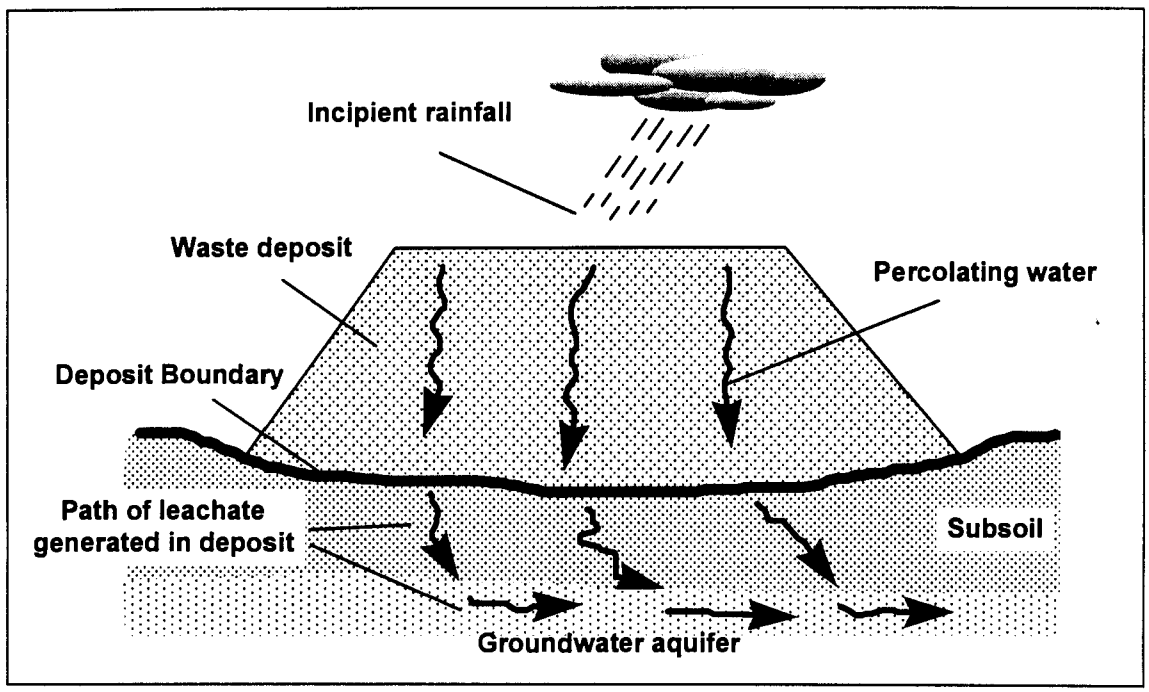

Figure 3-3: Conceptual process of leachate generation in a landfill waste deposit: (a) infiltration of rainwater; (b) release of species into percolating aqueous phase; (c) propagation as leachate plume in the subsoil and underlying aquifers.

In summary it can be said then, that pollution arises where contaminant species upset the delicate balances of natural ecosystems to such an extent that human well-being is affected. In most cases such contaminant species are contained in the waste streams of industrial activities. The degree of dispersion and hence location of impact of potential contaminants within wastes is directly linked to industrial waste management practice. With increased public awareness of the effects and causes of pollution, there is increasing pressure on the operators of industrial activities to both minimise the generation of waste and employ waste disposal strategies which minimise the risk of potentially harmful impact on the natural environment.

Waste minimisation can be achieved through the optimisation of process designs, choice of appropriate technology and efforts for waste recycling, i.e. return of waste material as

feed for other industrial processes. Where wastes cannot be avoided, environmentally responsible waste management must aim at containing potentially harmful constituents in waste streams in their least mobile form - usually solids - and ensure that disposal occurs in such a way that potential mobilisation from the deposit is minimised and stringently controlled.

In this sense sound waste disposal practice and an understanding of the chemical and physical processes that lead to contaminant mobilisation within solid waste deposits are critical. While the former is mostly concerned with maintaining a physical barrier between disposal site and the surrounding environment within the limits of manageable and not overly costly technology, understanding the mechanisms of leachate generation is important for meaningful assessment of the long-term environmental risk associated with a particular disposal site. Such risk assessments can in turn inform optimal waste management strategies and the combination ensures that the impact of industrial waste on the natural environment is minimal and able to be tolerated by the affected ecosystems.

3.2 Waste Disposal Practice in the Mining and Minerals Processing Industry

3.2.1 Introduction

Mining and associated mineral extraction and beneficiation operations world-wide result in large annual tonnages of various solid waste materials. These include waste rock, separation plant tailings, leach residues, smelter slags and flue dusts and residues from water treatment plants, amongst others.

Traditionally these wastes are disposed of in open heaps, piles, landfills or tailings impoundments on sites that are of convenient proximity to their source and that were considered unsuitable for alternative use or settlement. Because the large tonnages arising

out of a single operation, these deposits can grow to considerable dimensions, covering several hectares of ground and extending up to 100 m in height.

Table 3.1 gives averaged ore concentrations of various minerals mined and processed in the Republic of South Africa (Stewart and Petrie, 1997). The non-valuable fractions of the ores processed end up mostly as waste with only a small part being converted to useful by-products, such as sulphuric acid from roasted sulphide minerals. The total mass output from the South African minerals processing sector as a whole has been estimated at 655 million tons (Stewart and Petrie, 1996) for 1995. Only 14% of this output is as useful products, the rest being waste, a breakdown of which is given in Figure 3-4. It is likely that a similar product-waste breakdown applies to the minerals processing industry world-wide.

Table 3.1: Average ore concentrations of the of the feed to the South African minerals processing industry (Stewart and Petrie, 1997)

Sector	Metal	Average Concentration
Gold	Gold	4 g/t
PGMs	Noble Metals	5 g/t
Base Metals	Copper	1%
	Lead	6%
	Phosphate	8%
	Zinc	3%
Ferro-Alloys	Chromium	40%
	Iron	60%
	Manganese	40%
	Vanadium (as V2O5)	2%
Beach Sands	Titanium, Zirconium	1%

As Figure 3-4 indicates, most of the waste output from this sector is as solid waste, traditionally disposed in landfills. Exact inventories of amounts and nature of wastes stored in deposits throughout the world are extremely difficult to establish. This is mainly due to poor record-keeping by operators in the past and a continuing reluctance to do so still today where it is not strictly enforced by environmental legislation.

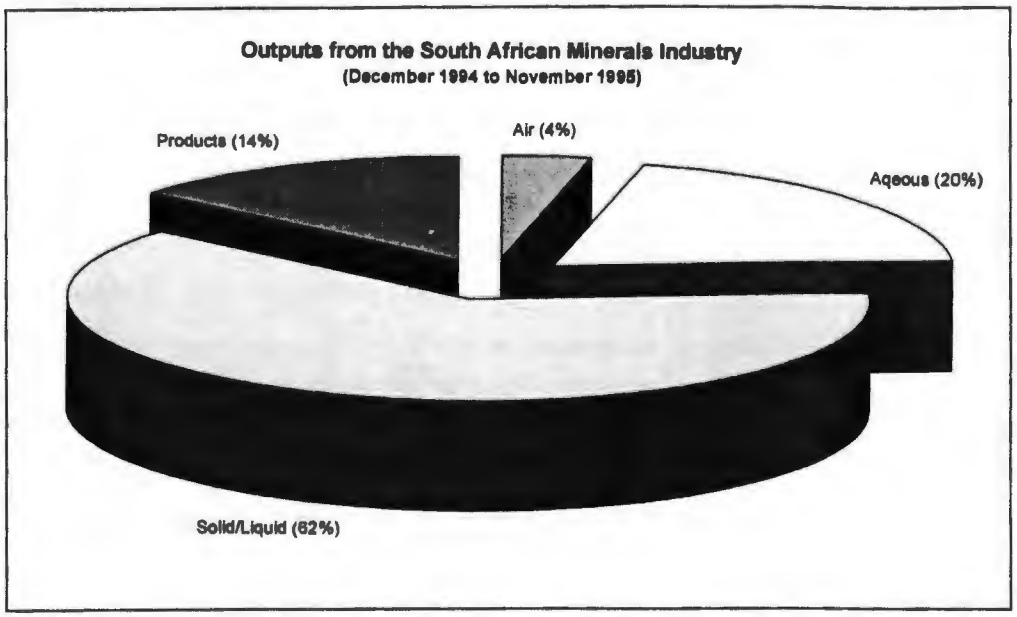

Figure 3-4: Breakdown of total mass output (655 Mt in 1995) from the South African minerals processing industry as a whole (Stewart and Petrie, 1997)

Until the middle of the century waste deposits were largely unengineered and the sites selected entirely on the grounds of proximity to a settlement or to the process plant that generated the waste (Daniel,1993). Geotechnical considerations, such as situation of aquifers, nature and stability of soil and substrata were seldom applied, and those concerns about stability which did exist, revolved solely around mechanical stability with respect to collapse. After closure of the operation, deposits were mostly abandoned and frequently forgotten.

Some of these disposal practices have led to catastrophic failures, of which only more recent examples have been well documented (for example Dobry and Alvares, 1967 as quoted in van Zyl, 1993). Since the 1960s these have led to the development of science around geotechnically safe mining and minerals processing waste disposal practice. Such practice includes construction of deposits with minimised risk of rockfall and landslides, stability with respect to ground movement and seismic events, amongst other.

In the 1970s, another set of reported catastrophes involving the leaching of contaminated water (Daniel, 1993) from forgotten deposits into surrounding soils and aquifers prompted

renewed environmental concerns around deposits of mining wastes. In the US and Western Europe a number of environmental techniques began to influence engineering design and waste management practice. These included minimising the percolation of water through the deposit by suitable compaction, the use of liners at the base of waste deposit as hydrodynamic barriers as well as leachate collection systems.

It is not known to what extent these improved practices are being applied in developing countries to which in recent years primary resource extraction and beneficiation has been moved due to declining resource in developing countries, but also due to the fact that environmental legislation is less-well promulgated and enforced in these countries (Petrie and Raimondo, 1997).

Environmentally sound design of waste deposits, however, is still a developing science. Although the fundamental understanding of leachate transport and, to a lesser extent, of leachate generation in and around waste deposits is reasonably well developed, many disposal practices and the technologies used are still relatively new and their long-term environmental effects not yet established. New technologies, such as liner materials and stabilisation methods keep emerging on the market, but only application in the field and monitoring over sufficiently long periods of time can establish their long-term environmental effectiveness.

Planning and construction of waste landfill deposits are traditionally civil engineering exercises, although knowledge from the fields of geotechnical and chemical engineering, geochemistry and even botany play significant roles. The following sections outline the main aspects of sound waste deposit engineering from site selection, site preparation by placing liners, leachate collection systems and monitoring wells. The main types of deposits, viz. dump heaps, tailings impoundments and mixed deposits, and some aspects relating to their operation are described. Ash disposal, heap leaching and methods of waste stabilisation are covered as they represent special aspects relating to waste disposal practice. Some comments on site closure are also given.

construction does not require extensive excavation work. Partially below or fully below ground disposal allow more efficient use of space, for example re-filling of old open cast mines or quarry. Also, below ground disposal will allow productive use of the surface after closure of the deposit, for example as a park.

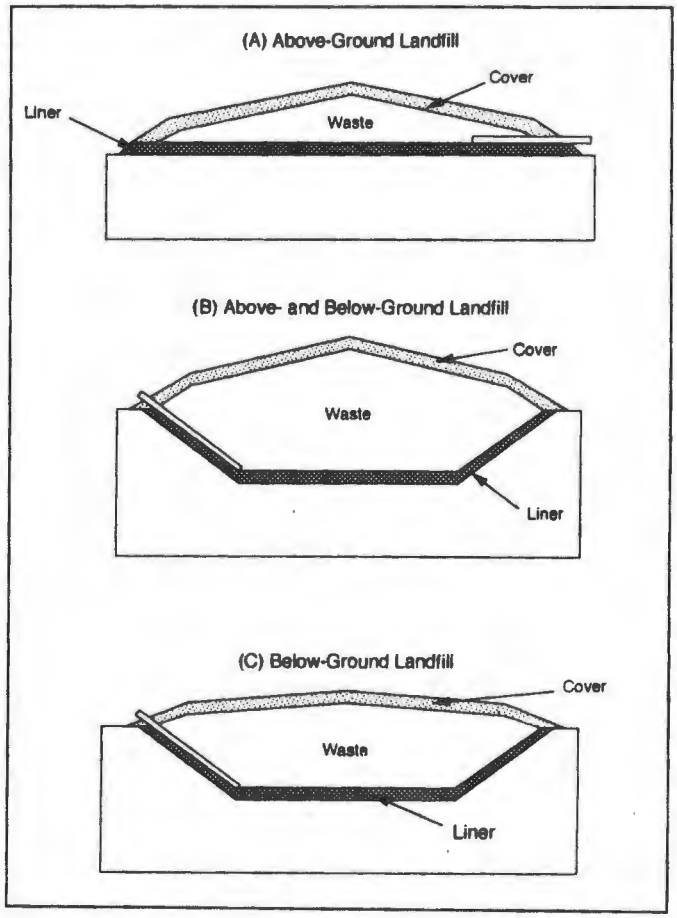

Figure 3-5: Types of landfills: (a) above-ground; (b) above- and below-ground; (c) below-ground (taken from Daniel, 1993)

3.2.3 Liners

Installation of a liner on site before waste is being placed is now common practice. A liner is essentially defined as a basin of low hydraulic conductivity material forming the base of a waste deposit. Any leachate percolating through the waste deposit will collect in this basin and only very gradually seep into the underlying sub-soil due to the hydraulic

resistance of the liner material. If a drainage or leachate collection system is in place collected leachate is largely removed through controlled channels before seepage occurs. Three types of liners are commonly used:

- naturally-occurring clay liners
- compacted soil or composite liners
- geosynthetic liners

Natural clay liners are naturally-occurring formations of low-hydraulic conductivity, clay rich soil, allowing direct waste disposal above them. Normally they are used as a back-up to additional engineered liners, but in can be found in older deposits as the only liner system present.

A major problem associated with natural liners is to ensure uniformly low hydraulic conductivity. In a natural formation, there may easily be smaller zones of higher conductivity or serious cracks and faults. Considering the large areas waste deposits cover, extensive pre-testing of such natural liners to detect and repair any potential faults is a costly exercise, a certain risk that potential leaks went undetected remains.

Compacted soil liners are constructed from natural soil materials which are, by means of compactors, mechanically compressed to minimise interstitial voids. These liners are usually constructed in successive layers of carefully prepared and compacted soil until the desired thickness is achieved. Great care needs to be taken in the compaction process to avoid cracking of the layer due to drying or freezing of the soil and in good bonding between individual layers to minimise the chance for horizontal flow in the interstice between two layers, thus potentially interconnecting cracks (Figure 3-6).

A lack of care and effort during preparation of compacted liners has resulted in frequent failures and their gradual replacement with the simpler and more robust geosynthetic liners. These are essentially large sheets of geotextiles with a layer of bentonite attached to

them. They are placed on-site with small overlaps, sealed with additional bentonite to form one large coherent sheet onto which some gravel and then the waste is placed.

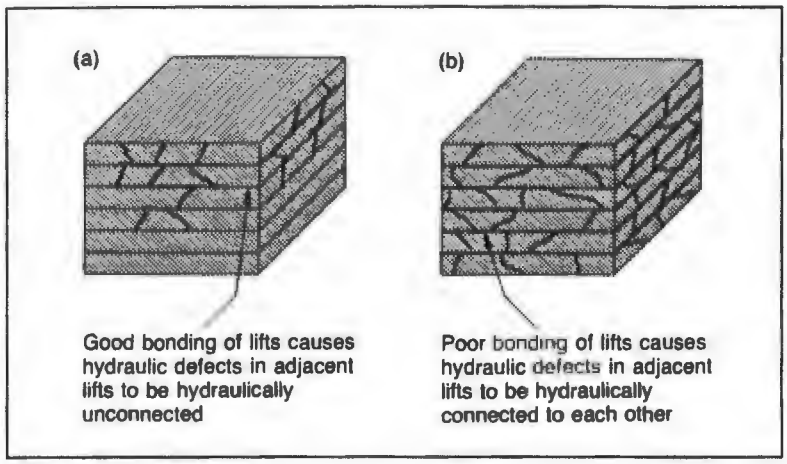

Figure 3-6: Effect of (a) good and (b) poor bonding between individual layers of a compacted clay liner(taken from Daniel, 1993)

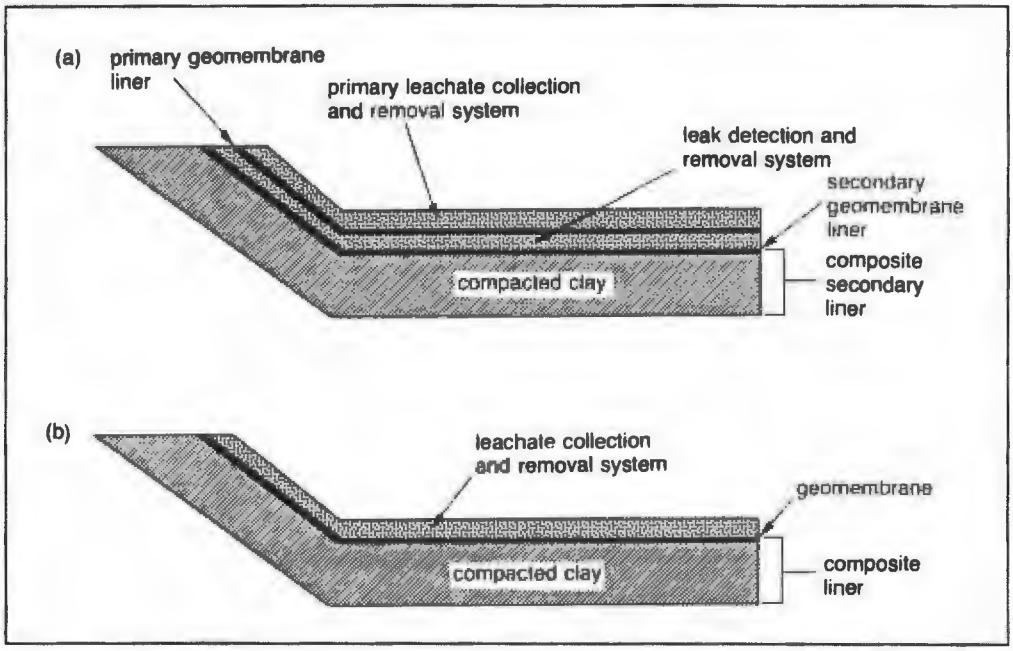

Figure 3-7: Minimum liner requirements of the US EPA: (a) for hazardous waste landfills; (b) for non-hazardous waste landfills (taken from Daniel, 1993)

Since geosynthetic liners can occasionally puncture or exhibit torn seams, it is advisable to place them on a back-up layer of natural clay or compacted soil to minimise the effects of these occasional leaks. By comparison, geosynthetic liners are simpler to install and more

robust than other liner types and therefore the preferred option. However, since they are a fairly recent invention, information on their long-term stability is not as yet available.

In the USA minimum containment requirements for hazardous and non-hazardous waste deposits are laid out in the Resource Conservation and Recovery Act, Subtitles C and D (Daniel, 1993). Hazardous waste deposits normally require a double liner system (Figure 3-7), consisting of a primary leachate collection and removal system above the first geoliner, followed by a secondary leak detection and removal system over a secondary geoliner which itself is placed on a compacted or natural soil liner as back-up. Non-hazardous waste sites still should have a single leachate collection and liner system.

3.2.4 Leachate Collection Systems

Leachate collection from a waste deposit is achieved by placing a drainage material, usually gravel, over the primary liner. Leachate percolating through the deposit collects in this layer and flows gravitationally along slopes towards a sump from where it is recovered by a submersible pump within a manhole or by large diameter pipes (Figure 3-8). Additionally a system of perforated collection pipes can aid the speedy removal of leachate from the drainage layer. In order to avoid clogging of drainage systems by fines carried in the moving liquid, the collection layer must be covered by a suitable filter layer, either sand or a geotextile.

In waste deposits with a double liner system a separate leachate collection system must be installed between the primary and secondary liner. Although ideally very little or no leachate should reach the secondary system, leachate can still be effectively removed in the case of a leak in the primary liner. Therefore this system is also referred to as the leak detection or witness drain.

Collected leachate is either directly recycled as process water if not too heavily contaminated or purified in a treatment plant with subsequent recycle or disposal, or pumped to evaporation ponds. Treatment on site is often uneconomic as the volumes of leachate generated are usually too small. Where many waste deposits are situated in close vicinity a central treatment plant, taking in all individual contributions, might be feasible, but pumping or haulage distances must be short to warrant such a set-up.

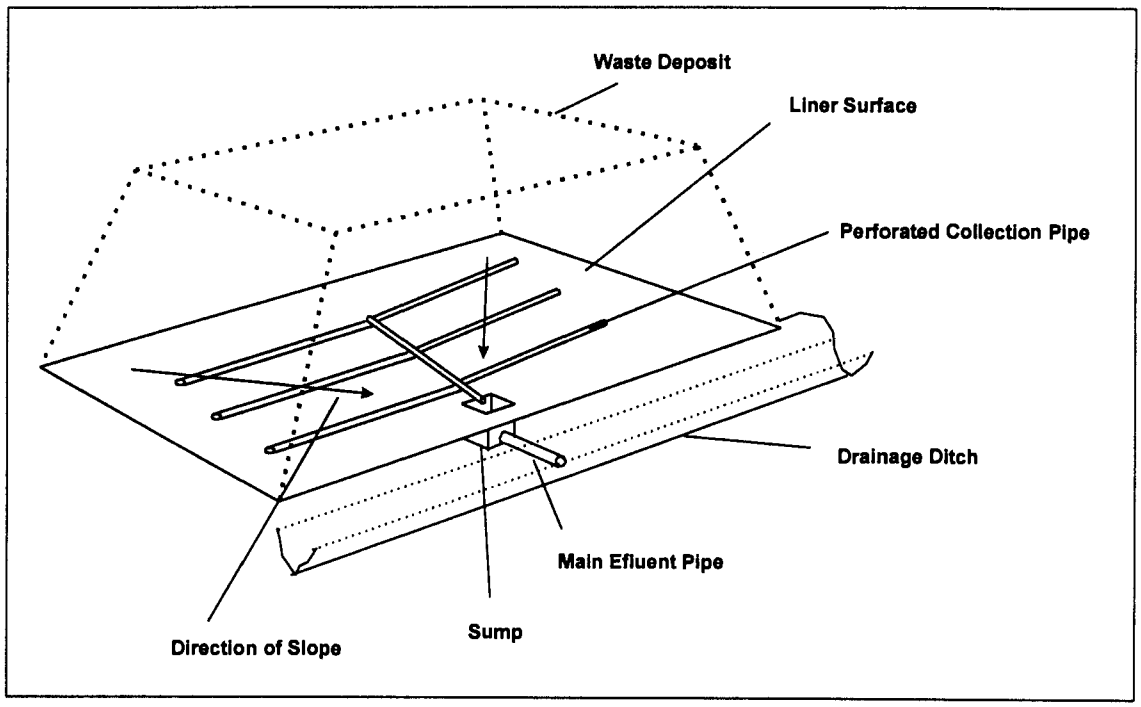

Figure 3-8: Layout of a leachate collection system at the base of a waste deposit

Evaporation ponds, essentially lined and sealed basins, allow contaminated water to evaporate, resulting in the dissolved solids to precipitate and collect at the bottom of the pond. From time to time the precipitate is scraped up and disposed of as hazardous waste. Here care needs to be taken that the precipitate is carefully disposed of, for example by encapsulation or cement based solidification (see Section 3.2.10), in order to avoid re-dissolution through the leachate inside yet another waste deposit. It is not clear to what extent such considerations are enforced in practice.

3.2.5 Monitoring Wells

Even in the most carefully designed and managed waste deposit there is always a certain risk that liner and leachate collection systems might fail or develop leaks. Only through on-going monitoring of the subsoil and aquifers in the vicinity of a waste deposit such leaks can be detected at an early stage and remedial action be taken before the contamination can spread out of control. This is achieved through regular sample taking from monitoring wells.

Appropriate placement and depths of monitoring wells requires a good knowledge of the soil strata and position and direction of groundwater flow underneath and in the vicinity of a waste deposit. A potential leachate plume might escape detection if wells are spaced too far apart, so that it can move between them or if wells are too shallow or too deep, so that the plume can move beneath or above (see Figure 3-9). Using a triple depth well system as depicted in Figure 3-10 has been recommended to avoid such problems, but increased installation, sampling and analytical costs may make this option prohibitive (Kent and Hemingway, 1993).

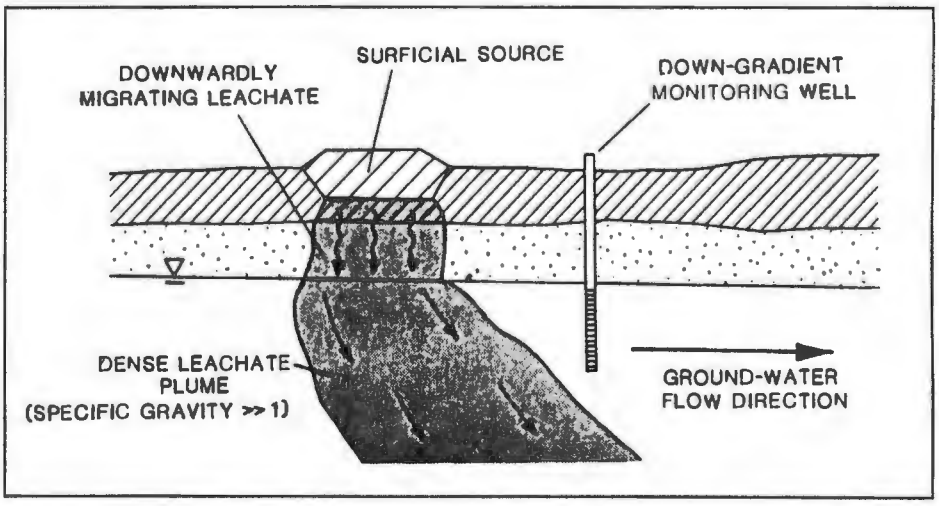

Figure 3-9: Scenario where a high density pollution plume migrates to the bottom of an aquifer escaping detection in the monitoring well, which does not protrude far enough into the layer (taken from Kent and Hemingway, 1993).

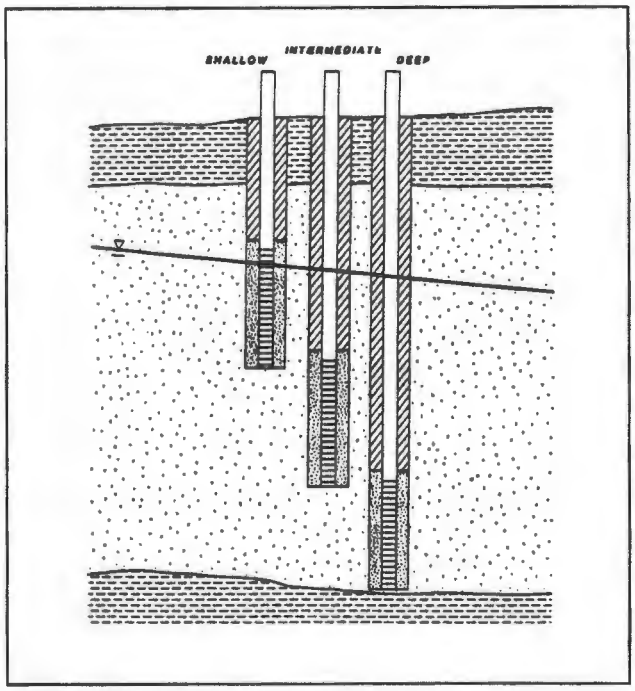

Figure 3-10:: Construction of an idealised monitoring well cluster (taken from Kent and Hemingway, 1993).

A thorough geophysical and hydrological assessment of a potential waste deposit site before construction commences, can contribute immensely to strategic placement of monitoring wells by minimising their number and maximizing the chances of early leak detection. (Kent and Mann, 1993).

3.2.6 Rock & Slag Deposits

Mining waste rock consists mainly of unmineralised rock resulting from mine propagation and overburden as well as rock containing low mineral grade ore not warranting exploitation. Depending on the geological nature of the mining operation these can vary greatly in composition, but are mostly competent, hard, durable rock consisting of particle sizes from 2m down to 1 μm, depending on the respective mining practice they originate from.

Smelter slags result from pyrometellurgical mineral processes and are mainly of a silicatious nature. Depending on fluxing agents used in the process they can be relative soft and brittle or extremely hard and glassified. Particles sizes ranges vary from process to process, but are largely similar to those of waste rock. Quench cooled slags are generally fairly uniform in size from granular to pebbly.

Disposal of these waste materials takes place by tipping from trucks or stacking using conveyor belts. The material is dumped over the face of a lift, which may be the full height of the dump (i.e. 100 m or more) or 15 to 30 m lifts with intermediate benches. The dumped materials cascades down the face, resulting in a segregation of particles with larger boulders rolling to the bottom while finer particles remain near the top. As a result, the bottom of the disposal facility consists frequently of free draining rock, while the upper elevations are less permeable. The top surface of the dumps are usually flat, gently sloping away from the face to ensure truck safety and avoid storm water run-off cascading over the face (van Zyl, 1993).

Major concerns in the construction of such deposits are both operational as well as long-term stability. Weathering of waste rock after deposition can result in loss of rock shear strength which can result in landslides at the face.

Since rock material is chemically relatively inert to draining rainwater, it is normally consigned to an unlined landfill. However, the phenomenon of acid rock drainage, the production of sulphuric acid from sulphide minerals through atmospheric oxidation, can provide an environment aggressive enough to leach hazardous constituents from rock deposits (Steffen, Robertson and Kirsten, 1989 as quoted in van Zyl, 1993). In an unlined landfill leachates such generated will migrate into the subsoil relatively unhindered.

Slag materials may contain toxic metals which can be solubilised under certain circumstances, particularly due to their often highly alkaline nature, but available information on slag disposal practice is scarce. Slags originating from the processing of

sulphide minerals may contain residual sulphur, which may give rise to acid mine drainage and consequently secondary mobilisation of heavy metal species.

3.2.7 Tailings Impoundments

Tailings are the products remaining after the extraction of metals from ore by physical (gravity separation, flotation) and chemical (leaching) methods. In these processes the ore is finely ground and slurried in water resulting in grain size often as much as 80% in the <75 μm fraction. Tailings are normally deposited as a slurry in specially designed impoundments. Design and disposal practice in such impoundments is well described in the literature (see van Zyl, 1993).

A tailings impoundment is formed typically by an embankment or dike constructed of suitable fill material or often of the tailings themselves. In this case the slurry is cycloned to obtain a coarser fraction for building the embankment whereas the fine fraction is deposited in the centre. The embankment can be a single wall closing a valley, three-walled on the side of a valley or on sloping ground, or a ring if the impoundment is constructed on flat ground (Robertson and van Zyl, 1980). Tailings disposal is into a pond at the centre of the impoundment, resulting in a gradually rising fill of consolidated material and the centre pond of standing, slowly draining and evaporating water (figure 3-11).

There are a number of different disposal methods mainly focusing on the way the slurry is fed to the impoundment (van Zyl, 1993):

- In "sub-aqueous deposition" the slurry is discharged under water, allowing the solids to settle as a soft bottom sediment and the liquid drains through it or evaporates.

- In "managed deposition" (also referred to as "subaerial deposition") the slurry is discharged to the pond above the water level from several points of discharge around the perimeter, resulting in the solids settling in deltas towards the centre of the pond. The clear supernatant liquid is either pumped for re-use or left to evaporate. The points of discharge are frequently moved to allow cyclic drying of the deposited solids.

- In "cycloned deposition" the coarser tailings are separated and used for building the embankment. The fine slurry is pumped into the pond by managed deposition (see above). Careful management is required in this process as the fine solid fraction does not drain and consolidate very easily.

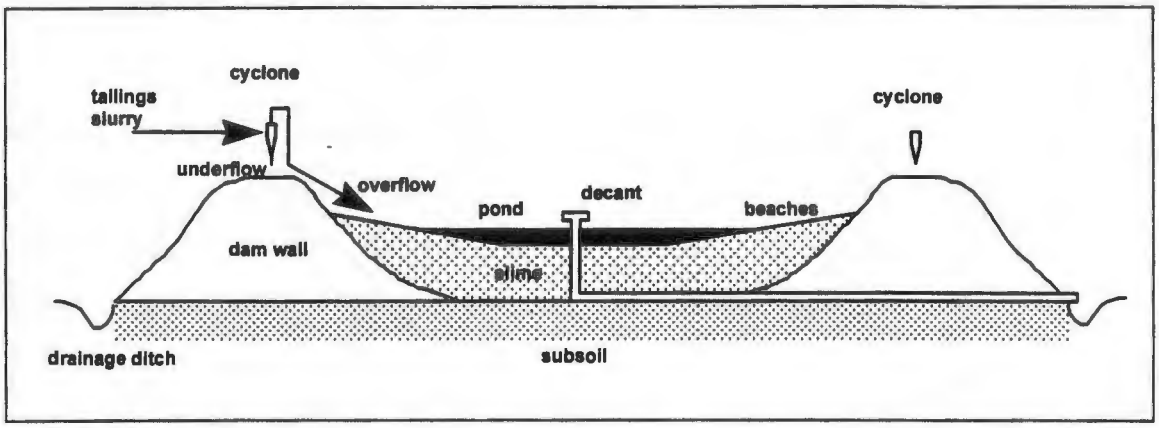

Figure 3-11: Cross-sectional view of a typical tailings impoundment commonly used in the South African gold mining industry.

Consolidation within a tailings impoundment is an on-going process. Tailings in lower levels are generally more consolidated than those more recently deposited due to the weight of the overlying layers. Depending on the method of deposition consolidation at the surface proceeds more or less rapidly. Using managed deposition surface settlement and drainage is more rapid and the surface becomes accessible for closure activities more rapidly and without the need for special construction measures.

Carefully managed deposition can result in highly consolidated solids with low hydraulic conductivities, effectively becoming liners in themselves. Drainage of pond water through

the deposit is thus very slow and most pond water is evaporated or can be removed through pumping. Nonetheless, a suitable liner and leachate collection system is highly recommended for tailings impoundments, since liquid seepage, however much restricted, still takes place.

Leachate from tailings impoundments is defined largely by the toxicity of the slurry liquid itself. Much concern, for example, was given to the cyanide contents of gold tailings, although subsequent research showed that cyanide is fairly quickly degraded by natural processes and may therefore at best be considered a "transient pollutant" (van Zyl 1993). Other, slow chemical processes, including acid rock drainage and its secondary leach effects (see Section 3.2.6), may well occur and can infringe on the long-term environmental stability of tailings impoundments. However, a more comprehensive understanding of the sometimes complex leachate generation processes is still lacking and should prompt further research. Some of this falls within the scope of the work presented herein.

3.2.8 Mixed Deposits

While the main types of wastes arising from a minerals processing operation are usually deposited in carefully engineered individual deposits, there are normally smaller quantities of other waste arisings that do not justify disposal in their own individual deposits. Such wastes include filter dusts, rinsing sludges, solid residues from waste water treatment operations, clean-up from spillages, general building rubble and scrap etc. Depending on their nature, such wastes may either be co-deposited within the main waste deposit or are consigned to mixed purpose deposit heaps.

Waste water treatment frequently involves the precipitation of dissolved solids and subsequent dewatering of the solids. The filter cake, normally dried to or just below of saturation, is then tipped by trucks or conveyors, resulting in piles with no pools of free-

standing solution. Depending on the nature and residual moisture of the cake residual drainage and consolidation of the pile will occur. If the cake material is very fine, slumping may occur, requiring some form of containment to avoid uncontrolled spreading.

Filter dusts arise from gas cleaning equipment, particularly of flue gases generated in pyrometallurgical processes. They are often extremely fine in size (smaller than 1 μm) and become easily airborne in open disposal. Thus, although they normally arise dry, they are often doused with water upon disposal to reduce the risk of rapid wind erosion. Due to the specific conditions that lead to dust generation within the process (as will be discussed in more detail in Section 3.3.1 for the case of chromium dusts), heavy metals tend to concentrate in these flue dusts, making them often highly toxic and hazardous.

Mixed or co-deposition of potentially hazardous small volume wastes poses a particular risk as careful design of such deposits is often neglected due to the small volumes involved. Contaminant release from hazardous co-deposited wastes may easily foul the leachate from an otherwise non-hazardous waste deposit, requiring large volume leachate treatment that could have easily been reduced to significantly smaller volumes, had the "culprit" been kept isolated. In the absence of careful waste management practice, it may be exactly these small volume wastes that can cause the greatest environmental damage.

Mixing of wastes of vastly different nature is therefore to be avoided where possible. In the case of contamination the material that causes it can then be easily isolated without the need for extensive remedial action on large volumes of waste.

3.2.9 Ash Deposits

Although the burning of coal in coal-fired power stations is not normally considered a minerals processing operation, the mineralogical and mainly inorganic nature of ash is

similar to that of other minerals processing wastes and so are its disposal to landfill deposits and the associated problems of potential leachate generation. It is therefore useful to include aspects of coal ash disposal in this review.

The high combustion temperatures in coal furnaces (in excess of 1600 °C) lead to decomposition, fusion and agglomeration of the mineral matter contained in the coal. Many trace metals tend to be volatilised and sulphides are converted to SO_2. While agglomerates tend to fall to the bottom of the combustion chamber as large clinkers (bottom ash), fine silicates and iron oxides are carried with the flue (flyash). Onto these many of the volatilised constituents tend to condense in cooler sections of the furnace. Thus flyash in particular contains significant concentrations of environmentally hazardous trace metals (Jones, 1995).

A majority of coal fired power stations operate wet ash disposal systems, i.e. the collected ash is slurried with water and pumped for disposal in tailings impoundments. Transport water is either discarded or recycled within the ash transport cycle. Slurrying of ash, particularly fly-ash can lead to the leaching of trace metal concentration already upon transport and further due to seepage through the deposit.

Therefore "dry" ash disposal, i.e. transport to disposal site by truck or conveyor and tipping onto the heap, is becoming increasingly more popular. This method not only avoids the production of large volumes of contaminated leachate, but the self-cementing properties of many flyashes can result in a waste mass of greatly reduced permeability to seeping rainwater (Jones, 1995). In fact many flyashes can be used for the solidification of other hazardous solid wastes (see section 3.2.10).

3.2.10 Waste Stabilisation/Solidification

Waste pre-treatment in through stabilisation/solidification (S/S) methods prior to disposal has gained a lot of attention over the last 15 to 20 years as a way of reducing the potential hazardousness of a waste. Since disposal in specially engineered hazardous landfills is costly, such methods can offer economic alternatives without compromising the environmental stability of the waste after placement.

Although usually referred to together, the terms "stabilisation" and "solidification" actually describe two different processes:

"Stabilisation" describes "*processes which limit the solubility of or detoxify the contaminate; the physical characteristic [of the waste] may or may not be improved or changed*" (Wiles, 1988). Toxic components are transformed to new, non-toxic compounds by chemical transformation. An alternative, more appropriate term frequently used is "chemical fixation", defined as the "*chemical technology used to detoxify, immobilise insolubilise or otherwise render a waste component less hazardous, or less capable of introducing itself into the environment* " (Conner, 1986).

"Solidification" is defined as "*a process in which materials are added to the waste to produce a solid*", usually "*as a monolithic block with high structural integrity*" (Wiles, 1988). This may or may not involve chemical bonding between the contaminant and the additive. "Encapsulation", as a special form of solidification, involves the complete coating or enclosure of a toxic particle or waste agglomerate with or within a new, non-hazardous substance.

Solidification methods do not in themselves modify the hazardousness of the waste material, but set up barriers between particle and environment limiting or restricting the transport of contaminants (Conner, 1986).

The most commonly applied S/S method is solidification based on the addition of Portland cement or pozzolanic substances, such as flyash (Arniella and Blythe, 1990; Cohen, 1997). The cementation reaction effectively incorporates waste particles into a solid matrix with minimal pore size and a much reduced surface area exposed to leaching. Residual moisture from solidified sludges or filter cakes is effectively consumed in the cementation reaction and thus prevented from leaching and transporting contaminants. The structural strength and permeability of the solidified waste depends on cement to waste ratios (usually 1:5 to 1:1), curing time and other factors, which must be carefully optimised for each type of waste.

Certain types of contaminants, such as borates, bichromates and many hydrocarbons can adversely interfere with the cementation reactions, resulting in low structural strength of the final product. On the other the high alkalinity of the solidified product can effectively immobilise many heavy metal species as hydroxides, that could otherwise be mobilised through leaching (Wiles, 1988)

The solidified waste is placed in a waste deposit either through casting into pads before setting occurs or through dumping of large size agglomerates in similar fashion as in rock dumps (see Section 3.2.6). In some cases the solidified material can also be used as construction material for road building or similar purposes.

Cement based solidification has been successfully applied particularly with inorganic wastes, although some organics can be solidified as well. Disadvantages of this method are the increase in mass and volume of waste through the cement addition and the additional cost of processing and additives used. Although containment of hazardous wastes in solidified matrices has proven successful in the period since their introduction (15 to 20 years), long-term degradation of the cement matrix may result in re-exposure of the contained waste. Therefore some care needs to be taken with respect to the long-term fate of cemented wastes.

Cement is also used in the encapsulation of waste agglomerates, such as drums or other containers, containing highly toxic wastes that do not lend themselves to direct solidification (particularly organic liquids). The drums are placed in a larger container constructed of cement slabs, the void is filled with casted cement and a lid is placed on top (Figure 3-12) . The monolith blocks are then buried or places in a monitored site.

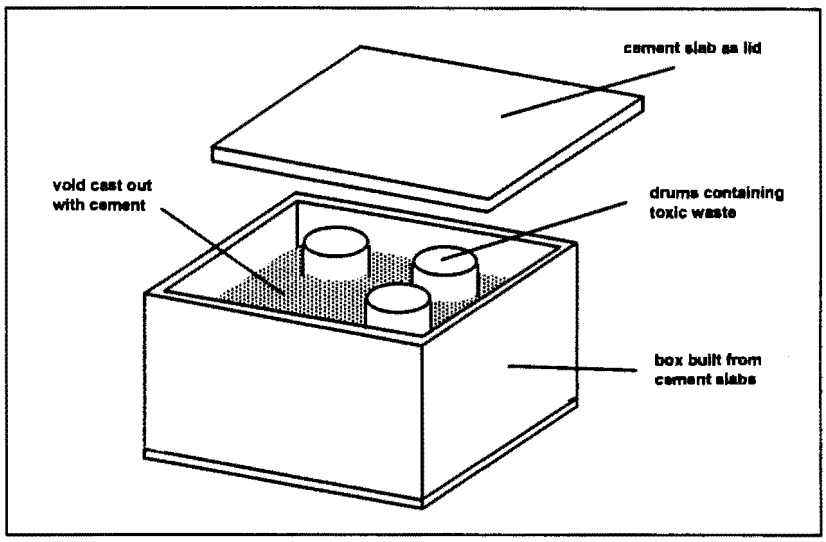

Figure 3-12: Cement encapsulation of toxic waste

Other solidification methods include the use of thermoplastics (bitumen, waxes, epoxies, etc.) as the solidifying agent. Although containment in these is often better than in cement, since a complete seal may be achieved, operating and material costs of these methods is often prohibitive. Hence these methods are restricted to use with highly toxic or radioactive, small volume wastes and as additional sealing of encapsulated waste monoliths.

Glassification of waste (also referred to as vitrification) is achieved by melting waste mixed with borosilicate glass in a furnace or in situ by melting the soil surrounding waste with the help of an electric arc (Arniella and Blythe, 1990). In either case an extremely stable and durable glass matrix results, effectively encapsulating waste particles. However, very high energy costs and problems with volatile contaminants escaping during the process have restricted this method mainly to use with nuclear wastes.

3.2.11 Site Closure

The end of the disposal operation at a particular site may come when the deposit has reached its design capacity and extension is not feasible or when the waste generation operation has come to an end. Historically this has often resulted in abandonment of the site with no further closure activities conducted. Depending on the type of deposit and envisaged future use, appropriate closure measures may include

- removal of all equipment from and fencing of the site
- draining of all surface ponds
- consolidation (compacting) of the deposit surface layer
- capping of deposit surface with liners or compacted soil
- placement of a soil layer and re-vegetation
- installation of suitable surface run-off systems
- continued collection and treatment of leachate
- continued sampling from monitoring wells

The infiltration of rain and drainage water into the deposit must be minimised in order to continuously keep the risk of contaminant mobilization as low as possible. This prompts the removal of all standing surface waters and "sealing" of the surface to maximise run-off of incipient rain water. In many cases lining of the surface may not be necessary, if construction of the deposit surface and placement of a soil surface are carefully engineered.

Re-vegetation of the deposit surface and site walls is recommended to avoid soil erosion by run-off waters and also to reduce the visual impact of a site. Since mineral waste materials usually offer little in terms of plant nutrients, soil layers placed should be sufficiently thick and plant species selected for re-vegetation sufficiently hardy to withstand the often adverse conditions the waste may impart on soil placed over it. Soil fixation on the often steep slopes of deposit side walls may require careful strategies to

avoid the risk of rapid erosion by run-off water and wind, particularly during the initial phases of re-vegetation.

Particularly in the initial period of time after closure seepage of residual drainage waters within the deposit will continue to generate leachate collecting in the drainage system, if one is in place. This may require further treatment beyond the closure of a site until such time that leachate flows become insignificant or sufficiently uncontaminated to allow direct discarding.

But even beyond that stage, there will always be a small risk of further, slow leachate generation within the waste deposit long beyond closure of a waste site. Therefore long-term monitoring of the leachates emanating from waste deposits is highly recommended. Furthermore, there may be a gradual release of leachate into the sub-strata of unlined deposits or lined deposit in which the liner has developed leaks. Long-term monitoring of groundwater in the vicinity through monitoring wells (see section 3.2.5) should therefore also continue for a long time after site closure. In case of a contamination, remedial action can be initiated before too much environmental damage is done.

3.3 Chromium Containing Wastes: Types, Treatment and Pollution

Having clarified principles of solid waste disposal practice with regard to the mineral processing industry, the focus is now turned on origin, characteristics and treatment (before and after disposal) of such wastes. Chromium containing wastes, particularly those arising from the ferro-alloy industry, are in many ways characteristic of solid waste types arising in the minerals processing industry as a whole. For this reason and the fact that experimental work in this study was conducted with such materials, the following discussion is mainly focused on this type of waste.

Essentially all industrial processes that produce or utilise chromium products (see Section 2.1.1) generate one or more types of chromium containing wastes, the majority of which are direct solid wastes or solids obtained from treatment processes of waste waters. Most of this solid waste is consigned to landfill deposition, historically without any of the precautionary measures indicated in Section 3.2. This has resulted in some cases of catastrophic pollution from chromium wastes requiring lengthy and costly remedial procedures, some of which are reported here.

The following sections give a survey of the major types and origin of chromium containing wastes, methods of chromium removal from waste waters, certain pre-disposal and in-deposit treatment technologies and recycle processes where these exist. Some case studies of catastrophic pollution, specifically from chromium containing wastes are reviewed and some commonly used remedial strategies are discussed.

3.3.1 Waste Types and Origin

Ferro-alloy slags

The pyrometallurgical processes beneficiating chromite ore to ferro-chrome and further to chrome steels essentially consist of a number of furnace stages. Chromite ore is reduced with a carbonaceous reductant in a submerged arc furnace to produce ferro-chromium (an iron-chromium carbide) of various compositions. In the stainless steel process ferro-chromium is melted together with other iron sources in an electric arc furnace (EAF) to yield a stainless steel product. This is usually further refined in further stages, such an argon-oxygen decarburizer (AOD) and a ladle, before being cast and rolled. Each furnace stage produces a slag phase consisting mainly of oxides of Ca, Mg, Al and Si but also smaller amounts of Cr and Fe as well as traces of other minerals. The slag is poured off and, after solidifying, usually disposed of as waste or used as construction material.

Mineralogical characterisation of slags varies from process to process and also with the charge materials used and is generally extremely complex. Chromium is mostly present as unaltered chromite or chromic oxides within a common matrix of Ca, Mg and Si oxides. Depending on the concentrations of these, the chromium is firmly incorporated in stable spinel type crystal structures or present as a separate oxide phase (Kilau and Shah, 1984). Calcium oxide is often present as a separate phase.

Oosthuyzen and Viljoen (1982) distinguish four distinct phases in their description of Transvaal (north eastern region of South Africa, now known as Mpumalanga) ferro-chromium slags:

- an amorphous, silica-rich glass phase (45 to 75 %)
- a spinel phase, containing mainly Al and Mg (10 to 25 %)
- partly reduced chromite grains, varying from almost unaltered chromite to Cr rich-iron poor varieties (15 to 30%). These are often referred to as partially altered chromites (PACs)
- metallic phases containing various amounts of chromium, iron and carbon (0.5 to 5%).

Ferro-alloy dusts

In each furnace stage in the ferro-chrome and stainless steel processes described above, flue dusts are generated through three possible mechanisms (Dreisinger et al., 1990; von Blottnitz, 1995):

- direct dusting during the melt-phase
- atomisation of molten metals in consequence of gas bubbling
- evaporation of metals (Zn, Pb, Cd etc.) which are volatile at the process operating temperature (>1500 °C). These later re-condense as flue gas cools.

These dusts are usually separated from the emission gases in electrostatic precipitators or bag-filters before the gas is released to the atmosphere. The collected dusts are disposed as waste to landfill where further treatment and recycling is not practised typically (see Section 3.3.4). Electric arc furnace dusts generated annually amount to some 500 000 tons in the United States alone (Hagni et al., 1991).

Steelmaking dusts can be characterised broadly as extremely fine spherical particles, usually less then 1 μm in diameter, frequently agglomerated into "fluffy" aggregates or "clumps" of 20 to 50 μm (Hagni et al., 1991; van Craen et al., 1983; Cox et al., 1985). Larger, angular particles up to 100 μm in size can also be found. While the smooth spherical particles are assumed to originate from atomised and condensed metals, the angular particles can be mostly attributed to dusting. The overall chemical composition of dusts is extremely complex and can vary widely, but consists mainly of Fe, Cr, Ca and Zn, with Pb, Cd and Ni present in smaller concentrations. The metals are usually present in the form of complex oxides (Hagni et al., 1991). Surface enrichment of certain metals as consequence of condensed volatiles, such as Zn, Pb and Cd, is widely reported (Lee et al., 1975; van Craen et al., 1983; Cox et al., 1985). Surface oxidation of Cr to Cr(VI) due to contact of the hot dust with oxygen has also been reported. Kornelius and Boegman (1994) showed that many of the metals are easily leachable in an aqueous environment, rendering dusts from both ferro-chrome and stainless steel processes hazardous.

Chromate process residues

The production of chromium chemicals from chromite involves roasting the finely ground ore with soda ash (sodium carbonate) in oil-fired rotary kilns at 1100 to 1200 °C (Dawson and Edwards, 1984):

$$(Mg,Fe)O{\cdot}(Cr,Al,Fe)_2O_3 + Na_2CO_3 + O_2 \rightarrow Na_2CrO_4 + Fe_2O_3 + MgO{\cdot}Al_2O_3 \quad \text{etc.}$$

The sodium chromate is recovered subsequently from the calcine by leaching in hot water, making use of its high solubility. The other constituents are largely insoluble and, after some recycling for increased chromate recovery, are disposed as waste.

The calcining stage is only about 85% efficient, leaving considerable amounts of chromium in the residue, most of it still unaltered in the chromite spinel state, but some also in other chromic oxides forms. Due to inefficiencies in the leach stage there may also be residual amounts of chromates. It is particularly these chromates which can be easily mobilised after disposal, sometimes with catastrophic consequences (Section 3.3.5). There is little information available about the generation and treatment of potential flue dusts from the calcining stage.

Process waste waters

There are numerous processes which employ or result in aqueous solutions of chromium chemicals for specific purposes, such as metal finishing, leather tanning and corrosion control. Spent process and rinse waters from such processes contain high concentrations of dissolved chromium, both in the trivalent and hexavalent forms. Historically such waste waters have been stored in evaporation ponds but are now mostly treated for chromium removal before being discharged or recycled as process water. Numerous treatment and removal processes are in place (Section 3.3.2), but they almost always result in a solid chromium-containing residue, which is consigned to landfill disposal.

Scrap metal

Most chromium used in metals ends up as scrap after the useful life span of the product and is consequently consigned to some form of landfill deposit. This is particularly true for metal values discarded within domestic waste. Although considerable portions of scrap metal is recycled as raw material in the metals industry, chromium, due to its ready availability as raw material, is not re-used on a large scale. In the United States only about

15% of chromium consumed were recycled from scrap metal in the 1970's (Nriagu, 1988), although this figure is likely to be higher today. Consequently most chromium produced in the metals industry is likely to end up ultimately as some form of solid waste.

Miscellaneous

Small amounts of chromium can probably be found in most other types of waste owing to its status as a trace metal (see Section 2.1). Of particular concern is fly ash from coal fired power stations which are mostly consigned to landfill (see Section 3.2.9). Although Cr concentration in these are low (for example, 20-60 ppm in some ashes from NSW, Australia (Jones, 1995)), the large tonnages of ash generated world-wide do give reason for concern.

Materials that were treated with or derived from chromium chemicals, such as wood treated with chromate based preservatives and many paints, pigments and dyes, will ultimately end up as disposed solid wastes. Again, the chromium concentrations in these materials are generally low, resulting in a high degree of dispersion, making effective recovery impossible.

Chromite is extensively used in the manufacture of refractory materials. Where these exceed their useful life-span, they become waste. However, since these materials are characterised by their extreme resistance to heat and chemical attack there is little concern with respect to their long-term environmental stability as wastes.

3.3.2 Chromium removal from waste waters

With rising environmental concern and strict legislation it is now common practice to remove heavy metals from industrial process and waste waters where they occur in concentrations exceeding certain limits. Particularly with respect to Cr(VI) great concern

is given to maintain concentrations in discharge water below the widely accepted drinking water standard of 0.05 mg/l. Several review papers (for example Beszedits, 1988; Raghu and Hsieh, 1989) indicate that there is a vast multitude of processes available for the removal of dissolved chromium species from waste waters. These can be broadly categorised as follows:

- reduction/precipitation: Cr(VI) is reduced through the introduction of a suitable reductant. Most common are bubbling with SO_2 gas, solutions of sodium bisulphite or ferrous iron (Fe^{2+}) obtained by introducing $FeSO_4$ or generating Fe^{2+} from a sacrificial iron electrode (see also Section 2.1.5). The reduced Cr(III) is precipitated by raising the solution pH to about 9 by addition of lime, caustic or limestone. All or almost all chromium reports to the precipitate, which can be filtered off and consigned to disposal or further treatment. Reduction with sulphide, introduced as sodium sulphide is also common. A combined reduction/precipitation effect can be achieved through the introduction of finely ground ferrous sulphide (FeS, Zouboulis et al., 1995). In waste waters free of sulphates, Cr(VI) can be directly precipitated with barium (Hartford, 1979).

- adsorption/complexation: The tendency of Cr(III), but also Cr(VI), to adsorb to mineral oxide surfaces or complex with certain organic groups, is exploited in these methods (see also Section 2.1.3). Good results have been achieved through the use of activated carbons and peat. The tendency of soils to adsorb significant quantities of metal ions, both onto soil minerals as well as soil organics is sometimes used in the "land-treatment" of waste waters (Fey, 1995), whereby controlled dispersion of dilute waste waters over soil results in the complete attenuation of the dissolved metal species.

- ion-exchange: organic resins with surface groups which can capture metal ions, both cations and anions, through ion exchange are commonly used in waste water treatment. The resins can be separated after loading and regenerated by removing the exchanged metals in a stripping operation, from where they can be further recovered. This way

ion-exchange acts as a concentration method. Metal specific resins have also been developed. Ion exchange can also be achieved with inexpensive starch xanthates, which can be disposed after loading.

- selective recovery methods: Solvent extraction methods and metal-specific ion exchange resins can be used to selectively recover chromium from a dilute waste water solution for recycle. Such methods are usually associated with high costs and are only feasible where considerable recoveries can be achieved or metal values are high.

- biological treatment: There are several biochemical methods which are feasible for the direct removal of Cr(VI). Sag and Kutsal (1989) report on the production of extracellular polymers using *Zoogloea ramigera*. Another method involves the removal and concentration of heavy metals including Cr(VI) using sulphate reducing bacteria to indirectly reduce the metals to insoluble metal-sulphide complexes (Apel et al (1990)), although poor results were achieved for Cr(VI) removal. Apel and Turick (1991) investigated the direct metabolic reduction of Cr(VI) using three different strains of *Pseudomonas* bacteria, with the isolate *Pseudomonas aeruginosa* PAO1 showing best results. Water hyacinths, a general nuisance plant, have been reported to rapidly and effectively extract heavy metal ions from water though their extensive root system (Beszedits, 1988).

- concentration methods: These are not treatment methods in themselves, but are used to concentrate dilute solutions of waste waters for further treatment as outlined above. Concentration can be achieved by reverse osmosis, electro-dialysis, evaporation, freeze separation and ion flotation.

3.3.3 Pre-disposal and In-deposit Treatment Practices

Once in a solid form, chromium-containing wastes are usually consigned to landfill where further recovery or recycling options are not considered economically attractive. To enhance the environmental stability of such wastes, a number of treatment practices are available, which are applied to the solid either prior to disposal or as an after-treatment on materials already deposited.

Cementation of wastes as a stabilisation method is frequently practised (Cohen, 1997; see Section 3.2.10). Particularly fine solids, such as emission dusts and dewatered sludges from treatment processes are incorporated effectively into a cement matrix through which migration of leach waters is greatly reduced. Furthermore certain metal cations tend to adsorb to the alumina silicates within the cement and are thus effectively attenuated. This method is also directly applicable to waste waters (i.e. without prior precipitation), which are used in the cement hydration reaction and effectively contains the dissolved metal ions.

Thermal alteration of wastes is aimed at containing chromium in spinel type crystal structures through careful adjustment of the Ca:Si ratio to about 2.0, melting and re-solidifying. A stable spinel, Uvarovite ($Ca_3Cr_2(SiO_4)_3$), is formed as well as calcium chromite $CaCr_2O_4$ (Kilau and Shah, 1984), this way reducing the possibility of atmospheric chromium oxidation in slag materials (see Section 2.3). Hattori et al. (1978) describe a similar method to stabilise treatment sludges obtained from a lime precipitation process by heating with silica. Beszedits (1988) reports on proprietary processes from Japan which obtain a ferrite spinel crystal from a chromium hydroxide sludge treated with ferrous iron through aerial oxidation. Vitrification (see Section 3.2.10) is the process of solidifying a waste material by encapsulation in a glass matrix. Glass forming material (such as silica) is mixed with the waste, melted and left to re-solidify as glass. The economic feasibility of thermal treatment processes is dubious due to the large energy

costs involved in the reheating/melting process, but the resulting chemical compounds are usually extremely stable and inert.

Solidification/stabilisation methods, including cementation and vitrification, can also be applied as an in-deposit treatment method, in which waste already deposited is locally mixed with solidifying agent, or into which the agent is injected. Cr(VI) containing wastes can also be co-deposited with a slow release reducing agent ensuring continued reduction should Cr(VI) become mobilised (Raghu and Hsieh, 1989).

Deposits equipped with an appropriately monitored double liner system may not require any specific pre-treatment of the waste as mobilised constituents can be collected with the leachate, which can in turn be treated like waste waters. In some instances the leaching of metals from waste deposits can actually be encouraged, where their recovery from collected leachate is feasible. Raghu and Hsieh (1989) report of an experimental procedure developed for chromium extraction from waste dumps. The waste site is trickled with an extraction agent, such as NaOCl or EDTA. Extracted chromium is then recovered from the extractant which is recycled.

3.3.4 Recycle Technologies

Ideally all chromium contained in waste materials that can potentially become mobilised from a disposal site, i.e. that is not in an ultimately environmentally stable form (such as a spinel type crystal structures), should be recycled to avoid burdening of natural environments (Section 3.1). Unfortunately, due to the ready availability of cheap chromium minerals, chrome waste recovery has historically enjoyed few economic incentives and recycling options are only practised when they become economically more advantageous over the disposal of hazardous wastes in special containments. The only operation that results in significant quantities of direct chromium metal recovery is the recycling of stainless steel scrap.

Solvent extraction and selective ion exchange resin processes can be used for the selective scavenging of chromium from waste water streams (Beszedits, 1988). The removed chromium is concentrated in the stripping solution, from where it can be recovered by appropriate processes. Such processes are usually only economical where relatively high concentrations of chromium are present in the waste stream, due to the high cost of appropriate extractants or resins, and these processes are therefore not widely practised.

The recovery of metal values from steel-making dusts is a particularly attractive route, since metal concentrations are usually high and disposal of the dust is often costly due to the high environmental toxicity associated with them. Technologies employed (see review by Kaltenhauser, 1987) involve pelletising or briquetting the waste and re-melting in a secondary furnace process (often using plasma arc technology). Volatile metals are allowed to evaporate and are subsequently recovered from the off-gases in scrubbing processes. The melt is reduced and separated in a mixed metal phase, mainly composed of Fe, Cr, Ni and Mo, and a non-hazardous slag phase which can be used as building material. The metal alloy is poured in ingots which can be re-used as feed material for stainless steel making processes. Pyrometallurgical processes have also been successfully employed in recovering metal values from treatment sludges (Hanewald et al., 1991).

Hydrometallurgical processes for the selective leaching of Pb and Zn from dusts and their recovery as a saleable product are also employed (Kaltenhauser, 1987). The solid residue, reduced in undesirable Pb and Zn, can in principle be pelletised and returned to the steel furnace (von Blottnitz, 1994). The use of spent steel plant pickling acid in the leach process is a good example for treating waste with waste.

A process recovering partially altered chromites (PAC, see Section 3.3.1) from ferro-chrome slags has been commissioned in South Africa (Coetzer *et al.*, 1994). The process involves milling the slag and a jigging plant for recovery of the PACs and metals which are pelletised and returned to the ferro-chromium process. The residue is essentially a

benign mixture of glassy and spinel type Al, Si and Ca oxides, which are consigned to landfill.

Baturay et al. (1991) describe a patented method by which chromium containing waste materials are milled and dried, mixed with sodium carbonate and ammonium nitrate and roasted in a reactor with a stoichiometric supply of oxygen in air at about 1000 °C. The product is cooled, re-sized and leached with water counter-currently in a four stage extraction process. All chromium is said to be recovered in the leach as Cr(VI), whereas the residual is supposed to be free of chromium. Since the process is essentially the same as the standard chromate process which has a limited recovery (see Section 3.3.1), the economic and environmental feasibility of this process is questionable.

3.3.5 Pollution Case Studies

The concept of environmental "time bombs" as proposed by Stigliani (1993) is a useful way of focusing attention on situations where hazardous chemicals may suddenly be released into the environment. This is exemplified in the rapid acidification of soils and lakes after their natural buffering capacity is exhausted, sometimes many years after the industrial operation causing the acidification has ceased. Similarly, heavy metals can be released and rapidly migrate after the natural attenuation capacity of a soil has been depleted. Common to these effects is the fact that a certain disposal practice may appear environmentally "safe" for a significant period of time before suddenly natural resistance to pollution breaks down - with potentially disastrous consequences. This concern must also be raised with many disposal practices relating to chromium containing wastes. Where there is a potential of chromium mobilisation, particularly as Cr(VI), there could be a gradual exhaustion of natural retention capacity, even if the effects may only become visible after many years. Some of the following reported case studies of catastrophic chromium pollution help to illustrate this point.

Hudson County, New Jersey, USA

Burke et al. (1991) describe, in detail, phenomena leading to the most severe case of Cr(VI) pollution in the USA to date: From 1905 to 1976 Hudson County was a centre for chromate and bi-chromate chemical manufacturing. Chromite ore was mixed with lime and soda ash and heated to convert insoluble trivalent compounds into the more soluble hexavalent compounds. These were then leached out with water twice before the residue, containing 2 to 7% chromium, was discarded. The residue was sold or given away for use as fill material and was widely used in construction of residential and commercial sites throughout the county. To date 130 chromium-contaminated sites have been identified as a direct result of this practice, most of them in the urban area of Jersey City.

In 1988 the New Jersey state medical examiner listed chromium toxicity as a contributory cause of death in the case of a man who worked for several years at a truck loading facility built upon chromite ore processing waste. Chromium levels as high as 53g/kg have been found in the soils near landfill sites. In a school, chromium was found in the ventilation system and in carpets throughout the building. A yellow chromate deposit was found at numerous basement walls near landfill sites. These effects are all due to the "chromate bloom" phenomenon described in Section 2.1.1. Increased incidences of skin ulcerations and respiratory problems amongst the local population have been reported

This case dramatically describes the effect of uncontrolled and unmonitored chromium disposal in a human environment. The costs of clean-up and containment of the waste have been estimated in the billion dollar range. This excludes any long-term health surveillance, nor does it address the potential need for remediation of residences and workplaces.

Nassau County, New York, USA

Calder (1988) accumulated information on an early case of Cr(VI) pollution in Nassau County, Long Island, New York:

Between 1941 and 1949 untreated wastes from an aircraft metal finishing plant, containing Cr(VI) at concentrations of ca. 40 mg/l, were discharged into disposal ponds near the plant. By 1949 the chromium contaminated groundwater had formed a cigar-shaped plume, whose front had travelled 1200 m from the disposal site and whose width was about 260 m. The maximum concentration of chromium in the groundwater remained at 40 mg/l. The chromium was migrating at approximately the same velocity as the groundwater (0.15-0.5 m/day). A treatment plant was installed in 1949 to remove Cr from the waste ponds. This remained only partially effective as concentrations of Cr(VI) remained as high as 35mg/l in 1962.

Nevertheless, chromium concentrations dropped markedly in the groundwater after installation of the treatment plant. The decrease in progression of the Cr plume after 1949 are not fully understood and are attributed to either increased adsorption of Cr(VI) at lower concentration or retarded reduction to Cr(III). Both explanations are plausible in the light of the theory exposed in Section 2.1, but they also highlight the difficulty of predicting the behaviour of chromium in soils.

Michigan State, USA

Calder (1988) reports groundwater contamination by chromium from a plastic chrome plating facility in south-western Michigan. Chromium concentrations of up to 14 mg/l, most of which was Cr(VI), were encountered in private water wells. A contaminant plume front extended approximately 1000 m from the plant facility. The source of the

contamination was not determined. The plant's process water discharge pond was allowed to contain Cr at concentrations only to a level of 0.05 mg/l.

The only other possible source could have been a sludge stockpile near the pond. This case particularly highlights the fact that Cr(VI) contamination can become excessive even although waste chromium disposal is being monitored.

Others

Burke et al. (1991) refer to a site near Bolton, England, where it was found that run-off from a chromite ore process residue landfill had adversely affected the biota of the river Croal. The residue was phytotoxic and highly alkaline. In Japan a chromate contamination of groundwater and ground surfaces in populated areas was found, where chromite ore processing residue had been used as fill material. Excessive dermatitis was reported during summer months amongst residents of communities who were in contact with the contamination.

Calder (1988) describe discharge of chromium containing wastes from a tailings pond at a plant near Telluride, Colorado, USA into the groundwater system. The groundwater velocity was very high (5m/day) and hence a plume developed at least 520 m in length containing Cr(VI) at concentrations up to 2.7 mg/l (pond concentration 8.8 mg/l) within two years.

3.3.6 Clean-up and Remedial Technologies

Pollution, where it has occurred and been detected, requires swift clean-up action, not only to prevent further spreading but also to rehabilitate the contaminated site. Even if there is no immediate danger for human health, uptake of pollutants into plants and thus into the food chain can result in indirect effects which must be avoid wherever possible.

Generally there is a series of remedial action strategies that can be applied, when a case of heavy metal contamination of soils and aquifers has been detected. Palmer and Wittbrodt (1991) list the following in the event of chromium contamination:

1. No Action Strategy: If a chromium contaminant is not likely to migrate from a site, then it might be decided take no immediate action other than closely monitoring the site with further steps to be taken only if these become necessary. This strategy is rarely applicable since contamination is usually a dynamic process and tends to spread with time, even if the source of contamination is removed. Also, bearing in mind the concept of environmental time bombs (Section 3.3.4), the capacity of a soil to attenuate future contamination may become exhausted. Such a situation should be avoided by timely remedial action.

2. Excavation of contaminated sites and deposition in a hazardous landfill site: This option is an improvement on the no action strategy, but the problem is simply moved from one site to another, on-going liability remains, the cost of landfilling is significantly increased and potential risk of exposure may be increased during the excavation process.

3. Pump and Treat Strategy: Contaminated groundwater is pumped to the surface and treated on site. This has two immediate effects: removal of contaminants from the subsurface for treatment, and maintaining gradient control so as to prevent the contaminants from migrating farther from the site. However, contaminants are only removed from the permeable layers in soils, whereas those from less permeable sites have to migrate into the permeable layers first, before they can be removed. It has been observed that, after termination of any pump and treat action, Cr(VI) contamination re-occurred after a certain period of time i.e. an on-going liability for remediation remained. Consequently pump and treat action may need to be applied for decades before all chromium is removed, the cost of which can become considerable.

4. Solidification/Stabilisation: A soil stabilisation process has two objectives; to put chromium in a chemical form that is leach resistant, and to reduce the permeability of the material, so that groundwater flows around the treated area rather than through it. Several soil solidification/stabilisation technologies have been developed (see also Section 3.2.10). These include cement solidification, silicate based processes, sorbent materials, thermoplastic techniques, surface encapsulation, organic polymer processes and vitrification. Leach resistance is a strong function of long term structural integrity of the solidified matrices. Failures in the past have been attributed to alkali-silica reactions and microbial attack, both of which result in crack formation and propagation.

5. Geochemical Barriers: These serve two purposes, to divert the flow of groundwater from a contaminated site and to retain contaminated leachate within the disposal site. Materials such as crushed limestone, or those promoting the reduction and subsequent precipitation of chromium are placed in the barrier. However, this strategy merely retards the migration of chromium, but never completely prevents it.

This list of remedial strategies clearly highlights that any clean-up action can easily become tedious, costly and long-winded and may have only limited success in containing or removing chromium pollution once it has occurred. The logical conclusion is to avoid pollution by appropriate disposal methods and continued monitoring of disposal sites. Furthermore, wherever recycle is feasible it should be the preferred method of waste management.

3.4 Closure

This chapter has offered a detailed introduction to numerous aspects of solid waste disposal practice with regard to wastes from the minerals processing industry, and more specifically chromium containing wastes, which are in many ways representative of other wastes arising in this industry.

It is important to point out that the concept of waste is an anthropogenic one, defining those materials that are unwanted within the chain of industrial processes. Such materials are returned to the natural environment by waste disposal, where they may begin to interact with the material cycles that form part of natural ecosystems and, in some cases, disturb the sensitive balances of these systems to adverse, even catastrophic effects. In these cases we refer to these interactions as pollution and the specific chemical species that cause the adverse interference as contaminants.

In the case of solid wastes the origin of potential pollution would be the mobilisation of contaminants from solid waste disposal sites by a process termed leachate generation. This results from the percolation of rain and process waters through the deposit matrix, which create an aqueous environment in which chemical reactions at the liquid-solid interface can result in the release of chemical species, which can become contaminating within natural ecosystems. These dissolved species can now migrate with and within the aqueous matrix towards the bottom of the deposit, where they can enter and spread in the underlying soil. It is here, where potential disturbances of natural ecosystems may occur.

Modern solid waste disposal practice is concerned with avoiding this scenario by maintaining some form of geo-technical barrier (liners) between deposit and the underlying soil and collect the leachate before it moves beyond this boundary. Historic deposits, where such practice was not in place, have frequently resulted in severe cases of pollution precisely by the mechanisms described above.

Furthermore, the increased awareness of the pollution potential of solid wastes has lead to a number of treatment options either before or after disposal, which aim at rendering the waste material less prone to the release reactions that lead to the formation of a potentially harmful leachate. And finally, reducing the amount of waste altogether - by optimising the processes that generate them and recycling - will inherently reduce the extent of potential leachate generation and thus adverse interference in natural ecosystems.

However, while much of modern waste disposal practice is concerned with preventing the leachate from solid waste deposits from entering the natural environment and rendering waste materials less prone to leaching, the process of leachate generation as a whole is as yet not fully understood. Lining waste deposits, leachate collection systems and waste treatment are costly operations with little direct economic benefit to their operators. The inability to predict the extent and duration of leachate generation can easily lead to operations that are either over-designed and therefore economically inefficient, or under-designed and thus environmentally inefficient. Moreover, with environmental efficiency increasingly becoming the liability of the operators of a waste generating operation, it can directly influence the economic efficiency of the operation as a whole.

The prediction of leachate generation, by use of an appropriate model, would be greatly beneficial in guiding the design of waste treatment and disposal operations from the outset for optimal economic and environmental performance. The development of such a model and the corresponding waste characterisation technique is the focus of the remainder of this thesis. Chromium containing waste materials from the ferro-alloy industry, which have been discussed to some extent in this chapter, have been used to test the proposed prediction technique.

4

Development of A Model to Simulate Leachate Generation and Transport in Solid Waste Deposits

As was pointed out in the previous chapter, a comprehensive modelling tool, specifically aimed at the prediction of leachate generation within waste deposits, is not available currently. Although there exist a multitude of hydro-transport and geochemical models, some of which were developed specifically for application to waste leach scenarios, these are mostly aimed at describing the transport of leachate *from* a deposit into surrounding soils and aquifers rather than the generation of leachate *within* the deposit. Also, by employing rigorous thermodynamic chemical equilibrium calculation routines, and simulation of two or three-dimensional flow fields, these models are extremely complex, requiring large computing capacities. This way they appear less suited for use in *a priori* waste leachibility assessment methods. For this reason waste assessment methods have to resort to simple laboratory-scale batch and column leach studies. But there appears to be a general lack of understanding how results from such laboratory tests can be correlated meaningfully - through the use of a suitable model - to allow prediction of the likely leach behaviour of a specific waste material in a full scale deposit scenario.

In this chapter a model aimed at accounting for this shortcoming is proposed and developed from first principles. The fundamental theory of aqueous flow through porous media, modes of release and transport of dissolved chemical species are briefly reviewed in Sections 4.1, 4.2 and 4.3. It will become clear that all existing models for contaminant release and transport are based on these fundamental principles to some extent, but with various degrees of simplification. Some such models are reviewed critically in Section 4.4.

It was found that models proposed for simulation of heap leach operations offer a promising route for adaptation to predictive waste leach modelling.

The heap leach model proposed by Dixon (1992) appears to be the most comprehensive approach to date and was therefore chosen as the point of departure for further development. The fundamental principles of this model are summarised and critically reviewed in Section 4.5. In Section 4.6, this base model is then extensively adapted and reworked to suit the more general requirements of waste leach scenarios. Particular focus falls on the inclusion of multiple reaction phenomena, for which detailed models are developed in Section 4.7. The model developed here has been translated into the WASTESIM computer code, the basic algorithms of which are presented in Section 4.8. A demo-version of the code is included on the disk attached to this volume and numerical methods are detailed in Appendix B.

Also contained in Section 4.8 is a preliminary study of the sensitivity of the model to a number of parameters, in terms of both, reaction behaviour and transport phenomena. This study is built on a hypothetical base case waste leach scenario, but gives valuable indicators to scenarios likely to occur in real waste deposits.

A summary of the model development and the main aspects of the model are given in Section 4.9. Some of the model limitations are also discussed here.

4.1 Hydro-transport Through Porous Media

In the context of leachate transport through solid waste deposits it is important to distinguish between the principles governing the flow of the bulk fluid (i.e. water) through the pores of the solid matrix, and those pertaining to the transport of dissolved chemical species with and within the aqueous phase. Although these two modes of transport are

closely interrelated, there are aspects individual to each which need to be addressed separately. This section introduces some fundamental principles of fluid flow through porous media, whereas contaminant transport is further investigated in section 4.2.

The flow of a fluid through porous media is usually described by Darcy's law:

$$v_D = \frac{Q}{A} = -K\frac{dh}{dx} \qquad (4.1\text{-}1)$$

where v_D is termed the specific discharge, K the hydraulic conductivity and dh/dx the hydraulic gradient. The specific discharge v_D is also referred to as Darcy velocity or superficial velocity (v_s). Implicit in this is the fact that although v_D is in units of velocity [m/s] it actually a volumetric flux [m^3/m^2s] or the velocity the fluid would have were there no particles in the bed (Bird *et al.*, 1960).

As shown in Figure 4-1, the hydraulic head h at a particular point P within the bed is the sum of two components, the elevation head z defined as the height of P with respect to some arbitrary datum line (for example sea level) and the pressure head ψ representing the height of fluid above P:

$$h = z + \psi \qquad (4.1\text{-}2)$$

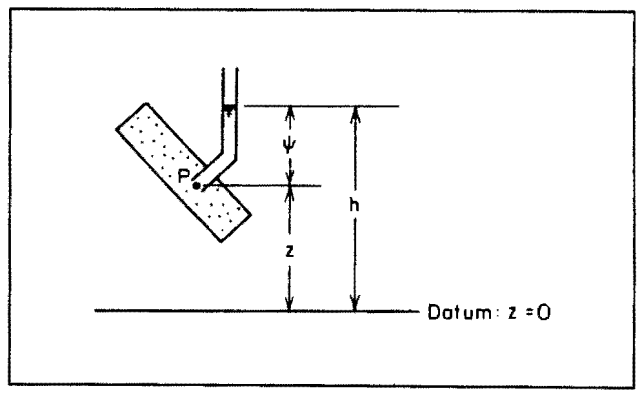

Figure 4-1: Hydraulic head h, pressure head ψ, and elevation head z at point P (taken from Freeze and Cherry, 1979)

In more general terms one would express the hydraulic gradient in terms of the gradient of fluid potential Φ, i.e. the change in mechanical energy per unit mass of fluid as a result of flow:

$$v_S = -K\frac{d\Phi}{dx} \tag{4.1-3}$$

Changes in fluid potential Φ are composed of contributions from changes of the potential (elevation) energy, kinetic (fluid velocity) energy and compression (fluid density) energy:

$$\Phi = gz + \frac{v^2}{2} + \int_{p_0}^{p}\frac{dp}{\rho} \tag{4.1-4}$$

In porous media flow of water the second term is neglected since flow velocities are usually very low. Also water is an incompressible fluid, resulting, after some re-arranging, in the simplified definition of Φ in the hydrological context:

$$\Phi = gh \tag{4.1-5}$$

Table 4.1: Range of values of hydraulic conductivity and permeability (taken from Freeze and Cherry, 1979)

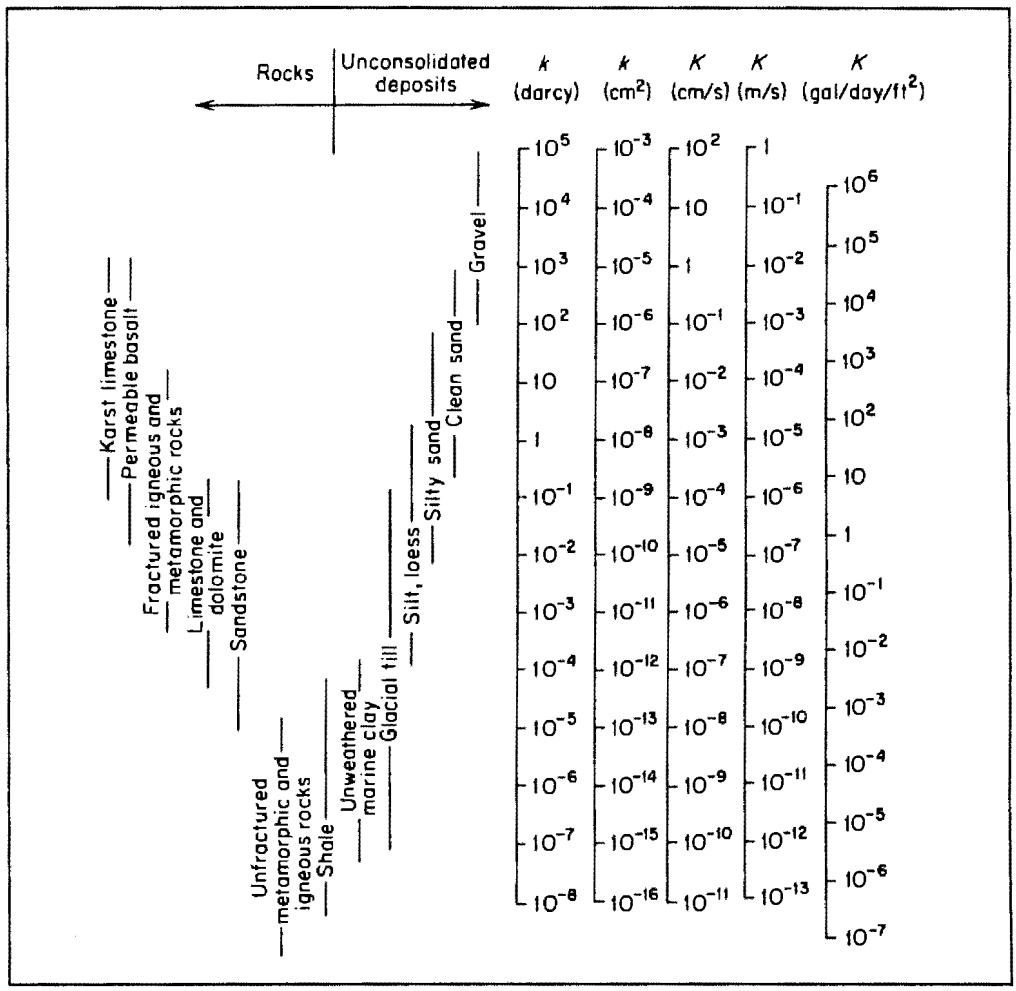

The hydraulic conductivity K is a characteristic parameter for the porous medium the fluid flows through - high for coarse, granular materials, such as sand or gravel, and low for fine-grained, densely packed materials, such as clays and silts and very low for non-porous materials such as rock. Table 4.1 gives an indication of values for K depending on the type of porous media.

The specific discharge v_D in Darcy's law describes flow on a macroscopic level (i.e. through a bed of particles), while on a microscopic level local flow patterns and velocity profiles can be extremely complex as the fluid winds its way between the individual particles (Figure 4-2).

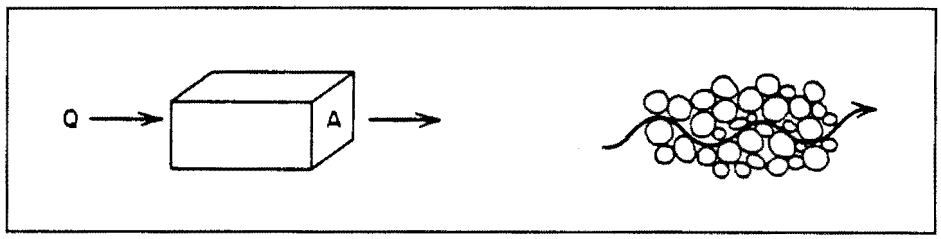

Figure 4-2: Macroscopic and microscopic concepts of flow through porous media (taken from Freeze and Cherry, 1979)

The average linear pore flow velocity v_{sp}, also known as seepage velocity is defined as

$$v_{sp} = \frac{v_D}{\varepsilon} \tag{4.1-6}$$

where ε is the bed voidage fraction or porosity.

Darcy's law is in principle an empirical correlation, providing a macroscopically averaged description of the microscopic behaviour (Freeze and Cherry, 1979). It has been shown, however, that, by theoretical development using fundamental principles of fluid flow (Navier-Stokes equations, see Bird *et al.*, 1960) and statistical methods for pore network characterisation, that Darcy's law is correct within certain limits of flow velocities (Bear, 1972) and that K can be correlated from properties of the porous medium.

The important hydraulic property of a bed of solids is its porosity ε, defined as the volume portion of solids V_{void} within a total volume element V_T of bed :

$$\varepsilon = \frac{V_{void}}{V_T} \tag{4.1-7}$$

Figure 4-3 shows the relation between various bed textures and porosity, Table 4.2 lists some values of porosity for various geologic materials. It becomes clear from these, however, that porosity in itself is not a good measure for the hydraulic conductivity of a material, as is illustrated in the example of the high porosity but low conductivity of clays.

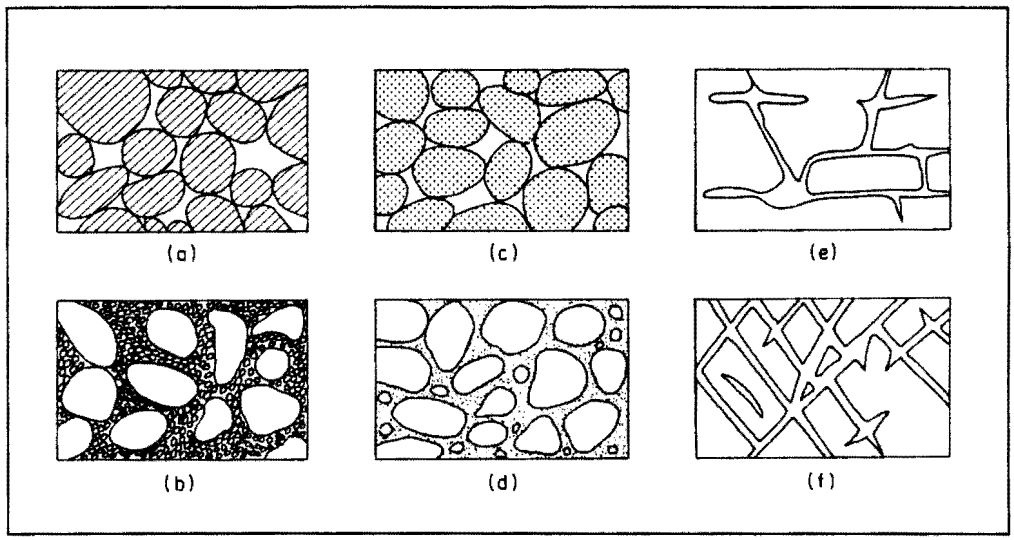

Figure 4-3: Relationship between texture and porosity. a) bed of uniform particles → high porosity; b) bed of mixed particle sizes → low porosity; c) bed of uniform particles which are porous themselves → very high porosity; d) bed with mineral matter deposited in interstitial spaces → reduced porosity; e) rock rendered porous by solution; f) rock rendered porous by fracturing (taken from Freeze and Cherry, 1979)

	n(%)
Unconsolidated deposits	
Gravel	25–40
Sand	25–50
Silt	35–50
Clay	40–70
Rocks	
Fractured basalt	5–50
Karst limestone	5–50
Sandstone	5–30
Limestone, dolomite	0–20
Shale	0–10
Fractured crystalline rock	0–10
Dense crystalline rock	0–5

Table 4.2: Range of values of porosity (taken from Freeze and Cherry, 1979)

Average particle size, size distribution, shape and randomness of packing all determine the nature of the pore network between particles in a bed in terms of factors such as pore size distribution and tortuosity. Clearly, a fluid flowing through a network of windy

capillary pores will experience much larger resistance to flow than if the pores were large and straight. Also, not all pores are conducive to flow as there might be "dead-ends" and pockets in which fluid will be practically stagnant (Figure 4-4). A detailed characterisation of the pore network within a particular bed of particles by calculation is generally not feasible and has been attempted only for highly idealised cases. Establishment of hydraulic conductivities, therefore, has to resort to empirical methods in most cases.

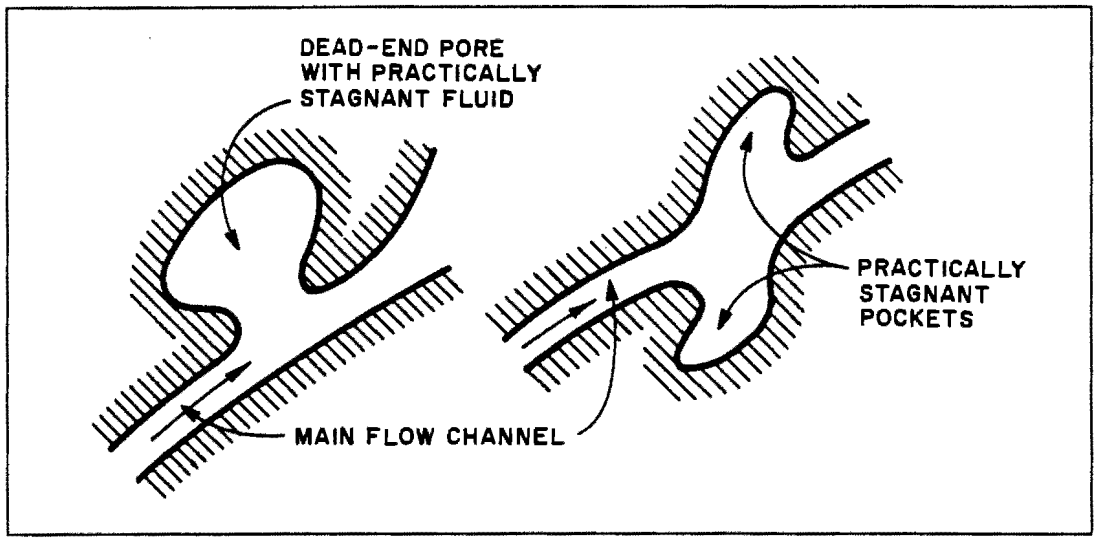

Figure 4-4: Dead end pores (after Bear, 1972)

The hydraulic conductivity of a bed material is not always independent of the direction of flow. Laminar materials, for example a packing of fibres, tend to exhibit preferential flow paths along the strands of the fibre rather than laterally between them. This phenomenon is called anisotropy and requires the establishment of a set of directionally dependent values for hydraulic conductivity (Freeze and Cherry 1979, Bear 1972).

Similarly, a bed of solid particles is not always homogeneous in types and packing of materials. In the case of waste deposits this might occur in mixed deposits, where different types of wastes are co-disposed in distinct regions. The equivalent in soils is the variation of layers of soil types with depth. Such beds are termed heterogeneous and require measurement of the various hydraulic conductivities attached to the different homogeneous zones within a heterogeneous bed.

Darcy's law as stated above can be extended into higher dimensions, here expressed in vector form for the most general case:

$$v = -\tilde{\mathbf{K}} \cdot \nabla\Phi \tag{4.1-8}$$

where $\tilde{\mathbf{K}}$ represents a hydraulic conductivity tensor (Bear, 1972), accounting for the directional dependency of $\tilde{\mathbf{K}}$ in the anisoptropic case. This can be established from the conductivities measured for the two or three principal directions (depending on the dimension of equation 4.1-8) and tensor geometry. If $\tilde{\mathbf{K}}$ is not directionally dependent (isotropic case) the tensor is replaced by the scalar value of K.

Although Darcy's law has been developed for flow through a saturated porous medium, i.e. the bed void space is completely filled with fluid, it can in principle also be applied for the unsaturated case, where the pores are only partially filled with fluid, the remainder being occupied by air. The moisture content θ is then defined as the fraction of the total bed volume occupied by the fluid volume V_f, i.e.

$$\theta = \frac{V_f}{V_T} \tag{4.1-9}$$

For saturated flow $\theta = \varepsilon$, for unsaturated flow $\theta < \varepsilon$.

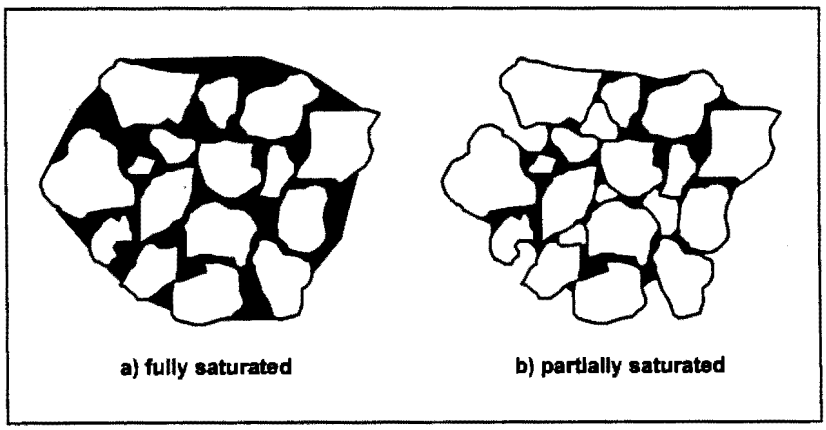

Figure 4-5: Water retention under (a) saturated and (b) unsaturated conditions. Note the fluid bridges between individual particles, holding the water under surface-tension forces.

In unsaturated beds the pressure head ψ takes a negative value. This reflects the fact that water in the unsaturated zone is held in the pores under surface-tension forces, while the air pressure remains atmospheric as is indicated in Figure 4-5 (Freeze and Cherry, 1979). For this reason it is also referred to as suction head or tension head.

Both, the moisture content θ and hydraulic conductivity K, are functions of the pressure head ψ and therefore also $K = K(\theta)$. Implicit in this is that a hydraulic head gradient, which is also a function of ψ (equation (4.1-2)), results in a gradient of moisture content (except for pure gravity flow). Darcy's law for an isotropic unsaturated bed in x direction can thus be written as:

$$v_{s,x} = -K(\psi)\frac{\partial h(\psi)}{\partial x} \tag{4.1-10}$$

Darcy's law describes only steady state flow, i.e. hydraulic head gradient and conductivity stay constant with time. Transient flow behaviour is particularly significant in the drying and wetting of unsaturated soils in consequence to seasonal rainfalls. In these cases the moisture content θ increases or decreases with time as the amount of water stored within a control volume changes.

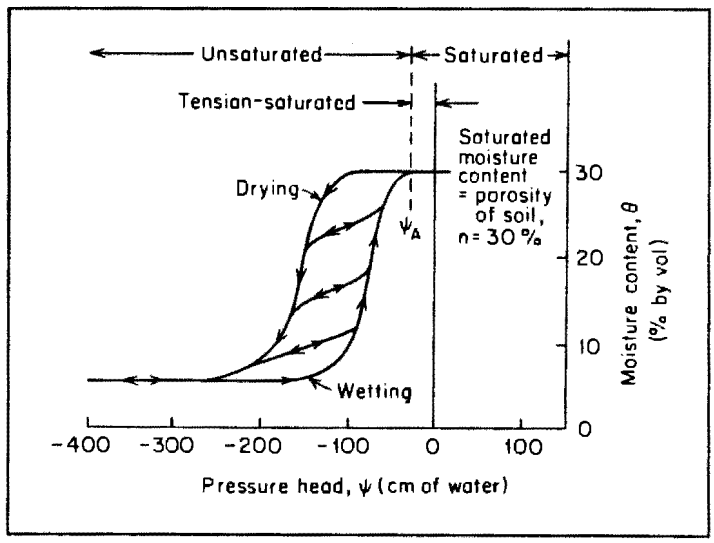

Figure 4-6: Typical drying-wetting curves for a sandy soil (taken from Freeze and Cherry, 1979)

For a specific bed medium one can define the specific moisture capacity C as

$$C = \frac{d\theta}{d\psi} \tag{4.1-11}$$

which needs to be established from experiment of measurement of θ versus ψ. Figure 4-6 shows a typical drying-wetting curve for a natural sand soil. Characteristic are the non-linear hysteresis shape of such curves and hence functions for C are non-linear also.

Darcy's law can be incorporated into the basic continuity equation for porous media thus:

$$-\nabla \cdot (\rho v) = \frac{\partial \varepsilon \rho}{\partial t} \tag{4.1-12}$$

which results in

$$\frac{\partial}{\partial x}\left[K(\psi)\frac{\partial h}{\partial x}\right] + \frac{\partial}{\partial y}\left[K(\psi)\frac{\partial h}{\partial y}\right] + \frac{\partial}{\partial z}\left[K(\psi)\frac{\partial h}{\partial z}\right] = \frac{\partial \theta}{\partial t} \tag{4.1-13}$$

It is more convenient to express this equation in terms of θ or ψ only. Using equations (4.1-2) and (4.1-11) , equation (4.1-13) can be converted to

$$\frac{\partial}{\partial x}\left[K(\psi)\frac{\partial \psi}{\partial x}\right] + \frac{\partial}{\partial y}\left[K(\psi)\frac{\partial \psi}{\partial y}\right] + \frac{\partial}{\partial z}\left[K(\psi)\left(\frac{\partial \psi}{\partial z} + 1\right)\right] = C(\psi)\frac{\partial \psi}{\partial t} \tag{4.1-14}$$

This equation, describing transient three-dimensional flow through unsaturated porous media, is often referred to as Richards Equation. This equation can be solved by suitable numerical methods in combination with the required experimental data for $K(\psi)$ and $C(\psi)$.

4.2 Contaminant Transport In Aqueous Flow

The transport of any dissolved chemical species i in a solvent, such as water, is most conveniently described by the continuity equation for mass transport:

$$- \nabla \cdot N_i + Q_{c,i} = \frac{\partial c_i}{\partial t} \tag{4.2-1}$$

where N_i is the flux of species i [mol/m^{2}s], $Q_{c,i}$ a source/sink (reactive) term and c_i the dissolved concentration of i. The concentration of i within a volume element changes with time according to the net balance of i transported in and out of this control volume and amounts of i generated or dissipated within. This mass balance is also valid for aqueous transport through porous media. Here, however, only part of a volume element is filled with fluid, the rest being occupied by solid (Figure 4-7).

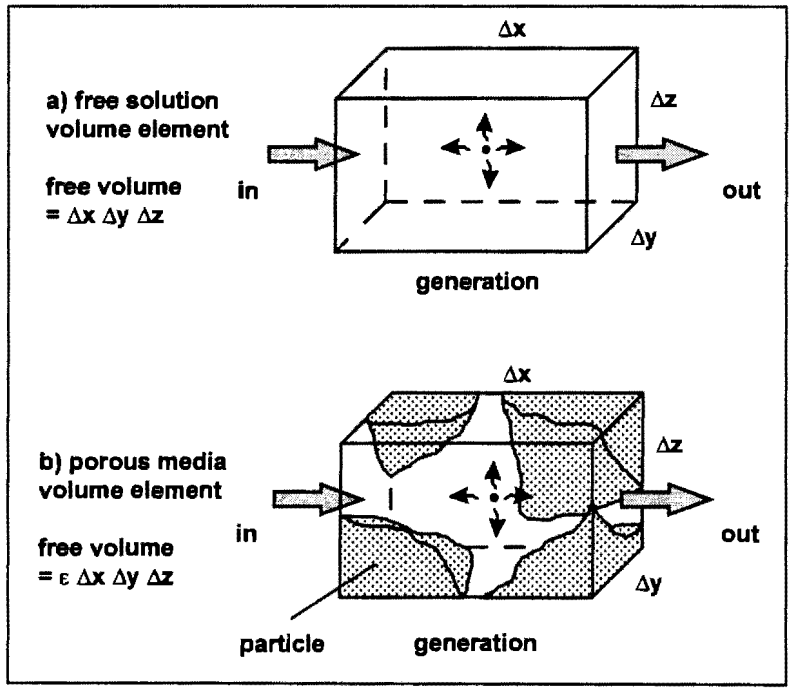

Figure 4-7: Concept of a volume element in (a) free solution, (b) porous media

While the flux and source/sink term in equation (4.2-1) are expressed in terms of unit total volume, the concentration in the accumulation is only in per unit fluid volume. Thus, for porous media, equation (4.2-1) is rewritten as

$$- \nabla \cdot N_i + Q_{ci} = \varepsilon \frac{\partial c_i}{\partial t} \tag{4.2-2}$$

Modes of transport, which are incorporated in the flux term N_i, depend on the physical environment considered. In flow through porous media these are normally attributed to three different effects: transport with the bulk liquid flow, molecular diffusion and mechanical dispersion.

The first refers to the transport of a dissolved concentration c_i with a fluid moving at a certain superficial bulk velocity:

$$N_i^{blk} = c_i v_s \tag{4.2-3}$$

Molecular diffusion results from the thermodynamic effect of minimising the free energy of a system that exhibits gradients of chemical potential of the solute. These gradients are mostly associated with concentration gradients of a dissolved species within the fluid. The resulting effect is migration of species from regions of higher concentration to those of lower concentration, even in the absence of any other transport mechanism. Molecular diffusion is described by Fick's Law:

$$N_i^{dif} = - D_i^* \nabla c_i \tag{4.2-4}$$

Here D_i^* is the molecular (sometimes referred to as "free solution") diffusion coefficient for species i, which is dependent on a number of factors, including ionic or molecular properties of i and the solvent as well as the concentrations of other dissolved species present. It is derived on the basis of un-restricted flow through a continuous fluid.

In the case of diffusion through porous media, however, this condition is not given. Not only is diffusive flux restricted by the areas available for diffusion (as governed by the porosity), but also by the fact that small pores are not straight tubes, but are likely to exhibit a degree of curvature or windedness, which lengthens the microscopic path a molecule has to travel to cover a certain distance on a macroscopic level (Figure 4-8). As a

result, macroscopic diffusion through porous media needs to be described by an effective diffusivity $D_{e,i}$ which encompasses microscopic effects imposed through the nature of the porous medium. One conventionally defines (Aris, 1975):

$$D_{e,i} = \frac{\varepsilon}{\tau_T} D_i^* \tag{4.2-5}$$

where τ_T is a tortuosity factor which is to account for the porous geometry. Although mathematical correlations for τ_T are available for simple geometries, in most cases it is reduced to a "fudge factor of greater or lesser sophistication" (Aris, 1975).

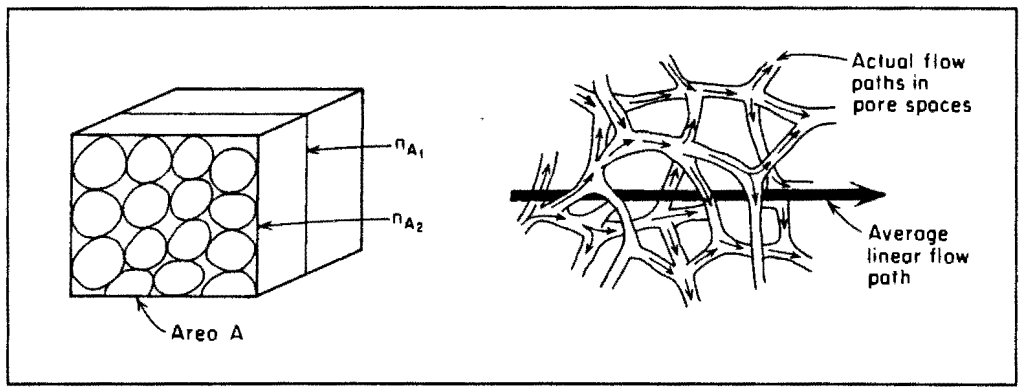

Figure 4-8: Effective diffusion governs macroscopic transport through porous media (taken from Freeze and Cherry, 1979)

Mechanical dispersion is not a transport process in itself, but the summary effect of a number of microscopic mechanical processes that take place when fluid flows through pores. The dissolved concentration of species i is dispersed longitudinally and (to a lesser extent) laterally to the direction of bulk flow. Three main effects are considered to play a role in mechanical dispersion as shown in Figure 4-9 (Freeze & Cherry, 1979; Shackleford, 1993):

a) dispersion due to a velocity profile in the channel of individual pores

b) dispersion due to different flow velocities in pores of different diameter

c) mixing effects related to the tortuosity, branching and inter-fingering of pore channels

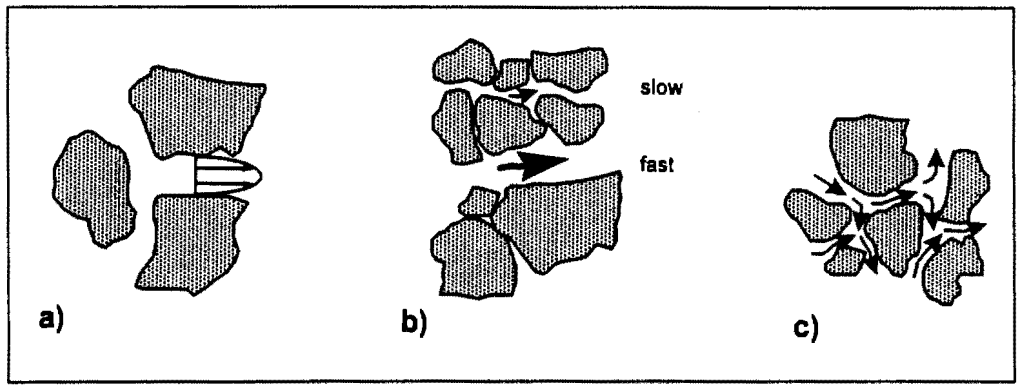

Figure 4-9: Mechanisms of mechanical dispersion: (a) velocity profiles in pores; (b) distribution of flow velocities; (c) branching and merging of pore channels

Mechanical dispersion is usually taken as a Fickian diffusion phenomenon and therefore described by an expression similar to Fick's Law:

$$N_i^{dsp} = -D_m \nabla c_i \tag{4.2-6}$$

It should be noted here that D_m is directionally dependent (i.e. anisotropic) and should therefore appear as a tensor quantity in equation (4.2-6). However mechanical dispersion is usually only considered in the principal direction of flow, with lateral dispersion rarely taken into account. Thus more correctly

$$N_{i,x}^{dsp} = -D_m \frac{\partial c_i}{\partial x} \tag{4.2-6a}$$

The mechanical dispersion coefficient D_m is a basically an empirical constant lumping the various dispersion phenomena listed above. It is, however, clearly dependent on the bulk flow (seepage) velocity v_{sp} since it directly dictates pore velocities at the microscopic scale. One can therefore often find

$$D_m = \alpha_L v_{sp} \tag{4.2-7}$$

where α_L represents a characteristic property of the porous medium, known as dynamic dispersivity (Freeze and Cherry, 1979).

In modelling the transport of dissolved constituents in flow through porous media the effects of effective molecular diffusion and mechanical dispersion are often lumped together in a single expression since they are both based on Fick's Law. The combined diffusion/dispersion constant is referred to as coefficient of hydrodynamic dispersion D_h:

$$D_h = D_m + D_e = \alpha_L v_{sp} + \frac{\varepsilon}{\tau_T} D^* \tag{4.2-8}$$

D_h has been shown to correlate well against the system Peclet number by comparing a large number of experimental data (Bear, 1972) as is shown in Figure 4-10.

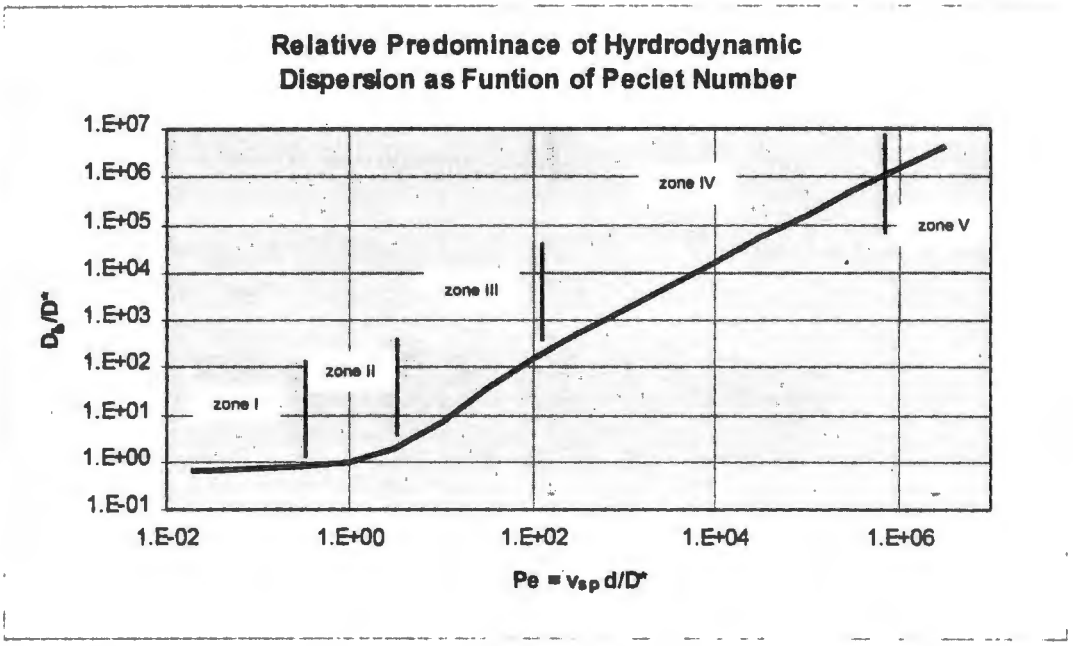

Figure 4-10: Relationship between hydrodynamic dispersion and molecular diffusion as function of system Peclet nymber (adapted from Bear, 1972).

The correlation is expressed as

$$\frac{D_h}{D^*} = \alpha_L Pe^m = \alpha_L \left(\frac{v_{sp} d}{D^*}\right)^m \tag{4.2-9}$$

where m is an empirical constant. d is a characteristic length, which is usually taken as the mean particle diameter, although it should be more correctly be mean pore diameter (Bear & Verruijt, 1987). It should also be pointed out here, that Peclet number and the ratio of

dispersion to diffusion coefficient are both expressed in terms of the molecular free-solution diffusion coefficient D^* and not of the effective diffusivity D_e which is already corrected for the porous medium, as indicated in equation (4.2-5). The graph in Figure 4-10 can be divided into 5 zones where different effects predominate, as detailed below:

- Zone I: At low Peclet numbers molecular diffusion predominates, since the average flow velocity is very small. D_h takes the value of D_e (not D^* !), explaining why the ratio D_h/D^* is smaller than 1.
- Zone II: At $0.4 < Pe < 5$ both diffusion and dispersion effects are of the same order of magnitude.
- Zone III: Here spreading is caused mainly by mechanical dispersion. In this zone $\alpha_L \approx 0.5$ and $1 < m < 1.2$.
- Zone IV: Mechanical dispersion is the predominant effect, increasing linearly with Pe, i.e. $\alpha_L \approx 1.8$ and $m = 1$.
- Zone V: This zone falls outside the range of validity of Darcy's law and mechanical dispersion is governed by effects of turbulence and inertia.

Thus, in summary, equation (4.2-2) can be re-written in terms of the various transport modes described above in linear x dimension:

$$- v_s \frac{\partial c_i}{\partial x} + D_h \frac{\partial^2 c_i}{\partial x^2} + Q_{c,i} = \varepsilon \frac{\partial c_i}{\partial t} \qquad (4.2\text{-}10)$$

or, in the general vectorized format, as:

$$- \nabla \cdot (v_s c_i) + \nabla \cdot (\tilde{D} \cdot \nabla c_i) + Q_{c,i} = \varepsilon \frac{\partial c_i}{\partial t} \qquad (4.2\text{-}11)$$

where $\tilde{D}$ refers to a dispersion tensor.

Equations (4.2-10) or (4.2-11) form the basis for transport of a dissolved species i with and within a bulk fluid moving through porous media. In combination with suitable hydrological models to describe the flow field of the bulk flow itself, such as given in equation (4.1-14), these equations can be used to comprehensively describe contaminant transport through waste deposits and underlying soils.

4.3 Reactions Leading to Contaminant Release or Removal

Equation (4.2-10) describes the transport of a dissolved contaminant species i through porous media. Release or removal of i from the dissolved state by any form of physico-chemical reaction is accounted for in the source/sink term $Q_{C,i}$. Such reactions can include:

- dissolution from or precipitation to a solid form
- sorption to or de-sorption from a solid surface, whereby sorption mechanism may encompass surface complexation, ion-exchange and surface precipitation
- chemical reaction with other species either dissolved or solid, such as redox reactions and leaching

As $Q_{C,i}$ is a summary rate term, the kinetic contribution from each reaction involving species i must be factored in individually:

$$Q_{C,i} = \sum_j R_i^j = R_i^{ads} + R_i^{rxn} + R_i^{dis} + \ldots \tag{4.3-1}$$

where a positive R_i^j represents the rate of production of species i due to reaction j. If i is consumed in a particular reaction, R_i^j must take a negative value.

Reactions that are found to be controlled by kinetic factors, for example the dissolution of a certain solid species by chemical attack by dissolved species (leaching), the formulation of a kinetic rate expression R_i^{kin} may take the form:

$$R_i^{kin} = \frac{dc_i}{dt} = f(k, c_i, c_x, \ldots) \tag{4.3-2}$$

where f represents some mathematical expression, k is a kinetic constant and c_x represents the concentrations of species other than i (both solid and dissolved) participating in the reaction. The nature of the rate expression and the relevant constants are usually established from suitable experiments.

Many chemical reactions, however, tend to proceed fast to some thermodynamic equilibrium, as is the case in dissolved phase redox and complexation reactions, dissolution/precipitation as well as many surface sorption reactions. For these, description by a kinetic rate expression would be pointless since kinetic constants are difficult to measure and the system is sufficiently well described by some thermodynamic equilibrium model. Prominent among these is the law of mass action:

$$K_{eql} = \prod_i a_i^{\nu_i} \tag{4.3-3}$$

where K_{eql} is the thermodynamic equilibrium constant at the given temperature, a_i represents the thermodynamic activity of species i participating in the reaction, and ν_i the stoichiometric coefficient of i in this reaction. The value of K is obtained from minimising the Gibbs free energy of the system or from tabulated experimental values. The activity of species in solution is obtained by

$$a_i = \gamma_i m_i \approx \gamma_i c_i \tag{4.3-4}$$

where γ_i is the activity coefficient of species i [kg/mol] and m_i the molality of i in solution [mol/kg], which, only for dilute aqueous systems, is approximately equal to the molar concentration of i. For ionic species, γ_i is usually obtained from suitable models such as the Debye-Hückel equation for dilute ionic solutions (ionic strength < 10^{-3} M). For higher concentrations γ_i can be modelled with the Lewis or other related equations.

In principle, all chemical reactions can be described by a thermodynamic equilibrium model. However, reactions which are kinetically inhibited are insufficiently accounted for in this manner as thermodynamics might describe an equilibrium condition which is not or only very slowly attainable in reality. Examples may include slow re-dissolution of an aged hydroxide or oxidation reactions with dissolved oxygen. For reactions like these a kinetic expression as given in equation (4.3-2) needs to be found. Furthermore, many systems, particularly surface sorption reactions, are difficult to describe thermodynamically requiring a large number of parameters from detailed surface characterisation.

Another drawback of equilibrium models is that their incorporation into a dynamic transport model is not straightforward. A rate term for the production or consumption of a species i can be obtained only indirectly by calculating the shift in an equilibrium within a discrete time interval Δt:

$$R_i^{equil} = \frac{\Delta e_i}{\Delta t} \tag{4.3-5}$$

where Δe_i represents the change in equilibrium concentration of i. This can only be achieved by numerically solving the highly non-linear equilibrium model equation, making analytical solution of the combined reaction-transport equation (4.2-10) impossible.

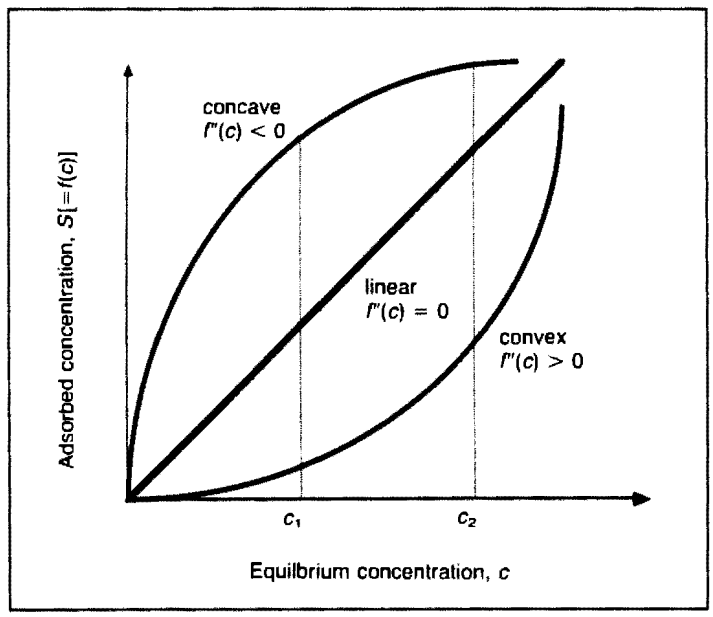

Figure 4-11: General types of adsorption isotherms (taken from Daniel, 1990)

An exception has been the use of a simplified linear sorption model, which is incorporated in the transport equation in the form of a term

$$R_i^{sorp} = -\rho_b \frac{\partial S_i}{\partial t} = \rho_b \frac{\partial S_i}{\partial c_i} \frac{\partial c_i}{\partial t} \tag{4.3-6}$$

where ρ_b is the solid bulk density [kg/m^3_{bed}] and S_i the sorbed concentration of i per unit mass solid [mol/kg_{solid}]. The term dS_i/dc_i describes the change of adsorbed concentration of i in equilibrium with changing dissolved concentration which is obtained from an experimentally measured equilibrium isotherm. These are usually represented as curves of adsorbed versus dissolved concentration of a particular species at equilibrium, such as shown in Figure 4-11.

Where this isotherm is linear one can write

$$\frac{\partial S_i}{\partial c_i} = \text{const} = K_{d,i} \tag{4.3-7}$$

where $K_{d,i}$ denotes the partition or distribution coefficient of component i. In this case the sorption rate term can be incorporated into the transport equation (4.2-11) as follows:

$$-\nabla\cdot(v_s c_i) + \nabla\cdot(D_h \nabla c_i) = \varepsilon(1+\frac{\rho_b}{\varepsilon}K_{d,i})\frac{\partial c_i}{\partial t} \tag{4.3-8}$$

The term $(1 + \rho_b/\varepsilon\ K_{d,i})$ is referred to as the retardation factor R_d. This name originates from the concept that the advance of a dissolved contaminant is retarded through the effects of adsorption. R_d is constant only where adsorption isotherms are linear or taken as linear in the concentration range of interest, as is shown in Figure 4-12. In the latter case K_{di} is obtained from the slope of a secant across the isotherm. For non-linear isotherms R_d can be expressed as a function of the form $R_d = f(c_i)$ (Shackleford, 1993; Freeze and Cherry, 1979).

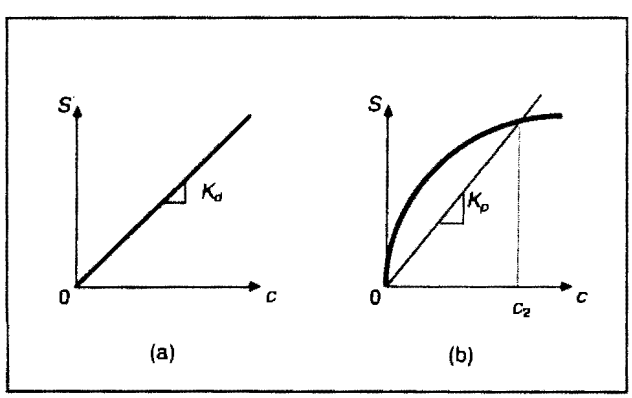

Figure 4-12: Obtaining K_d from a given adsorption isotherm: (a) linear; (b) secant formulation for concave isotherm (taken from Daniel, 1990).

Commonly used adsorption models are the Freundlich and Langmuir isotherms (which represent the concave type).

The Freundlich isotherm is written as

$$S_i = b c_i^m \tag{4.3-9}$$

where b and m are constant coefficients. For m = 1 the isotherm becomes linear and $K_{d,i} = b$.

The Langmuir isotherm is written as

$$S_i = \frac{\alpha c_i}{1 + \beta c_i} \tag{4.3-10}$$

where α and β are constant coefficients.

Isotherm models are limited, however, in their ability to describe variable degrees of surface complexation, solids with heterogeneous sorption sites and ion-exchange reactions (Mangold and Tsang, 1991). Mass action models can account better for these type of reactions, but they do require more parameters. A third class of reaction models to describe surface sorption phenomena is that of surface complexation or electric double-layer models, which are the most rigorous in describing all ionic surface interactions within one unifying theory (see for example Dzombak and Morel, 1990), but require a large number of parameters and rigorous surface characterisation, which has prevented their wide-spread use as equilibrium models (Mangold and Tsang, 1991).

A simplified, but frequently employed dissolution model is the external film transfer model. Which describes those cases where the release of contaminant situated at the solid surface into the moving fluid is controlled by the diffusional resistance of a liquid surface "film":

$$R_i^{dis} = k_c(\rho_b S_i - c_i) \tag{4.3-11}$$

where S_i and c_i represent the solid surface and bulk concentrations respectively, and k_c is a film mass transfer coefficient. The underlying assumption in this model is that the contaminant is dissolved instantly within the surface, but only gradually released into the

bulk fluid. Although the film mass transfer concept has its sound theoretical foundations (see Bird *et al.*,1960), the film transfer model of equation (4.3-11) is often used as a method of empirically lumping a number of reaction and diffusional effects into a single parameter, which is measured from experiment. Since film transfer is a strong function of the specific hydrodynamic conditions, such empirical values are usually unsuitable for direct scale-up.

The review in this section clearly shows that there is a number of approaches to the incorporation of chemical reactions into the modelling of dynamic transport systems, either on the basis of kinetic or equilibrium models. Since in real systems both types are occurring, a more unified approach is sought, which allows incorporation of any type of reaction into dynamic modelling. Such an approach is proposed in Section 4.7.

4.4 Review of Existing Contaminant Transport Models

The fundamental equations governing hydro-transport, contaminant transport and mechanisms of contaminant release/attenuation in the context of flow through porous media have been introduced in the preceding sections. These have been applied by numerous workers in attempts to model contaminant transport by groundwater flow from a source of contamination (such as the boundary of a deposit site) through surrounding soils and aquifers, and, to a lesser extent, through various forms of waste deposits themselves. It is useful to review the various models employed in the context of the theory in order to gain an insight in how each may be used to best model contaminant release from waste deposits. Table 4.3 gives a survey of a number of models developed in the context of pollution modelling and related areas and identifies the techniques and degree of sophistication employed on the levels of hydro-transport, solute transport and reaction models. Further aspects of these models are discussed in the following.

Rowe (1988, 1990) and Booker (Rowe and Booker, 1985a, 1985b, 1990, 1991) have modelled contaminant migration from waste deposits through a variety of liners, hydraulic barriers, fractured till and soil in one and two dimensions. The transport equations used in their modelling approach is essentially the transient convection-dispersion model of equation (4.2-11). Hydro-transport is assumed at steady state with predetermined seepage velocities. The approach taken to reaction is that of the retardation factor for modelling linear adsorption as given in equation (4.3-8). The initial concentration of the migrating leachate at the deposit boundary is predetermined and only its spread and attenuation away from the deposit are modelled. The authors justify this on the grounds that contaminant migration through deposit liners and underlying soil is a long-term process relative to the construction and initial leach period of the deposit. Model equations with suitable boundary conditions were solved by Laplace and Fourier transforms.

Korfiatis *et al.* (1984) describe modelling unsaturated one-dimensional flow patterns through a column filled with municipal refuse exposed to a period of artificial rain. The model equations used were a combination of the one-dimensional transport equation (4.2-10) with no reaction term $Q_{C,i}$ and the Richards equation for unsaturated flow (4.1-14). The model allowed successful reproduction of flow results from the column study. Demetracopoulos *et al.* (1986) expand on this study in terms of leachate generation within the column. A simplified film transfer source term as indicated in equation (4.3-11) was included as well as a similar term taking account of bacterial decomposition. While the model results capture the column leach data qualitatively, the difficulty of obtaining meaningful kinetic parameters, particularly for bacterial activity in municipal refuse deposits, was given as the reason for the lack of a better quantitative correlation.

A number of complex geochemical models combining unsaturated two- or three-dimensional hydro-transport with chemical equilibrium modelling, have been applied in the context of modelling contaminant transport from waste sites and details can be found in the review by Mangold and Tsang (1991).

Table 4.3: Models developed for simulating leachate generation and contaminant transport

Source	Type of Model	Application	Transport Modelling	Reaction Modelling	Remarks
Rowe and Booker (1985-1991)	hydro-transport	leachate transport through ground surrounding a waste deposit	1D and 2D convective flow, saturated	retardation, no generation	
Korfiatis (1984) Demetracopoulos (1986)	hydro-transport/ hydro-chemical	transport through and biological activity within municipal waste deposits	1D convective flow, unsaturated	film dissolution, bio-reaction	transport modelling successful, reaction modelling poor
Mangold and Tsang (1991)	equilibrium (MINTEQ)	groundwater analysis, nuclear waste disposal	None	equilibrium chemistry including sorption and precipitation	verified in numerous cases
	hydro-transport (SATURN)	groundwater contamination studies	2D convective flow, dispersion, diffusion	sorption, dissolution	propriety software
	hydro-chemical (FASTCHEM)	modelling of power-station ash deposits	1D convective flow, dispersion, diffusion	includes MINTEQ	EPRI software
Vogt and Herrling (1990)	hydro-chemical	hydro-chemical/ contaminant transport trough an infiltration passage	2 D convection/ dispersion	equilibrium solution chemistry	
Cote and Bridle (1986) Batchelor (1990)	diffusion	leachate generation from cemented wastes	diffusion only	dissolution	empirical acid leach index
Bartlett (1992), Dixon (1992), Davies (1995)	hydro-chemical	heap leach modelling, also applcable to waste heap modelling	1D convective flow in bulk, diffusion in particle pores	kinetic reactions	separates between bulk and particle phenomena

In terms of reaction modelling most of these models focus on thermodynamic equilibrium calculations as indicated in equations (4.3-3) and (4.3-4), although kinetic reactions can sometimes also be incorporated. The initial leachate concentration at the source (i.e. at the boundary of a waste deposit) is mostly assumed as given, although Jones (1995) indicates that rigorous models of this type (particularly FASTCHEM) have also been used to model leachate mobilisation within coal ash deposits, but only with limited success. This was attributed to the lack of appropriate kinetic models for certain non-equilibrium reactions, such as slow dissolution and leaching.

Another example for the rigorous transport-equilibrium model approach is the work by Vogt and Herrling (1990). They describe large-scale simulation of contaminant transport through an infiltration passage, a numerical solution strategy for which was developed by Leismann (Leismann and Frind, 1989). During simulation, chemical equilibrium between all participating species is calculated at each node and for each time step of the iteration. Although numerically trivial, the large number of thermodynamic species means that the calculations can become very cumbersome, necessitating the use of a high capacity vector computer. Vogt indicates that kinetic reaction expressions can be easily incorporated into the model, but would require lengthy laboratory tests not conducted in his study. It thus becomes clear that the exclusive use of chemical equilibrium models insufficiently accounts for interactions at the solid-liquid interface leading to contaminant release.

A somewhat different approach emerges from the modelling of leachate generation from wastes that have been solidified into monolithic structures by cementation (see Section 3.2.10), such as described by Cote and Bridle (1986) and Batchelor (1990). Due to the small pore size in such structures, contaminant migration is governed primarily by diffusion. In this case equation (4.2-10) essentially reduces to Fick's second law, i.e. omitting the convective and reactive terms and reducing dispersion to molecular diffusion.

This is commonly solved analytically for semi-infinite one-dimensional geometry and zero surface concentration as (Crank, 1975):

$$L(t) = c_i^0 \left(\frac{D_e}{\pi t}\right)^{1/2} \qquad (4.4\text{-}1)$$

where L(t) is the time-dependent leach rate (at the monolith surface), c_i^0 the initial, uniformly distributed contaminant concentration in the block and D_e is the effective pore diffusivity, governed by porosity of the structure, pore size and tortuosity.

This approach presupposes that the contaminant is uniformly dissolved in the pore solution of the structure. Contaminants that are insoluble due to fixation within the cement matrix are assumed to only be solubilised through acid attack. Model approaches to take account of this phenomenon include the formulation of a "leachibility index" to replace D_e in equation (4.4-1) (Bishop, 1986; Batchelor, 1990) or by formulating an alternative leach rate expression in terms of acid transport to the waste and its acid neutralisation capacity (Cote and Bridle, 1986). In both cases the parameters are established from various waste testing procedure outlined in in a review in Section 5.1.1 (for example, see Stegemann and Cote, 1991). Needless to say, the formulation of such leach parameters is purely empirical and simplistic.

Nonetheless, it is worth considering the following point: Taking blocks of porous cemented waste as large "particles" and a flow of groundwater past it as liquid bulk flow, then the postulated pore diffusion-reaction concept can be taken as a starting point for modelling contaminant release at the particle level. This concept is particularly relevant in the modelling of leachate generation from heap leach operations (Davies, 1995)

Heap leaching is a further area in which groundwater flow modelling combined with the transport of dissolved species has found some use. This low-cost minerals processing operation finds application in the hydrometallurgical extraction of values from low grade ores. Leach liquor flows through a porous bed of ore particles, which can be considered

porous in themselves. On its way, it interacts with the solids by chemical reaction and transports the released dissolved minerals very similarly to the way contaminants are transported through waste deposits. For this reason modelling work conducted in this area merits further consideration.

The focus of heap leach modelling rests more on the mechanisms and kinetics of the release reactions, particularly at the level of an individual particle, than appears to be the case with waste models. In a review by Bartlett (1992) various approaches by a number of workers are summarised. The common feature is formulating the transient diffusion equation (i.e. equation (4.2-10) without the convective term) for porous spheres (emulating a single particle, figure 4-13):

$$\varepsilon \frac{\partial c_i}{\partial t} = D_e[\frac{\partial^2 c_i}{\partial r^2} + \frac{2}{r}\frac{\partial c_i}{\partial r}] + Q_{c,i} \qquad (4.4\text{-}2)$$

with all terms as defined previously.

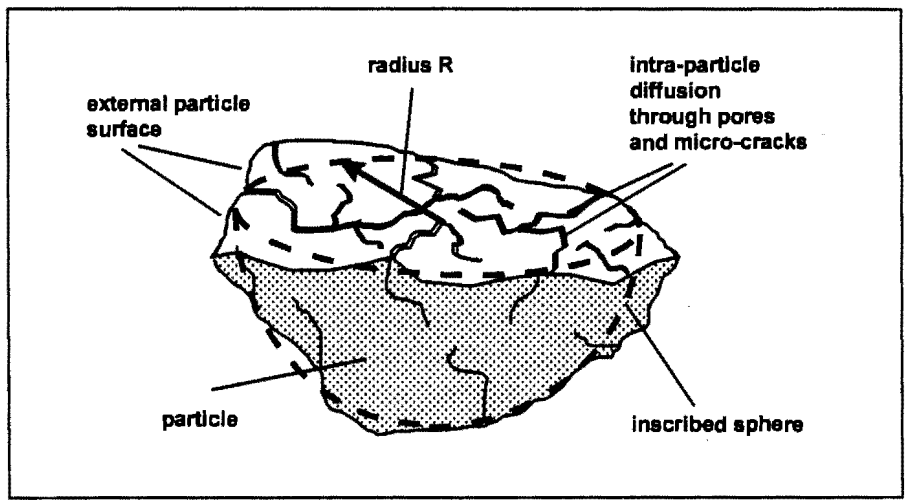

Figure 4-13: Conceptual modelling of an individual porous particle

This equation is then interpreted according to various (simplifying) assumptions:

- diffusion controlled release: Reaction in the particle pores is assumed to proceed fast relative to the diffusional transport, therefore the reaction term $Q_{c,i}$ in equation (4.4-2) is

omitted. The mineral species i is assumed to be completely and uniformly dissolved within the particle pore matrix at time t_0 and is transported by diffusion only. This model can be solved analytically (Crank, 1975). This approach is the same in principle as the one formulated for diffusional release from monolithic cement blocks.

- pseudo steady-state diffusional release: The mineral i dissolves from a retreating internal front (shrinking core model) controlled by the availability of reactant diffusing into the particle. This approach was for example attempted by Roman et al. (1974). The shrinking core model is well described in chemical engineering literature (Levenspiel, 1972).

- mixed kinetic release: Here a suitable kinetic term needs to be found for the dominant chemical reaction(s) and substituted for $Q_{C,i}$ in equation (4.4-2), thus making it a reaction-diffusion model at the particle level. Reaction rate constants need to be established by experiment. The model requires numerical solution (Bartlett, 1992).

- pseudo steady-state mixed kinetic release: The shrinking core model is applied to the case where both diffusion and chemical reaction, expressed in a suitable kinetic term in $Q_{C,i}$, are considered. This approach was taken by Madsen and Wadsworth (1981), and an analytical solution has been described by Bartlett (1992).

In all these models the bulk transport of the leachate is simulated in a "CSTR in series" manner. The heap is conceptualised as a column that can be sub-divided into a number of "compartments" or disks, each containing a mass of particles fully in contact with a volume of bulk liquid in a "well mixed" fashion (Figure 4-14). The dissolved species concentration at the particle surface (as calculated from the relevant particle scale model) is set equal to its bulk concentration and the fractional release into the bulk fluid within a discrete time interval is calculated via a mass-balance (Davies, 1995). In the next interval the volume of bulk liquid within each compartment is completely replaced by the volume from the one above and the calculation is repeated. This approach is justified by the

assumption that reaction processes within the particle pores are slow relative to the bulk release process. In the comprehensive heap leach model proposed by Dixon (Dixon, 1992; Dixon and Hendrix 1993a, b) the approach at the particle level is in essence the mixed kinetic release model described above, but at the bulk level particle release is linked to a one-dimensional transport model, along the lines of equation (4.2-10), although omitting the dispersion term on the assumption of ideal plug flow. Bulk flow is assumed as saturated and steady state.

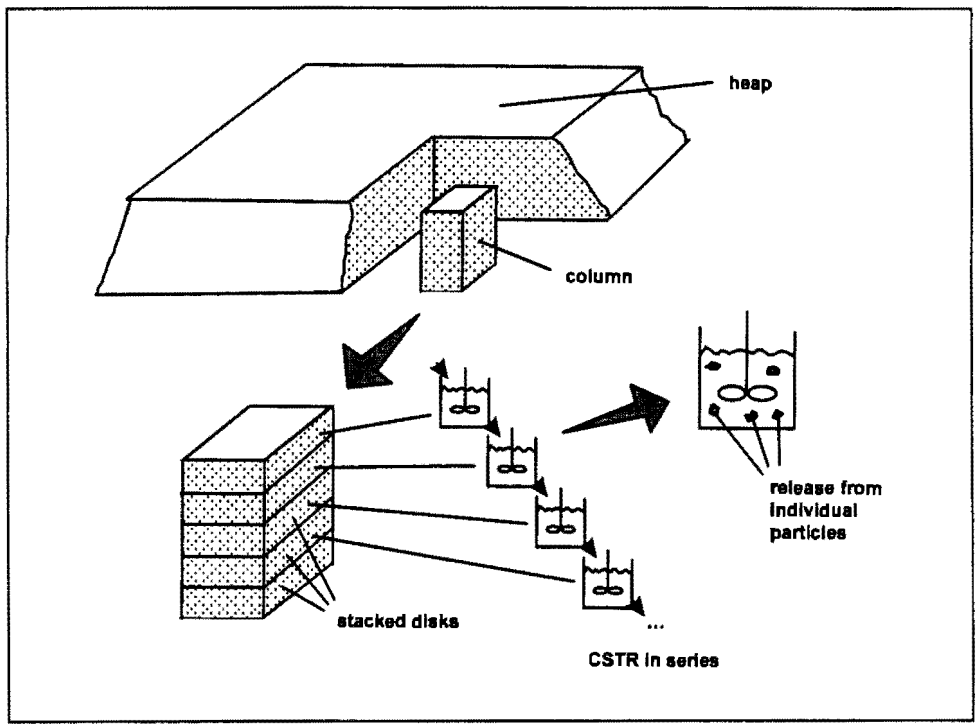

Figure 4-14: Conceptual subdivision of a waste heap column into a series of CSTRs

In summary, it becomes clear that all modelling work reviewed here relies on the fundamental transport equation (4.2-11), but the various terms of this equation are accounted for in a number of different ways:

- Flow (convective term): On the hydro-transport side flow is modelled either by rigorous multidimensional, unsteady-state, unsaturated flow (equation (4.1-14)), by a pre-determined steady-state flow field or it is assumed stagnant (as is the case in pore diffusion models).

- Dispersion: Various approaches have been employed, either full hydrodynamic dispersion (see Section 4.2), diffusion only (for stagnant liquids) or it is omitted altogether (as is the case in the Dixon approach).

- Reaction (source/sink term): All aspects reviewed in Section 4.3 have been incorporated in the various models, but with different preferences. Geo-hydrological models focus mainly on equilibrium models, either by use of the simplistic retardation factor or fully comprehensive multi-reaction, multi-speciation thermodynamic models, which appear hampered by their computational complexity. Heap leach models, by nature of their main focus, employ mainly kinetic reaction models or dissolution-diffusion within the particle pores.

It appears, furthermore, that rigorous geochemical transport models with their insistence on comprehensive chemical equilibrium modelling, are probably overly ambitious (particularly considering their limited success thus far), while none of the simplifications encountered in the other approaches seems to properly satisfy the conditions for sensible waste leach modelling. Hence a "healthy compromise" to appropriately model release-transport from waste deposits is still sought. In developing such a model, which will be the subject of the following sections, one can draw on some insights from existing approaches.

4.5 The Dixon Heap Leach Model

Dixon (1992) investigated the kinetics of heap leaching of one or several solid reactants by a single dissolved reagent using an unsteady-state particle scale model which is incorporated into an unsteady-state one-dimensional heap model. Davies (1995) has extensively reviewed this model and pointed out ways of adapting it to suit the modelling of contaminant release from granular waste deposits. Since this approach is pursued further in this work, it is useful to briefly elaborate on the modelling concepts employed in Dixon's original work, including some of the steps he has taken towards expressing the model equations in a non-dimensional form.

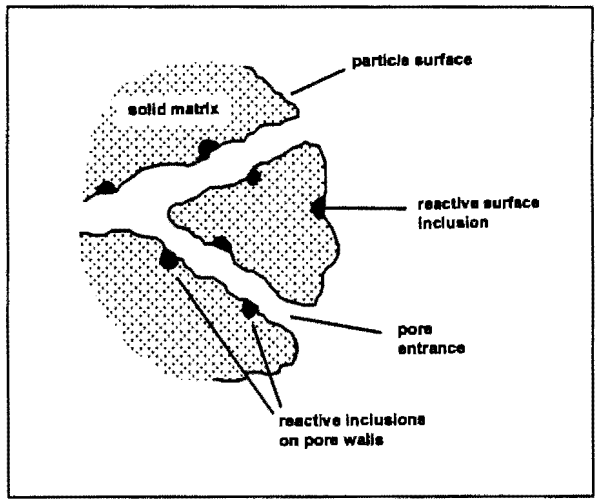

Figure 4-15: Distribution of discrete grains of solid reactive species on the pore walls (after Dixon, 1992)

As has already been pointed out in Section 4.4, one particularly interesting aspect of heap leach modelling work is the separation of diffusion-reaction within the pores of an individual particle and the diffusion of dissolved species into and out of the pores into the moving bulk fluid in which they are transported. Accordingly, in Dixon's work the equations are derived separately for a single particle and then for the heap as a whole. The particle is assumed as a porous sphere of inert material, in which grains of the reactive solid species are well distributed on the pore walls throughout the particle (Figure 4-15).

Important in this context is that the amount of leachable constituents is small relative to the matrix material and that porosity and particle size are not significantly affected through the leach process.

4.5.1 Reaction Modelling

The model is mainly concerned with specific kinetic leach reactions of a single dissolved reactant A which can react with one or several solid reactants B_i according to known stoichiometry:

$$A + \sum_i b_i B_i \rightarrow \text{dissolved products} \qquad (4.5\text{-}1)$$

where b_i is the stoichiometric coefficient. For the kinetic rate of dissolution of the solid reactant B_i the following rate expression is proposed:

$$\frac{d c_{pi}}{dt} = - k_{pi} c_{pi}^{\phi_i} c_A \qquad (4.5\text{-}2)$$

where c_{pi} indicates the solid concentration [mol/kg] of B_i in the particle pores, k_{pi} the reaction kinetic constant and ϕ_i the reaction order, the choice of which is discussed in more detail by Dixon. c_A represent the dissolved concentration of reactant A [mol/m^3], which is taken to be of first order. Dixon offers no explanation why c_A should not also be of variable oder, but it is assumed that first order was chosen for simplicity of the development to follow and that the derrivation can easily be reiterated incorporating a variable order for c_A as well.

A similar reaction term can also be written for reaction at the particle surface:

$$\frac{d c_{si}}{dt} = - \frac{3 k_{si} c_{si}^{\phi_{si}} c_{A,s}}{R \rho_t (1 - \varepsilon_p)} \qquad (4.5\text{-}2)$$

where c_{si} is the solid reactant concentration at the surface [mol/kg], R the particle radius, ρ_t the true solid density, and ε_p the particle porosity. The other parameters are defined as

before with the index s indicating that they are relating to the particle surface. It is not quite clear why there is a need for a separate rate constant for reactions on the external particle surface, since clearly both the nature of the reaction as well as its mechanism should be the same irrespective of where it occurs. Thus the reaction constant should remain the same and only the surface concentration needs to be defined separately. This aspect is discussed further in section 4.7. For clarity of the development to follow reactions at the particle surface are not considered further for the remainder of this section.

4.5.2 The Particle Pore Model

The mass balance of transport and reaction of the dissolved reactant A is given through the continuity equation (4.2-11) formulated for diffusion in radial direction in a porous spherical matrix:

$$D_{e,A}\left[\frac{\partial^2 c_A}{\partial r^2} + \frac{2}{r}\frac{\partial c_A}{\partial r}\right] - \rho_t(1-\varepsilon_p)\sum_i \frac{k_{pi} C_{pf}^{\phi_{ri}} c_A}{b_i} = \varepsilon_p \frac{\partial c_A}{\partial t} \qquad (4.5\text{-}4)$$

where $D_{e,A}$ is the effective pore diffusivity for species A. The introduction of $\rho_t(1-\varepsilon_p)$ (porous solid density) before the reactive term results from the fact that the solid concentration of B_i, in terms of which the rate equations (equation 4.5-2) are expressed, is defined in units of mass (or moles) per unit mass solid, whereas the dissolved concentration of A is expressed in mass (or moles) per unit volume liquid in touch with the solid. The ratio $\rho_t(1-\varepsilon_p)/\varepsilon_p$ would effectively represent the solid mass to liquid volume ratio present in the particle pores.

Equation (4.5-2) and (4.5-4) are sufficient to describe reaction and diffusion of A through the particle. For transport of each dissolved species i equation (4.5-4) is re-written, assuming a one-to-one molar correspondence between the solid and dissolved state:

$$D_{ei}\left[\frac{\partial^2 c_i}{\partial r^2} + \frac{2}{r}\frac{\partial c_i}{\partial r}\right] + \rho_t(1-\varepsilon_p) k_{pi} c_{pf}^{\phi_{ri}} c_A = \varepsilon_p \frac{\partial c_i}{\partial t} \qquad (4.5\text{-}5)$$

Suitable boundary and initial conditions for reactant A or any dissolved species i are:

$$c_i(r,0) = c_i^0$$

$$c_i(R,t) = c_{b,i}$$

$$\frac{\partial c_i}{\partial r}(0,t) = 0 \qquad \text{(4.5-6 a,b,c)}$$

where c_i^0 is some initial concentration (usually zero or some initial dissolved concentration) and $c_{b,i}$ is the reagent or dissolved species concentration in the bulk solution at the particle surface. For the solid constituents B_i one can further write

$$c_{pi}(r,0) = c_{pi}^0 \qquad \text{(4.5-6 d)}$$

For solution of this system Dixon suggests non-dimensionalising the system in order to group the relevant parameters of the model. The following set of dimensionless variables is defined:

$$\chi_i = \frac{c_i}{b_i c_A^0} \qquad \chi_A = \frac{c_A}{c_A^0} \qquad \text{(4.5-7 a,b)}$$

$$\chi_{b,i} = \frac{c_{b,i}}{b_i c_A^0} \qquad \chi_{b,A} = \frac{c_{b,A}}{c_A^0} \qquad \text{(4.5-7 c,d)}$$

$$\sigma_{pi} = \frac{c_{pi}}{c_{pi}^0} \qquad \delta_i = \frac{D_{e,i}}{D_{e,A}} \qquad \text{(4.5-7 e,f)}$$

$$\xi = \frac{r}{R} \qquad \tau = \frac{D_{e,A}\, t}{\varepsilon_p R^2} \qquad \text{(4.5-7 g,h)}$$

where c_A^0 is some reference reagent concentration.

The model equations (4.5-2), (4.5-4) and (4.5-5) can then be expressed in dimensionless terms:

$$\frac{d\sigma_{pi}}{d\tau} = - \kappa_{pi}\beta_i \sigma_{pl}^{\phi_{pi}} \chi_A \tag{4.5-8}$$

$$\frac{\partial^2 \chi_A}{\partial \xi^2} + \frac{2}{\xi}\frac{\partial \chi_A}{\partial \xi} - \sum_i \kappa_{pi} \sigma_{pl}^{\phi_{pi}} \chi_A = \frac{\partial \chi_A}{\partial \tau} \tag{4.5-9}$$

$$\delta_i \left[\frac{\partial^2 \chi_i}{\partial \xi^2} + \frac{2}{\xi}\frac{\partial \chi_i}{\partial \xi}\right] - \sum_i \kappa_{pi} \sigma_{pl}^{\phi_{pi}} \chi_A = \frac{\partial \chi_i}{\partial \tau} \tag{4.5-10}$$

which defines the following two dimensionless groups:

$$\beta_i = \frac{\varepsilon_p b_i c_A^0}{\rho_t (1-\varepsilon_p) c_{pi}^0} \tag{4.5-11}$$

$$\kappa_{pi} = \frac{\rho_t (1-\varepsilon_p) k_{pi} (c_{pi}^0)^{\phi_{pi}} R^2}{b_i D_{e,A}} \tag{4.5-12}$$

The boundary conditions both for A and i become

$$\chi_i(\xi,0) = 0$$

$$\chi_i(1,\tau) = \chi_{i,b} \tag{4.5-13 a-c}$$

$$\frac{\partial \chi_i}{\partial \xi}(0,\tau) = 0$$

and

$$\sigma_{pi}(\xi,0) = 1 \qquad (4.5\text{-}13\ d)$$

The dimensionless group β represents a stoichiometric ratio, which indicates the reagent strength relative to the initial concentration of solid reactant i. For a particle of given porosity a value of $\beta_i = 1$ would indicate there is sufficient initial reagent concentration to dissolve all of the particular B_i (Davies, 1995). κ_{pi} represent the ratio of kinetic reaction rate to the rate of diffusion within the particle pores and in this sense becomes a Damköhler number of the second type (Aris, 1975). Equations (4.5-8) to (4.5-10) thus describe in non-dimensionalised form the reaction diffusion process within the pores of a single spherical particle of radius R in terms of two characteristic numbers β_i and κ_{pi}.

4.5.3 Bulk Transport Model

Dixon proceeds further by describing transport of the leachate on the heap level as a one-dimensional advection process through a (porous) column of particles. Reactant and reaction products interact with this bulk flow on the particle surface and through diffusion into and out of the particle pores. This is achieved by formulating the general transport equation (4.2-11) in direction (z), indicating height within the column, considering advection as the only mode of transport (i.e. ignoring dispersion effects altogether) and replacing the source/sink term with the combined effects of surface reaction and surface pore diffusion for product species i:

$$- v_s \frac{\partial c_{b,i}}{\partial z} + \frac{3(1-\varepsilon_b)}{R}\left[k_{si}\, c_{si}^{\phi_{si}}\, c_{b,A} - D_{e,i}\left(\frac{\partial c_i}{\partial r}\right)_{r=R}\right] = \varepsilon_b \frac{\partial c_{b,i}}{\partial t} \qquad (4.5\text{-}14)$$

and for the reactant A:

$$- v_s \frac{\partial c_{b,A}}{\partial z} - \frac{3(1-\varepsilon_b)}{R}\left[\sum_i \frac{k_{si}\, c_{si}^{\phi_{si}}\, c_{b,A}}{b_i} + D_{e,A}\left(\frac{\partial c_A}{\partial r}\right)_{r=R}\right] = \varepsilon_b \frac{\partial c_{b,A}}{\partial t} \qquad (4.5\text{-}15)$$

where ε_b represents the heap porosity, i.e. the voidage between the particles in the bed excluding the internal particle porosity. In this form the equations only consider release from a single particle size of radius R. Dixon has indicated how this can be easily extended to account for a distribution of particle sizes, by introducing a further summation over the combined surface reaction - pore diffusion term. This has been elaborated in more detail by Davies (1995).

The set of boundary conditions for equation (4.5-14) is

$$c_{b,i}(z,0) = 0 \qquad c_{b,i}(0,t) = 0 \qquad (4.5\text{-}16\ a,b)$$

and for (4.5-15)

$$c_{b,A}(z,0) = 0 \qquad c_{b,A}(0,t) = c_A^0 \qquad (4.5\text{-}17\ a,b)$$

It must be pointed out here, that the bulk level equations appear somewhat simplistic. The reason given by Dixon for not including a dispersion term in equations (4.5-14) and (4.5-15) is the assumption of ideal plug flow, implying the likely effects of dispersion are too minor to warrant inclusion. The validity of this assumption is not further substantiated. Likewise mass transfer between bulk fluid and particle surface and pores is assumed ideal, i.e. film effects are negligible, which again is not further substantiated.

Defining the further dimensionless variables:

$$\zeta = \frac{z}{Z} \qquad \vartheta = \frac{v_s t}{\varepsilon_b Z} \qquad (4.5\text{-}18\ a,b)$$

where Z is the total height of the column, the model equations (4.5-14) and (4.5-15) can be expressed as

$$-\frac{\partial \chi_{b,i}}{\partial \zeta} - \omega\left[\delta_i\left(\frac{\partial \chi_i}{\partial \xi}\right)_{\xi=1} - \frac{\kappa_{si}}{3}\sigma_{si}^{\phi_{si}}\chi_{b,A}\right] = \frac{\partial \chi_{b,i}}{\partial \vartheta} \qquad (4.5\text{-}19)$$

and

$$-\frac{\partial \chi_{b,A}}{\partial \xi} - \omega\left[\left(\frac{\partial \chi_A}{\partial \xi}\right)_{\xi=1} + \sum_i \frac{\kappa_{si}}{3}\sigma_{si}^{\phi_{si}}\chi_{b,A}\right] = \frac{\partial \chi_{b,A}}{\partial \vartheta} \qquad (4.5\text{-}20)$$

which defines the dimensionless group ω:

$$\omega = \frac{3(1-\varepsilon_b)D_{e,A}Z}{v_s R^2} \qquad (4.5\text{-}21)$$

which is discussed in some more detail in section 4.5.4 below. The boundary conditions (4.5-16 a, b) and (4.5-17 a, b) become

$$\chi_{b,i}(\zeta,0) = 0 \qquad \chi_{b,i}(0,\vartheta) = 0 \qquad (4.5\text{-}22\ a,b)$$

and

$$\chi_{b,A}(\zeta,0) = 0 \qquad \chi_{b,A}(0,\vartheta) = 1 \qquad (4.5\text{-}22\ c,d)$$

This defines, in non-dimensionalised form, the transport of dissolved species A and i through the bed with direct interaction at the surface of particles (here taken as uniform size, although this can be expanded to size distributions). In combination with the equations governing the diffusion reaction within the spherical particles (equations (4.5-8) to (4.5-13)) within a suitable numerical scheme effective modelling of heap leaching can be achieved as Dixon (1992) has demonstrated in his work.

4.5.4 Some Critical Comments

Some critical comments need to be levelled at the dimensionless parameter ω, which represents the ratio of porous diffusion of reactant A to bulk convective flow, and thus, according to Dixon, corresponds to the inverse of the Peclet number Pe for mass transfer.

This is, however, an unusual definition of the Peclet number, since here two transport phenomena are related to each other which are in fact unrelated. In the conventional definition of Pe,

$$Pe = Re \cdot Sc = \frac{v\,d}{D^*} \qquad (4.5\text{-}23)$$

convection (indicated through v) over a characteristic length d is set in relation to diffusion (indicated through molecular diffusivity D*). Thus the magnitude of the Peclet number suggests, which of the two transport mechanism dominates in a given system. This has already been indicated in the discussion of the effect of mechanical dispersion effects relative to molecular diffusion in Section 4.2 and especially Figure 4-10.

Dixon's ω, however, relates bulk convection (expressed through v_s and bed length Z) to pore effective diffusion (characterised through D_{eA} and particle radius R). The remaining terms in the definition of ω (equation 4.5-21), $3(1-\varepsilon_b)/R$, correspond to the total particle surface area to bulk volume ratio of the given bed.

In essence ω thus relates two transport processes that occur in *different* systems - bulk and particle pores - which are not directly related. Only if the number relates convection to diffusion within the *same* system would this parameter have real physical significance. This would be the case, had Dixon allowed for bulk dispersion.

However, the alleged correspondence of ω to the system Peclet number is not entirely incorrect, since the effective pore diffusivity $D_{e,A}$ is directly related the molecular diffusivity D_A^* (see equation (4.2-5)), as is the bulk diffusivity (see equation (4.2-8)). Thus, indirectly, ω is indeed related to the Peclet number for bulk flow, but the actual physical significance of ω remains dubious. By way of explaining discrepancies in experimental to modelled results, Dixon admits that ω is in fact a function of system parameters, such as bulk flow rate, particle size distribution etc. He further introduces an empirical model for the dependency of an apparent value for ω, termed ω_{app}, on the system

Reynolds number, thus indirectly allowing for dispersion effects (i.e. departure from the ideal flow assumption made earlier). It is felt that the inclusion of a dispersion term in the governing bulk flow equations and/or surface diffusion effects at the particle level would have accounted for this correction in a more meaningful way. Further discussion of the potential significance of Peclet numbers in porous flow systems is given in Section 4.5.2.

The non-dimensional approach to the model equations also needs to be examined more critically. Its obvious attractiveness is to lump model parameters into physically significant dimensionless groups, thus allowing system comparison, independent of scale. In his work, Dixon compares a number of modelling scenarios on this basis, without scale parameters, such as particle size and porosity, entering into it. Modelling the heap as a chemical reactor, studies of heap effectiveness as a function of the non-dimensional parameters β_i, κ_i and ω allows for easy optimisation of the overall process.

In the modelling of real systems, however, little is gained by such an approach, since all physical parameters that inform β_i, κ_i and ω need to be determined individually. Davies (1995) has shown how the model equations can be used to fit results from a small scale leach experiment by optimising κ_i. This, however, first requires the individual pre-determination of the rate constant k from the experiment, so that effectively only the effective diffusivity $D_{e,A}$ is optimised for. Thus, non-dimensionalising the model equations offers no real benefit in this context. In actual fact, through the definition of the dimensionless time τ (equation (4.5-7 h)) requiring a value for $D_{e,A}$, fitting experimental data becomes unnecessarily cumbersome if $D_{e,A}$ itself is the target variable for optimisation. For this reason Dixon has later suggested partial non-dimensionalisation of the model equations keeping the time variable dimensional (Dixon, 1996). The dimensionless groups defined previously are changed to a number of "time constants" as is demonstrated here for the modified form of equation (4.5-10):

$$\frac{\delta_i}{\tau_D}\left[\frac{\partial^2 \chi_i}{\partial \xi_2} + \frac{2}{\xi}\frac{\partial \chi_i}{\partial \xi}\right] + \frac{\beta_i \sigma_i^{\phi_i} \chi_A}{\tau_R} = \frac{\partial \chi_i}{\partial t} \qquad (4.5\text{-}24)$$

with

$$\tau_{R,i} = \frac{1}{k_i c_A^0 (c_{pi}^0)^{\phi_{pi}-1}} \tag{4.5-25}$$

and

$$\tau_D = \frac{\varepsilon_p R^2}{D_{e,A}} \tag{4.5-26}$$

While this method has the same capacities as the fully non-dimensionalised approach, it allows for easy handling of real time data. In effect however, the partial non-dimensionalisation reduces to a simple normalisation of the space and concentration variables, with the only benefit being ease of comparative studies. While it is straightforward to normalise the space variables r and z against particle radius R and bed height Z, respectively, normalisation of concentration variables remains complicated. In the Dixon model, with its simple and clearly defined stoichiometric interdependency of the species involved this is relatively easy (see equation 4.7-7 a-d), allowing expression of all reference concentrations in terms of the feed concentrations of a single reagent species. On the other hand, in complex systems with many interacting species, which will be the focus of the development to follow (Sections 4.6 and 4.7), such simple relationships do not exist and selection of suitable reference concentrations may become a matter of arbitrary choice. In this case even the partial non-dimensionalisation of model equations offers no benefit in the application of the model.

It was therefore decided to not further pursue non-dimensionalisation as part of model development at this stage, since the focus of work presented here is on establishing and confirming the usefulness of a rigorous modelling approach in extracting parameters from experimental data and applying these in the prediction of the behaviour of existing waste heap scenarios. It should be stated, however, that the non-dimensional approach does merit further consideration when conducting studies on optimisation of waste heap design parameters with a view to minimising leachate generation. This is, however, beyond the scope of the present work.

4.6 Formulation of the Fundamental Waste Leach Model

As has been indicated in the preceding sections, Dixon's heap leach model was considered a good starting point for the development of model equations describing the release of contaminants from heaps of granular mineral waste. The model involves separating the process into two domains, reaction-diffusion at the level of individual particles and diffusion-convection at the heap level.

4.6.1 Particle Level Model

The particle is modelled as a porous sphere. Reaction can take place both on the internal pore walls and the external particle surface. Transport of dissolved species is by diffusion only. Hence the model concept of equation (4.4-2) is retained here:

$$D_{e,i}\left[\frac{\partial^2 c_i}{\partial r^2} + \frac{2}{r}\frac{\partial c_i}{\partial r}\right] + \varepsilon_p \sum_j R_i^j = \varepsilon_p \frac{\partial c_i}{\partial t} \qquad (4.6\text{-}1)$$

using the same notation for the reactive term as was introduced in Section 4.3 (equation (4.3-1)). As the reactive term is formulated as rate of production/consumption of species i per unit *fluid* volume, the factor ε_p before the reactive term is introduced to relate this to the *total* particle volume in terms of which the equation is formulated (see also Figure 4-7).

In departure from Dixon's model, which was preoccupied with distinct kinetic leach reactions, the model has to provide for a number of reaction types, both kinetic and equilibrium, as has been highlighted in Section 4.3. Equation (4.6-1) is formulated in terms of one particular dissolved species i, so the reactive term has to include all reactions j in which species i is either consumed or produced. For each species considered in the system, the equation has to be re-written with the respective reactive terms.

As has already been indicated in Section 4.3, there are essentially two paths for incorporating the contributions determined from the individual reaction models. Kinetic reactions, such as those formulated by Dixon are simply expressed as in equation (4.3-2):

$$R_i^{kin} = \frac{dc_i}{dt} = f(k_{kin}, c_i, c_x, \ldots) \tag{4.6-2}$$

For all other types of equilibrium reactions only indirect formulation of a rate term is possible, as was indicated in equation (4.3-6). The shift in equilibrium through the introduction of some imbalance (change in the dissolved concentration following diffusive migration or competing kinetic reaction) can be found by solving the appropriate equilibrium model. If the concentration shift in species i due to equilibrium reaction j is expressed as Δc_i^j, it can be incorporated in a reaction term as

$$R_i^{equil} = \frac{\Delta c_i^j}{\Delta t} \tag{4.6-3}$$

assuming this shift occurs kinetically fast within a time interval Δt. This in effect presumes that equilibrium reactions proceed in discrete time intervals, with the overall diffusion-reaction process in the particle pore progressing in time via a series of equilibrium steps. This indirect method precludes an analytical solution to the model equations which will have to be obtained by numerical methods. An in-depth discussion of reaction models and details of a unified method for their incorporation into a numerical model solution scheme is given in Section 4.7.

4.6.2 Particle Surface Model

Equation (4.6-1) in combination with the suitable reaction models describes the reaction-diffusion process within the pores of a spherical particles. In the Dixon model this is directly linked with the bulk transport equation, assuming no further mass transfer resistance between particle surface and the moving bulk fluid. In practice this assumption is not always realistic.

Boundary layer theory suggests that there exists a zone or "film" near a solid surface in which a concentration profile exists between surface and bulk fluid concentrations some distance away from the surface (Figure 4-16). The net rate of mass transfer across this zone is a function not only of the concentration gradient between surface and bulk, but also of bulk flow conditions and the local geometry. The resistance to mass transfer across this film is usually expressed in terms of a simplified "film" mass transfer coefficient k_c:

$$N_i^{film} = k_c(c_{b,i} - c_{s,i}) \tag{4.6-4}$$

where $c_{B,i}$ represents the bulk concentration and $c_{S,i}$ the surface concentration of species i.

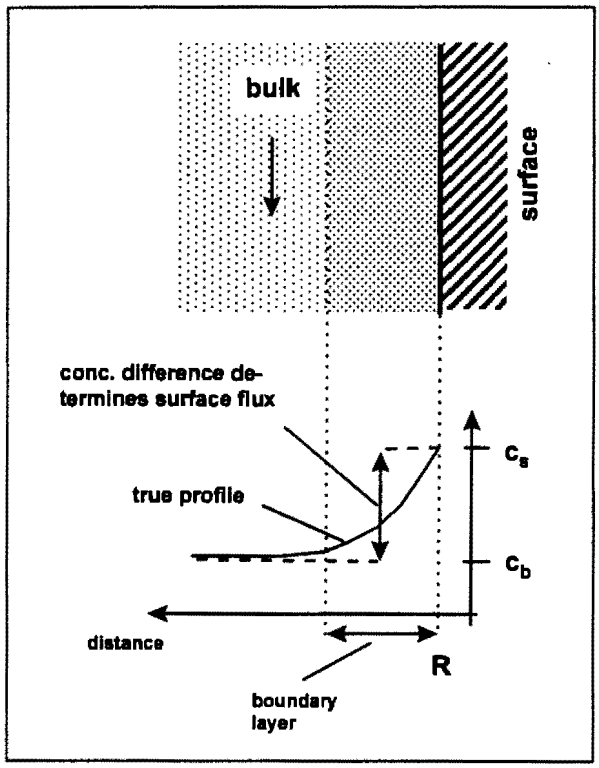

Figure 4-16: Concentration boundary layer between particle surface and bulk fluid.

Values for the film mass transfer coefficient k_c can be obtained from theoretical considerations only for simple geometries, otherwise from experiments, whereby experimental parameters are usually normalised in terms of characteristic dimensionless numbers and correlations between these are established for more complex geometries. Due to the analogy of heat and mass transfer (Bird *et al.*, 1960) at this level, many such correlations established for heat transfer can also be used for mass transfer problems. Commonly one finds k_c described either in Sherwood number (Sh):

$$Sh = \frac{k_c d}{D^*} = f(Re,Sc) \tag{4.6-5}$$

or in terms of the Chilton-Colburn factor j_D:

$$j_D = Sh\ Re^{-1}\ Sc^{-\frac{1}{3}} = \frac{k_c}{v_{sp}}\left(\frac{\mu_f}{\rho D^*}\right)^{\frac{2}{3}} = f(Re) \qquad (4.6\text{-}6)$$

So, for example, for mass transfer from particles in a packed bed one can find (Bird *et al.*, 1960):

$$j_D = 0.91\ Re^{-0.51}\ f_{sh} \quad (Re < 50) \qquad (4.6\text{-}7)$$

where f_{sh} represents a particle shape factor.

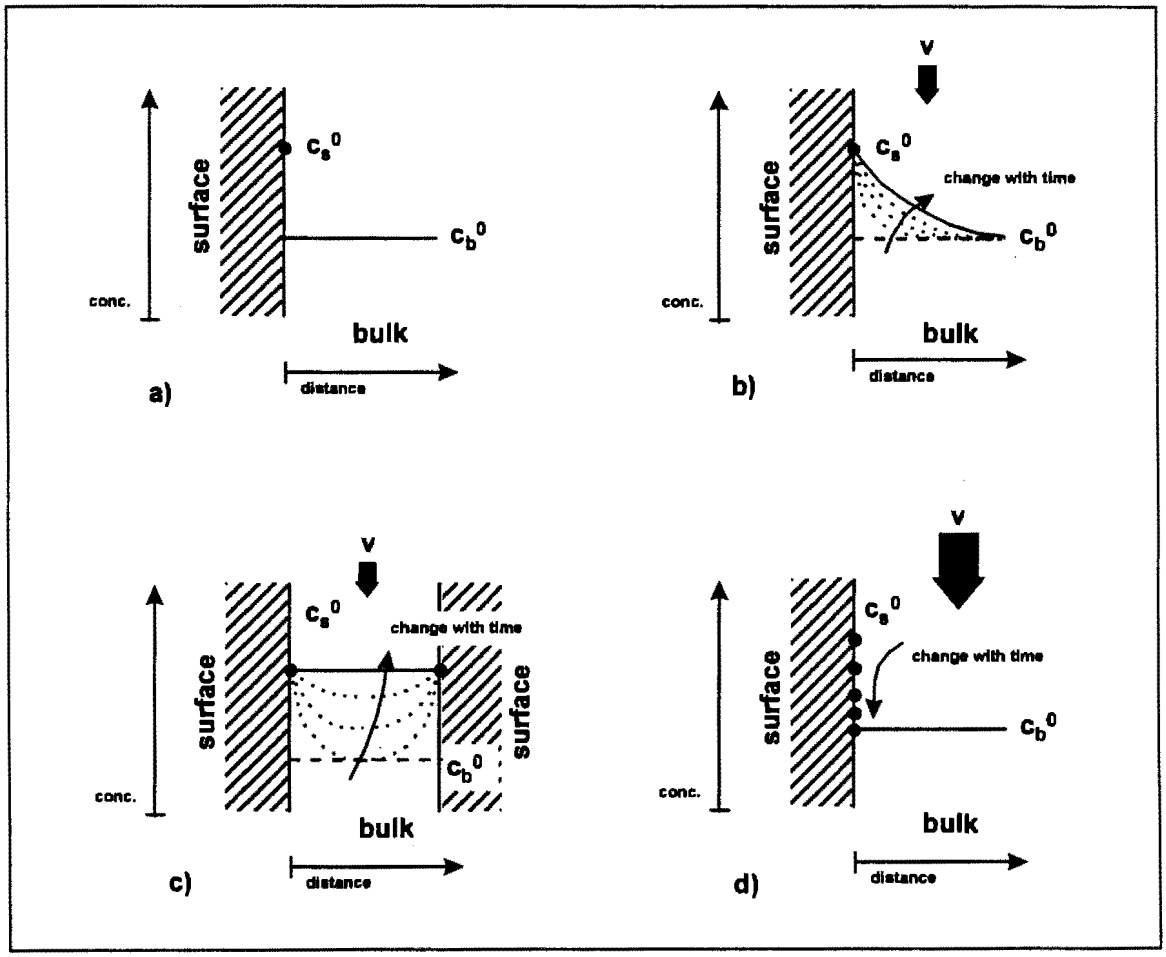

Figure 4-17: Establishment of surface-bulk profiles. a) initial gradient; b) film profile; c) bulk equalisation due to limited bulk volume; d) surface equalisation due to rapid bulk removal

The film concept is based on the assumption that mass transport from the surface is into a large body of fluid in which case the rate of transport does not significantly affect the rate of change of the bulk concentration some distance away from the surface, as is illustrated in Figure 4-17. Starting from an initial concentration gradient (Figure 4-17a), a steady state profile is established as indicated in Figure 4-17b. There are, however, two limiting cases to this concept, where film transport does not apply.

The first case occurs if the body of fluid is small, as may be the case in the narrow pores of a packed bed. In this case the net transport from the surface results in a rapid increase of the bulk fluid concentration and thus in an elimination of the concentration gradient between surface and bulk and consequently the bulk concentration becomes equal to that of the bulk (Figure 4-17c).

The second limitation is reached if bulk flow velocities are high and thus the rate of transport from the surface becomes high. In this case the surface concentration is depleted rapidly resulting in an elimination of the concentration gradient between surface and bulk (Figure 4-17d). Consequently also in this case the surface concentration can be assumed to equal that of the bulk.

In the modelling of transport through a packed bed there exists the possibility of flow situations where neither of these limiting cases is given. For example, in the case of saturated groundwater flow through a bed of pebbles, the interstitial pore volume may be large enough and flow velocities low enough to maintain a concentration gradient between surfaces and bulk.

It would be useful to identify situations which fall between the two limiting cases by some system characteristic number. Best suited would appear to be the Peclet number (Pe), which relates convective to diffusive effects. High values would indicate high seepage velocities and consideration of film diffusion effects may not be required. Furthermore, if the characteristic length d in the Peclet number was replaced by the ratio of bulk volume

to surface area, a better indicator might be obtained whether the body of fluid can indeed be considered as "large" enough to maintain a surface-bulk concentration gradient:

$$Pe = \frac{v\,d}{D^*} = \frac{v_{sp}}{D^*}\frac{\overline{R}}{3(1-\varepsilon_b)} \qquad (4.6\text{-}8)$$

where $\overline{R}$ represents the average particle radius. For low values of this modified Peclet number (small seepage velocities, small particles, low bulk voidage) small pore volumes are in contact with a large particle surface area and the equalisation between bulk and surface concentrations is highly likely.

The question that remains unanswered at this point is which values of the modified Peclet number constitute the upper and lower limits between which film transport is a relevant mechanism. This could probably be established from a detailed experimental study, but is not pursued further here. It is, however, interesting to note that the definition of Peclet number proposed in equation (4.6-8) is similar to the factor ω defined by Dixon (see Section 4.5.3 , equation (4.5-21)). Although, as was critically remarked in Section 4.5.4, the physical significance of ω is somewhat dubious, the discrepancy between Dixon's (ideal case) ω and that apparent from experimental results, ω_{app} , could be taken as an indication that a surface film resistance was indeed present in his studies. In his experiments Dixon used relatively coarse particles ($\overline{R}$ = 5-8 mm), but moderate bulk flow velocities (v_{sp} = 2.3 - 5.6 $\cdot 10^{-5}$ m/s) resulting in a range of the modified Peclet number from 34 to 130. This may be taken as a first indication of the range where film mass transfer may be significant.

Thus, clearly, there exist cases where diffusion across a surface film can influence the transport of species from the particle surface into the moving bulk fluid. For these cases it is then necessary to formulate an additional equation which can incorporate this effect into the overall reaction-transport model. For this it is assumed that there exist local zones of stagnant fluid "trapped" on the surface of particles. This is particularly valid if the particles are angular in shape and exhibit a certain degree of surface roughness.

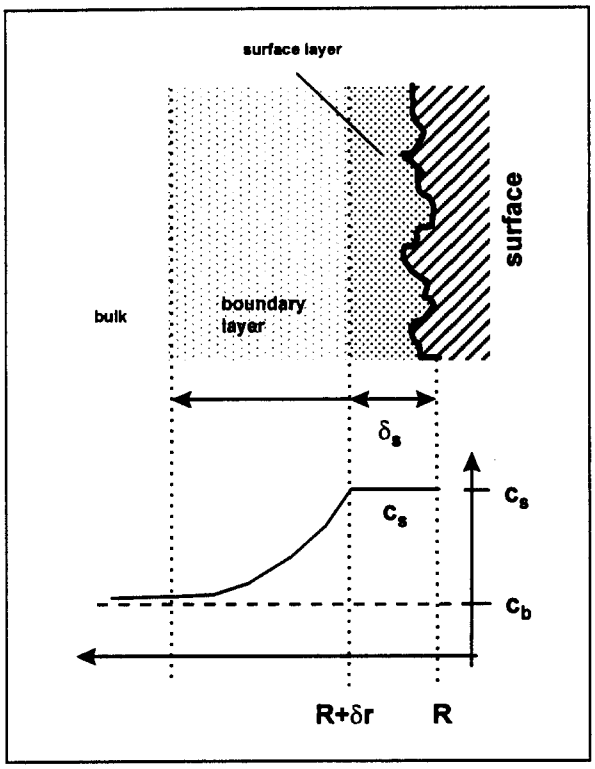

Figure 4-18: Close-up of particle surface, showing a fluid surface layer "trapped" in surface unevenness

Thus a thin, stagnant fluid "hull" exists around the particle separating it from the moving bulk fluid, as is shown in Figure 4-18. This hull is seen to represent a separate surface layer the only requirement of which is that it be sufficiently thin to allow assumption of constant concentration throughout, i.e. concentration changes as a result of mass transport from either side of the layer (particle surface and surrounding bulk fluid) are more or less instantaneous across the layer.

For clarity it should be pointed out that this surface layer is distinctly different from the boundary layer or diffusion film discussed before. While the former describes a stagnant thin zone at the physical particle surface (Figure 4-18), the boundary layer describes concentration and flow profiles in the bulk fluid near the stagnant particle surface (Figure 4-16) and no statement about its actual thickness is made. For the surface layer, however, we need to define the thickness of this surface layer δ_s. Then we can write for continuity across the surface layer:

$$k_c(c_{b,i} - c_{s,i}) - D_{e,i}\varepsilon_p\left(\frac{\partial c_i}{\partial r}\right)_R + \delta_s \sum R^j_{s,i} = \delta_s \frac{\partial c_{s,i}}{\partial t} \qquad (4.6\text{-}9)$$

where the first term on the LHS describes the film mass transfer flux of species i from the bulk as indicated in equation (4.6-4), the second term the diffusive flux into the particle pores (and therefore expressed in terms of the effective pore diffusivity), and the third term sums all surface reactive terms involving i. The RHS represents the accumulation of i in the surface layer of thickness δ_s.

It would be more correct to understand δ_s as the ratio of the fluid volume of the surface layer to particle surface area, which is equal to the layer thickness. The choice of a value for δ_s is fairly arbitrary as long as it is small. The argument here is that the rate of transport across the surface is large relative to accumulation within it if the volume is small, and hence the accumulation term has little effect on the overall balance. If, for example, some measure of the surface roughness exists (very similar to that measured for pressure drop calculation in pipes) then this value could be used for δ_s.

The pore flux term of equation (4.6-9) describes the flux into or out of the particle pores as governed by the concentration gradient at the particle surface and thus retains the definition given by Dixon (equation (4.5-14)). Through the introduction of the surface equation (4.6-9), this term no longer describes the flux of i from the pores into the bulk fluid but merely from inside the pores to the surface, which is conceptually more correct.

The reactive terms $R_{s,i}^{j}$ are defined as rates of production of species i per unit surface volume due to reaction j [mol/m^{3}s], acknowledging that the surface layer is conceptually in contact only with the particle surface (as opposed to a discrete volume, as was conceptualised in the particle pores). Therefore a different definition of solid surface concentrations is required, which is not necessarily related to the volumetric solid concentration defined before. The surface reactive term will be discussed in more detail in Section 4.7. It should be pointed out again that the inclusion of the surface layer model in the overall reaction-transport model is optional, depending on whether such surface effects are relevant in each particular scenario considered.

4.6.3 Bulk Flow Transport Model

The basic transport equation for flow through a porous bed of particles has already been given in equation (4.2-11). As illustrated in Section 4.4, various modelling strategies employ this equation to various degrees of rigour. For example, the Dixon approach

ignores the effects of dispersion on the assumption of ideal flow, although this was later put into question by experimental results (see Section 4.5.4). It was therefore decided to employ the unmodified, one-dimensional formulation of equation (4.2-10) as the basic transport model for bulk flow transport in waste deposit heaps. Although a 3-dimensional model would of course allow more rigorous modelling of the transport process, it is assumed here that the principal direction of flow in heaps is downwards and that transverse transport is small. Also, in order to keep the overall model reasonably simple, it was decided that expansion into higher dimension is not crucial at this stage.

Re-stating equation (4.2-10) in terms of the heap height variable (z) thus gives:

$$- v_s \frac{\partial c_{b,i}}{\partial z} + D_h \frac{\partial^2 c_{b,i}}{\partial z^2} + Q_{c,i} = \varepsilon_b \frac{\partial c_{b,i}}{\partial t} \qquad (4.6\text{-}10)$$

where the subscript b indicates concentrations in the bulk fluid (as opposed to those in the pores or on the surface). ε_b is the bulk fluid volume fraction, i.e. the fractional volume of the bed that is filled with fluid (excluding particle pores) and thus corresponds to the moisture content θ introduced in Section 4.1 (equation (4.1-9)). ε_b can be perceived as the product of bulk bed porosity (i.e. excluding particle porosity) ε_h, also known as heap voidage ratio, and the saturation factor f_{sat}, which ranges from 0 for completely dry to 1 for fully saturated pores:

$$\varepsilon_b = \varepsilon_h f_{sat} = \frac{V_{pores}}{V_{pores} + V_{particles}} f_{sat} \qquad (4.6\text{-}11)$$

The source/sink term $Q_{c,i}$ in equation (4.6-10) needs to be replaced by a flux term indicating the transport of species i from the particle film boundary into the bulk and summing over the particle population in the bed. Thus equation (4.6-10) becomes:

$$- v_s \frac{\partial c_{b,i}}{\partial z} + D_h \frac{\partial^2 c_{b,i}}{\partial z^2} - \sum_n \frac{3(1-\varepsilon_h) w^{(n)}}{R^{(n)}} k_{c,i} (c_{b,i} - c_{s,i}^{(n)}) = \varepsilon_b \frac{\partial c_{b,i}}{\partial t} \qquad (4.6\text{-}12)$$

where the counter (n) indexes particle size class and $w^{(n)}$ indicates the mass fraction of particles in this size class. It should be pointed out that for a homogeneous material with

constant density the mass fraction of particles in a particular size class corresponds to its volume fraction, but mass fractions are more easily measured.

Equation (4.6-12) presumes that the particle surface constitutes the only source/sink for any species i relative to the bulk flow. While this is correct for any type of reaction involving interactions with a solid surface, such as adsorption, dissolution or leaching, it does not hold true for interactions between species within the dissolved phase, such as hydrolysation, complexation and those involving dissolved gases. Where such bulk reactions may be of significant consequence to the overall leach behaviour of the heap it is necessary to also include reaction terms in the overall bulk level equation:

$$- v_s \frac{\partial c_{b,i}}{\partial z} + D_h \frac{\partial^2 c_{b,i}}{\partial z^2} + \varepsilon_b \sum_j R^j_{b,i} - \sum_n \frac{3(1-\varepsilon_h) w^{(n)}}{R^{(n)}} k_{c,i} (c_{b,i} - c^{(n)}_{s,i}) = \varepsilon_b \frac{\partial c_{b,i}}{\partial t} \qquad (4.6\text{-}13)$$

where $R^j_{b,i}$ represent the individual reactive contributions to the change of bulk concentration. Again the same reaction models that can be used for pore and surface reactions (excluding those involving a solid species) can be incorporated into the model equation, which is discussed further in Section 4.7.

For situations where surface film diffusion is not considered to be a relevant mechanism (as discussed in Section 4.6.2), i.e. where bulk concentration can be taken to equal surface concentration, the summation term in equation (4.6-13) needs to be replaced by the summation of the pore diffusive fluxes and the surface reaction terms:

$$- v_s \frac{\partial c_{b,i}}{\partial z} + D_h \frac{\partial^2 c_{b,i}}{\partial z^2} + \varepsilon_b \sum_j R^j_{b,i} - \sum_n \frac{3(1-\varepsilon_h) w^{(n)}}{R^{(n)}} D_{ei} \left(\frac{\partial c_{p,i}}{\partial r} \right)_{R^{(n)}} + \varepsilon_b \sum_j R^j_{s,i} = \varepsilon_b \frac{\partial c_{b,i}}{\partial t} \qquad (4.6\text{-}14)$$

with the surface reaction term $R^j_{s,i}$ as discussed before. Again, reference to Section 4.7 is made where reaction mechanisms at pore, surface and bulk level are discussed in detail.

4.6.4 Batch Model

Although the central model equations were derived for the overall process of leachate generation and transport in a heap, they can easily be modified to describe the process of batch leaching in a stirred tank reactor (STR). This is particularly useful in the context of establishing reaction parameters, such as kinetic and adsorption constants, for a particular waste material from laboratory scale leach tests. The particle level processes should remain the same within these as they would be in a full scale heap scenario, with only the process on bulk level being different. With the model suitably adapted, the particle level parameters can be extracted from suitable batch leach tests and then be incorporated into the full scale model without loss of applicability.

The process in an optimally operated STR assumes good mixing between the particles and the bulk fluid, i.e. there should be no external mass transfer resistance between the particle surface and the bulk solution and the bulk concentration of any dissolved species is the same throughout, i.e. there are no concentration gradients within the bulk fluid. In this context only the particle level equation (equation (4.6-1)) applies as before, but the surface equation (4.6-9) is replaced by a bulk solution mass balance and the heap transport equation falls away altogether.

Hence we have on the particle level as before:

$$D_{e,i}\left[\frac{\partial^2 c_i}{\partial r^2} + \frac{2}{r}\frac{\partial c_i}{\partial r}\right] + \varepsilon_p \sum_j R_i^j = \varepsilon_p \frac{\partial c_i}{\partial t} \qquad \text{(4.6-1) or (4.6-15)}$$

with all parameters as defined in Section 4.6.1.

On the bulk level we can write

$$- V_{part} \sum_n w^{(n)} \frac{3 D_{e,i}}{R^{(n)}} \left(\frac{\partial c_{p,i}}{\partial r}\right)_{R^{(n)}} + V_{liq} \left[\sum_j R_{s,i}^j + \sum_j R_{b,i}^j \right] = V_{liq} \frac{d c_{B,i}}{dt} \tag{4.6-16}$$

where V_{part} is the total volume the particles take in the STR (including pore volume) and V_{liq} is the bulk fluid volume (excluding fluid help up in pores).

Since the total particle surface is now in well mixed contact with the entire fluid volume, the thin surface layer conceptualised in Section 4.6.2 falls away with the entire bulk fluid effectively becoming the surface volume in the STR case. It is for this reason that in above equation (4.6-16) the surface reactive terms $R_{s,i}^j$ are not summed with the pore contributions from the individual particle size classes, but taken as a total surface contribution, since the surface concentration will be the same for all particle size and is equal to the bulk concentration.

Thus the layer thickness δ_s, which was defined as the ratio of surface volume to surface area at the particle level, could be replaced by

$$\delta_{STR} = \frac{V_{liq}}{A_{part}} = \frac{V_{liq}}{V_{part}} \frac{1}{\sum_n \frac{3w^{(n)}}{R^{(n)}}} = \frac{M_{part}}{M_{liq}} \frac{\rho_f}{\rho_t (1 - \varepsilon_p)} \frac{1}{\sum_n \frac{3w^{(n)}}{R^{(n)}}} \tag{4.6-17}$$

where the ratio M_{part}/M_{liq} represents the mass solid to liquid ratio (S:L ratio) commonly encountered in batch experiments, with ρ_f the fluid mass density (usually taken as 1000 kg/m^3 for water). While δ_{STR} does not appear in equation (4.6-16) it is used in the calculation of the reaction contributions R_{si}^j, which is elaborated in more detail in Section 4.7. Equation (4.6-16) can now be used to model leach tests conducted in a batch laboratory experiment and thereby extracting various model parameters by suitable optimisation.

4.6.5 Boundary and Initial Conditions

The pore and bulk level equations (4.6-1) and (4.6-12,13 or 14) are partial differential equations of concentration of second order in space and of first order in time dimensions. As such they require two boundary and one initial conditions each. The surface level equation (4.6-9) and batch model equation (4.6-16) are differential equations of first order in time only and hence require one initial condition. These can be defined as follows.

Pore level equation:

$$c_{p,i}(r,0) = c^0_{p,i} \qquad c_{p,i}(R,t) = c_{s,i} \qquad \left.\frac{\partial c_{p,i}}{\partial r}\right|_{0,t} = 0 \qquad \text{(4.6-18 a-c)}$$

The initial condition (4.6-18a) requires that the initial solution concentration of each species i in the pore solution must be known. This is usually achieved by assuming it is zero or corresponds to some initial equilibrium condition which needs to be determined. This is discussed further in the context of reaction modelling in Section 4.7. The surface boundary condition (4.6-18b) states that the pore concentration at the surface corresponds to the surface concentration for each species i. The second pore level boundary condition (4.6-18c) suggest that the concentration gradient at the centre of the sphere is zero because of total symmetry at this point.

Surface level equation:

$$c_{s,i}(t-0) = c^0_{s,i} \qquad \text{(4.6-19)}$$

The initial condition for the surface level equation simply suggests that the initial surface concentration is known. By similar argument to above this could be either zero or some pre-determined equilibrium value.

Batch model equation:

$$c_{b,i}(t = 0) = c^0_{b,i} \tag{4.6-20}$$

Similar to the initial condition for the surface level equation, the batch model equation assumes the initial bulk concentrations must be known, either by equilibrium calculations or from initial feed concentrations in the liquid charge to the STR.

Bulk level equation:

$$c_{b,i}(z,0) = c^0_{b,i}$$

$$v_s c_{feed,i} = v_s c_{b,i}\Big|_{z=0} - D_h \frac{\partial c_{b,i}}{\partial z}\Big|_{z=0} \tag{4.6-21 a-c}$$

$$v_s c_{b,i}\Big|_{z=Z} - D_h \frac{\partial c_{b,i}}{\partial z}\Big|_{z=Z} = v_s c_{exit,i}$$

The initial condition for the bulk level equation (4.6-21a) again states that the initial concentration of each species i must be known throughout the bulk fluid. The inlet boundary condition (4.6-21b) states that the concentration at the influx of species i in the feed liquor into the column at $z=0$ is equal to the flux of i transport further into the column by the combination of convection and dispersion. Likewise the exit boundary condition (4.6-21c) at $z=Z$ states that the flux to the bottom of the column of i by a combination of convection and diffusion is equal to the flux of liquor removed from the bottom of the column. It should be pointed out that both inlet and exit boundary conditions are variable and depend on the geometric scenario that is being modelled. Equations (4.6-21b) and (4.6-21c) describe the case where the feed liquor is dripped onto the bed and the effluent drips away from the bottom of the bed, which describes the scenario used in some of the lysimeter experiments employed in this study (see Section 5.3). For other scenarios, for example the continuous migration of leachate from a waste deposit into the underlying soil, the boundary conditions need to be formulated accordingly.

4.7 Multiple Reaction Modelling

Types of reactions that require consideration in the modelling of contaminant release from waste particles have already been discussed in Section 4.3. Ways of incorporating various reaction models into an overall reaction transport model were indicated in Sections 4.3 and 4.6.1. In this section an attempt is made to devise a somewhat more unified strategy for the incorporation of a number of reaction types:

- kinetic leach reactions
- Langmuir and Freundlich adsorption equilibrium
- surface processes described by mass action type equilibrium constants
- auto-hydrolysis of water (pH)

which will be discussed in more detail. This list of reactions is by no means exhaustive in terms of possible reaction modes, but it is felt that it is sufficiently universal to cater for the most common reaction phenomena.

4.7.1 A General Reaction Mechanism

For all reactions considered within this model development one can write the following universal reaction equation:

$$sS + aA + bB \rightarrow cC + dD \tag{4.7-1}$$

where S represents the solid species (if present), A and B the dissolved reactive species and C and D the dissolved product species. s, a, b, c, d represent the stoichiometric coefficients ν_i. One can define the stoichiometric coefficient vector for a reaction j as

$$\nu^j = (-s, -a, -b, c, d) \tag{4.7-2}$$

Furthermore, we define the concentration of the solid species as c_S in units of mass per unit solid mass (for example in [mg/g]), and those of the dissolved species i=A..D as c_i in units of mass per unit liquid volume (for example in [mg/l]), which is the most common way of reporting concentrations.

As a reaction proceeds, the concentration of the reagent species decrease and those of the product species increase in proportion to the stoichiometric ratio stipulated by the underlying reaction equation. It is thus possible to express the change in concentrations of the species participating in a reaction in terms of a single variable e, referred to as the reaction extent. For convenience we choose e_C, the change in concentration of the product species C, as the extent variable for the general reaction model. This is a logical choice as any type of reaction will have at least one product species, while some may only have a solid reactant, some only dissolved reactant(s) and others both or more and therefore choosing any of the reagent species for the extent variable would be less suitable.

If we now let the reaction proceed to a certain extent, we arrive at a new concentration of product species C, $c'_C = c_C + e_C$. For the new concentrations of the other dissolved species participating in this reaction we can then write

$$c'_A = c_A - \frac{a}{c}\frac{M_A}{M_C}e_C \qquad c'_B = c_B - \frac{b}{c}\frac{M_B}{M_C}e_C \qquad c'_D = c_D + \frac{d}{c}\frac{M_D}{M_C}e_C \qquad (4.7\text{-}3)$$

where M_i represents the molecular mass of species i. The ratio of the molecular masses needs to be introduced in this notation if all concentrations are taken as mass, rather than molar, concentrations, which is more commonly the case. If all concentrations are expressed in terms of molar concentrations, the ratio can be omitted.

For the solid species S we can write

$$c_s' = c_s - \frac{s}{c}\frac{M_S}{M_C}\mu\, e_C \qquad (4.7\text{-}4)$$

where μ represents the liquid to solid ratio in the given system. This ratio needs to be included since solid concentrations are reported as per unit solid mass rather than liquid volume. The introduction of μ thus relates the change in a dissolved concentration to the corresponding change in solid concentration. Some care needs to be taken define μ correctly for the system under consideration, which is discussed in some further detail in Section 4.7.4.

Using the stoichiometric vector introduced in equation (4.7-2), we can summarise equations (4.7-3) and (4.7-4) to

$$\Delta c_i = \left(c_i' - c_i\right) = \beta_i e_C \qquad \text{with} \quad \beta_i = \frac{\nu_i}{\nu_C}\frac{M_i}{M_C}, \quad \beta_S = \frac{\nu_S}{\nu_C}\frac{M_S}{M_C}\mu \qquad (4.7\text{-}5)$$

where β_i denotes what is essentially a stoichiometric extent coefficient. Carefully note that the stoichiometric coefficients ν for the reagent species (S, A and B) are defined as negative numbers and also that by inserting the values for species C, β_C becomes equal to 1.

4.7.2 Reaction Rates

Describing the rate of change of the concentration of species i due to a *single* chemical reaction j, we can define the rate term

$$R_i = R_i^j = \left(\frac{dc_i}{dt}\right)_j \qquad (4.7\text{-}6)$$

However, when several reactions simultaneously contribute towards the rate of change of species i, clear distinction must be made between the overall rate of change of c_i and that effected by the *individual* reaction j:

$$R_i = \frac{dc_i}{dt} = \sum_j R_i^j = \sum_j \left(\frac{dc_i}{dt}\right)_j \qquad (4.7\text{-}7)$$

This distinction is subtle but important to recognise, as in multiple reaction modelling the contributions of individual reactions j to the change of c_i are often influenced by the overall rate of change of c_i.

If all reactions considered are expressed as kinetic rate expressions of the form

$$R_i^j = \left(\frac{dc_i}{dt}\right)_j = f_j(k, c_i, c_x, \ldots) \qquad (4.7\text{-}8)$$

then summation of the individual reaction rate expressions to define the overall rate equation is straightforward. If, however, any of the reactions considered is a non-kinetic (i.e. very fast) equilibrium reaction they can not be incorporated in the summation in this way as no rate expression of above format can be formulated.

This problem can be circumvented by introduction of a discretised equilibrium shift. Within a given discrete time interval Δt an equilibrium reaction will proceed from the initial concentrations of the participating species at the beginning of the interval (t) to the concentrations which satisfy equilibrium conditions. Even if the reaction is complete before the end of the interval ($t + \Delta t$), one can attribute this concentration shift to the entire interval and thus define a "rate" of reaction as

$$R_i^j = \left(\frac{\Delta c_i}{\Delta t}\right)_j \qquad (4.7\text{-}9)$$

This approach essentially "smoothes" a reaction that proceeds in an more or less instantaneous step change into one proceeding at a continuous rate and is particularly

useful for the numerical solution of reaction models in which time dependent processes are modelled in discrete time steps anyway.

Combining equation (4.7-9) with the concept of the generalised reaction extent introduced in the preceding section (equation (4.7-5)), we can then formulate

$$R_i^j = \beta_i^j \frac{e_C^j}{\Delta t} \tag{4.7-10}$$

with the extent variable e_C and the stoichiometric coefficient β_i for each reaction j as defined before. When solving each reaction model, the e_C of equilibrium reactions is calculated from some mathematical expression describing equilibrium:

$$f_f(c_i + \beta_i e_C) = K \tag{4.7-11}$$

where K represents some equilibrium constant. For discretised kinetic reactions the extent can also be extracted by re-formulating equation (4.7-8):

$$\frac{dc_i}{dt} = f(k, c_i, c_x, \ldots) = \frac{\Delta c_i}{\Delta t} = \beta_i \frac{e_C}{\Delta t} \tag{4.7-12}$$

In both cases e_C needs to be calculated only once for each reaction and can then be apportioned to the concentration changes of the participating species.

Modelling both kinetic and equilibrium reactions using the approach of discretised reaction extents has been successfully employed in the overall solution algorithm used for the model developed in Section 4.6. More specific ramifications of this are discussed in Appendix B.

4.7.3 Reaction Models

Having introduced a generalised approach to reaction modelling in terms of the reaction extent variable e_C, we can now focus on how this variable can be determined for each of the reaction types considered in the context of this work.

Kinetic Leach/Dissolution Reaction

These are usually formulated in terms of rate of change of the solid species S as some function of solid and dissolved reagent and/or product concentrations and one or more reaction constants:

$$\frac{dc_S}{dt} = f_{kin}(k, c_S, c_A, c_B, c_C, \ldots) \tag{4.7-13}$$

For example, consider the leach reaction

$$S + aA \rightarrow cC + dD$$

Postulating this reaction proceeds first order with respect to both, solid and dissolved reactant concentrations, but is not a function of the product concentrations, the corresponding reaction model would be

$$\frac{dc_S}{dt} = -k\, c_S c_A \tag{4.7-14}$$

This model corresponds to the reaction model used by Dixon in the development of his heap leach model (Section 4.5). It should be pointed out that both c_S and c_A can be of any order, but only first order is considered at this stage for simplicity.

Another example would be the kinetic dissolution reaction

$$S \rightarrow cC + dD$$

Again, assuming first order kinetics in terms of the solid concentration, the corresponding reaction model would be

$$\frac{dc_S}{dt} = -kc_S \tag{4.7-15}$$

In this manner one can formulate kinetic rate equations for any type of reaction with any dependency on the concentrations of the species involved and at any order. Where such kinetic reactions are considered, it is important to select the appropriate reaction model (in terms of the proposed rate equation) on the basis of available experimental data.

However, irrespective of the kinetic reaction model chosen, its incorporation into numerical modelling of the overall leach process can always be easily achieved using the reaction extent variable approach introduced in the preceding section by the following method:

1. Calculate e_C from the kinetic model equation, combining equations (4.7-10) and (4.7-13)

$$e_C = \frac{1}{\beta_S}\left(\frac{\Delta c_S}{\Delta t}\right)\Delta t = \frac{1}{\beta_S} f_{kin}(k, c_S, c_A, c_B, \ldots)\Delta t \tag{4.7-16}$$

   bearing in mind that the concentrations c_S, c_A, c_B, etc. are to be taken as those at time (t).

2. Determine the reaction rates for all participating species as stipulated in equation (4.7-10):

$$R_i^j = \beta_i \frac{e_C}{\Delta t} \tag{4.7-17}$$

Adsorption Reactions

Chemical adsorption of a dissolved species onto a solid offering sites for adsorption can be simply expressed as

$$S_{ads} \rightleftharpoons C_{dis}$$

This is an equilibrium reaction, which is suitably described by adsorption isotherms as was detailed in Section 4.3. Although there is a multitude of such characteristic isotherm models, we limit ourselves here to the Langmuir and Freundlich isotherms, both two parameter models which find common use in describing adsorption of dissolved species in aqueous solutions.

The Langmuir isotherm is written as

$$\frac{c_S}{c_{S,max}} = \frac{Kc_C}{1 + Kc_C} \tag{4.7-18}$$

which can be re-formulated in terms of the extent variable e_C as

$$\frac{(c_S + \beta_S e_C)}{c_{S,max}} = \frac{K(c_C + e_C)}{1 + K(c_C + e_C)} \tag{4.7-19}$$

Given the (non-equilibrium) concentrations of both dissolved species (in [mg/l]) and adsorbed solid form (in [mg/g]) at a time (t), equation (4.7-19) can be solved for the extent e_C by which the concentrations have to change to reach a new equilibrium. In this case this reduces to solving a simple quadratic equation:

$$e_C^2 + \left(\frac{\beta_S + K(\beta_S c_C + c_S - c_{S,max})}{K\beta_S} \right) e_C + \left(\frac{c_S + K(c_C c_S - c_C c_{S,max})}{K\beta_S} \right) = 0 \tag{4.7-20}$$

The Freundlich isotherm is written as

$$c_S = b(c_C)^m \tag{4.7-21}$$

and reformulated in terms of the extent variable e_C as

$$(c_S + \beta_S e_C) = b(c_C + e_C)^m \tag{4.7-22}$$

Again, given the non-equilibrium concentrations of c_S and c_C at a time (t), this equation can be solved for the extent e_C. If the exponent m=1 this reduces to a linear equation and for m=2 a quadratic needs to be solved. For any other values of m solution of equation (4.7-22) requires a non-linear root finding method.

Having found the equilibrium extent e_C from solving either equation (4.7-20) or (4.7-22), depending on which model is being used, the rate of change in concentration of the participating species within a given discrete time interval can now be obtained from equation (4.7-10) as before.

Solubility Product Reactions

For the equilibrium dissolution/precipitation of a solid the general reaction equation can be written as

$$S \rightleftharpoons cC + dD$$

implying the salt S is of composition C_cD_d. The equilibrium is suitably described by the solubility product:

$$(c_C)^c(c_D)^d = K_{sol} \tag{4.7-22}$$

where K_{sol} represents an equilibrium constant.

This equation can again be re-formulated in terms of the extent variable e_C:

$$(c_C + e_C)^c(c_D + \beta_D e_C)^d = K_{sol} \tag{4.7-23}$$

Given the non-equilibrium concentrations of the participating species at time (t), equation (4.7-23) can be solved for e_C using non-linear root finding methods. The rate of change of each participating species over the discrete time interval Δt is obtained from equation (4.7-10) as before.

One special kind of solubility product is that describing the auto-hydrolysis of water:

$$H_2O \leftrightharpoons H^+ + OH^-$$

which is important in the modelling of any aqueous system. The solubility product for water is given by

$$(c_{H^+})(c_{OH^-}) = K_{H_2O} \tag{4.7-24}$$

The extent variable e_C (here = e_{H+}) and the rates for the participating species can be calculated in the same manner as before. It should be borne in mind, however, that particularly H^+ concentrations are not usually reported in mg/l, but rather in mol/l or pH, and care needs to be taken to use the appropriate conversions, when incorporating this reaction with others.

General Equilibrium Type Reactions

Similar principles as those for solubility product reaction type also apply for solution of any type of equilibrium reaction

$$sS + aA + bB + ... \leftrightharpoons cC + d\,D + ...$$

which is described by the law of mass action in its most general form

$$\prod_i (c_i)^{\nu_i} = K_{eql} \tag{4.7-25}$$

Again this can be expanded using the extent variable e_C, bearing in mind that even in this universal reaction the will always be at least one product species:

$$(c_C + e_C)^c \prod_{i \neq C} (c_i + \beta_i e_C)^{\nu_i} = K_{eql} \tag{4.7-26}$$

As before, given the non-equilibrium concentrations of all participating species, this equation can be solved for e_C using non-linear root finding methods and the rate of change of the participating species determined from using equation (4.7-10).

4.7.4 Modelling Pore, Surface and Bulk Reactions

As was indicated in equation (4.7-4), the stoichiometric extent coefficient for the solid species, β_S, needs to incorporate the liquid to solid ratio μ for the system under consideration. This is necessary since the concentration of the solid species c_S is given in terms of mass or moles per unit total solid mass, whereas all dissolved concentrations are reported in mass or moles per unit volume of fluid. In a particular system the decrease or increase in solid concentration is linked to the decrease or increase of dissolved concentrations of the corresponding species not only by the reaction stoichiometry but also by the amount of fluid relative to the total solid mass present in the system under consideration, which is contained in the parameter μ.

In the context of the general reaction-transport model developed in Section 4.6 it is crucial to ensure appropriate choice of μ for meaningful incorporation of reaction mechanisms. The model distinguishes between processes at particle, surface and bulk level and the definition of μ is different in each case.

At the particle level, the liquid volume of fluid that is in contact with the solid particle mass is held up in the particle pores. Assuming that the pores are fully saturated with fluid, the total pore volume can be calculated from the particle porosity via

$$V_{pore} = \varepsilon_p V_{particle} = \varepsilon_p \frac{M_{particle}}{\rho_{particle}} \tag{4.7-27}$$

where the dry particle density $\rho_{particle}$ corresponds to the solid mass per unit volume of particle (including the volume occupied by pore spaces). This is related to the true solid density of the particle material ρ_t, which is the value usually determined in experimental studies, via

$$\rho_{particle} = \rho_t(1 - \varepsilon_p) \tag{4.7-28}$$

and thus combining equations (4.7-26) and (4.7-27) we obtain for the pore liquid to solid ratio μ_p:

$$\mu_p = \frac{V_{pore}}{M_{solid}} = \frac{\varepsilon_p}{\rho_t(1 - \varepsilon_p)} \tag{4.7-29}$$

acknowledging that the dry particle mass is identical to the dry solid mass of the particle. Note that this definition of μ is independent of particle dimensions, providing porosity and true solid density are identical for all particle size classes.

The particle surface level model, introduced in Section 4.6.2, is based on the assumption that there exists a thin film of fluid of thickness δ_s in contact with the particle surface, within which a surface concentration of dissolved species can enter reactions with solid species contained in the solid surface. The dissolved concentrations can be different from those in the bulk fluid if a diffusion resistance between bulk and particle surface exists, which is governed by bulk flow velocity and bed geometry. If no such resistance exists because of good local mixing, as is assumed in a batch reactor scenario (see Section 4.6.4), the surface concentration of dissolved species is equal to the bulk concentration. It is

important to recognise that, depending on which case is present, the surface liquid to solid ratio would be defined quite differently.

A further difficulty is introduced through the way surface solid concentrations are defined, particularly in relation to the solid concentrations associated with the particle pores. The external surface area (i.e. the surface of a sphere of the same radius as the particle) of highly porous particles is small compared to the internal surface area made up of the pore walls. If the particle is homogeneous, the amount of a solid species located on the outside surface would be marginal compared to that located on the inside of the particle and there would be little benefit to define this as a separate quantity. In this case it is sufficient to model all solid liquid reactions within the pore model whilst these reactions can be safely ignored on the external surface. However, if there is evidence of surface enrichment of a particular solid species, then this should be attributed to a separate surface concentration and taken into account in surface reaction modelling. If the particle is relatively non-porous, the entire concentration of a solid species can be attributed to the surface and separate pore modelling is not required.

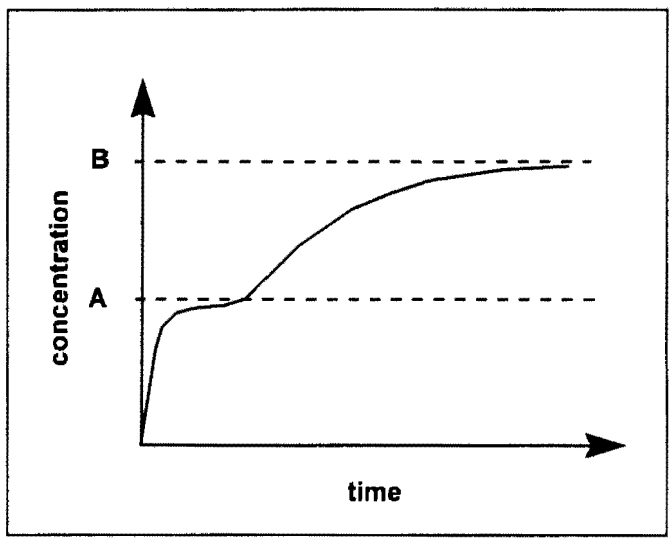

Figure 4-19: Hypothetical leach experiment indicating the existence of separate pore and surface concentrations of the leached species

Only in the rare case where internal and external surface area of a homogeneous material are of similar magnitude, some trade-off has to be made as to what portion of the reactive solid concentration is attributed to the surface and what portion to the internal pores. This could potentially be identified experimentally in the following manner: Consider a batch leach experiment of the solid species in question with a leach curve as given in Figure 4-19. The curve clearly

indicates two separate release processes, the first proceeding relatively fast to concentration level A and the second more gradually further to level B. In this case it is conceivable that the first release is attributable to a surface reaction, whereas the second release results from a pore reaction which is slowed by pore diffusion effects. The concentration level A can then be attributed to a surface concentration and the residual level (B-A) to the pore concentration of the solid species. It must, however, be established clearly, whether the two releases can be indeed attributed to the *same* reaction. Repeating the experiment with different particle size classes may provide more evidence in this context. If a surface concentration is defined, it is common to express this in terms of unit mass per unit particle (external) surface area, for example in [mg/m^2]. This is not strictly necessary, but more convenient as will become clear in the argument to follow. To translate a solid mass concentration into the corresponding solid surface concentration one would divide by the total (external) surface area per unit mass, which can be determined from a given particle size distribution:

$$c_S\,[\mathrm{mg/m^2}] = \frac{\rho_t(1-\varepsilon_p)}{\sum_n \frac{3w^{(n)}}{R^{(n)}}} \cdot c_S\,[\mathrm{mg/g}] \qquad (4.7\text{-}30)$$

where $w^{(n)}$ refers to the mass fraction of particles in class (n). For the surface layer model the surface layer thickness δ_s has been defined in Section 4.6.2. Understanding the particle as a sphere of radius R, then the volume of this layer becomes $V_S = 4\pi R^2\delta_S$ and the ratio of particle surface area to surface liquid volume simply

$$\frac{A_S}{V_S} = \frac{4\pi R^2}{4\pi R^2\delta_S} = \frac{1}{\delta_S} \qquad (4.7\text{-}31)$$

Acknowledging, that for surface reaction modelling the liquid volume to solid mass ratio μ would have to be replaced by a liquid volume to solid surface area ratio, if surface rather than mass concentration of the solid species are used, the factor μ' for surface reaction modelling is then

$$\mu_S = \delta_S \tag{4.7-32}$$

If, however, the solid surface concentration remains defined as moles or mass per unit solid mass as was done for pore modelling, μ would have to take account of the fact that the ratio of surface area to mass of an individual particle changes with the radius:

$$\mu_S = \frac{V_S}{M_{paticle}} = \frac{3 \cdot 4\pi R^2 \delta_S}{4\pi R^3 \rho_t (1-\varepsilon_p)} = \frac{3\delta_S}{R\rho_t (1-\varepsilon_p)} \tag{4.7-33}$$

and thus μ would become a function of R, which is less convenient in the actual modelling of surface reactions.

For the batch reactor model (Section 4.6.4) the surface area of the entire solid charge is in contact with the bulk fluid in the reactor and the total surface area to volume ratio is

$$\mu_{STR} = \delta_{STR} \tag{4.7-34}$$

with δ_{STR} as defined in equation (4.6-17) in Section 4.6.4. In this particular case it is less important, whether the surface concentration of solid species is defined in terms of mass per unit surface area or per unit mass of solid since the solid surface concentration of all particle size classes would be the same at all times. Here μ can be defined as

$$\mu_{STR} = \frac{V_{liq}}{M_{part}} \tag{4.7-35}$$

which corresponds to the inverse of the solid to liquid ratio employed in the batch reactor.

For the bulk model as presented in Section 4.6.3, no separate definition of μ is required since, through the presence of the surface layer with the associated surface model, no solid-liquid reactions can take place in the bulk fluid. If, however, the surface layer model is not employed, particularly when surface film diffusion effects can be considered

negligible, then solid surface reactions would directly interact with concentrations in the bulk fluid. In this case the solid surface concentration to bulk fluid ratio becomes

$$\mu_B = \frac{V_{bulk}}{A_{part}} = \frac{\varepsilon_b}{(1-\varepsilon_h)\sum_n \frac{3w^{(n)}}{R^{(n)}}} \tag{4.7-36}$$

or if the solid concentration at the surface is defined per unit mass the following ratio is employed:

$$\mu_B = \frac{V_{bulk}}{M_{part}} = \frac{\varepsilon_b}{\rho_t(1-\varepsilon_p)(1-\varepsilon_h)} \tag{4.7-37}$$

with the heap voidage ε_h and bulk volume fraction ε_b as defined in Section 4.6.3.

4.8 Model Sensitivity Study Using WASTESIM

The model equations developed in Section 4.6 describe the continuity of a dissolved species i for an individual porous particle (equation (4.6-1)), for diffusion transport between particle surface and bulk fluid across a stagnant surface film (equation (4.6-9)), for a packed bed with one-dimensional downward bulk flow (equation (4.6-13)), and for a batch reactor loaded with a distribution of particle sizes (equation (4.6-16)). Release and attenuation of various species as well as the chemical interactions between them can be described mathematically by a number of reaction mechanisms, some of which have been discussed in Section 4.7.

Quite clearly the mathematical complexity even of a relatively simple system precludes analytical solution of the underlying equation and solution by numerical methods with the help of a computer is required. All equations developed within this study have been translated into the comprehensive computer algorithm WASTESIM, which offers a user-

that have been developed within this study have been devised. These have been incorporated into the WASTESIM computer code, which offers a user-friendly platform for the entry and manipulation of all model parameters, such as particle density, size distribution, porosity and effective diffusivity, bed height, flowrates, saturation, dispersivity, species characteristic parameters as well as reaction types and constants.

The simulation package of the code models the particle level equation, either alone, in combination with the batch equation, or with the column bulk flow equation. The (optional) particle surface equation can be switched in, if so required. The time dependent changes of species concentrations are displayed graphically during the simulations and the results are stored on file for manipulation in other computer programs.

A brief introduction to the WASTESIM code in its central modelling modes, PARTICLE, BATCH and COLUMN is given in Section 4.8.1. Details on program functionality, numerical methods and solution algorithms can be found in Appendix B. A demo-version of the program can be found on the disk attached to this volume.

Using the WASTESIM code, a sensitivity study on a simple base case is conducted. A number of model parameters are varied, one by one, over a range of values, in order to demonstrate the models robustness and, at the same time, show the significance certain variables have on the resulting leach curves. The parameters investigated can be grouped as particle characteristic parameters (particle size and distribution of sizes, porosity and effective pore diffusivity factor, Section 4.8.3), reaction characteristic parameters (reaction type and constants, Section 4.8.4) and bed transport characteristic parameters (bed height, feed flow rate, dispersivity and saturation, Section 4.8.5).

4.8.1 Computer Simulations Based on the Model Equations

As was already indicated before, the model equations developed in Section 4.6 together with the reaction modules of described in Section 4.7 can only be solved numerically and evaluated and applied in computer simulations. The DOS based code WASTESIM, of which a demo-version can be found on the attached disk, includes modules for the solution of all model equations introduced thus far. Description of program functionality, numerical methods and solution algorithms is given in Appendix B.

The program consists of a menu-based data entry platform on which all current model parameters are displayed and manipulated. The structure of the WASTESIM platform is briefly outlined in Appendix B. Table 4.4 lists all parameters that can be specified and also indicates which parameters are required for which type of simulation. The entire set of parameters is saved in a run-file (*.rmf) and can be re-called in later program runs.

Table 4.4 : Model Parameters in WASTESIM

Parameter	Symbol	Units	Remarks
Species Parameters			
molecular mass	M_i	g/mol	
initial concentration	c_i^0	mg/g	for solid
		mg/l	for dissolved species
ini. surface concentration	$c_{s,i}^0$	mg/g	(solid species only)
feed concentration	$c_{f,i}$	mg/l	(dissolved spec. only)
species diffusivity	D^*	m^2/s	(dissolved spec. only)
Material & Particle Parameters			
true solids density	ρ_t	kg/m^3	
particle porosity	ε_p	-	
effective diffusivity fact.	d_{eff}	-	corresponds to ε/τ
particle radius	R	mm	NB: not diameter
size class mass fraction	$w^{(n)}$	kg/kg	specify up to 5 size classes

Table 4.4 (cont.)

Parameter	Symbol	Units	Remarks
System Parameters			
bed height	Z	m	
bed area	A_{bed}	m^2	cross-sectional area
fluid flow rate	Q	l/day	in feed (can be variable)
bed porosity	ε_h	-	
fract. saturation	f_{sat}	-	
effect. bed diffusivity fact.	d_{bed}	-	
batch reactor fluid volume	V_{fluid}	litres	only required for BATCH mode
total batch solids charge	M_{tot}	kg	not required for COLUMN
Reaction Parameters			
stoichiometric coefficients	ν_i	-	
kinetic dissolution, kinetic reaction	k	s^{-1}	first order rate constant
	c_S^0	mg/g	ini. solid conc.
instant dissolution	c_S^0	mg/g	ini. solid conc.
adsorption	K	l/mg	Langmuir constant
	c_{max}	mg/g	max. adsorbed conc.
	c_S^0	mg/g	ini. adsorbed conc.
solubility product	K	$(l/mg)^{(a+b)}$	solubility product
	c_S^0	mg/g	ini. solid conc.
Simulation Parameters			
simulation time increment	Δt	s	initial value, variable during simulations
plot interval	p.i.	-	number of time intervals after which a data point is generated
run mode	PARTICLE, BATCH, COLUMN		simulation mode
surface only modelling	on/off		sets the inclusion of particle pore modelling
surface film modelling	on/off		sets the inclusion of the surface layer model

Three types of simulations are possible, which are set using the RUN MODE switch in the Parameters/System menu: PARTICLE, BATCH and COLUMN, the operation of which is described below. Simulation runs are started from the platform and the ongoing output of the simulations is displayed graphically on-screen.

In the PARTICLE mode only the processes within the pores of a single particle are modelled, based on equation (4.6-1) and fixed, pre-defined surface concentrations. While this of little use for modelling real systems, it is useful for studying the interactions between various reaction modes and diffusion transport within the pores. The graphic screen output of WASTESIM in PARTICLE mode is shown in Figure 4-20.

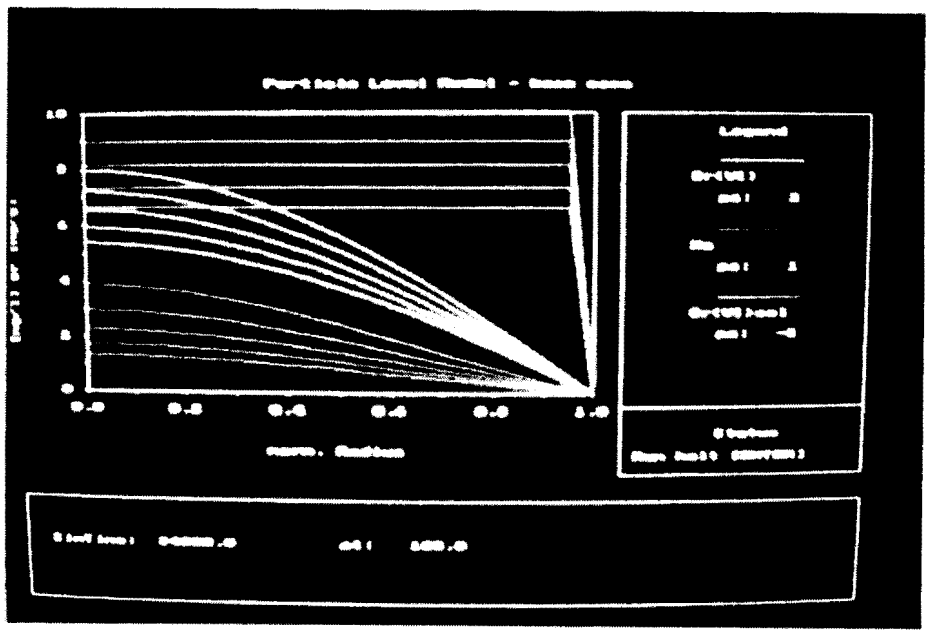

Figure 4-20: Screen output of WASTESIM in PARTICLE Model

Simulations in BATCH mode combine modelling the particle pore processes of one particle size or a distribution of sizes with the batch reactor equation (4.6-16). Module output is the time-dependent change of concentrations in the batch liquor, which is also saved as a result-file on disk (*.res). The graphic screen output of WASTESIM in BATCH mode is shown in Figure 4-21. Here the particle pore profiles for one size class are shown on the left hand side (only one is shown due to space limitations, but any size class can be

selected for display) and the time dependent bulk concentration profiles on the right. Particle pore modelling can also be switched off (on the Parameters|System screen), in which case all reactions are modelled as surface reactions.

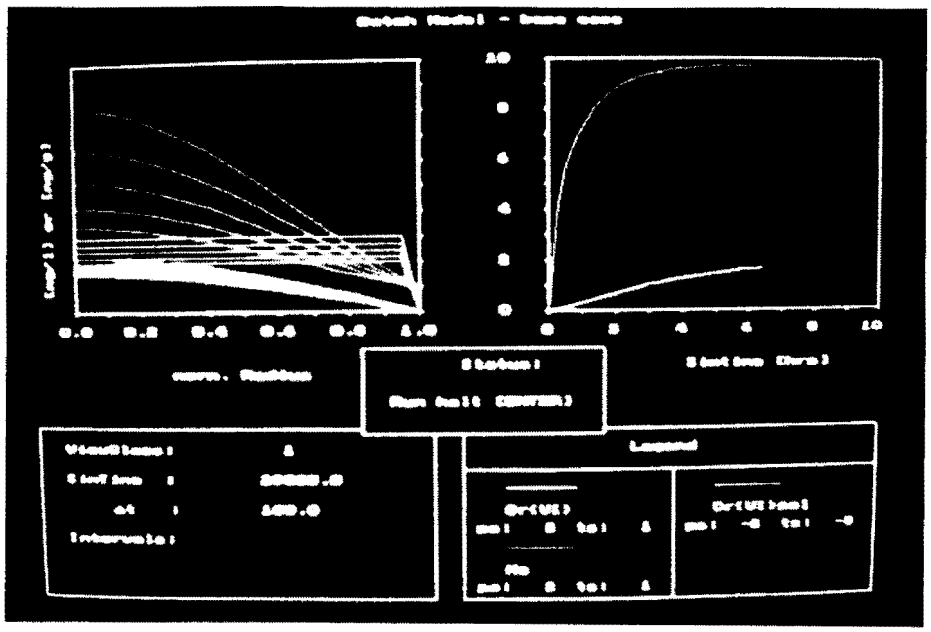

Figure 4-21: Screen output of WASTESIM in BATCH Mode

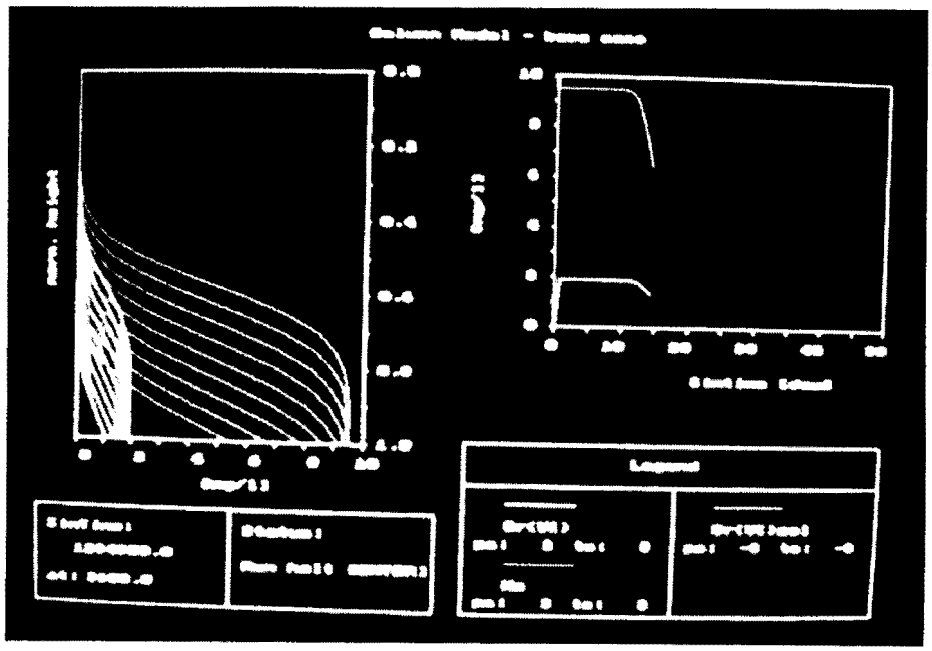

Figure 4-22: Screen output of WASTESIM in COLUMN Mode

Simulations in COLUMN mode combine particle pore modelling with the column bulk transport equation (4.6-13). The particle surface layer equation (4.6-9) can be switched in if so required (on the Parameters|System screen). Again particle modelling can be restricted to surface only processes if so desired. The module output is the time dependent change in concentrations in the effluent from the column, which is displayed graphically (Figure 4-22) and also stored in a result file. As can be seen in Figure 4-22, the graphic display also shows the concentration profiles of selected species as a function of height in the column. Additional features of the COLUMN mode are the incorporation of variable feed flow-rates (by reading from a data file) and a BATCH-COLUMN combination, which allows modelling of a specific experimental set-up detailed in Section 5.4.

4.8.2 A Base Case for Model Evaluation

In the following the various model equations, as encoded in the WASTESIM computer program, are evaluated with regard to their sensitivity to a number of model parameters. This is done in order to obtain a preliminary feel for the model's capabilities and to give an indication of which parameters are most likely to influence the time-depended release behaviour of contaminant species in waste deposits.

All the following simulations are conducted on the basis of a hypothetical waste material, with characteristics as detailed below. Although this base case is made up, many parameters chosen (see Table 4.5) closely relate to those observed for real waste materials investigated in Chapters 6 and 7.

For the base case material it is assumed that Cr(VI) and Na are the only species that are released in any significant concentrations. It is assumed further that Cr(VI) release is described by a kinetically controlled first order dissolution mechanism with a half-life of approximately 2 hours (i.e. $k=10^{-4}$ s^{-1}) and that of Na by instant dissolution. The total dissolvable concentration of Cr(VI) in the material is 0.2 mg/g and that of Na is 1 mg/g.

The material has a true density of 3000 kg/m^3 and consists of more or less mono-sized particles 10 mm in diameter with a porosity of 5%. When the material is tested in batch leach experiments, 100 g of solids are usually mixed with 1 litre of solution. In a laboratory scale column (16 cm in diameter) the material is packed to a height of 1 m and exhibits a packing porosity of 50%. The bed is sprinkled with distilled water at a flow rate of approximately 200 ml/day. All base case parameters are listed in Table 4.5 and are available in the demo-model on the accompanying disk in the file "basecase.rnf". Although hypothetical the base case used for a preliminary model sensitivity study here exhibits may features of the real waste materials investigated later in this study.

Figures 4-20, 2-21 and 4-22 in the preceding section showing screen outputs of WASTESIM simulations in PARTICLE, BATCH and COLUMN mode are in fact runs of the base case scenario.

Table 4.5 : Base Case Model Parameters

Parameter	Symbol	Base Case Value	Units
true solids density	ρ_t	3000	kg/m^3
particle radius	R	5	mm
particle porosity	ε_p	0.05	-
species diffusivity	D*	Na: $1.35 \cdot 10^{-9}$ Cr(VI): $1.13 \cdot 10^{-9}$ (sorce: CRC,1992)	m^2/s
effective diffusivity fact.	d_{eff}	0.025 (= $\varepsilon_p/2$)	-
Cr(VI) kinetic dissolution	k	$1 \cdot 10^{-4}$	s^{-1}
	c_0	0.2	mg/g
Na instant dissolution	c_0	1.0	mg/g
total STR solids charge	M_{tot}	0.1	kg
STR fluid volume	V_{fluid}	1.0	litres
bed height	Z	1.0	m
bed area	A_{bed}	0.02	m^2
fluid flow rate	Q	0.2	l/day
bed porosity	ε_h	0.5	-
fract. saturation	f_{sat}	0.3	-
effective bed diffusivity factor	d_{bed}	0.5	-

4.8.3 Batch Studies: Particle Size, Size Distribution and Pore Diffusion

The influence of particle size and effective diffusivity in the particle pores on the time depended leach curves is demonstrated using the base case in BATCH mode. Figure 4-23 shows the leach curves for a charge of mono-sized particles of 2, 5, 10 and 20 mm diameter with all other parameters unchanged. Also shown is a leach curve for 10 mm particles generated in the surface-only mode, i.e. assuming the particle to be non-porous.

For Na this instant surface dissolution results in a flat profile, while dissolution combined with pore diffusion results in leach profiles which are increasingly more protracted as particle size increases, and the pore diffusion of Na becomes rate limiting to the overall release mechanism.

For the kinetically controlled dissolution of Cr(VI) the effect of particle size is only marginal. This is due to the fact that the reaction rate is rate controlling for the release and pore diffusion is fast by comparison. Only for the largest size class (20 mm) does pore diffusion protract the overall release by a small margin.

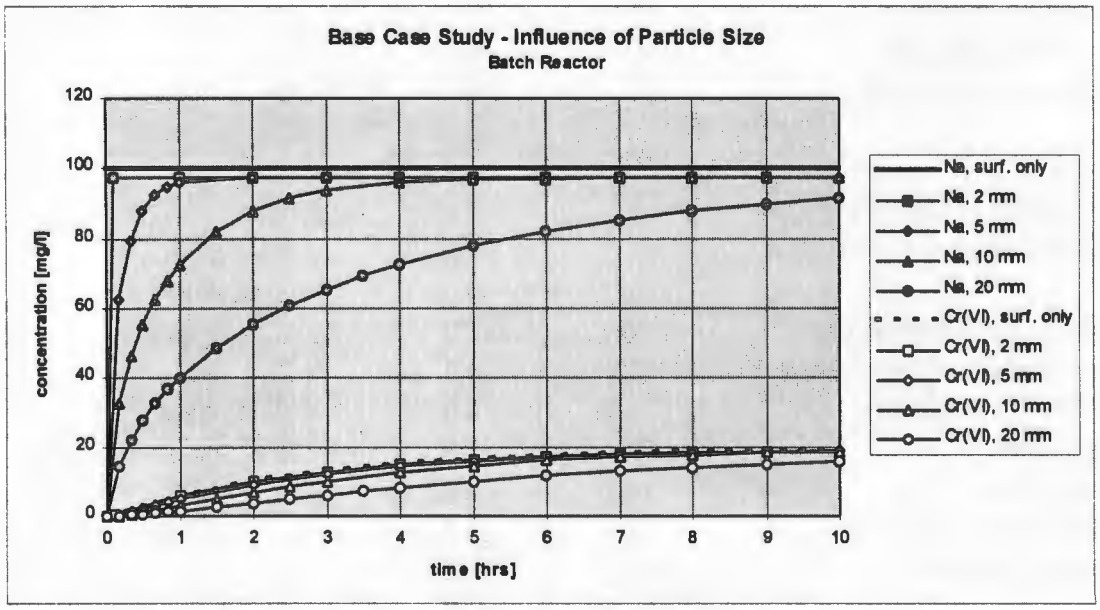

Figure 4-23: Effect of particle size on batch leach curves

Figure 4-24 shows the simulated leach curves for a charge composed of a mixture of 5, 10 and 20 mm particles at various distributions as indicated. The resultant leach curves for Na clearly show, how the overall kinetic effect becomes more pronounced as the fraction of larger particles (for which pore diffusion is more rate limiting) increases. Again, for the Cr(VI) curves the distribution effect remains insignificant as overall release is dominated by the kinetics of the release reaction rather than diffusion effects.

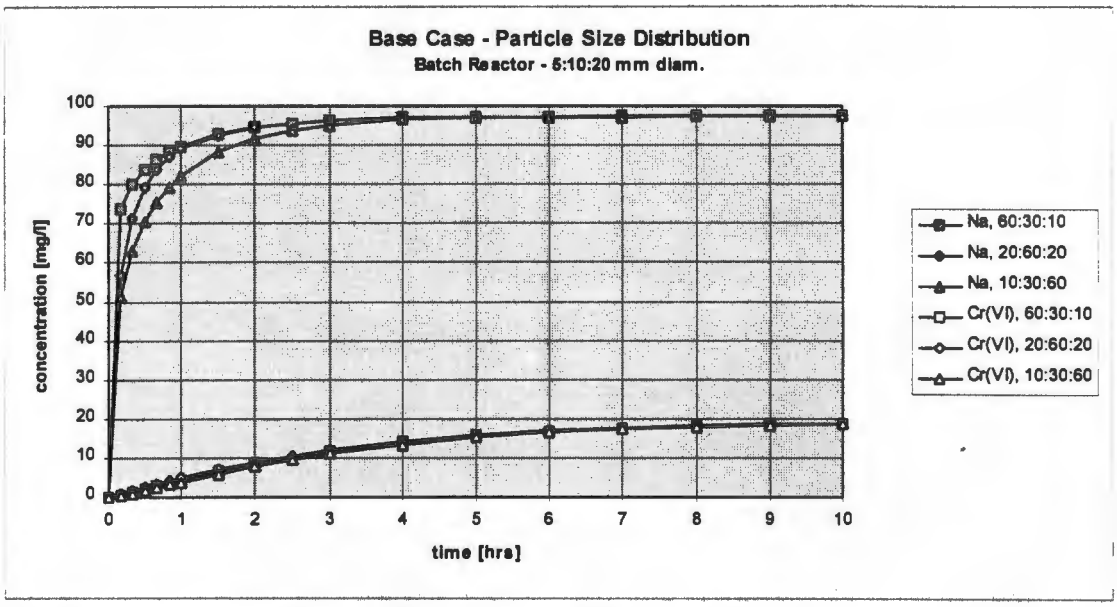

Figure 4-24: Leach curves of various particle size distributions

Pore diffusion is described in term of an effective pore diffusivity, which, according to equation (4.2-5), can be taken to be the product of a factor ε/τ (porosity over tortuosity) and the free solution diffusivity D*, which is usually taken from literature values (for example CRC, 1992). A value of 2 is normally taken as a rule-of-thumb estimate for τ (Bartlett, 1992). In the WASTESIM program ε/τ corresponds to the effective diffusivity parameter d_{eff}, which can be manipulated in order to allow for more accurate estimation of this parameter when simulating batch leach data.

Figure 4-25 shows simulated leach curves for the base case 10 mm particles with d_{eff} set to values of 0.1, 0.025 ($=\varepsilon_p/2$) and 0.01 and all other parameters unchanged from the base case. Similarly to increasing the particle diameter, decreasing the effective pore diffusivity

(i.e. assuming more tortuous pores) more and more protracts Na release as diffusion out of the pores becomes increasingly more inhibited. For Cr(VI) release the effects is not as significant, but starts to become noticeable for the lowest pore diffusivity factor (d_{eff}=0.01) as the diffusion resistance becomes increasingly more controlling over the kinetic reaction.

It needs to be seen in practice, however, to what extent this deliberate manipulation of the effective diffusivity factor is valid relative to the rule-of-thumb value of ε/2. Some care needs to be taken that the effective diffusivity is estimated from an independent experiment and not used as a "fudge factor" for fitting curves to experimental results.

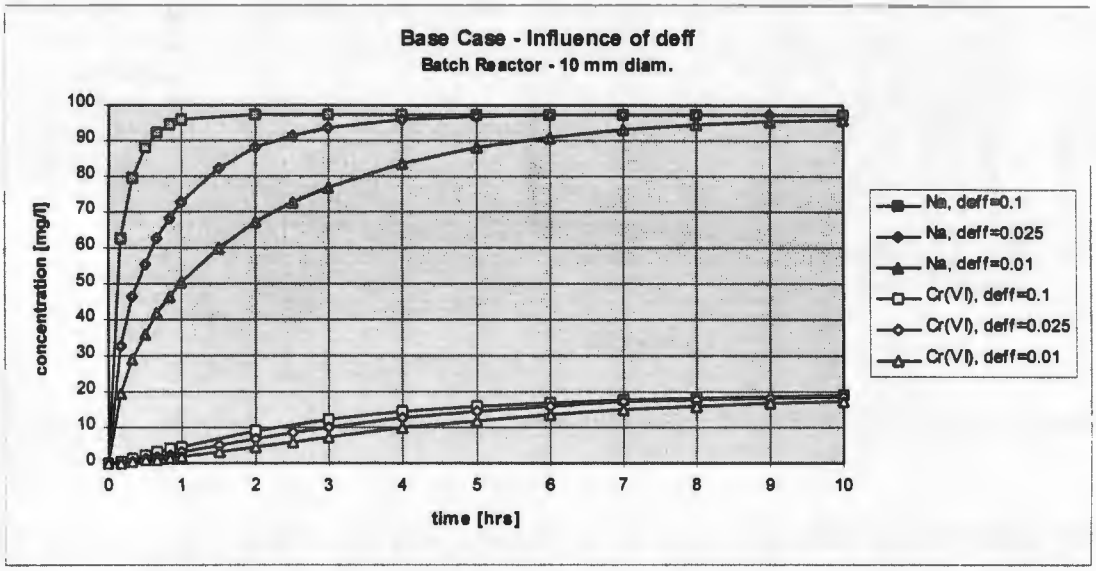

Figure 4-25: Effect of effective pore diffusivity on leach curves

Comparing the release curve for Na modelled for the large size particle with the Cr(VI) release curves (which are more or less independent of size in the range considered here), one could be led to conclude that both release mechanisms are kinetic in similar fashion, overlooking that the one is governed by pore diffusion and the other by kinetic reaction. In practice this effect can only be disseminated through experiments with different size classes. However, if a material is relatively mono-sized, it may be feasible to express instant dissolution plus pore diffusion more simply as a kinetic dissolution reaction (with the rate constant established experimentally for the given particle size) and ignoring pore

effects by taking the particle as a non-porous sphere (i.e. model it in the surface-only mode).

The modelled curves shown in Figure 4-23 also indicate that particle size effects become effectively negligible for particles smaller than 2 mm for the effective diffusivities considered here. In practice this means that there is little point to model small particles as porous spheres as any pore diffusion effects are too insignificant to warrant this - and this reduce computational effort significantly. In this regard, however, the critical particle size requires careful evaluation in terms of its dependence on effective pore diffusivity and particle porosity.

4.8.4 Testing of Reaction Types and Their Influence on Leach Scenarios

The various reaction mechanisms catered for by the model (see Section 4.7) and incorporated in WASTESIM are studied - in terms of their sensitivity to the associated input parameters and their influence on the simulated leach scenarios - in the following. This was done using simulations in COLUMN mode as this more clearly demonstrates the relative effects of the various reaction effects on the time dependent leach behaviour of waste materials in a deposit scenario.

Kinetic Dissolution

Figure 4-26 shows model runs using the base case (i.e. kinetic dissolution of Cr(VI) and instant dissolution of Na), for a number of values of the kinetic dissolution constant. For the base case time constant ($k=10^{-4}$ s^{-1}) Cr(VI) release reaches completion before any significant amounts of effluent have left the bed and the effluent leach curve therefore is similar to that of Na, which represents instant dissolution. Thus, the kinetic dissolution becomes effectively instantaneous when considering the time scale of fluid residence in the bed (15 days for base case conditions).

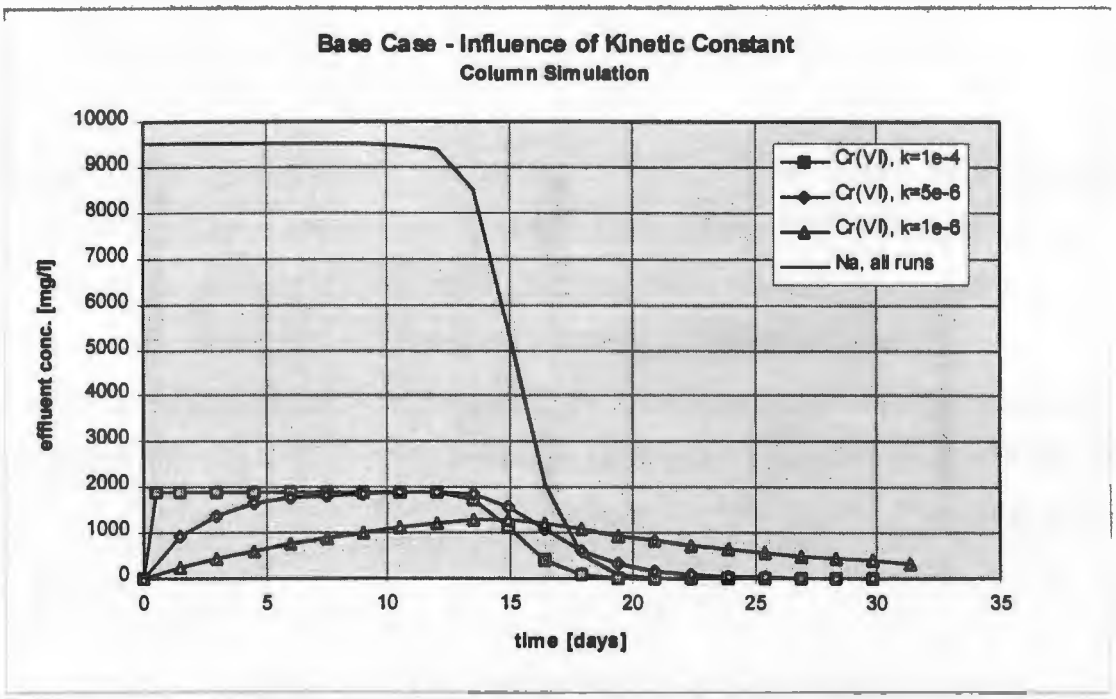

Figure 4-26: Column leach curves for kinetic release at various time constants

For lower reaction constants the release curve shows a more gradual increase and a more protracted decrease. With Cr(VI) being released more slowly, concentrations in the bulk fluid - and hence the effluent - reach peak levels only after some effluent has already left the bed. The more protracted this kinetic release is, the more bed dispersion will take effect (see Section 4.8.5), which explains the longer tail-ends.

A rapid fall-off of concentrations can be observed for the Na curve and is typical for bed leach scenarios. Under "plug flow" conditions the fluid containing dissolved concentrations is pushed out of the bed by the clear liquid entering the bed. Once the front fresh fluid has travelled to the bottom of the column, effluent concentrations will drop dramatically. A small tail-end effect is observed as small quantities of the dissolved species migrate backwards against the direction of flow due to bed diffusion effects. This is discussed in more detail further below.

These trends are significant also with respect to comparing batch and column experiments. At the time scale of batch leach experiments (usually a few hours or days), the base case

Cr(VI) dissolution appeared as slow relative to the Na dissolution (Figure 4-23), while at the time scale of the column simulation (30 days) Cr(VI) dissolution does not appear to be kinetic at all (Figure 4-26). On the other hand, very slow reactions, that are significant at the column scale (as is clearly the case for $k=10^{-6}$ s^{-1}) can be so slow in batch experiments that they may go unnoticed, or the experiment needs to be conducted sufficiently long (half life at $k=10^{-5}$ s^{-1} is 20 hours, at $k=10^{-6}$ s^{-1} this is 200 hours).

In this regard, particle pore diffusion effects also need to be seen critically when scaling from batch leach to column scenarios. Only for relatively large particles or very small diffusivities are these effects likely to play a role at the time scale of column scenarios. As neither is the case for the base case scenario it is justified to model column scenarios taking the particles as non-porous (as is done here henceforth). When working with real waste materials, however this needs to be assessed in each case studied.

Langmuir Adsorption

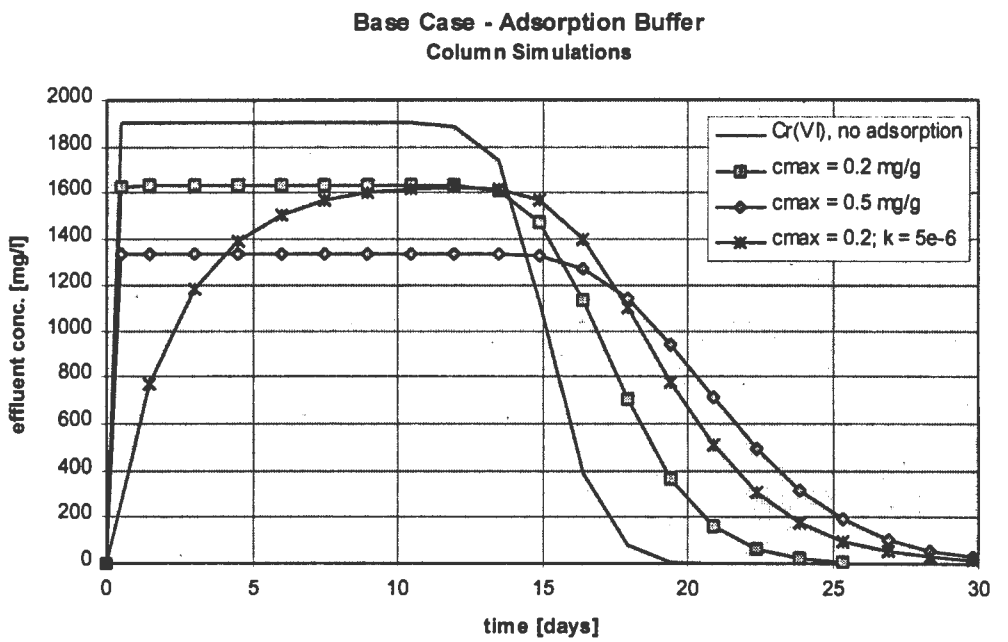

Figure 4-27: Effect of adsorption on Cr(VI) release curve

In the next study the kinetic release of Cr(VI) has been combined with a Langmuir type adsorption isotherm for Cr(VI) (Section 4.3s and 4.7). Figure 4-27 shows the simulated leach curves for the combined reactions at the various values of the adsorptive capacity, c_{max}, as well that obtained for the kinetic release alone. Clearly adsorption acts as a buffer to the Cr(VI) released by dissolution alone, with the fall-off of the leach curves becoming increasingly more protracted as the buffer capacity increases. This phenomenon can be explained as follows: As Cr(VI) is released by dissolution, some is adsorbed onto the particle surface, keeping dissolved concentrations lower than would be expected without the adsorption reaction. Once the release reaction has come to completion, the adsorbed concentrations are re-released into the fresh bulk fluid flowing from the top of the bed, thus resulting in a protracted effluent leach curve. This falls off gradually as the adsorptive capacity is depleted, and the fall-off period is longer the higher this adsorptive capacity is.

Also included in Figure 4-27 is a Cr(VI) leaching/adsorption curve for a smaller kinetic time constant (relative to the base case) to illustrate the effect of loading the adsorption buffer. The increase of Cr(VI) concentrations is more gradual and it goes to smaller extents when compared to an unbuffered reaction (see Figure 4-26). Thus the net effect of the adsorption buffer is a dampening of the peak concentrations expected from the dissolution reaction and a stretching of the leach profile with time. It should be pointed out that the areas under all leach curves in Figure 4-27 are identical and correspond to the 0.2 mg/g Cr(VI) originally present in the material.

Solubility Product Dissolution

In the next study the effect of instant dissolution is compared to dissolution limited by solubility (as expressed in a solubility product). For this the Na instant dissolution reaction in the base case is replaced with solubility type dissolution reaction:

$$NaX \rightarrow Na^{+} + X^{-}$$

The solubility limit of Na from dissolution of the hypothetical NaX salt is 9000 mg/l. All parameters characterising the reaction are listed in Tale 4.6.

Table 4.6: Parameters for NaX Solubility Product

Parameter	Value
Molar mass of NaX :	73 g/mol
ini. solid conc. of NaX :	1-2.5 mg/g
solubility product K_{NaX} :	$1.76 \cdot 10^8$ $(mg/l)^2$

Figure 4-28 shows simulated Na leach curves for instant dissolution and solubility product dissolution with various initial concentrations of the NaX salt. All other parameters were kept at base case values. Clearly the solubility product reaction acts as a release buffer maintaining the Na concentrations at the 9000 mg/l solubility level until all salt has dissolved. Where the initial salt concentrations are too low to reach the solubility limit (as is the case for 1 mg/g NaX, as shown in Figure 4-32) all salt dissolves instantly and the effluent leach curve shows the same behaviour as that modelled for instant dissolution. If the salt concentration just corresponds to the 1 mg/g Na of the base case (at 1.6 mg/g NaX) the leach curves allow direct comparison. The instant dissolution curve shows a smoother fall-off profile, while the solubility curve falls off more abruptly.

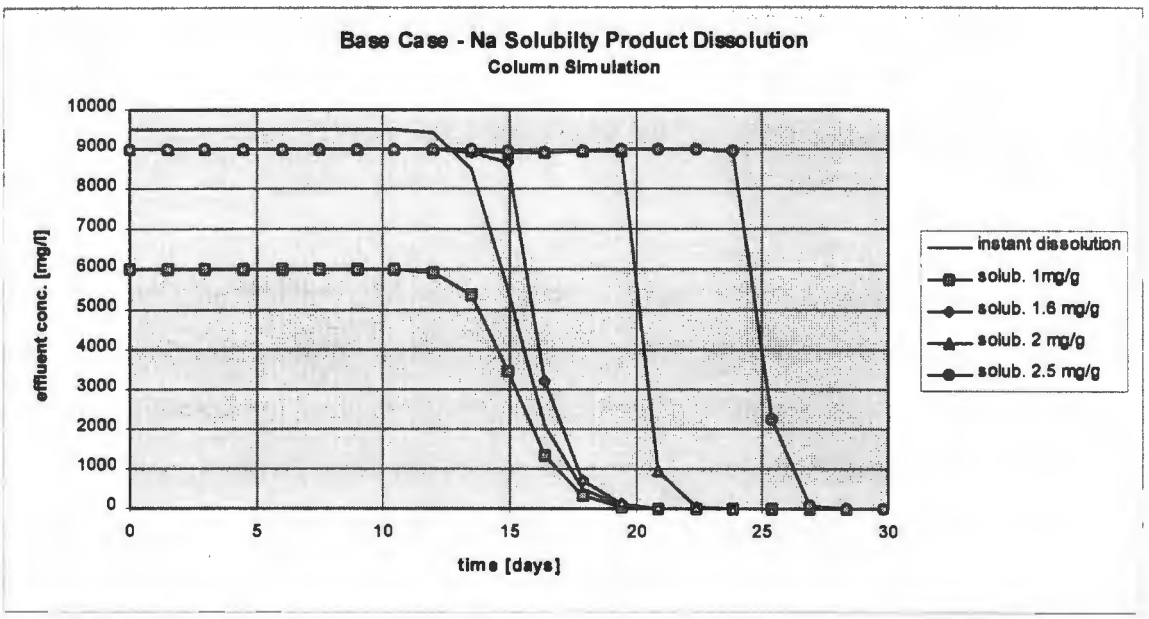

Figure 4-28: Influence of solubility controlled dissolution on Na leach profile (various NaX concentrations)

This can be explained as follows: When fresh fluid enters the bed the dissolved Na migrates backwards against the direction of flow due to bed diffusion effects (see further below) resulting in a "smearing" of the initially sharp concentration front, which results in the smoothed fall-off curve, once this has reached the bottom of the bed. The solubility buffer, on the other hand, maintains the Na concentration at a constant level and thus effectively preventing the "smearing" effect until the salt is depleted. When the leach front reaches the bottom of the bed, the fall-off corresponds more or less to a step change with only some backward migration following salt depletion.

Kinetic Dissolution Involving a Reactant

The next study focuses on a kinetic leach reaction involving a reactant species. Here it is assumed that Cr is released in kinetic fashion through the action of acid (i.e. H^+), which is consumed in the reaction. H^+ is introduced as an additional species in the simulation and the kinetic Cr(VI) dissolution reaction is replaced by the kinetic leach reaction mode with the first order rate constant k varied between $1 \cdot 10^{-7}$ and $1 \cdot 10^{-8}$ s^{-1}. All other model parameters were kept the same as the base case. Figure 4-29 shows the leach curves generated by WASTESIM for a constant feed concentration of H^+ (100 mg/l) and varied kinetic constants. Figure 4-30 shows the simulated leach curves for cases where the feed acid concentration is varied, but the kinetic constant kept constant at $1 \cdot 10^{-7}$ s^{-1}.

A small kinetic constant and thus rate of reaction results in a low rate of consumption of acid and production of Cr. Consequently the Cr leach curve appears drawn out, whereas the acid, which is not fully consumed on its path through the bed breaks through more or less after one bed residence time (15 days, see above) has passed, with a small degree of "smearing" as a result of bed diffusion (see below). It then tapers off more gradually as the slow Cr leaching reaction continues and it reaches the feed concentration level once this reaction is completed. For increased reaction rates the acid is consumed more rapidly and consequently breakthrough appears later. At the same time the Cr leach curve appears more in the form of a peak as the time for total Cr dissolution becomes shorter.

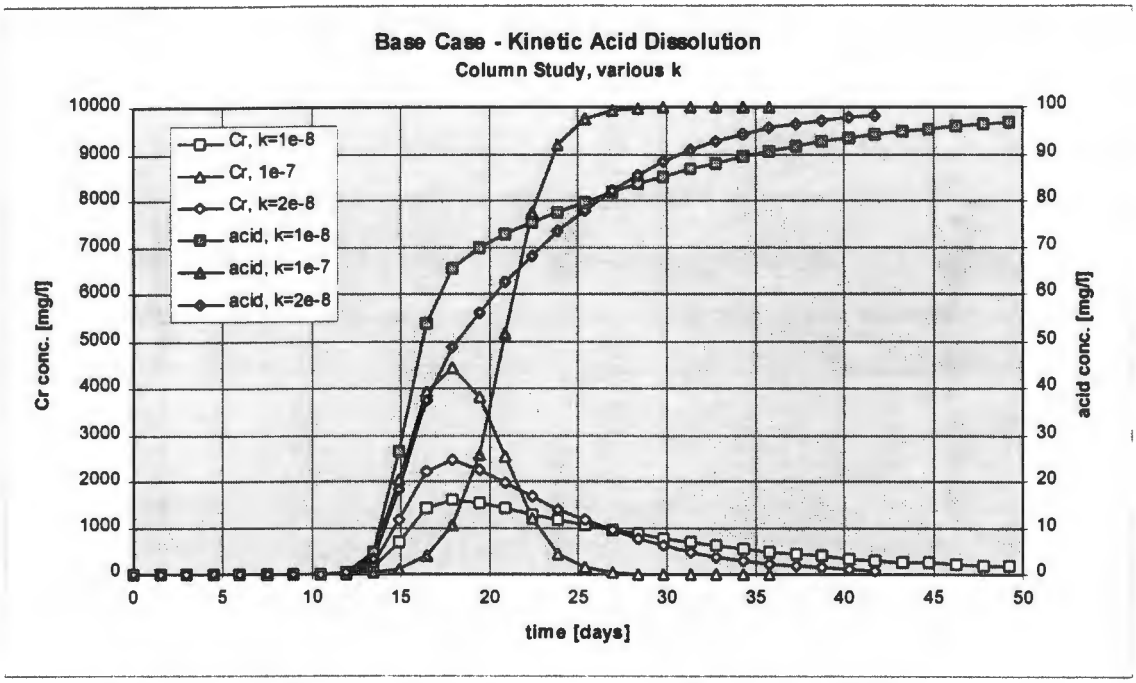

Figure 4-29: Effect of various kinetic leach constants for the acid dissolution of Cr

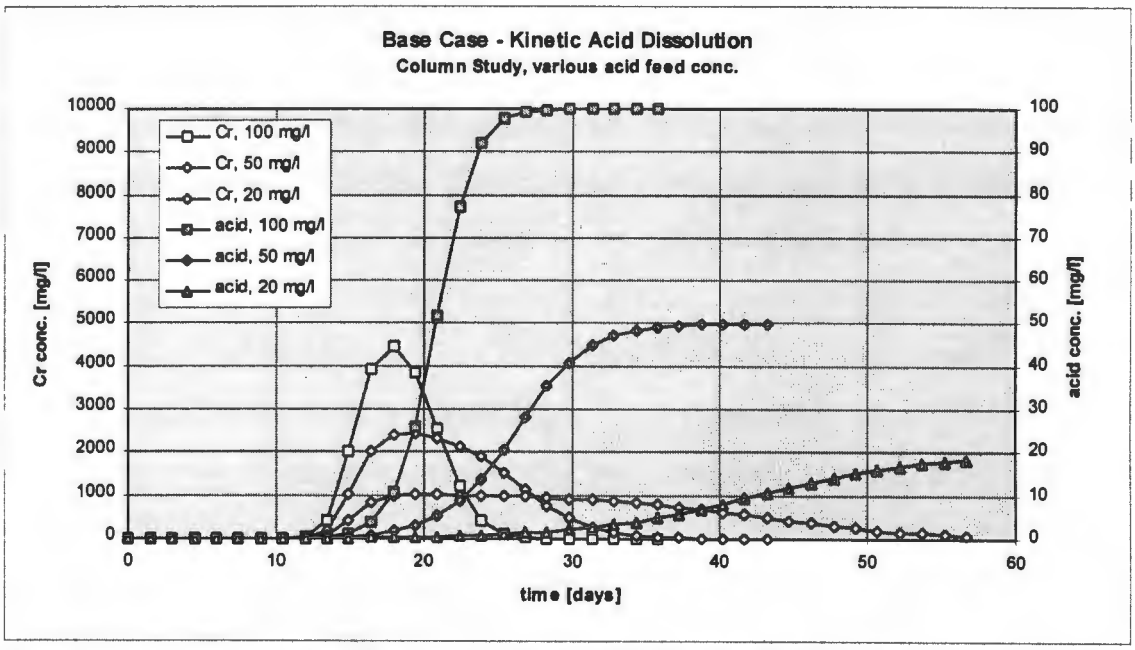

Figure 4-30: Effect of various feed acid concentrations on the kinetic dissolution of Cr

Decreasing the feed concentration of acid results in slower dissolution of Cr (despite the relatively high rate constant) as acid concentrations become limiting in the bed. Thus fresh acid will have to be continuously supplied through the feed before the reaction can

proceed further. Consequently the Cr leach curves become more drawn out the lower the feed acid concentration and acid breakthrough appears increasingly later due to increasingly complete consumption in the bed. It should be pointed out, again, that the area under all Cr leach curves in Figures 4-29 and 4-30 are identical and correspond to the 0.2 mg/g initial Cr concentration in the material. It should also be remarked here, that this scenario corresponds to the approach commonly used to model heap leaching and an extensive discussion of kinetic leach reaction phenomena is given by Dixon (1992) and Davies (1995).

4.8.5 Column Studies: Bed Residence Time, Bed Saturation and Dispersion

As was indicated in several of the studies above, the parameters describing fluid transport through the bed also influence the dynamic nature of the effluent leach curves. The total residence time of fluid in the bed corresponds to the ratio of total fluid volume held up in the bed pores and the feed flow rate. This volume is, in turn, determined by bed cross-sectional area and height, bed porosity and pore saturation with fluid. Figure 4-31 shows modelling runs of the base case with three different residence times as determined by varying bed height and feed flow rate.

The figure clearly indicates that the change of bed residence time mainly results in a shift of the fall-off points of the leach curves as would be expected. It is worth noting, however, that the fall-off becomes more protracted with increasing residence time. This can be explained by the increased effect of bed dispersion, which is a time dependent phenomenon, i.e. the longer the fluid resides in the bed, the more the concentration difference between what is dissolved in the bed initially and the fresh fluid entering the bed becomes "smeared" by diffusion against the direction of flow.

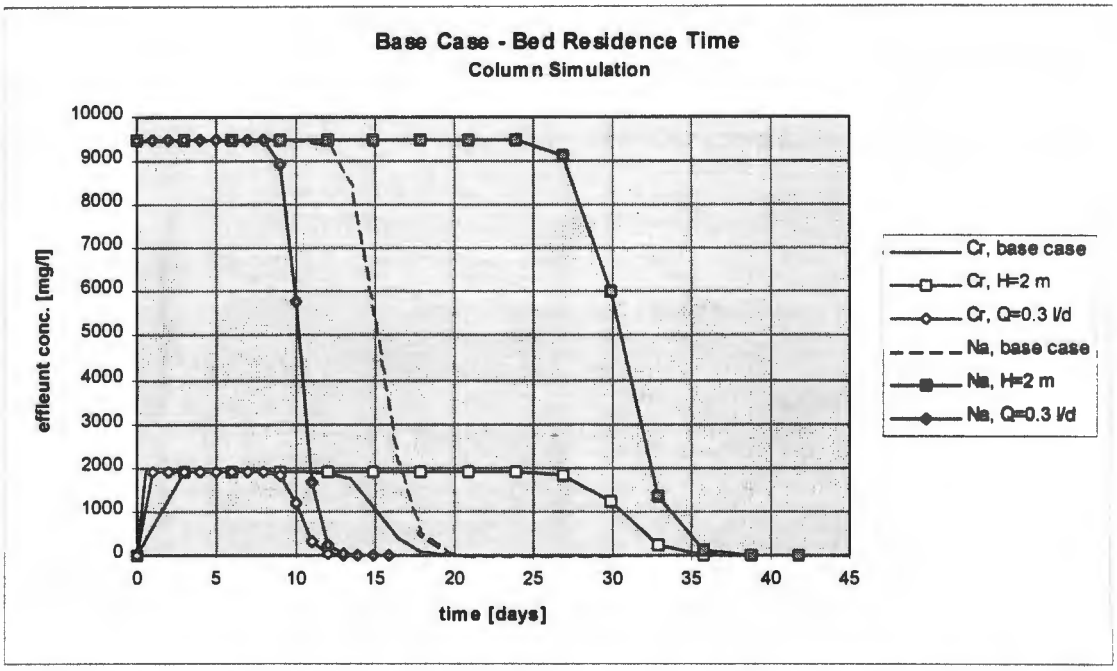

Figure 4-31: Study of various bed residence times on the base case leach curves

Bed dispersion is governed by a combination of hydro-dynamic effects, such as micro-mixing, and molecular diffusion (see Section 4.2). In the WASTESIM code this is taken into account through a bed dispersion factor d_{bed} with which the free solution diffusivity is multiplied to achieve an "effective bed diffusivity", similarly to that defined for particle pore diffusion. It must be stressed, however, that bed dispersion is different from pore diffusion in as much as it is not only governed by geometry, but also flow conditions and bed saturation. Figure 4-10 (in Section 4.2) gives an indication of the relationship between bed dispersivity and hydrodynamic conditions in saturated beds. For flow through unsaturated beds estimation of this effect is generally difficult and has to resort to empirical means (for example through tracer studies, which is discussed further in Section 5. 6).

For purpose of demonstrating the model sensitivity to variation of this effective bed diffusivity, the base case scenario has been modelled varying the bed diffusivity factor d_{bed}. This is shown in Figure 4-32. Clearly, increased bed dispersion at the base case flow rate (Q=0.2 l/day) results in an increased "smearing" of the leachate front exiting the bed in consequence to increased backward migration of the dissolved concentrations into the

fresh feed liquor. This effect becomes more pronounced for simulations with a reduced flow rate (Q=0.1 l/day, also shown in Figure 4-32), which results in double the bed residence time. This illustrates that bed dispersion is a residence time dependent phenomenon.

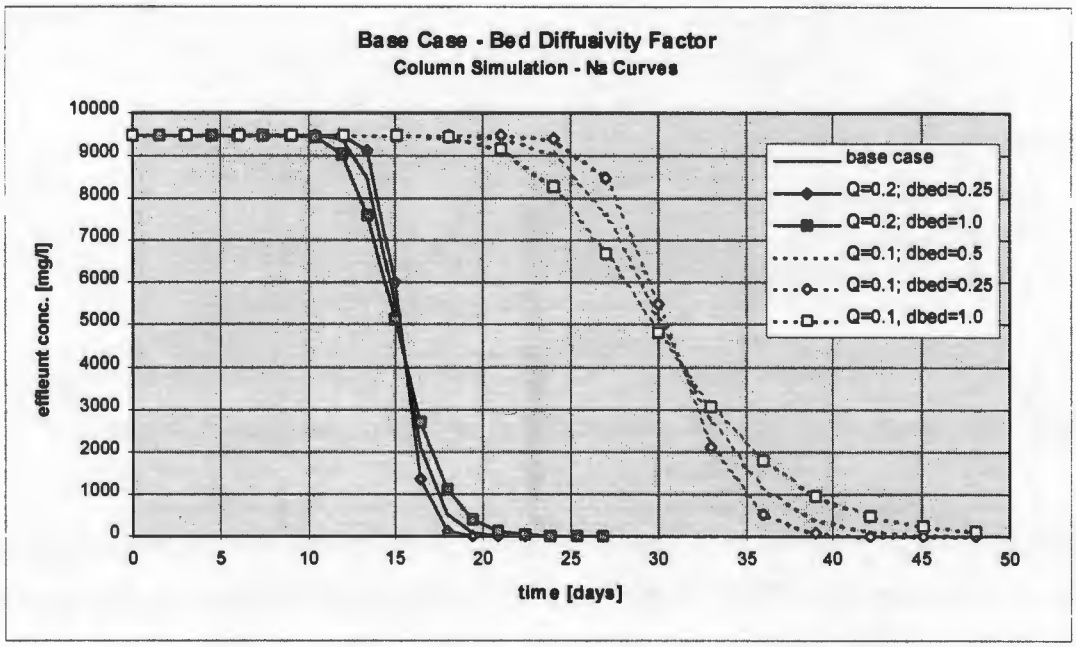

Figure 4-32: Influence of effective bed dispersion on the modelled leach curve for Na for base case flow rate of 0.2 l/day and reduced flow at 0.1 l/day

Besides bed dimensions and feed flow rate, the bed residence time is also governed by bed porosity (in terms of the interstitial voids between particles through which flow can occur) and the degree of fluid saturation of these pores. But furthermore, these two factors also determine the effective solid to liquid ratio in the bed, i.e. the amount of fluid present in the bed relative to the mass of solid particles it is in contact with. This, in turn, directly affects the release behaviour of dissolving constituents into the bulk fluid, in terms of both, actual concentrations achieved and the dynamics of chemical reactions (which are dependent on solution concentrations). This effect is demonstrated in Figure 4-33, which shows the modelled leach curves of the base case scenario with the fractional bed saturation varied.

Clearly, increased bed saturation, resulting in both an increased bed residence time (as more fluid is held up in the bed) and a decreased solids to liquid ratio, has quite a marked effect on the effluent leach profiles, as they become significantly more protracted and dilute. Again, the area under the leach curves is the same in all cases and corresponds to the initial concentrations present in the material.

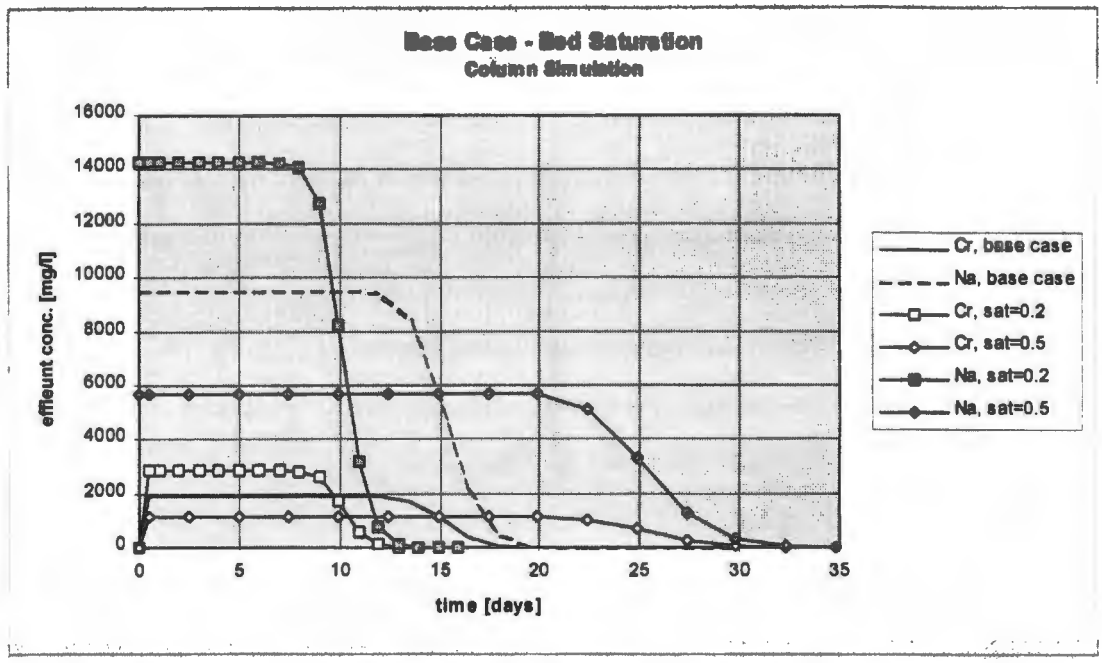

Figure 4-33: Influence of varied bed saturation on base case leach profiles.

Determination of bed saturation in unsaturated beds is, however, not a straightforward exercise. Not only is this dependent on factors such as bed packing, particle size distribution, particle shape and surface characteristics, but may also be a function of time as seasonal drying and wetting of a bed exposed to the elements directly influences the amount of fluid present in the bed (Section 4.1). This is significant in terms of the stated purpose to use the model in predicting leach scenarios from waste deposits, the majority of which are likely to exhibit unsaturated conditions (see Chapter 3). With small errors in the estimation of bed saturation leading to significantly different leach scenarios in terms of time dependence and concentrations of the effluent profiles, correct estimation of the hydrodynamic conditions in the bed are crucial. This aspect is elucidated further in the context of the experimental studies in the following chapters.

4.9 Summary and Further Aspects

4.9.1 Summary

A detailed review of modelling approaches to hydro-transport through porous media, including transport of species dissolved in the aqueous phase, the underlying theory as well as background on the incorporation of chemical reaction modelling is given in Sections 4.1 to 4.4. There appears to be large number of geochemical transport codes, some of which include comprehensive chemical equilibrium models, which can be used to model the migration of a contaminant plume through a porous soil matrix. However, for modelling the actual release of contaminants from the solid matrix, as would be required to describe the leachate generation behaviour of solid waste deposits, these codes appear less well adapted and , moreover, often overly rigorous considering that full chemical characterisation of the solid material is mostly not possible.

Using modelling tools developed for heap leaching appear to be a better approach given the similarity between waste leach and heap leach scenarios. These models usually employ chemical reactor theory at the level of individual particles and combine this with a simplified one-dimensional transport model at the overall heap level. There is, however, considerable variance in the degree of rigour employed for reaction modelling and, given that these models were developed for heap leaching, they focus almost exclusively on one principal kinetic leach reaction. The heap leach model developed by Dixon (1992), reviewed in detail in Section 4.5, offers the most rigorous approach and was chosen as the basis for expansion to incorporate effects considered important in the modelling of waste deposits.

The fundamental equations governing this expanded leach model are developed in Section 4.6 The model operates at three different levels, the pores of an individual particle, the particle surface and the porous bulk matrix. The pore model (equation (4.6-1)) has been introduced by Dixon and was retained unaltered. It models the individual particle as

porous spheres, with the only mode of transport through the pores being molecular diffusion described by an effective diffusivity, which accounts for pore tortuosity.
The surface level equation (4.6-9) was introduced in departure from the Dixon model in order to account for surface film diffusion effects if these exist. This is justified as under certain flow conditions removal from the particle surface may be hindered by diffusional migration into the moving bulk fluid, which is corroborated by Dixon's experimental results. Identification of whether such conditions exist may be achieved on the basis of a modified system Peclet number (equation (4.6-8)).

Transport of dissolved species into and with the moving bulk phase is described by equation (4.6-13), or, if surface effects are absent, by equation (4.6-14). In departure from Dixon's model, a bulk dispersion term has been introduced, which may become relevant in slow moving systems, where diffusional migration through the bulk fluid is of a similar order of magnitude as convective transport. Bulk transport is described in the vertical direction only as it is felt that this would be the principal direction of flow in any type of heap.

Although aimed at providing a comprehensive model for reaction-transport of leachate from waste deposits, a model equation for stirred tank batch reactors is also derived (equation (4.6-16)). This is useful for modelling laboratory scale experiments which are conducted in order to identify particle level reaction and transport parameters. Here the particle level reaction-diffusion model remains the same as before, but on the bulk level the transport model is essentially replaced by a dynamic mass balance.

The model equations allow incorporation of reactive contributions at all three levels considered. A unified approach to the calculation of these reaction contributions on the basis of dissolved and solid concentrations of the participating species is introduced in Section 4.7. This relies on the formulation of a reaction extent variable e_C and stoichiometric coefficients β_i for all participating species (equation (4.7-5)). Some care

needs to be taken for reactions involving solids which need incorporation of the local solids to liquid ratio. This is covered in detail in Section 4.7.4.

Two main types of reactions are distinguished, those proceeding fast to some thermodynamic equilibrium and those for which a kinetic reaction model can be formulated. While incorporation of the latter into a dynamic model is straightforward, equilibrium models require discretisation, assuming equilibrium is reached within a given time step and the resulting changes in concentration of the participating species can be expressed as their "rate" of change in this time interval. This approach precludes analytical solution of the model equations, but this is not considered problematic as the overall reaction-transport model is too complex for analytical solution in any event and will have to resort to numerical methods.

Detailed explanation how to calculate the extent variable for each time step for a number of both, kinetic and equilibrium, reaction types within each discrete time step is given in Section 4.7.3. These include kinetic leaching and dissolution as well as equilibrium adsorption, dissolution/precipitation and the solubility product of water. It should be pointed out again, that this list is by no means exhaustive of possible reaction types, but contains what is considered most important for the modelling work in the present study, and is sufficiently indicative of how other reaction types can be incorporated.

The model equations thus presented in Sections 4.6 and 4.7 represent the basis for an extremely versatile tool for modelling a large number of deposit and laboratory leach scenarios incorporating multi-species, multiple reaction modelling. These have been translated into the WASTESIM computer code, the basic numerical algorithms of which are detailed in Appendix B. A MS-DOS based prototype version of the code WASTESIM is included on the disk accompanying this volume. The basic layout of the program and its various simulation modes are described in Section 4.8.1.

Model operation and its sensitivity to a number of model parameters is tested with a base case study in Sections 4.8.2 to 4.8.5. The sensitivity study clearly demonstrates the extreme versatility of the modelling approach in terms of incorporating various reaction and transport modes and switching between batch and column leach scenarios. The study highlights the extent to which transport parameters, such as effective pore and bed diffusivity as well as bed residence time (as determined by bed geometry and flow-rate), can influence the dynamic leach curves in batch and column scenarios. Direct comparison between batch and column studies also show that kinetic effects significant at batch scale may appear more or less instantaneous in the column study and inversely, kinetic effects observed at the column scale may be so slow that they may go unnoticed at the batch scale, which is normally operated over much shorter periods of time. This is significant in the light of the aim of this work to use laboratory scale studies to predict the leachate generation behaviour of full scale deposits. Also significant is the influence of column saturation on predicted leach curves, considering that this quantity is difficult to measure in practice.

4.9.2 Model Limitations

The model developed in this chapter is an attempt to be as inclusive as possible while maintaining model complexity at a reasonable level. While much of the model's success for a given scenario much depends on a sensible choice of relevant species and reactions and the material characterisation that goes with it, there are a number of phenomena that can potentially occur in a waste deposit scenario, for which the model does not cater at its current state of development. Some of these are listed below:

- Complex bulk flow characteristics: the model is only one-dimensional in its description of the bulk flow, which is justified by the assumption that the principal direction of flow in a waste deposit will be vertically downwards. If transverse flow is significant (i.e. the flow field is 3 dimensional), the model is likely to fail. Likewise the model

assumes well distributed flow over a cross-section of the bed. If there is a significant amount of flow channelling, i.e. preferential flow paths where the bulk flow moves fast relative to other areas, then the model's applicability is limited. One could, in principle, sub-divide the heap into a "bundle" of parallel columns with different flow velocities in each and model these individually, but that would not account for transverse migration (by diffusion) between the columns. It would furthermore be difficult, if not impossible, to determine the distribution of flow channels in a bed *a priori*. A further aspect of unsaturated bulk flow is the changing moisture content in consequence to seasonal wetting and drying, which would affect in essence the bulk fluid void ratio ε_b. The bulk flow model would have to be reformulated in terms of the Richards equation (4.1-14) to account for this phenomenon.

- Changing particle characteristics: One important assumption for the model at the particle level is that particle characteristics remain constant during the leach process in terms of particle size distribution and porosity. This presumes that the amounts of leachable constituents are small relative to the total particle volume, so that their removal would not result in a reduction in particle size (shrinking particle concept) nor in a significant increase in the internal pore volume. Materials, that do not fulfil these criteria cannot be effectively accounted for by the current model. It would be possible, in principle, to cater for a changing porosity and include a population balance in the model, but this would seriously compromise its ease of solution. Also, quantification of these effects is not straightforward, since shrinking particles would have a secondary effect on bed packing and thus on flow profiles through it.

- Bed silting: precipitation of salts in consequence to super-saturation is unlikely to occur on the pore walls of a particle in as well distributed a fashion as dissolution. More likely it will lead to the formation of suspended nuclei in bulk and pore fluid, which will eventually settle and potentially block particle and bulk pore spaces, which could significantly restrict transport of other dissolved species. Such effects are not taken account of in the model.

- Temperature effects: changing temperatures affect essentially all physical parameters describing the bed, flows and reactions. While it is not a problem to correct all of these for changing temperatures, the model in its current state is not set up to incorporate this, which is a limitation considering that seasonal changes in temperature in parts of the world can be as much as 50 °C.

- Non-ideal Solution Thermodynamics: All model and reaction equations introduced in Section 4.6 and 4.7 have been formulated in terms of species concentrations, which is logical for maintaining continuity. However, as was indicated in Section 4.3, equilibrium reaction models are usually described in terms of the thermodynamic activities of the participating species rather than their concentrations. Similarly, diffusion processes are more correctly described on the basis of gradients of chemical potential, rather than concentration.

  Activities for dissolved species are related to their concentration via activity coefficients, which can be calculated from suitable thermodynamic models, such as the Debey-Hückel law for ionic species in dilute solutions, but such calculations are cumbersome in many cases and require knowledge of the concentrations of all other species involved. The current model formulation allows modelling of the fate of a selected number of species, although other species may be present in the system. If activity calculation was incorporated into the model, which is not problematic in principle, this selective modelling is no longer possible as the concentrations of all species at all times need to be known. For many modelling scenarios this would seriously compromise processing speed necessitating the need for powerful computing equipment, which contradicts the stated objective of numerical simplicity. It needs to be seen to what extent omission of activity coefficients affects the capabilities of the present model.

- Dissolved gaseous species: Although the model equations are not restricted to the concentrations of ionic species, the adsorption of gaseous species, such as O_2 and CO_2 from the gas phase present in unsaturated beds is currently not considered, although the role of carbonates and atmospheric oxidation reactions are of considerable importance in the modelling of waste deposits (for example the oxidation of sulphide minerals in the context of acid rock drainage, see Section 2.2.6). In principle, gaseous dissolution can be incorporated into the model by means of a suitable gas adsorption isotherm, such as Henry's Law, but the gas phase in unsaturated beds would then have to be considered as an additional bulk phase with a separate transport equation and can no longer be handled as "dead" volume. Dixon (1996) has indicated that this is not particularly problematic, but currently such modelling of gas phases is not considered further.

5

An Integrated Waste Assessment Methodology: Experimental Methods and Analytical Tools

The comprehensive model developed in the previous chapter provides a framework within which the modelling of contaminant release from a waste material, and subsequent transport of leachate through the waste deposit, can be achieved. For any specific waste material under investigation a number of input parameters to the model are required, which characterise the release behaviour of the material with respect to various chemical species of interest and further some aspects of their transport behaviour within a deposit.

In line with the objectives set out in the introduction (Chapter 1), these parameters must be found from a suitably designed set of laboratory experiments on the material in question. Methods for the laboratory assessment of waste leach potential have been proposed by numerous workers and some form part even of regulatory frameworks. Some of these are reviewed in Section 5.1.1. While such tests allow some insight into the waste leach behaviour under laboratory conditions, they are rarely directly applicable to full scale waste deposit scenarios, other than by giving general trends. A more systematic approach is therefore required that allows the establishment of characteristic parameters from laboratory experiments, which are then used with the model to predict realistic full scale waste leach scenarios as a function of time. An integrated assessment and modelling methodology is proposed in Section 5.1.2, which is aimed at achieving this systematic approach.

This methodology has been developed through detailed experimental and modelling studies with two real waste materials with specific focus on the release of chromium. Detailed accounts of the full experimental investigations and modelling studies for each of

the two materials tested in this thesis are given in Chapters 6 and 7. Since the methods and tools used for the interpretation of the data are similar in each case and follow the general methodology laid out here, these are introduced and discussed in general terms in this chapter. This includes general material characterisation (Section 5.2), lysimeter studies (5.3), batch leach experiments (5.4) and adsorption studies (5.5). The use of the models, which form the core of the WASTESIM code (Chapter 4) is elaborated in some detail for extraction of parameters from laboratory experiments (leach kinetics, Section 5.4) and column tracer studies (Section 5.6). The chapter concludes with a brief introduction of common aspects of the two experimental studies (Section 5.7).

5.1 Methodological Approach to Waste Leachibility Assessment

As was illustrated in Chapter 3, the potential of a waste material to generate a harmful leachate within a deposit scenario has led to the introduction of a number of measures to minimise the migration of leachate beyond the boundaries of a deposit, for example through the use of liners and leachate collection systems. The rigour of such measures is determined by a preliminary assessment of the leachate generation potential of the waste material on the basis of laboratory experiments. Section 5.1.1 gives a brief review of the types of analyses commonly conducted in this context.

One significant draw-back of such experimental assessments is, however, that they are restricted to the laboratory or, at best, pilot-plant scale and little guidance is offered how to translate the information obtained into leach scenarios in full scale waste deposits. In the absence of a better understanding of the complex and time-dependent chemical and physical processes occurring within waste deposits, many assessment techniques resort to establishing the maximum possible - or "worst case" - release behaviour for the material under consideration. The philosophy behind the latter approach is the assumption that, if contaminant release is acceptably small under fairly aggressive (worst case) conditions (usually in terms of leachate pH), then it will be the same or less under more realistic

(usually in terms of leachate pH), then it will be the same or less under more realistic conditions. In this way such methods are more in aid of waste "typing" than assessing their dynamic potential to generate leachate. Furthermore, the definition of "acceptably small" contaminant release is in itself a matter of debate as continuous release of small contaminant concentrations over long periods of time may in some cases offset release of large concentrations over a relatively short period

The model developed in Chapter 4 offers an important tool to avoid such shortcut methods by allowing a rigorous description of the time-dependent leachate generation process in terms of a number of significant parameters, both in terms of chemical release and transport behaviour, for a given waste material. These parameters still need to be established from suitable laboratory experiments, but they can now be correlated in a meaningful way to allow scaling to full scale waste deposits. Thus an integrated waste assessment methodology can be formulated in which experimental laboratory assessment is combined with the modelling tool. This methodology is put forward in Section 5.2.2.

5.1.1 Review of Existing Waste Assessment Methods

Laboratory waste leach test procedures currently practised fall into two main categories - batch leach tests and column (lysimeter) tests. While batch leach procedures are usually cheap and fairly rapid to conduct, lysimeter experiments, depending on their scale (in terms of the size of the waste bed), can be considerably more expensive to set up and maintain. Jackson et al. (1984) compared results of a sequential batch leach procedure (see below) and a small scale column test on various wastes under comparable conditions and concluded, that, while the batch extraction method offer greater reproducibility and simplicity, the column test was more realistic in simulating conditions which occur under field conditions. It appears that the judicious manipulation of solid to liquid ratio, pH and redox conditions in a series of relatively inexpensive batch tests can identify the reactions controlling the chemical release process, and enable the thermodynamic and kinetic parameters of the governing processes to be identified. Column systems complement the

results from batch tests by providing critical information on the effect of moving concentration boundaries on the dissolution of solutes (Jones, 1995). In this sense, batch leach procedures should be designed to emulate likely field conditions as they might be identified from suitable lysimeter experiments and further pinpoint the release mechanisms relevant to the waste material under consideration. Van der Sloot *et al.* (1990) point out that tests yielding a more fundamental understanding of waste leach behaviour allow a more rational approach to establishing the environmental quality of a particular waste material. Current standardised leach tests have a limited rational basis in this regard.

There are a number of such standardised leach procedures devised by licensing authorities in order to establish base case waste characterisation methods, but the extent to which these would suffice to assess true waste leach behaviour under field conditions must be seriously questioned. Prominent amongst these standardised tests is the Toxicity Characteristic Leaching Procedure (TCLP) as devised by the US EPA (US Federal Code of Register, 1992).

In the TCLP a charge of waste material, pre-sized to less than 9 mm, is leached in an acetic acid buffer solution in a Zero Headspace Extractor (ZHE), a container with no air space between liquid and its walls, tumbled in a rotary device for 18 hours. The leachate is then analysed for concentrations of certain organic and heavy metal constituents. If any one of these exceeds certain limits, which derive from arbitrarily multiplying drinking water standards by 100, then the waste material is classified as toxic, requiring deposition in a hazardous waste landfill with double liner system (see Section 3.2). The kinetics of contaminant release are not established in this procedure. In essence the TCLP thus constitutes at best a "worst case" assessment, merely suitable for waste typing, as indicated above.

The TCLP superseded the older EP Tox procedure which was an acetic acid leach controlled at pH 5, but did not allow for the measurement of a number of volatile organics

(Dietrich et al., 1993). The use of the ZHE in the TCLP enables the trapping of the organics in the leachate at the expense of pH control. Thus the emphasis of the test shifted from the determination of metals to the determination of organics (Drews and Mahote, 1994). Clearly the TCLP is designed for assessment of municipal domestic and mixed light industrial wastes which characteristically have a high organic content, but appears misplaced for primarily inorganic solid wastes as those from the minerals processing and mining industries. Furthermore, the fairly aggressive leach environment poorly reflects the contaminant release behaviour encountered in a realistic deposit scenario, even if kinetics are taken into account. Seemingly arbitrary choice of particle size limitations, leach time, leachant type and concentration are further factors that make the universal applicability of the TCLP questionable (Drews and Mahote, 1994). Nonetheless, the TCLP enjoys widespread use as the sole waste assessment procedure.

Other standardised batch leach procedures include:

- pH and/or redox controlled agitated leach tests (Ruhr-Universität Bochum, 1991): As opposed to the TCLP, pH is controlled at a specific value (usually between 3 and 5) using nitric acid to avoid organic complexation. Alternatively the redox potential of the eluate is controlled, although this is more difficult to maintain. The use of the acid leach environment is justified by the assumption that in the long-term the deposit will assume the pH of the incipient rain-water and must remain stable under these conditions. In this sense, this test is also a worst case assessment.

- Immersion leach tests (van der Sloot *et al.*, 1987, 1990): Larger specimens of a waste product are immersed in a given volume of leach solution, which is refreshed from time to time and analysed for dissolved constituents. Such experiments are particularly aimed at establishing the diffusion controlled release from larger waste particles.

- Sequential chemical extraction leach test (Stegemann and Cote, 1991): A charge of finely ground waste material is subjected to a series of successive extraction and leach

tests, which increase in their aggressiveness, ranging from ion exchange with lithium chloride to total digestion with hydrofluoric acid. This test is aimed at broadly categorising the various degrees to which selected hazardous constituents can be mobilised.

- Serial batch leach tests (Dynamic Leaching Procedure, ANS, 1986): A charge of waste material is contacted with fresh leach liquor (normally distilled water) in a number of successive leaches. This is aimed at modelling the changing leachate composition draining from the top layer of a hypothetical landfill or soil. This test was compared to lysimeter experiments run under similar conditions by Jackson et al. (1984) with mixed results.

- Acid Neutralisation Capacity (ANC): A test to assess the amount of acid or base equivalent that is required per gram of solid waste to maintain it at a specific pH. Leached concentrations are not measured in this test, but are sometimes correlated from ANC data for the leach behaviour of cemented wastes (Cote and Bridle, 1986).

Common to all these procedures is the establishment of maximum release behaviour of a particular waste material under intense if not aggressive conditions. Careful dissemination of individual release mechanisms and effects of particle properties, such as size, is largely absent. In this sense, such tests must be seen as creating "worst case" scenarios and the usefulness of test results in realistically modelling leachate release and transport through waste deposit must be viewed with circumspection.

Jones (1995) reviews the experimental assessment of trace metal leachibility from coal combustion flyash conducted by a large number of workers over the last 20 years. It becomes clear, that meaningful assessment cannot be achieved by a few isolated leach tests, but requires a carefully designed test program to appreciate fully all major effects of concern. Jones states in this regard:

"Leach test methods for solid wastes are often criticized on the grounds that the results produced are either not reliable, or not able to be extrapolated to a disposal environment. However, the lack of agreement between the results of leaching tests and measurements in the field are probably more often the result of inadequate specification of the physical and chemical conditions used for the test, than inherent shortcomings of the methods themselves. It is essential that the reasons for carrying out a leach test be clearly identified from the start, to enable the correct method and operating parameters to be specified, and to permit the potential effects of unique features (for example, groundwater composition and redox potential) of the prospective waste disposal to be considered."

5.1.2 The Integrated Waste Assessment Methodology

The statement above clearly highlights two central aspects that need to be taken into account for meaningful waste assessment:

- Careful experimental investigation of the leach behaviour of the waste material being investigated under the chemical conditions it is likely to experience within a full scale deposit scenario
- Careful scaling (extrapolation) of the laboratory leach data to the full scale deposit scenario on the basis of meaningful parameters

In this sense, the approach to waste leachibility assessment needs to be methodical and carefully planned from the outset. The model of the leachate generation and transport process, which forms the core of the WASTESIM computer code, offers a valuable tool for the meaningful scaling of laboratory data to full scale scenarios. As indicated in Chapter 4, the particular strength of the modelling approach lies in the distinction of particle level reaction and bulk level transport mechanisms., which allows the establishment of the chemical reaction parameters in batch leach experiments without loss

of validity in a column leach scenario. An integrated assessment methodology combining laboratory tests with the modelling tool is proposed in the following. Figure 5-1 illustrates this approach.

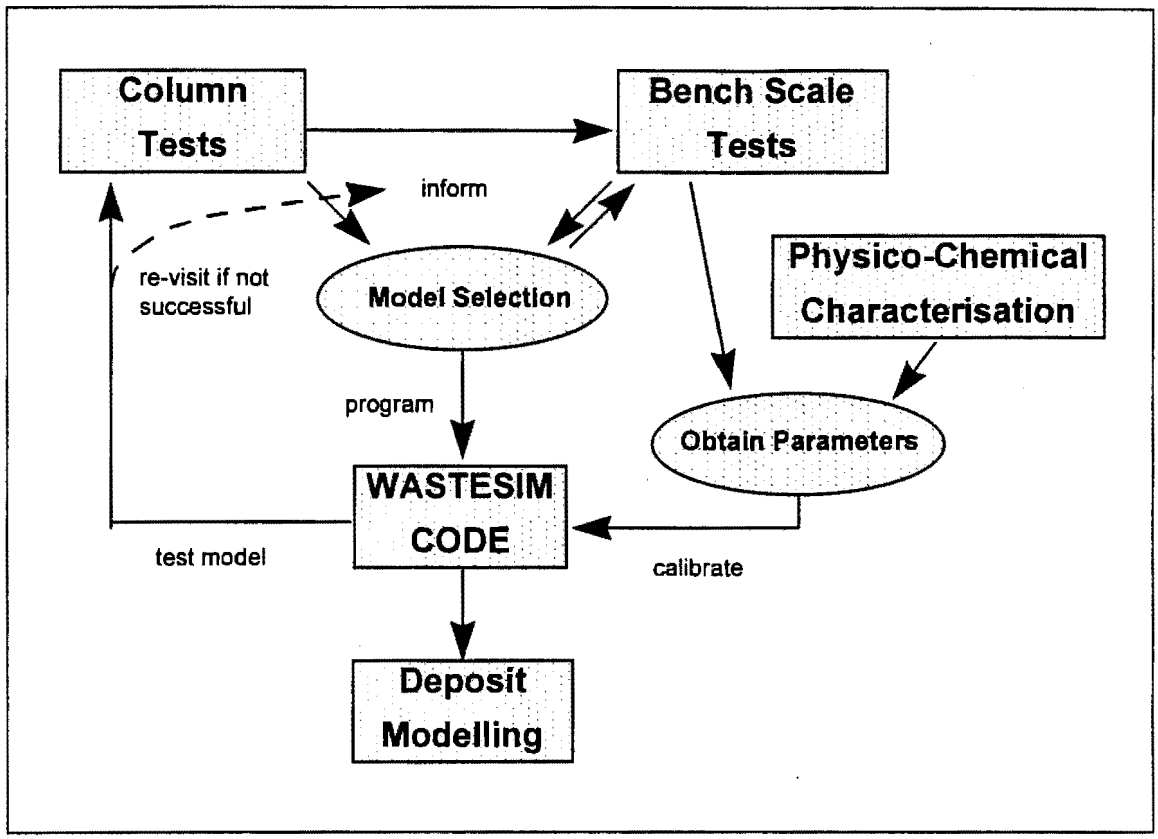

Figure 5-1: The integrated assessment methodology

As the statement by Jones (1995) indicates, the leach behaviour of a waste material should be investigated under chemical conditions likely to prevail in the deposit scenario the material is ultimately placed in. These conditions are more realistically established in lysimeter column studies than batch leach experiments (Jackson *et al.*, 1984). Therefore the proposed methodology suggests to investigate the leach behaviour of the waste material in medium scale lysimeter column studies. Not only do the results obtained from such experiments reveal a great deal about the chemical conditions in the bed, but also provide a set of time-depended leach curves, against which the results of the laboratory assessment can be tested later, using the modelling code.

Having established an "initial feel" for the prevailing chemical and hydrodynamic conditions and the predominant species that merit further consideration, a series of bench-scale experiments and tests is initiated which aims to further discriminate and quantify individual reaction mechanisms at the particle level. Such tests include dynamic leach experiments, adsorption studies and the establishment of particle pore diffusion effects through suitable leach experiments. The WASTESIM code in BATCH mode (see Section 4.8), which is based on a mathematical model for batch leach scenarios, can be used to extract kinetic leach parameters and pore diffusivities from experimental data by optimisation methods.

The sensitivity study of the model (Section 4.8) has clearly identified that model predictions are also strongly dependent on parameters which describe the transport behaviour of the fluid through the deposit bed. Thus the transport characteristics of the material under investigation in a deposit scenario also require careful examination by experiment. This includes physical characterisation of the particles in terms of size distribution, shape, bulk packing behaviour and so forth. But more importantly the hydrodynamic characterisation of the deposit bed needs to be established. It is proposed here that this can be achieved by tracer studies in laboratory scale columns which are modelled using the WASTESIM code in the COLUMN mode (see Section 4.8).

Once sufficient characterisation of the material in terms of its chemical reaction and transport behaviour has been achieved, a model is assembled from this information, which is thought to adequately describe the leach process in the initial column study. The model is programmed in the WASTESIM code by selecting the appropriate simulation and reaction modes and is calibrated using the experimental data from the bench scale experiments, tracer studies and physico-chemical characterisation. It should be pointed out that all calibration parameters have to be established by *independent* experiments and none is derived directly from the initial column study, which was aimed only at providing an initial indication of the prevailing chemical conditions.

This initial column experiment is now simulated using WASTESIM, programmed and calibrated in this way, and the simulation results are carefully compared with the experimental data. If this comparison is favourable it can now be assumed with some confidence that model selection and calibration are adequate to account for full scale scenarios, given the mathematically rigorous model components, and calibration on the basis of an extensive experimental study.

If, however, this intial simulation yields poor results, then both the model selection and laboratory assessment stages need to be revisited. Usually, the discrepancies between simulated and measured data will already reveal where the shortcomings of the current approach arise. These can then be addressed by appropriate modifications to the model and re-calibration on the basis of additional experiments. It must be stressed, again, that any modification of model parameters must be supported by further *independent* experiments and that the original lysimeter data must be kept as an independent test case, to avoid undue empiricism in the overall approach. This approach of fine-tuning the model is continued until satisfactory simulation of the initial column study is achieved.

As illustrated in Figure 5-1, once this assessment procedure has produced a satisfactory model of the test material in a small scale lysimeter experiment, it can be used to model full scale scenarios merely by changing the parameters that describe the different geometry and boundary conditions, while maintaining the central model components which describe the bulk hydrodynamic and particle level reaction-transport behaviour. The great advantage of this approach is that a number of deposit scenarios can be simulated without much additional information, which allows for the optimisation of waste disposal strategies in terms of their likely environmental impact.

A concern that needs to be raised regarding the approach presented here is the question of time scales. One aim of the laboratory assessment methodology is to achieve characterisation of the chemical release reactions with relatively short-term and simple experiments. Some release reactions may, however, be kinetically slow and therefore

overlooked in short term test. In a full scale deposit scenario, however, such reactions may potentially contribute significantly to the overall release of a particular species, but would not be accounted for in the model. This was already indicated in the sensitivity study of the model (Section 4.8) in the study of the influence of the kinetic constant of a particular reaction. This effect should be borne in mind, when studying the time dependent release behaviour of a material under laboratory conditions.

The various stages of the laboratory assessment and use of the model in data correlation and verification is elaborated in the following sections. It should be noted that all the work conducted in this thesis must be seen as in development of the methodology and some of the methods proposed and attempted here were later found to be insufficient or unsuitable. This is appraised more carefully in the concluding chapter (Chapter 8), where routes for further development are explored also.

5.2. Material Characterisation Methods

The materials under investigation in this study were characterised broadly as received with respect to the following categories:

- physical appearance: bulk appearance, dry bulk density, colour, smell, moisture content, etc.
- particle characterisation: size distribution, density, porosity, shape, BET specific surface area, etc.
- chemical characterisation: elemental composition, acid neutralisation capacity, water and TCLP leach behaviour

Physical assessment was conducted mainly by observation. Moisture content was established by drying overnight at 105 °C, dry bulk density by weighing a measuring cylinder filled with the respective material.

Physical particle characterisation was conducted by study of electron micrographs. Particle size distribution of samples was assessed by sieve analysis for the coarser slag material (Chapter 7) and laser diffraction analysis for the fine material studied in Chapter 6. True solid density was measured using a helium pycnometer.

In terms of the chemical characterisation, elemental composition was assessed by fusion with sodium peroxide and subsequent analysis of metals using atomic absorption spectroscopy. This method was preferred over XRF analysis due to the complex nature of the waste materials and the lack of appropriate matrix standards. Acid neutralisation capacity (ANC) was established by titration with nitric acid. Water washes entailed tumbling a charge in distilled water at 1:20 solid to liquid ratio for 24 hours and subsequently analysing the leachate. The TCLP followed the standard method as devised by the US EPA (1992). All analytical tools employed are detailed further in Appendix A.

5.3 Lysimeter Studies

Column studies are a commonplace method to assess the potential for leachate generation of a particular waste material. As was indicated in Section 5.1.1, they are considered to be more realistic in simulating conditions which occur in the field and can help identify experimental parameters for more specific batch leach experiments, such as prevalent leach pH and species concentrations. Many models for leachate transport away from deposits also rely on the knowledge of leachate composition at the bottom of the deposit as a function of time, for which lysimeter studies can give a reasonably good insight.

A drawback of lysimeter studies is the considerable amount of time and cost involved in setting these up and running them. A further aspect of the work presented here was, therefore, to investigate the effects of accelerating and down-sizing the lysimeter tests, and to what extend this could be accounted for by the model. Indirectly, in this way, additional base cases for the different materials were created against which model scale-up or scale-down could be tested.

Two types of lysimeter were employed in this study:

- **Constant Head Lysimeter** (Figures 5-2 and 5-3): These were designed for leaching of the fine materials for which it is assumed that their hydraulic conductivity under saturated conditions is sufficiently low to require a hydraulic head to drive liquid through them at sufficient rates. The unit consists of a 225 mm ID glass pipe with conical base, filled with glass marbles as base support. These are covered by a sheet of glass fibre onto which the material (slurried to a paste with distilled water) is carefully layered to achieve a homogeneous, saturated packing of the required height. The top of the packing is covered with another sheet of glass fibre and glass marbles to act as ballast to ensure bed compaction. The hydraulic head of leach liquor is achieved by either a 1 m head pipe over the bed which is connected to an adjustable reservoir bucket as indicated in Figure 5-2 a and b or by a connection to a compressed air line with pressure regulator if higher heads (at the expense of exact pressure control) were required (Figure 5-3 a and b).

- **Percolator Lysimeters** (Figure 5-4 a-c): These were used for coarser materials (LCS and MS) with hydraulic conductivities sufficiently high for the bed to remain unsaturated at the required flow rates. The unit consists of a 225 mm ID glass pipe with a conical base. Bed support is achieved either by the same type of glass marble packing as used in the constant head units or by a glass support plate covered with glass marbles. The material is packed onto a glass fibre sheet placed on the support to the required height by sprinkling small random charges evenly over the bed cross-section to the required height. The top bed surface is open to the atmosphere. Leach liquor is fed to the bed via a sprinkler mechanism, which consists of a peristaltic pump arrangement and a mechanical lever arm moving a dripping pipette fairly evenly over the bed surface in a rosette-like movement (Figure 5-4b). This was designed in order to ensure good surface distribution at the low flowrates required in the experiment.

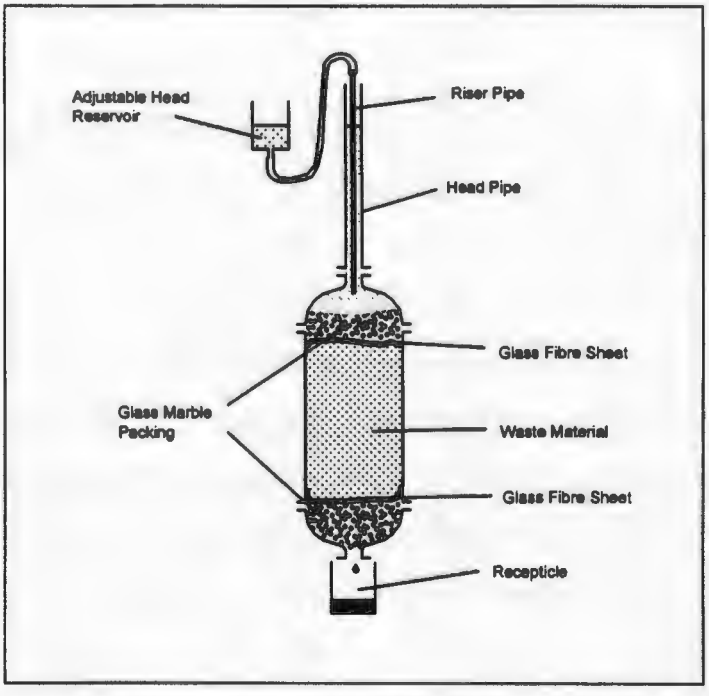

Figure 5-2a: Constant Head Lysimeter with head pipe and bucket arrangement (schematic)

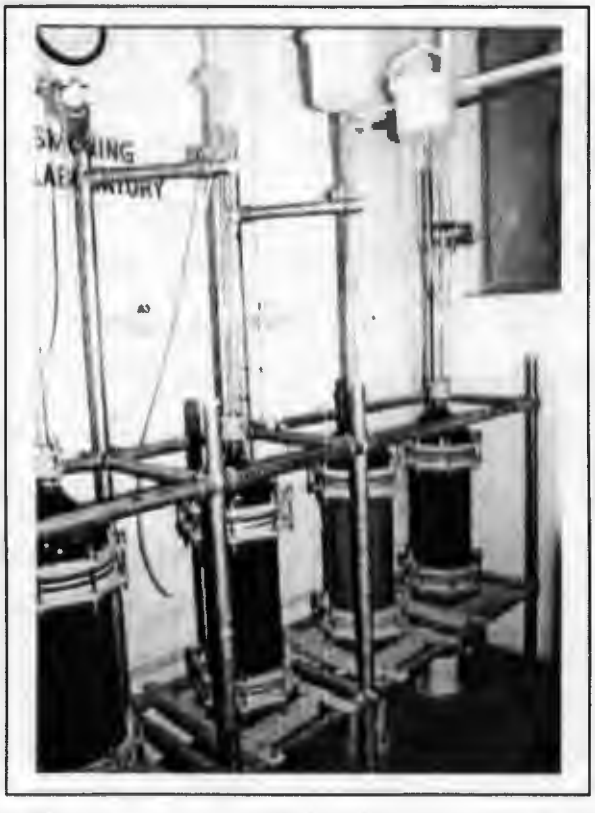

Figure 5-2b: Constant Head Lysimeter with head pipe and bucket arrangement (charged with fine dust material)

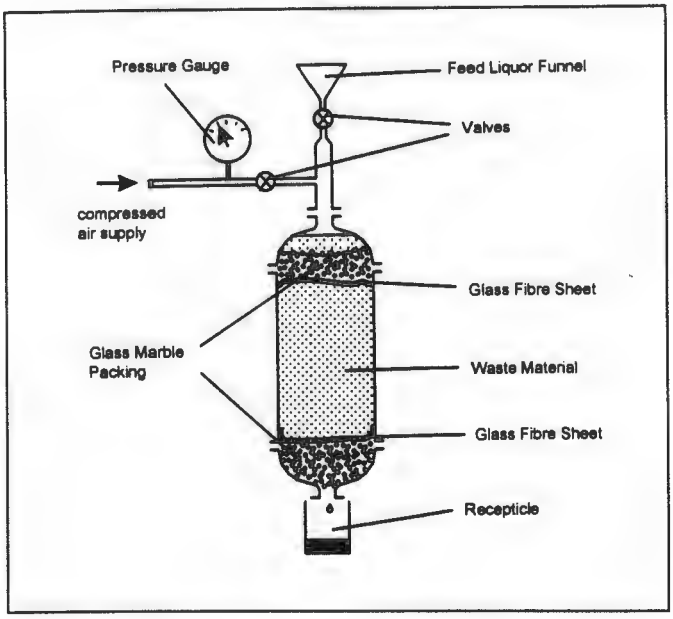

Figure 5-3a: Constant Head Lysimeter with air pressure arrangement (schematic)

Figure 5-3b: Constant Head Lysimeter with air pressure arrangement (charged with fine dust material)

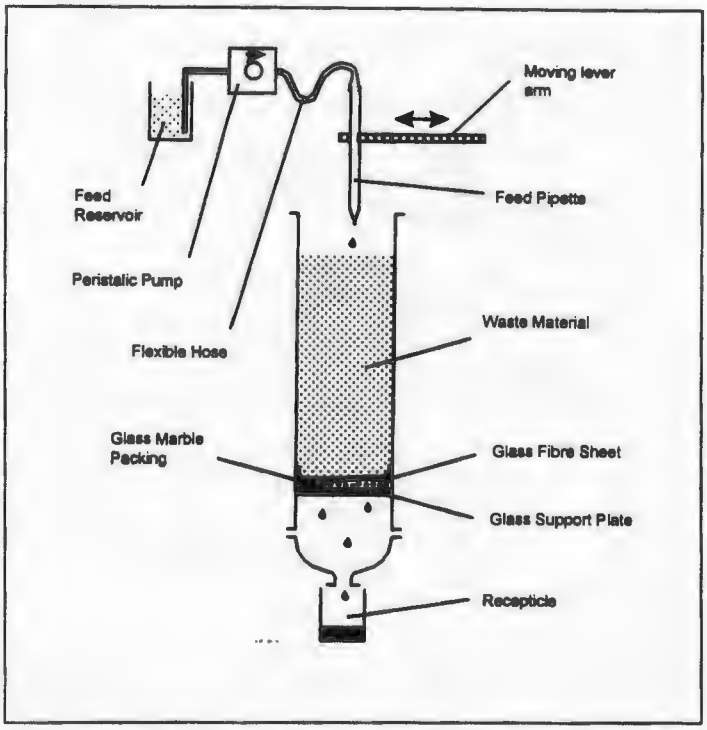

Figure 5-4a: Percolator Lysimeter (schematic)

Figure 5-4b: Sprinkler mechanism

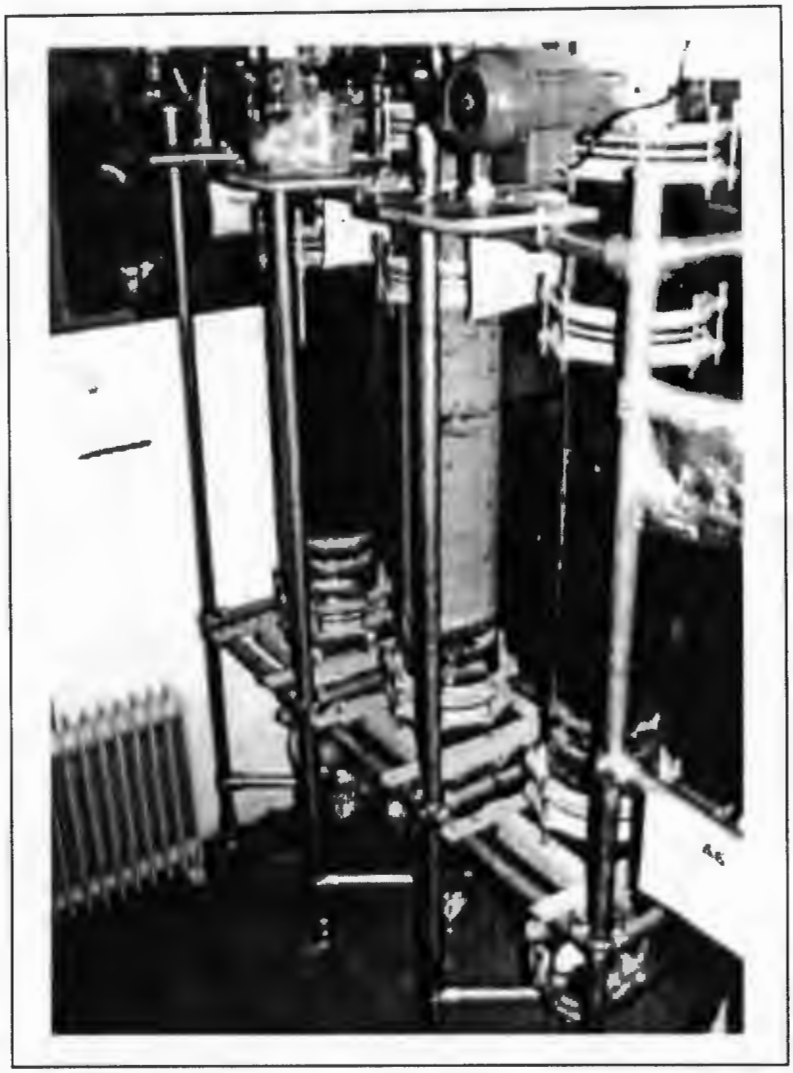

Figure 5-4c: Percolator Lysimeter(filled with various materials)

Both lysimeter types were constructed from QVF® glassware components. The effluent collecting at the bottom of the bed drains fairly rapidly through the base support and is collected in sample beakers placed underneath the column. In order to minimise evaporation losses of the sample, the beaker is packed into a plastic bag tied to the bottom outlet. The units were positioned in an enclosure in which the temperature was kept reasonably constant at 22 ± 2 °C.

After placement of the respective materials, the bed was left to settle for about 1 week before commencing the supply of leach liquor. The leach liquor used in all lysimeter

experiments was artificial "acid rain", distilled water acidified with a 6:4 mixture of sulphuric acid to nitric acid to a pH of 4.0 ± 0.05 and well aerated to ensure good dissolution of CO_2. The feed rate, which varied from experiment to experiment, was monitored only for the slag percolator units, since the unsaturated conditions in the bed resulted in some loss to evaporation within the bed. Due to the low target flow rates in the slag percolators, the feed was supplied in intermittent intervals (4x2 hours) over a 24 hr period. In the saturated dust units feed rates were assumed to equal the recoveries at the bottom of the bed. The hydraulic head in these units was measured daily, either by measuring the height of the liquid level in the head pipe or by reading the pressure gauge in the air supply line.

Leachate collected in the sample beakers was collected in regular intervals, daily in the initial phase of the run, and then less frequently but at least once a week thereafter. Upon sampling effluent volume and mass were established and the pH was measured. The samples were subsequently analysed for various metals by the methods detailed in Appendix A. As all effluent samples were clear, no filtration prior to analysis were conducted.

5.4 Batch Leach Experiments

While column studies give a good indication of the leach processes likely to occur in a full scale waste deposit, it is difficult to relate these back to processes occurring at the level of the individual particles without a number of comparative experiments. Furthermore, column studies are expensive and time-consuming to conduct.

Batch leach experiments on small samples of a particular waste material, on the other hand, are quick and relatively simple to conduct, which is why they find widespread use as

tools for easy characterisation of a waste's potential to generate leachates, as was indicated in Section 5.1.1.

It is the stated objective of this work to combine results from batch leach experiments and other bench scale tests on a particular waste material with those from a column study through the model developed in Chapter 4 to obtain a powerful tool to predict the potential leachate generation of this waste material in a full scale deposit scenario.

The extraction of reaction parameters from batch leach experiments follows is based on careful interpretation of the leach curves obtained under various conditions to disseminate between instant dissolution, solution equilibria and kinetically controlled release mechanisms of the species under consideration. The WASTESIM code in BATCH mode (see Section 4.8), is a useful tool for extracting kinetic parameters from batch leach data. Method and types of leach experiments are described in Section 5.4.1 and aspects of data interpretation in Section 5.4.2.

5.4.1 Methods and Types of Batch Leach Experiments

General Method

All batch leach experiments were conducted by contacting a charge of solid material with a lixiviant in a glass container providing adequate agitation. Agitation is necessary to remove external diffusional mass transfer resistance between particles and fluid and ensure good mixing of the bulk phase. This way the kinetics of any release mechanism can be attributed purely to effects at the particle level and it can be assumed that the bulk liquid concentrations are equal to those at the particle surface.

Most tests conducted in the context of this work were run in 2 l glass bottles with screw caps tumbled top over bottom in a rotating device at 30 rpm (Figure 5-5).This arrangement

was preferred for its smooth and clean operation and excellent agitation. Only where rapid access to the suspension was required, experiments were conducted in glass beakers with overhead stirrers (usually at 800 rpm), although agitation of coarse grained materials proved difficult with this set-up.

Figure 5-5: The rotating bottle device with 2l glass bottles

Depending on the type of experiment conducted, lixiviant, solids to liquid ratios (S:L), particle size distribution of the charge, leach period and other reaction conditions were varied, as is discussed below. All leaches were conducted at room temperature at 20 ± 2 °C. In experiments where the time-dependend leach behaviour was of interest small samples (usually 10 ml) were taken from the reactor vessel at regular intervals (usually 15 min, 30 min, 1 hr, 2hr, 4hr, 8hr, etc. after experiment start), filtered over 0.45 µm filter paper and analysed for pH, before storing in a sample bottle at 6 °C until further analysis. Chemical species in the context of this work analysed usually included Cr(VI) and total Cr, Na, K and Ca. Other species such as Mg, Fe, Mn Zn, Pb, Mo, Ni and Cd were also analysed in many cases, but results for these are mostly not reported in the text, in order to

maintain the focus on the behaviour on chromium. Information about laboratory instrumentation used for sample analysis can be found in Appendix A.

Acid and TCLP Leaches

The classic Toxicity Characteristic Leaching Procedure (TCLP, US EPA, 1992) still finds widespread use as a simple method for assessing the leach potential of a particular waste material as was discussed in Section 5.1.1. Although some criticism can be levelled at the choice of acetic acid as leachant for materials not deposited in municipal waste landfills, it was nonetheless decided to apply this leach tests to the materials under consideration in this work in order to substantiate or refute these criticisms. The tests were, however, conducted in a kinetic fashion, i.e. samples were taken at regular intervals during the run in order to obtain kinetic leach curves as functions of time. Acetic acid is normally chosen for the TCLP test since it buffers the pH at a value around 4, which is considered the "worst case" condition that could potentially arise in a waste deposit. For comparison identical experiments employing 0.1 M HCl, which is a strong acid, as leachant instead of the 0.1 M acetic acid stipulated in the TCLP procedure were also run.

All experiments were conducted at a S:L ratio of 1:20 in the rotating bottles as was outlined above. The Zero Headspace Reactor (ZHR) stipulated in the TCLP procedure (see Section 5.1.1), used for retaining volatile compounds in solution, was not used in the present experimentation as no volatile gases were expected and the (ZHR) restricts agitation of suspension of fine solids. Although the TCLP procedure suggests to leach for 18 hours before taking one single sample, the tests were run for 24 hours with regular sampling in order to allow assessment of kinetic effects.

As will be seen from the acid leach test results for the individual materials (Chapters 6 and 7), these tests are of little use if the acid neutralisation capacity (ANC) of the tested material is high, resulting in rapid neutralisation of the leach liquor (buffered or

unbuffered), rendering particularly the TCLP unsuitable in terms of its objectives and some form of continuous acid addition would be required to maintain pH levels low. This aspect notwithstanding, the acid leach curves give a good indication of leach potential of the various metal species under aggressive leach conditions.

Water Washes

Although the leachant used in the column experiments was acidic (Section 5.3), the high ANC of all the materials tested (Chapters 6 and 7) would suggest that this initial acidity is neutralised rapidly with little influence on the leaching of metal species. It was therefore decided to conduct leach experiments of the various materials in a distilled water leach in order to investigate the release of metal species in the absence of acid reagents.

Water washes were conducted initially at S:L ratios 1:20 with samples taken at regular intervals over a 24 hour period. Other tests were conducted with various S:L ratios (from as low as 1:50 up to 1:1), individual particle size classes of a particular material, with added reagents (particularly in the adsorption studies, see Section 5.5) and over extended periods of time (up to 1 week).

Alkali Leaches

The column studies on one of the materials tested resulted in effluent pH values significantly higher than those observed in the water washes. This is can be attributed to concentration effects, since the pH is determined largely by the instant dissolution of soluble alkali salts in the pore fluid, which is at a much higher solids to liquid ratio in the bed than in the batch experiment. With the much higher pH values prevailing in the pore fluid as it passes through the bed, it is of interest to investigate what effect this has on the dissolution of other metal species, particularly Cr(III) which is known to become soluble at pH values above 12. For this reason an alkali leach in solutions of NaOH was conducted for this material.

Strong alkali leaches were also used for the total extraction of Cr(VI). As it was the principal species of interest in this work, and is easily mobilizable, it was of interest to establish the maximum releasable concentration of this species under aggressive conditions, for which repeated caustic leaching was found suitable, under which conditions Cr(VI) dissolution is maximised and retention by adsorption minimised.

In these tests a 50 g charge of each of the materials was slurried in 1litre of a 1 M NaOH solution (thus resulting in a 1:20 solids to liquid ratio) for 24 hours using the bottle tumbling arrangement as before. After the leach, a sample of the leach liquor was taken for Cr(VI) analysis. The slurry was then filtered in a pressure filter to recover the solid residue. This was then rinsed with a further 50 ml of distilled water in order to remove any residual Cr(VI) retained in the pore solution. The solid residue was then again slurried in 1 litre of 1 M NaOH for 24 hours and the procedure repeated 4 times. Each time the amount of Cr(VI) measured in the leach liquor was determined.

Pore and Bed Diffusion Experiments

Agitated batch leach experiments are aimed specifically at removing the external mass transfer resistance between particle and the fluid moving around it. Diffusion effects, if these exist, are restricted to the porous matrix of the particle. The effective porous diffusivity of a particular species can be described as the product of its free solution diffusivity and a pore geometric coefficient $d_{eff} = \varepsilon/\tau$ (equation (4.2-5)). Conducting a series of identical leach experiments with only the particle size class varied will reveal pore diffusional effects, since with increasing particle size the pore diffusional resistance to release of a particular species becomes more pronounced and can be quantified with the help of a suitable analytical technique. This is discussed in the following section.

Similarly to diffusion through particle pores, dissolved species diffuse through the interstitial spaces between particles in a packed bed if these are filled with water. If this bulk pore fluid is moving, the main mode of transport will be convection with some

dispersion as result of mechanical effects (see Section 4.2). However, if the fluid is stagnant or moves at very slow velocities, transport through the bed is mainly governed by molecular diffusion, as is indicated in Figure 4-10. For beds of very fine particles (as were encountered in the experimental work, Chapter 6), the interstitial pore spaces are likely to become narrow and increasingly convoluted. Diffusion through these pores may then be restricted in same fashion as may be the case in particle pores.

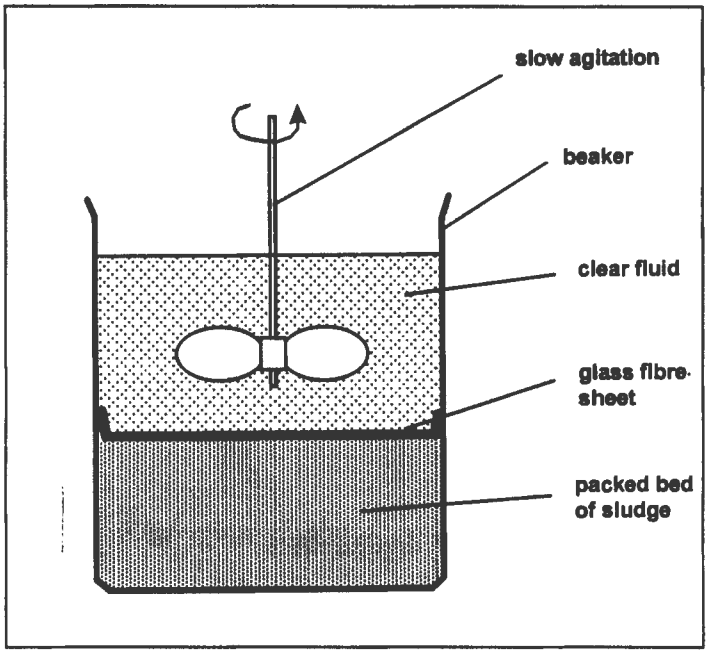

Figure 5-6: Set-up of the stagnant bed leach experiment

This effect can be established and quantified with a stagnant bed leach experiment. Here, the material under investigation is mixed with water into a thick paste and carefully layered into the bottom of a glass beaker (Figure 5-6) to form a bed of certain height. This is covered with a thin sheet of glass fibre turned up at the edges. A measured volume of water is carefully poured over this sheet and gently stirred with an overhead stirrer to achieve mixing. The glass fibre sheet was used to prevent particles from being drawn up into the clear liquid and at the same time allow unhindered diffusion of dissolved species through it, both of which were achieved effectively. Small samples were taken regularly from the clear supernatant liquor and analysed for some selected species. The

interpretation of the time dependent diffusion into the supernatant fluid requires use of the COLUMN mode in the WASTESIM code (see Section 4.8), which has been modified in such a way so as to account for the supernatant fluid as a batch reactor present at one side of the column. This is discussed further below.

5.4.2 Interpretation of Batch Leach Experiments

While batch leach experiments are a quick and simple method to characterise the release behaviour of a waste material under given conditions, some careful interpretation of the data obtained from such experiments is required. This is particularly the case if batch data are to be compared to effects occurring in a deposit scenario, where considerably higher solids to liquid ratios are usually present, even if the chemical conditions in terms of solution pH are similar.

A series of carefully conducted batch experiments on a waste material under investigation can help identify, disseminate and quantify species release and the governing types of chemical reactions. Key aspects of this analysis the are detailed in the following list:

- Prominent species. Species that are released in concentrations sufficiently high to merit concern are easily identified, but it must be borne in mind that the usually low S:L ratios employed in batch experiments can result in considerable dilution effects.

- Kinetic nature of the release. Kinetic effects can be clearly identified from time-dependent leach profiles. Figure 5-7 shows three characteristic leach profiles, instantaneous release, rapid release, that can be taken as near instantaneous, and kinetically controlled release. Care must be taken that slow kinetic releases are actually picked up within the relatively short leach period of the experiment.

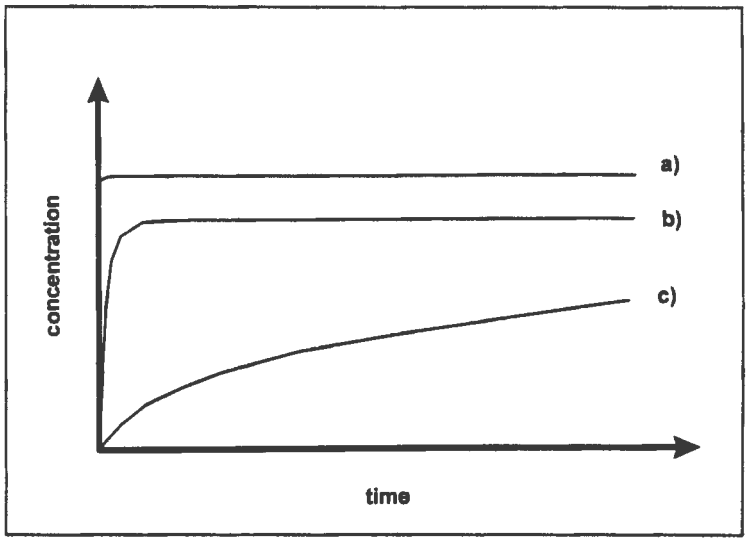

Figure 5-7: Characteristic leach curves observed in batch leach experiments. a) instantaneous release, b) fast equilibrium release, c) kinetic release

- Influence of pH. Conducting leach experiments on the same material at different pH levels helps to identify which release reactions are influenced by pH and to what extent.

- Multiple mechanisms. The release of a species may be controlled by several simultaneous mechanisms, such as instantaneous release and subsequent kinetic release or by instantaneous release and subsequent removal by adsorption, as indicated in Figure 5-8. If this is the case additional experiments under slightly different conditions may enhance one reaction mechanism over the other and thus allow better dissemination.

- Diffusion effects. Although batch experiments are aimed specifically at removing external mass transfer resistance to release from the particle surface, internal diffusion in particle pores can nonetheless take place. Although these release mechanisms may appear as apparently kinetic (Figure 5-7), they may very well be related to slow diffusion from particle pores. This can be easily verified by conducting batch experiments with different particle sizes. Diffusion effects will be less pronounced in small particles, whereas true kinetic effects are independent of size class. This effect was also identified in the model sensitivity study (see Section 4.8).

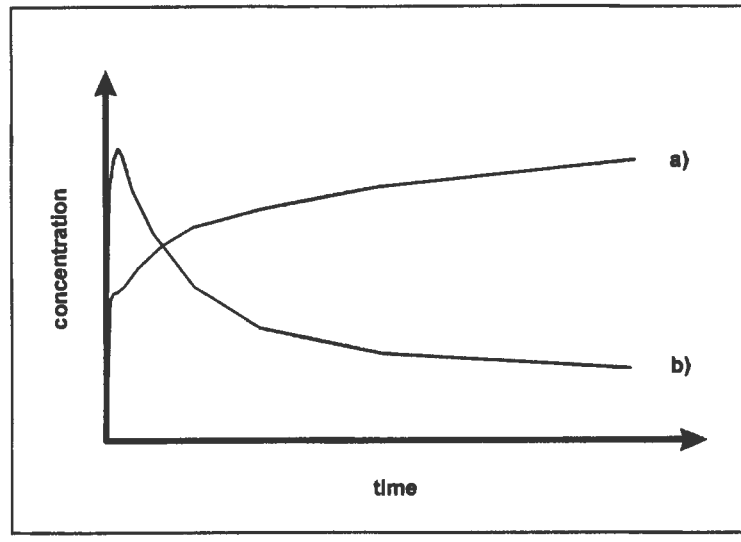

Figure 5-8: Leach curves of dual release mechanisms. a) instant release and subsequent kinetic release. b) instant release and subsequent slow removal.

- Concentration effects. Many equilibrium release mechanisms, particularly adsorption, are governed by the solution concentration of a particular species. In the dilute environment of many batch experiments these effects may become negligible, whereas in tests run at higher solids to liquid ratios under otherwise identical conditions such concentration effects may become more pronounced and thus identifiable.

This list quite clearly illustrates that one single experiment is insufficient to fully disclose all release mechanisms of the predominant species and usually a series of tests needs to be run, varying solution pH, solid to liquid ratios and, where possible, particle size, in order to fully disclose all relevant aspects of the release of the main species.

Instantaneous release and equilibrium effects can be identified and quantified directly from the concentrations measured under various leach conditions, providing the experiment has been conducted for long enough to ensure equilibrium. Description of equilibrium conditions can then be achieved by selecting and parameterising a set of relevant equilibrium reactions in the WASTESIM code, either with tabulated equilibrium constants, where available, or those calculated from the experimental data (particularly for

adsorption studies, see Section 5.5). This process is demonstrated in detail in Chapters 6 and 7 where test results on the individual materials are analysed.

Kinetic and diffusion phenomena, however, require a different type of analysis. Here single point equilibrium values are insufficient to quantify the relevant parameters and a time-dependent leach curve needs to be established. This is used to obtain a kinetic reaction (or diffusion) parameter for the model usually by fitting the experimental data by some form of regression analysis. In the present work the WASTESIM code in BATCH mode (Section 4.8) is used for this purpose.

Figure 5-9 shows a set of data points which indicates the kinetic release of a particular species. Using the WASTESIM code a series of leach curves can be generated for the given system by manipulating the value of the kinetic constant of the reaction under consideration. The value for which the best fit is obtained is then taken as the correct value for the kinetic constant for that particular reaction.

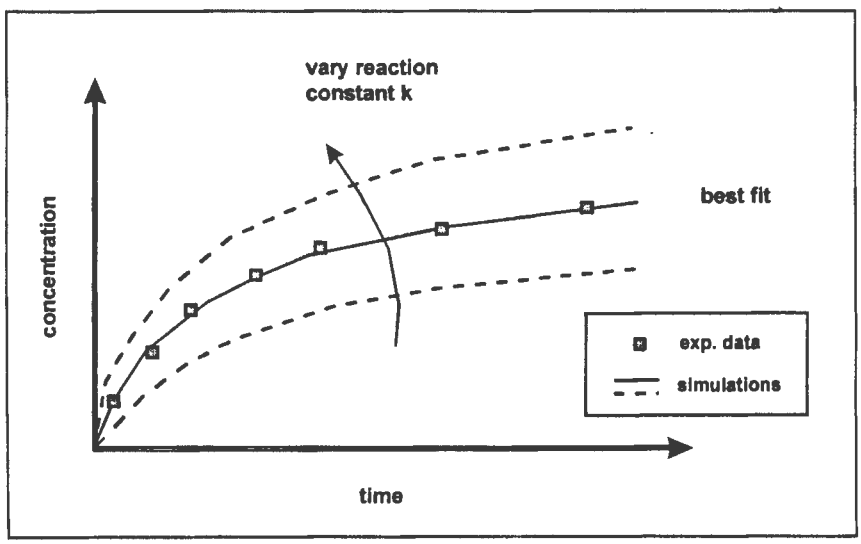

Figure 5-9: Fitting kinetic data by varying the kinetic constant in batch modelling runs

Similarly for diffusion modelling, the free solution diffusivity of a species is established from the literature (for example CRC, 1992) and the effective pore diffusivity parameter d_{eff} (see Section 4.8) is determined by varying its value until the best fit is obtained for a

given set of data. The advantage here is that this parameter is purely geometric and therefore valid for all species. Hence it needs to be determined only once.

It must be stressed, however, that this curve fitting approach using the model is only valid if only one parameter (either the effective pore diffusivity parameter or a kinetic constant) is fitted per set of data. This means that for diffusion modelling the underlying release mechanism must be either non-kinetic or already quantified by some other means, and likewise for kinetic modelling the diffusivity must be already known, or not relevant.

The modelling tool can also be used for establishing effective bed diffusivities from the according type of experiment described in Section 5.4.1. Here transport through the bed of particles is modelled using the WASTESIM code in COLUMN mode with the superficial velocity set to zero and dilution into the stirred batch volume as the modified exit boundary condition (using the BatchColumn switch, see Appendix B). If particle level release behaviour is already fully quantified (by suitable batch leach experiments and modelling), then the only unknown parameter in this system is the bulk diffusivity coefficient d_{bed} (again, the free solution diffusivity can be taken from literature values, see Section 4.8), which can be obtained by fitting simulated curves to a set of experimental data. Again, this coefficient is purely geometrical and therefore valid for all species considered.

Interpretation of batch leach data by careful interpretation and modelling is essential for successful prediction of column (and thus full scale deposit) leach behaviour, as is demonstrated for the materials under investigation (Chapters 6 and 7).

5.5 Cr(VI) Adsorption Studies

One reaction mechanism that requires particular attention is that of adsorption equilibria of a dissolved species with the particle solid interface. Simple leach experiments are insufficient to reveal more detail about this phenomenon. As adsorption reactions are usually equilibrium reactions and therefore likely to proceed fast, desorption may appear similar to salt dissolution. Similarly, adsorption, occurring simultaneously with other release mechanisms, may actually re-capture some of the released species, and concentrations measured in the leachate appear lower than what was originally released. Solution concentration and adsorbed concentrations are in an equilibrium, which can be described by suitable isotherms, as was highlighted in Section 4.3.

While this is of no further consequence in the batch leaches, adsorption/desorption equilibria may become significant in the columns or full scale waste deposits. Here dissolved concentrations in the bulk fluid are displaced by the moving bulk flow. If adsorption equilibria exist, this may prompt more of a particular species to be released into the bulk fluid as bulk concentrations are depleted. In the absence of such equilibria, dissolved concentrations would not be replenished as the bulk fluid is moved through the bed. Consequently adsorption/desorption equilibria can significantly protract the active leachate generation capacity of a particular waste material in a deposit environment and hence act as a release buffer.

It is therefore important to study in more detail the adsorption/desorption of the various materials under investigation in order to obtain a full appreciation of this phenomenon. The focus of the work conducted in the context of this work has been on the adsorption of Cr(VI), but it is acknowledged that other species may also participate in adsorption reactions, although these were not studied further.

Experiments that can reveal more detail about the ad/desorption behaviour of Cr(VI) include adsorption from solutions artificially spiked with Cr(VI), desorption from solids

repetitively leached in fresh solution, and buffered leach capacities observed in batch leach experiments run at increasing solids to liquid ratios, which are outlined in Section 5.5.1.

From each experiment conducted a data point is obtained relating a Cr(VI) solution concentration to a adsorbed solid concentration. Several of such data points taken together can then be used to fit an adsorption isotherm, which is described in Section 5.5.2.

5.5.1 Experimental Methods

Adsorption and Desorption Experiments

For the adsorption experiments the materials investigated were washed at 1:20 solids to liquid (S:L) ratio in aqueous solutions pre-loaded with various concentrations of Cr(VI) (by dissolving appropriate amounts of $K_2Cr_2O_7$ in distilled water) for 24 hours in the tumbling bottle device as used in the batch leach experiments. Dissolved Cr(VI) concentrations were measured from samples taken before charging the solids and at the end of the leach run.

This method of experimentation is, however, limited to materials which show significant adsorption uptake at the low S:L ratios employed. For weak adsorption the amounts removed from solution, irrespective of the spiked concentrations, may be too small to significantly change the solution concentration and may thus go unnoticed. For these cases experiments have to be run at higher solids to liquid ratios, resulting in larger amounts being adsorbed (although being the same per unit mass or surface area of particle) and thus a measurable change in solution concentration.

In the desorption experiments the materials were washed 1:20 solids to liquid ratio in distilled water for 24 hours similarly to the aqueous leaches described in Section 5.4. Final leachate concentrations Cr(VI) were measured. At the end of the leach, the slurry was

filtered in a pressure filter and the filter cake immediately re-slurried in a fresh charge of distilled water as before. Care was taken to recover as much of the solid as possible with minimal loss. After a further 24 hour wash the procedure was repeated for a third time. The rationale here was similar to the extraction leaches described in Section 5.4 but using a non-aggressive leach environment with pH values closer to those observed in the column studies. This way it was hoped to obtain an estimate of the adsorbed concentrations initially present in the material.

Concentration Leaches

Most batch experiments usually employ a solid to liquid ratio of 1:20 by mass. This ratio is commonly employed in standardised leach tests, such as the TCLP, and chosen mainly to ensure good solids mixing so that extra-particle diffusion resistances become negligible. However, dilution effects likely to occur in the relatively large volume of leachate may create a chemical environment which may be significantly different from that in the pore solution in the deposit of the same waste material, where solids to liquid ratios are much higher.

This is of particular significance with respect to adsorption. At higher solids to liquid ratios the available solid surface area per unit volume fluid increases and so does the available adsorptive capacity. Thus a material which exhibits only a limited adsorption behaviour in dilute leach experiments may be able to adsorb quite considerable amounts of a particular dissolved species at high concentrations. It should be pointed out that equilibrium adsorption per g solid does not increase at higher S:L ratios, but the total removal from solution is increased and therefore more easily quantifiable.

A series of batch leach experiments at various solids to liquid (S:L) ratios can thus provide further data points for the adsorption isotherm of Cr(VI) for the different materials considered in this study. An added advantage of this method is that adsorption data could also be obtained for other species that dissolve from a particular material within the same

series of experiments without the need to use solutions spiked with the various species at various concentrations and may hence reduce experimental effort considerably. As the focus was on Cr(VI), this is, however, not further pursued here.

The tests were essentially identical to the water washes in rotating bottles, described in section 5.4, but with different S:L ratios than the usually employed 1:20, such as 1:50, 1:10, 1:5, 1:2 and even 1:1, where possible. Since only the conditions at equilibrium, but not short term kinetic effects, were of interest, tests would be run for 24 hours and only one sample drawn at the end of the experiment, filtered and subjected to Cr(VI) analysis.

5.5.2 Fitting Adsorption Isotherms

Adsorption isotherms describe the equilibrium partition between the amount of a species adsorbed per unit mass solid and that dissolved in the contacting fluid per unit volume. Plots of adsorbed concentration versus concentration in solution are often referred to as adsorption isotherms. The curves are usually obtained by experiment and subsequently mathematically expressed by a suitable model.

While there is a multitude of such models, kinetic or equilibrium, the Langmuir and Freundlich isotherm models are most commonly encountered in the adsorption of ions from solution (see Section 4.3). Although originally derived for gas adsorption, the Langmuir model has in many cases been found to describe solution adsorption phenomena quite well. For ion adsorption the Freundlich model is generally taken to be more closely related to the actual physico-chemical interactions at the solid surface (see Sections 4.3 and 2.1.3), although Freundlich isotherms may not necessarily differ by much from the Langmuir isotherms for the same situation.

Both models require two parameters, the maximum adsorbable concentration $c_{S,max}$, and an empirical equilibrium constant K for the Langmuir isotherm (see equation (4.3-10)), and a

constant b and exponent m for the Freundlich isotherm (see equation (4.3-9)). In both cases these must be obtained from experiment by fitting the experimental data points plotted as adsorbed concentration c_S versus concentration in solution c.

This exercise is conducted here for the Cr(VI) adsorption isotherms for the three materials in order to illustrate the procedure. Other isotherms, where of relevance, can be established in similar fashion, if sufficient data is available.

Fitting the Langmuir isotherm is achieved by rearranging equation (4.3-10):

$$\frac{1}{c_S} = \frac{1}{Kc_{S,max}} \cdot \frac{1}{c} + \frac{1}{c_{S,max}} \qquad (5.5\text{-}1)$$

which is of the form Y = aX + b and can therefore be used to extract both empirical parameters $c_{S,max}$ and K by linear regression on available experimental data.

Likewise the Freundlich isotherm equation (4.3-9) can be re-arranged:

$$\ln(c_S) = m \cdot \ln(c) + \ln(b) \qquad (5.5\text{-}2)$$

which, again, is of the form Y = aX + b and can therefore be used to extract both parameters b and m by linear regression of experimental data points.

It was decided to attempt fitting both models to the experimental data obtained for the three materials in order to allow comparison (see Chapters 6 and 7).

5.6 Hydrodynamic Characterisation Using Tracer Studies

5.6.1 Residence Time Distributions

Bulk convective transport of fluid through the column bed is characterised in the model by factors such as feed flow rate (or feed flux), bed porosity and saturation. These determine the seepage velocity of fluid flow through the porous matrix.

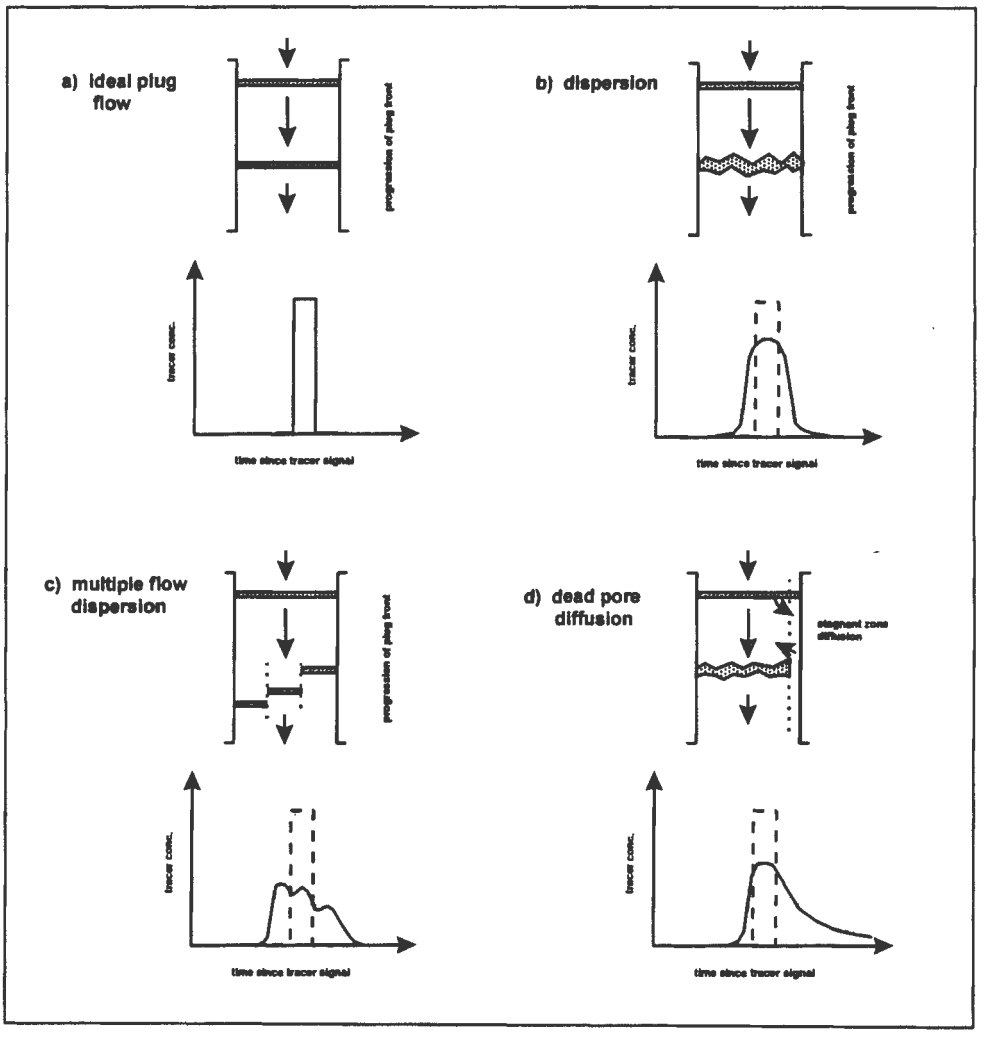

Figure 5-10: Ideal plug flow and distortions of a moving plug front due to various dispersion effects.

The residence time of the fluid is determined by the ratio of the total fluid volume held up in the bed and the feed flow rate. This residence time determines the time taken for a front of fluid entering the bed to travel through the bed exactly once and dissolved species would travel through the bed in ideal plug-flow fashion (Figure 5-10a).

In real systems the flow through a porous matrix is unlikely to follow ideal uniform flow conditions. As indicated in Section 4.2, dispersion effects result in a "smearing" of the plug front, i.e. the smoothing of concentration profiles around the moving front, due to micro-scale diffusion and mixing effects (Figure 5-10b). This effect becomes more pronounced with increasing residence time in the bed.

Flow through a packed bed can also be governed by a zones of different hydraulic conductivities and stagnant pockets (Section 4.1). Fluid flow may exhibit significantly different seepage velocities through these zones (from high velocity in channels to completely stagnant in dead pores) and hence flow through the bed may exhibit a distribution of residence times. Portions of a concentration front entering such a bed travels through the bed over different periods of time and therefore appear as a dispersed profile (Figure 5-10c). Different to dispersion at the micro-scale, this phenomenon is due more to macro-scale effects.

A further effect influencing macro-scale dispersion is that of dead pore diffusion. Dissolved species transported in the bulk flow may diffuse into dead zones and only very gradually diffuse back into the bulk once concentrations have dropped there. This retention can result in significant time-delays in the transport of dissolved species through the bed. In this case a moving plug front is distorted with a long tail-end (Figure 5-10d) This phenomenon is particularly evident in unsaturated beds of unevenly shaped particles and therefore likely to be encountered in waste deposit scenarios.

The phenomenon of residence time distributions is well known in chemical reactor theory (Levenspiel, 1972) and can be accommodated in the model description of a process, if this

distribution is determined by tracer experiments. In these an alien species (i.e. one that does not participate in any reactions taking place within the bed) is injected into the feed stream, either as a short-term spike or a sudden step change, as is illustrated in Figure 5-11. Responses to these tracer "signals" at the bottom of the bed reveal information about the residence time distribution in the bed .The various dispersion scenarios illustrated in Figure 5-10 can in fact be seen as responses to injection of tracer pulses. Methods of tracer experiments conducted in the context of this study are detailed in Section 5.6.2.

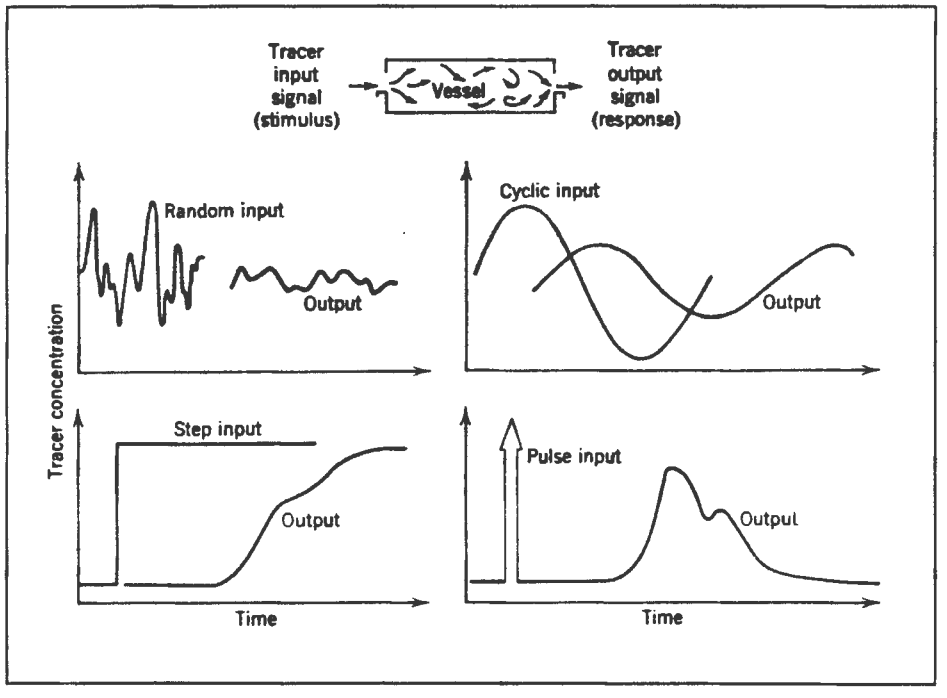

Figure 5-11: Typical signal-response curves in tracer studies (after Levenspiel, 1972)

The model developed in Chapter 4 allows for the inclusion of a bulk dispersion term (equation 4.6-14) using the lumped dispersivity term D_h (see also Section 4.2). Tracer response curves are usually translated into a dispersion coefficient, similar to D_h, from an integral analysis of the response curve. Details of this analysis are elaborated by Levenspiel (1972) and are not repeated here. This term alone, however, caters poorly for macro-scale dispersion effects due to a distribution of flow velocities through the bed and for dead pore diffusion. In the present study approximation to a distribution of flows is

attempted with a two-modelling approach, which is described in more detail in Section 5.6.3. Incorporation of dead pore diffusion effects is, however, not considered at this stage, but potential exists to expand the model developed in Chapter 4 in this regard.

5.6.2 Experimental Set-up of Tracer Studies

For two of the materials under consideration in this study tracer tests have been conducted. The tracer of choice was Li^+ (as Li_2SO_4) which is highly soluble at all pH levels and therefore not likely to be artificially retarded by precipitation within the bed. The studies were conducted by starting the leach run with the acid rain feed liquor and then suddenly stepping up the Li concentration in the feed to fairly high concentrations (about 900 mg/l), then continuing with the Li feed for a while before suddenly returning to the unspiked feed liquor. This way the response to two separate step changes could be investigated within the same experiment. A preliminary experiment with a simple tracer injection (pulse signal) indicated that tracer concentrations would become too diluted within the relatively large bed volume. Therefore this commonly applied type of tracer study was not used in the experiments presented here. The leachate was collected frequently throughout the run and analysed in order to ensure accurate accounting for all Li^+ recovered at the bottom of the bed. The collection of leachate was continued until residual Li concentrations had become sufficiently small (here taken as 1% of the feed concentration) so that the test could be considered to be completed.

Independent Li adsorption studies (see Section 5.5) on the materials were conducted in batch experiments, where Li solutions at various concentrations were contacted with the solid material over extended periods of time. This was done to ensure that Li adsorption on the solid matrix is not interfering with the fate of the tracer on its way through the column.

The response curves obtained for two small columns set-ups (Chapter 6 and 7) were analysed using the two-stream modelling approach (see Section 5.6.3 below) and modelled using the WASTESIM code.

5.6.3 Two Flow Analysis Using WASTESIM

The applicability of residence times obtained on the basis of purely mathematical analysis of the response curves is somewhat limited in as much as it attributes flow non-idealities (macro-scale velocity distributions in the bed) to dispersion effects, which strictly apply only at the micro-scale (bed diffusion and micro-mixing). Thus a residence time distribution resulting from a distribution of flow velocities in the bed is taken as equivalent to the "smearing" effect around a moving plug front (as was described in Section 5.6.1), which is, strictly speaking, incorrect, but may be acceptable for a system of given dimensions and flow conditions.

When considering scale-up to a geometrically similar system, macro-scale effects, such as the relative predominance of slow and fast moving zones, may very well remain the same, whilst micro-scale dispersion, the extent of which is a function of actual residence time in the system, may become much more pronounced. The sensitivity study in Section 4.8 has indicated how leach profiles become more protracted with increasing residence time as dispersion effects become more pronounced.

However, the residence time distribution of a tracer in a given system is not necessarily identical to the distribution of flow velocities in the bed, but is more likely to be a combination of micro- and macro-scale effects. Therefore a meaningful modelling approach to the hydrodynamic conditions in a real bed should take account of both effects. Dead pore diffusion, which was identified as a third factor influencing bed residence times (Section 5.6.1), is not considered in the present study. The potential distribution of flows through the bed is approximated through a two-stream approach, i.e. it is assumed that the

real distribution can be described sufficiently well in terms of one fast and one slow moving stream.

To this end, the measured tracer response curves is analysed in the following manner. The response curve was initially simulated with the WASTESIM code in COLUMN mode (see Section 4.8 and Appendix B) on the assumption of uniform flow, given all parameters describing the bed, such as dimensions, net porosity (established from total solid mass filled, bed dimensions and true solid density), fractional saturation (established from a mass balance of water filled, fed and retrieved from the system), profiles of daily flowrates measured and Li concentrations in the feed (incorporating the timing of the step changes), all of which were available from the experimental records. The ideal case curve generated in this fashion was compared to the measured curve, to identify the degree of congruence.

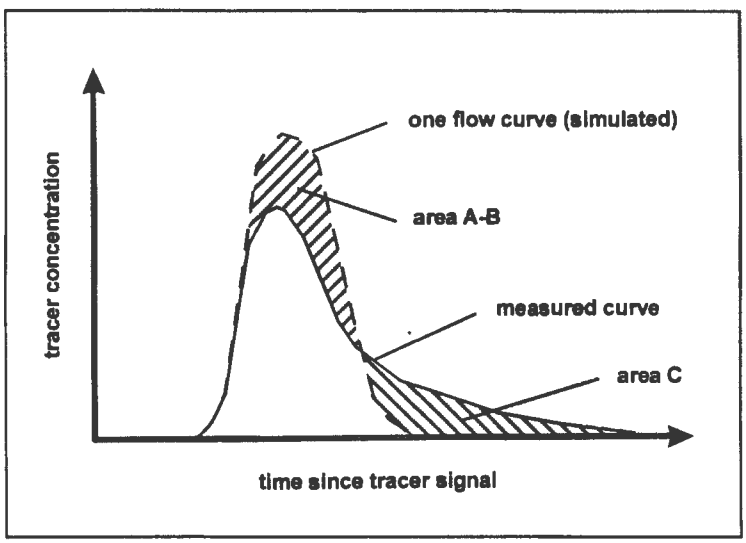

Figure 5-12: Area analysis of modelled ideal case and measured tracer curves reveal information about slow and fast moving portions of the flow

Subsequently both curves were integrated to establish the areas of overlap as is illustrated in Figure 5-12. The difference between the two curve areas (A-B) is taken to correspond to the total amount of Li that is travelling with a second, slower stream and thus corresponds the tail-end area C. If the bed is assumed to consist of two parallel beds of equal cross-

section (and hence volume), the ratio of the areas (A-B) to (B) then corresponds to the split ratio of the total flow Q_{tot} rate between slow and fast streams in the two "half-beds" .

Since the WASTESIM code at its current stage of development can only accommodate one single stream, the two-stream approach is modelled by two separate runs with half the original bed area and the flow rates apportioned to the slow and fast streams and subsequently "mixing" the resulting data points. This is done by calculating for each pair of data points (as generated by the two runs) the average weighted proportionally to the flow rate split.

This approach is demonstrated using the same base case parameters as were used in the model sensitivity study in Section 4.8 (Table 4.5), with the only modification being a change of the kinetic constant of the Cr(VI) dissolution reaction from 10^{-4} to $5 \cdot 10^{-6}$ s^{-1} in order too better demonstrate the effect of the split flow approach on the leach curve of this reaction (as can be seen from Figure 4-26, this value results in a more hump-shaped leach curve). In the split flow modelling runs the bed area was reduced from 0.02 to 0.01 m^2 and the feed flow rate from 0.2 l/day to the values corresponding to the splits attempted (0.133 and 0.067 l/day for the 2:1 split and 0.12 and 0.08 l/day for the 3:2 split). The model was run for each of the two flow rates and the results (concentration-time data) of the two runs added together on a spreadsheet with weights according to the split ratio (i.e. 0.67 and 0.33 for the 2:1 split and 0.6 and 0.4 for the 3:2 split).

The resulting leach curves are plotted in Figures 5-13 for Cr(VI) and 5-14 for Na. As can be seen, the two-stream approach results in an earlier but more protracted fall-off of the concentration levels when compared to the results of the single stream simulation, similarly to what was observed when changing the bed dispersion coefficient d_{bed} (Figure 4-36, Section 4.8), but much more pronounced. Increasing the split ratio increasingly reveals the existence of two distinct flows as indicated by the plateau in the concentration-time curve. In the modelling of real systems with a wide distribution of different flow

regimes this approach becomes somewhat limiting as two streams may be insufficient to approximate the true distribution in a meaningful way.

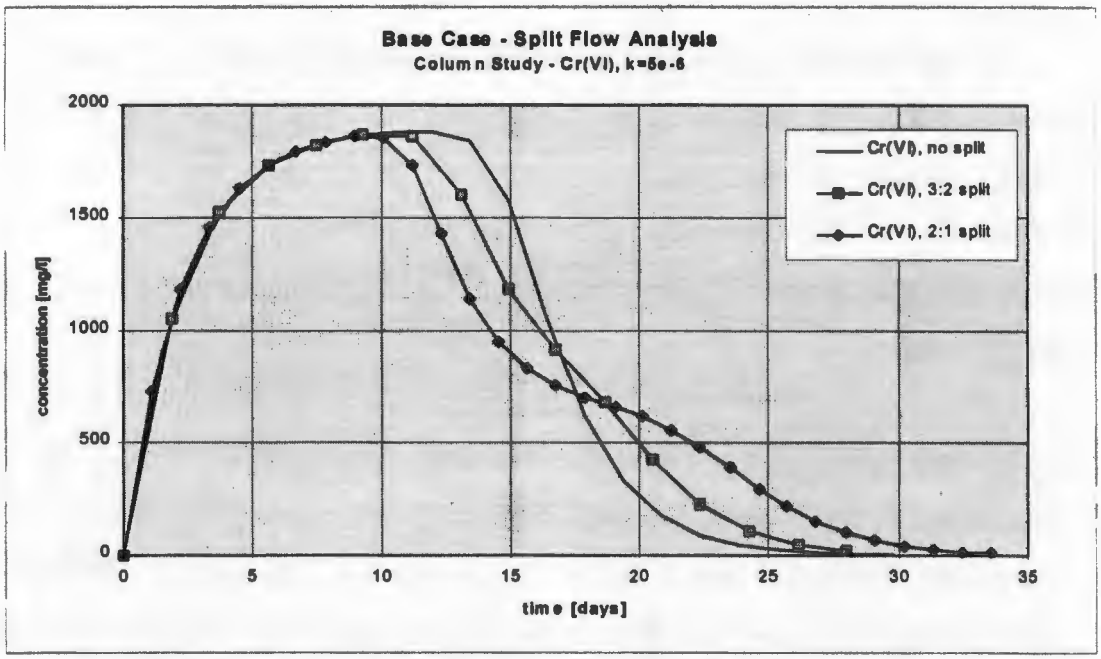

Figure 5-13: Simulated base case Cr(VI) (with $k=5 \cdot 10^{-6}\ s^{-1}$) leach profiles for single-flow and two-flow approaches with different split ratios

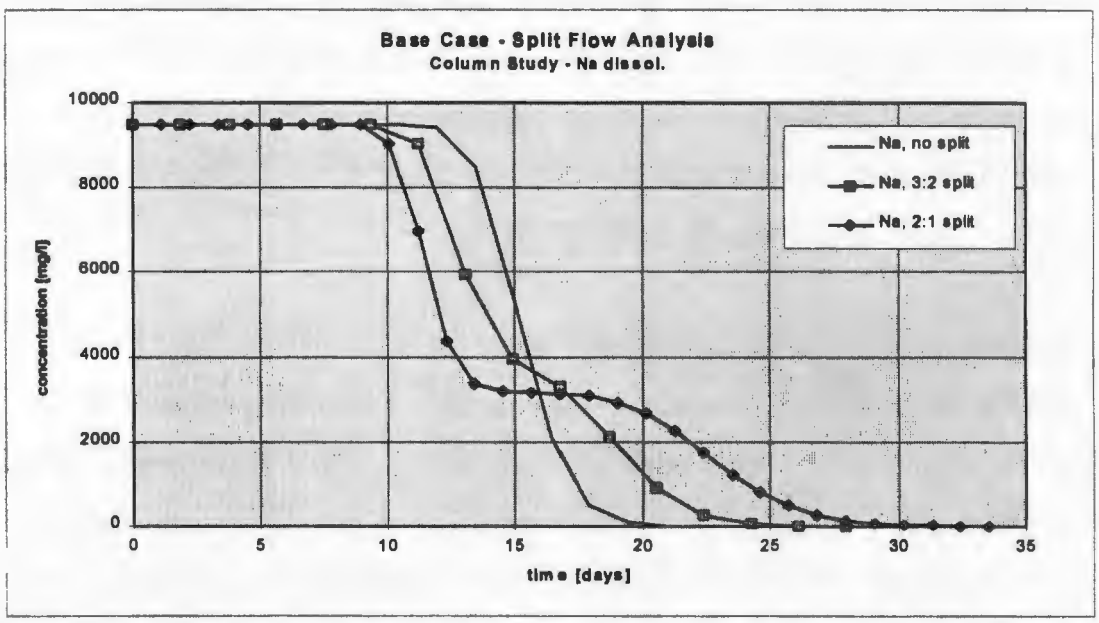

Figure 5-14: Simulated base case Na leach profiles for single-flow and two-flow approaches with different split ratios

It should be pointed out again, that the two-stream approach allows to distinguish between micro-scale and macro-scale dispersion effects and thus avoids the more or less empirical lumping of all dispersion effects into a single parameter. As noted above, however, the approach is less suitable if the distribution of flows is very wide. Also, the effect of dead pore diffusion is not considered currently.

5.6.4 Further Avenues for Analysing Tracer Studies

The two-flow method illustrated in the preceding section is clearly a simplistic approach to model the complex hydro-dynamic behaviour of fluid in unsaturated packed beds. While it may offer a reasonable first step towards accounting for a possible distribution of flow velocities through zones of different hydraulic conductivity and channelling, it does disregard the effect of dead pore diffusion. It is questionable, however, whether this omission can be justified with regard to the materials investigated in this study. Particularly the experimental work conducted on the granular, highly porous slag material investigated in Chapter 7 clearly suggests otherwise. It is therefore appropriate to investigate briefly avenues for future model expansions to account for this effect.

Fluid caught up in dead pores can be perceived as small "pockets" of stagnant fluid held in narrow interstitial spaces between particles as well as in crevices and indentations in the surface of irregularly shaped particles. Through these stagnant volumes large parts of the particle surfaces are thus separated from the moving bulk fluid. This concept is congruent with the stagnant fluid "hull" postulated for the surface zone model put forward in Section 4.6.2, where it was stated that this hull consist of fluid "trapped" in the surface roughness of the particles. It was postulated that this stagnant layer be sufficiently thin to assume a constant surface concentration throughout. Relaxing this postulate somewhat would allow a portion of the total fluid held up in the bed to be assigned to this stagnant surface layer, and thus it can be assumed to correspond to the volume of fluid caught up in dead pore spaces. Diffusion through dead pore spaces can thus be simulated as diffusion through an

expanded surface layer. In the model in its current state of development this would simply require to choose a value for δ_s, the surface layer thickness, or, more correctly, the ratio of stagnant fluid volume to total particle surface area, that considers the total volume of fluid assumed to be trapped in dead pore spaces.

This approach is, however, limited by several constraints:

- The partition between stagnant and mobile fluid volume in the bed needs to be established from a suitable experiment or set of experiments.

- The surface zone model postulates that the surface of the entire body of particles in the bed is covered with the surface film. This would result in the film thickness to remain still relatively thin and the contact surface between stagnant and moving fluid rather large, making this scenario appear far removed from the concept of distinct "pockets".

- A film diffusion coefficient, which adequately represents diffusion from stagnant pores needs to be established from a suitable experiment.

The step change tracer response experiment used in the present study is insufficient to yield the required information, and the approach was therefore not pursued further in the present context.

A more realistic approach to modelling dead pore diffusion in the rinsing of spent heaps has been proposed by Illerbrun and Dixon (1996) based on work by Turner. Also here the fluid volume held up in the bed is divided between stagnant and moving fluid, but the stagnant fluid is assigned to a distribution of zones of different lengths and cross-sectional areas, which are assumed cylindrical for modelling purposes (Figure 5-15). Dead pore diffusion is modelled as diffusion along "branches" of discrete volume and length. Thus, additional to a distribution of particles with possible internal pore reaction-diffusion

effects, the overall heap model includes a distribution of these cylindrical pockets of dead volume with associated axial diffusion effects, both interacting with the bulk flow.

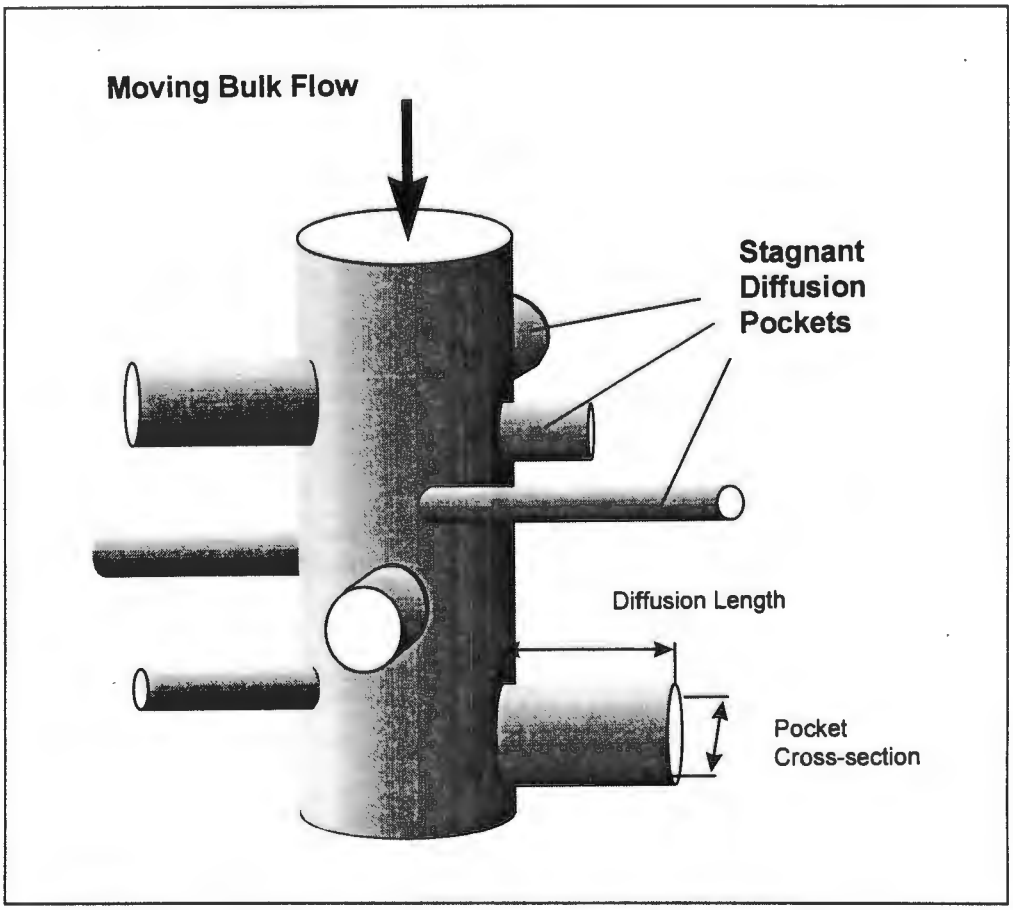

Figure 5-15: "Turner structure" as proposed by Illerbrun and Dixon (1996) to account for a distribution of cylindrical dead pore pockets along the path of moving bulk fluid

Illerbrun and Dixon claim success with establishing the length and size distributions of theses pockets as well as the fraction of total fluid volume held up in stagnant pores from a series of frequency response tracer experiments. Although the mathematical analysis of these tests involving Fourier analysis appears cumbersome, the procedure yields more rapid and complete information over the conventional impulse or step change tracer tests.

It appears thus that modelling dead pore diffusion is possible in principle, but requires significant expansion of the overall modelling approach. This has not been pursued further in the context of the present study, but, considering the model limitations regarding the

hydrodynamic behaviour encountered in the experimental studies (See Chapters 6 and 7), it is considered to be an important aspect that should be addressed in future work.

5.7 Introduction to the Experimental Studies

The general methodology for a systematic investigation into the experimental assessment and modelling of waste materials in deposit scenarios has been introduced in Section 5.1.2. This has been put to the test with two chromium containing waste materials from the ferro-alloy industry, more specifically an emission control dust from a stainless steel smelter (referred to as Metallurgical Dust, Chapter 6) and a granular slag material from the production of ferro-chromium (Low Carbon Slag, Chapter 7). Although these two materials originate from the same type of industry and both from high-temperature metallurgical processes, they are nonetheless completely different in physical nature, chemical and mineralogical composition as well as in their tendencies to generate and promote transport of a hazardous leachate in a deposit situation. The only similarity lies in the fact that for both materials the release of chromium, particularly Cr(VI), is the most significant contributor for the generation of a potentially harmful leachate, although by significantly different release mechanisms. The two investigations must therefore be seen as separate case studies and comparisons are only drawn as far as successes and limitations of model and methodology are concerned. These are mostly confined to the concluding discussion in Chapter 8.

Both materials originate from a ferro-alloy producer located in the Mpumalanga Province in South Africa. Since all samples were collected run of production on a specific day, rather than over an extended period of time, their representativeness within the context of the process they originate from remains questionable. Within the context of this work, however, this is only of marginal interest. All experiments, analyses and attempts to model these were conducted on the same homogeneous, well mixed batches of samples and should therefore be fairly representative within themselves. Care needs to

be taken only when extrapolating findings to the overall waste bodies the individual samples would report to within the industrial context. This is, however, beyond the scope of the present work.

The experimental work follows in broad terms the methods and modelling approaches outlined in this Chapter, although there are some specific modifications, which are discussed in more detail in the individual studies. A large number of experimental data points have been collected within the studies as the leach behaviour of a number of species was investigated in numerous experiments. Only relevant data is presented in the following chapters, mostly in graphical presentation. All data is, however, available in tabulated form in Microsoft ™ Excel spreadsheets contained on the disk accompanying this volume. A table of contents is given in Appendix C.

NB: pages 264-268 deleted, text continues on page 269

6

Experimental Study 1: Metallurgical Dust

An experimental methodology which can be used to characterise waste materials with respect to their potential for leachate generation in a landfill scenario is proposed and elaborated in Chapter 5. This methodology was tested with two solid waste materials originating in the ferro-alloy industry.

Dust carried in the emission gases from high temperature furnaces are one common type of waste material generated in this industry. As indicated in Section 3.3.1 these result from direct dusting of the furnace charge, atomisation of the melt and re-condensed vapours of volatile metals such as Pb, Zn and Cd. They are usually extremely fine in nature and characterised by high metal content. In general such dusts are regarded as hazardous wastes requiring disposal in appropriate landfill or re-processing in secondary furnace processes.

One such material (in the following referred to as Metallurgical Dust, MD) is the material of focus in this chapter. The MD material is an emission control dust from a combined electric arc furnace and argon oxygen decarburisation plant, which forms part of a ferro-alloy process located in the Mpumalanga Province of South Africa. Origin and general characterisation of the sampled MD material is given in Section 6.1.

The MD material has been subjected to the full suite of lysimeter column and laboratory experimental studies outlined in Chapter 5. Results from two lysimeter studies are detailed in Section 6.2. A brief outline is given how these helped to identify further laboratory

studies required to characterise the leach behaviour of the material more closely, particularly with respect to chromium leaching, which is the focus of the present work.

All batch leach and adsorption studies are detailed in Section 6.3 and the interpretation of the results, including correlation of Cr(VI) adsorption data, is elaborated. Through this analysis a reaction matrix for use in the computer model was established and verified against the batch leach data.

Section 6.4 describes the results from a stagnant bed leach experiment and an attempt to model results using the reaction matrix established before and extract, if necessary, a bed diffusion parameter.

A tracer study was conducted on an accelerated lysimeter column, which is detailed in Section 6.5. The tracer response curve was interpreted using the WASTESIM computer algorithm and the split flow analysis as described in Section 5.6. This analysis gives a good indication of the dispersion behaviour likely to occur in flow through beds of this material.

Finally, with all reaction and transport parameters sufficiently characterised from the laboratory experiments, the computer model is applied to simulate the leach curves of the two column studies. Results of this simulation are described and critically discussed in Section 6.6.

6.1 Origin and Characterisation of the Material

As outlined in Section 5.8, the Metallurgical Dust (MD) is the joint emission dust from the EAF and AOD furnaces of a stainless steel smelter. Both the electric arc furnace (EAF) and the argon-oxygen decarburizer (AOD) vessels are located within the same building.

Dusts arising during the smelting campaigns are directed to the ceiling of the building were they are jointly removed in the ventilation system and subsequently recovered in the emission control plant which employs bag filters. Thus, although originating from two different processes, the dust arises only as a single mixed phase, which is disposed of by tipping on a open disposal site near the smelter plant. It should be pointed out that the process employs mainly scrap as iron source with the associated problems introduced by heavy metals, such as Pb, Zn and Cd in protective coatings. Due to their volatile nature these tend to report to the gas phase in the process and subsequently re-condense as fine dust.

The process alternates between two types of steel produced, austenitic and ferritic, the difference being mainly the higher addition of alloying metals, such as Cr, Ni, Mn and Mo, to the austenitic type. A sample of the dust generated in each campaign has been taken and subjected to initial analysis separately (referred to as MD Aust and MD Ferr). Since in the real process the two dusts are co-disposed, all further experiments were conducted on a mixture of the two types. This was meant to be at a ratio 1:1.5 Ferr:Aust by mass, which is related to the production of the respective types of steel, but was taken at 1:1.14 Ferr:Aust by mass, due to an error at the beginning of experimental work. In order to ensure consistency, the mixture recipe was kept at this erroneous ratio in all later work.

Both dusts are very similar in physical appearance. MD occurs as a very fine, heavy, chocolate-brown powder of very fine dust-like particles. It emits a noticeable foul smell, reminiscent of acetylene, which could be attributed to reactions involving calcium carbides, a likely by-product of the electric arc furnace process. Upon contact with water the foul smell becomes noticeably stronger, which supports this theory. On skin contact the powder is very sticky with a tendency to smudge. Handling the material results easily in dusting and requires care, as the dust acts as a respiratory irritant. The samples as received had a negligible moisture content of 0.61% for MD Aust and 0.42% for MD Ferr.

Individual MD particles can only be observed under the electron microscope. Two main types of particles are observed:

- agglomerates of extremely small spheres (Figure 6-1a): These agglomerates range in size from a few micron up to 50 micron, while the individual spheres are mostly sub-micron in size (commonly around 100 nm, as shown in the close-up in Figure 4-1b), although a few larger spheres can be found. The perfect spherical shape of these particles supports the theory that they originate from condensing metal vapours and atomised liquid metal droplets, as was suggested in Section 3.3.1.

- larger individual particles of irregular shape (figure 6-2): These are not very frequent, but distinctly different from the agglomerates, which in some case can even be condensed on them. In size they range from about 1 micron up to 50 microns. These particles are assumed to originate from direct dusting off the arc furnace charge, which was also suggested in section 2.6.1.

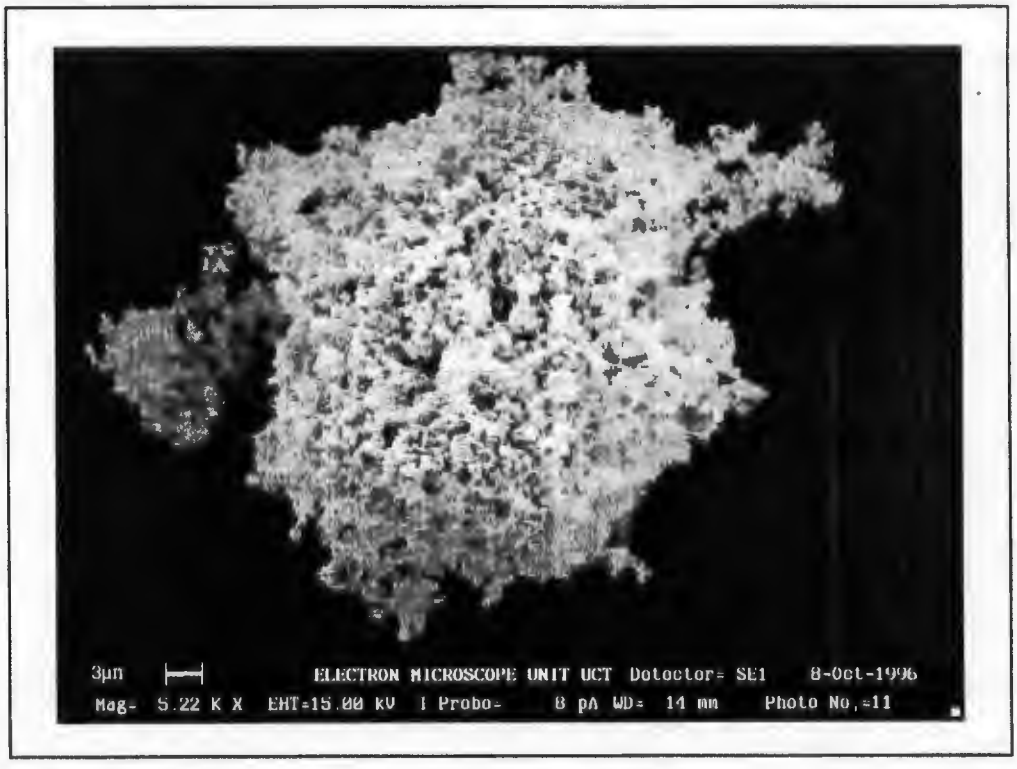

Figure 6-1a: Metallurgical Dust: Agglomerate "particle" of micro-spheres

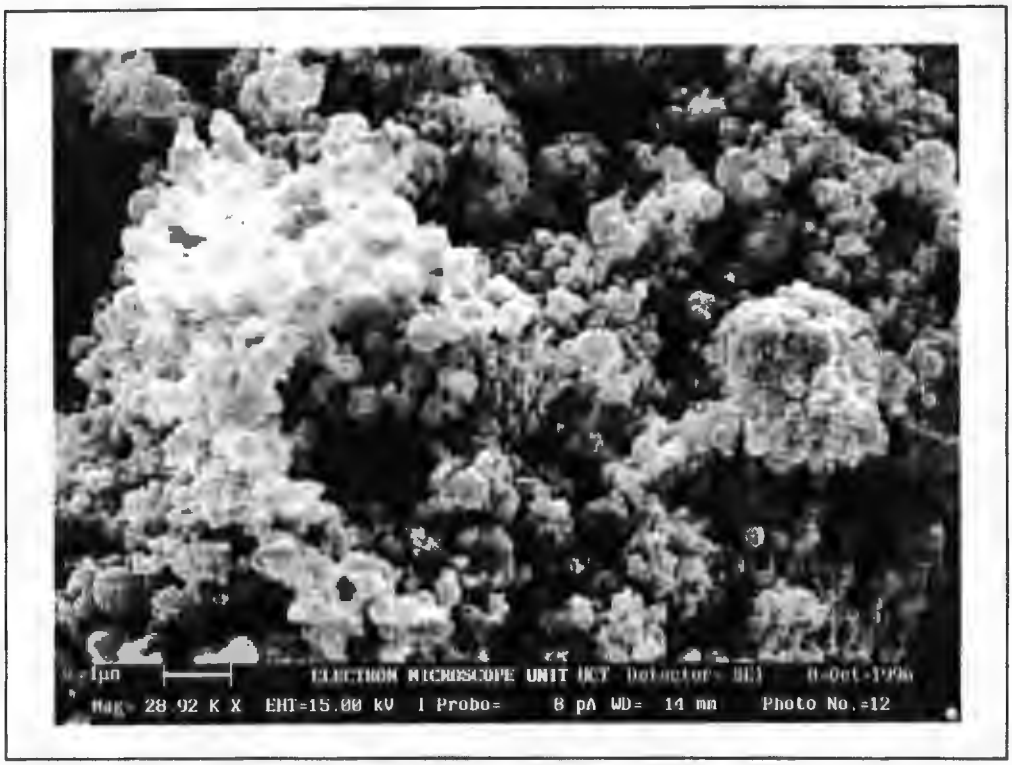

Figure 6-1b: Close-up on micro-spheres within agglomerate

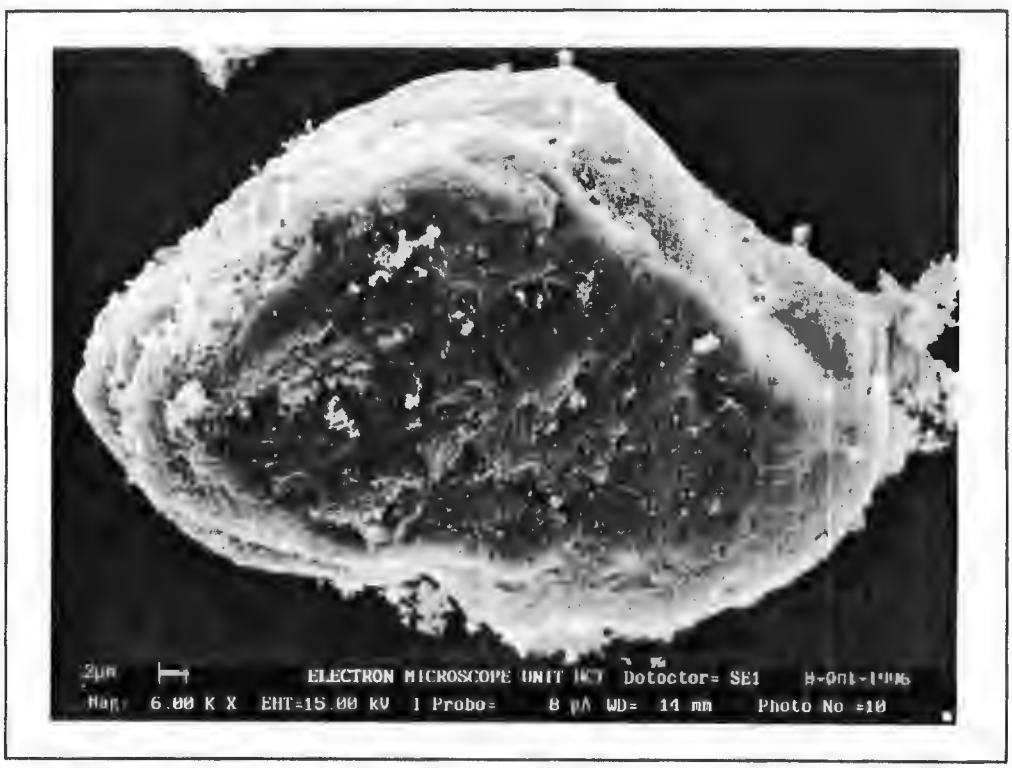

Figure 6-2: Metallurgical Dust: Angular dust particle

The particle size distributions, established from laser diffraction analysis, are given for MD Aust and MD Ferr in Figures 6-3a and 6-3b respectively. A significant fraction of larger particles up to 500 micron were found in these analyses if the dust was freshly suspended in water. These disappeared completely after the suspension was exposed to ultrasound for 5 minutes. This can be taken as an indication that particles show a strong tendency to agglomerate to the larger clusters that were observed under the electron microscope.

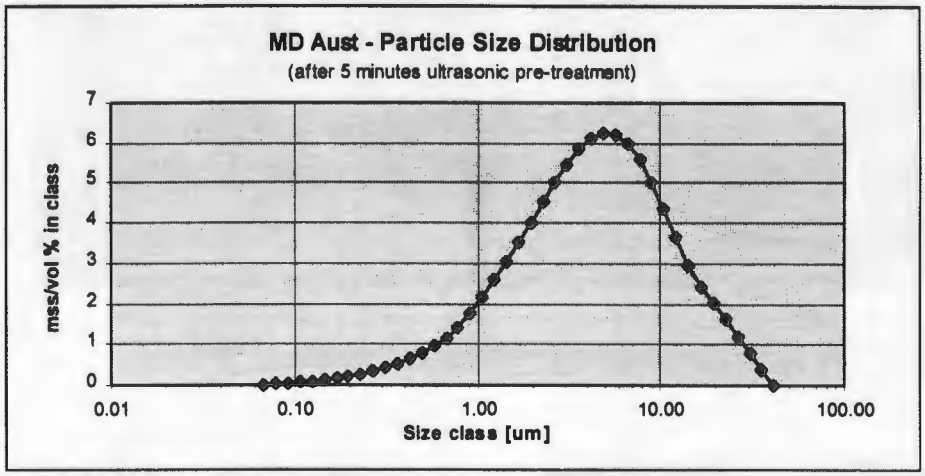

Figure 6-3a:Particle Size Distribution of MD Aust

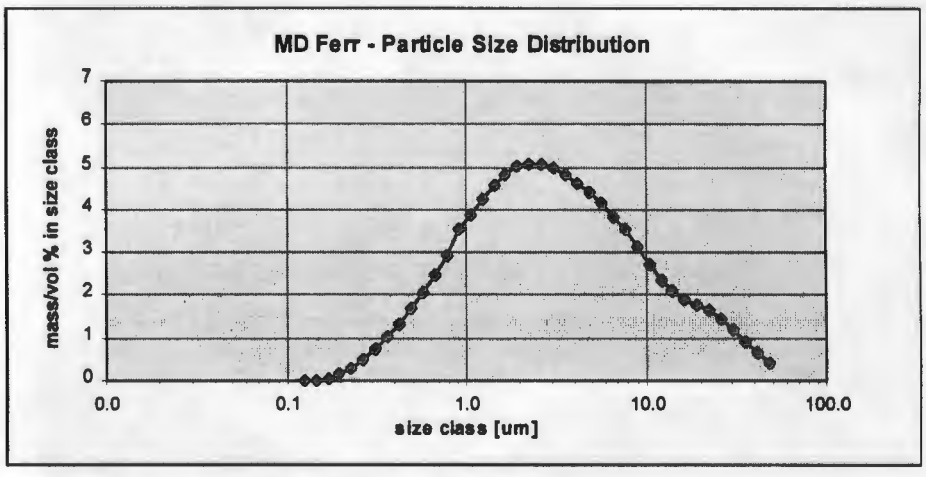

Figure 6-3b: Particle size Distribution of MD Ferr

Bulk characterisation of the two MD types and the mixture is given in Table 6.1. The high true solid densities indicate that the material is metallic to a significant degree. The

relatively low settled dry bulk density in turn indicates a high dry bulk porosity, which is explained by both the large interstitial voids within the agglomerates (see Figure 6-1) and the poor packing achieved through the irregular shape of these agglomerates. Somewhat better packing is achieved with the slurried material, possibly due to a break-up of the larger agglomerates upon wetting. BET surface area characterisation indicates a moderately large surface area per unit mass of particles, but due to the extremely complex nature of the solid, it is difficult to establish, how much of this (if any) reports to internal particle pores. However, since the particles are mainly agglomerates of sub-micron size globules, it is unlikely that diffusion through intra-particle pores plays any significant role in the kinetic behaviour of such a fine grained material.

Table 6.1: Bulk characteristics of MD Material

	MD Aust	MD Ferr	Mix
true density [kg/m^3]	4362	4397	4378
dry bulk density [kg/m^3]	1040	1275	
dry bulk voidage	0.76	0.71	
residual moisture [%]	0.61	0.42	
slurry moisture [%]	ca. 25	ca. 22	ca. 27
wet bulk density [kg/m^3]	ca. 2100	ca. 2300	ca. 2200
wet bulk voidage	0.67	0.62	0.64
BET surface area [m^2/g]	5.731	4.097	

Elementary analysis of the common metals for both MD Aust and MD Ferr, established from fusion digests, is given in Table 6.2. It should be noted here that Na is not included in this table, since the use of sodium peroxide as the fusion agent prohibits accurate analysis (see Section 5.2). Other analyses suggest it should be in the region of 0.5% by mass for both materials. The analysis confirms the origin of the two dusts, with MD Ferr showing significantly lower concentrations of the alloy metals Cr, Ni, Mn and Mo. The significant concentrations of the volatiles Pb and Zn in both materials again confirm that at least some of the dust originates from condensation from the gas phase. They are also indicative of the problems associated with the introduction of scrap iron into the process as

was indicated above. The balance of MD mass (ca 33%) is assumed to be made up mostly of oxygen, which would indicate that most metals are in an oxidised state, rather than elemental metal.

Table 6.2: Elementary Composition of MD Material*

	MD Aust	MD Ferr	Mix (calc.)
% of total	53.3	46.7	100
Fe	27.88	32.29	29.94
Cr	11.95	8.45	10.32
Mn	7.43	4.54	6.08
Ni	1.93	0.47	1.25
Mo	1.12	0.18	0.68
Ca	7.29	8.6	7.90
Mg	4.12	4.61	4.35
K	0.38	0.36	0.371
Zn	2.75	4.88	3.74
Pb	0.46	0.9	0.665
Ti	0.11	0.11	0.110
Cu	0.11	0.11	0.110
Sn	0.05	0.02	0.036
V	<0.01	<0.01	<0.01
Cd	0.005	0.0070	0.0059
Hg	0.0009	0.0008	0.0009

* all data reported in % of total

MD is a highly alkaline material resulting in an nearly instantaneous solution pH of 12.4, when slurrying 1:20 with distilled water. This is attributed to the easily soluble oxides of Na and K and the alkali buffers of CaO and MgO. The acid neutralisation curves (Figure 6-4) show the large buffer capacity of the material over the entire pH range, resulting from the acid dissolution of the various metal oxides at the various pH levels.

The results of an 24 hour water leach on the MD mixture (Table 6.3) indicate the concentrations the metals easily soluble upon contact with water, which are, as suggested above, mainly Na, K and Ca. Important are also the dissolution of significant amounts of Cr (as chromates, accounting for more than 98% of the total Cr assay) and Mo (assumed

as molybdates), which are oxoanions, soluble at all pH levels (see Section 2.1.2). All other metal concentrations are small, owing to their low solubility at the high solution pH.

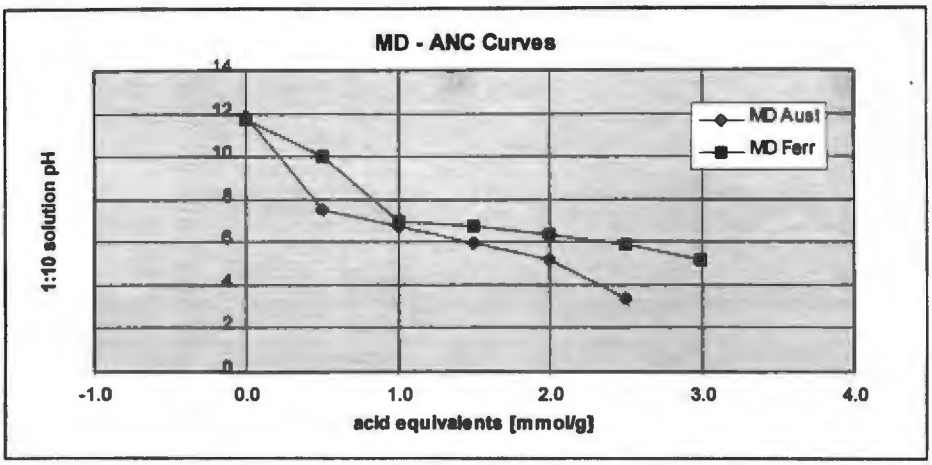

Figure 6-4: Acid neutralisation curve for Metallurgical Dust

Table 6.3: Water wash and TCLP results on MD material

	Water Wash		TCLP	
Element	mg/l	mg/g_{dust}	mg/l	mg/g_{dust}
Na	292	5.8	320	6.4
K	605	12	650	13
Ca	114	2.3	716	14.3
Mg	0.036	0.001	452	9.0
Cr_{tot}	77	1.5	69	1.4
Cr(VI)	76	1.5	69	1.4
Mo	38	0.76	8.0	0.16
Fe	0.010	neg.	0.30	0.006
Zn	0.50	0.01	311	6.22
Pb	1.1	0.022	0.060	0.001
Cd	0.003	neg.	0.70	0.014
pH	12.45		7	

The TCLP test results on the MD mix confirm the instant solubility of Na and K which are at similar levels to the water wash. The introduction of the acid affects mainly the dissolution of Ca, Mg and Zn, whereas the concentration levels of the other metals change only marginally when compared to the water wash. It is important to take note of the final solution pH at 7, which indicates the acid capacity of the TCLP mixture has been

exhausted during the leach, which is understandable considering the high ANC of the dusts described above. This also indicates that the TCLP is essentially unsuitable for this type of material.

6.2 Lysimeter Studies

Two lysimeter studies were conducted with the MD material as indicated in Table 6.4. The first labelled MD1 was conducted in a Constant Head Lysimeter with head pipe as described in Section 6.3. The extremely small flow rates achieved through this column resulted in a very long experimental period. A second experiment under accelerated conditions (smaller bed and higher driving pressure) was therefore conducted in order to obtain leach curves more quickly. This experiment was also used as a second test case for the waste characterisation methodology to follow. Detailed account of all results from experiment MD1 and MD2 are given in the following.

Table 6.4: Experimental Parameters of MD Lysimeter Column Studies

Material(Code)	Lysimeter	Bed Height [mm]	Daily Flowrate [ml]	Hydraulic Head	Duration [days]
MD (MD1)	CHL, head pipe	524	varied, 40-500	125 cm	400
MD (MD2)	CHL, pressure	270	varied, 350-1000	50 kPa	30

6.2.1 Experiment MD1

As indicated in Table 6.4 in this experiment a 524 mm bed of the mixed MD material was continuously flushed with the "acid rain" feed mixture under a constant hydraulic head of around 125 cm for a period of 400 days.

Over this period the daily flow rate through the bed (Figure 6-5) dropped significantly from an initial 94 ml to as low as 41 ml after 85 days, whereafter it recovered back to 94 ml after 211 days and dramatically increased to levels fluctuating between 400 and 600 ml per day. This behaviour is not clearly understood, but it is speculated that two competing mechanisms might occur here. During the downturn phase, pore spaces might become blocked by bed consolidation, whereas in the subsequent upturn phase preferential flow paths (channelling) gradually open.

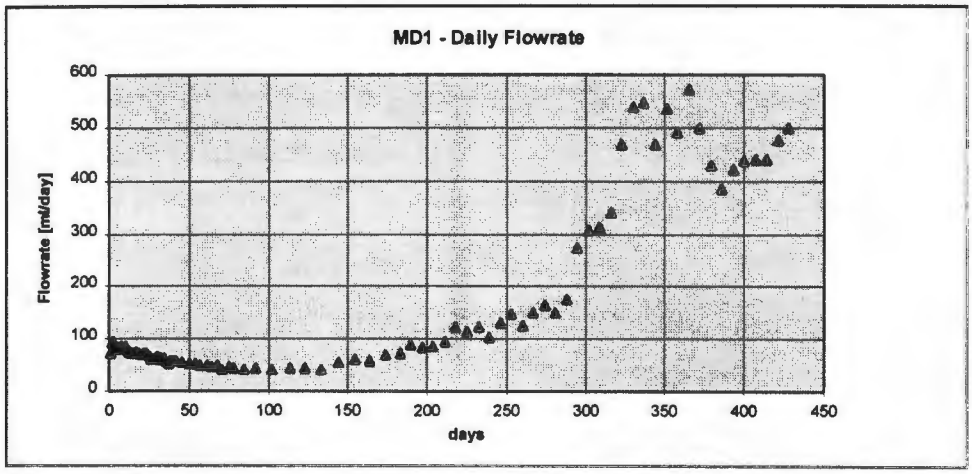

Figure 6-5: Daily flowrate development in experiment MD1

The development of effluent pH and concentration profiles for chromium (both total and Cr(VI)), as well as Na and K, are shown in Figure 6-6 a-c. The considerable degree of scatter in the pH curve is attributed to unstable readings of the pH instrument initially used (see Appendix A), but a trend is nonetheless clearly recognisable. Starting from an initial level of around 13.9 the pH more or less linearly decreases until it reaches a level of around 12 after 350 days, where it remains more or less constant.

The high initial pH levels are associated with the instant dissolution of the alkali metals as hydroxides, which was already evident in the preliminary water wash experiments on the MD material (Table 6.3). For similar reasons the very high levels of Na, K and Cr(VI) are associated with their instantaneous dissolution into the bed fluid in which they are flushed out with the effluent.

Also interesting to note are the initially slightly higher total Cr relative to Cr(VI) concentrations in the effluent, indicating that Cr(III) does dissolve to a small degree during this phase, which is possible considering the initially high pH which is conducive to Cr(III) dissolution. These and other aspects of chemical interactions in the MD bed are discussed further in Section 6.3.

Significant effluent concentrations were observed for Na, K and Cr as displayed here, as well as for Zn, Pb, Mo, Cu and Cd for which data is available on the disk attached to this volume (Appendix C). The concentration versus time curves of all of these are similar in shape, i.e. the high initial levels only very gradually decrease with time until after about 200 days a sharp decrease is observed to much lower levels, and then a gradual tapering off for the remainder of the experiment.

The sharp decrease can easily be explained by the fact that after about 200 days the total volume that has flown through the bed corresponds to the volume of pore fluid initially present in the bed (from placing it as a wet paste). Thus, assuming plug flow behaviour, the fluid volume in the bed has been replaced exactly once and the initially dissolved concentrations of species have all been flushed out, resulting in the sudden decrease. Deviations from perfect plug flow (by dispersion) are indicated by the fact that the drop does not come as a step change but more gradually over about 100 days. This is discussed further in the context of the tracer study detailed in Section 6.5.

The residual tapering off of concentrations is then the combined effect of secondary dissolution and the flushing out of concentrations that have diffused backwards against the direction of the flow, as well as of those trapped in dead pores. The existence of this backward migration is also illustrated by an interesting observation made during the experiment: The clear leach liquor standing in the head pipe of the lysimeter gradually turned yellow (indicating the presence of Cr(VI)) from the top of the bed upwards.

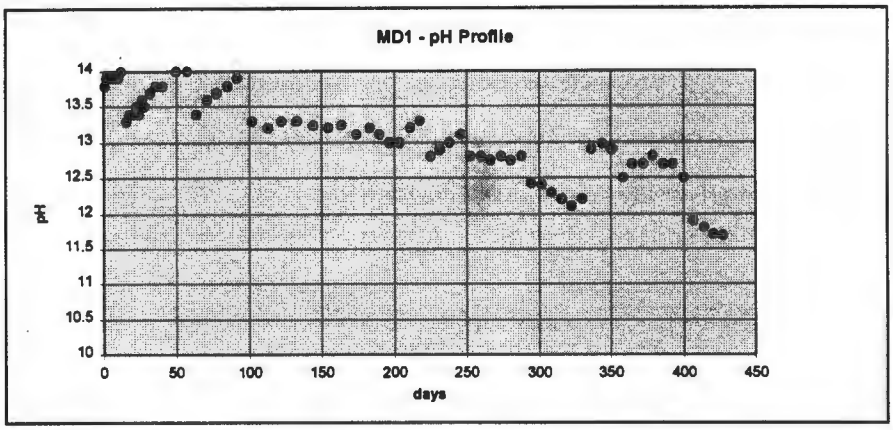

Figure 6-6a: pH profile in effluent of experiment MD1

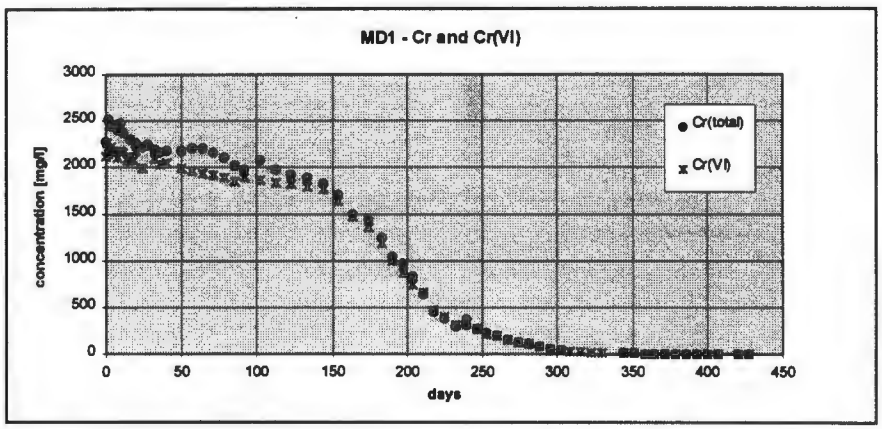

Figure 6-6b: Concentration profile of Cr and Cr(VI) in effluent of MD1

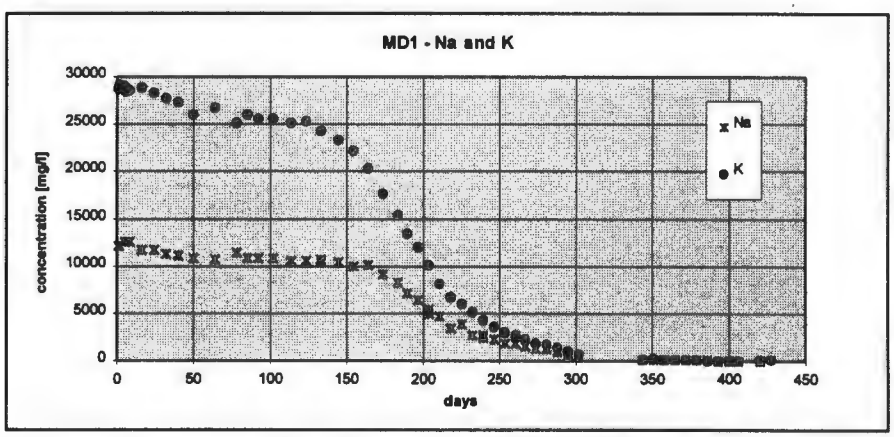

Figure 6-6c: Concentration profile of Na and K in effluent of MD1

This indicates that the flowrates were small enough to result in a net flow of Cr(VI) counter to the direction of flow. This was further supported by the fact that at the end of the experiment, when flow rates began to increase significantly, the yellow colour in the head pipe very quickly disappeared again. These observations are discussed in more detail in context of model results in Section 6.6.

An average initial flowrate of 85.8 ml/24hrs (first 5 days) was used to calculate the hydraulic conductivity of the bed as approximately 10^{-8} m/s, which puts the material into the category of clayey, impervious substances (see Table 4.1 in Section 4.1). This is an interesting finding in as much as the low permeability of this material, which is desirable from an environmental point of view, is completely offset by the extremely high concentrations of soluble constituents mobilised at such low flowrates. This aspect supports the fact that the MD material is completely unsuitable for landfill disposal without at least some form of pre-treatment.

6.2.2 Experiment MD2

The long duration of experiment MD1 was considered prohibitive for effective waste characterisation on a laboratory scale for this type of material with low hydraulic conductivity. In an attempt to accelerate lysimeter experiments, it was decided to repeat the experiment using a shorter bed and a higher hydraulic head as driving force.

As indicated in Table 6.4, in this experiment the bed height of the MD mixture was reduced to 270 mm and an air pressure of about 50 kPa was applied to the liquid feed, which was replenished daily to ensure that there was a level of fluid above the top of the bed at all times. All other experimental conditions remained the same as in experiment MD1. The experimental period was reduced to 30 days.

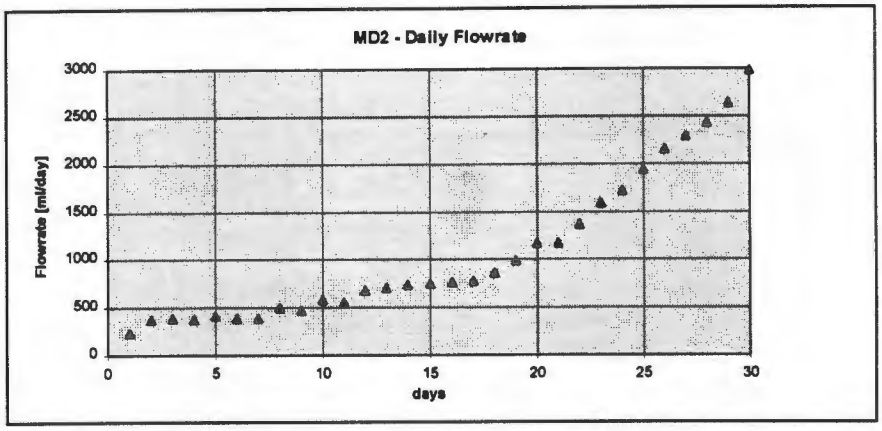

Figure 6-7: Daily flowrate development in experiment MD2

As in experiment MD1 the flow rate through the bed (Figure 6-7) started at initially low levels around 400 ml/day and increased only gradually for the first 17 days, whereafter it increased more rapidly until the end of the experiment. It is interesting to note that the average flow rate during the "flat" phase of the profile (i.e. over the first 10 days) is about 8 times higher than the average flow rate in experiment MD1 in this period (first 200 days), which is in good correspondence to the fact that the bed height is reduced by half and the driving pressure quadrupled here, and hence the hydraulic conductivity of the material is approximately the same in both beds as would be expected. Also, in both experiments the pore volume of the bed is flushed out exactly once within this "flat" phase, indicating that the cause for initial hydraulic resistance is removed after this phase resulting in a significant increase of flow rates thereafter. This is possibly related to the establishment of preferential flow channels. Again, this is discussed further in the context of the tracer studies in Section 6.5.

The development of effluent concentrations versus time is given in Figure 6-8 a-c for pH, total Cr and Cr(VI), Na and K. All data for these and other metal concentrations (Pb, Zn, Mo etc.), not shown here, are included in the disk accompanying this volume (Appendix C). All profiles are very similar to the ones observed in experiment MD1 with very similar starting concentrations. An exception is maybe the pH profile which started at somewhat lower levels (13.1) and never exceeded 13.4.

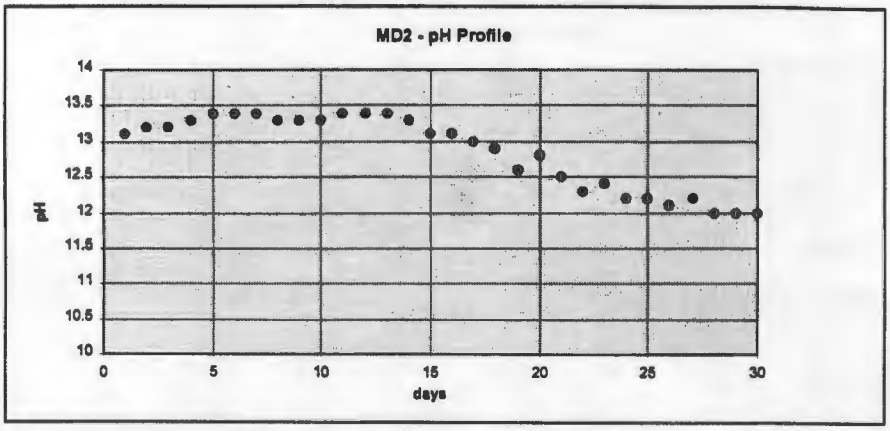

Figure 6-8a: pH profile in effluent of experiment MD2

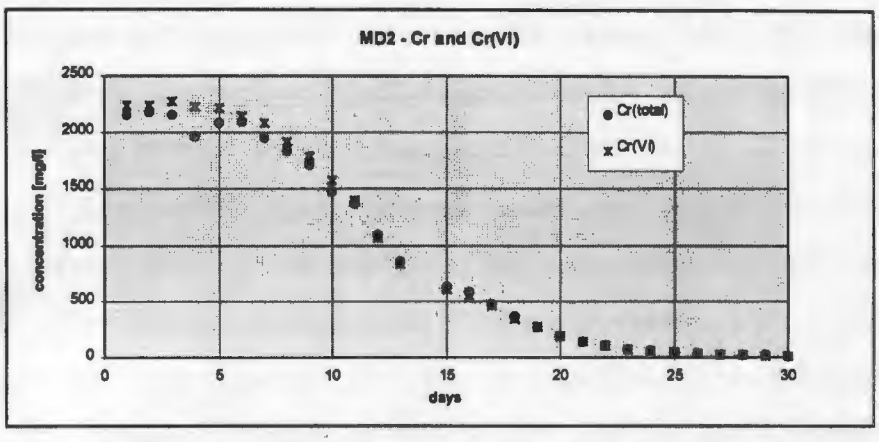

Figure 6-8b: Concentration profile of Cr and Cr(VI) in effluent of MD2

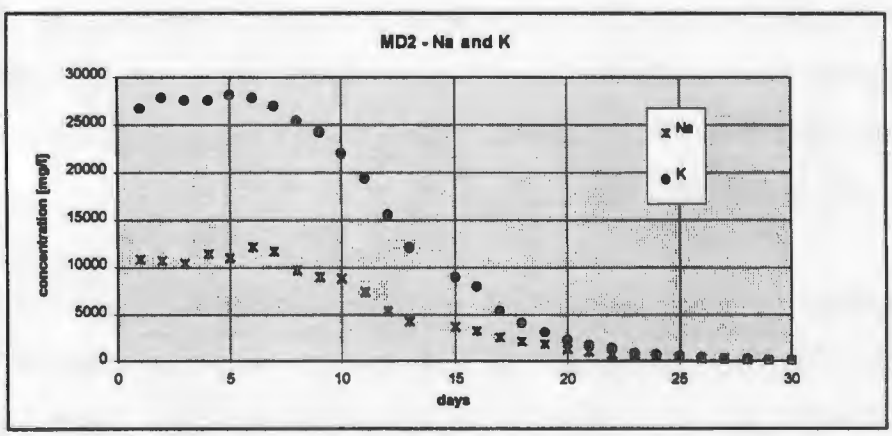

Figure 6-8c: Concentration profile of Na and K in effluent of MD2

As was indicated above, the sharp drop in concentrations after 10 days corresponds to the point in time at which the pore volume of the bed has been flushed out exactly once. This confirms the assumption, that the high initial concentrations result from instant dissolution into the fluid phase when the material is placed in the lysimeter as a wet paste which is then displaced by the percolating leach liquor in a plug flow fashion.

A more in depth comparison between the two MD experiments, particularly in terms of comparing the different time scales is given in Sections 6.5 and 6.6.

6.2.3 Summary

Both lysimeter studies show leach behaviour similar in trend with respect to the main constituents found in the effluent. Prevailing pH levels are extremely high in both experiments indicating the dissolution of hydroxide salt, probably those of Na and K, as these species occur in similarly high concentrations. The pH levels are high enough to be conducive to the dissolution of various heavy metal species, such as Pb, Zn and Cr(III) due to their amphoteric character and these species were indeed found in significant concentrations in the effluent. Predominant, however, is the presence of remarkably high concentrations of Cr(VI) in the order of g/l, which is several orders of magnitude higher than what is acceptable in terms of environmental concerns (drinking water limit is 0.05 mg/l).

Further characterisation of the MD material should therefore focus on the two key aspects, origin and quantification of the high pH levels and its influence of the release behaviour of chromium species.

On the level of transport behaviour fluid flow through the MD bed exhibits somewhat peculiar characteristics which need careful investigation to ensure successful modelling of leachate generation. One possible explanation relates to the extremely high concentrations

of dissolved species removed within the first flushing of the bed in both experiments. In experiment MD 2, for example, the sum total amounts of Na and K removed from the bed in the first 10 days are approximately 150g, which corresponds to about 0.9% of the total solid mass in the bed (16.8 kg). As this still discounts the corresponding anions (OH- in all likeliness) and other ionic species, total solid removal from the bed in the first ten bed would be in the order of 1-2%. The scenario is similar for experiment MD1. This is significant and could explain a gradual opening of pores with a subsequent decrease of resistance to flow. However the drastic increases in flowrate observed in the experiments are unlikely to be explained by this observation alone.

6.3 Bench Scale Studies

In line with the experimental methodology outline in Chapter 5, the preliminary findings from the column studies should give a good first indication of chemical conditions prevailing in a bed situation, which are then to investigated in small scale experiments.. All batch leach experiments conducted on the MD material are described in Sections 6.3.1.to 6.3.4, Cr(VI) adsorption studies are described in Section 6.3.5 and an isotherm is quantified from the available data. The information gathered from all experimentation thus far is reviewed in Section 6.3.6 and the reaction scheme considered for further modelling is formulated and tested in a number of scenarios.

6.3.1 Acid and TCLP Leaches

Although the MD lysimeter experiments indicated very high solution pH values in the pore solution, it was nonetheless decided to test the material in an acid leach environment. As was indicated in Section 5.4 this is useful for gathering evidence on whether certain reactions are pH controlled or not. A 24 hr leach was conducted in each 0.1 M HCl and the TCLP acetic acid buffer. The pH curves for both of these leaches is given in Figure 6-9. These clearly indicate that for both types of acid the strong alkalinity of the MD material

immediately neutralises all acid present and drives the resulting pH into the neutral region. This clearly contradicts the objective of the TCLP to maintain a buffered low pH for leaching.

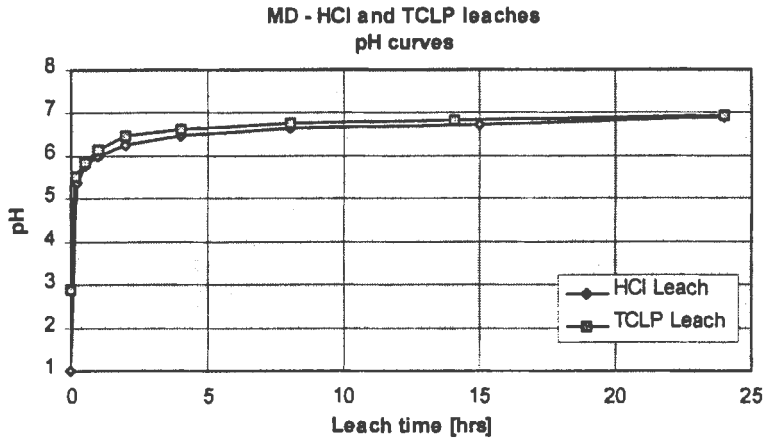

Figure 6-9: pH curves vs. time for MD HCl and TCLP leaches

Leach curves from the TCLP and HCl leaches were more or less identical for this material. Figure 6-10 a shows the TCLP leach curves for Na, K, Ca, Mg and Zn, which all leached in concentrations above 200 mg/l, Figure 4-33b shows those of total Cr, Cr(VI) and Mo, which leached at smaller, but appreciable concentrations. All other metals leached at concentrations below 2 mg/l and are not reported here, but data is available in tables on the disk attached to this volume.

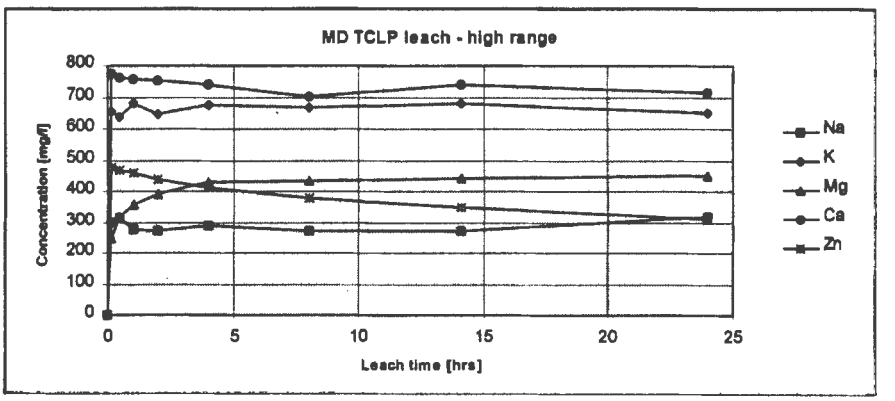

Figure 6-10a: Leach profiles of Na, K, Mg, Ca and Zn in TCLP on MD material

The leach curves for Na, K, and Ca rise to their high levels almost instantaneously and remain there without much further change. This behaviour indicates fast dissolution of soluble salts or kinetically fast leaching. The Mg curve shows a somewhat more gradual leach reaction, nearing completion only towards the end of the 24 hour leach period. The initial jump in leached concentrations within the first 15 minutes of the experiment coincides with the drastic rise in pH and the associated consumption of initial acid.

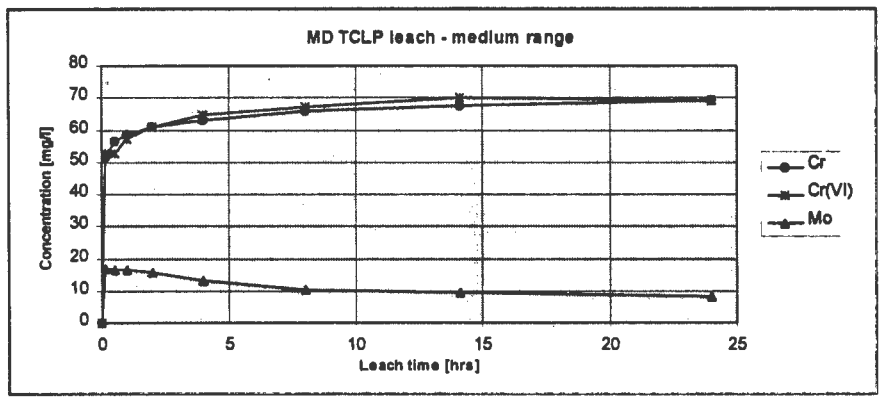

Figure 6-10b: Leach profile of Cr, Cr(VI) and Mo in TCLP on MD material

The leach curve of Zn gradually drops from the high initial level. Here it can be assumed that acid leaching leads to the instant liberation of Zn into solution, followed by gradual re-precipitation as $Zn(OH)_2$ in consequence to the pH rising to higher levels at which this compound is insoluble. The Mo curve shows similar behaviour.

The Cr leach curves indicate that all Cr in solution is present as Cr(VI), which is somewhat surprising since some acid leaching of Cr(III) at the initial stages could be expected. It could, however, be speculated that the available acid is rapidly consumed by those species which show fast leaching kinetics (Ca, Mg, Zn) before significant amounts of Cr(III) can be leached. The subsequent rise in pH would furthermore support the re-precipitation of Cr(III) as its hydroxide. Therefore only Cr(VI), whose dissolution is not driven by acid reaction or pH goes into solution gradually. Being an anion, chromates might show a tendency to initially adsorb to other metal oxides present in the solid and later desorb as the pH levels rise.

6.3.2 Water Wash

Although starting at a neutral pH level a water wash was considered as a suitable test environment as the strong alkalinity of the MD material is likely to drive leach pH rapidly to high levels more comparable to those encountered in the columns.

The pH profile for this experiment is given in Figure 6-11 and indeed shows that pH levels almost instantaneously rise to a level of 12.4 and remain there for the rest of the experiment.

The water wash leach curves for all metal species released from this material have essentially all the same shape with an initial jump to a certain concentration level where they remain more or less constant for the remainder of the experiment.

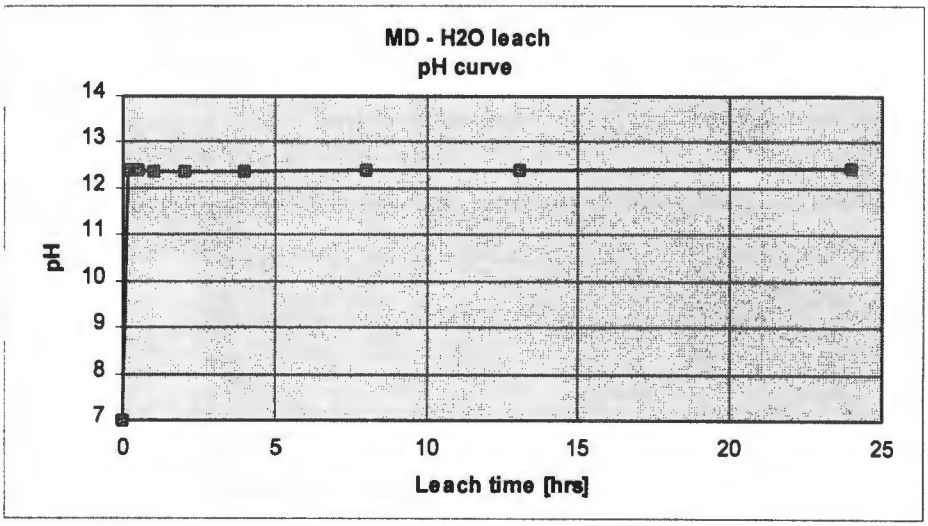

Figure 6-11: pH vs. time curve for H_2O leach on MD material

The leach curves of Na, K and Ca, which exhibited high concentration levels are given in Figure 6-12a and those of total Cr, Cr(VI) and Mo at moderate concentration levels in Figure 6-12b. All other species analysed, including Pb, Zn, Cd, Mg and Fe, leached in concentrations smaller than 2 mg/l.

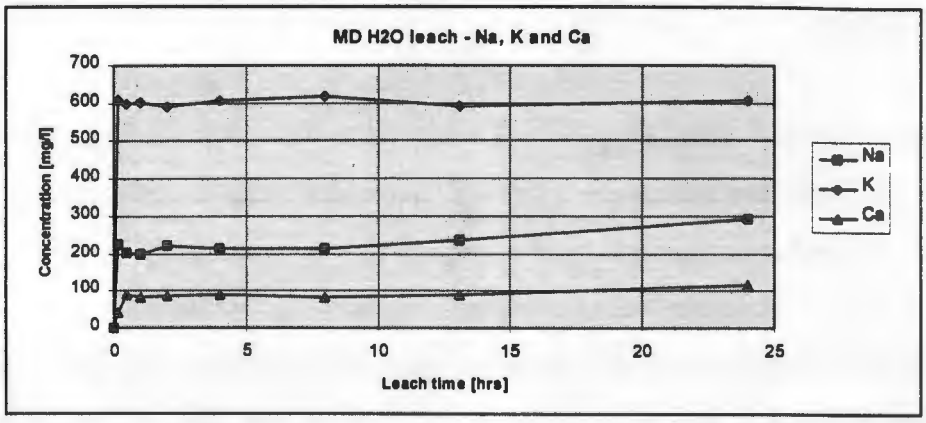

Figure 6-12a: Leach profiles of Na, K and Ca in H_2O leach on MD material

The high levels of Na, K dissolving more or less instantly and the high pH of the MD wash (around 12.4) are a strong indication that these dissolve from their oxide/hydroxide forms. In fact, taking all Na and K dissolved after the first 15 minutes as their hydroxides, the resulting OH^- concentration after dissolution would correspond almost exactly to the pH of 12.38 measured in the experiment at this point. Also, final K and Na concentrations are at similar levels to those observed in the acid leaches, indicating that these dissolve irrespective of the leachant (and hence solution pH) used.

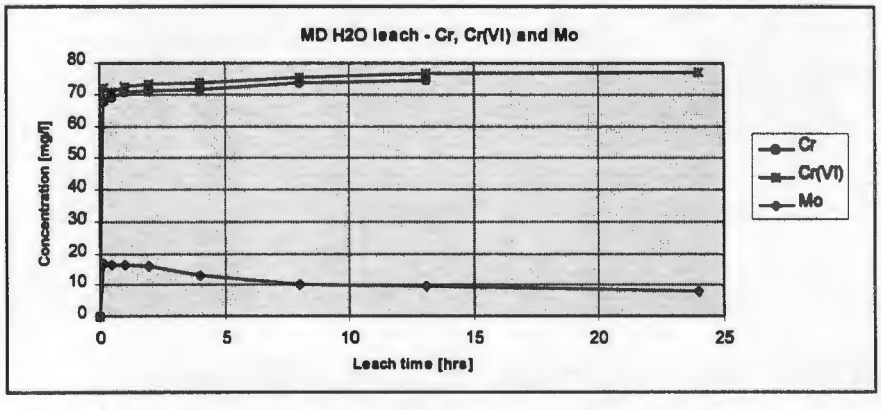

Figure 6-12b: Leach profile of Cr, Cr(VI) and Mo in H_2O leach on MD material

Similarly it is assumed Ca is present mainly in its oxide/hydroxide forms. The solubility of this compound is, however, much more limited, resulting in relatively small concentration in the water wash when compared to the acid leaches, where Ca is actively leached.

Cr dissolves exclusively as Cr(VI), which is soluble at all pH levels. After the initial jump there is only a marginal increase over the remainder of the experiment indicating some slower dissolution, which might be related to diffusion from particle pores or to a slower secondary release which is kinetically controlled. It is interesting to note that Cr(VI) levels observed in the water wash are about 10% higher than those measured in the acid leaches, which could be taken as an indication that there is some adsorption of the chromate anion at the lower pH levels in these.

6.3.3 Alkali Leaches

Considering the high effluent pH in the lysimeter column experiments, alkali leaches at similar solution pH should be the obvious choice to study release behaviour on a comparable basis.

Leach curves for the MD alkali wash in 1 M NaOH (nominal, pH constant at 13.7 constant throughout the leach) are given in Figure 6-13a and b. Values for Na are not plotted due to its use in the leach liquor. It is important to compare these curves to those obtained from the water wash, which exhibited a pH of around 12.4. One can notice immediately the high levels of Zn, Pb and Mo going into solution at this pH, which must be explained by their amphoteric behaviour and solubility at high pH levels.

Also the levels of total Cr and Cr(VI) are up when compared to the water wash with the discrepancy between the two indicating an increased release of Cr(III) in the alkali region. The increased level of Cr(VI) dissolving at higher pH is, however, somewhat surprising, since its ready solubility should not be a function of pH. It must therefore be speculated a some sort of desorption or ion-exchange mechanism leads to the release of more Cr(VI) at higher pH levels.

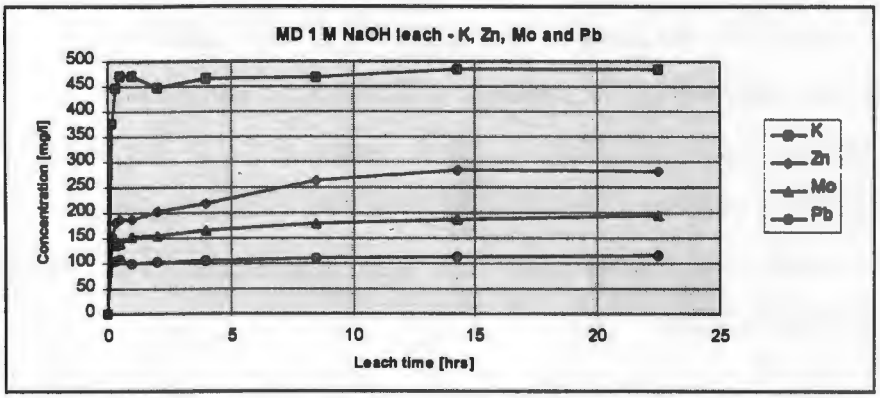

Figure 6-13a: Leach profile of K, Zn, Mo and Pb in alkali leach on MD material

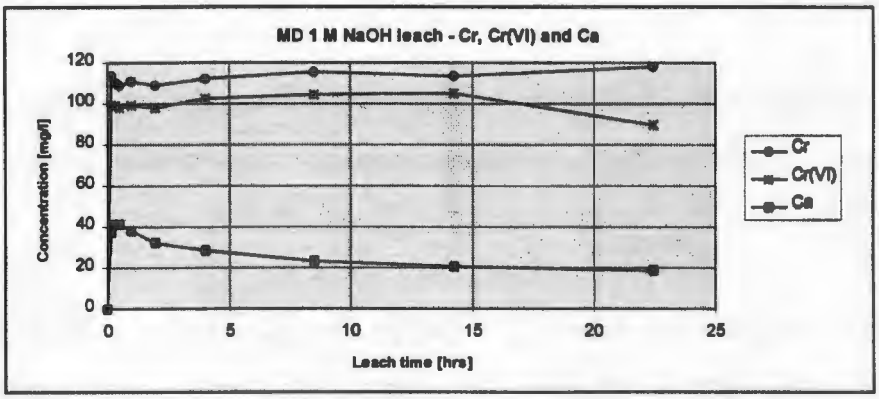

Figure 6-13b:Leach profile of Cr, Cr(VI) and Ca in alkali leach in MD material

On the other hand, concentration levels of K and Ca are down by comparison with the water wash curves. In the case of Ca this could be taken as an indication that due to the limited solubility of $Ca(OH)_2$ dissolution is oppressed by the high solution pH. The oppression of K dissolution is, however, not fully understood if it is assumed to be present in the solid in its oxide/hydroxide form as was speculated previously.

6.3.4 Cr(VI) Extraction Leach

As the release of Cr(VI) appears to play an important role in the leach behaviour of the MD material and furthermore appears to be involved in a number of release reactions, it was considered to have some measure of total Cr(VI) releasable from the material.

The material was therefore subjected to the Cr(VI) extraction leach procedure as described in Section 5.4. Results from this test are given in Table 6.5. Clearly the amounts of releasable Cr(VI) are much higher then experienced in any of the leaches nor in the column experiments and there thus appears to be a portion of Cr(VI) which is very strongly bound the solid and is only released under repeated aggressive conditions. This could be explained by a strong adsorption mechanism although the high pH levels would suggest anion adsorption is not usually strong here.

Table 6.5: MD Cr(VI) Alkali Extraction Leaches*

Leach No.	Cr(VI) conc. in leach solution [mg/l]
1	113
2	6.84
3	4.69
4	2.25
total Cr(VI) removed from solid [mg/g]	2.54

* successive 24 hour leaches in 1 M NaOH, S:L = 1:20

6.3.5 Cr(VI) Adsorption Studies

Quite clearly adsorption of Cr(VI) onto the solid material does play a role in its release from the MD material and was therefore investigated further.

Initial adsorption experiments for this material were conducted in a 1:20 S:L slurry with initial Cr(VI) solutions ranging from 0 to over 1000 mg/l. These high values were chosen since the material releases fairly high Cr(VI) concentrations by apparent dissolution and it was felt that additional adsorption would only be noticeable if this was significantly exceeded. Results from these tests (not shown here) remained inconclusive as the changes

in solution concentrations after accounting for the expected additional release of Cr(VI) from the solids were too small to measure accurately. This was attributed to the low solids concentration used, which would adsorb only small quantities of Cr(VI) without changing the high solution concentrations by much.

It was therefore decided to repeat the experiments with a S:L ratio of 1:2 in order to boost the adsorption effect. For technical reasons these were conducted in a beaker with overhead stirrer in order to achieve good mixing of the resulting thick slurry. A further aspect that requires careful investigation in this context is that of solution pH. Different to the other materials, the solution pH of MD slurries is governed by the direct dissolution of alkalis (as was indicated in Section 6.3.2) and therefore increases with increasing solids to liquid ratios. This in turn affects the amount of Cr(VI) released per g of solids, which also increases with increasing pH, and may - as yet to be verified - also influence the adsorption behaviour which is likely to decrease with increasing pH. As the pH measured in the effluent from the MD lysimeter columns was in the range of 12 to 14, this potential combined release/adsorption effect requires careful investigation in this range.

In a preliminary experiment the MD material was slurried 1:20 in distilled water for 2 hours and the solution pH measured. The pH was then driven up by addition of a few drops of concentrated NaOH solution and slurried for a further 2 hours before pH was measured again and then increased again. After each step a small sample was taken, filtered and analysed for Cr(VI). This way the increased Cr(VI) release with increasing solution pH was measured. The same titration experiment was conducted in the opposite direction by slurrying the solids 1:20 in 1 M NaOH and driving the pH down in steps by addition of concentrated HNO_3 while measuring Cr(VI) concentrations after each step.

The results of these titration experiments are plotted in Figure 6-14. Quite clearly the release of Cr(VI) (here expressed as mg per g solid) increases with increasing pH between 12.2 and 13.4, beyond which it stays more or less constant. This release is irreversible as the downwards titration data indicate. Once released, Cr(VI) concentrations in solution

remain unchanged irrespective of the solution pH. A simple linear model for the Cr(VI)-pH relationship is proposed further below. It should be noted that the maximum release at around 2 mg/g is considerably lower than the 2.5 mg/g established from the total extraction experiment detailed in Section 6.3.4

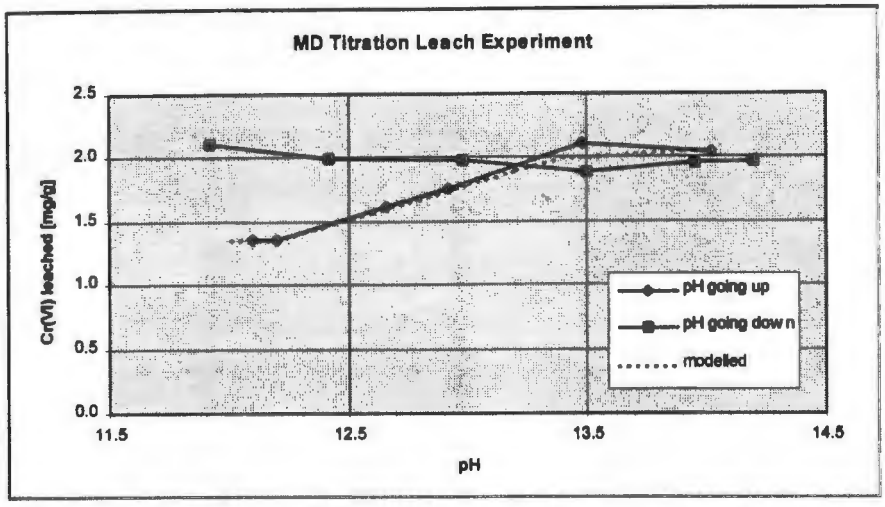

Figure 6-14: Effect of pH on Cr(VI) release from MD material

Adsorption of Cr(VI) was now measured by slurrying MD 1:2 in Cr(VI) solutions of around 800, 2200 and 4400 mg/l and adjusting the pH immediately to levels around 12.5, 13 and 13.5 in different experiments. The mixture was then slurried for 2 hours before re-measuring the pH (which tended to shift slightly off the initial target value) and taking a sample for Cr(VI) analysis.

The raw results of these experiments are presented in Table 6.6. Here the total expected amount of Cr(VI) was calculated by adding to the Cr(VI) concentration spiked to the charge the amount likely to be released from the solid at the prevailing solution pH. It should be noted here that the slurry pH before pH adjustment was always around 13 and that the amount of Cr(VI) released at this pH would remain in solution even if the pH was subsequently driven down - as was shown in the titration experiments above. The difference between expected total and measured concentrations was then assumed to make up the amount of Cr(VI) adsorbed onto the solids, which is expressed as mg per g solid in the table. These data show a clear trend for Cr(VI) adsorption. Adsorption increases with

increasing solution concentration and at each concentration level there is a trend of decreasing adsorption with increasing solution pH, as would be expected. The raw data from these experiments is further correlated into an adsorption isotherm model for this material as follows.

Table 6.6: Results from Cr(VI) adsorption experiments on MD material *

Cr(VI) spiked to charge	final pH	Cr(VI) expect. from leach	total Cr(VI) expected	total Cr(VI) measured	difference adsorbed
mg/l		mg/l	mg/l	mg/l	mg/g
0	12.48	900	900	656	0.488
0	13	893	893	696	0.395
0	13.42	1000	1000	782	0.436
808	12.6	893	1701	1358	0.686
808	12.94	877	1685	1390	0.591
808	13.4	1000	1808	1541	0.534
2212	12.7	893	3105	2529	1.151
2212	12.97	885	3097	2612	0.970
2212	13.44	1011	3222	2773	0.898
4423	12.25	893	5316	4608	1.417
4423	12.92	872	5295	4642	1.307
4423	13.4	1000	5423	4853	1.140

* 2 hr washes at given pH, 1:2 S:L ratio

The date points given in Table 6.6 have been grouped in three sets according to the values of final solution pH (<12.7, around 13 and >13.4) and are displayed on a graph adsorbed concentration versus solution concentration in Figure 6-15. Quite clearly there is a trend in all three sets to show a concave type adsorption behaviour and that the adsorption tendency decreases with increasing pH. Isotherms were therefore modelled as both Langmuir and Freundlich isotherms for each set independently. The results of the regression fits (as outlined in Section 5.5.2) are given in Table 6.7 and the modelled isotherms are also indicated in Figure 6-15.

The regression coefficients r^2 indicate good fits for all sets using either model. It is interesting to note that the value for $c_{S,max}$ is very similar around 2 mg/g for all three pH regions, indicating that the maximum absorbable amount of Cr(VI) (and thus the number

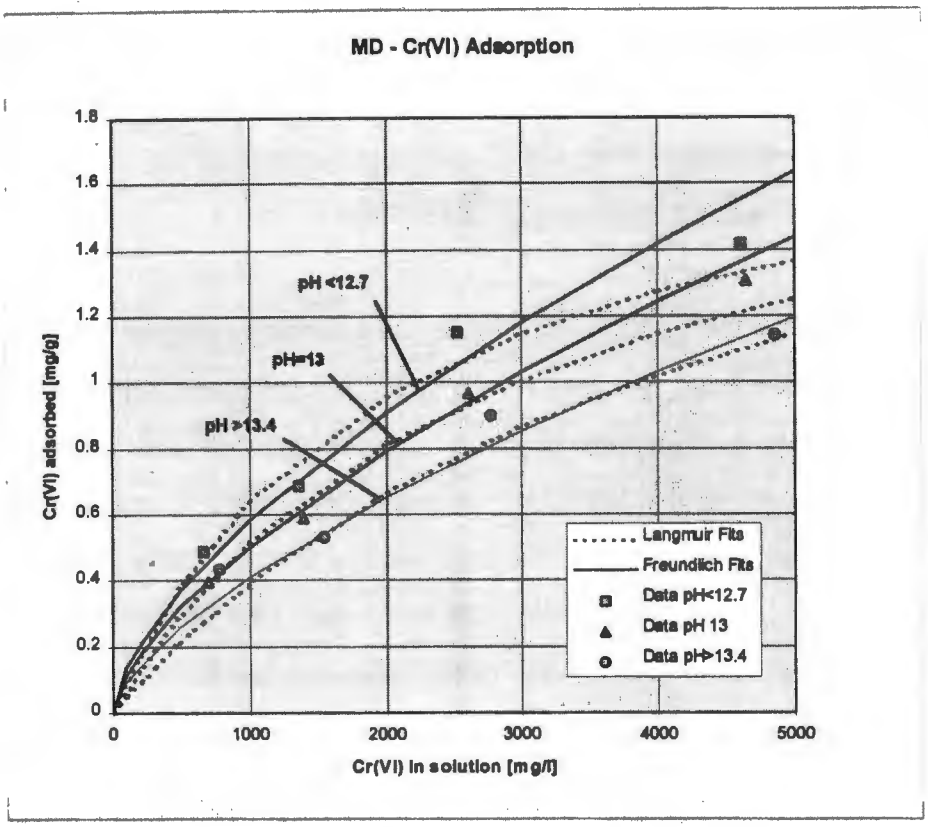

Figure 6-15: Cr(VI) adsorption on MD material - raw data

Table 6.7: Best fitted data for Langmuir and Freundlich adsorption isotherms for MD

	Langmuir Isotherm			Freundlich Isotherm		
	$c_{s,max}$	K	r^2	b	m	r^2
pH < 12.7	1.904	0.00051	0.966	0.0070	0.64	0.959
pH = 13	1.966	0.00035	0.985	0.0057	0.65	0.995
pH > 13.4	2.212	0.00021	0.985	0.0043	0.66	0.962
correlation	$K = 5.1 \cdot 10^{-4} - 1.9 \cdot 10^{9} \cdot (10^{-12.7} - 10^{-pH})$			$b = 0.007 - 0.0039 \cdot (pH - 12.7)$		

of adsorption sites) is not greatly influenced by the solution pH. The Langmuir adsorption constant K is a linear function of H^+ concentration (not pH!) in the range considered. Similarly, the exponents m of the Freundlich isotherm are all nearly identical around 0.65 (which may be related to the number of Cr(VI) ions per adsorption site) and the coefficient b is in fact a linear function of pH in the range considered.

Also, when comparing the measured data to the fitted isotherms (Figure 6-15), both types appear to fit the data equally well for Cr(VI) solution concentrations below 3000 mg/l. At higher concentrations the Langmuir isotherm begins to taper off , while the Freundlich isotherms continue to fit the high data set reasonably well. As the highest Cr(VI) concentrations encountered in any of the column experiments never exceeded values of 3000 mg/l, it is of little importance which of the models best represents the adsorption isotherm. In general, however, the Freundlich isotherm model should be given the preference as it represents the physico-chemical mechanisms of adsorption better.

6.3.6 Reaction Modelling

In summary of the batch leach on the MD material experiments, it can be stated that in an alkaline environment most release reactions are more or less instantaneous, with final concentrations mostly reached after 2 hours and only marginal changes thereafter. The release of alkalinity appears to be driven mainly by the dissolution of Na and K hydroxides. The release of Ca is a function of pH, with concentrations decreasing with increasing pH, supporting a $CaO/Ca(OH)_2$ buffer system. Acid leaches with their rapid change of pH to neutral are poor indicators of the likely leach behaviour in the alkaline environment encountered in the beds.

Cr(VI) release, although instantaneous, is a function of increasing pH, particularly in the region between pH 12 to 14. An interesting finding is the fact that the release reaction is irreversible, i.e. Cr(VI) released at high pH would not re-precipitate once the pH is

and measured data on the basis of these flat curves. More convenient is to compare the calculated equilibrium values with averaged measured values within a table.

The WASTEMD code was used to simulate the H_2O batch leach curves for different values of the initial Cr(VI) solid concentration that would go into solution (according to reaction 5). The calculated equilibrium concentrations and measured data are given in Table 6.8. The first modelled set (for $c_{Cr(VI)}^0$ =2.0 mg/l) corresponds to the data shown in Figure 6-16. As can be seen from the table, pH and concentrations of Na, K and Cr correspond very well (within 5%) to the measured values. Ca concentrations are somewhat over-predicted by the model, but, as Ca was not a species of interest, this is considered acceptable here. Changing the initial Cr(VI) solid concentration by as much as 20% does have only very marginal effect on the resulting equilibrium value. This trend can be explained by the buffering capacity of the Cr(VI) adsorption reaction.

Table 6.8: Experimental and Modelled Equilibrium Values for 1:20 H2O leach

	measured	modelled solid Cr(VI) at		
		2 mg/g	1.8 mg/g	1.6 mg/g
pH	12.4	12.5	12.5	12.5
Na	220	230	230	230
K	600	600	600	600
Ca	115	149	149	149
Cr(VI)	72	73.4	70.9	68.4
Crtot	72	76.7	74.2	71.7

As a further test of the proposed MD reaction matrix, the results of the batch leach experiment in 1 M NaOH have been modelled and compared to the experimental data (Table 6.9). As can be seen, model predictions begin to differ from the measured value except for Cr(VI), the release behaviour of which has been closely investigated in the pH range from 12 to 14. While the predictions are still acceptable for pH, Na and K, the

Table 6.9: Measured and Modelled Equilibrium Values for 1:20 1 M NaOH Leach

	measured	modelled
pH	13.7	14.0
Na	21000	20230
K	480	600
Ca	20	0.15
Cr(VI)	100	97.5
Crtot	118	202

* all data in mg/l

discrepancy of predicted and measured Ca concentrations is significant. The model (through reaction 2) assumes Ca dissolution would be completely suppressed at very high pH values, whereas in reality other reactions involving Ca may play a role. The high over-prediction of total Cr levels results from the solubility product employed in reaction 7. As was stated in Pourbaix (1966), the exact determination of Cr(III) solubilities is extremely fickle. Thus the comparison shows quite clearly that reasonably accurate predictions over a range of conditions are possible only if the system is closely characterised in terms of the prevailing reactions and species.

6.4 Bed Diffusion Experiment and Modelling

Having established a general reaction scheme describing the release of chromium and other species from the MD material, this can now be tested further with the material in a bed situation. As MD is characterised by extremely small particles (see Section 6.1) and exhibits considerable hydraulic resistance to flow through the packed matrix, there is reason to believe that the inter-particle porous structure of the material is sufficiently convoluted to exhibit resistance also to diffusion transport of dissolved species. This was tested using the stagnant bed leach experiment described in Section 5.4.

Parameters for this experiment are given in Table 6.10. The resulting concentration-time curves of Cr(VI), Na and pH are given in Figure 6-17. All curves exhibit expected behaviour, with supernatant concentrations increasing rapidly initially while the

lowered. Measurable Cr(VI) adsorption occurs only at very high solution concentrations and, again, is a function of solution pH in the region pH 12 to 14. Experimental data can be fitted reasonably well with both Langmuir and Freundlich adsorption isotherms.

Careful evaluation of the results of various experimental studies conducted on the MD material give a fairly good insight into the chemical interactions which determine the release behaviour of the material in a deposit situation as was discussed in Section 5.4.2. The parameters for instantaneous release and equilibrium reactions relevant to the present case can be extracted from an analysis of experimental data and tested with the computer model, which has a module for calculation of simultaneous equilibrium reactions.

Although a large number of reactions may be required to fully describe the system, the assumption is made that, if focus is concentrated on the main species under consideration, only those reactions that directly pertain to these need to be considered, providing interference of other species is not significant. The selection of significant species and reactions requires careful evaluation of the experimental evidence from lysimeter and batch leach experiments. The validity of the selection needs to be tested ultimately within the methodology applied here and may have to be revised if other significant factors become significant during subsequent work. In the present study focus was placed on the release of chromium species. For the MD material this is, however, strongly influenced by solution pH. Therefore those reactions which have a significant influence on solution pH need to considered as well.

The following system of 7 reactions was chosen to describe instantaneous and equilibrium release behaviour (particularly that of Cr species) of MD. Reaction type (according to the types described in Section 4.7.3) and the relevant parameters as well as their source (from experiment of literature), are listed below:

1. $H_2O \leftrightarrows H^+ + OH^-$

Reaction Type:	Solubility product of water	
Reaction Constant:	$K = 1.7 \cdot 10^{-7}$ mg²/l²	(converted from $K_w = 10^{-14}$ mol²/l²)

2. $Ca(OH)_2 \leftrightarrows Ca^{2+} + 2OH^-$

Reaction Type:	Solubility product of hydrated lime	
Reaction Constants:	$K = 4.624 \cdot 10^{7}$ mg³/l³	calculated from literature value (CRC, 1992)
	$c_{Ca(OH)2}^{0} = 60$ mg/g	taken as larger in order to allow neutralisation of 0.1 M acid

3. $NaOH \rightarrow Na^+ + OH^-$

Reaction Type:	Instant full dissolution of sodium hydroxide	
Reaction Constants:	$c_{NaOH}^{0} = 8$ mg/g	calc. from batch leach exp.: 230 mg/l Na from 50 g solids (Figure 6-12a)

4. $KOH \rightarrow K^+ + OH^-$

Reaction Type:	Instant full dissolution of potassium hydroxide	
Reaction Constants:	$c_{KOH}^{0} = 17$ mg/g	calc. from batch leach exp.: 600 mg/l K from 50 g solids (Figure 6-12a)

As indicated, the initial solid concentrations values have been estimated from batch experimental data. Equilibrium constants, where relevant, have been taken from the literature or, in the case of the Cr(VI) adsorption isotherm, have been correlated from experimental data. Although reaction 1 to 4 do not involve Cr species, which are the primary focus of the work here, they strongly influence the prevailing solution pH, which in turn influences Cr release behaviour and they can therefore not be ignored.

5. $Cr(VI)_{solid}$ $\{+H^+\}$ $\rightarrow$ $Cr(VI)_{aq}$

Reaction Type:	pH dependent, irreversible dissolution of Cr(VI)
Reaction Model	$mg\,Cr(VI)_{aq} = \begin{cases} 1.36 & pH < 12.2 \\ 1.36 + \frac{([Cr(VI)_{solid}] - 1.36)}{(13.4 - 12.2)}(pH - 12.2) & pH\ 12.2 - 13.4 \\ [Cr(VI)_{solid}] & pH > 13.4 \end{cases}$
Reaction Constant	$c_{Cr(VI)}^{\ 0} = 2.0$ mg/g

This model was derived by evaluating the data of the Cr(VI) titration experiment (Figure 6-15) by linear regression in the range 12.2 < pH < 13.4

6. $Cr(VI)_{ads.}$ $\leftrightharpoons$ $Cr(VI)_{aq}$

Reaction Type	Cr(VI) Langmuir adsorption
Reaction Constants:	$K_{ads} = \begin{cases} 5.1 \cdot 10^{-4} & pH < 12.7 \\ 5.1 \cdot 10^{-4} - 1.9 \cdot 10^{9} \cdot (10^{-12.7} - 10^{-pH}) & pH\ 12.7 - 13.4 \\ 2.1 \cdot 10^{-4} & pH > 13.4 \end{cases}$
	$c_{ads}^{\ 0} = 0.0$ mg/g
	$c_{max} = 2.0$ mg/g

All parameters as given in Table 6.7

7. $Cr(III)$ oxides $\leftrightharpoons$ $Cr(III) + H^+$

Reaction Type:	Solubility product of chromic oxide	
Reaction Constants:	$K = 1 \cdot 10^{-9}$ mg^2/l^2	calc. from literature value (Pourbaix, 1966)
	$c_{CrOx}^{\ 0}$: arbitrary	dissolving conc. will be small

The release of other heavy metal species, on the other hand, is not seen to influence pH or the release of Cr to any significant extent and are not considered further. It must also be pointed out that all reactions defined are instantaneous or equilibrium, and kinetic reactions are not considered further as there was little experimental evidence for these.

The matrix of reactions defined for the MD system is quite complex and involves two reactions (5 and 6) that are not catered for by the reactions available in the standard form of the WASTESIM code (see Sections 4.7 and 4.8). Therefore a modified version of the code was prepared in which reactions 1-4 and 7 were defined in the user interface, while reactions 5 and 6 were hard-coded (i.e. manipulation of reaction parameters from the user interface was not possible). This modified version is available on the disk accompanying this volume as WASTEMD (see Appendix C).

As a first test it was attempted to model the H_2O batch leach experiment with the BATCH module of the code (see Section 4.8) and the reaction matrix entered or hard-coded as indicated above. According to the experimental conditions, the liquid volume was set to 1 litre and the solid charge to 50 g. The particles were modelled as non-porous, since, as was argued in Section 4.8, leaching a material exhibiting very small particle size is unlikely to result in significant pore diffusion effects. The results of this modelling run are shown in Figure 6-16.

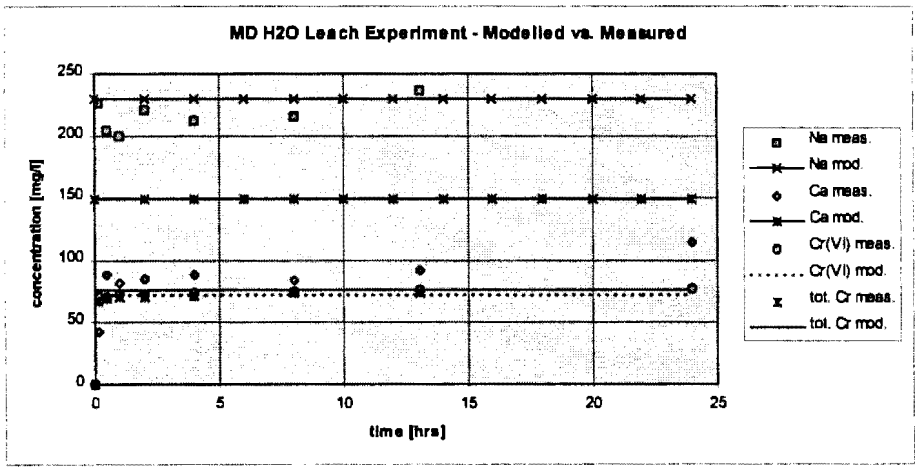

Figure 6-16: Modelled and measured leach curves of the MD H_2O leach experiment

Since no kinetic effects (kinetic reactions or pore diffusion) are considered here, all model curves appear as flat lines, with all concentration values corresponding to the initial equilibrium calculated. This corresponds in trend to most batch leach curves observed in the experiments. There is, however, little benefit in comparing the modelled

concentration gradient between bed and fluid is still large, and then gradually levelling off as bed and supernatant concentrations become more and more equal.

Table 6.10: Parameters for bed diffusion experiments on MD

Material:	MD mix
dry mass filled [g]	400.5
total mass filled [g]	546.4
bed volume [ml]	275
bed area [cm^2]	78.5
bed height [mm]	35
supernatant vol. [ml]	500

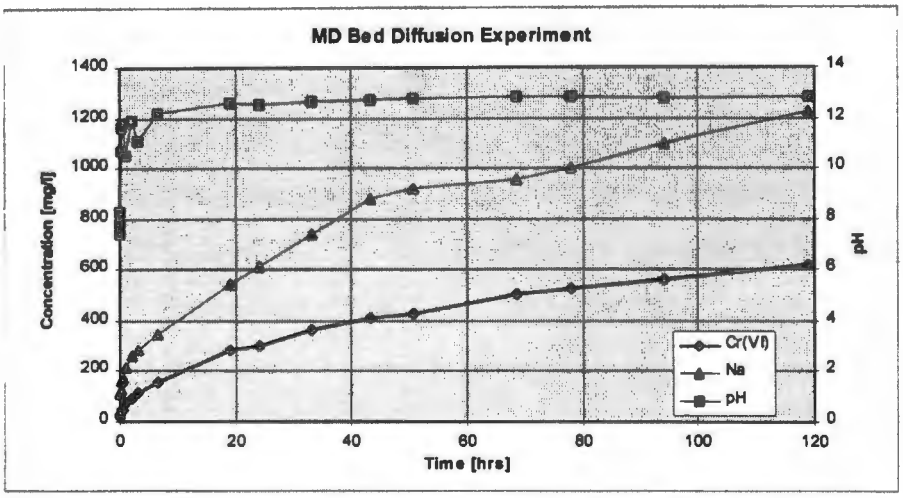

Figure 6-17: Concentration profiles for the MD stagnant bed leach experiment

As described in Section 5.4.2, the WASTESIM code has a modification which allows the COLUMN mode to be combined with the BATCH mode to allow modelling of the stagnant bed leach experiments. All experimental parameters indicated in Table 6.10, have been entered into the code as well the reaction matrix as detailed in Section 6.3. The parameters that required further attention are bed porosity ε_h, fractional bed saturation f_{sat} and the effective bed diffusivity factor d_{bed}. As was discussed in Section 4.8 these parameters are significant in determining bed transport behaviour.

The total bed voidage, calculated from bed volume, solid mass and solid true density, was 0.69, a value that seems rather large, but compares well to that calculated for other MD column studies. An explanation would be the agglomerated nature of the dust particles, composed of many sub micron sized globules with large interstitial spaces (see electron micro-graph, Figure 6-1a). This could, in principle, be taken as internal particle "pores", rather than attributed to the bulk voidage, but it is felt that the void space between particles is likely to be of the same order of magnitude as the void space enclosed within agglomerates and it would therefore be valid to lump the two as bulk voidage. If there is increased diffusion resistance due to small pore sizes (and hence tortuosity), then this would apply equally for the bulk and can be modelled for a given bed diffusivity coefficient d_{bed}.

It was also noted that the volume of water used to slurry the dust was less than required to fill the calculated bed pore volume and hence a bed saturation of only 80% was achieved, with the rest assumed to be filled with air. Again this finding was surprising, but can be explained by the fact that air in the narrow spaces within the dry agglomerates is not likely to be displaced immediately upon contact with water and is consequently trapped in the paste that is used to form the bed. The aspects of bulk voidage and saturation are more critically discussed in the context of the tracer studies detailed in Section 6.5.

Hence, for purpose of modelling the stagnant bed experiment, bed voidage was taken as the calculated 0.69 and saturation fraction as 0.8. As initial guess for effective diffusivity coefficient, the rule-of-thumb value $d_{bed} = \varepsilon/2 = 0.35$ was used.

Modelled curves are plotted together with the experimental data points in Figure 6-18. In trend all curves follow the experimental values closely. The pH curve is over-predicted by about 0.5 pH units, but it appears that the measured values are rather low considering the very high solid to liquid ratio achieved within the system (i.e. solids in the bed relative to bed moisture and supernatant fluid combined, 1:1.6).

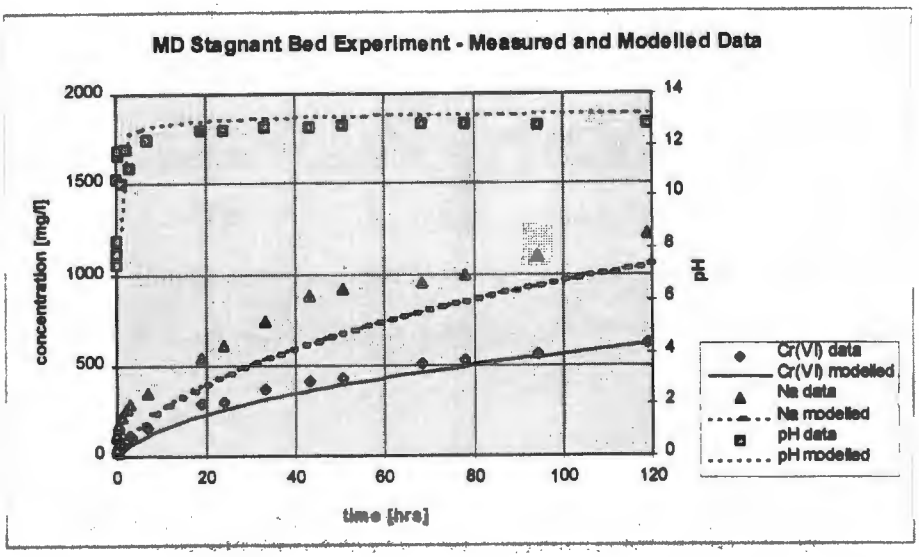

Figure 6-18: Modelled and experimental curves for MD stagnant bed experiment

Both, Na and Cr curves, are somewhat under-predicted, but the slope of the simulated curve follows that of the measured data in both cases. This is taken as an indication that the bed diffusivity has been estimated correctly, since increased or reduced pore diffusion would change the slope of the leach curve noticeably, as was demonstrated in the sensitivity study in Section 4.8 (although there a look is taken at the influence of changing the *particle* pore diffusion coefficient, this analysis is equally valid for the *bed* diffusion coefficient in the stagnant bed experiment.

The measured curves appear offset against the simulated curves by a small margin. It is noted that the initial rise of the measured data (over the first 20 minutes or so) is very steep and appears unrelated to the slower diffusion release later in the experiment. A plausible explanation for this behaviour would be that the top layer of the bed, closest to the glass fibre sheet and stirred supernatant, experiences some degree of bulk fluid movement resulting from turbulences carried through the sheet. Consequently the dissolved concentrations in this top layer are carried into the supernatant more rapidly. To account for this the bed might be taken as slightly shorter and the concentrations associated with the top layer taken as dissolving instantaneously. Taking the dissolved concentrations after 20 minutes as corresponding entirely to this top layer, then, from an

estimate of the expected initial bulk concentrations (see Section 6.3.6), the thickness of this top layer can be calculated to be about 2 mm or 5% of the bed.

A second modelling run has therefore been attempted, in which the bed height is reduced to 33 mm and the offset concentrations of Cr(VI) and Na were set to 50 mg/l and 160 mg/l respectively (corresponding to measured concentrations after 20 minutes). All other model parameters are unchanged from the previous run. The results of this run are shown in Figure 6-19.

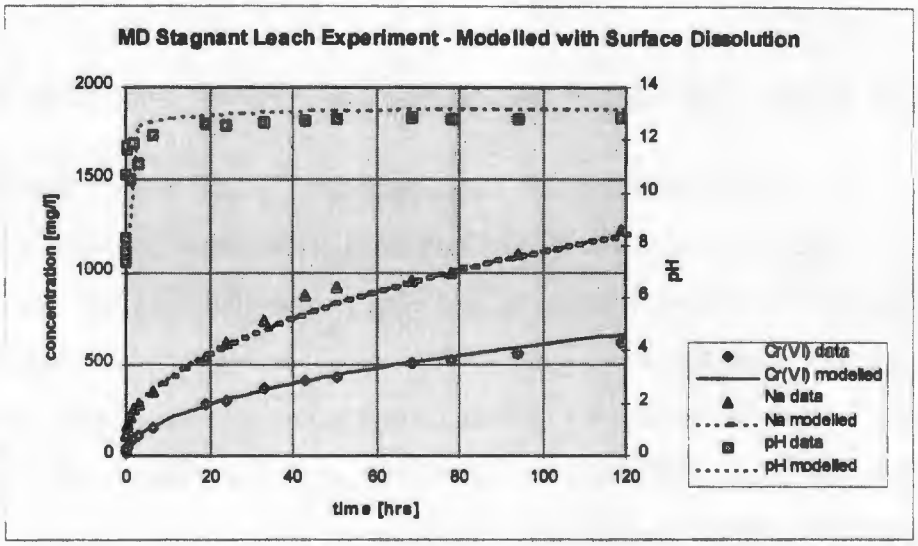

Figure 6-19: Modelled MD stagnant bed leach experiment accounting for instant dissolution from the top layer

As can be seen the speculated instant dissolution of the top-layer of the bed would account well for the discrepancies of the initial modelling run. Excellent closure between modelled and measured data is achieved in this case, which supports the earlier statement that the effective bed diffusivity co-efficient d_{bed} is well approximated by 0.35. It is possible, in principle, to manipulate d_{bed} further to achieve even better closure between measured and modelled data, but this is not considered to achieve much in the present context.

6.5 Column Tracer Study

The tracer study for the MD mixture was conducted in an accelerated Constant Head Lysimeter (Section 5.3) experiment with a short bed and pressurised liquid feed similar to experiment MD2 (Section 6.2). Ideally this experiment should have been conducted in the same bed as either experiment MD1 or MD2, but since the permeability in both these experiments change considerably towards the end of the experiment, these were not considered suitable for comparison. Therefore a fresh accelerated experiment has been undertaken (experiment MD3). Experimental conditions are listed in Table 6.11.

The experiment was started with unspiked leach liquor (acid rain mixture) and run for 8 days to allow establishment of bulk flow conditions. The feed liquor standing over the top of the bed was then completely drained and replaced by liquor spiked with around 900 mg/l Li^+. The experiment was continued on this basis for 7 days, before all residual spiked liquor was again drained and replaced by regular acid rain mixture, with which the experiment was continued until Li concentrations in the effluent had dropped below 5 mg/l at which stage the tracer study was considered complete. The effluent flow rate was carefully monitored (Figure 6-20) and found to change over the duration of the experiment, similar to what was experienced in experiments MD1 and MD2. A possible explanation for this has been offered in Section 6.2.3.

Table 6.11: Experimental Parameters of MD Tracer Column Study

Material(Code)	Lysimeter	Bed Height [mm]	Daily Flowrate [ml]	Hydraulic Head	Duration [days]
MD (MD3)	CHL, pressure	200	670 - 1000	50 kPa	60

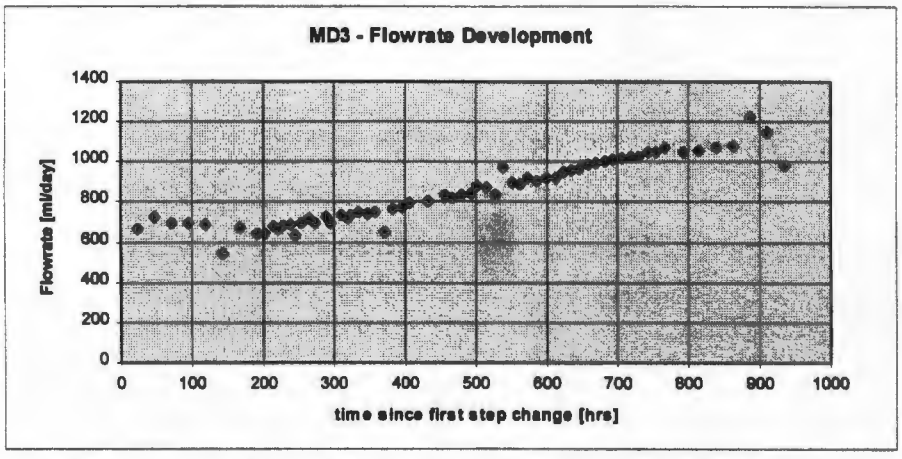

Figure 6-20: Flow rates through the lysimeter in experiment MD3

Li concentration in the effluent versus time are given in Figure 6-21. The seemingly smooth profile with one distinct peak must not detract from the fact that this curve is in fact the response to two step changes in the experiment (although this could in fact be interpreted as one extended pulse). The location of the peak is also in no relation to the actual average residence time in the bed. Assuming plug flow through the bed, the liquid volume (4.75 l) in the bed should have been flushed out once after around 170 hours given the actual sample throughput measured. At this point in time, however, the effluent Li concentration has only reached 145 mg/l and the peak only occurs after about 290 hours. Therefore the curve requires some more careful explanation.

Total Li feed and recovery were calculated by multiplying throughput per sample period with the respective Li concentrations. These are plotted in Figure 6-22, which indicates a mass balance closure in excess of 98% and thus near total recovery of all Li fed into the system. This can also be interpreted as an absence of dead pores in which tracer gets permanently trapped.

Possible scenarios for dispersion of flow through packed beds were discussed in some detail in Section 5.6. It was indicated that this effect can result from micro-scale effects such as diffusion and micro-mixing, from a distribution of flow through the bed (through

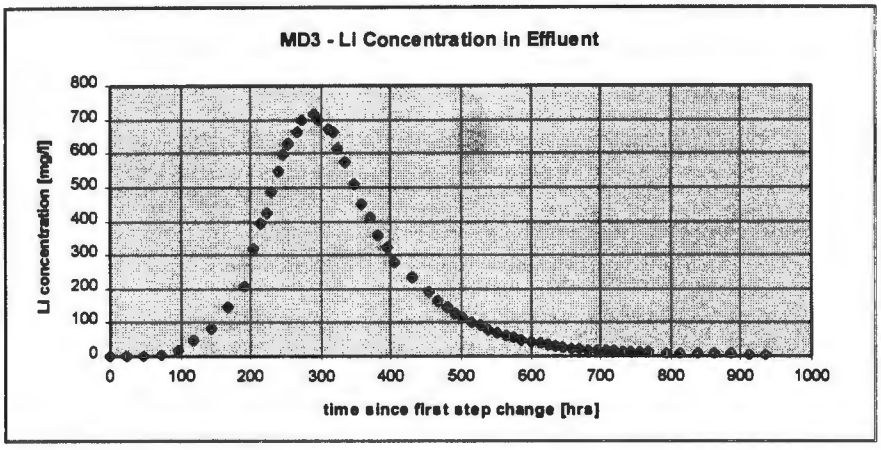

Figure 6-21: Li recovery profile in experiment MD3

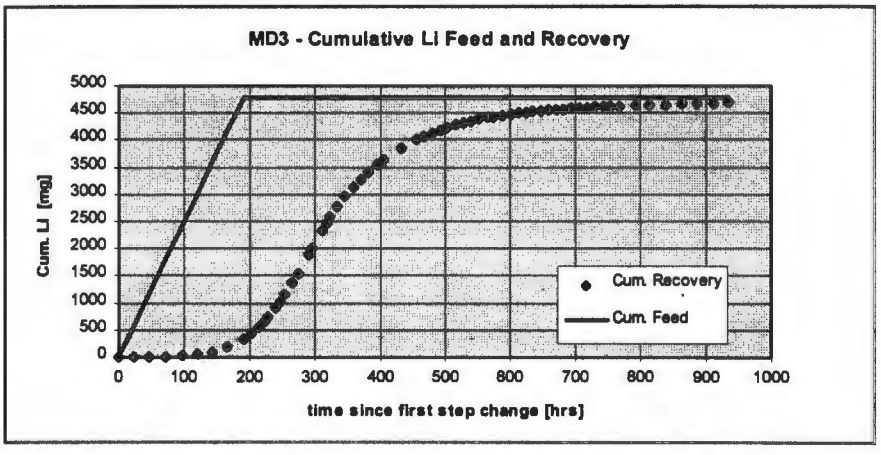

Figure 6-22: Cumulative Li feed and recovery in experiment MD3

zones of different hydraulic conductivity) and from dead pore diffusion. In real beds it is likely that a combination of all effects may be encountered.

In the present study it was attempted to model the Li tracer curve with the WASTESIM code to identify which combination of factors is most suitable to emulate the measured trends. This included using the split flow analysis introduced in Section 5.6.

Initially the Li flow through the bed was simulated the packing information available from the experimental set-up. Again the bulk voidage was calculated at the large value of 0.69 as was already found in the stagnant bed experiment (Section 6.4) and the fractional saturation likewise at 0.8, indicating the presence of a considerable volume of air in the bed. As was explained before, this could be related to agglomerated nature of the MD particles where air can easily be trapped in the agglomerates when slurrying the material with water. The bed diffusion factor d_{bed} was kept at 0.35 as confirmed by the stagnant bed leach experiment (Section 6.4). The changing flow-rate measured during the duration of the experiment (Figure 6-20) was accounted for during the simulation by varying the flowrate variable accordinng to the programmed data. The simulated Li response curve is plotted, together with the experimental data in Figure 6-23. For comparison the same run was also conducted with a fractional saturation of 1.0, which is also shown in the figure.

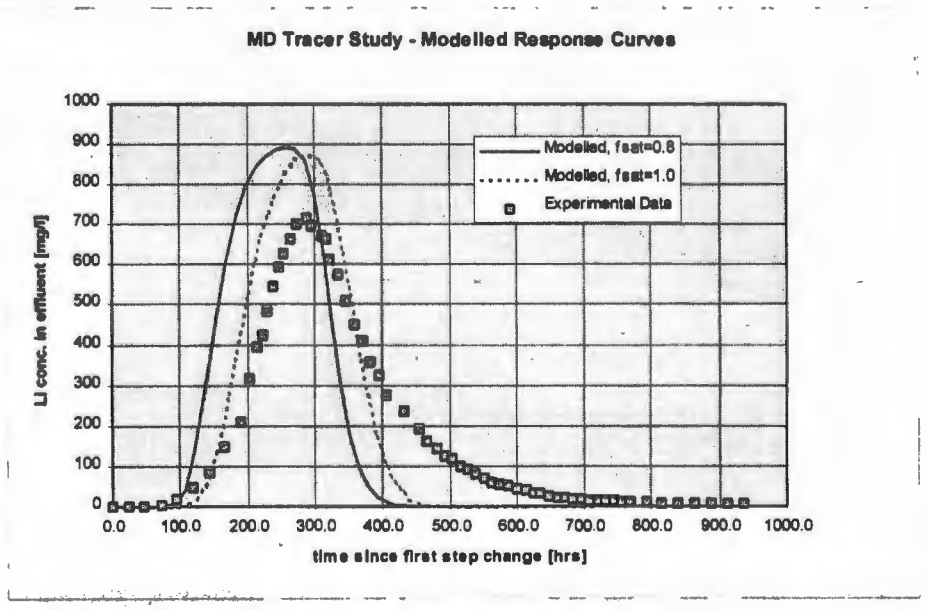

Figure 6-23: MD3 tracer data and modelled response curves

Quite clearly both simulated curves show a much narrower spread of the response curve than the measured data and a correspondingly higher peak value. The area under all three curves is, however, identical (which was checked for model confirmation) as would be expected. The first conclusion that can be drawn from this is that Li dispersion by

diffusion can alone not account for the spread of the observed response curve. What is more surprising, however, is the fact that time of the peak of the curve modelled for saturated flow corresponds to the time of the measured peak, while the peak under unsaturated conditions appears early, although packing information suggests that the bed was initially not saturated.

It is therefore speculated that bed saturation with fluid changes in the course of a leach run. If it is assumed that the air trapped in the bed is in small pockets within the particle agglomerates and no free surface flow occurs, then the trapped air could gradually become displaced by or dissolved in the bulk fluid and replaced by liquid. Through this removal not only the area available for flow gradually increases, but also the resistance to flow is likely to decrease as the net seepage velocity becomes smaller. This may then result in increasingly higher flow rates under a given driving pressure, a phenomenon that has been observed in all MD column experiments. Careful mass balance between inflowing and outflowing liquid would indicate whether there is in fact net accumulation of fluid in the bed, but unfortunately such information could not be extracted from the experimental records (only effluent but not feed flow was monitored in the constant head type lysimeters, see Section 5.3).

The onset of full saturation could be taken as the point where flowrates begin to increase. In the present tracer study this point unfortunately occurs right in the middle of the run (after about 250 hours). Since the column was run for 8 days before commencing the tracer study, it can be assumed that the saturation process is already far progressed and the assumption of fully saturated flow will be maintained for further analysis. It should be pointed out that the WASTESIM code at its current state of development can take account of changing flow-rates, but not of fluid bulk accumulation. Simply varying the fractional saturation during the run would result in erroneous simulations.

For the split flow analysis, as was described in Section 5.6, the area between the modelled (for f_{sat} = 1.0) and measured curves (Figure 6-23) was calculated by integrating both

curves and subtracting the areas to the point of intersection. This area is taken to correspond to the total amount of Li that travels through the bed more slowly and the ratio between this area and the area under the residual would correspond to the flow split between fast and slow moving fluid. In the present case this has been calculated to be approximately 2:1.

As was pointed out in Section 5.6.3, split flow is modelled by conceptually dividing the column into two smaller columns, each with half the cross-sectional area and the same height. The available flow-rate is split 2:1 between these two columns and the Li response curve calculated individually for both columns. The resulting concentrations are then apportioned into the joint effluent by calculating the weighted average. The results from this exercise are plotted in Figure 6-24.

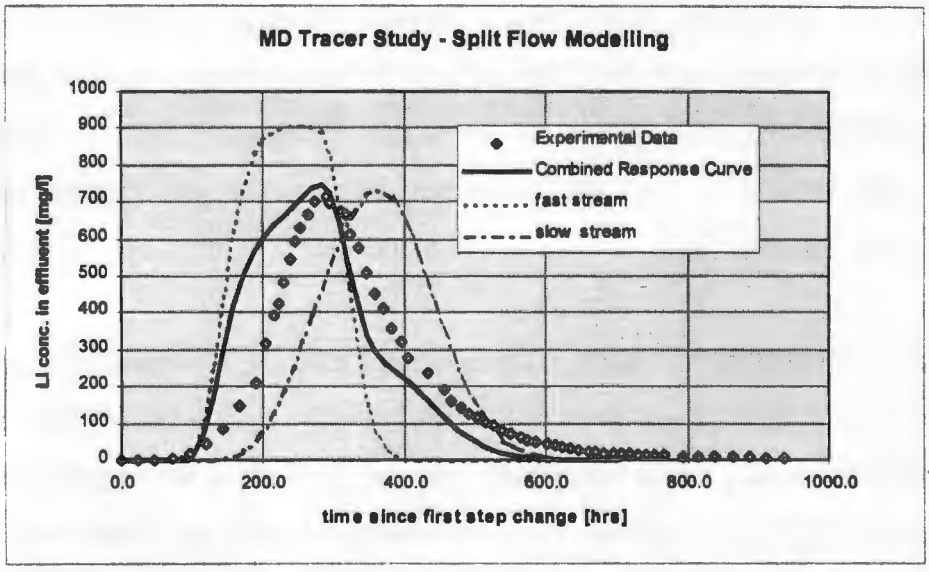

Figure 6-24: MD tracer data and response curves modelled using split flow analysis

As can be seen, the combined response curve thus modelled corresponds to the measured data very closely, both in the location and height of the peak and the shape of the tail-end. The modelled curve is, however, slightly early relative to the experimental data and this requires some further explanation.

In his treatise on residence time studies, Levenspiel (1972) cites reasons for a measured tracer curve appearing later than expected as

- inaccurate measurement of flow rates
- inaccurate account of volumes available for flow
- adsorption of the tracer onto the bed material

All these three reasons merit consideration in the present study. Flowrate measurement, which was conducted by weighing the effluent beaker during sampling, was relatively crude in the present study and could easily account for flowrates being slightly inaccurate. Pore fluid volumes could easily have been slightly miscalculated by inaccurately weighing the solid mass actually placed in the column (although great care was taken in doing so). Also, the residence time of fluid in the support packing at the bottom of the column (see experimental set-up in Section 5.3) has not been taken into account. As this consists of relatively large glass-beads, the hold-up in this section may still contribute, albeit marginally, to a delay of the effluent.

Adsorption of the Li tracer onto the MD material was in fact investigated prior to commencement of the study and found to be marginal at less than 1mg/g in the concentration range considered. But nonetheless, such marginal adsorption may contribute to a small delay in the measured tracer response curve. The effect of this potential adsorption delay has been built into the split flow modelling by assuming a Langmuir type adsorption isotherm for Li, which emulates the few data points that were obtained during this preliminary study. The modified combined response curve is plotted, together with the experimental data, in Figure 6-25. Quite clearly this marginal adsorption does not contribute to any significant extent for the time discrepancy still residual after conducting the split flow analysis. However, as too few data points were measured with respect to Li adsorption and other delaying effects listed above have not been quantified, this result should be viewed with some care.

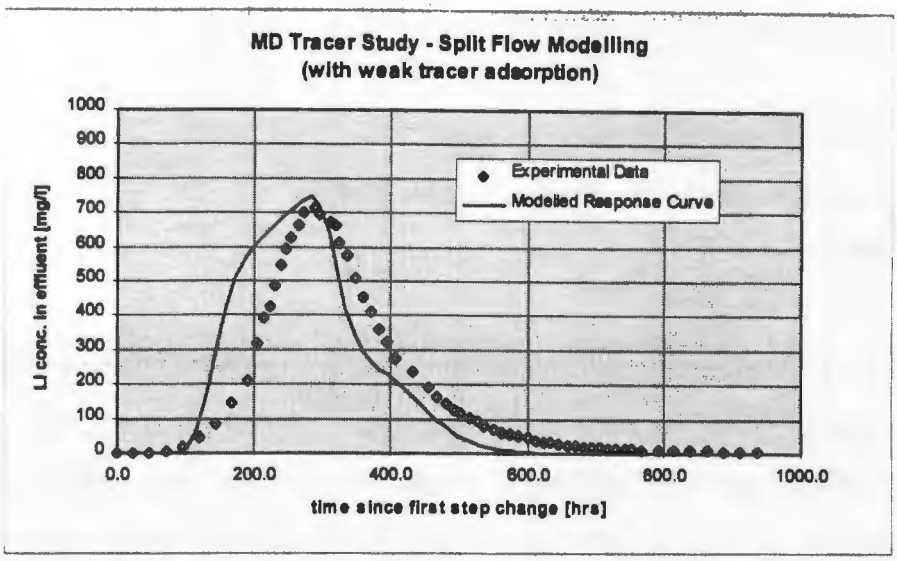

Figure 6-25: MD tracer data with modelled split flow response curve taking account of minor tracer adsorption

Another effect not taken into account in the split flow assumption is that of cross-zone diffusion, i.e. lateral diffusion between zones of different hydraulic conductivity, and the effect of dead pores. In packed bed systems, migration of tracer (and thus any dissolved species) in and out of stagnant zones in the bed is considered an important contributor to delay of species transport. As was indicated in Section 5.6, the model is, in its current form, not suitable to take account of such effects, but there is scope for their inclusion at a later stage.

6.6 Column Modelling

The release behaviour of the MD material has been characterised in terms of Cr species and alkalinity by batch leach experiments, as was described in Section 6.3. The stagnant bed diffusion experiment (Section 6.4) has indicated that bed diffusion is well described by the rule-of-thumb $d_{bed} = \varepsilon/2$ (=0.35 here). It was also indicated that intra-particle diffusion effects are negligible due to the very small particle sizes of this material. The

tracer study MD3 has shown that there is, at least for the conditions in the accelerated lysimeter, a strong evidence for a distribution of flow rates through zones in the bed of higher or lower hydraulic conductivity. Tracer work has also shown that the bed saturation is likely to change with time as air trapped in the porous matrix is gradually displaced or dissolved in the bulk fluid, and that this could serve as an explanation why flowrates significantly increase after some time.

It is now attempted to validate the information gathered by modelling the expected leach profiles of the two lysimeter studies MD1 and MD2, which are described in Section 6.2, and comparing the result with experimental data. Results from this modelling work are discussed in Sections 6.6.1 and 6.6.2 respectively.

6.6.1 Modelling of MD1 Data

The WASTESIM code in COLUMN mode (see Section 4.8) has been applied using the reaction matrix as formulated in Section 6.3.6. The bed characteristic parameters are given Table 6.12. As was indicated in Section 6.5, bed saturation appears to be a function of time, but this cannot be incorporated into the model equations at this point in time. Two modelling runs were therefore conducted, one taking the fractional saturation at the value of 0.9 as calculated from the packing information and the second one taking this value as 1.0 assuming saturation is achieved rapidly enough to not affect the leach curves. In addition the run was also modelled using the split flow approach with a split ratio of 2:1, as identified in Section 6.5, and full saturation. The varying flow rates through the bed, as given in Figure 6-5, have been incorporated into the modelling. Only the first 320 days of the run were simulated since

Table 6.12: Bed Characteristic Parameters for Experiment MD1

Bed Area	0.04 m^2
Bed Height	0.524 m
Dry Solid Mass Filled	32.2 kg
Mass Water Filled	12.0 kg
Fractional Bed Porosity	0.65
Fractional Bed Saturation	0.89

flow-rates develop dramatically after this point and the concentration of most species has dropped to low values. The results of the modelling runs are given in Figure 6-26a to d by plotting modelled curves together with the measured data for pH, Na and K and Cr and Cr(VI).

The predicted pH curve corresponds to the measured data well in trend, but slightly over-predicts the measured values. However, it is pointed out in Section 6.2 that the large degree of scatter of the measured pH data points was due to an inaccurate instrument and should therefore be treated with some care. In this regard the agreement of measured and simulated trends is of greater significance that the actual values.

The agreement between modelled and measured Na curves is remarkably good and fair for K. In both cases the curve modelled using the split flow approach gives the best results and the one using single flow at a fractional saturation of 0.9 the worst. As was shown in the sensitivity study of the model (Section 4.8), changing the value of f_{sat} does not only affect the residence time in the bed, but also the effective solid to liquid ratio and thus the concentrations of dissolving species. This is confirmed here as for f_{sat} = 0.9 effluent concentrations are higher but the concentration drop (appearing at the end of one residence time) appears earlier and exhibits a steeper slope (Figure 6-26b). In terms of this slope the curve modelled for f_{sat} = 0.9 emulates the measured trend better than the one for saturated conditions, but the actual concentrations remain too high. This observation again underlines the sensitivity of the model to this factor and that measurement rather than estimation of bed saturation is essential.

The split flow approach generates better fits than single flow modelling, capturing tail-end effects better. While this gives excellent agreement for Na, the tail end of the K curve tends to over-predict actual trends. There is no clarity as to where this discrepancy originates.

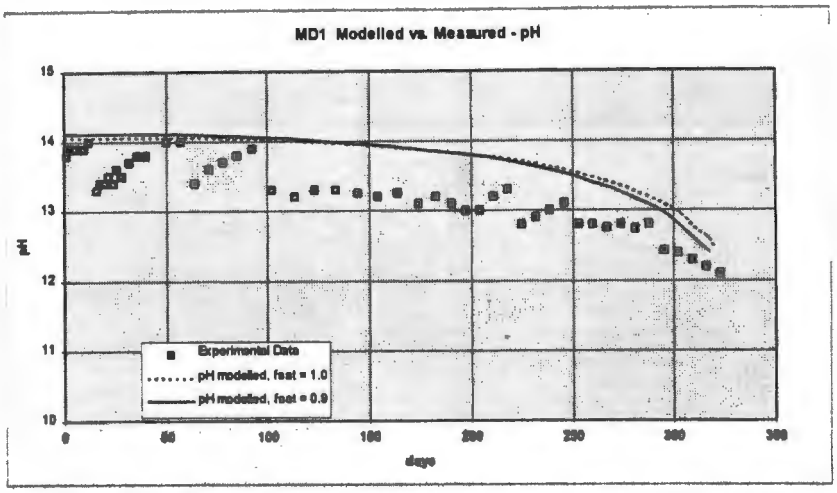

Figure 6-26a: Modelled and measured pH profile in experiment MD1

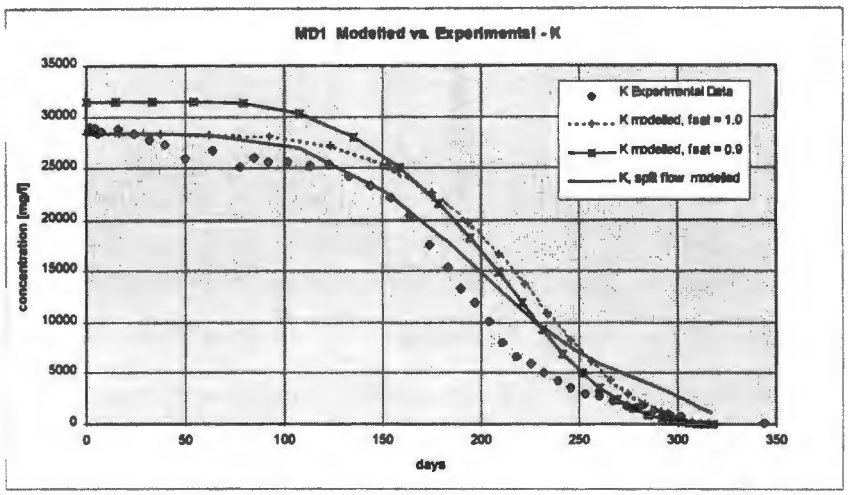

Figure 6-26b: Modelled and measured concentration profiles of K in experiment MD1

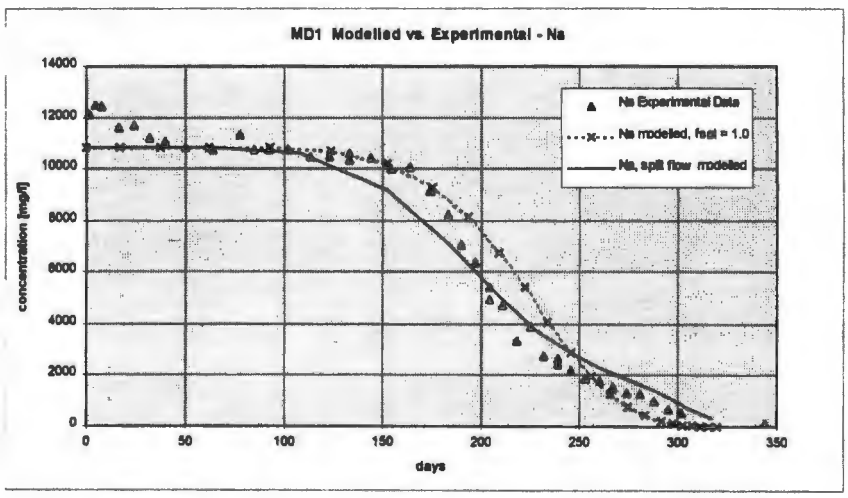

Figure 6-26c: Modelled and measured Concentration profiles of Na in experiment MD1

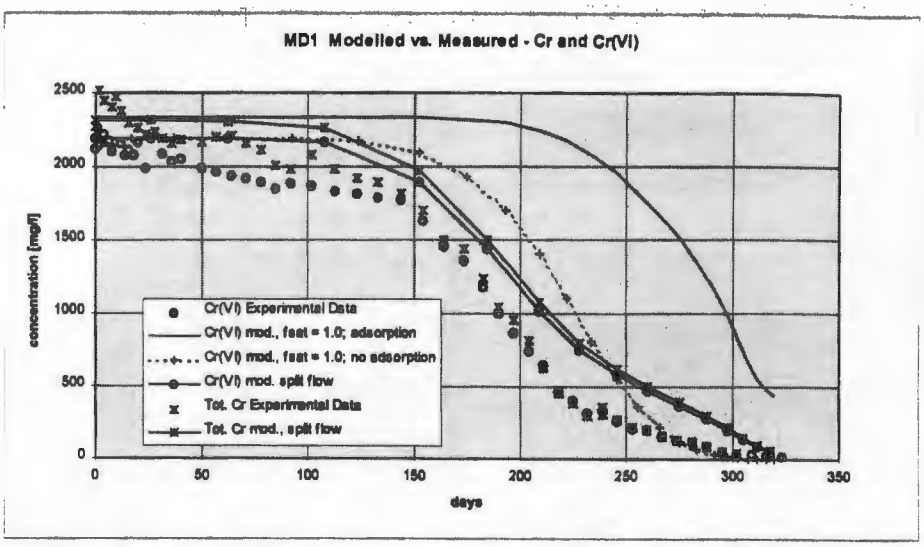

Figure 6-26d: Modelled and Measured concentration profiles of Cr and Cr(VI) in experiment MD1

For the Cr(VI) and total Cr curves (Figure 6-26d) the leach curve was initially modelled using the full reaction matrix as established in Section 6.3.6, i.e. considering Cr(VI) dissolution and adsorption as well as Cr(III) dissolution. However, in this case the modelled curve (for f_{sat}=1.0) and measured data are in good agreement only over the very initial phase. The modelled curve begins to drop off at a much later point in time than the measured data. As the sensitivity study in Section 4.8 has shown, this effect is attributed to the adsorption/desorption of Cr(VI) which essentially acts as a Cr(VI) buffer (Figure 4-27). When Cr(VI) concentrations in the bed begin to drop as the initial concentrations are flushed out of the bed, more is released by desorption and Cr(VI) levels in the effluent begin to drop only once this buffer is exhausted. In the MD1 column experiment this desorption buffering behaviour does not appear to be present, although it was clearly established from the batch experiments (Section 6.3).

For confirmation the Cr(VI) curve was re-modelled with the adsorption/desorption reaction set dormant and the initial dissolution of Cr(VI) manipulated such that initial bed concentrations would correspond to the measured values. This also shown in Figure 6-26d. This curve corresponds much better to the measured data, with the same protraction

of the modelled curve relative to the data, as was observed with Na and K. Quite clearly this would suggest that Cr(VI) desorption does not take place in the bed or, in other words, Cr(VI) adsorption appears irreversible. While this may be plausible and may have been overlooked during adsorption studies (all experiments focused on adsorption, but none on desorption), it would then be surprising to find good agreement between model and data from the stagnant bed leach experiment (Section 6.4). Clarity in this regard can only be obtained from further experimental work. It is, for example, possible that what was perceived as the combination of Cr(VI) dissolution and adsorption, both a strong function of pH, is in reality one single surface-complex reaction (see Section 2.1.3 on Cr surface chemistry).

The Cr(VI) and total Cr curves modelled using the split flow approach (but ignoring desorption) again gives the best fit to the measured data (Figure 6-26d), particularly by emulating the tail end trend quite well, but still over-predicting actual concentrations in this region. It is interesting to note that the initial discrepancy between total Cr and Cr(VI) (assumed to correspond to dissolved Cr(III)) and the later closure of the two curves is captured well by the model.

6.6.2 Modelling Experiment MD2

The WASTESIM computer code has been applied to the data from the accelerated leach experiment MD2 in much the same fashion as has been done with those of experiment MD1. As results were very similar, only the most salient points are discussed in the following. The bed characteristic parameters are given in Table 6.13.

Table 6.13: Bed Characteristic Parameters for Experiment MD2

Bed Area	0.04 m^2
Bed Height	0.27 m
Dry Solid Mass Filled	16.8 kg
Mass Water Filled	6.2 kg
Fractional Bed Porosity	0.64
Fractional Bed Saturation	0.9

Again, the initial saturation factor has been calculated as 0.9, but as flowrates through this system gradually increase (Figure 6-7), similarly to the other MD columns studied, there is reason to believe that the bed gradually reaches full saturation. Thus the data has been modelled for both fractional saturations of 0.9 and 1.0, bed diffusivity was kept at 0.35 as before. The split flow modelling approach, using a split ratio of 2:1, f_{sat}=1.0 and d_{bed}=0.35, has also been attempted. The results of all modelling runs are plotted, together with the experimental data, for K and Cr(VI), respectively, in Figure 6-27a and b.

Similarly to study MD1, the modelled curves for K indicate that a fractional saturation of 0.9 would over-predict the initial concentration (relative to taking it as 1.0) due to the higher solids to liquid ratio, but drop off more rapidly due to the shorter residence time in the bed. For f_{sat}=1.0 the modelled and measured curves correspond well in trend, but concentrations remain slightly over-predicted. The split flow approach again generates the best fit, particularly in terms of capturing the tail end effect observed.

The various modelled leach curves for Cr(VI) (Figure 6-27b) indicate much the same trends as was already observed in the study of the MD1 experiment. Again it is found, that the Cr(VI) adsorption reaction established from the bench-scale experiments is not reversible, but that good agreement between simulated and measured curves is achieved, if only Cr(VI) dissolution is considered. Also, the curve modelled with the split flow approach generates the closest fit, capturing the tail-end of Cr(VI) release better than the one-flow modelling runs.

The results obtained from modelling experiment MD2 are of very similar quality compared to those achieved for MD1. This is an important and encouraging outcome considering that the two experiments were run under significantly different conditions and that all model parameters (in terms of both reaction behaviour and transport phenomena) were obtained from independent studies. The overall assessment methodology, put forward in Section 5.1.2, postulates that the lysimeter studies only be used as a test case for the model parameters established from laboratory experiments.

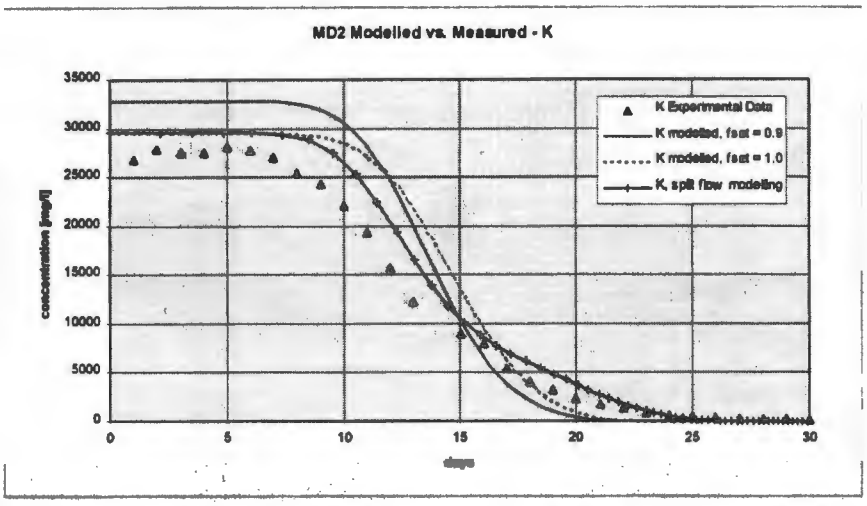

Figure 6-27a: Measured and modelled profiles for K for experiment MD2

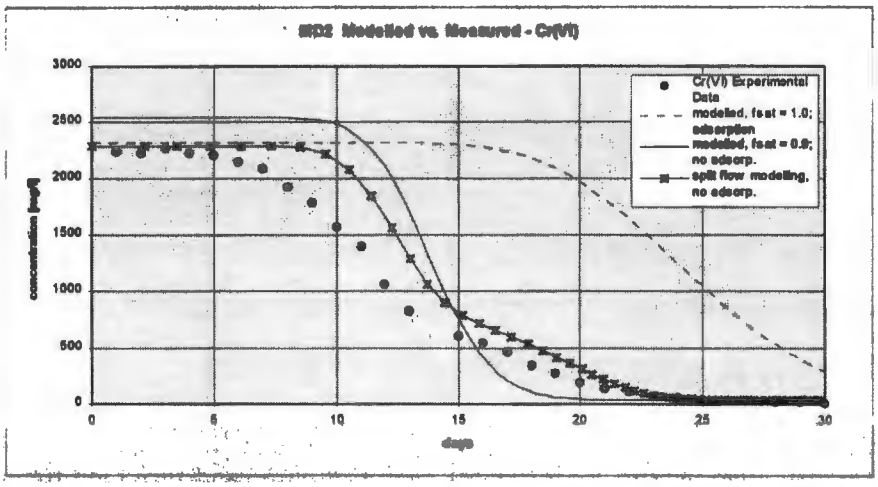

Figure 6-27b: Measured and modelled profiles for Cr(VI) for experiment MD2

If this model test is successful then the parameters obtained can be used with reasonable confidence to model deposit scenarios at a much larger scale. The fact that the model was successfully tested against two test cases, significantly different in scale and operation, is a clear indicator that this approach is valid and that the model is indeed an excellent tool to correlate laboratory scale waste assessment with the behaviour of the material studied in deposit situations.

However, in terms of the behaviour of Cr(VI) it should be acknowledged that in the present study the bench-scale assessment has indicated an adsorption/desorption reaction

mechanism that was not confirmed when tested with the column experiments. Although column modelling was successful when this reaction was ignored, this step nonetheless violates the overall methodology, which postulates that all reaction parameters used in the column model must first be confirmed by independent experiments. Thus more clarity with respect to the Cr(VI) adsorption/desorption must be achieved, before the data could be used to model the behaviour of the MD material in a full scale deposit scenario.

6.7 Closure

This chapter gives detailed account of all experimental and modelling work conducted on one particular waste material from the ferro-alloy industry, an emission control dust termed Metallurgical Dust (MD). The approach taken followed the methodology laid out in Chapter 5..1.2, which aims to collect sufficient information about the leachate generation potential of a waste material through laboratory scale experiments and compare these against test cases obtained through lysimeter studies on the same material, which need to be characterised only in terms of their transport properties.

Two lysimeter tests were conducted to create such test cases and provided the initial feel for the prevailing chemical conditions to inform more detailed batch experiments. As the first test proceeded too slowly, a second column was run under accelerated conditions in order to test whether acceleration would compromise the quality of the leach data obtained.

The material was then subjected to a number of batch leach and Cr(VI) adsorption tests which were carefully interpreted in order to identify a matrix of reactions which characterise the release behaviour independent of scale. As chromium was the species of focus in the present study, only those reactions that are directly or indirectly relevant Cr release were studied. For the MD material Cr(VI) release and adsorption behaviour is

closely linked to solution pH, which in turn is determined by dissolution of the hydroxide salts of Na and K and a $Ca(OH)_2$ buffer. All reactions were taken to be fast and equilibrium controlled, and no evidence for kinetically controlled reactions was found in the batch experiments within the experimental time frame. Likewise, the very small particle size of the material supports the assumptions that intra-particle diffusion effects are negligible.

On the other hand, the small particle size may suggest resistance to diffusion through the interstitial pores in a packed bed situation as these may be small and convoluted. A short-term stagnant bed-diffusion experiment confirmed this suggestion and the effective diffusivity parameter in the bed (d_{bed}) was found to correspond well to the rule-of-thumb value of $\varepsilon/2$.

A column tracer study was conducted in order to identify typical flow patterns through a bed packed with MD material. Results showed a flow behaviour not uncommon in flow through packed beds indicating a distribution of flow velocities and hence residence times though the bed. Using the split flow analysis approach described in Section 5.6, the measured curves could be modelled reasonably closely. Furthermore, model results gave strong indication that the initially unsaturated bed is likely to become saturated as leaching progresses. This coincides with a dramatic increase of the hydraulic conductivity of the bed, which has been observed in all column experiments.

Both lysimeter experiments were modelled using the material specific and bed operational parameters established in the experiments. Agreement between modelled and measured data was generally good for Na and K, but poor for Cr(VI), if adsorption/desorption established from laboratory tests was allowed. Result improved significantly if adsorption was taken as irreversible, which does, however, require further confirmation by independent experiments.

Model predictions employing the split flow method generated the closest fit to measured data, particularly in terms of accounting for tail-end effects, and can therefore be seen as a useful approach to modelling the complex flow behaviour of waste beds.

The overall assessment methodology has been validated by obtaining reasonably good agreement between modelled and measured data for two systems operating at significantly different scales with all material related parameters obtained from independent laboratory studies. It is acknowledged, however, that the adsorption/desorption behaviour of Cr(VI) requires further investigation by independent laboratory experiments, before the assessment the of MD material with respect to its Cr leach potential is completed and the parameters obtained can be applied to model full-scale deposit scenarios.

7

Experimental Study 2: Low Carbon Slag

The experimental methodology employed to characterise waste materials with respect to their potential for leachate generation in a landfill scenario is elaborated in Chapter 5. This methodology was tested with two solid waste materials originating in the ferro-alloy industry. While a pyrometallurgical emission control dust is investigated in the previous Chapter, a smelter slag is the material of focus in this chapter.

Slags arising from smelting and pyrometallurgical reduction processes constitute by far the largest volumes of waste generated in the minerals processing industry (see Section 3.1). As was already indicated in Section 3.3.1 these material usually exhibit a complex mineralogy consisting of amorphous silica-rich glass phases, Al and Mg spinel structures, free CaO and various metallic phases.

One such slag material (in the following referred to as Low Carbon Slag, LCS) is the material of focus in this chapter. This material originates from a ferro-chromium smelter, which forms part of a ferro-alloy process located in the Mpumalanga Province of South Africa. Origin and general characterisation of the sampled LCS material are given in Section 7.1.

The LCS material has been subjected to the full suite of lysimeter column and laboratory experimental studies outlined in Chapter 5. Results from two lysimeter studies are detailed in Section 7.2. A brief outline is given how these helped to identify further laboratory studies required to characterise the leach behaviour of the material more closely, particularly with respect to chromium leaching, which is the focus of the present work.

All batch leach and adsorption studies are detailed in Section 7.3 and the interpretation of the results, including correlation of Cr(VI) adsorption data, is elaborated. Through this analysis a reaction matrix for use in the computer model was established.

Section 7.4 describes the results from experiments conducted to establish the particle level diffusion characteristics of the material. These are analysed, together with the results of a kinetic batch leach experiment, with the help of the computer modelling tool. Results from this analysis give some indication of the likely particle level and bed diffusion characteristics of this material.

A tracer study was conducted on a short lysimeter column, which is detailed in Section 7.5. The tracer response curve was interpreted using the computer algorithm and the split flow analysis as described in Section 5.6. This analysis gives a good indication of the dispersion behaviour likely to occur in flow through beds of this material.

Finally, with all reaction and transport parameters sufficiently characterised from the laboratory experiments, the computer model is applied to simulate the leach curves of the two column studies. Results of this simulation are described and critically discussed in Section 7.6.

7.1 Origin and Characterisation of the Material

The Low Carbon Ferrochrome Slag originates from a submerged arc furnace in which chromite ore is refined to a ferro-chromium product. The slag is quenched in water after pouring from the vessel resulting in a coarsely granular and highly porous material. This is disposed, after dewatering, to landfill or milled for use as agricultural lime for the local farming community owing to the high lime content of the material

LCS appears as grey-blue porous granules nearly spherical in shape. The material is fairly brittle and the larger particles can be crushed between the fingers. Doing so reveals that many of the larger particles are hollow on the inside. It is speculated that this is a result of the formation of bubbles of water vapour when the molten slag is quenched. The particle size distribution (by sieve analysis) of the sample as received is given in Figure 7-1 indicating the bulk of the particles is between 2 and 4 mm in diameter. It was furthermore observed that particles below 2 mm in diameter were mostly debris from broken larger particles and more angular in shape. Figure 7-2a shows an electron micro-graph of an unbroken particle. Clearly visible is a number of pore openings on the otherwise smooth surface. Figure 7-2b shows a micro-graph of the inside surface of a smaller debris particle. This appears almost sponge-like with a large number of crevices and pockets.

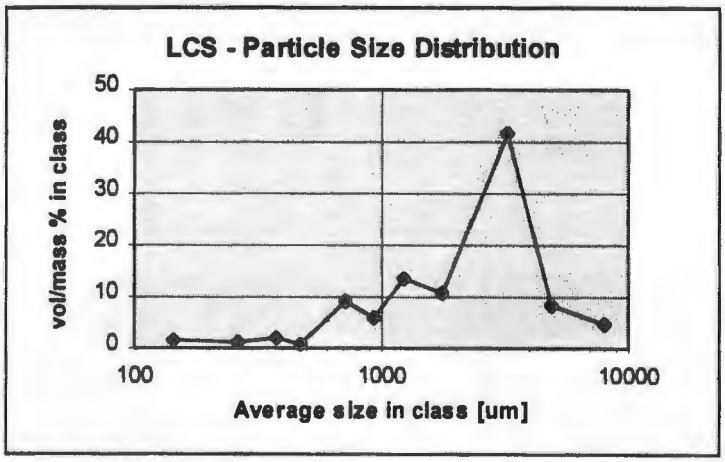

Figure 7-1: Particle size distribution by sieve analysis on LCS material

Table 7.1: Bulk characteristics of LCS material

true density [kg/m^3]	2900
dry bulk density [kg/m^3]	910
dry bulk voidage	0.69
residual moisture [%]	19.7
slurry moisture [%]	n/a
moist bulk density [kg/m^3]	1000
moist bulk voidage	0.72
BET surface area [m^2/g]	9.35

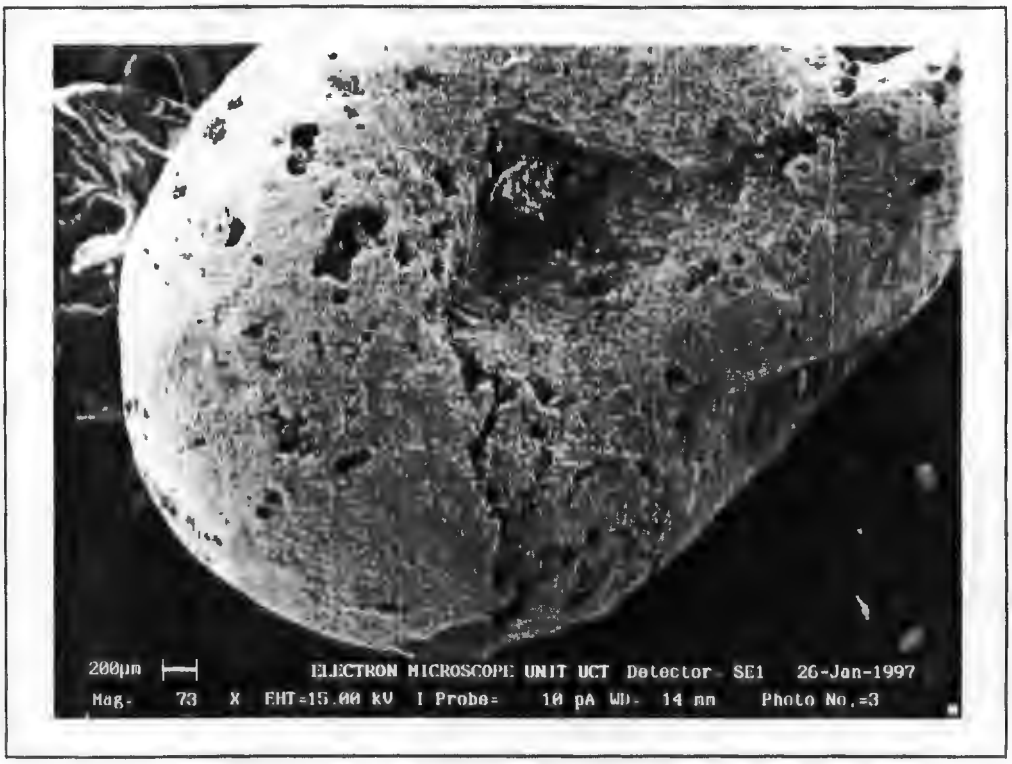

Figure 7-2a: Typical unbroken LCS particle, note the smooth surface with pore openings

Figure 7-2b: Debris LCS particle, note the sponge-like appearance

Bulk characterisation of the LCS sample is given in Table 7.1. The relatively low true solid density is indicative of a lower content of heavy metals when compared to the Metallurgical Dust (Section 6.1). The low settled bulk density (and hence high bulk porosity) results from both the poor packing achieved between the relatively equisized particles and the high internal particle porosity. This was established separately by carefully weighing out a counted number of particles in the 2-4 mm size class (Table 7.2). The value is only approximate, since the variance between the individual measurement was large and the exact average particle diameter could only be estimated. This was done by assuming that particle volumes (and hence masses) were evenly distributed over the range and that the volume averaged diameter was representative of the average particle diameter. BET surface analysis shows a high specific surface area, which is not surprising considering the high porosity of the material.

Table 7.2: Establishment of LCS particle porosity

averg. mass 100 parts.*	averg. part. diameter.**	vol. of 100 particles	mass of 100 solid parts.	voidage
[g]	[mm]	[l]	[g]	
2.223	3.2	0.00172	4.987	0.554

* average of 10 batches of exactly 100 particles
** volume average diameter, assuming continuous distribution over range

The elementary analysis of LCS established by fusion digest is given in Table 7.3. It should be noted that Na is absent from this table due to its presence in the sodium peroxide reagent, but its concentration is assumed to be in a similar region to that of K at about 0.1% by mass. The analysis shows that LCS is composed mainly of the alkali earths Ca and Mg. If these are assumed to be present in their oxide form, CaO and MgO would account for over 80% of the total LCS mass. The other metals account for only 2.65% (about 4% if assumed as their common oxides) of the total mass, leaving about 15% unaccounted for. This is assumed to be made up by alumina-silicates, which were not analysed for, but are common components in slag materials.

Table 7.3: Elementary analysis of LCS*

Fe	0.17	Pb	<0.01
Cr	1.89	Ti	0.40
Mn	0.07	Cu	<0.01
Ni	0.04	Sn	<0.01
Mo	<0.01	V	<0.01
Ca	47.4	Ag	0.0005
Mg	9.61	Cd	<0.0001
K	0.080	Hg	n/a
Zn	<0.01		

*all values in percent

Figure 7-3 shows that the acid neutralisation capacity of the LCS is high, which is understandable considering its high lime content. In fact a continuous acid leach at pH 3 resulted in the near complete dissolution of the entire LCS sample. It is this high lime content which justifies the use of the material as agricultural lime. The lime content is also the primary reason for the high solution pH if LCS is slurried 1:20 with distilled water.

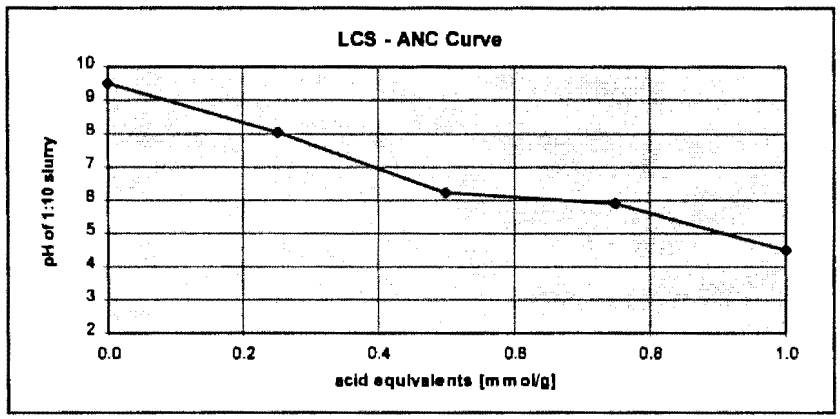

Figure 7-3: ANC curve for LCS material

Results from water wash and TCLP for LCS are given in Table 7.4. There appears to be a small, directly soluble fraction of Na and K, which is similar in both leaches. Metal dissolution in the water wash is restricted to Cr and Fe, with all other metals assayed dissolving at concentrations below detection. It is important to note that most Cr dissolves as Cr(VI) at concentrations which are high considering that this material is used as agricultural lime.

Table 7.4: Water wash and TCLP results on LCS material

	Water Wash		TCLP	
Element	mg/l	mg/g_{dust}	mg/l	mg/g_{dust}
Na	13.6	0.27	15.8	0.32
K	6.64	0.13	6.43	0.13
Ca	23.7	0.47	1050	21
Mg	0.95	0.0190	311	6.2
Cr_{tot}	0.32	0.0064	6.29	0.13
Cr(VI)	0.31	0.0062	0.95	0.0190
Fe	0.04	0.0008	0.27	0.0054
pH	11.4		5.7	

Acid leaching affects mainly the dissolution of Ca and Mg - to be expected considering their high concentrations in the material. Also the dissolution of Cr increases significantly, but the fraction of total Cr which is Cr(VI) becomes much smaller when compared to the water wash, indicating that most Cr liberated by the acid would be Cr(III). Considering the ready solubility of Cr(VI), it is surprising to find that a significantly higher amount is released through the acid leach, suggesting that some Cr(VI) is locked in the particle matrix and only liberated under more aggressive leach conditions. The leaching of other metals, including Fe, is not affected significantly by acid leaching owing to their low concentration in the slag.

The relatively high final pH at the end of the TCLP leach again suggests that this test is essentially unsuitable for the LCS due to its high acid neutralisation capacity.

7.2 Lysimeter Studies

Two lysimeter studies were conducted with the LCS material as indicated in Table 7.5. Both experiments, labelled LCS1 and LCS2, were conducted in the open type Percolator Lysimeters as described in Section 5.3. In order to simulate conditions likely to occur in full scale waste deposits, the daily feed flow rate was kept deliberately low at around 200

ml/day (target flow rate). Under these conditions the bed matrix is only partially saturated as was observed through the glass walls of the lysimeter, with the interstitial spaces between particles largely occupied by air. As the low flow rates employed result in extended fluid residence times in the long bed of experiment LCS1, a second experiment was conducted in a much shorter bed but under otherwise similar conditions. This was to be used as a second test case for the assessment methodology as lined out in Chapter 5 and also to identify how an experiment accelerated in this way would compare to a more long-term scenario.

Table 7.5: Experimental Parameters of Lysimeter Column Studies on LCS

Material(Code)	Lysimeter	Bed Height [mm]	Daily Flowrate [ml]	Hydraulic Head	Duration [days]
LCS (LCS1)	PL	1740	181	--	160
LCS (LCS2)	PL	500	200	--	45

7.2.1 Experiment LCS1

All bed and flow specific information on experiment LCS1 is given in Table 7.6. The lysimeter column of the experiment was charged with a total mass of about 70 kg of the moist (17% by mass) LCS material by carefully sprinkling subdivided charges over the cross-section of the bed to a height of 1740 mm above the base plate. After leaving to settle for about a week, which resulted in no visible changes in the bed, the bed was sprinkled with daily charges of around 181 ml of the "acid rain" mixture, applied over four 2 hour intervals within a 24 hour period. This intermittent supply of feed solution appeared to be effectively buffered within the column since the effluent flowrate at the bottom of the bed was continuous and relatively constant throughout the day.

Table 7.6: Bed Flow and Packing Information for LCS1

dry solid mass filled	58.5 kg
moisture water filled	12.0 kg
fill height	1.74 m
total bed volume	69.2 l
water hold-up after breakthrough	16.8 l
bed porosity excl. particle pores	35.2 %
bed porosity incl.. particle pores	70.5 %
bed saturation	34.4 %
average feed flow rate	181 ml/d
average effluent flow rate	141 ml/d
average recovery	78 %
average residence time	120 d

The consumption of feed liquid as well as the recovery at the bottom of the bed were monitored carefully and are given in Figure 7-4. The feed curve is essentially a straight line with the slope of around 185 ml/day, which corresponds to the average daily feed. The two little steps at days 104 and 143 relate to pump stoppage as a consequence of power failure. The recovery curve starts after 26 days, which corresponds to the saturation period of the bed, i.e. the time it takes to saturate pore spaces sufficiently to allow continuous flow through the bed. At this point the total liquid volume held up in the bed was calculated as 16.8 l, which corresponds to approximately 34% saturation of all available pore space in the bed (as made up by particle and interstitial pores).

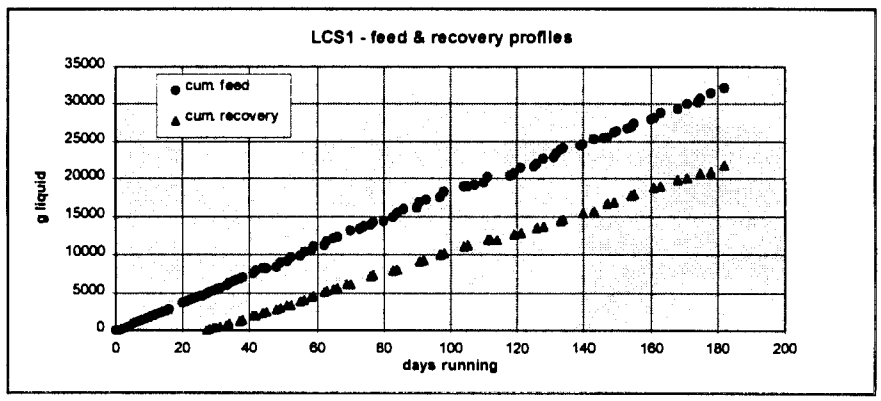

Figure 7-4: Cumulative feed and recovery profiles in experiment LCS1

It must be pointed out that the saturation period is not the same as the bed residence time, since a large portion of liquid was already present in the bed at the beginning of feed supply and no information is available, as to how much of the fluid held up in the bed is actually mobile.

The recovery curve is also a fairly straight line, but shows a flatter slope than the feed curve, which indicates that some fluid (in the order of 22%) is continuously lost on the passage through the bed, either by chemical uptake (unlikely considering the amounts) or through evaporation into the unsaturated pore spaces. A small inflection in the recovery curve can be found around day 112, which is likely to be in response to the pump failure on day 104 mentioned above, and could be taken as an indication that fluid residence time is in the order of 8 days.

The development of effluent concentrations for pH, total Cr and Cr(VI) and Na, K as well as Ca are given in Figure 7-5 a-c. All curves are plotted against time since the day of breakthrough, which corresponds to the day the first drop of effluent appeared at the bottom of the bed (day 26). No other metals of significant concentrations were found in the effluent. The pH profile (Figure 7-5a) shows an initial plateau around pH 9 for the first 40 days, whereafter it gradually increases over the next 60 days. After day 100 the pH levels remain relatively constant between pH 10 and 10.5 for the rest of the experiment.

The leach curves for total Cr and Cr(VI) identically show a concentration plateau around 13 mg/l for the first 40 days since breakthrough, whereafter they very gradually drop to a lower level around 4 mg/l where they remain constant after 140 days. Total Cr levels appear to be about 10% higher than Cr(VI) levels for the first 100 days before the gap closes towards the end. This is somewhat surprising considering the extremely limited solubility of Cr(III) at the pH levels encountered.

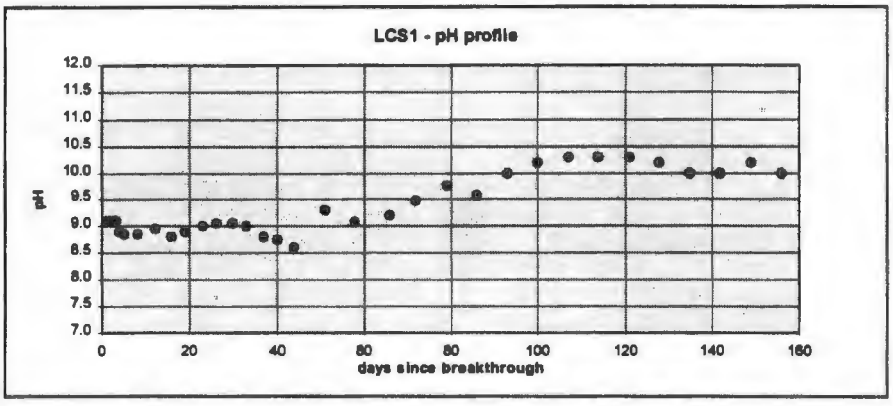

Figure 7-5a: pH profile in effluent of experiment LCS1

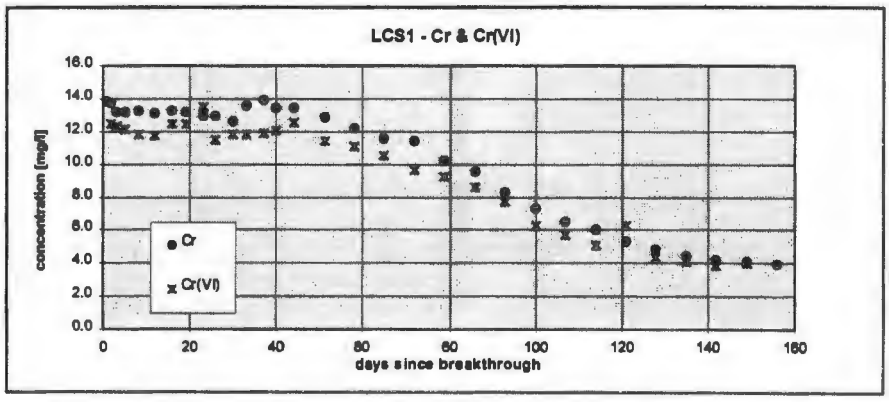

Figure 7-5b: Concentration profile of Cr and Cr(VI) in effluent of LCS1

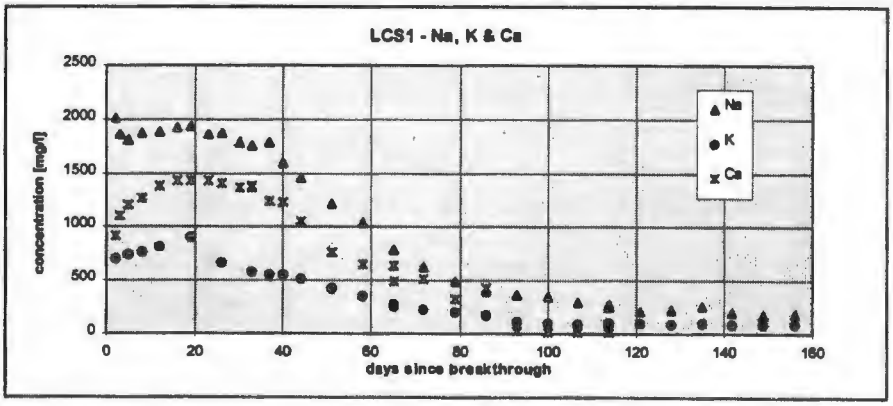

Figure 7-5c: Concentration profile of Na, K and Ca in effluent of LCS1

The leach curves for the alkalis Na, K and Ca all show similar leach profiles with a small initial rise, reaching a peak after 20 days, then dropping to a lower level over the next 60 days. After 80 days Na continues to drop gradually from 400 to just under 200 mg/l, which is still about 10 % of the initial concentration. K concentrations become virtually constant at around 100 mg/l after 80 days and Ca concentrations become altogether negligible.

Conceptually the leach profiles for the granular LCS material look similar to those obtained from the saturated percolator units (as used for the MD material, Chapter 6) with high initial levels dropping off to lower residual levels. This indicates both a higher degree of dispersion in the LCS bed as well as time-dependent release due to intra-particle diffusion. It is also interesting to note that extent and duration of the drop phases of the various concentration curves vary, but that they all appear to start around day 40 after breakthrough. It is not quite clear what the significance of this day is, since it does not seem to correspond to a flushing out of the fluid volume held up in the bed as was noted for the dust experiments. This aspect will have be clarified from modelling the column leach scenario, which is discussed in Section 7.6.

7.2.2 Experiment LCS2

The long duration (6 months) of the experiment LCS1 in the long column gave reason to attempt a lysimeter study on the same material in a much shorter column to obtain results under accelerated conditions. It was decided, however, to maintain the feed flow rate at the same level as before in order to avoid undue dilution of dissolving concentrations in the higher fluid volumes passing through the bed and to maintain similar conditions of bed saturation for better comparison.

In experiment LCS2 a short column was packed with the moist LCS material in the same fashion as in LCS1 to a height of 50 cm and again left to settle for one week before

sprinkling with leach liquor started. All bed and flow characteristic information for experiment LCS2 is given in Table 7.7. Feed flowrate of the "acid rain" mixture was on average around 210 ml/day. The experiment continued for a period of 45 days.

Table 7.7: Bed Flow and Packing Information for LCS2

dry solid mass filled	17.0 kg
moisture water filled	3.0 kg
fill height	0.5 m
total bed volume	19.9 l
water hold-up after breakthrough	4.2 l
bed porosity excl. particle pores	34.4 %
bed porosity incl.. particle pores	70.5 %
bed saturation	30 %
average feed flow rate	210 ml/d
average effluent flow rate	175 ml/d
average recovery	83 %
average residence time	24 d

Consumption of feed liquor as well as recovery at the bottom of the bed were recorded and are given in Figure 7-6. As observed in experiment LCS1, both represent straight lines with the slopes indicating the feed and recovery flow rates. Breakthrough, i.e. the first drop of effluent at the bottom of the bed, occurred after 6 days, whereafter the flow was continuous at a relatively constant rate throughout the day, unaffected by the interval nature of the feed. The volume of fluid held up in the bed at this point was calculated as 4.2 litres, which corresponds to about 30% saturation of all available pore space in the bed and is thus somewhat lower as the saturation achieved in experiment LCS1.

The slope of the recovery curve is flatter than that of the feed curve, again indicating a loss to evaporation in the order of 17%. Considering that this is in the same order of magnitude as in experiment LCS1 despite much shorter residence times in the bed, could be an indication that evaporation mainly occurs near the open top end of the bed which is likely to be well aerated.

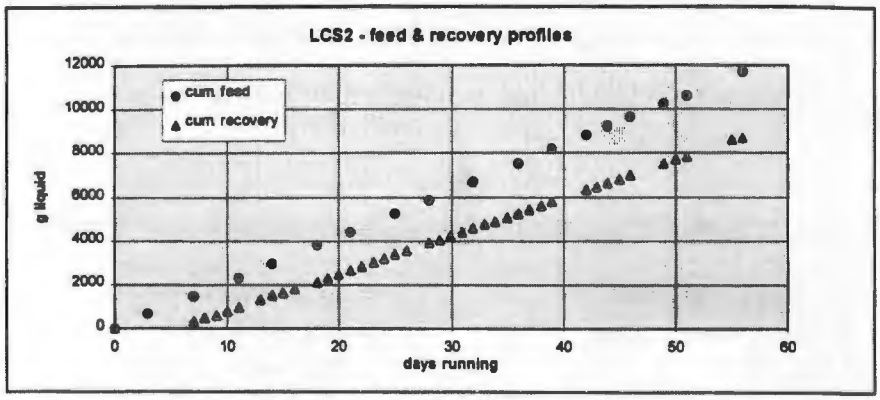

Figure 7-6: Cumulative feed and recovery profiles in experiment LCS2

Effluent leach profiles are given for pH, total Cr and Cr(VI) as well as Na, K and Ca in Figure 7-7 a-c. The pH curve shows a development similar to that in experiment LCS1, but seemingly "shifted" by one pH step, starting with a plateau around pH 10, then increasing to between 11 and 11.5 where it would settle. The reason for this shift is not obvious and needs to be discussed in the light of the discussion of chemical reaction behaviour of the LCS material, given in Section 7.3.

The Cr leach curves (Figure 7-7 b) both show a gradual increase to a maximum around 14 mg/l, before dropping off and settling at a residual level at 4 mg/l. The significantly higher total Cr reading (20%) over the first 15 days would confirm a trend already observed in experiment LCS1, but the sudden drop to the same levels as the Cr(VI) thereafter may give rise to the suspicion that analytical error was present, since Cr(III) dissolution should remain insignificant, even at the slightly higher pH levels observed in this experiment. Although the Cr curves appear differently to those observed in experiment LCS1, it is interesting to note that the peak and residual concentration are identical at just under 14 mg/l and 4 mg/l respectively. The gradual initial increase indicates a kinetically controlled release from the solid. In the long column this effect could be potentially masked by the longer fluid residence time in the bed, so that Cr(VI) peak concentrations are already reached before the first fluid leaves the bed.

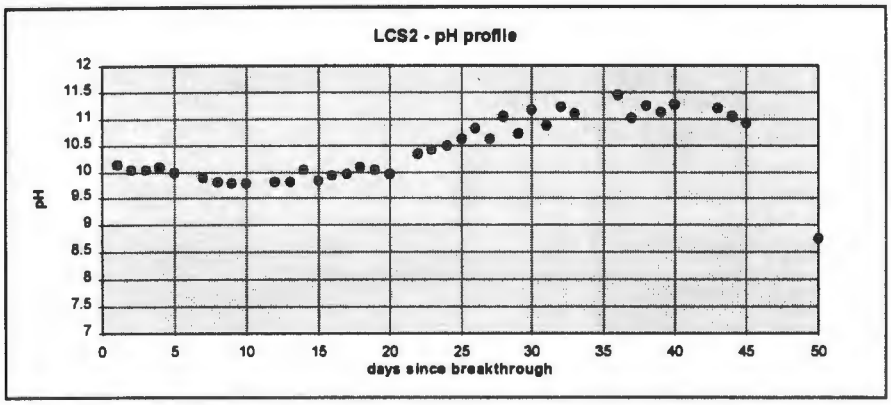

Figure 7-7a: pH profile in effluent of experiment LCS2

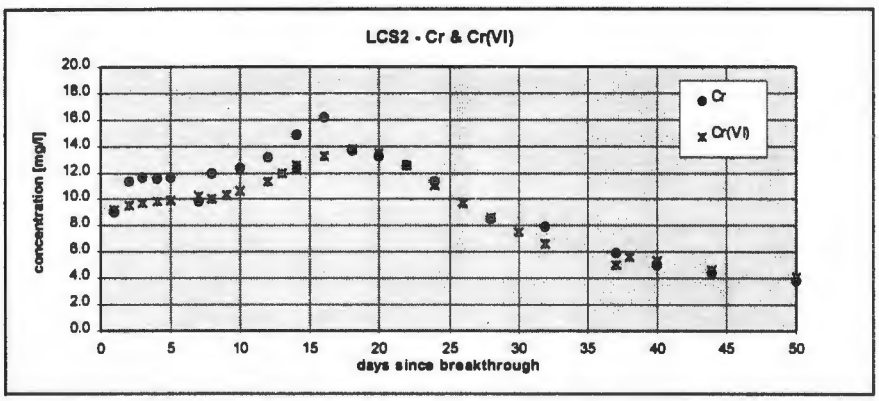

Figure 7-7b: Concentration profile of Cr and Cr(VI) in effluent of LCS2

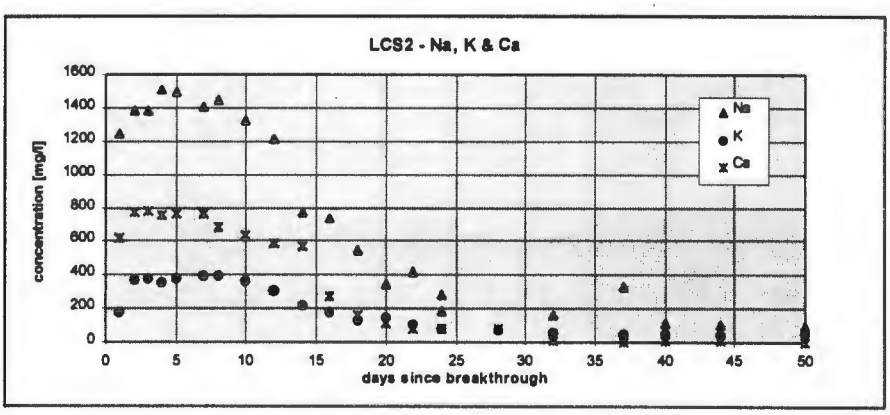

Figure 7-7c: Concentration profile of Na, K and Ca in effluent of LCS2

The alkali leach curves for experiment LCS2 (Figure 7-7 c) are all very similar in shape and relative proportion to those obtained in experiment LCS1, apart from a more pronounced initial rise for all three metals over the first few days. All curves reach a peak level after 5 days and then drop off to low residual levels over the next 20 days. The peak level concentrations, however, are somewhat lower than those observed in the long column. Again the residual Ca levels suddenly drop to values near zero towards the end of the experiment.

A more in-depth comparison between the two LCS experiments, particularly in terms of the different bed dimensions and consequently leach time scales is given in Sections 7.5 and 7.6.

7.2.3 Summary

Both lysimeter studies show comparable leach behaviour with respect to the main constituents found in the effluent. In both experiments the pH levels remained at a plateau before gradually increasing by about 1 pH unit towards the end of the experiment. The pH curve obtained from the shorter column (pH 10 to 11) was, however, one pH unit higher than that obtained from the longer column. The reasons for this phenomenon need further clarification.

The only species to dissolve in significant quantities in either experiment were Na, K, Ca and chromium, mostly in the form of Cr(VI). While the leach curves of the alkalis all show similar trends with short-term initial increases followed a relatively rapid fall-off, the Cr(VI) curves from both experiments appears more protracted and - at least in the case of experiment LCS2 - a clear gradual increase followed by a gradual decrease. Peculiar to all leach curves is the residual levels still present in the effluent at the end of the experiment with no or very little tendency to decrease with time.

Further characterisation of the LCS material should therefore focus mainly on the release mechanisms of Cr(VI), which appear to be an interaction of several mechanisms, such as slow kinetic release and retardation by adsorption at the moderate pH levels observed in the experiment. Although the discrepancy of the pH curves between the two experiments requires further study, it still needs to be seen to what extend this interferes with the release behaviour of chromium species, on which the work is focused here.

The characterisation of transport behaviour of fluid flow through an unsaturated matrix of highly porous granular material, such as distributions of flow across the bed and diffusion in and out of particle pores, remains a challenge. An extremely careful investigation is required in order to allow meaningful modelling of leachate generation within these.

7.3 Batch Experiments

In line with the experimental methodology outlined in Chapter 5, the preliminary findings from the column studies should give a good first indication of chemical conditions prevailing in a bed situation. Small scale experiments should thus focus on characterising the behaviour of individual species further by clearly targeted experiments. All batch leach experiments conducted on the LCS material are described in Sections 7.3.1.to 7.3.4, Cr(VI) adsorption studies are described in Section 7.3.5 and an isotherm is quantified from the available data. The information gathered from all experimentation thus far is reviewed in Section 7.3.6 and the reaction scheme considered for further modelling is formulated and tested in a number of scenarios.

7.3.1 Acid and TCLP Leaches

Although the LCS lysimeter experiments indicated very high solution pH values in the pore solution, it was nonetheless decided to test the material in an acid leach environment. As indicated in Section 5.4, information from such acid leach tests may be useful for gathering evidence on whether certain reaction are pH controlled or not.

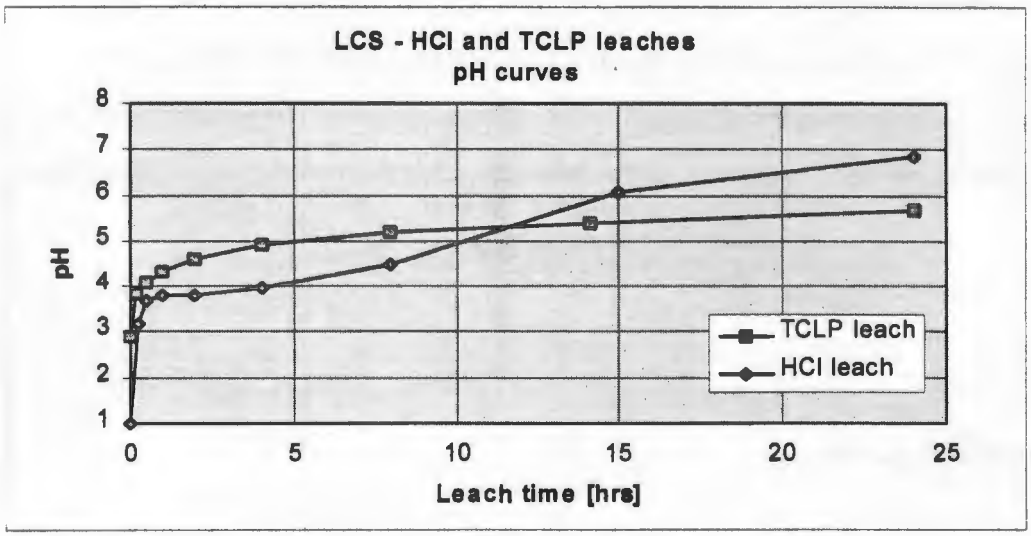

Figure 7-8: pH curves for HCl and TCLP leaches on LCS material

A 24 hr leach was conducted in each, 0.1 M HCl and the TCLP acetic acid buffer. The pH curves for both these leaches is given in Figure 7-8. As can be seen the LCS material showed somewhat differing behaviour. In the HCl leach the pH level jumps to pH 3.9 and remains there before later gradually increasing to just under pH 7. This behaviour could suggest a two phase reaction mechanism, with fast initial leaching and a secondary, much slower leach reaction. The TCLP pH curve shows the normal kinetic development, but levelling at pH values below 6.

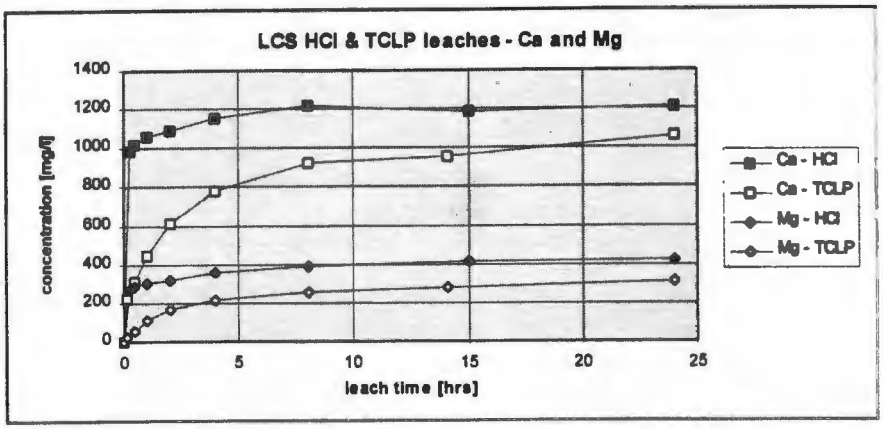

Figure 7-9: Ca and Mg leach curves from HCl and TCLP leaches for LCS material

The leach curves for Ca and Mg for both experiments, which are the major species going into solution, are jointly shown in Figure 7-9. The HCl curves show an initial jump for both species in similar concentrations to those achieved only towards the end of the TCLP run (around 1000 mg/l for Ca and 300 mg/l for Mg). After this initial jump, which must be explained by rapid acid leaching, the curves increase only very gradually, which is in line with the pH curve observed.

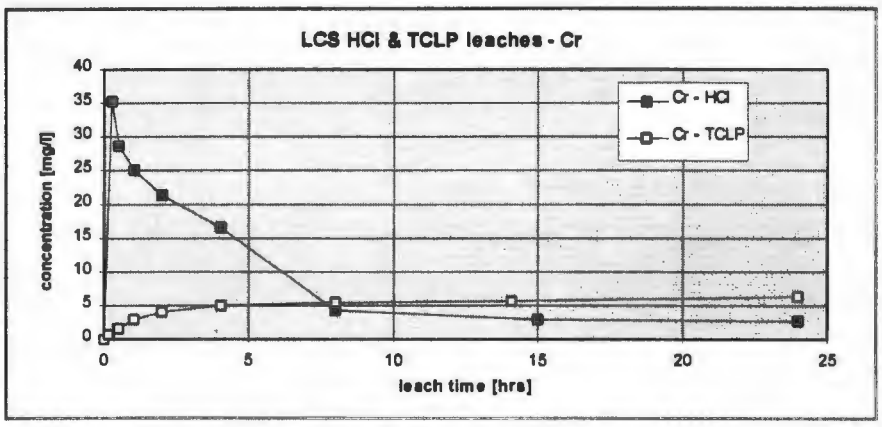

Figure 7-10a: Cr leach profiles in LCS HCl and TCLP leaches

The leach curves for total Cr and Cr(VI) for both experiments are given in Figure 7-10 a and b. Here the behaviour in the two experiments is quite different. In the HCl experiment the total Cr level jumps to an initially high level at 35 mg/l from where it then drops again to a final level of only 3 mg/l. This can be explained by rapid initial acid leaching with a

subsequent drop due to re-precipitation (presumably as $Cr(OH)_3$) as the pH increases in the experiment. The Cr(VI) concentration remains small with an initial jump to 2.5 mg/l from where it increases only very marginally.

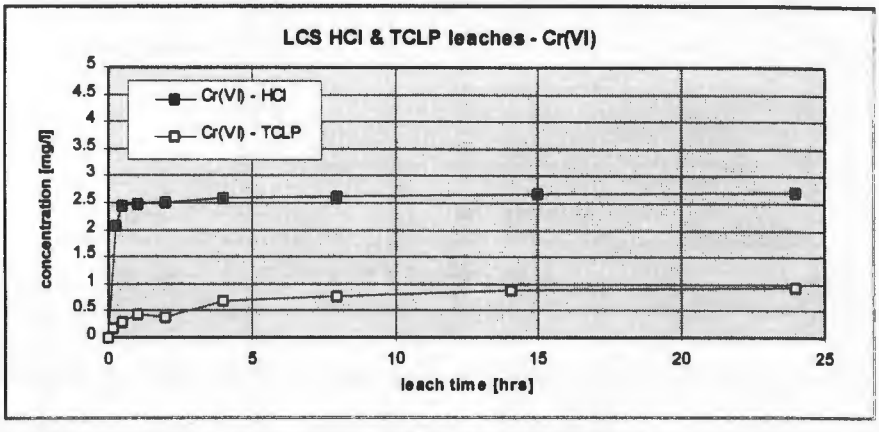

Figure 7-10b: Cr(VI) leach profiles in LCS HCl and TCLP leaches

In the TCLP experiment the total Cr curve develops in a normal first order fashion (Figure 7-10a) reaching a final level around 6 mg/l. Here, the Cr(VI) concentration remains below 1 mg/l at all times. The rapid Cr leach as observed in the HCl experiment is not encountered since the pH conditions are not as aggressive in the TCLP leach (initial pH at 2.9 as compared to 1). It is not quite clear, however, why the Cr(VI) levels remain smaller in this experiment.

Other than Ca, Mg and Cr, only Na and K leached from the LCS material in significant concentrations (in both experiments at around 35 mg/l and 8 mg/l respectively). Other metal species detected in the leachates were at concentrations well below 1 mg/l.

7.3.2 Water Wash

Although the prevailing pH in the LCS column studies was in the alkaline region, it was decided to test the leach behaviour in a wash in distilled water as it was expected some release reaction would drive the alkalinity into similar regions as those observed in the column.

The pH profile for this experiment is given in Figure 7-11. As can be seen, pH levels immediately jump to around pH 10, from where they continuously increase to around pH 11.4 over the duration of the experiment. This appears to be a clear indication of a kinetic process taking place.

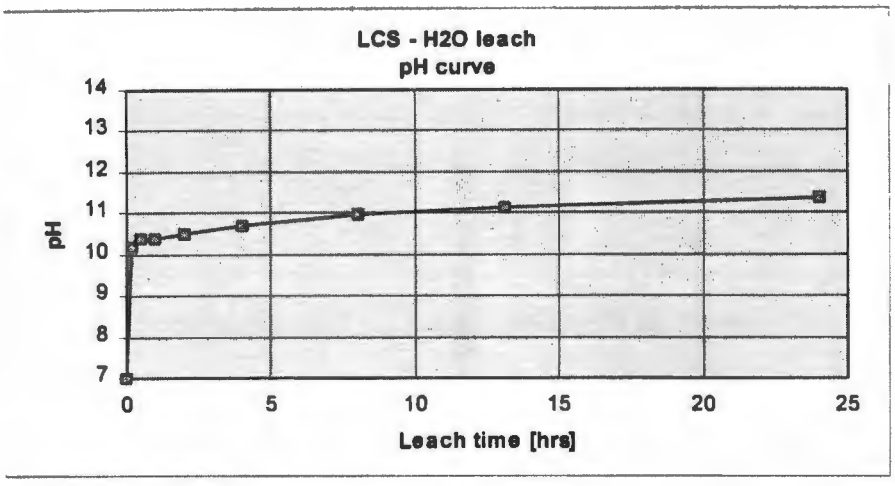

Figure 7-11: pH profile of H_2O leach on LCS

The leach curves of metal species dissolved in the LCS water wash are given in Figure 7-12 and b. Only Na, K and Ca dissolved at appreciable concentrations, whereas Mg, total Cr and Cr(VI) remained at concentrations below 1 mg/l. No other metal species were detected in the leachate.

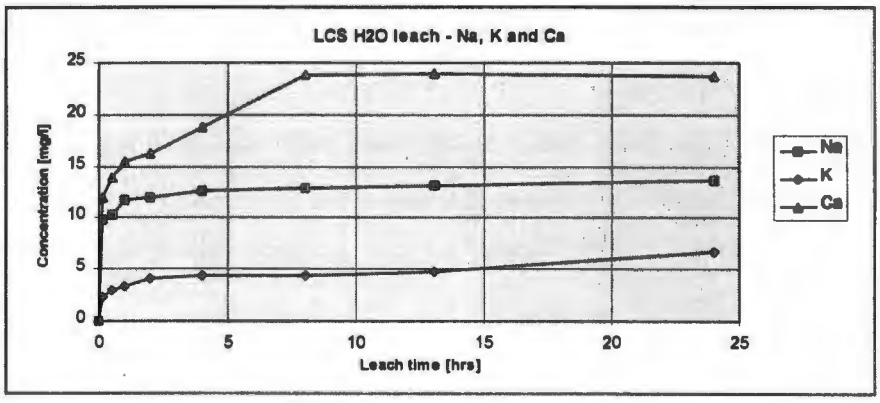

Figure 7-12a: Leach profile of Na, K and Ca in H_2O leach on LCS material

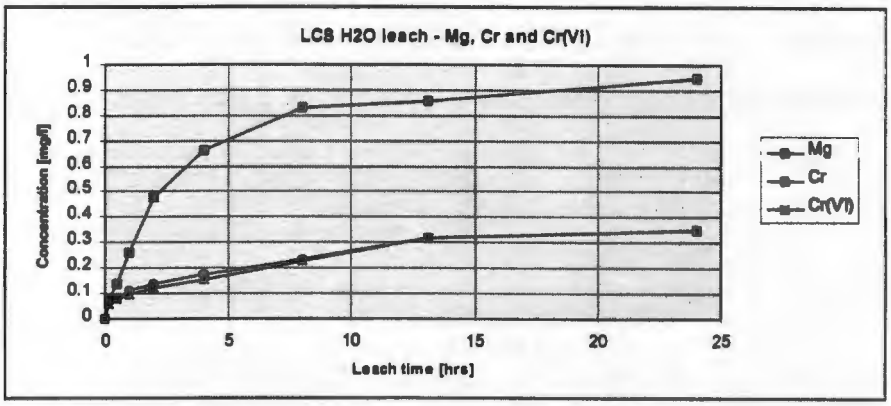

Figure 7-12b: Leach profile of Mg, Cr and Cr(VI) in H_2O leach on LCS material

The leach curves of all species show time a dependent release behaviour over the first few hours, which can be taken as an indication that diffusion through the particle pores has an influence on leach kinetics. While the leach curves for Na, K and Ca settle at final concentrations after the first 6 hours of leaching, those of Mg, Cr and Cr(VI) rise more gradually and do not settle on final concentrations after 24 hours. This scenario compares well to that simulated for the hypothetical base case in the model evaluation in Section 4.8.3, especially as shown in Figure 4-23, and can therefore be taken as an indication that the release of Na, K and Ca is instant dissolution, controlled by pore diffusion, while the release of Cr and Mg is controlled by a kinetic reaction mechanism.

The levels of Na and K are comparable (although slightly lower) to those achieved in the acid leaches, indicating that these are likely to originate from the dissolution of salts, possibly hydroxides, independent of pH. The low Ca and Mg levels can again be explained by the limited solubility of Ca compounds which dissolve much better under acid attack. With respect to Cr(VI) leaching a small initial offset in the order of 0.1 mg/l is noted. This is attributed to a small degree of instant dissolution from the surface as opposed to the slower kinetically controlled release described above.

7.3.3 Alkali Leaches

The leach curves of a LCS leach in 0.1 M NaOH (nominal, pH 12.8, which stayed constant throughout) are given in Figure 7-13a and b. Note that concentrations of Na are not reported due to its presence in the leach liquor.

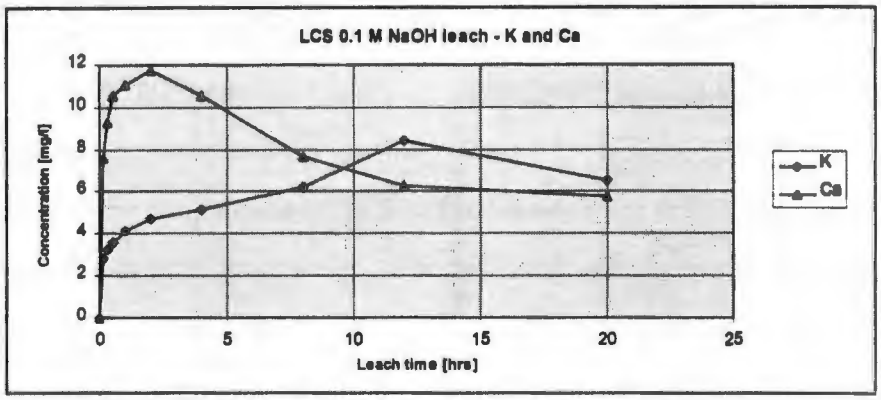

Figure 7-13a: Leach profile of K and Ca in alkali leach on LCS material

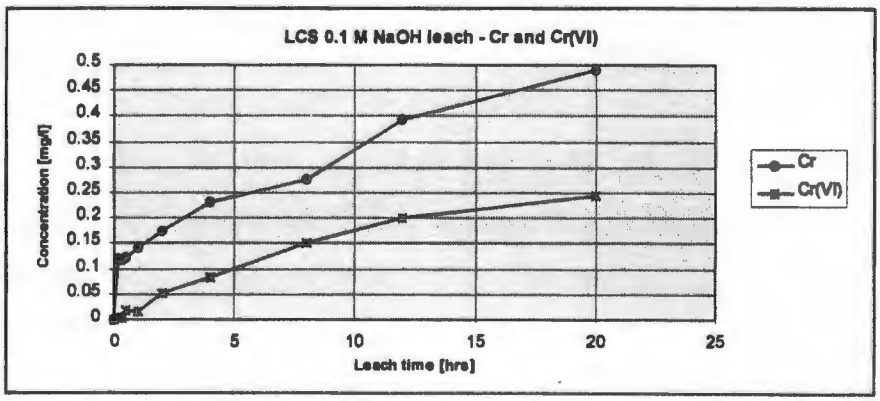

Figure 7-13b:Leach profile of Cr and Cr(VI) in alkali leach on LCS material

While the release of K is in a similar order of magnitude to that observed in the water wash, the leach curve of Ca shows a significantly different behaviour. Concentration levels initially rise to a peak of about 12 mg/l. This level corresponds in order of magnitude to that observed in the water wash in the same leach period (see Figure 7-12a), but where concentrations further increase in the water wash, they gradually drop back to a level around 6 mg/l in the alkali leach. This behaviour could be attributed to re-

precipitation of Ca as hydroxides due to the high pH levels introduced by the leachant. It is not quite clear, why the initial dissolution takes place irrespective of the high pH, which is present from the beginning of the experiment, but could be attributed to the kinetics of the precipitation process.

The leach curves of total Cr and Cr(VI) show similar behaviour to that observed in the water wash, but the discrepancy between the two curves indicates that a certain amount of additional Cr(III) goes into solution, probably as a result of increased Cr(III) solubility at high pH (Section 2.1.2), whereas the Cr(VI) release remains more or less unchanged. Again it becomes clear that the kinetics of the Cr(VI) release are relatively slow and release has not reached completion at the end of the experiment, further substantiating the speculation that Cr(VI) release is governed by reaction kinetic effects..

7.3.4 LCS Long-term Leach

The various batch leach experiments conducted with the LCS material indicate that the release of Cr(VI) is controlled by reaction kinetic effects and Cr(VI) release has not reached completion within the 24 hour experiments. Also, the Cr(VI) concentrations measured in the effluent from the LCS column studies (see Section 7.2) suggest that much higher amounts of Cr(VI) are removed from the material than the short-term batch leach experiments would suggest.

It was decided to investigate the Cr(VI) release from the LCS material over an extended leach period. The experimental conditions were essentially the same as in the water wash with the material washed at 1:10 S:L in distilled water in the tumbling bottle device over a 7 day period. Samples were taken twice daily and analysed for Cr(VI). One repeat run was conducted for comparison of reproducibility.

The Cr(VI) leach curves for these long-term water washes are given in Figure 7-14. As can be seen, Cr(VI) does indeed leach only very slowly from the material with very good reproducibility between the two runs. Although the curves level off after about 4 days, the release reaction does not appear to have reached a final value even as long as 7 days of continuous leaching.

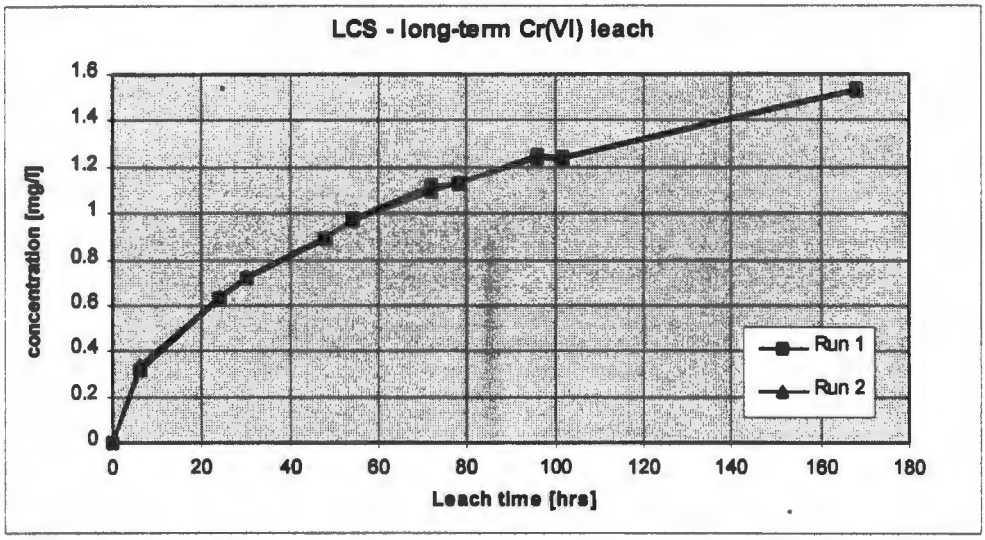

Figure 7-14: Leach profile of Cr(VI) in long-term H_2O leach on LCS material

It should be remarked, that the experiment was not conducted for a longer period due to attrition of the particles exposed to the continuous tumbling of the relatively brittle material. Therefore, although the leach curves indicate a clear trend, the results should be treated with some care as they may be a direct consequence of particle attrition and consequently the higher solid surface area exposed to leaching.

Nonetheless, the results of this experiment show clearly that for this material the release of Cr(VI) is indeed controlled by a kinetically much slower mechanism which would go unnoticed in the standard 24 hr leach experiments. This could possibly be related to matrix diffusion effects, i.e. Cr(VI) is not present as discrete inclusions at the surface of the particle pores, but is present within the solid matrix of the particle and can therefore migrate to the particle surfaces (internal and external) only very slowly. This is discussed in more detail in Section 7.4.

7.3.5 Cr(VI) Extraction Leach

As the release of Cr(VI) appears to play an important role in the leach behaviour of the LCS material, it was considered useful to quantify the total amount of Cr(VI) releasable from the material by the caustic leach method described in Section 5.4. The LCS material was tested as the original mix of different size particles as well as for the 2-4 mm and <500 micron size fractions, the results are presented in Table 7.8.

Table 7.8: LCS Cr(VI) Alkali Extraction Leaches*

	LCS Cr(VI) concentration in leach solution [mg/l]		
Leach No.	mix	2-4 mm	< 500 μm
1	0.75	0.78	3.30
2	0.50	0.59	2.14
3	0.81	0.89	2.39
4	0.41	0.47	1.26
total Cr(VI) removed from solid [mg/g]	0.049	0.054	0.182

* successive 24 hour leaches in 1 M NaOH, S:L = 1:20

The results for the LCS material seem to indicate that a larger amount of Cr(VI) is contained in the <500 micron size fraction than in the larger particles or the mix (which consists mainly of the larger particles, see Figure 7-1). However, considering the slow Cr(VI) release kinetics of this material illustrated in the previous section, the 24 hour tests may have been too short to effect complete release from the larger particles. In the smaller particles the time needed for the Cr(VI) to migrate to the particle surface may be considerably shorter and hence more is released within the same period of time, unaffected by the aggressive leach medium. More experimentation would be required to clarify this aspect, but was not conducted as it was felt that knowledge of the total amount of extractable Cr(VI) is not crucial for the purpose of further modelling.

7.3.6 Cr(VI) Adsorption Studies

The lysimeter experiments on LCS (Section 7.2) have shown that the release curves for Cr(VI) appear more protracted relative to those of the alkalis, which, as was demonstrated in the model study in Section 4.8 (Figure 4-27), could be taken as an indication that some retardation by adsorption may be present in the system. The adsorption behaviour of the material towards Cr(VI) was therefore investigated by adsorption tests using solutions spiked with Cr(VI) and concentration leaches, as stipulated in Section 5.5. pH was not found to influence the adsorption behaviour in the range likely to be encountered in the bed.

Table 7.9: Results from Cr(VI) adsorption experiments on LCS material

Initial Cr(VI) mg/l	Final Cr(VI) mg/l	Expected mg/l	Cr(VI) ads. mg/g
0.0	0.6	0.6	0.0000
2.0	2.4	2.6	0.0044
5.0	5.3	5.6	0.0058
10.7	10.7	11.3	0.0136
18.8	18.7	19.4	0.0130
40.7	40.6	41.3	0.0130
81.0	80.9	81.6	0.0152

* 24 hr water washes at 1:20 S:L ratio

Only few adsorption runs were conducted at 1:20 S:L ratio in Cr(VI) solutions ranging from 0 to 80 mg/l. Results are presented in Table 7.9. As stated before, it can be assumed that no Cr(VI) is initially adsorbed onto this material. The amount of Cr(VI) released by leaching over the 24 hour experimental period is indicated by the first run in unspiked solution. This was assumed to be the same in all experiments. The total expected Cr(VI) concentration was calculated by adding the expected leached concentration to the initial Cr(VI) concentration of the leach solution. The difference between expected and actually measured concentrations was assumed to have adsorbed. This is expressed as mg per g solid in the table. Quite clearly from these values there is a trend for increasing Cr(VI) adsorption with increasing solution concentration.

Concentration leaches for the LCS material were conducted at S:L ratios of 1:10, 1:5 and 1:2. At higher ratios the charge of this coarsely granular material would no longer be entirely covered by liquid and it was doubted that leach efficiencies in the bottle tumbler would yield comparative results. Furthermore it was feared that attrition would significantly alter the particle size distribution over the 24 hour leach period at high solids concentrations.

Table 7.10: Release of Cr(VI) from LCS at various S:L ratios*

S:L Ratio	Cr(VI)
1:20	0.0130
1:10	0.0107
1:5	0.0101
1:2	0.0087

* expressed as mg released per g dry solid

The leachate concentrations of Cr(VI) were measured at the end of the 24 hour leach runs. Concentrations released, expressed as mg per g solid are given in Table 7.10. Solution pH values were around 11 for all runs and solution pH was therefore not considered to be a variable in these experiments.

For this material Cr(VI) concentrations (expressed as mg/g dry solid) show a slightly decreasing tendency with increasing S:L ratios. Thus it can be presumed that this material shows some adsorption tendencies, which become more pronounced as S:L ratios increase.

The Cr(VI) adsorption behaviour of the LCS material was characterised by fitting both Langmuir and Freundlich isotherms to the available data. Since all data points represent adsorption and pH was not a variable for this material, no further subdivision of data was necessary.

The experimental data (given in Tables 7.9 and 7.10) was fitted with the two methods by regression as before and the fitted parameters are given in Table 7.11. Figure 7-15 shows experimental data together with the two adsorption models. While both isotherms fit the

Table 7.11: Best fitted data for Langmuir and Freundlich adsorption isotherms for LCS

Langmuir Isotherm		
$C_{S,max}$	K	r^2
0.012	0.201	0.922
Freundlich Isotherm		
b	m	r^2
0.0025	0.46	0.938

experimental data well in the low concentration range (<10 mg/l Cr(VI)), experimental data obtained at higher concentrations show a large degree of scatter, which is reflected in the relatively low r^2 values for both methods, but too few data points have been measured to ascertain whether this scatter is due to experimental error or to the fact that neither isotherm model adequately reflects the Cr(VI) adsorption behaviour of this material. Nonetheless, since the Cr(VI) concentrations measured in the column studies of the LCS material fall mostly in the low concentration range, it is assumed here, that either isotherm describes adsorption behaviour onto the LCS material sufficiently well in this region.

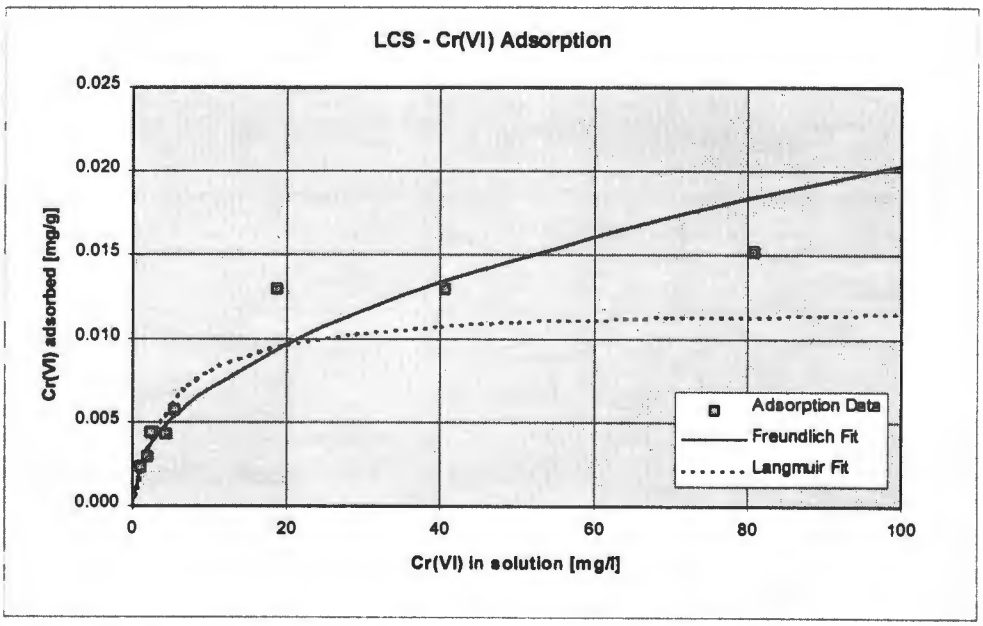

Figure 7-15: Cr(VI) adsorption on LCS - experimental data and fitted isotherms

7.3.7 Reaction Modelling

In summary of the batch leach experiments conducted on the LCS material it can be stated that the release of chromium species, which are the main focus of work here, is driven by at least three simultaneous mechanisms: instant dissolution, slow kinetic release and adsorption. None of these release mechanisms appears to be strongly influenced by the solution pH at the levels encountered in aqueous batch leach experiments and in the lysimeter studies. Thus, unlike the MD material investigated in Chapter 6, only those reactions pertaining directly to the release of chromium need further consideration for modelling purposes. The set of reactions considered here is thus

1. $\mathbf{Cr(VI)_{solid} \rightarrow Cr(VI)_{aq}}$

Reaction Type:	Instant Cr(VI) dissolution	
Reaction Constant:	$c_{Cr(VI)}^{0}$ = 0.002 mg/g	calc. from batch leach exp.: 0.1 mg/l from 50 g solids (Figure 7-12b)

2. $\mathbf{Cr(VI)_{solid} \rightarrow Cr(VI)_{aq}}$

Reaction Type:	Kinetic Cr(VI) dissolution	
Reaction Model:	first order in solid Cr(VI) conc.	
Reaction Constants:	$k = 3.2 \cdot 10^{-6}\ s^{-1}$	extracted from long term leach experiment (see Section 7.4)
	$c_{Cr(VI)}^{0}$ = 0.02 mg/g	estimated from long term leach experiment

3. $\mathbf{Cr(VI)_{ads} \rightleftharpoons Cr(VI)_{aq}}$

Reaction Type:	Cr(VI) Langmuir adsorption
Reaction Constants:	K_{ads} = 0.201 l/mg
	c_{ads}^{0} = 0.0 mg/g
	c_{max} = 0.012 mg/g

All parameters as given in Table 7.11

The kinetic constant needs to be investigated carefully in combination with modelling the pore diffusivity of the material, which is discussed in more detail in Section 7.4. The value for k given here is the optimised number extracted from the long-term leach data (Figure 7-14).

The set of reactions given here does not include Cr(III) release. Although some evidence for this was found in the lysimeter studies (Section 7.2), Cr(III) release could not be confirmed in the batch leach experiments. Cr(III) solubility at the pH levels encountered in the column experiments are too low for any noticeable Cr(III) concentrations to be expected in solution and the possibility of analytical error could not be ruled out.

The release of Na and K from LCS material appeared to be controlled mainly by more or less instant dissolution from the solid at approximately 0.3 mg/g and 0.1 mg/g respectively. Although only of marginal interest in this study, these species were found to be useful for testing the trends of model predictions in the study of the MD material detailed in Chapter 6, and the effect of instant Na dissolution has also been studied extensively in the preliminary evaluation of the WASTSIM code in Section 4.8. Therefore the release of these species was incorporated into the simulations for comparative purposes.

The release of Ca, on the other hand appears to be controlled by solution pH. The existence of dissolution from $Ca(OH)_2$, as postulated for the MD material (Chapter 6), is not supported by the low solution concentrations and pH values found in the water leach experiments. It is therefore assumed that Ca is present in the material in other mineralogical forms, with different solubility characteristics. This was, however, not further investigated in the present study and modelling of Ca release was omitted.

Since the beds in the LCS column studies were only partially saturated with water, and air is likely to be present as a continuous gas phase throughout the bed, adsorption of CO_2 into the liquid phase may be of considerable significance here. Formation of carbonate

species in solution may influence pH and also give rise to precipitation of carbonate salts of dissolved species, particularly Ca. Although effluents from the lysimeter studies were not analysed for carbonates, evidence for their presence was found in the frequent formation of a white precipitate on the walls of glass equipment, which easily dissolved in acid under the formation of bubbles. It would thus be of great interest to investigate the interactions of Ca and CO_2 in unsaturated beds, but this is not pursued further here.

7.4 Particle Pore Diffusion and Modelling of Kinetic Constant

Low Carbon Slag is a coarsely granular material with distinct individual porous particles (Section 7.1). In a packed bed situation it is plausible to assume that the moving bulk fluid moves in the interstitial spaces between individual particles, while chemical release into the bulk is governed by diffusion through the internal pores of the particles. If these pores are narrow and convoluted, intra particle diffusion is governed by an effective diffusivity, which is the product of the free solution diffusivity of a species and a factor, d_{eff}, which accounts for these geometric effects (Equation (4.2-5)). As the LCS material consists of porous particles, it was attempted to quantify this effective diffusivity factor by a Cr(VI) adsorption experiment, which is detailed in Section 7.4.1. A value for the diffusivity parameter is obtained by simulating the experiment using the WASTESIM code for various values of d_{eff} until the best fit for the experimental data is found.

As the kinetic release of Cr(VI), detailed in Section 7.3.4, interferes in the experiment, extraction of the diffusivity parameter had to be done in parallel with establishing a kinetic constant for this reaction, since it needed to be ensured that diffusion effects be clearly distinguished from the "true" kinetic effects. This was done by simulating the long term Cr(VI) leach experiment, detailed in Section 7.3.4, for various values of the kinetic constant k until the best fit was obtained. As both experiments involve both parameters,

d_{eff} and k, this curve fitting had to be done alternately. Details of this iterative parameter estimation exercise are given in Section 7.4.2.

7.4.1 Particle Diffusion Experiment

The model developed in Chapter 4 can be applied to a batch reactor scenario (Section 4.6.4) and the WASTESIM code in BATCH mode allows simulation of such scenarios (Section 4.8). If particles are all of the same size, and well mixed, the release (or consumption) of a species is governed solely by the dynamics of the reactions it is involved in and the rate at which it diffuses in or out of the particles, which in turn is governed by the effective particle diffusivity. If the reaction mechanisms can be described by suitable reaction models the only unknown parameter is this effective diffusivity, which can then be obtained by simulating the experiment with WASTESIM for various values of this effective diffusivity until the simulated curve is obtained that best fits the experimental data.

This approach was followed to establish the effective diffusivity of the LCS particles using the adsorption of Cr(VI) onto this material. An Cr(VI) adsorption isotherm for LCS has been established in Section 7.3.6. The Cr(VI) adsorption equilibrium is assumed to be established rapidly, i.e. there are no kinetic effects associated with this reaction. Hence, if a concentration of Cr(VI) is introduced at the beginning of a leach experiment, this should be adsorbed rapidly, unless hindered by diffusion resistance in the particle pores. As was shown in Section 4.8.3, this pore diffusion effect is a function of both particle size and effective diffusivity. If the particles present in the experiment are all of similar known size, the observed rate of the Cr(VI) adsorption should then be directly proportional to the rate of diffusion of Cr(VI) into the particle pores and thus the effective pore diffusivity is the only unknown quantity. With the help of the WASTESIM code a value for this can be established by manipulating the effective diffusivity parameter, d_{eff}, until the best fit to the experimental data is obtained.

It must be borne in mind, however, that the kinetic release of Cr(VI), as described in Section 7.3.4, will interfere in the LCS system. As this reaction proceeds slowly relative to pore diffusion (see Figure 6-12 and the discussion in Section 7.3.2) it is assumed that this interference is only marginal within the time frame of the adsorption-diffusion experiment, but will nonetheless have to be considered in order to isolate a value for the effective pore diffusivity.

The Cr(VI) adsorption experiment was conducted on two particle size fractions of the LCS material, >2000 to ≤ 4000 μm and >1400 to ≤ 2000 μm. These were obtained from sieving the dried original LCS mix. 250 g of the size fraction were slurried in 1 l distilled water (thus resulting in a 1:4 S:L ratio) for 15 minutes in the tumbling bottle device. This initial wetting was conducted in order to saturate particle pores with water and in order to wash off soluble species, including the Cr(VI) which does dissolve immediately in small concentrations (see Section 7.3.7). A small sample was then taken to establish this initial Cr(VI) concentration.

Approximately 10 ml of a 1000 mg/l Cr(VI) concentrate solution was then poured into the reactor, which was immediately closed and tumbled to disperse the concentrate to result in an approximately 10 mg/l Cr(VI) solution. Small samples (so as to not alter the S:L ratio too significantly over the experimental period) were then drawn, frequently over the first 30 minutes of the experiment, and then from time to time. The experiment was continued over a 24 hour period. Samples were filtered and stored for Cr(VI) analysis.

The Cr(VI) concentration versus time curves for the two size fractions are given in Figure 7-16. Both curves behave exactly as expected. The initial concentration drops rapidly as Cr(VI) is adsorbed onto the solids and level out after a short while as this process goes to completion. Levels then start to pick up again much more gradually as the continuous leaching of Cr(VI) from the material starts to become significant. For the smaller size fraction Cr(VI) levels drop more rapidly as diffusion into the smaller particles should

proceed faster here. Final levels after 24 hours are more or less the same as observed for the larger size fraction.

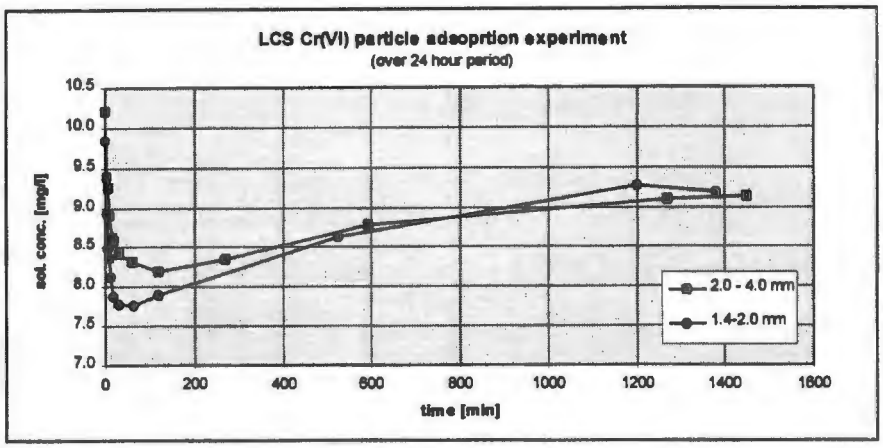

Figure 7-16: Cr(VI) adsorption-leach profile on 2 LCS particle size classes

7.4.2 Establishment of Diffusivity and Kinetic Reaction Parameters

Since the diffusivity experiment investigated the combined effect of Cr(VI) adsorption and kinetic release in porous particles, knowledge of the characteristic of these reactions is required for the establishment of the effective diffusivity parameter by curve fitting. While adsorption has already been characterised in terms of suitable isotherm models (Section 7.6) and is assumed not to be governed by kinetic effects, establishment of a kinetic reaction constant for Cr(VI) release on the basis of the experimental data given in Section 7.3.4 is still outstanding. The kinetics of this reaction are a combination of the "true" kinetic release from the solid and the kinetic effects of diffusion of the released Cr(VI) through the particle pores into the bulk fluid. Although the model study in Section 4.8.3 did indicate that the influence of pore diffusion resistance on slow kinetic reactions is marginal, this needs to be confirmed in the present situation.

The kinetic reaction constant for the Cr(VI) release reaction can be established by using the WASTESIM code to generate a number of simulated curves for various values of this constant and choose the one that best fits the experimental data, as was described in

Section 5.4.2 and Figure 5-9). In the present case this does, however, require a value for the effective pore diffusivity, which still needs to be established from the diffusion experiment detailed in the previous section. This, in turn, requires a value for the kinetic Cr(VI) release, which interferes in the experiment. Thus the establishment of the two parameters becomes an iterative procedure.

A kinetic constant was first obtained by fitting the experimental data given in Figure 7-14 using the WASTESIM code in BATCH mode (as outlined in Section 5.4.2), taking the effective pore diffusivity factor d_{eff} at unity. The best fit was obtained for $k = 3.0 \cdot 10^{-6}$ s^{-1}. Some of the modelled curves, together with the experimental data are shown in Figure 7-17.

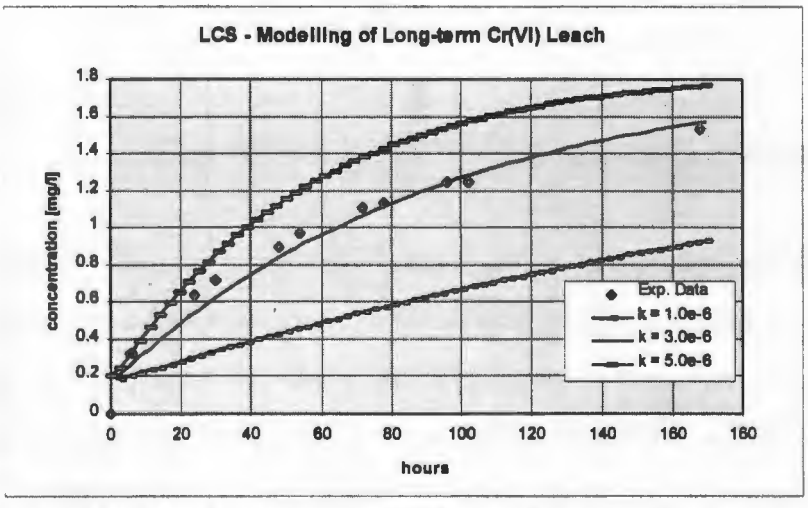

Figure 7-17: Modelled Cr(VI) long-term leach for LCS, assuming $d_{eff} = 1$

Using this value, the experimental data from the pore diffusion experiment (Figure 7-16) for the 2-4 mm size fraction was fitted by modelling the given experimental conditions and varying the effective diffusivity factor d_{eff}. The modelled curves for some values are shown in Figure 7-18, together with the experimental data. Clearly a good fit of the initial data points is obtained for $d_{eff} = 0.5$, but the slope of the modelled curve beyond the first 200 minutes (not shown here) appears somewhat flatter than the experimental data would suggest.

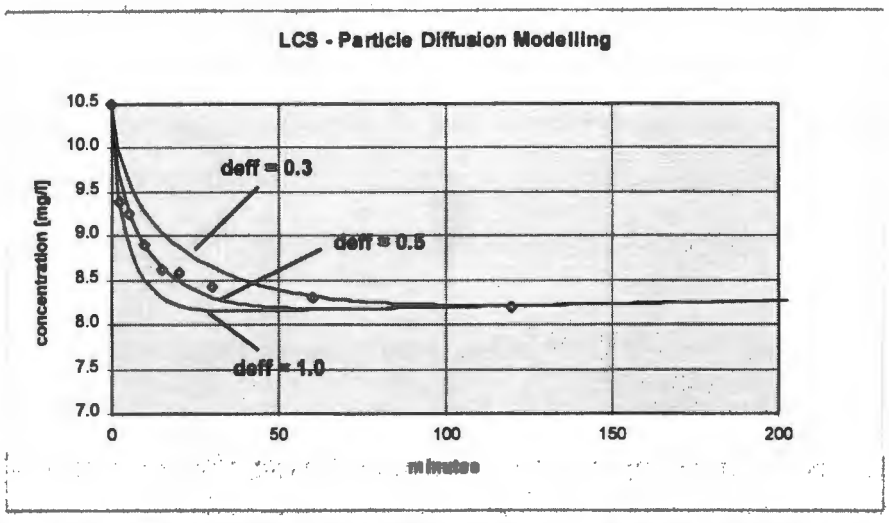

Figure 7-18: Modelled pore diffusion experiment with various d_{eff} and $k=3.0 \cdot 10^{-6}\ s^{-1}$. Only the first 200 minutes of the experiment are plotted for clarity.

The kinetic reaction was therefore re-modelled, this time using a pore diffusivity modified by the estimated factor d_{eff}=0.5 and a new best fit was obtained for k = $3.2 \cdot 10^{-6}\ s^{-1}$. This value was then again used to re-model the pore diffusion experiment and a slightly improved fit of the data is obtained. It was then attempted to further optimise the value of d_{eff}, but the changed value of k had little influence on the early part of the curve and thus the value of d_{eff} = 0.5 was accepted. The final modelled curve is shown in Figure 7-19.

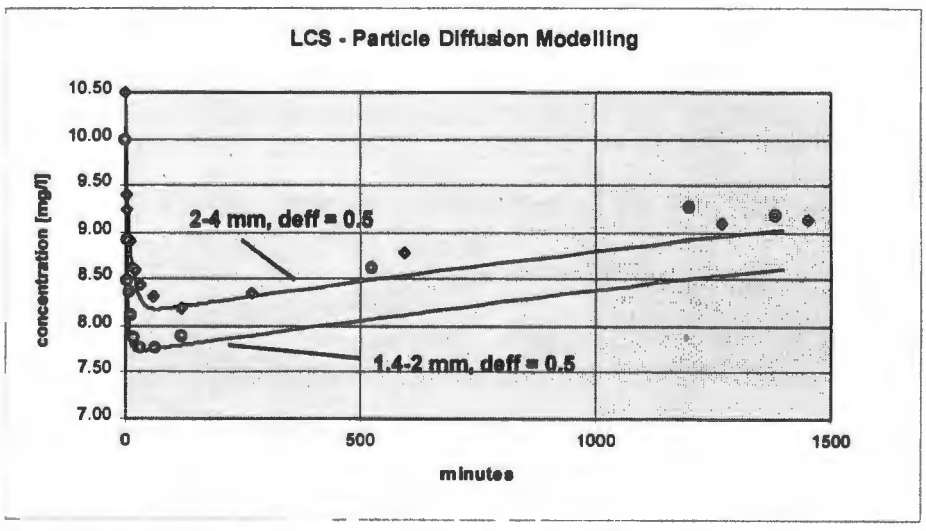

Figure 7-19: Plot of modelled curves and experimental data for the particle diffusion experiment on LCS

The same parameters obtained were now applied to model the diffusion experiment of the smaller particle size fraction, data and the modelled curve are also shown in Figure 7-19. Good fit of the measured data is obtained over the initial period, where the adsorption and diffusion of Cr(VI) into the particle pores dominates. Clearly the smaller particle size fully accounts for the faster drop of Cr(VI) levels as pore diffusion proceeds more rapidly.

However, the residual curve beyond 200 minutes does not match the experimental data well. It has, however, the same slope as that of the curve modelled for the larger particle size. The fact that the curve appears shifted downwards is simply due to the slightly lower initial Cr(VI) concentration achieved in this experiment (10 mg/l as opposed to 10.5 mg/l). After the initial adsorption equilibrium is reached at a correspondingly lower level, subsequent release is mainly governed by the kinetic reaction, which is taken as a function of solid concentration of Cr(VI) only and should therefore proceed according to the given rate constant irrespective of the actual solution concentrations.

The fact that the experimental data for the smaller particle size suggest a steeper slope, at least until the same concentration levels as in those measured for the larger particles is reached, could be taken as an indication that the kinetic release reaction may also be governed by solution concentration of Cr(VI). This appears unlikely, considering that long-term leach and diffusion experiments were conducted at considerably different solution concentration of Cr(VI) and the kinetic constant fits both sets of data well, at least for the larger particle size. It could be speculated, however, that the kinetic constant remains a size dependent quantity, although pore diffusion effects have already been taken account of.

As was indicated in the formulation of the kinetic reaction model (Section 7.3.6), the slow release mechanism of Cr(VI) could be linked to slow migration through the solid matrix. In this context one might want to distinguish between macro-porous and micro-porous structure of the LCS material. The macro-porous structure refers to the large channels and crevices visible under the electron microscope (see Figure 7-2), attributed to the formation

crevices visible under the electron microscope (see Figure 7-2), attributed to the formation of vapour bubbles during the quenching process from which this material originates (Section 7.1). Most of the high particle porosity ($\varepsilon_p = 0.55$) is associated with these large pores. The effective pore diffusivity factor $d_{eff} = \varepsilon/\tau$ (equation (4.2-5)) was established as 0.5, indicating that the tortuosity τ would be near unity in this case, or, in other words, that the relatively large pore channels are insufficiently convoluted to influence the effective diffusivity through the LCS particles.

Micro-pore effects, on the other hand, refer to migration through much smaller pores (micron sized and smaller) and through the crystal lattice, which may not necessarily be governed by diffusion through an aqueous matrix. As it is difficult to describe these effects separately, one usually resorts to express such processes in terms of a kinetic expression, in which the kinetic constant essentially lumps all reaction kinetic and diffusion effects for want of more detailed information. This was done in the present case by assuming the slow kinetic release of Cr(VI) from the LCS material to be first order in solid concentration only. If the kinetic dissolution is a micro-pore process, as is postulated here, the kinetic constant may well be a function of particle size and the reaction may be governed by solution concentrations in the macro-pore solution as well. More evidence for this effect would have to be gathered by suitable experimentation, such as studying the release reaction in solutions of various Cr(VI) concentrations and for various individual size classes, but this was not conducted within in the present study.

However, the chosen kinetic model and established constant appear to describe the Cr(VI) release from the 2-4 mm size class well, which is considered acceptable given that this size class makes up over 40% of the LCS material. It needs to be seen, whether this simple model is sufficient to account for effects in a deposit situation, This is discussed further in Section 7.6.

7.5 Tracer Study

The tracer study conducted on the LCS material was done in continuation of experiment LCS2 in the same bed. Since conditions in the bed in terms of permeability do not appear to change significantly in the course of the previous experiment, it is expected that results from a tracer study would directly reflect the flow conditions of experiment LCS2 and would allow conclusions to be drawn with respect to those prevailing in experiment LCS1.

The tracer experiment (termed LCS3) started immediately at the end of LCS2 (after 45 days of monitoring) by replacing the acid rain mixture in the feed beaker with a solution of approximately 830 mg/l Li^+ (as Li_2SO_4) and continuing percolation at an average daily feed rate (applied in 4 x 2 hours intervals over a 24 hour period, see Section 5.3) of approximately 205 ml/day. This was continued for a period of 36 days by which time Li concentrations in the effluent began to reach peak levels. The feed liquor was then switched back to unspiked acid rain mixture and daily feeds continued as before. The Li concentrations as well as effluent flow-rates were carefully monitored for a further 113 days after Li supply was stopped. The average effluent flow-rate over the entire experimental period was 177 ml/day, which corresponds to 86% fluid recovery, with the balance assumed lost to evaporation the bed.

Figure 7-20 shows Li concentration in feed and effluent versus time. As can be seen, the Li levels in the effluent drop extremely slowly towards the end of the experiment, which is why it was stopped although residual concentrations were still as high as 15 mg/l. Although this would mean that significant amounts of Li may still have been held up in the bed, data gathered was considered sufficient to allow an assessment of the residence time distribution within the bed. The curve indicates two equal peaks in short succession, separated by a phase of irregular Li recoveries. This is taken as indicative of a distribution of flow fronts arriving at the bottom of the bed in relatively short succession.

The protracted tail-end of the response curve is not uncommon in tracer tests of packed beds (Levenspiel, 1972) and is attributed to slow migration in near-stagnant zones of the bed and continued release from fluid trapped in dead pores, as was discussed in more detail in Section 5.6.

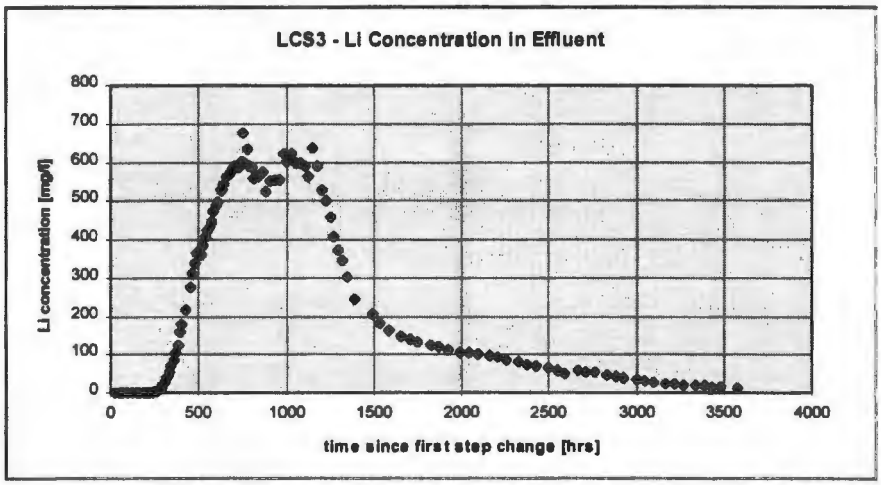

Figure 7-20: Li recovery profile in experiment LCS3

Multiplying the Li concentrations in the effluent with the volume of effluent recovered within each sample period allows to calculate the cumulative recovery of Li with time, and likewise for the feed. This has been plotted in Figure 7-21. The recovery curve is useful to establish the total amount of tracer recovered and still held in the bed at each point in time, as well as mass balance closure at the end of the experiment. In the present case this is only about 82 %, corresponding to about 1000 mg Li still held up in the bed, which is high considering the low effluent concentrations at the end of the experiment and too high to be explained by analytical error. A possible explanation would be permanent Li adsorption to the solids in the order of 5 mg per 100 g. This was not confirmed in initial batch adsorption studies of Li on the LCS material over the concentration range employed, even over extended periods of time.

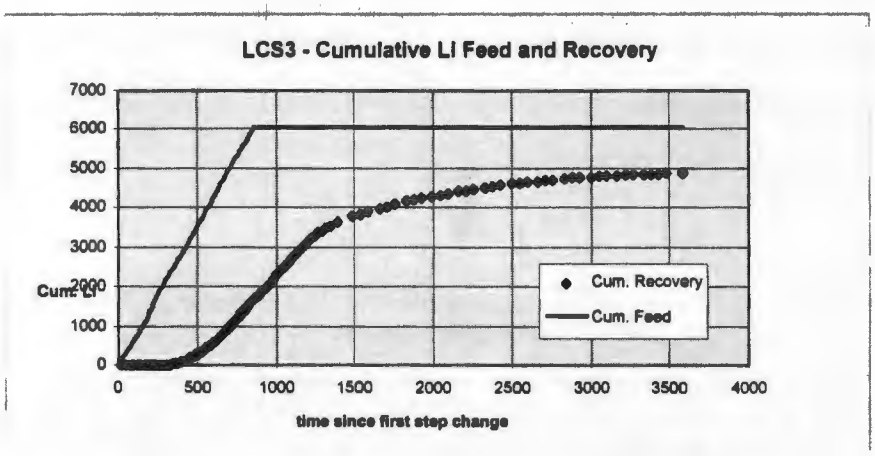

Figure 7-21: Cumulative Li in feed and recovery in experiment LCS3

It was noted, however, that total Li recovery over the experimental period corresponded very closely to the total fluid recovery (82% vs. 86%). As was stated above, fluid loss is attributed to evaporation within the bed, which at all times is only partially saturated and thus allows free flow of air through it. This, in itself, would not explain a loss of ionic species dissolved in this fluid, as these would be left behind and simply concentrate in the remaining fluid.

It is, however, plausible to assume that a significant portion of fluid is "trapped" in dead pores, given the highly porous nature of the LCS material (Section 7.1). Exchange of dead pore fluid with the moving bulk fluid is marginal or non-existent (Section 4.1). Although most dead pores should have become saturated in the course of experiment LCS2, which preceded LCS3, it is plausible to assume that the major loss to evaporation is from the stagnant fluid in dead pores, which can therefore be replenished continuously. In this scenario the high concentrations of Li carried in the tracer fluid may remain permanently trapped in the dead pores and have little opportunity to migrate into the moving bulk fluid, even if their concentrations in the pores continuously increase. Consequently the apparently poor mass balance closure of the tracer experiment may indeed be related to the accumulation of tracer to dead pores and is of similar magnitude as the total fluid loss if evaporation is assumed to proceed mainly from these dead pores. This scenario requires to

be substantiated by further experimentation, which was not conducted in the context of the present work.

The tracer response curve from experiment LCS3 was simulated using WASTESIM (see Section 5.6), based on the assumption that effluent flow rates represent the net transport of Li through the system and that all Li carried in the lost feed liquor is permanently trapped in the system and thus need not be accounted for.

A further model assumption was that the large macro-pore volume of the particles can be attributed to the bulk fluid. As was indicated in Section 7.4, diffusion resistance to migration of species in and out of these pores is of the same order of magnitude as resistance to bulk diffusion through a porous matrix of similar porosity. Furthermore, it was stated in Section 7.1 that the majority of particles appear to be debris of larger, hollow granules (see also electron-micro-graphs in Figure 7-2 a and b) and their "porosity" is more attributable to the raggedness of their external surface rather than internal pores. Thus fluid trapped in these "pores" is likely to be in full contact with the bulk fluid and may in fact be moving albeit at a lower velocity than fluid nearer to the free surfaces in the unsaturated bulk pores. This argument does not extend to diffusion through micro-pores present in the solid matrix material, but, as discussed in Section 7.4, micro-pore effects can be taken account of by suitable "lumped" kinetic models. Therefore, modelling of particle pore effects was not included. Thus assuming the particle macro-pores to report to the bulk voidage, the total bulk porosity has been calculated to be 70.5%, a large value, but plausible in the light of the forgoing argument.

Another question that needs to be addressed carefully in the context of modelling LCS beds is that of bed saturation. This can be obtained from analysing the initial packing information of experiment LCS2 and the saturation period before the first fluid breaks through after percolation commences (Table 7.7). From this data the fractional saturation was calculated as approximately 0.30, if it is assumed that no further accumulation occurs after the first breakthrough of fluid. Whether this assumption is valid remains

questionable, however. The fractional recovery of fluid during experiment LCS2 was approximately 82% on average, which is somewhat lower than that observed for the same bed in experiment LCS3 (86%). It is therefore plausible, that some fluid apparently lost to evaporation is in fact continuously accumulated in the bed until maximum saturation is reached well into experiment LCS2. This accumulation could result in the fractional bed saturation to become as high as 0.35. Again, this effect remains speculative and would require closer investigation.

The tracer response curve for the given system was thus modelled, initially assuming uniform bulk flow throughout the bed. The modelled curve is shown, together with the experimental data in Figure 7-22. The peaks of modelled curve and measured data coincide well, indicating that the bulk residence time in the bed is captured well in the model, but the modelled curve significantly exceeds measured concentration levels and does not capture the protracted tail end.

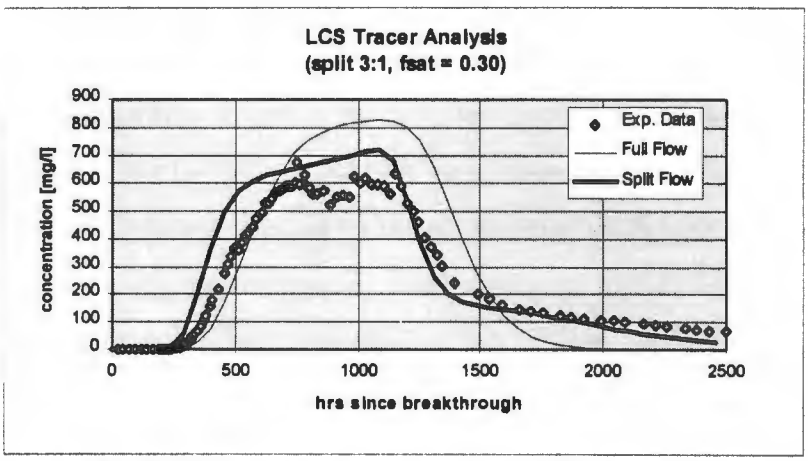

Figure 7-22: Modelled and measured Li tracer response curves

It was therefore decided to conduct the split flow analysis as stipulated in Section 5.6. Comparing the areas under modelled and measured curves between the points of intersection results in a split ratio of approximately 3:1 between faster and slower moving fluid fractions. Thus the bed was re-modelled as consisting of two columns of half the cross-sectional area each and the total flow-rate split 3:1 between these. The Li response

be substantiated by further experimentation, which was not conducted in the context of the present work.

The tracer response curve from experiment LCS3 was simulated using WASTESIM (see Section 5.6), based on the assumption that effluent flow rates represent the net transport of Li through the system and that all Li carried in the lost feed liquor is permanently trapped in the system and thus need not be accounted for.

A further model assumption was that the large macro-pore volume of the particles can be attributed to the bulk fluid. As was indicated in Section 7.4, diffusion resistance to migration of species in and out of these pores is of the same order of magnitude as resistance to bulk diffusion through a porous matrix of similar porosity. Furthermore, it was stated in Section 7.1 that the majority of particles appear to be debris of larger, hollow granules (see also electron-micro-graphs in Figure 7-2 a and b) and their "porosity" is more attributable to the raggedness of their external surface rather than internal pores. Thus fluid trapped in these "pores" is likely to be in full contact with the bulk fluid and may in fact be moving albeit at a lower velocity than fluid nearer to the free surfaces in the unsaturated bulk pores. This argument does not extend to diffusion through micro-pores present in the solid matrix material, but, as discussed in Section 7.4, micro-pore effects can be taken account of by suitable "lumped" kinetic models. Therefore, modelling of particle pore effects was not included. Thus assuming the particle macro-pores to report to the bulk voidage, the total bulk porosity has been calculated to be 70.5%, a large value, but plausible in the light of the forgoing argument.

Another question that needs to be addressed carefully in the context of modelling LCS beds is that of bed saturation. This can be obtained from analysing the initial packing information of experiment LCS2 and the saturation period before the first fluid breaks through after percolation commences (Table 7.7). From this data the fractional saturation was calculated as approximately 0.30, if it is assumed that no further accumulation occurs after the first breakthrough of fluid. Whether this assumption is valid remains

curves were modelled individually for both these columns and the resulting concentration profiles then added as weighted averages. The resulting curves are shown in Figure 7-22.

The split flow response curve thus modelled captures the trends of the measured data quite well, both with respect to the peak plateau and the protracted tail end. The modelled curve does, however, appear early relative to the measured data, indicating that simulated flow-velocities in the bed are higher than in reality and thus that the residence time of the faster flow appears shorter than measured.

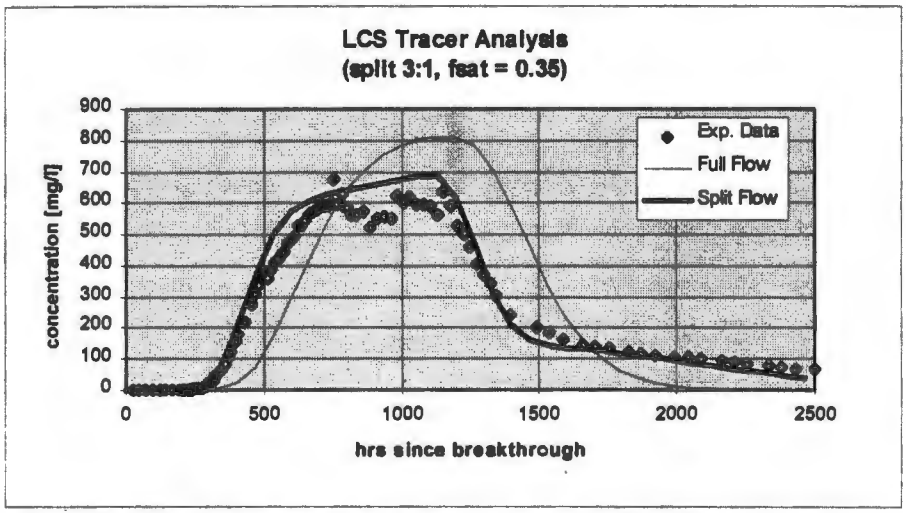

Figure 7-23: Modelled and measured Li tracer response curves for f_{sat}=0.35

It can be shown that changing the split ratio would not improve the modelled response curve as it would appear even earlier if the split ratio is raised or would tend to the curve modelled for uniform flow (Figure 7-22) if it is lowered. However, keeping the split ratio as 3:1 and increasing the value for fractional saturation to 0.35, which may be justified as discussed above, results in a modelled response curve remarkably close to the measured data, as shown in Figure 7-23. Higher saturation and hence bulk fluid volume results in lower flow velocities in both streams for given flow-rates and hence the response curve appears more delayed and more protracted relative to that obtained for a lower saturation.

7.6 Column Modelling

The release behaviour of the LCS material has been characterised in terms of Cr(VI), Na and K by batch leach experiments, as was described in Section 7.3. As pH does not to govern the release behaviour in the pH range encountered in the column experiments, reactions that may influence column pH are not considered further. The release of Cr(VI) is governed by the combined effect of instant initial release, a weak adsorption isotherm and a slow kinetic release, assumed to be related to slow diffusion from the particle micro-porous structure (Section 7.3). A kinetic reaction model, first order in solid concentration of Cr(VI), has been chosen to represent this release and a kinetic constant has been obtained from modelling available experimental data (Section 7.4).

Although the material is coarsely granular, the high internal particle porosity and the rugged shape, particularly of the smaller particles, give rise to the assumption that in a packed bed situation this porosity can be attributed to the bulk porosity of the bed rather than a separate particle porosity and particle level modelling is not required. This is confirmed by the outcomes of the column tracer study detailed in Section 7.5. Also, results from the particle diffusion experiment (Section 7.4) suggest that diffusion through these macro-pores is not hindered by the convolution of the pores, but corresponds to that of migration through large interstitial pores.

The tracer study (Section 7.5) has indicated that bed saturation (including the particle macro-pores) is in the order of 30-35%, and may change slightly as flow through the bed is established. Column experiments (Section 7.2) have shown that there is a significant discrepancy between flow volumes supplied to and recovered from the columns. Although the tracer study indicates that most of this is likely to be lost due to evaporation from dead pores in the bed, it could not be established with clarity to what extent bed accumulation (and consequently saturation) is also present. The tracer study furthermore indicated, by way of the split flow analysis (Section 4.5), that at least 25% of the bulk flow can be

associated with a slow moving phase, likely to be that moving through or close to the particle macro-pore structure.

It is now attempted to validate the information gathered by modelling the expected leach profiles of the two lysimeter studies LCS2 and LCS1, which are described in Section 7.2., and comparing the result with experimental data. Results from this modelling work are discussed in Sections 7.6.1 and 7.6.2 respectively.

7.6.1 Modelling Experiment LCS2

It was decided to consider modelling of experiment LCS2 first, since information gathered from the tracer study, which was conducted in the same bed, is likely to be more directly applicable to this experiment. Scale-up to the larger column of LCS1, on the other hand, requires more careful consideration.

As indicated above, mainly the release and transport behaviour of Cr(VI) on the basis of the reaction mechanisms established by separate laboratory experiments, was considered. Leach profiles of Na were also modelled for comparison, since its release appears to be governed solely by instant dissolution, which is relatively simple to simulate.

The WASTESIM code was applied in the COLUMN mode (Section 4.8) employing the reaction scheme as laid out in Section 7.3.6. Modelling runs conducted were on the assumption of the average flow rate to be present throughout the bed and on the basis of split flow at a split ratio of 3:1 (Section 7.5). The effective bulk diffusivity factor d_{bed} was taken at 0.5, which corresponds to the value established from the pore diffusion experiments (Section 7.4) and is taken to apply also if the particle macro-pores are taken as bulk pores. For comparison a value of $d_{bed} = 0.25$ was also used. The modelled curves, together with the experimental data of experiment LCS2 are shown for Cr(VI) in Figures 7-24 a and for Na in Figure 7-24b.

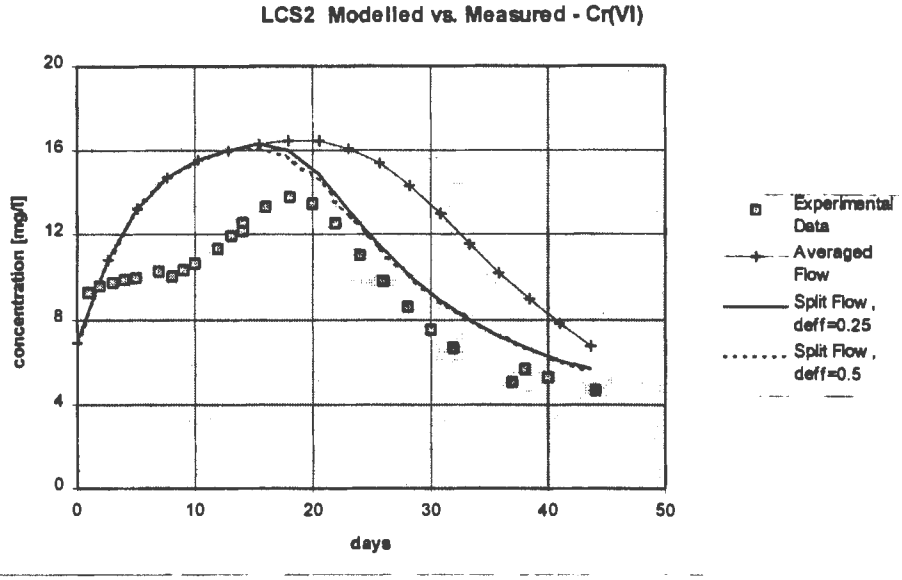

Figure 7-24a: Modelled and measured Cr(VI) profile in LCS2

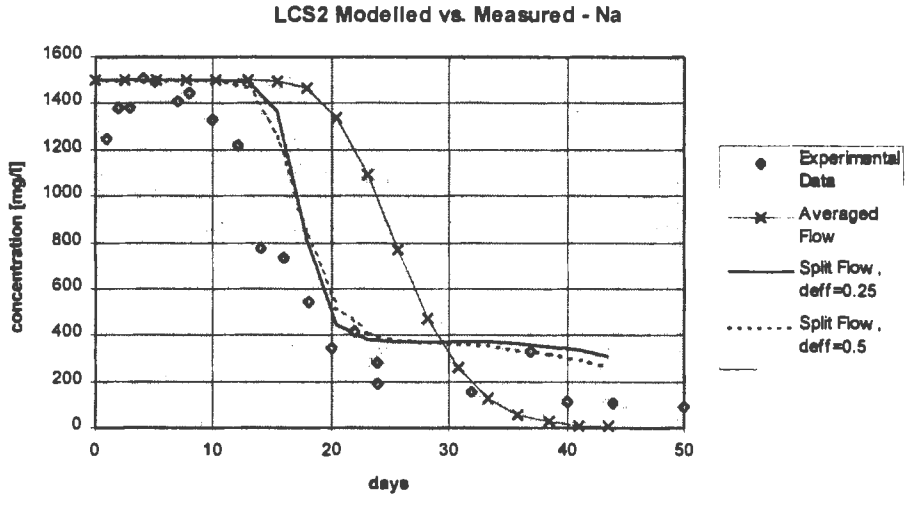

Figure 7-24b: Modelled and measured Na profiles in LCS2

For both Na and Cr(VI) the modelled curves correspond to the experimental data in order of magnitude and general trends, but acceptable agreement is only achieved when using the 3:1 split flow approach. But even then there remain significant discrepancies between modelled and measured data in the order of 10-20%, which is discussed in the following. The value of the effective diffusivity factor d_{bed} has only marginal effect on the simulated leach curves. This trend was already observed in the context of the model sensitivity study

(Section 4.8) and is attributed to the relatively short residence time in the LCS2 bed, which does not give bed diffusion sufficient time to progress.

The modelled Cr(VI) curve (Figure 7-24 a) shows an initial steep rise phase resulting from the slow kinetic release reaction. which settles, once the corresponding solid concentration is exhausted, and the gradually decreases as the adsorption buffer replenishes Cr(VI) that is transported out of the bed. This combination of Cr(VI) kinetic release and adsorption was already described in the model sensitivity study (Section 4.8.4).

In the present case released concentrations significantly exceed the measured values and peak levels are reached much faster, although buffered by the adsorption reaction. This is taken as an indication either that adsorption in the system is somewhat stronger than was measured in the batch experiment, or that the release reaction proceeds slower than the batch leach experiment would suggest, or that the kinetic release of Cr(VI) is also a function of solution concentration and therefore slower if these are high. As was indicated in Section 7.4, insufficient experimental data was gathered to confirm this trend and use of an alternative reaction model was not attempted. As stated in Section 7.2.2, the drop-off phase is more protracted for Cr(VI) than for Na, a trend which is well captured by the modelled curve as a result of the adsorption buffer.

The modelled Na curve (Figure 7-24 b) over-predicts the initial Na concentrations by some 10%, indicating the bulk solids to liquid ratio in the bed was actually higher than was calculated from the initial saturation data (Table 7.7) and therefore resulting in a stronger dilution effect. Also, the modelled curve does not emulate the initial rise phase observed in the experimental data. This is not surprising, since Na release was taken as instant dissolution with no other kinetic effects present, but some clarification is needed to explain this trend.

The onset of drop-off of the modelled curve occurs later than it does for the measured data, and modelled concentration levels are higher. The influence of bed saturation on

modelled leach curves has already been discussed in the context of the model sensitivity study in Section 4.8.5. It was shown, that increasing the fractional saturation parameter results in both decreased concentrations (due to the lower bed solids to liquid ratio) and increased bed residence time. For the modelled Na curve to fit the experimental data better, bed residence time and concentration levels would both have to be reduced (to effectively move the modelled curve in Figure 6-24b down and left), but this can not be achieved by manipulating the bed saturation alone.

Quite clearly the characterisation of the bed in terms of an assumed uniform saturation and a simple two phase flow model is insufficient to account for all effects taking place in experiment LCS2. The tracer study (Section 7.5) has already indicated that flow through the bed is more likely to consist of a broad band of faster moving streams and a long tail-end of slow streams, rather than two distinct phases, although these can be used to emulate the true distribution reasonably well. Furthermore, it is likely that slower and faster streams flow alongside each other, for example, slower through the rugged and porous particle surfaces, and faster on top of these through the interstitial spaces. In this case there would be continuous exchange between the phases, both in terms of actual fluid mixing and diffusion between phases.

This scenario can help to explain some phenomena observed in the experiment. The initial rise phase of the Na curve could, for example be related to slow diffusion exchange between the slow moving phase near the particle surfaces, where Na is initially concentrated and the faster moving fluid further away. Likewise explained is the more protracted rise of the Cr(VI) curve, where concentration will initially rise closer to the particle surfaces and only gradually migrate to the faster bulk stream.

Modelling of these effects is possible, in principle, if the bed is characterised as a complex network of plug flow and CSTR reactors (Levenspiel, 1972), but such characterisation is tedious and largely empirical with little value for scale-up to another system, as was indicated in Section 5.6. It is felt, however, that using the two stream approach, but

allowing diffusion exchange between the two phases, may suffice to describe such systems reasonably well. Such interface exchange could easily be characterised by some lumped mass transfer coefficient similar to what has been postulated for the exchange between stagnant and moving fluids in the surface film model formulated in Section 4.6.2. It would be relatively easy to reformulate the surface equation (4.6-9) as a secondary bulk equation and model both bulk streams simultaneously. Such a modification offers opportunities for further model development, but is not considered within the present work.

7.6.2 Modelling Experiment LCS1

As indicated in the preceding section, modelling of the short column experiment was considered first as more information on the hydrodynamic conditions in this bed were available through the tracer study. Nonetheless, this bed characterisation appeared unsatisfactory for the model to fully emulate the measured experimental data resulting in some significant discrepancies both in terms of concentration levels and time scale. It needs to be seen now to what extend this trend is confirmed in the much longer bed of experiment LCS1.

The WASTESIM code in COLUMN mode was applied employing the reaction scheme as laid out in Section 7.3.6. Similar to what was done in the modelling of experiment LCS2, runs were conducted on the assumption of the average flow rate to be present throughout the bed and on the basis of split flow at a split ratio of 3:1 (Section 7.5). The effective bulk diffusivity factor d_{eff} was taken at 0.5, which corresponds to the value established from the pore diffusion experiments (Section 7.4) and is taken to apply also if the particle macro-pores are taken as bulk pores. The modelled curves, together with the experimental data of experiment LCS1 are shown for Cr(VI) in Figures 7-25 a and for Na in Figure 7-25 b.

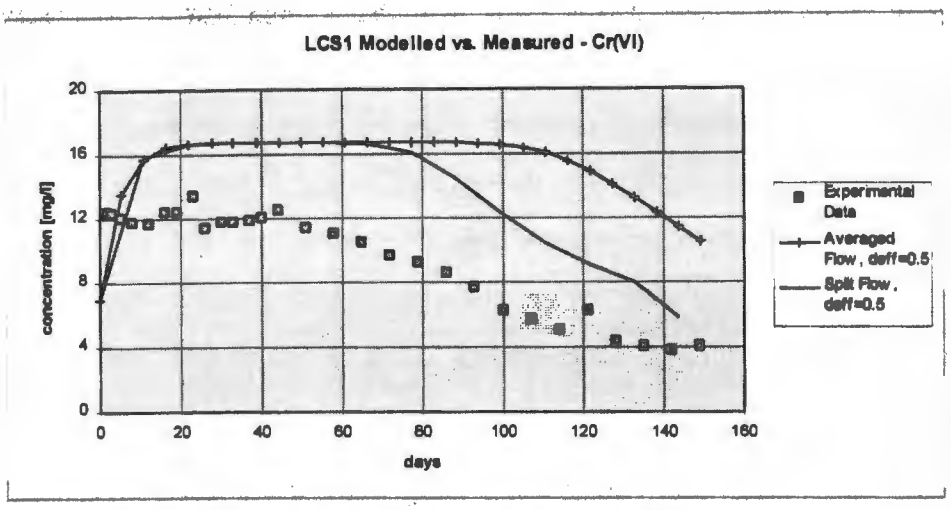

Figure 7-25a: Modelled and measured Cr(VI) profiles in LCS1

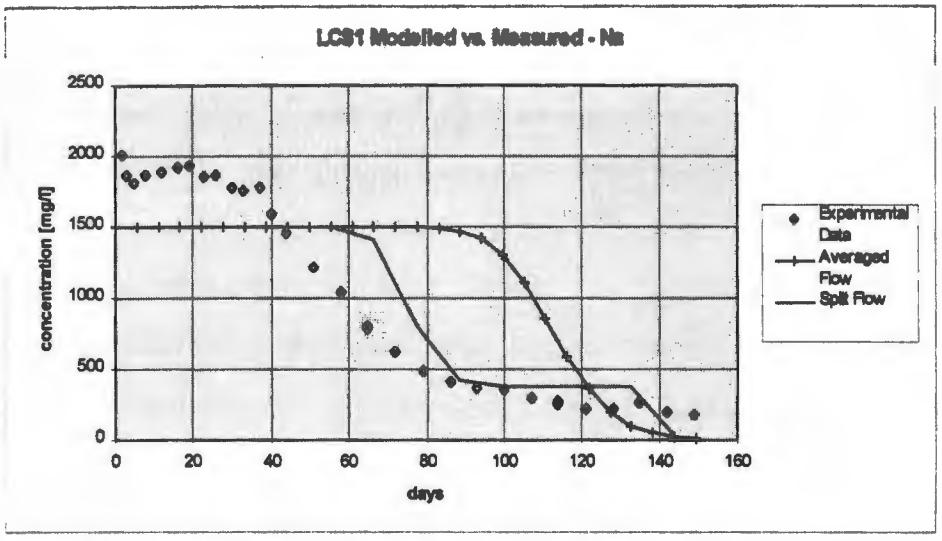

Figure 7-25b: Modelled and measured Na profiles in LCS1

Quite clearly only the curves modelled on the basis of the split flow approach by and large correspond to the trends of the experimental data, although the level of congruency is relatively poor and errors up to 30% are present. Despite the split flow approach, the slower stream does still not account for the extended tail end as particularly evident in the Na curve (Figure 7-25 b). The onset of the concentration drops is also significantly later than experimental data would suggest. In principle these observations are an indication that the stream split is more likely to be in the order of 4:1 or even 5:1, but it must be

questioned whether such splits are still physically realistic. It is speculated here that, beside a distribution of flows through the bed, diffusion from stagnant zones and dead pores becomes increasingly more significant with increasing residence time in the bed. A larger portion of fluid held up in the bed is associated with a non-moving phase than was assumed in the case of LCS2. This is plausible, since the estimated hold-up for LCS1 is proportionally slightly higher, and the longer bed could well prevent the evaporation of fluid from dead pores as may have still been possible in the short LCS2 column (see Section 7.5). This is supported by the fact that the net loss of fluid from both columns is of very similar magnitude and the observation that, after completion of experiment LCS1, the top 30 cm of the de-commissioned bed dried out much faster (as observed through a change in colour) than the lower regions.

The modelled Cr(VI) curve (Figure 7-25 a) suggests an initial rise phase which was not observed from the experimental data. It was already speculated in Section 7.2 that rise following kinetic release may be masked by diffusion effects in the bed, which are not accounted for by the model in its present form. Similar to what was observed in experiment LCS2 the measured Cr(VI) concentrations are up to 30% lower than those modelled. This is either an indication that the bed saturation is higher than initially assumed (although this is unlikely to account for as much as 30% dilution), or that the chosen kinetic reaction model does not appropriately represent the release of Cr(VI).

The latter argument is more plausible considering that the material was charged to the bed wet and left to settle for as long as two weeks (see Sections 7.2 and 5.3). If the release reaction was solely driven by the solid concentration of Cr(VI), then there is no reason why the reaction should not have gone to completion long before the lysimeter experiment began. Since this is obviously not so, it can be assumed that the kinetic release of Cr(VI) is indeed driven by dissolved Cr(VI) concentrations and could in fact be some form of kinetically controlled desorption reaction.

The modelled Na curve (Figure 7-25 b) predicts significantly lower concentrations than the experimental data would suggest, and the observed initial concentration rise is not captured. This would again indicate that mobile fluid volumes in the bed are actually lower than what was calculated from the initial saturation data (Table 7.6) and that diffusion from stagnant or slow moving zones of the bed is present, as was discussed in detail in the context of experiment LCS2 in Section 7.6.1.

The quality of model predictions under unsaturated bed conditions, such as encountered in the lysimeter studies of the LCS material, has thus been shown to be strongly dependent on the characterisation of bed saturation and the apportionment of bed fluid to stagnant zones, zones with slow bulk movement and those with faster bulk movement. While much of this information can be obtained from column tracer studies for each particular case, it may not necessarily be applicable to a scenario of different scale. The model in its current form is not well suited to account for bed diffusion effects between the various bulk zones, but it is possible to expand this further. It is unclear, however, to what extent bed characterisation at laboratory scale is applicable to full scale deposit scenarios, even with an expanded modelling tool.

The LCS study presented in this chapter has also shown that considerable care needs to be taken when characterising chemical reactions at the laboratory scale. In the present case the assumption that Cr(VI) release is a kinetic function of solid Cr(VI) concentrations only, was only questioned once this reaction model was tested against the lysimeter data. In the context of the assessment methodology put forward in Chapter 5, further experimental work and confirmation through modelling of the column test cases is required, before the model can be used to simulate leach behaviour of this material from full scale waste deposits.

7.7 Closure

This chapter has given detailed account of all experimental and modelling work conducted on one particular waste material from the ferro-alloy industry, a ferro-chromium smelter slag termed Low Carbon Slag (LCS). The approach taken followed the methodology laid out in Chapter 5, which aims to collect sufficient information about the leachate generation potential of a waste material through laboratory scale experiments and compare these against test cases obtained through lysimeter studies on the same material, which need to be characterised only in terms of their transport properties.

Two lysimeter tests were conducted to create such test cases and provided the initial feel for the prevailing chemical conditions to inform more detailed batch experiments. As the first test involved a comparatively tall column with correspondingly long residence times of fluid in the bed, a second column experiment was conducted which involved a much shorter bed but was run under similar flow conditions as the first experiment. This was done in order to test whether this down-scaling would compromise the quality of the leach data obtained. Both experiments revealed protracted saturation periods, unsaturated bed conditions and significant loss of the permeating fluid attributed to evaporation.

The material was then subjected to a number of batch leach and Cr(VI) adsorption tests which were carefully interpreted in order to identify a matrix of reactions which characterise the release behaviour independent of scale. As chromium was the species of focus in the present study only those reactions that are directly or indirectly relevant Cr release, were studied. For the LCS material Cr(VI) release was found to be controlled by a combination of instant dissolution, adsorption/desorption and a comparatively slow kinetic release mechanism attributed to diffusion through the micro-porous structure of the solid. These were quantified by suitable analysis of the available batch leach data.

Cr(VI) release reaction mechanisms do not appear to be a function of solution pH in the range likely to be encountered in deposits. Reactions contributing to solution pH were

therefore not considered further. No release of chromium species other than Cr(VI) were identified in batch experiments, which would be expected as pH levels encountered in the columns are too low to allow significant Cr(III) concentrations in solution.

As the LCS material consists of highly porous granules, experiments were conducted to establish the effective pore diffusivity governing migration from the particles into the surrounding bulk fluid. This was achieved by simultaneously optimising data obtained from a kinetic Cr(VI) leach experiment and a Cr(VI) adsorption experiment. Findings suggested that diffusion through the relatively large macro-pores of the particles is of a similar order of magnitude to what would be expected in flow through a packed bed of similar porosity. It was therefore assumed that it is reasonable to attribute the macro-porosity of the particles to the bed porosity in a packed bed situation. The kinetic release is probably controlled by micro-pore diffusion which can be effectively lumped in a kinetic reaction constant and thus particle pore modelling is unnecessary in a packed bed situation.

A column tracer study was conducted in order to identify typical flow patterns through a bed packed with LCS material, which, due to its large bed porosity and particle sizes is highly permeable and only partly saturated with fluid. Results indicated a wide distribution of flow velocities and hence residence times though the bed with a protracted tail end associated with slow diffusion from dead pores. Significant tracer loss due to permanent capture in dead pores was encountered . Nonetheless, using the split flow analysis approach described in Section 5.6, the measured curves could be modelled reasonably closely, if tracer loss is assumed to be permanent.

Both lysimeter experiments were modelled using the material specific and bed operational parameters established in the experiments. For the small column agreement between modelled and measured data (in terms of Cr(VI) and Na) was reasonable in terms of onset, slope and bottom levels of the drop-off curve, but poor in predicting initial behaviour of both species considered. For Cr(VI) this was attributed to poor choice of reaction model,

necessitating further experimental investigation, and for Na to inaccurate assessment of bed saturation and mixing effects between slow and fast moving phases currently not considered in the model.

Model predictions were generally poor for the data of the larger column. This is attributed to poor assessment of bed saturation and the likeliness of significant dead pore volume. It also shows, that the results of the tracer analysis of the smaller column are not directly scaleable to the situation in the larger column and more sophisticated characterisation of the hydrodynamic conditions in unsaturated beds is required. These can be taken into account if the model is suitably expanded.

The unsatisfactory correlation between modelled and measured data is, however, not taken as a failure of the overall modelling and assessment strategy put forward in Chapter 5. It merely indicates that the model formulated in Chapter 3 requires expansion to take account of effects occurring in unsaturated bed situations and that suitable assessment methods need to be drawn up which characterise the hydrodynamic behaviour of such beds independent of scale.

8

Conclusions

The main objective of the work presented in this thesis is the development of a mathematical model which describes the process of leachate generation and transport in solid waste deposits. Such a model allows insight into the time-dependent development of concentrations of environmentally harmful constituents in the effluent from such waste deposits.

It is postulated in the Introduction (Chapter 1) that the model can be used to assess the leachate generation potential of a particular waste material in a full scale deposit scenario *a priori* on the basis of a systematic laboratory investigation. The particular attractiveness of such an approach is that it allows predictive modelling of leachate generation for a number of different deposit scenarios and can thus inform the selection of appropriate waste management strategies to minimise the risk of adverse environmental impact.

The laboratory assessment methodology that was proposed, and which is illustrated in Figure 8-1, involves subjecting the waste material under investigation to a lysimeter column study to obtain an initial feel for the chemical conditions prevailing in a deposit situation, as well as a test case against which the model can be verified later. More specific bench scale investigations are then conducted to assess the chemical release behaviour of the material under consideration with regard to the constituents of concern. The hydrodynamic behaviour of the material in a deposit situation is also assessed through tracer studies in column experiments. From the experimental data, characteristic reaction and transport parameters, with which the model is calibrated, are derived. The

transport parameters, with which it is calibrated, are derived. The leach curves of the initial lysimeter studies are then simulated and compared with the experimental data. If good agreement is achieved it can be assumed with some confidence that the assessment is completed. The calibrated model can now be used to predict leach scenarios in full scale deposits of the material tested.

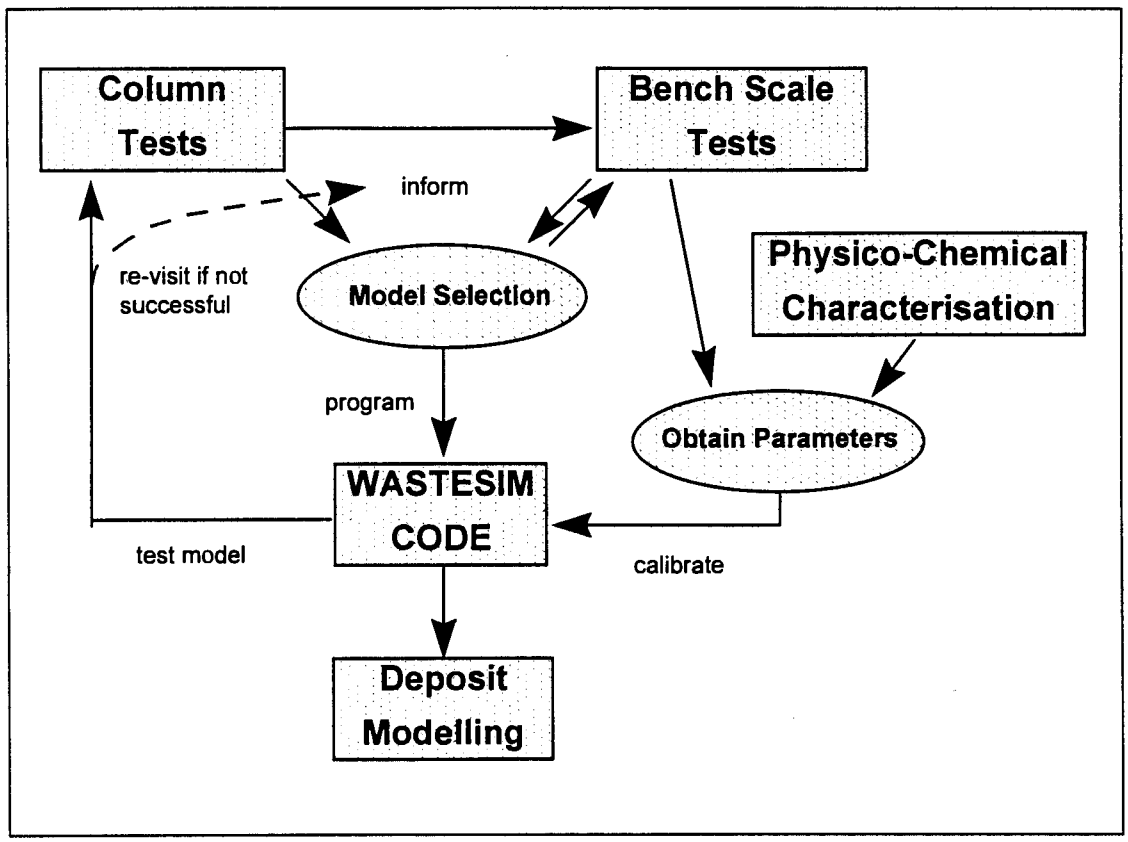

Figure 8-1: The waste assessment methodology

In order to test this methodology and hence prove or disprove the hypothesis, extensive experimental work was conducted with two waste materials from the ferro-alloy industry, a steel-making furnace dust and a ferro-chromium smelter slag. The primary contaminant of environmental concern in both of these materials is chromium, especially in its toxic hexavalent form. Chromium was therefore taken as the focal species in this work.

The approach taken in this work was first to obtain a solid background understanding of chromium chemistry and the interaction of chromium in the environment (Chapter 2) as well as an appreciation of waste management practice regarding solid waste disposal - both in general, and more specifically concerning the nature, handling and treatment of chromium-containing waste materials (Chapter 3). Chapter 4 continues with a review of the theory underlying contaminant transport through porous media and of existing approaches to model these, before embarking on the development of a more refined model used in this study. In Chapter 5 the proposed assessment methodology is discussed in terms of both experimental methods to be used and ways to analyse the results to obtain waste characteristic model parameters. Chapters 6 and 7 then give detailed account of the experimental and modelling studies conducted with the two waste materials tested.

In this concluding chapter the work presented in this thesis is summarised in terms of the specific approaches taken and the key findings (Section 8.1). This is followed, in Section 8.2, by a critical discussion of the significance of specific findings and the work as a whole. In Section 8.3 recommendations are made as to where further development of both model and assessment approach should go next. Finally, Section 8.4 explores areas and ways in which the work presented herein might ultimately find application.

8.1 Summary

As outlined above, the central objective of the work was to develop a mathematical modelling tool for leachate generation in minerals processing waste deposits. A set of appropriately chosen laboratory tests provides sufficient parameters for this model to allow predictive modelling of the time-dependent leachate generation behaviour of this material in full scale waste deposit scenarios. This combined assessment and modelling strategy was put to the test with two chromium containing waste materials from the ferro-alloy industry.

Chapter 2

The release of chromium species was the main focus within the test work conducted. In order to have full appreciation of the various reaction mechanisms that contribute to release (or attenuation) reactions, a good understanding of chromium chemistry in general is required. This is provided in the detailed review contained in Chapter 2. The main points here are that chromium is mostly present either in its trivalent or hexavalent oxidation state. While the former is largely insoluble in the pH range from 5 to 12, Cr(VI) is mobile at all pH values and considered highly toxic and carcinogenic due to its nature as a strong bio-oxidant. Aqueous chemical reactions involving chromium comprise dissolution / precipitation, adsorption / desorption and oxidation / reduction between the two oxidation states. In natural environments, such as soils, lakes and oceans, all these mechanisms are involved in complex chemical cycles.

Of particular interest, however, is the oxidation of Cr(III) to Cr(VI) through the action of atmospheric oxygen. Although this reaction is thermodynamically feasible, it appears to proceed extremely slowly under ambient conditions and has therefore been largely overlooked in environmental studies. In waste deposits containing trivalent chromium this reaction could, however, lead to the long-term release of Cr(VI) into the leachate. An experimental study of this oxidation reaction with chromic oxide-lime mixtures and with a chromium-containing waste material has confirmed that the reaction takes place in the presence of alkalinity and calcium with a half life in the order of 5 to 10 years.

Chapter 3

The environmental impact of solid waste deposits is directly linked to the leachate generation process within the deposit. Rainwater percolating through the porous matrix of the deposit creates an aqueous environment into which chemical species such as chromium can be released and within which they can migrate to the base of the deposit and from there further into the surrounding environment. An understanding of solid

waste management practice with regard to deposit construction, liners and leachate collection systems can give a good insight into the specific aspects relevant to the leachate generation process in such deposits. Chapter 3 gives a detailed review of these aspects. It becomes clear that modern practice is mainly concerned with maintaining geo-technical barriers between deposit and the surrounding environment and with collecting and treating the leachate before it can cause harm. Little clarity appears to exist, however, with respect to the exact dynamic nature of the leachate generation process itself. Considering that deposit liners and leachate collection systems are costly operations and are not always in place, it is argued that meaningful prediction of leachate generation on the basis of a sound model can greatly help to optimise the efficiency of such operations, both from environmental and economic points of view.

Chapter 4

In the development of a model to describe leachate generation within a porous solid matrix, one would have to combine two aspects of this process - the chemical release of contaminant species from the solid matrix and their transport with and within the moving aqueous matrix. The latter aspect can draw from a substantial body of knowledge available from the modelling of groundwater flow. The relevant theory in this regard, which is reviewed in Sections 4.1 and 4.2, clearly indicates that contaminant migration is governed by convective flow, mechanical dispersion and diffusion. Groundwater modelling generally focuses on saturated flow conditions and the description of unsaturated beds is complicated by the variation of saturation due to seasonal drying and wetting.

The modelling of chemical reactions in aqueous solution can be divided into two main approaches, that of equilibrium calculations on the basis of solution thermodynamics and that based on kinetic rate equations (Section 4.3). While the former is commonplace in the modelling of geo-chemical systems, the latter is usually used for the description of leach processes. A combination of the two approaches appears to be rarely attempted.

A number of computer codes are available which combine chemical reaction modelling with modelling of hydro-transport processes (Section 4.4). These have found application in the modelling of contaminant transport through groundwater and for modelling heap leaching. As heap leaching bears a striking resemblance to the process postulated for leachate generation in solid waste deposits, the heap leach model developed by Dixon (1992) was more closely investigated for adaptation (Section 4.5). This model distinguishes between reaction-diffusion at the level of the individual particle and convection transport in the bulk fluid of a bed packed with such particles. The governing transport equations at both levels are based on the continuity equation and reaction modelling is accounted for by kinetic rate terms.

The model developed in the present study (Section 4.6) expands on the Dixon approach, retaining the particle level model, but incorporating a dispersion term into the bulk equation. A surface zone model is introduced as an additional level to provide a step between the particle and bulk level equations. This allows for the incorporation of surface film diffusion effects, which may need to be accounted for under certain bulk flow conditions, as may be defined by a modified system Peclet number (Section 4.6.2). The model has been formulated also for a batch leach scenario. Here the particle level equation is retained as before, but the bulk level transport equation is replaced by a simple mass balance accounting for accumulation in the leach liquor.

As in the Dixon model, reaction modelling in the present approach is mainly focused on the solid liquid interactions at the particle level, although provision for bulk level reactions is also made. In departure from the Dixon approach, a way has been devised (Section 4.7) to combine reactions described by kinetic rate equations with those described by thermodynamic equilibrium equations (for which it is assumed that equilibrium is established fast). Such reactions include dissolution governed by solubility products, Langmuir and Freundlich adsorption isotherms and the auto-hydrolysis of water (governing pH).

The present modelling approach has been translated into the WASTESIM computer code, which is introduced in Section 4.8.1 and described in some more detail in Appendix B. This code allows simulations of multi-species, multi-reaction processes in porous or non-porous particles of single size or a distribution of sizes in batch leach reactors or various column leach scenarios, and is thus an extremely versatile tool for modelling the processes thought to govern leachate generation. This has been demonstrated in a model sensitivity study, described in Section 4.8.2. Starting from a base case, the simulated leach curves of a hypothetical waste material (which in many ways resembles the real waste materials tested in the context of this work) are compared on the basis of various modifications to the model parameters, such as particle size, size distribution, pore diffusivity, reaction types and constants, factors affecting bed residence time, bed dispersion and bed saturation.

Many significant aspects emerged from this study, but two key aspects merit specific mention. One is the influence of particle pore diffusion on the time-dependent release behaviour of a dissolving constituent. While this may significantly influence the leach curves in a batch leach scenario, this effect becomes negligible in a column scenario if particle sizes are small and bed residence times long. The other aspect is that of bed saturation, which influences both solid to liquid ratio in the column bulk fluid and fluid residence time in the bed. This aspect has quite a marked effect on the simulated leach curves, but is difficult a quantity to measure in practice. These aspects are more critically discussed in Section 8.2.

Chapter 5

For a model to generate meaningful predictions of the leaching behaviour of a waste material in a deposit situation, model components and the parameters with which it is calibrated must be obtained from a rigorous laboratory assessment of the waste material in question. While a number of such waste assessment techniques have been in use for the typing of potentially hazardous waste materials, often on the basis of worst case

assumptions involving comparatively aggressive leach media, these techniques offer little insight into the dynamic leach characteristics of a material in a deposit situation. The laboratory assessment methodology put forward in Section 5.1 (and re-iterated in the introduction to this chapter) is aimed at providing a more meaningful approach in this regard. The basic philosophy of this approach is to conduct all reaction characteristic experiments in an environment that is chemically similar to that likely to occur in a waste deposit (which is established from an initial lysimeter experiment) and test the outcome of this study immediately against an independent test case (such as the initial lysimeter study) with the help of the model. This way the waste characterisation can be confirmed before modelling of a full scale deposit is attempted. Various experimental methods for this waste assessment methodology in terms of lysimeter column and batch leach studies, adsorption and diffusion experiments are described in Chapter 5, and guidelines are given for the interpretation of experimental data in terms of model parameters. In some instances the WASTESIM code in the batch simulation mode can actually be used to obtain these parameters by curve fitting the experimental data (Section 5.4).

The hydrodynamic conditions in the deposit bed in terms of bed saturation, bed residence time and flow distribution are equally important for the meaningful prediction of leach scenarios. Tracer studies are a useful method to reveal information about these. Although the model in its current state of development is not equipped to handle flow distributions, a method is proposed to interpret the results from column tracer studies in terms of a two flow approach in which the column is conceptually divided into two parallel "half-columns" with different flow-rates. These can be modelled separately and the respective effluent concentrations conceptually mixed by calculating the weighted average. This approach is described in Section 5.6. Dead pore diffusion is, however, not adequately modelled by this approach and some avenues are explored how this can be accounted for in future model expansions.

The proposed laboratory assessment methodology and validation using the model is put to the test with two chromium-containing waste materials from the ferro-alloy industry. Each of these has been subjected to a whole suite of lysimeter studies, batch leach and adsorption experiments, column tracer tests, etc., the results of which are detailed in Chapters 6 and 7, respectively. For both materials the focus was on the release of chromium, particularly Cr(VI), but the release of other species (particularly those of Na and K) was also considered, where directly relevant. It should be pointed out, however, that the two materials were completely different in physical and chemical nature, and the two studies should only be compared in terms of successes and limitations of model and methodology.

Chapter 6

For the first material, an emission control dust from a stainless steel smelter, the release of Cr(VI) appeared to be controlled by a combination of pH-dependent dissolution and adsorption and that of Cr(III) by pH-dependent solubility. The material is characterised by its strong alkalinity, mainly attributed to the dissolution of Na and K hydroxides. As it consists entirely of micron-sized particles, pore diffusion effects were assumed to be negligible as observed dissolution effects appeared more or less instantaneously. The reaction parameters of the model were calibrated on the basis of the experimental data, and batch leach experiments were successfully reproduced in WASTESIM computer simulations.

In a column situation the material exhibited high hydraulic resistance due to the small particle size. Bulk transport was assumed to be mainly governed by the slow bulk convection and molecular diffusion. The effective bed diffusion coefficient was assessed in a stagnant bed leach experiment and was found to correspond well with the rule-of-thumb value of $\varepsilon/2$. A column tracer study was conducted in a lysimeter experiment to establish the hydro-dynamic conditions, which indicated a narrow distribution of residence times with a small tail-end. Some difficulty was experienced in assessing the

degree of bed saturation, which appeared to change from 80% to fully saturated in the course of the experiment. Modelling the tracer response curve with the WASTESIM code yielded best results assuming a fully saturated bed. The two flow approach was attempted, resulting in very good emulation of the measured response curve, although the modelled curve showed a slightly shorter time lag than the experimental data.

The leach curves obtained from two independent lysimeter experiments (MD1: 52 cm high, flowrate < 80 ml/day; MD2: 27 cm high, flowrate > 500 ml/day) were simulated with the WASTESIM code calibrated entirely with parameters obtained from other laboratory experiments. For Na and K very close agreement was obtained for both columns, assuming saturated bed conditions and using the split flow approach. For Cr(VI) good agreement was only achieved if the adsorption reaction, as observed in the batch leach experiments, was taken as irreversible. No clarity exists as to why this should be so and further experimentation would be needed to clarify this observation.

The modelling approach was nonetheless considered successful, as it predicted the leach curves of the two lysimeter experiments equally well, although they were run under significantly different conditions. This is taken as a strong indication that the model can indeed be used to predict the leach behaviour in larger scale scenarios on the basis of small-scale laboratory studies.

Chapter 7

The second material, a ferro-chromium smelter slag, is characterised by small, highly porous granules with a mean particle size of around 2 mm. For this material the release of chromium was found to be controlled by a combination of some instant dissolution, a slow, kinetically controlled release and adsorption. None of these reactions appeared pH-controlled in the region considered. The release of Na, which was entirely attributed to instant dissolution, was also monitored for comparison. Although the material consists of porous particles, particle pore diffusion effects were found to be negligible,

as the very high porosity (>50%) and relatively small particle size do not seem to offer significant resistance to pore diffusion. A kinetic constant for the release of Cr(VI) was established through curve-fitting using WASTESIM simulations of a batch leach experiment.

The hydrodynamic conditions in beds of this material were not easily assessed, as the bed exhibited low and varying degrees of saturation (around 30%) and a significant loss (15-20%) of the percolating fluid to evaporation. A column tracer study indicated a wide distribution of flows; a protracted tail-end associated with slow diffusion from stagnant zones; and significant tracer loss assumed to be due to retention in dead pores. The tracer response curve could, however, be modelled reasonably well using the two flow approach.

The leach curves obtained from two independent lysimeter experiments (one 50 cm and one 174 cm column, same flow rate) were simulated with the WASTESIM code calibrated entirely with parameters obtained from other laboratory experiments. For the small column, agreement between simulated and measured curves was reasonable, but slightly over-predicted. This was mostly attributed to unsatisfactory determination of bed saturation. For the tall column, model predictions compared to the measured data only in trend, but the actual concentrations differed by as much as 30%. Again, this is attributed to insufficient hydro-dynamic characterisation. Additionally, here the effect of dead pore diffusion may strongly influence the leach profiles due to the longer residence times in the bed.

Also in this case study, the discrepancies between modelled and measured curves are not seen as a failure of the overall assessment and modelling approach, but merely highlight the fact that meaningful description of hydrodynamic phenomena, particularly in unsaturated beds, is of the same importance as chemical characterisation. The model in its current state of development is as yet not sufficiently equipped to handle these effects.

8.2 Concluding Discussion

As formulated in the introduction to this work, there is currently no comprehensive method or tool which allows the assessment of the potential for leachate generation in solid minerals processing waste deposits. The development of such a tool was the central objective of this thesis, and it was hypothesised that the combination of a rigorous mathematical model - describing the reaction and transport processes likely to occur in waste deposits - with a methodical laboratory study of the waste material in question, will achieve this objective. In the present work such a study has focused on the release and transport of chromium species from chromium-containing waste materials from the ferro-alloy industry.

Modelling the Leachate Generation Process

Existing laboratory methods to assess the leach potential of solid waste material tend to focus on establishing maximum possible - or "worst case" - leach potential, often by leaching in comparatively aggressive leach media. These methods, however, mostly fail to take cognisance of the time-dependent nature of the leach process. This time-dependence is introduced through the kinetic nature of some release reactions, but, more importantly, through the dynamic transport of dissolved constituents through and with the aqueous matrix in the bed. These transport processes, which include diffusion, convection and hydrodynamic dispersion, can best be appreciated with the help of a rigorous mechanistic model.

The model developed in Chapter 4, which is based on a careful review of existing approaches found in the modelling of groundwater flow and heap leaching, offers a unique approach, as it combines equation (4.6-1), which describes reaction-diffusion in the pores of the individual particle, with equation (4.6-13), which describes one-dimensional convection-dispersion in the bulk fluid. These two model levels can be linked directly or via a surface zone equation (4.6-9), which would account for surface

to bulk mass transfer resistance. Whether these are significant, can potentially be established by analysis with a modified Peclet number, but this avenue and use of the surface zone equation has not been explored further in modelling work within this work.

Also in terms of reaction modelling the present approach offers a unique combination of reaction types that can be described by a kinetic rate equation with those described by a thermodynamic equilibrium model (Section 4.7). This is a significant advantage as previous work has indicated that neither reaction type alone is sufficient to describe the chemically complex and dynamic reaction processes at the solid-liquid interface.

The model equations have been expressed in numerical form and integrated into the WASTESIM computer code, which offers a user-friendly platform on which a large variety of waste leach scenarios can be created by specifying a number of characteristic parameters which relate directly to those employed in the various transport and reaction model equations. Once fully specified, WASTESIM can immediately simulate a leach scenario and displays the time-dependent leach curves on-screen. Thus WASTESIM is an extremely versatile and interactive tool for the modelling of the rather complex leachate generation process.

For meaningful modelling runs, however, the characteristic parameters that determine the reaction and transport behaviour need to be obtained for a particular waste material in a particular deposit scenario. This can only be achieved through a rigorous assessment of the material in question and such an assessment will need to be done through laboratory experimentation. The key questions that need to be addressed in this context can be formulated as follows:

- How are laboratory experiments best designed to reveal as much relevant information as possible with the least experimental effort?
- How is experimental data used to devise and calibrate an appropriate model ?
- How can the model, calibrated with these parameters, be tested?

Experimental Design

As was already indicated above, many existing waste characterisation procedures, such as the TCLP, establish the worst case behaviour of the waste material under relatively aggressive conditions. As such they are of little use in helping to calibrate a model that is specifically aimed at describing the leach process under *real* conditions. This was clearly shown in the two experimental studies. The TCLP leach was conducted with both materials, although the results of these tests had no bearing on the calibration and testing of the model. In the case of the LCS material the TCLP test would have actually passed this material as environmentally acceptable with the Cr(VI) concentrations just below the 5 mg/l limit after the recommended 18 hour leach period. These results demonstrate that tests such as the TCLP have in fact little value in the meaningful prediction of leachate generation in deposit scenarios, at least for the materials investigated here, although they are commonly employed as yardsticks for precisely this purpose.

The assessment methodology put forward in Chapter 5 suggests that realistic conditions are best established from lysimeter studies, which are likely to mimic conditions in full-scale waste deposits. Such studies can inform the design of more specific laboratory experiments, which are likely to produce meaningful results. The experimental methods described in Chapter 5 were employed in the present study, but it is acknowledged that not all of these were successful in revealing the desired information. The methods proposed here need to be seen as preliminary and their applicability needs to be assessed in each particular case study.

Data Interpretation

Regarding the interpretation of experimental data, a significant feature of the model is the distinction between reaction-diffusion processes at the level of the individual particle and the various transport processes at the bulk level. This allows the particle

level model to be "disconnected" and combined with another bulk model describing the mass balance of a batch reactor (equation 4.6-16). All model parameters relating to particle level processes (such as all reaction parameters and the effective diffusivity through the particle pores) will remain unchanged, irrespective of whether a batch or column leach scenario is being modelled. This feature can be exploited to establish parameters from batch experiments which are equally valid in a full-scale deposit. This approach has been demonstrated for the establishment of the effective pore diffusivity and a kinetic leach constant from batch experimental data (Chapter 7).

The COLUMN mode of WASTESIM can be used to obtain model parameters from experimental data, particularly for the interpretation of tracer study results. Column tracer studies were found to be a particularly useful method for the establishment of hydro-dynamic conditions in packed beds of the waste material under investigation. This has been demonstrated in both case studies (Chapters 6 and 7). Flow through such beds is likely to result in a distribution of flows through zones of varied permeability and effects relating to diffusion from dead pores. In unsaturated beds the degree of bed saturation significantly influences the bulk transport characteristics. To account for the distribution of flows the two flow analysis approach, presented in Section 5.6, can be employed. This approach allows the use of the WASTESIM code to model such columns, although it is only designed for one single flow velocity. This has been successfully demonstrated for the MD waste material (Chapter 6). Dead pore diffusion effects, however, can not be incorporated into the model at its present state of development. This was found to be a limitation in the modelling of the LCS material, for which this effect was likely to be significant (Chapter 7). Possible avenues for model expansions to account for this effect have been investigated in Section 5.6.3.

Thus the work in this thesis has clearly shown how model parameters determining both reaction and transport behaviour of a particular waste material can be obtained entirely from laboratory scale experimentation and how the model can itself be used in the interpretation of experimental data. The overall assessment methodology (Figure 8-1)

put forward in Chapter 5 offers a way to bridge the gap that has thus far existed between laboratory waste characterisation and the leachate generation process in full-scale waste deposit scenarios.

Testing Model and Calibration

The model parameters obtained from extensive laboratory assessment, as well as the chosen model itself, need to be put to the test by comparison of time-dependent leach data from a large scale deposit scenario against curves simulated using WASTESIM, which incorporates the chosen transport and reaction models calibrated with the corresponding parameters. The assessment methodology proposed that this was to be done initially with data gathered from an independent lysimeter study. This way possible shortcomings of the assessment could be detected and improved upon through further experiments and/or model modifications.

In the present study this approach has been fairly successful for the MD material (Chapter 6) with close agreement achieved between modelled and measured effluent pH and concentration profiles of Cr(VI), Na and K, which were the species on which the assessment focused. But for Cr(VI) this agreement was only achieved when adsorption, which was identified in bench-scale experiments, was taken as an irreversible reaction (which corresponds to a correction of the chosen model), which has not yet been confirmed in independent experiments. This should not, however, be seen as a failure of the overall approach as it can be attributed to insufficient characterisation of the reaction behaviour of the material in question. This can be improved through further experimental work.

Testing model and calibration for the LCS case (Chapter 7) was less successful, with significant discrepancies between modelled and measured data for all species considered (Cr(VI), Na and K), although the general trends corresponded well. These discrepancies were more attributed to insufficient characterisation of the hydro-dynamic conditions of

the bed than the chemical characterisation of the material. As indicated above, transport through unsaturated beds is characterised by a distribution of flows as well as dead pore diffusion. The model is not equipped to handle the latter effect, but it is considered to be a significant factor in beds of the LCS material, with its highly porous and irregularly shaped particles. Thus the study with this material has identified a shortcoming of the model which will have to be addressed by further development. The slow kinetic release of Cr(VI), however, should also be investigated more closely to ensure that insufficient characterisation of this effect has not also contributed to the poor modelling results.

The unsatisfactory closure between modelled and measured data is insufficient to disprove the central hypothesis of this work, that modelling of deposit scenarios on the basis of a systematic laboratory assessment is possible *in principle*. It merely highlights the need for ongoing development of both model and laboratory methods to improve the quality of predictions.

The central aims of this work have therefore been achieved. A rigorous mathematical model, which describes the leachate generation process in waste deposits, has been formulated and implemented in a computer modelling code. It was hypothesised that this model can predict in a meaningful way the release and transport of hazardous constituents from waste materials in a deposit situation - on the basis of calibration with parameters obtained from a methodical assessment of the waste material in question. Proof of this hypothesis has been achieved through extensive investigations with two chromium containing waste materials. It is acknowledged that both model and experimental methodology require further expansion and refinement, but the overall approach is valid and merits further consideration.

The Way Ahead

In terms of the methodology illustrated in Figure 8-1 the experimental work presented in this thesis has followed the assessment loop (lysimeter study - bench scale study -

model selection - parameter determination - model testing) through one cycle. The results from the initial model tests were sufficiently encouraging to accept that the approach should be pursued further. The next stage would be to return to bench scale experiments and model development to achieve improvement of the model predictions, but keeping in mind that any new or revised parameter needs to be supported by independent experimentation.

Once model and calibration have been shown to perform satisfactorily within the assessment procedure, it still needs to be seen whether predictions will be successful when the model is taken to the full scale. Although no full scale experimental work has been conducted in the context of this work, experimental work and the model sensitivity study (Section 4.8) have highlighted two aspects in this regard, which need to be considered carefully before embarking on a full scale study.

Long Term Effects

The first of these aspects is the question of scaling in time. Most batch leach experiments conducted in this study were conducted over 24 hours or at best over a few days. The lysimeter column studies, which reflect deposit scenarios, were conducted over anything between 30 days and 14 months. The life span of a full scale waste deposit is more likely to be indefinite, but even if it is assumed that active leaching from such deposits ceases after some time (and there is as yet no basis for this assumption), then, still, this time frame would likely be in the order of decades. This difference in scale has some significant implications for the relative importance of some mechanisms of the overall leach process over others.

The model sensitivity study (Section 4.8) has shown that time-dependent processes, such as particle pore diffusion or kinetic leaching, which appear significant in a 24 hour batch leach experiment, appear to be more or less instantaneous when the same material

is modelled in a small scale lysimeter experiment with a residence time of 15 days. It is conceivable that this effect would appear even more pronounced in a full scale scenario. On the other hand, mechanisms that may go unnoticed in batch leach studies, such as a very slow reaction mechanism with a half life in the order of months or years, may start to become significant in full scale deposit scenarios exhibiting long residence times. This effect was clearly demonstrated in the context of the long-term atmospheric oxidation of chromium (Section 2.3). This reaction was difficult to establish in a 5 day batch reactor experiment, but clearly evidenced over a 2 year period in a column study with a real waste material. In order to account for such long-term reactions in model predictions in full scale deposits, the question that still requires clarification is how these effects can be appropriately established and quantified through laboratory experiments.

Conditions in Full Scale Deposits

The second aspect that needs to be considered when taking the information from laboratory assessment to full scale modelling is that of scaling in space. While this should not have any implication for the particle level reaction modelling, it may significantly affect the hydro-dynamic characterisation of the bed, particularly under unsaturated conditions. The comparison of model predictions for the small and the large LCS lysimeter column (Chapter 7) has indicated that predictions at the larger scale are worse than those for the smaller scale, for which the hydrodynamic conditions had been established through a tracer study. This has been attributed to increased influence of dead pore diffusion and general uncertainty regarding the degree of bed saturation, which may in fact be variable, non-uniform and a function of bed dimensions and further of local climatic conditions (Section 4.1). The model sensitivity study has shown that the degree of bed saturation, even if it is taken as constant and uniform throughout the bed, strongly influences the shape of the modelled leach curves. Thus there exists some doubt whether laboratory scale characterisation of hydro-dynamic parameters such as the distribution of flows and bed saturation can be simply extrapolated to describe the

conditions in a full scale deposit. The underlying theory of flow through unsaturated porous media needs to be carefully re-evaluated and, if necessary, the model needs to be expanded.

Closure

This work has shown that predictive modelling of leachate generation in waste deposits is possible in principle. Model predictions can, however, only be as good as the parameters on which the model is based. Meaningful parameters can be established through a systematic laboratory investigation of the waste material in question, but validation of these parameters by testing against independent lysimeter studies is recommended, before full scale modelling is attempted. But even if such validation is obtained, care needs to be taken that long-term reaction effects as well as full-scale hydrodynamic characterisation are appropriately accounted for. Further development work will have to address the latter aspects in particular.

8.3 Recommendations for Further Work

The preceding section has clearly stated that the overall modelling and assessment approach is valid and that further development should be pursued in order to address the shortcomings that have been identified through the experimental study. The main areas of further developments are briefly discussed in the following.

Expansion to other contaminant species and multi-species modelling

The present work has focused primarily on the release and transport of chromium species, mainly Cr(VI), from waste materials in which these were the contaminants of

concern. Release and transport of other ionic species (mainly Na and K) was only considered where these directly or indirectly influenced the release of Cr. The model (and the WASTESIM code) is, however, not limited to these particular species and can also be used for non-ionic dissolved species (such as organics). The assessment methodology is also not restricted to chromium, although some of the experiments conducted within this study were specifically aimed at the interactions of chromium species. Multi-species modelling has to some extent already been employed in the present studies. Reactive interaction between species were, however, restricted to the control of pH. The model's robustness with respect to multi-species, multi-reaction modelling has not yet been put to the test.

It is recommended that the modelling and assessment approach is tested with respect to heavy metal species other than chromium and that the experimental methods employed in this study are critically revisited with respect to their applicability to these. This expansion, particularly if it is combined with the simultaneous modelling of other species, requires thorough understanding of the underlying chemistry. Background studies, similar in extent to what was investigated for chromium, should be conducted for these before specific experimental methods are designed.

Expansion and categorisation of reaction mechanisms

Reaction modelling is currently restricted to the reaction types described in Section 4.7. Although it was indicated that other reaction types can be incorporated in similar fashion to these, this work is currently still outstanding. With respect to the modelling of interactions in waste deposits, reactions leading to the phenomenon of acid rock drainage (Section 3.2.6) and the resulting secondary leach reactions need to be given serious attention. Likewise, avenues should be explored for the incorporation of reactions resulting from biological activities (such as oxidising bacteria).

As was indicated in Section 4.9, equilibrium reaction modelling does not at this stage consider non-ideal solution thermodynamics, which may be a considerable drawback for complex multi-species reaction systems. Incorporation of these should be considered, although this may seriously compromise the current numerical simplicity of the WASTESIM code. However, some clarity needs to be obtained on the extent to which rigorous thermodynamic modelling does improve the quality of model predictions, considering the quality of material characterisation that can realistically be achieved.

As indicated in the discussion in the preceding section, particular attention needs to be given to kinetically slow reactions, which may not be noticed in short term laboratory experimental studies. Given that there is generally a time constraint on a waste characterisation programme, it is unrealistic that such assessment can be achieved for each material studied. The establishment of a database of slow kinetic reactions could therefore be considered, as well as the development of some simple method of establishing which of these reactions are likely to apply for a particular waste material. It needs to be seen to what degree such an approach would remove the uncertainties associated with the prediction of these slow reaction mechanisms.

Modelling and assessment of transport in unsaturated beds

As was indicated in the preceding section and Section 4.9, the model's capabilities with respect to phenomena in unsaturated bed scenarios are currently fairly limited. While the two flow approach offers significant improvement over single flow modelling, this approach has not as yet been fully explored and still requires incorporation into the WASTESIM code. Multiple flow modelling could also be considered in this regard.

Modelling of dead pore diffusion still requires incorporation into the model. To account for this effect, modification of the surface zone model (equation (4.6-9)) could be

considered, although this has not yet been put to the test in the present studies. Gas adsorption and transport through the gas phase in a deposit are another aspect that have not yet been considered, although Dixon (1996) has already given indications as to how this could be achieved with relative ease. In this context it would be interesting to see to what extent CO_2 adsorption and the interactions of carbonates can be predicted by the model. The assessment of hydrodynamic conditions in full scale deposits also needs to be re-evaluated. It is not clear at this stage to what extent laboratory scale studies can be extrapolated meaningfully in this regard.

Full scale validation of the approach

The ultimate test for model and assessment methodology is validation of a full scale scenario with field data. It is felt, however, that such a validation exercise should be deferred until model and methodology have been expanded and tested sufficiently at the laboratory scale to a point that very good agreement between simulated and measured data is achieved at this level. It is likely that scaling to full deposit scenarios will always introduce a level of uncertainty into the model predictions. In order to assess this uncertainty, it should be ensured that as little uncertainty as possible is introduced through the laboratory assessment on the basis of which this scale-up is conducted.

8.4 Future Applications of the Model and the Assessment Methodology

The work presented in this thesis lays the foundation for a comprehensive modelling and assessment strategy aimed at providing a tool for the prediction of leachate generation in waste deposits. It is now worth looking at the future applications such a tool could potentially have.

Environmental Risk Assessment

As was already outlined in the Introduction to this thesis, industry is faced with increasing pressures to maintain environmentally sound operations, and the legal liability for cases of pollution arising out of a particular process is more and more commonly placed with its operators. In terms of waste deposits this liability does not cease with the closure of a particular operation, but is usually maintained until sufficient certainty exists that the risk of future adverse environmental impact is minimal. In the interim the former operator has to ensure that appropriate monitoring and, if necessary, leachate collection is maintained.

The risk of environmental impact during industrial activity and beyond is an operational risk and, with the liability for any costly clean-up action resting with the operators, it is also an economic risk. As the environmental risk associated with solid waste deposits is directly linked to the process of leachate generation, the proposed modelling and assessment methodology would be an invaluable tool for risk assessment. It would inform the operators of a disposal activity about whether and when to expect the emergence of a hazardous leachate at the bottom of a deposit. It could also help licensing authorities to establish when the risk of future leachate generation of a particular deposit is sufficiently minimal so that a closure certificate can be issued.

Optimising Waste Disposal Strategies

The modelling and assessment strategy allows the prediction of leachate generation from a deposit scenario entirely on the basis of a laboratory scale investigation. Thus full scale deposit scenarios can be modelled even before they are constructed. An opportunity exists, therefore, to attempt modelling of a number of full scale deposit scenarios to allow comparison of the leachate generation behaviour as indicated in Figure 8-1. Such comparisons can be used to identify optimal disposal strategies for minimising the leachate generation potential, for example in terms of deposit height and area covered, packing method, comminution of particles and so forth. It is even

conceivable that deliberate leaching (i.e. operating a waste deposit like a heap leach) could achieve quick down-wash of the dissolvable constituents and may therefore be preferable to slow leaching at ambient conditions.

Another optimisation that could possibly be achieved indirectly from conducting systematic waste assessments is that of process technology. The presence of problem species (often present in traces) that is identified for a particular waste material can often be related back to inefficiencies in the process that generated this material. Through appropriate modification or substitution of process technology these problem species might no longer exist in the waste material or in much reduced concentrations, rendering the waste less hazardous or even environmentally benign.

Modelling Heap Leaching

The model developed within this study was originally derived from models developed for heap leaching, as heap leach scenarios are in many ways similar to waste leach scenarios. There is no reason, however, why the model (and the WASTESIM code) should not continue to find application in the modelling of heap leach scenarios. The expansions to the Dixon model (Section 4.5) appear well suited to more realistically account for flow and transport conditions in unsaturated heaps.

Modelling Transport Through Soils

The model is also not restricted to describing the process of leachate generation, but could well be used to describe the process of leachate attenuation when it migrates through the porous structure of unsaturated soil zones. This would be useful to model pollution scenarios and the spread of a contaminant plume down from the source of pollution towards the groundwater level. While the spread of contaminants in groundwater is well described in groundwater modelling software, description of generation and migration through the unsaturated soil at the source site is not yet well covered, and the present approach could find potential application in this context.

The minerals processing industry, which is by far the largest generator of solid mineral wastes world-wide and is challenged with increasingly stringent environmental pressures, should welcome the development of a tool that allows meaningful assessment of leachate generation potential and thus the environmental risk associated with its waste deposits. The fundamental structures of this tool have been developed and tested in the present work and avenues for further expansions and refinements have been explored. The application of the modelling approach in optimisation studies can potentially lead to much improved waste disposal strategies being employed in the future.

References

Aldrich, J.R. (1997) Sludge Generation from Ferrous/Sulfide Chromium Treatment. Air Force Eng. Serv. Cent., Eng. Serv. Lab., Technical Report ESL-TR-84-27 (Tyndall Air Force Base, Florida 32403, U.S.A.).

Alloway, B.J. and Ayres, D.C. (1993) *Chemical Principles of Environmental Pollution*, London: Blackie Academic & Professional.

Anderson, N.J., Bolto, B.A. and Pawlowski, L. (1984) A Method for Chromate Removal fromm Cooling Tower Blowdown Water. *Nuclear and Chemical Waste Management* **5**, 125-129.

Aoki, T. and Munemori, M. (1982) Reduction of Chromium(VI) by Iron(II) Hydroxide in Alkaline Solution. *Bull. Chem. Soc. Jpn.* **55**, 730-732.

Apel, W.A. (1990) Separation and Concentration of Hazardous Metals from Aqueous Solutions Using Sulphate Reducing Bacteria. *Bioprocess Engineering Symposium 1990.* Vol. **16**, 75-80.

Apel, W.A. and Turick, C.E. (1991) Bioremediation of Hexavalent Chromium by Bacterial Reduction. *Minerals Bioprocessing 1991*, Smith, R.W. and Misra,. M (Eds.) pp. 376-387.

Aris, R. (1975) *The Mathematical Theory of DIffusion and Reaction in Permeable Catalysts - The Theory of the Steady State*, Oxford: Claredon Press.

Arniella, E.F. and Blythe, L.J. (1990) Solidifying Traps Hazardous Waste. *Chemical Engineering* 92-102.

Baes, C.F. and Mesmer, R.E. (1976) Chromium. In: *The Hydrolysis of Cations*, pp. 211-219. New York: John Wiley and Sons.

Barcza, N.A. (1996) The Role of Pyrometallurgy in the Development of South Africa. *SAIMM* **96**, 229-239.

Bartlett, R.J. (1991) Chromium Cycling in Soils and Water: Links, Gaps and Methods. *Environmental Health Perspectives* **92**, 17-24.

Bartlett, R.J. and James, B.R. (1979) Behaviour of Chromium in Soils: III. Oxidation. *J. Environ. Qual.* **8**, 31-35.

Bartlett, R.J. and James, B.R. (1988) Mobility and Bioavailabilty of Chromium in Soils. In: Nriagu, J. (Ed.) *Chromium in the Human and Natural Environment*, pp. 267-304. New York: John Wiley and Sons .

Bartlett, R.J. and Kimble, J.M. (1976) Behaviour of Chromium in Soils: I. Trivalent Forms. *J. Environ. Qual.* **5**, 379-382.

Bartlett, R.J. and Kimble, J.M. (1976) Behaviour of Chromium in Soils: II. Hexavalent Forms. *J. Environ. Qual.* **5**, 383-386.

Bartlett, R.W. (1992) Simulation of Ore Heap Leaching Using Deterministic Models. *Hydrometallurgy* **29**, 231-260.

Batchelor, B. (1990) Leach Models: Theory and Application. *J. Hazard. Mater.* **24**, 255-266.

Baturay, O., Shirk, J.E. and Sigerson, A.L. (1991) Method for Removing Chromium from Chromium Containing Waste Material. US Patent 5,007,960. Application No. 421,136. (Apr 16, 1991).

Bear, J. (1972) *Dynamics of Fluids in Porous Media*, New York: American Elsevier.

Beszedits, S. (1988) Chromium Removal From Industrial Waste Waters. In: Nriagu, J. (Ed.) *Chromium in the Human and Natural Environment*, pp. 231-265. New York: John Wiley and Sons .

Bird, R.B., Stewart, W.E. and Lightfoot, E.N. (1960) *Transport Phenomena*, New York: John Wiley & Sons.

Bishop, P.L. (1986) Prediction of Heavy Metal Leaching Rates from Stabilized/Solidified Solid Wastes. *Mid-Atlantic Industrial Waste Conference 1978*. Boardman, G.D. (Ed.) pp. 236-252.

Burke, T., Fagliano, J., Goldoft, M., Hazen, R.E., Iglewizc, R. and McKee, T. (1991) Chromite Ore Processing Residue in Hudson County, New Jersey. *Environmental Health Perspectives* **92**, 131-137.

Calder, L.M. (1988) Chromium Contamination of Groundwater. In: Nriagu, J. (Ed.) *Chromium in the Human and Natural Environment*, pp. 215-229. New York: John Wiley and Sons .

Coetzer, G., Giesekke, E.W. and Guest, R.N. (1994) Hexavalent Chromium in the Processing of Ferrochrome. MINTEK pp. 93-104.

Cohen, B. (1997) Cement-Based Solidification of Ferro-Alloy Solid Wastes. PhD Thesis. University of Cape Town, Cape Town, South Africa.

Conner, J.R. (1986) Fixation and Solidification of Wastes. *Chemical Engineering* **86**, 79-85.

Conner, J.R. (1993) Stabilising Hazardous Waste. *CHEMTECH* **93**, 35-44.

Cote, P.L. (1986) Contaminant Leaching From Cement-Based Waste Forms Under Acidic Conditions. PhD Thesis. McMasters University,Canada.

Cote, P.L. and Bridle, T.R. (1987) Long-Term Leaching Scenarios For Cement-Based Waste Forms. *Waste Management & Research* **5**, 55-66.

Cox, X.B., III and Linton, R.W. (1985) Determination of Chromium Speciation in Environmental Particles, Multitechnique Study of Ferrochrome Smelter Dust. *Environ. Sci. Technol.* **19**, 345-352.

Crank, J. (1975) *The Mathematics of Diffusion*, 2nd edn. Oxford: Claredon Press.

CRC (1992) *CRC Handbook of Chemistry and Physics*, 73rd edn. Boca Raton, Fl., USA: CRC Press.

Daniel, D.E. (1993) *Geotechnical Practice for Waste Disposal*, London: Chapman & Hall.

Davies, G.M. (1995) Prediction of Leachate Generation from Minerals Processing Waste Deposits. MSc Thesis. University of Cape Town, Cape Town, South Africa.

Dawson, M.F. and Edwards, R.I. (1984) An Alternative Route for the Production of Chromium Chemicals from Chromite. *Report MINTEK* M50.

Deltombe, E., De Zoubov, N. and Pourbaix, M. (1966) Chromium. In: Pourbaix, M. (Ed.) *Atlas of Electrochemical Equilibria*, pp. 256-271. Pergamon Press.

Demetracopoulos, A.C., Sehayek, L. and Erdogan, H. (1986) Modeling Leachate Production from Municipal Landfills. *J. Environ. Eng.* **112**, 849-866.

Dixon, D.G. (1992) Predicting the Kinetics of Heap Leaching with Unsteady-State Models. University of Nevada, Reno, USA.

Dixon, D.G. (1996) Revised Equations for Dixon's Heap Leach Model Involving One Gaseous and One Aqueous Reagent.(private communication Sep 10, 1996).

Dixon, D.G. and Hendrix, J.L. (1993) A Mathematical Model for Heap Leaching of One or More Solid Reactants from Porous Or Pellets. *Metallurgical Transactions B* **24B**, 1087-1102.

Dixon, D.G. and Hendrix, J.L. (1993) A General Model for Leaching of One or More Solid Reactants from Porous Ore Particles. *Metallurgical Transactions B* **24B**, 157-169.

Dreisinger, D.B., Peters, E. and Morgan, G. (1990) The Hydrometallurgical Treatment of Carbon Steel Electric Arc Furnace Dusts by the UBC-Chaparral Process. *Hydrometallurgy* **25**, 137-152.

Drews, S.C. and Mahote, S.I. (1994) Laboratory Leach Tests for Modelling Hazardous Waste Containment. Research Report. Department of Chemical Engineering, University of Cape Town.

Dzombak, D.A. and Morel, F.M.M. (1990) *Surface Complexation Modeling - Hydrous Ferric Oxide*, New York: John Wiley & Sons.

Eary, L.E. and Rai, D. (1987) Kinetics of Chromium(III) Oxidation to Chromium(VI) by Reaction with Manganese Dioxide. *Environ. Sci. Technol.* **21**, 1187-1193.

Eary, L.E. and Rai, D. (1988) Chromate Removal from Aqueous Wastes by Reduction with Ferrous Ion. *Environ. Sci. Technol.* **22**, 972-977.

Elderfield, H. (1970) Chromium Speciation In Seawater. *Earth Planet Sci. Lett.* **9**, 10-16.

Espenson, J.H. (1970) Rate Studies on the Primary Step of Reduction of Chromium(VI) by Iron(II). *J. Am. Chem. Soc.* **92**, 1880-1883.

Espenson, J.H. and King, E.L. (1963) Kinetics and Mechanisms of Reactions of Chromium(VI) and Iron(II) Species in Acidic Solution. *J. Am. Chem. Soc.* **85**, 3328-3333.

Farrow, C.J. and Burkin, A.R. (1973) Alkali Pressure Leaching of Chromium(III) Oxide and Chromite Mineral. *Leaching and Reductive Hydrometallurgy [Hydrometallurgical Meeting] 1973.* pp. 20-27.

Fendorf, S.E. and Zasoski, R.J. (1992) Chromium(III) Oxidation by MnO2. 1) Characterisation. *Environ. Sci. Technol.* **26**, 79-85.

Freeze, R.A. and Cherry, J.A. (1979) *Groundwater*, Englewood Cliffs, NJ: Prentice-Hall.

Fruchter, J.S., Rai, D. and Zachara, J.M. (1990) Identification of Solubility-Controlling Solid Phases in A Large Fly Ash Field Lysimeter. *Environ. Sci. Technol.* **24**, 1173-1179.

Gmelin (1962) Chrom(III)-Hydroxyhydrate. In: Pietsch, E.H.E. (Ed.) *Gmelins Handbuch der Anorganischen Chemie*, 8th edn. pp. 60-81. Weinheim/Bergstrasse, Germany: Verlag Chemie GMBH.

Hagni, A.M., Demars, C. and Hagni, R.D. (1991) Mineralogy of Electric Arc Furnace Dusts. *EPD Congress '91*. Gaskell, D.R. (Ed.) pp. 801-809.

Hanewald, R.H., Munson, W.A. and Schweyer, D.L. (1991) Metal Recovery from Spent Acid Solutions and Baghouse Bags Using the Inmetco Process. In: Reddy, R.G., Imrie, W.P. and Queneau, P.B. (Eds.) *Residues and Effluents- Processing and Environmental Considerations*, pp. 842-857.

Hartford, W.H. (1979) Chromium Compounds. In: *Kirk & Othmer Encyclopedia of Chemical Technology*, 2nd edn. pp. 82-120.

Hattori, M., Yaku, K. and Nagaya, K. (1978) Treatment of the Sludge Containing Chromium and Calcium by Heating with Silica. *Environ. Sci. Technol.* **12**, 1431-1434.

Ipatiew, W.W. and Platonowa, M.N. (1932) Oxidation von Chromhydroxyd und Chromeisenstein durch Luft-Sauerstoff in Gegenwart von Alkali. *Ber. dt. chem. Ges.* **65B**, 572-575.

Jackson, D.R., Garrett, B.C. and Bishop, T.A. (1984) Comparison of Batch and Column Methods for Assessing Leachability of Hazardous Waste. *Environ. Sci. Technol.* **18**, 668-673.

Jacobs, J.H. (1992) Treatment an Stabilisation of Hexavalent Chromium Containing Waste Material. *Environ. Prog.* **11**, 123-126.

James, B.R. and Bartlett, R.J. (1983) Behaviour of Chromium in Soils: VII. Adsorption and Reduction of Hexavalent Forms. *J. Environ. Qual.* **12**, 177-181.

James, B.R. and Bartlett, R.J. (1983) Behaviour of Chromium in Soils: V. Fate of Organically Complexed Cr(III) Added to Soil. *J. Environ. Qual.* **12**, 169-172.

James, B.R. and Bartlett, R.J. (1983) Behaviour of Chromium in Soils: VI. Interactions Between Oxidation-Reductionand Organic Complexation. *J. Environ. Qual.* **12**, 173-176.

Johnson, C.A. and Xyla, A.G. (1991) The oxidation of chromium(III) to chromium(VI) on the surface of manganite (g-MnOOH). *Geochim. Cosmochim. Acta* **55**, 2861-2866.

Jones, D.R. (1995) The Leaching of Major and Trace Elements from Coal Ash. In: Swaine, J. and Goodarzi, F. (Eds.) *Environmental Aspects of Trace Elements in Coal*, pp. 221-262. Kluwer Academic Publishers.

Kaltenhauser, R. (1987) Recycling Furnace Dust. *Industrial and Scientific Metallurgy* **87**, 23-26.

Kent, B. and Hemingway, M.P. (1993) Monitoring Wells. In: Daniel, D. (Ed.) *Geotechnical Practice for Waste Disposal*, pp. 607-650. London: Chapman & Hall.

Kent, B. and Mann, P. (1993) Recovery Well Systems. In: Daniel, D. (Ed.) *Geotechnical Practice for Waste Disposal*, pp. 497-519. London: Chapman & Hall.

Kilau, H.W. and Shah, I.D. (1984) Chromium-Bearing Waste Slag: Evaluation of Leachability When Exposed to Simulated Acid. *Hazardous Industrial Waste Management and Testing, Third Symposium.* ASTM STP 851. Jackson, L.P., Rohlik, A.R. and Conway, R.A. (Eds.) pp. 61-81.

Korfiatis, G.P., Demetracopoulos, A.C., Bourodimos, E.L. and Nawy, E.G. (1984) Moisture Transport in a Solid Waste Column. *J. Environ. Eng.* **110**, 780-796.

Kornelius, G. and Boegman, N. (1994) Water Soluble Components in Dust From Ferro-Alloy Production. *NACA Conference, Somerset West, South Africa.* pp. 1-7.

Leismann, H.M. and Frind, E.O. (1989) A Symmetric-Matrix Time Integration Scheme for the Efficient Solution of Advection-Dispersion Problems. *Water Resources Research* **25**, 1133-1139.

Levenspiel, O. (1972) *Chemical Reaction Engineering*, 2nd edn. New York: John Wiley & Sons.

Madsen, B.W. and Wadsworth, M.E. (1981) A Mixed Kinetics Dump Leaching Model for Ores Containing a Variety of Copper Sulfide Minerals. Report RI 8547, U.S. Department of the Interior, Bureau of Mines.

Mangold, D.C. and Tsang, C. (1991) A Summary of Subsurface Hydrological and Hydrochemical Models. *Review of Geophysics* **29**, 51-79.

Mayer, L.M. (1988) Geochemistry of Chromium in the Oceans. In: Nriagu, J. (Ed.) *Chromium in the Natural and Human Environment*, pp. 173-187. New York: John Wiley & Sons.

McGrath, S.P. and Smith, S. (1990) Chromium and Nickel. In: Alloway, J. (Ed.) *Heavy Metals in Soils*, pp. 125-150. Glasgow and London: Blackie.

Moran, J.M., Morgan, M.D. and Wiersma, J.H. (1986) Ecosystems: The Flow of Energy and Materials. In: *Introduction to Environmental Science*, 2nd edn. pp. 29-61. New York: Freeman & Co.

Nakayama, E. (1981) Chemical Speciation of Chromium in Seawater. Part 2: Effects of Manganese Oxides and Reducible Organic Materials on the Redox Process of Chromium. *Anal. Chim.* **130**, 401-404.

Nakayama, E. (1981) Chemical Speciation of Chromium in Seawater. Part 1: Effect of Naturally Occurring Organic Material on the Complex Formation of Chromium (III). *Anal. Chim.* **130**, 289-294.

Nakayama, E., Tokoro, H., Kuwamoto, T. and Fujinaga, T. (1981) Dissolved State Of Chromium in Seawater. *Nature* **290**, 768-770.

Nieboer, E. and Jusys, A.A. (1988) Biologic Chemistry of Chromium. In: Nriagu, J. (Ed.) *Chromium In the Human and Natural Environment*, pp. 21-79. New York: John Wiley and Sons.

Nriagu, J.O. (1988) Production and Uses of Chromium. In: Nriagu, J.O. (Ed.) *Chromium in the Human and Natural Environment*, pp. 81-103. New York: John Wiley and Sons.

Nriagu, J.O. and Pacyna, J.M. (1988) Quantitative assessment of worldwide contamination of air, water and soils by trace metals. *Nature* **333**, 134-139.

Nyholm, R.S. (1947) The Aerial Oxidation of Trivalent Chromium In Aqueous Solution. *Journal of Science in the Chemical Industry* **66**, 449-451.

Oosthuizen, E.J. and Viljoen, E.A. (1982) Quantitative Mineralogy Applied to a Study of the Process Involved in the Production of Ferrochromium from Transvaal Chromite Ore. *XIV International Minerals Processing Congress.* Toronto, Canada. Vol. **VIII**, p. 6.1-6.17.

Palmer, C.D. and Wittbrodt, P.R. (1991) Processes Affecting the Remediation of Chromium-Contaminated Sites. *Environmental Health Perspectives* **92**, 25-40.

Petersen, J. (1994) Chromium Interconversions in Natural Environments - Potential Implications for Hazardous Leaching from Industrial Waste Landfills. Research Report. Department of Chemical Engineering, University of Cape Town.

Petersen, J. and Petrie, J.G. (1997) A Modelling Strategy to Predict Leachate Generation Within Minerals Processing Waste Deposits. *XX International Minerals Processing Congress*. Aachen, Germany. von Blottnitz, H. (Ed.) Sep 1997. Vol. **5**, 81-90.

Petrie, J.G. and Paxton, R.G. (1996) Integrated Technologies for Treating Liquid and Solid Wastes from Ferrochrome and Stainless Steel Production. *Technical Solutions for Pollution Prevention in the Mining and Minerals Processing Industries*. Palm Coast, Florida. Richardson, P.E., Scheiner, B.J. and Lanzetta, F.J. (Eds.) pp. 329-338.

Petrie, J.G. and Raimondo, J.P. (1997) Attempts to Close Material Cycles in Industrialised Countries: Threat, Challenge or Opportunity for Minerals Exporting Countries. *XX International Minerals Processing Congress*. Aachen, Germany. von Blottnitz, H. (Ed.) Sep 1997. Vol. **5**, 9-25.

Raghu, D. and Hsieh, H. (1989) Origin, Properties and Disposal Problems of Chromium Ore Residue. *Intern. J. Environmental Studies* **34**, 227-235.

Rai, D., Sass, B.M. and Moore, D.A. (1987) Chromium(III) Hydrolysis Constants and Solubility of Chromium(III) Hydroxide. *Inorg. Chem.* 345-349.

Richard, F.C. and Bourg, A.C.M. (1991) Aqueous Geochemistry of Chromium: A Review. *Water Reserves* **25**, 807-816.

Roman, R.J., Benner, B.R. and Becker, G.W. (1974) Diffusion Model for Heap Leaching and its Application to Scale-up. *Transactions, Society of Mining Engineers, AIME* **256**, 247-249.

Ross, D.S., Sjogren, R.E. and Bartlett, R.J. (1981) Behaviour of Chromium in Soils: IV. Toxicity to Microorganisms. *J. Environ. Qual.* **10**, 145-148.

Rowe, R.K. (1988) Eleventh Canadian Geotechnical Colloquium: Contaminant Migration through Groundwater - the Role of Modelling in the Design of Barriers. *Can. Geotech. J.* **25**, 778-798.

Rowe, R.K. (1991) Contaminant Impact Assessment and the Contaminating Lifespan of Landfills. *Can. J. Civ. Eng.* **18**, 244-253.

Rowe, R.K. and Booker, J.R. (1985) 1-D Pollutant Migration in Soils of Finite Depth. *J. Geotech. Eng.* **111**,

Rowe, R.K. and Booker, J.R. (1985) Two-Dimensional Pollutant Migration in Soils of Finite Depth. *Can. Geotech. J.* **22**, 429-436.

Rowe, R.K. and Booker, J.R. (1990) Contaminant Migration Through Fractured Till into an Underlying Aquifer. *Can. Geotech. J.* **27**, 484-495

Rowe, R.K. and Booker, J.R. (1991) Pollutant Migration Through Liner Underlain by Fractured Soil. *J. Geotech. Eng.* **117**, 1902-1919.

Ruhr-Universitaet Bochum (1991) Entwicklung eines Routinetests zur Elution von Schwermetallen aus Abfaellen und belasteten Boeden. Research Report. Ruhr-Universitaet Bochum & Landesamt fuer Wasser und Abfall NRW, Bochum, Germany.

Sag, Y. and Kutsal, T. (1989) The Use of Zoogloea ramigera in Wastewater Treatment Containing Cr(VI) and Cd(II) Ions. *Biotechnology Letters* **11**, 145-148.

Saleh, F., Parkerton, T., Lewis, R., Huang, J. and Dickson, K.L. (1989) Kinetics of Chromium Transformations in the Environment. *The Science of the Total Environment* **86**, 25-41.

Sandell, E.B. (1950) Chromium. In: *Colorimetric Determination of Traces of Metals*, 2nd edn. pp. 257-270. New York: Interscience Publishers

Schroeder, D.C. and Lee, G.F. (1975) Potential Transformations of Chromium in Natural Waters. *Water, Air and Soil Pollution* **4**, 355-365.

Shakelford, C.D. (1993) Contaminant Transport. In: Daniel, D. (Ed.) *Geotechnical Practice for Waste Disposal*, pp. 33-65. London: Chapman & Hall.

Sheehan, P.J., Meyer, D.M., Sauer, M.M. and Paustenbach, D.J. (1991) Assessment of the Human Health Risks Posed by Exposure to Chromium Contaminated Soils. *Journal of Toxicology and Environmental Health* **12**, 161-201.

Spiccia, L. and Marty, W. (1986) The Fate of "Active" Chromium Hydroxide, Cr(OH)3. 3H2O, in Aqueous Suspension. Study of the Chemical Changes Involved in its Ageing. *Inorg. Chem.* **25**, 266-271.

Stegemann, J.A. and Cote, P.L. (1991) Investigation of Test Methods for Solidified Waste Evaluation - A Cooperative Program. Report EPS 3/HA/8, Environment Canada - Wastewater Technology Centre, Ontario, Canada.

Stewart, M. and Petrie, J.G. (1996) Waste Management and Disposal in Minerals Processing. In: *Planning for Closure - Best Practices in Managing Ecological Impact from Mining* (in print).

Stigliani, W. and Salomons, W. (1993) Our Father's Toxic Sins. *New Scientist (12)*, 38-42.

Stollenwerk, K.G. and Grove, D.B. (1985) Adsorption and Desorption of Hexavalent Chromium in an Alluvial Aquifer Near Telluride, Colorado. *J. Environ. Qual.* **14**, 150-155.

Stunzi, H. and Marty, W. (1983) Early Stages of Hydrolysis of Chromium(III) in Aqueous Solution. 1) Characterisation of a Tetrameric Species. *Inorg. Chem.* **22**, 2145-2150.

UCT (1994) Environmental Stability of Chromium Bearing Wastes: Leaching and Potential Oxidation. Research Report. Petersen, J. and Petrie, J.G. (Eds.) Department of Chemical Engineering, University of Cape Town, South Africa.

US EPA (1992) The Toxicity Characteristics Leaching Procedure. USA Code of Federal Regulations 40th edn. Part 261, app. II., Washington, D.C.

van Craen, M.J., Denoyer, E.A., Natusch, D.F.S. and Adams, F. (1983) Surface Enrichment of Trace Elements in Electric Steel Furnace Dust. *Environ. Sci. Technol.* **17**, 435-439.

van der Sloot, H.A. (1990) Leaching Behaviour of Waste & Stabilized Waste Materials: Characterization for Environmental Assessment Purposes. *Waste Management & Research* **8**, 215-228.

van der Weijden, C.H. and Reith, M. (1982) Chromium (III)- Chromium (VI) Interconversions in Seawater. *Marine Chemistry* **11**, 565-572.

van Zyl, D. (1993) Mine Waste Disposal. In: Daniel, D. (Ed.) *Geotechnical Practice for Waste Disposal*, London: Chapman and Hall.

Vanysek, P. (1992) Ionic Conductivities and DIffusion at Infinite Dilution. In: Linde, D.R. (Ed.) *CRC Handbook of Chemistry and Physics*, 73rd edn. pp. 5-111-5-112. Boca Raton: CRC Press.

Vogel, A.I. (1960) Chromium. In: Vogel, A.I. (Ed.) *A Textbook of Quantitative Inorganic Analysis*, pp. 651-652. London: Longmans.

Vogt, M. and Herrling, B. (1990) Simulation of Coupled Geochemical and Transport Processes of an Infiltration Passage Introducing a Vectorized Multicomponent Transport-Reaction Model. *VIII International Conference on Computational Methods in Water Resources*, Venice, Italy. pp. 399-404.

von Blottnitz, H.B. (1994) Development and Assessment of a Hydrometallurgical Process to Treat Chromium-Containing Dusts. MSc Thesis. University of Cape Town, Cape Town, South Africa.

Weng, C.H., Huang, C.P., Allen, H.E., Cheng, A.H.-D. and Sanders, P.F. (1994) Chromium Leaching Behavior in Soil Derived from Chromite Ore Processing Waste. *The Science of Total Environment* **154**, 71-86.

Wiles, C.C. (1988) Solidification and Stabilization Technology. In: Anonymous *Standard Handbook of Hazardous Waste Treatment & Disposal*, pp. 7.85-7.101. New York: McGraw Hill.

Wood, J.K. and Black, V.K. (1916) Aphoteric Metallic Hydroxides. Part III. Chromium Hydroxide. *J.Chem.Soc.* **109**, 164-171.

Yassi, A. and Nieboer, E. (1988) Carcinogenity of Chromium Compounds. In: Nriagu, J. (Ed.) *Chromium in the Human and Natural Environment*, pp. 443-479. New York: John Wiley and Sons.

Zoubolis, A.I., Kydros, K.A. and Matis, K.A. (1995) Removal of Hexavalent Chromium Anions from Solutions by Pyrite Fines. *Wat. Res.* **29**, 1755-1760.

Appendix A

Analytical Equipment and Methods

Metal Analysis Using AA Spectroscopy

For the analysis of metals in solution Atomic Adsorption (AA) Spectroscopy was used. The instrument employed throughout was a Varian SpectrAA 30. The instrument was calibrated before the analysis of each element using standards prepared from commercial standard solutions. The samples were diluted such that the anticipated concentration of the species in question would fall into the optimal instrument calibration range. Some interference was anticipated with some samples from the MD lysimeter experiments (Chapter 6) which exhibited very high concentrations of Na and K. These were checked with test solutions and not found to be significant. Analytical error was found to be in the order of ± 5% .

Fusion Digests

The analysis of metal concentrations in solids were analysed using a sodium peroxide fusion digest. The solid sample is finely ground with pestle and mortar or in a rod mill to -100 μm. 500 mg (carefully weighed) of this powder is intimately mixed with 5 g NaO in a zirconium crucible, which then heated with a gas flame until the mixture ignites. The reaction is then left to proceed until it ceases. The crucible is left to cool down before the residue is carefully washed out with 1 M HCl into a 100 ml volumetric flask and the recovered solution made up to the mark with distilled water. The metals of interest can now be analysed using AA spectroscopy as outlined above and their concentration in the original sample calculated.

Cr(VI) Analysis Using Spectrophotometry

Cr(VI) was analysed using the Diphenyl-carbazide Method as suggested by Sandell (1950). The carbazide analytical solution is prepared by dissolving 0.2 mg diphenyl-carbazide crystals in 50 ml ethanol, mixing this with 250 ml 0.5 M H_2SO_4 in a 500 ml volumetric flask and making up to the mark with distilled water. For analysis 5 ml of the sample solution, diluted to a Cr(VI) concentration of less than 2 mg/l, are mixed with 7.5 ml of the carbazide mixture. A deep purple colour indicates the presence of Cr(VI), the intensity of which is analysed on a Spectrophotometer set to 543 nm wavelength. The instrument used in throughout this work was a Varian Cary 1E UV Spectrophotometer. The instrument was calibrated with standards prepared from a commercial standard solution before each run of analyses. Analytical error was in the order of ± 2% or better. Interference from dissolved Fe species is well known in this type of analysis, but as Fe concentrations in all samples were significantly lower than Cr(VI), this was not a problem in the present study.

True Density Measurement Using A Pycnometer

The true solids density (i.e. the mass of the solid per unit volume excluding all pore volume) was measured using a helium pycnometer. The instrument used throughout this study was a Micromeritics AccuPyc 1330.

pH Measurement

All pH measurements were conducted using a standard Corning combination electrode with a display instrument. The instrument used initially during the experimental work (most lysimeter studies) was a Hanna Instruments 8525. This instrument was calibrated with reference pH electrolytes regularly, but due to a circuit fault, calibration was not stored automatically and therefore the measured pH values were somewhat uncertain (in the order of ± 0.2 pH units, but as much as ± 0.5 pH units for pH > 13.5). After this fault

was detected, the instrument was replaced by a Corning Ion Analyser 250, which performed without any problems and with an accuracy in the order of ± 0.02 pH units.

Electron Microscopy

All electron-micrographs presented in this thesis were taken at the UCT Electron Microscope Unit on a custom built unit.

BET Surface Area Analysis

These were conducted on a Micrometrics ASAP 2000.

Appendix B

An Introduction to WASTESIM,

Model Solution Algorithms & Numerical Methods

WASTESIM - A Brief User Manual

This appendix briefly outlines the functionality of the WASTESIM modelling code, its broad structure, the underlying model solution algorithms and the numerical methods employed. A proto-type DOS based version of the WASTESIM (© UCT, 1998) modelling code is included on the disk attached to this volume. At the DOS prompt either type A:\WASTESIM\WASTESIM.EXE to run the program directly from the disk, or copy the entire contents of the A:\WASTESIM\ directory into a directory on your local hard-drive or network. Note that all files in this directory must be copied.

The program consist of a parameter entry platform and several modelling modules which are called directly from the platform. The layout of the platform is described in terms of the main menus in Figure B-1.

The PARAMETER menu calls the various screens on which the various model parameters can be directly entered. The complete list of all model and simulation parameters that can be manipulated in WASTESIM is given in Table 4.4 (in Section 4.8). The various screens are fairly self-explanatory, so only a brief summary of these is given here. Some of the screens are record screens i.e. they are rewritten for each item defined (this applies for information on dissolved and solid species, particle size classes and reactions). Use Previous and Next on the menu to switch between records, AddRec to add, DeleteRec to delete a record.

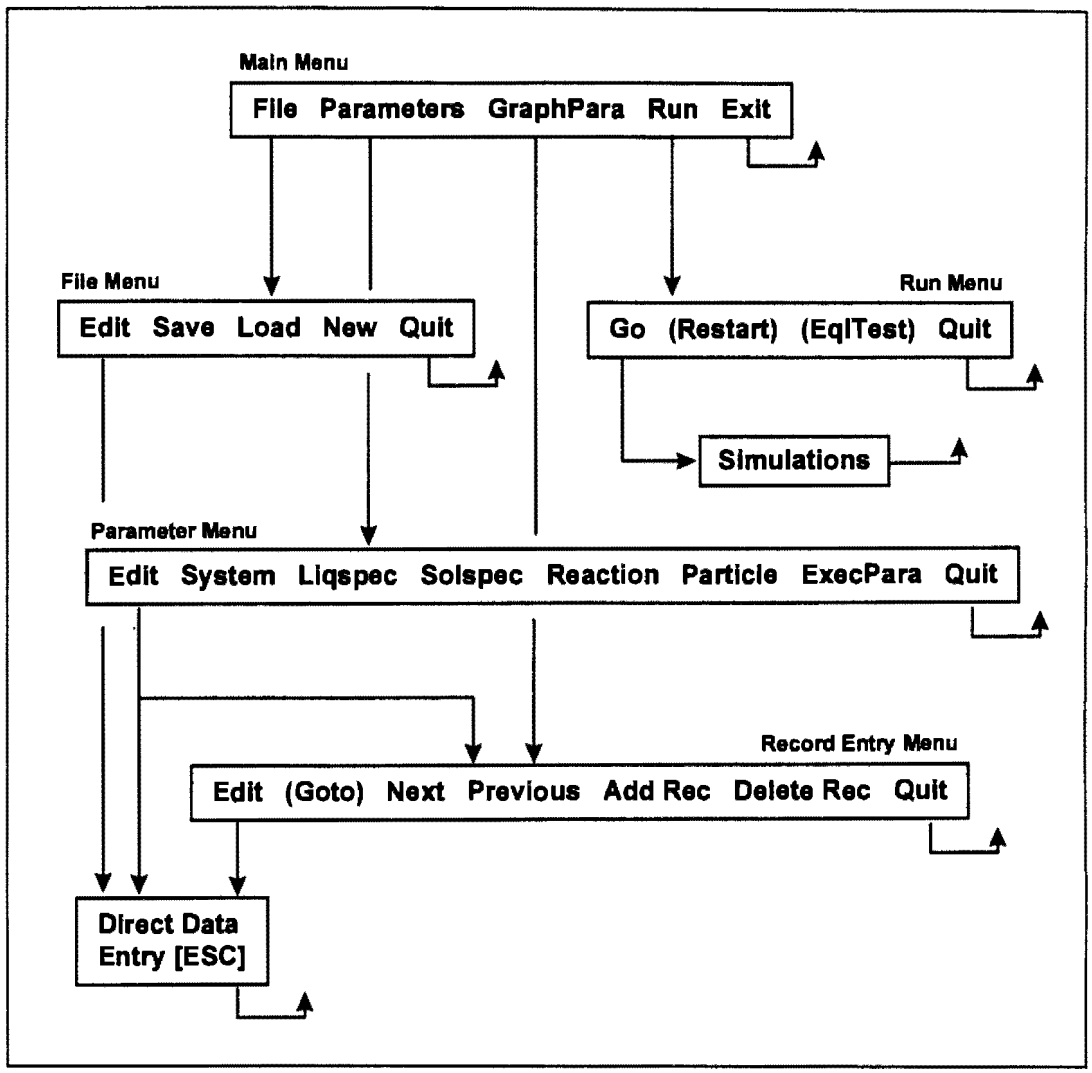

Figure B-1: Menu structure of the WASTESIM data platform

- SYSTEM: Here the modelling mode (PARTICLE, BATCH or COLUMN, see Section 4.8) is set and all parameters describing the column (bed height, bed area, feed flow rate, etc.) or the batch reactor (liquid volume, solid charge mass) are entered. Ensure all parameters are entered in the units as indicated. Also on the SYSTEM screen there are a number of switches to enable/disable particle pore modelling, surface film modelling and the batch column mode (which is a combination of column and batch modes used to model the stagnant bed leach experiment (Section 5.4).

- LIQSPECS: Here all parameters for each dissolved species considered are set, such as name, molecular mass, zero concentration (i.e. concentration at the beginning of a run), feed concentration (i.e. concentration in the feed to a column or initial bulk concentration in a batch reactor) and free solution diffusivity (values for these can be found in CRC, 1992). Note that this screen is a record screen.

- SOLSPECS: Similar to the LIQSPEC menu all parameters defining a solid species considered are entered (name molecular mass, initial solid concentration, surface concentration).

- REACTION: On this record screen individual reactions are defined by setting the reaction type (see Section 4.7), participating species, stoichiometric coefficients and a reaction constant (kinetic or equilibrium).

- PARTICLE: Here all particle and material specific parameters are entered. The include the true solid density, porosity and the effective pore diffusion factor d_{eff}, as well radii and mass fractions of the various size classes in a distribution. Only these two parameters can be varied from record to record. Care needs to be taken that the mass fractions do add up to 1.

- EXECPARA: On this screen some simulation parameters are set, such as the initial time increment, the number of time steps before a point is plotted and the total simulation time

On the FILING menu directories and names for files are set. The files associated with the program are run files (*.rnf) and result files (*.res). In the run files all parameters defined on the user screens are stored (use the SAVE command to save and LOAD to recall). The file blankrun.rnf contains the default values.

On the GRAPHPARA menu the species for which the concentration profiles will be displayed during the simulations are set. Also a set of up to 10 data points can be defined, which will be displayed (useful if the program is used for curve fitting).

The actual simulation runs are started from the RUN menu with the GO command. Depending on the run mode chosen (PARTICLE, BATCH or COLUMN, on the Parameters:System screen) different simulation screens will be displayed (see Figures 4-20 to 4-22 in Section 4.8). On these the concentration profiles through the particle (or column) and the time dependent concentration profiles in the effluent (or batch bulk liquor) will be displayed for those species selected on the GraphPara screen. In each run the required solution modules are loaded and the system is initialised before the user is prompted to begin the run. During the run the total simulation time and the current time increment are continuously displayed as well as a counter indicating the current simulation interval. All curves are updated after the number of intervals specified on the Parameters:ExecPara screen. The run continues until the specified stop time or halted if any key is pressed. If the run was halted a menu will appear which lets the user change the time increment, continue or exit the run. If the run is exited (either after completion or interruption), the time dependent effluent (or batch fluid) concentration profiles will be written to the result file (*.res) as specified on the File screen. The program will then automatically return to the data entry platform.

Solution Algorithms and Numerical Methods

The WASTESIM modelling code is entirely based on the mathematical model presented in Section 4.6 and the reaction equations detailed in Section 4.7. The following is a general description of the way the various equations have been discretised, the numerical calculation methods employed as well as the generalised solution algorithms. The WASTESIM code was originally developed in Turbo Pascal ™, but detailed code listings are not given here.

Discretisation

Numerical solution of the model equations requires discretisation in both space and time. Space is approximated by a grid of nodes for which concentrations are defined, and progression in time is taken in discrete steps of given length. A space differential can then be approximated by the difference between two nodes and thus differential equations can be reduced to linear difference equations, which can be solved arithmetically for each time step.

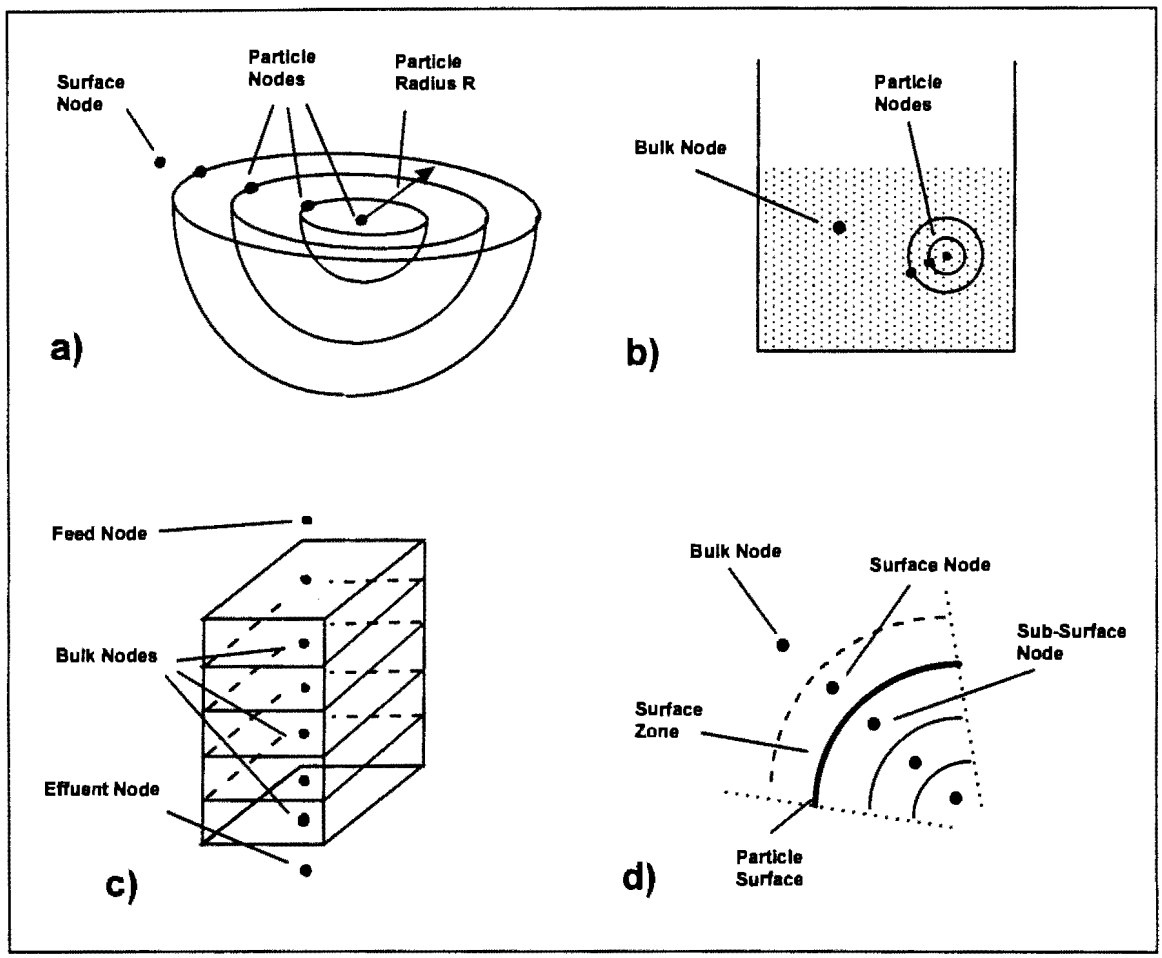

Figure B-2: Model discretisation for a) particle, b) batch reactor, c) column disks and d) surface zone

The present modelling approach distinguishes between the individual particle and bulk conditions. The individual particle is taken as a porous sphere, with transport in radial direction only (Equation 4.6-1). Therefore the inner particle space is subdivided into radial

nodes, each representing a homogeneous shell of the particle space (Figure B-2.a). This node sub-division is applied for particles from each size class considered. The number of particle nodes is currently fixed at 20.

The concentrations immediately at the surface of the particle are contained in a further node, the particle surface node. For the batch model (Equation 4.6-16) this represents the only node outside the particle as concentrations in the bulk fluid of a batch reactor are assumed to be well mixed and homogeneous (Figure B-2.b)

The waste column is taken as a stack of disks, each of which is taken as a node with concentrations representative of the disk (Figure B-2.c). This node is termed a bulk node. The number of disks (and hence bulk nodes) can be selected on the Parameters:System screen in the WASTESIM platform). If the particles within each disk are in direct contact with the bulk fluid, the bulk node represents the surface node for each particle class in this disk. If, however, a surface zone is assumed (Section 4.6.2), then a node is assigned for each particle size class in each disk and this surface zone node steps in between particles and the bulk node as shown in Figure B-2.d.

Solving the Reaction Matrix

For each node the concentrations of all species participating in the system are stored. This applies to both, species dissolved in the fluid associated with the node and those in the solid matrix associated with the node. As indicated in Section 4.7, each species can undergo a large number of reactions which involve a number of other species, both solid and dissolved. Distinction was made between reactions described by a kinetic expression and those described by thermodynamic equilibrium.

As was shown in Section 4.7, the progression of a kinetic reaction or the shift in an equilibrium reaction can be calculated for each discrete time step in terms of the extent

variable e_C, which can be translated into a contribution of each reaction to the change in concentration of all species involved (see equation 4.7-7).

When solving a matrix of reactions for a multi-component system, both kinetic and equilibrium reactions occur simultaneously and are likely to interfere with each other in terms of influencing the total solution concentrations of the species involved, making the calculation of concentrations after each time step for each node not a trivial exercise.

The present approach is illustrated in Figure B-3. The kinetic and equilibrium reactions are calculated separately. First only the change in concentrations of the species involved in kinetic reactions is calculated on the basis of the concentrations at the beginning of the time step. Subsequently an overall equilibrium of all species is calculated using an equilibrium solver module, which simultaneously optimises all equilibrium reactions (see Appendix B for numerical methods). This is taken as a first guess for the concentrations at the end of the time step. The procedure is now repeated, calculating the kinetic contributions on the basis of both the concentrations at time t and the temporary forward estimate, giving a better approximation in terms of the modified Euler method (equation (B.1), which represents the linearised version of equation (4.7-14)).

$$\frac{c_S^{(t+\Delta t)} - c_S^{(t)}}{\Delta t} = -\frac{k}{2}\left(c_A^{(t)} c_S^{(t)} + c_A^{(t+\Delta t)} c_S^{(t+\Delta t)}\right) \qquad \text{(B.1)}$$

Subsequent to this, again equilibrium is calculated, improving the forward estimate. This is continued until kinetic contributions no longer change. The final equilibrium contributions are then calculated on the basis of the last temporary concentrations.

This procedure generates two sets of information - the final concentrations of all species at the end of each time step and the contributions *each* reaction in the matrix has made to the changes within this time step. This reaction-by-reaction approach offers great advantage in under-specified systems, as mass balance consistency between solid and dissolved species

can be maintained without knowing the fate of the associated counter-ions. The reaction contributions can also directly feed into the source/sink terms of the various transport equations.

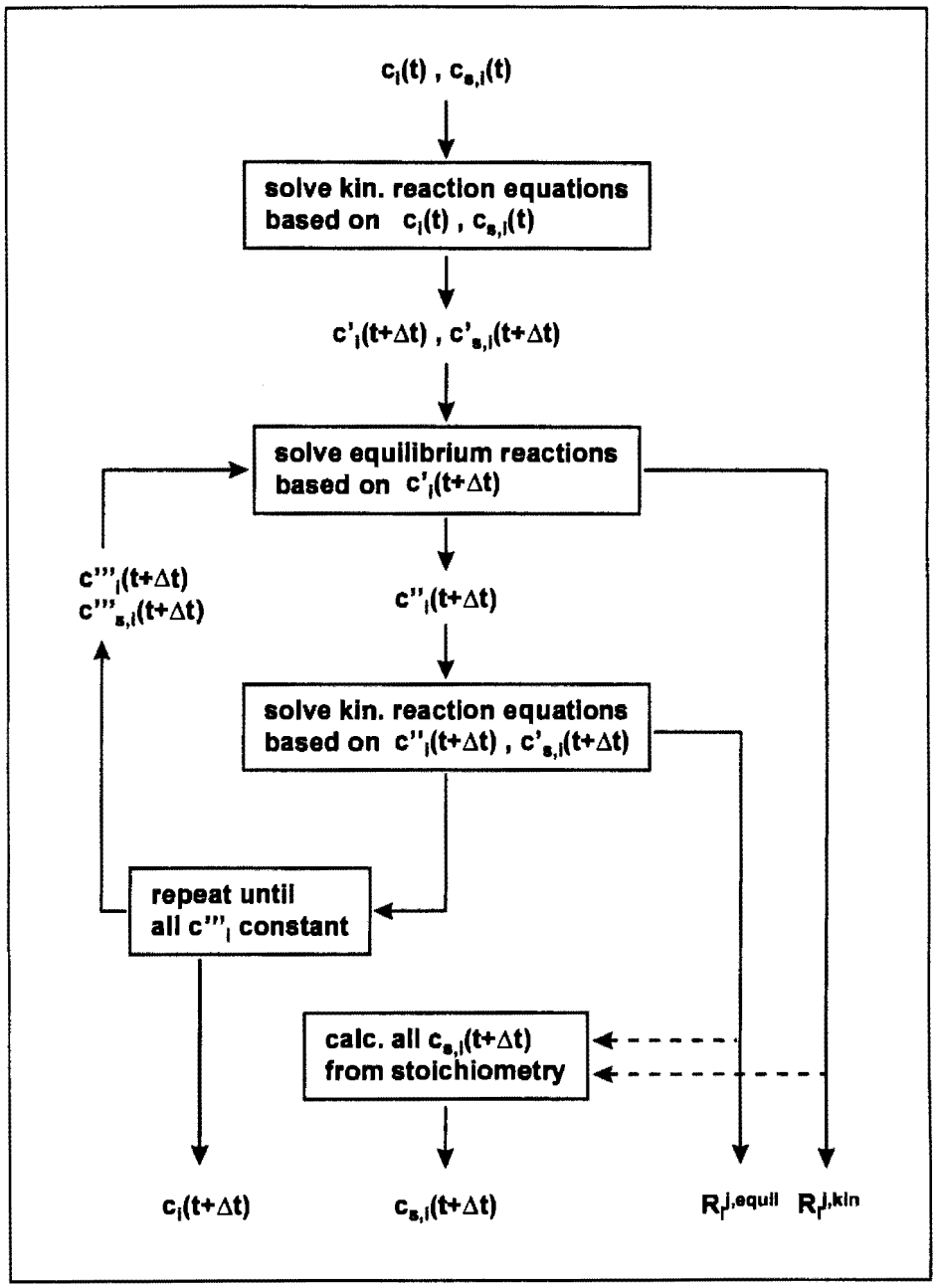

Figure B-3: General solver algorithm for multi-reaction systems

Solving the Particle Equation

The particle level equation (4.6-1), which is a second order partial differential equation in radial direction and time is approximated numerically by a Crank-Nicholson algorithm, which offers sound numerical stability (Davies, 1996). Equation (B.2 a) gives the numerical version for equation 4.6-1 for the centre node (node counter s = 0), equation (B.2 b) for all internal nodes (s = 1 to N-1) and equation (B.2 c) for the surface node (s = N). These equations represent a set of N equations in N unknown concentrations $c_i^{(t+\Delta t)}$ and can be solved using a tri-diagonal matrix inversion scheme.

a) for centre node s=0:

$$\frac{D_{ei}}{2}\left[\frac{3}{\left(\frac{\Delta r}{2}\right)}\left(\frac{c_{pi}^{1,t}-c_{pi}^{0,t}}{\Delta r}+\frac{c_{pi}^{1,t+1}-c_{pi}^{0,t+1}}{\Delta r}\right)\right]+\varepsilon_p\sum_j R_i^j=\varepsilon_p\frac{c_{pi}^{0,t+1}-c_{pi}^{0,t}}{\Delta t}$$

b) for nodes s=1 to N-1:

$$\frac{D_{ei}}{2}\left[\left(\frac{c_{pi}^{s+1,t}-2c_{pi}^{s,t}+c_{pi}^{s-1,t}}{(\Delta r)^2}+\frac{c_{pi}^{s+1,t+1}-2c_{pi}^{s,t+1}+c_{pi}^{s-1,t+1}}{(\Delta r)^2}\right)+\frac{2}{s\Delta r}\left(\frac{c_{pi}^{s+1,t}-c_{pi}^{s-1,t}}{\Delta r}+\frac{c_{pi}^{s+1,t+1}-c_{pi}^{s-1,t+1}}{\Delta r}\right)\right]+\varepsilon_p\sum_j R_i^j=\varepsilon_p\frac{c_{pi}^{s,t+1}-c_{pi}^{s,t}}{\Delta t}$$

c) for surface node s=N: $c_{pi}^{N,t}=c_{si}^{t}$ (B.2)

This approach determines the new concentrations of a species i for all internal nodes on the basis of the concentrations at the beginning of the time step, the reaction contributions calculated by the reaction solver and an estimate of the concentration at the (external) surface, and thus a new concentration profile for i through the particle is established.

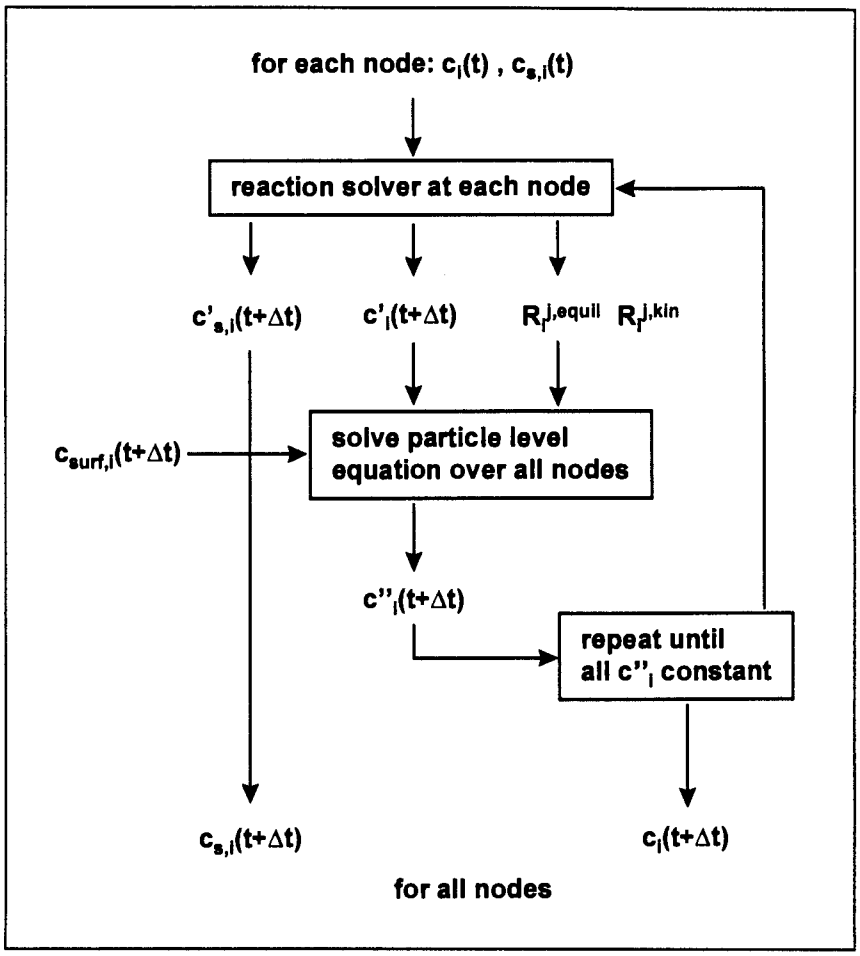

Figure B-4: Solver algorithm for particle level equation

A schematic of the solution algorithm for the particle solver module is given in Figure B-4. As the concentrations of each species at each node may change through diffusion transport during each time step, which in turn effects the reaction contributions, the solution algorithm involves an iterative procedure between calculating reaction contributions at each node for all species and solving the transport equations for each species over all nodes. Reaction and transport modelling are closely interlinked in this way.

Solving the Batch Equation

The batch reactor equation (4.6-16) is essentially a mass balance equation accounting for the change of each species in the reactor bulk fluid on the basis of migration into and out of particle pores and reaction on the particle outer surface. As such it is a first order differential equation in time only and can be solved by a simple forward modified Euler method (equation (B.3)).

$$-\frac{YD_{ei}\varepsilon_p}{2}\sum_n \alpha_n\left(\frac{c_{Bi}^t - c_{N-1}^{(n),t}}{\Delta r^{(n)}} + \frac{c_{Bi}^t - c_{N-1}^{(n),t}}{\Delta r^{(n)}}\right) + \sum_j R_i^j = \frac{c_{Bi}^{t+1} - c_{Bi}^t}{\Delta t}$$

$$\text{with} \quad \sum_n \alpha_n = \sum_n \frac{3w^{(n)}}{R^{(n)}}, \quad Y = \frac{M_{part}}{\rho_t(1-\varepsilon_p)V_{liq}},$$

thus

$$c_{Bi}^{t+1} = \frac{c_{Bi}^t\left(1 - \frac{YD_{ei}\varepsilon_p\Delta t}{2}\sum_n \frac{\alpha_n}{\Delta r^{(n)}}\right) + \frac{YD_{ei}\varepsilon_p\Delta t}{2}\sum_n \frac{\alpha_n}{\Delta r^{(n)}}\left(c_{N-1}^{(n),t} + c_{N-1}^{(n),t+1}\right) + \Delta t\sum_j R_i^j}{1 + \frac{YD_{ei}\varepsilon_p\Delta t}{2}\sum_n \frac{\alpha_n}{\Delta r^{(n)}}}$$

$$\text{also} \quad \Delta r^{(n)} = \frac{R^{(n)}}{N_{pore}} \quad \text{with } N_{pore} \text{ number of pore nodes} \tag{B.3}$$

Interfacing with the particle level equation is achieved by estimating the concentrations at the first sub-surface node of each particle size class, which thus requires iterative switching between solving the particle level equations and the bulk level equation. This is shown in Figure B-5. Incorporation of reactions at the (external) surface is done in a similar fashion as for the particle level model, with iterative switching between the reaction calculation at the bulk node and solution of the bulk equation.

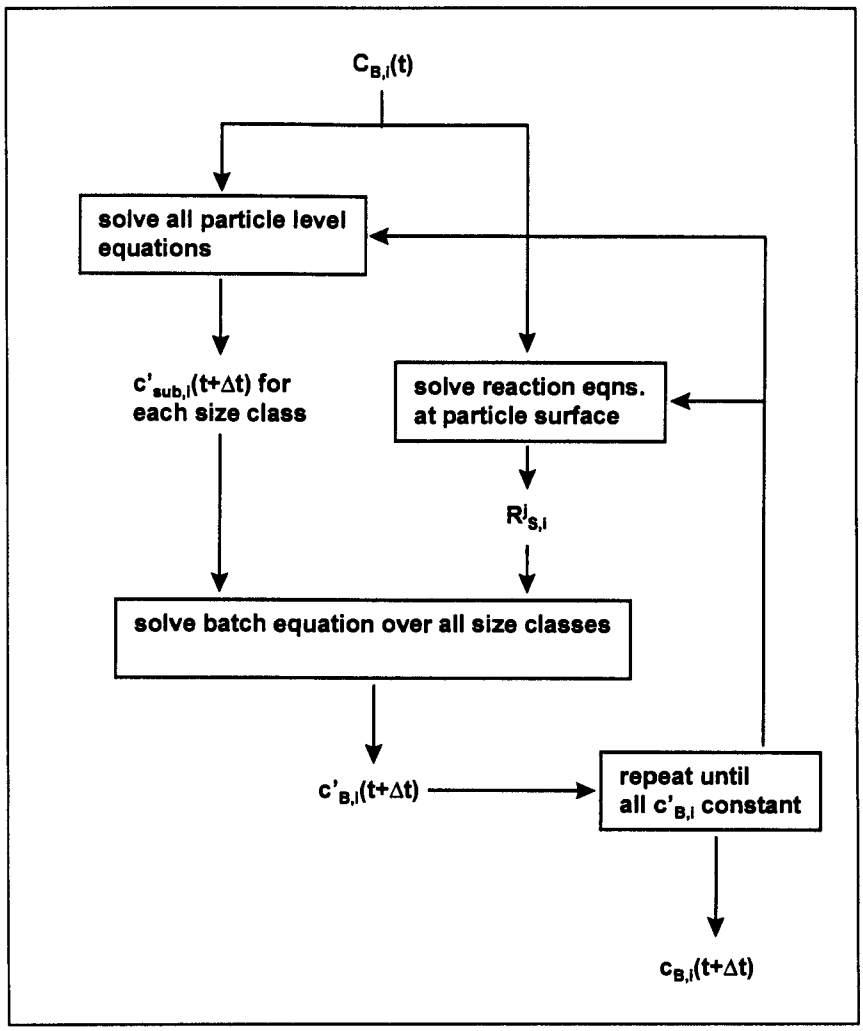

Figure B-5: General solution algorithm for batch modelling

Solving the Column Model

The column bulk transport equation (4.6-14) is a second order partial differential equation in axial direction and time, similar to the particle level equation. Here, however, convective bulk fluid transport also needs to be taken into account, which is de-coupled from the reaction-diffusion part of the equation in order to separate transport by diffusion from transport by bulk movement. Thus, for solution of the bulk transport equation only the diffusion-reaction part of the equation is solved, using a Crank-Nicholson algorithm similar to that applied for the particle level equation. Equation (B.4 a) gives the numerical

version for equation 4.6-12 for the first disk, equation (B.4 b) for all intermediate disks and equation (B.4 c) for the bottom disk. Again, these equations represent a set of N equations in N unknown concentrations $c_i^{(t+\Delta t)}$ and can be solved using a tri-diagonal matrix inversion scheme.

a) for disk 1:

$$\frac{D_{hi}}{2}\left(\frac{(c_{Bi}^{2,t}-c_{Bi}^{2,t})}{(\Delta z)^2}+\frac{(c_{Bi}^{2,t+1}-c_{Bi}^{2,t+1})}{(\Delta z)^2}\right)+$$
$$\frac{k_{ci}}{2}\sum_n \alpha_n\left[\left(c_{Bi}^{1,t}-\left(c_{Si}^{1,t}\right)^{(n)}\right)+\left(c_{Bi}^{1,t+1}-\left(c_{Si}^{1,t+1}\right)^{(n)}\right)\right]$$
$$+\varepsilon_b\sum_j R_{Bi}^j = \varepsilon_b\frac{c_{Bi}^{1,t+1}-c_{Bi}^{1,t}}{\Delta t}$$

b) for disks 2 to N-1:

$$\frac{D_{hi}}{2}\left(\frac{(c_{Bi}^{s-1,t}-2c_{Bi}^{s,t}+c_{Bi}^{s+1,t})}{(\Delta z)^2}+\frac{(c_{Bi}^{s-1,t+1}-2c_{Bi}^{s,t+1}+c_{Bi}^{s+1,t+1})}{(\Delta z)^2}\right)$$
$$\frac{k_{ci}}{2}\sum_n \alpha_n\left[\left(c_{Bi}^{s,t}-\left(c_{Si}^{s,t}\right)^{(n)}\right)+\left(c_{Bi}^{s,t+1}-\left(c_{Si}^{s,t+1}\right)^{(n)}\right)\right]+\varepsilon_b\sum_j R_{Bi}^j = \varepsilon_b\frac{c_{Bi}^{s,t+1}-c_{Bi}^{s,t}}{\Delta t}$$

c) for disk N:

$$\frac{D_{hi}}{2}\left(\frac{(c_{Bi}^{N-1,t}-c_{Bi}^{N,t})}{(\Delta z)^2}+\frac{(c_{Bi}^{N-1,t+1}-c_{Bi}^{N,t+1})}{(\Delta z)^2}\right)$$
$$+\frac{k_{ci}}{2}\sum_n \alpha_n\left[\left(c_{Bi}^{N,t}-\left(c_{Si}^{N,t}\right)^{(n)}\right)+\left(c_{Bi}^{N,t+1}-\left(c_{Si}^{N,t+1}\right)^{(n)}\right)\right]$$
$$+\varepsilon_b\sum_j R_{Bi}^j = \varepsilon_b\frac{c_{Bi}^{N,t+1}-c_{Bi}^{N,t}}{\Delta t}$$

with $$\sum_n \alpha_n = \sum_n \frac{3(1-\varepsilon_h)w^{(n)}}{R^{(n)}} \qquad \text{(B.4)}$$

For each time step this requires knowledge of the bulk node concentrations at the start of the interval and all contributions from the particles in the disk (both in terms of reaction and diffusion from the particle surface). Bulk flow movement is effected only after a number of intervals, the total time of which corresponds to the time necessary for the fluid to move exactly by one node (as determined by node spacing and bulk velocity). At this point the concentrations of each node are moved one step downwards, which corresponds to the assumption that all the fluid contained in one disk is moved to the next one down entirely. Thus continuous bulk movement is resolved into steps.

As the overall solution of the column bulk transport equation is directly linked to the solution of the particle level equations describing the distribution of particle sizes in each disk, some care needs to be taken to achieve the numerous iterations in this process in the most economic manner, as computing time may become prohibitive at this level. The current approach is shown in Figure B-5. Here the intermediate results from each step of the particle level simulation in each disk are used immediately to calculate the contributions to the bulk equation and thus calculate new intermediate bulk concentration, which are the taken as new boundary conditions of the next round of particle level calculations. This double loop is continued until convergence of some key concentrations is achieved. If the surface level equation (4.6-9) is to be used, this is simply switched between solving particle level and bulk equations.

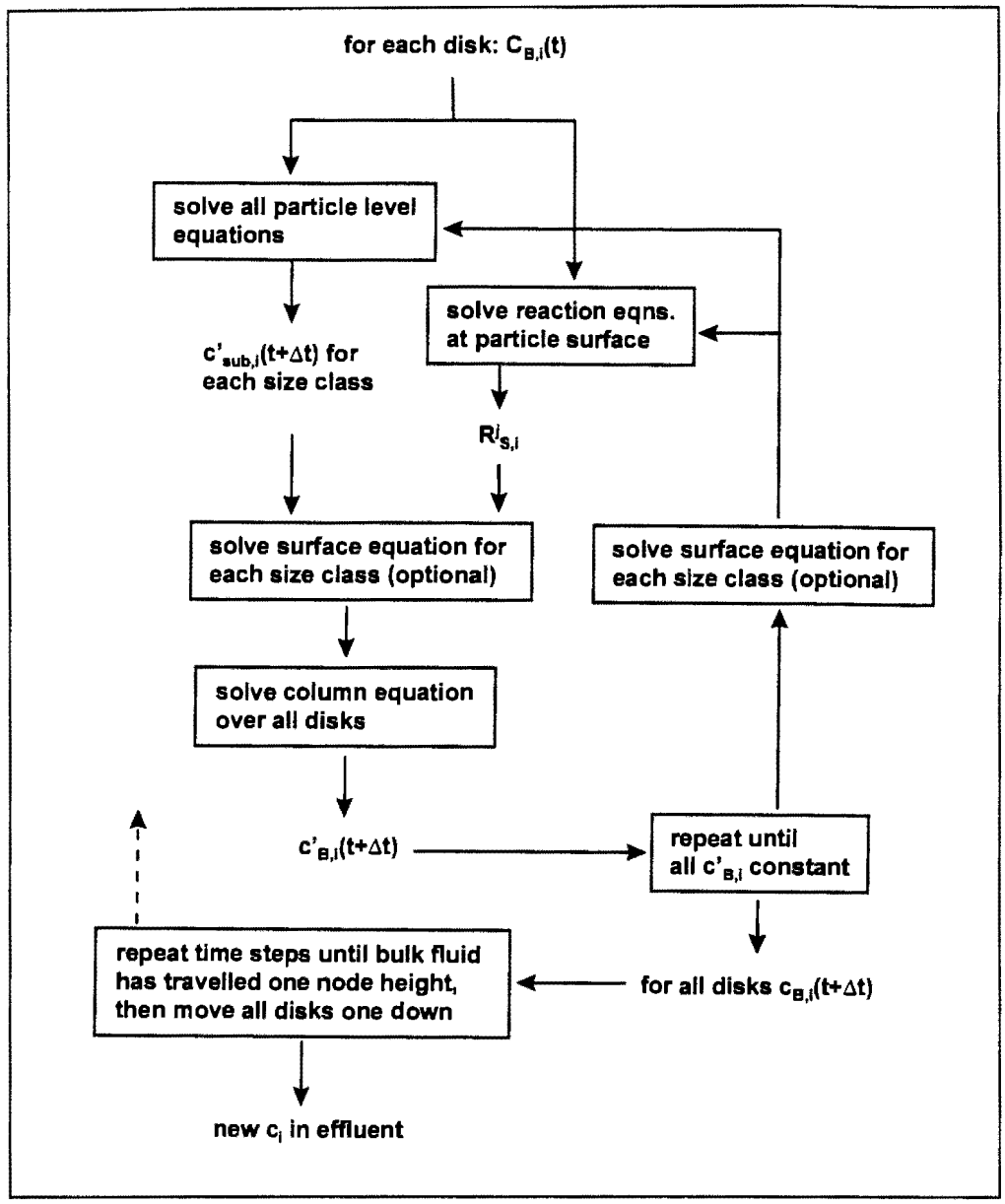

Figure B-6: Solution algorithm for column simulations

Appendix C

Table of Contents - Data Files and WASTESIM Code

A 3.5" disk, labelled DATA & WASTESIM, containing all data files and a proto-type version of the WASTESIM modelling code, is attached to the back of this volume.

Experimental Data Files

The folder DATA contains the zip file Alldata.zip which comprises data files of all experimental data and modelling results pertaining to this thesis as well as most of the graphs used in the text. All data files are Microsoft Excel™ spreadsheets. A detailed table of contents is given below.

File Adsorption.xls

Contains experimental data of Cr adsorption studies on the various materials as well as Freundlich and Langmuir regression analysis and graphs

Sheet	Contents
Cr MD Ads	data for adsorption study on MD material
Cr LCS Ads	data for adsorption study on LCS material

File Bcresults.xls

Contains all modelling results of the sensitivity study based on variations of the base case parameters (Section 4.8) as well as all graphs

Sheet	Contents
PS Mono	batch simulations for various single particle sizes
PSD	batch simulations for some particle size distributions
deff	batch simulations for various effective diffusivity coefficients
k	column simulations for various Cr(VI) dissolution reaction constants

Diffusion.xls (cont.)

Sheet	Contents
adsorption	col. simulations for combined kinetic Cr(VI) dissolution and Langmuir adsorption reaction with various c_{max}
solubility	col. simulations for solubility controlled Na dissolution with various initial solid concentrations of the salt NaX
kin.reac.	col. simulations for Cr(VI) leach reaction for various kinetic constants and reagent concentrations
RT & sat	col. simulations for various bed heights, flow velocities and bed saturations
beddiff	col. simulations for various values of the bed diffusivity coefficient
split flow	col. simulations using split flow approach for various spit ratios

Files ColLCS1.xls, Col LCS2.xls, ColMD1.xls, ColMD2.xls, ColMS123.xls

Contain experimental data of lysimeter studies LCS1, LCS2, MD1 and MD2 as well as all graphs representing the data. The lysimeter study MS123 was used for demonstration of the long-term Cr oxidation effect (Section 2.3)

Sheet	Contents
Info & Flow Data	packing information and all measured flow rates
Anal. Data	all analytical results of effluent concentrations of various metal species and pH
Graphs	all graphs

File ColTrace.xls

Contains experimental data of the tracer studies conducted with the LCS and MD materials as well as all graphs

Sheet	Contents
MDSum	data for tracer study MD3 (flow rates, Li conc in feed and effluent, daily and cumulative), graphs
LCSSum	data for tracer study LCS3 (flow rates, Li conc in feed and effluent, daily and cumulative), graphs

File CroxBall.xls

Contains experimental results from long-term Cr oxidation experiments using moist balls of Cr2O3 (Section 2.3)

Sheet	Contents
Summary	Summary results of all ball experiments, graphs
Ca-1, Ca-2, pH13-1, pH13-2, MnO2-1, MnO2-2	experimental record sheets for the various ball experiments (see Section 2.3 for details)
blank	blank record sheet
calcs	calculations for the estimation of a first order reaction constant and half-life for the Cr oxidation reaction

File CroxBtch.xls

Contains experimental results for the batch Cr oxidation experiments (see Section 2.3)

Sheet	Contents
Crox1 - alkali	data for exp. series Crox1 - oxidation in alkali solution, graphs
Crox2 - acid	data for exp. series Crox2 - oxidation in acidic solution, graphs
Crox 3-Conc.	data for exp. series Crox3 - oxidation at various initial Cr concentrations (in acid solution), graphs
Crox4 - MnO2	data for exp. series Crox4 - oxidation in the presence of MnO_2, graphs
Conv.-pH	graph for oxidation conversion after 100 hrs vs. solution pH

File Diffusion.xls

Contains experimental data of the MD bed diffusion and the LCS particle pore diffusion experiments as well as the results of modelling these and all graphs

Sheet	Contents
MD Bed	experimental data for MD bed diffusion experiment and modelling results
LCS part. diff.	experimental data for LCS pore diffusion experiment (time-dependent adsorption of Cr(VI))
LCS Cr(VI) kinetic	modelling results for kinetic Cr(VI) dissolution from LCS material (see file LCSBatch.xls for experimental data)
LCS Pore Diff.	modelling results for LCS pore diffusion experiment

File LCSBatch.xls

Contains experimental data of various LCS batch leach experiments and all graphs

Sheet	Contents
LCSdata	experimental data for all leach experiments (TCLP, HCl, H2O, high and low alkali)
pH profiles, LCS TCLP, LCS HCl, LCS H2O, high alkali, low alkali	graphs of all experimental data and pH profiles from TCLP, HCl, H2O, high alkali and low alkali leaches
LCS conc.	experimental data for H2O leaches of LCS at various S:L ratios
LCS Endur	experimental data for long-term LCS Cr(VI) leach experiment

File LCSMod.xls

Contains column modelling results for LCS material (LCS1, LCS2 and tracer study) as well as all graphs

Sheet	Contents
LCS1 Mod	various modelling results for LCS1 column study, exp, data, graphs
LCS2 Mod	various modelling results for LCS2 column study, exp. data, graphs
Tracer	modelling results for LCS3 tracer study, single flow, split flow and exp. data, graphs

File Material.xls

Contains all data resulting from the physico-chemical characterisation (Section 5.2) of the various materials, tables and graphs

Sheet	Contents
MD Data	all data for the MD material
LCS Data	all data for the LCS material
MS Data	all data for the Metallurgical Slag material used in the long-term Cr oxidation study (Section 2.3)

File MDBatch.xls

Contains experimental data of various MD batch leach experiments and all graphs

Sheet	Contents
Mddata	experimental data for all leach experiments (TCLP, HCl, H2O, high and low alkali)
pH profiles, MD TCLP, MD HCl, MD H2O, high alkali, low alkali	graphs of all experimental data and pH profiles from TCLP, HCl, H2O, high alkali and low alkali leaches
MD conc.	experimental data for H2O leaches of MD at various S:L ratios
MD Mod	modelling results for MD H2O and high alkali leaches

File MDMod.xls

Contains column modelling results for MD material (MD1, MD2 and tracer study) as well as all graphs

Sheet	Contents
MD1 Mod	various modelling results for MD1 column study, graphs
MD2 Mod	various modelling results for MD2 column study, graphs
Tracer one flow	modelling results for MD3 tracer study, assuming single flow, graphs
Tracer split flow	modelling results for MD3 tracer study using the split flow analysis, graphs
MD1, MD2, Tracer exp. data	experimental data for model comparison used in graphs (from files ColMD.xls and ColTrace.xls)
integration.	numerical integration of tracer results to obtain split ratio

WasteSim Files

The folder WasteSim contains all files relating to the WASTESIM modelling code. These can be divided according to their file extensions as is listed overleaf.

Executables (*.exe)

Files on Disk: WasteSim, WasteMD

WasteSim contains both the data entry platform and the simulation engine. A brief user manual is given in Appendix B. Both the base case study and the LCS simulations can be run from this. WasteMD is a modified version to incorporate the more complex reaction mechanisms involved in modelling the MD material. Only the Md1Sim.rnf run file can be run on this platform .

Screen Files (*.scr)

Files on Disk: FilePage, Legend, LiqSpec, Particle, Reaction, RunPara, SolSpec, System, Welcome

These contain the screen layout for the various levels of the WASTESIM data entry platform and should always be kept together with the main WasteSim program code.

Run Files (*.rnf)

Files on Disk: BlankRun, BaseCase, MD1Sim, LCS2Sim

These are the data files that contain all parameters defined for a specific run. A set of parameters is loaded or saved from the File menu in the WASTESIM main program. BlankRun.rnf contains default parameters and should always be kept with the main WASTESIM code. BaseCase.rnf contains the parameters of the base case study (Section 4.8), MD1Sim.rnf all parameters for the MD1 modelling runs (these MUST be run in the modified WasteMD code). LCS2Sim.rnf contains all parameters for the LCS2 modelling runs.

Result Files (*.res)

Files on Disk: Results

The results of a simulation (time-concentration data) are written to ASCII space delimited files as specified in the File menu of the main WASTESIM code. Results.res is the default file name.

Flow Files (*.dat)

Files on Disk: MD1Flow

These contain data for varying feed flow rates for a column simulation. MD1Flow.dat is used in conjunction with run file MD1Sim.rnf in the WasteMD program.